frontiers | Research Topics

Metabolomics in crop research – current and emerging methodologies, volume III

Edited by
Marta Sousa Silva and Carlos Cordeiro

Coordinated by
Ute Roessner

Published in
Frontiers in Plant Science

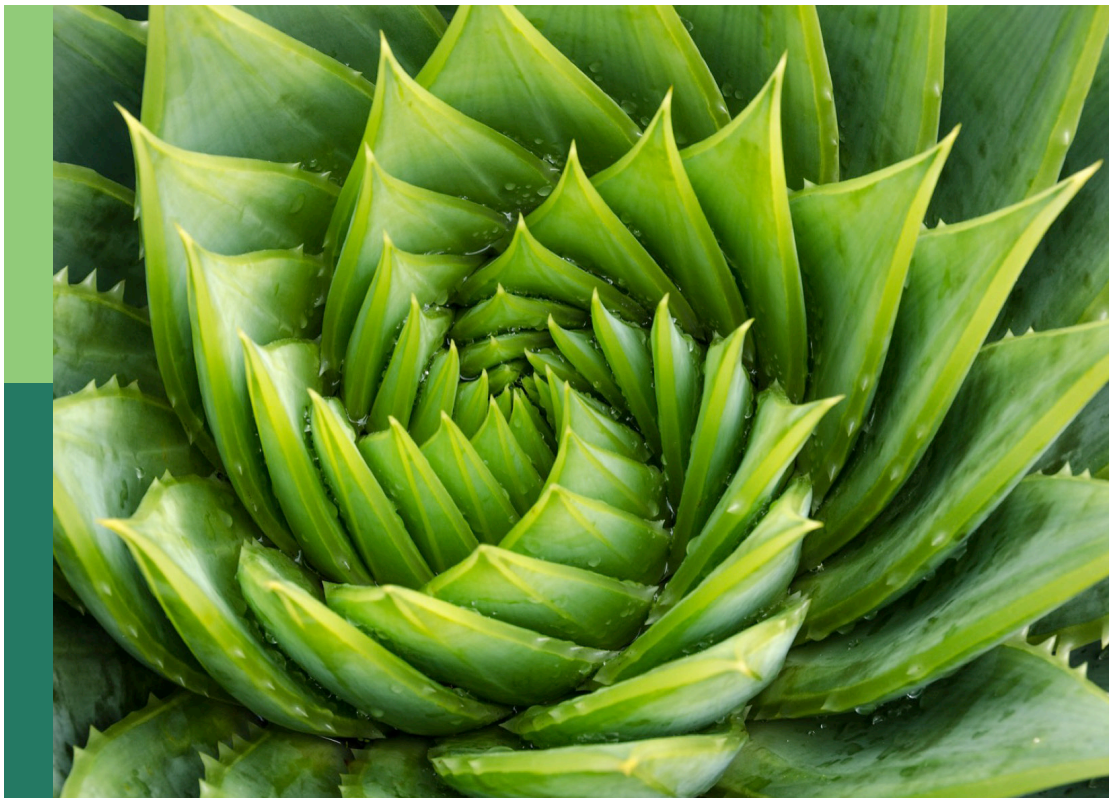

ISSN 1664-8714
ISBN 978-2-8325-6466-0
DOI 10.3389/978-2-8325-6466-0

About Frontiers

Frontiers is more than just an open access publisher of scholarly articles: it is a pioneering approach to the world of academia, radically improving the way scholarly research is managed. The grand vision of Frontiers is a world where all people have an equal opportunity to seek, share and generate knowledge. Frontiers provides immediate and permanent online open access to all its publications, but this alone is not enough to realize our grand goals.

Frontiers journal series

The Frontiers journal series is a multi-tier and interdisciplinary set of open-access, online journals, promising a paradigm shift from the current review, selection and dissemination processes in academic publishing. All Frontiers journals are driven by researchers for researchers; therefore, they constitute a service to the scholarly community. At the same time, the *Frontiers journal series* operates on a revolutionary invention, the tiered publishing system, initially addressing specific communities of scholars, and gradually climbing up to broader public understanding, thus serving the interests of the lay society, too.

Dedication to quality

Each Frontiers article is a landmark of the highest quality, thanks to genuinely collaborative interactions between authors and review editors, who include some of the world's best academicians. Research must be certified by peers before entering a stream of knowledge that may eventually reach the public - and shape society; therefore, Frontiers only applies the most rigorous and unbiased reviews. Frontiers revolutionizes research publishing by freely delivering the most outstanding research, evaluated with no bias from both the academic and social point of view. By applying the most advanced information technologies, Frontiers is catapulting scholarly publishing into a new generation.

What are Frontiers Research Topics?

Frontiers Research Topics are very popular trademarks of the *Frontiers journals series*: they are collections of at least ten articles, all centered on a particular subject. With their unique mix of varied contributions from Original Research to Review Articles, Frontiers Research Topics unify the most influential researchers, the latest key findings and historical advances in a hot research area.

Find out more on how to host your own Frontiers Research Topic or contribute to one as an author by contacting the Frontiers editorial office: frontiersin.org/about/contact

Metabolomics in crop research – current and emerging methodologies, volume III

Topic editors
Marta Sousa Silva — University of Lisbon, Portugal
Carlos Cordeiro — University of Lisbon, Portugal

Topic coordinator
Ute Roessner — The University of Melbourne, Australia

Citation
Sousa Silva, M., Cordeiro, C., Roessner, U., eds. (2025). *Metabolomics in crop research – current and emerging methodologies, volume III*.
Lausanne: Frontiers Media SA. doi: 10.3389/978-2-8325-6466-0

Table of contents

05 Editorial: Metabolomics in crop research – current and emerging methodologies, volume III
Marta Sousa Silva and Carlos Cordeiro

08 Comparative transcriptomic and metabolomic analyses reveal differences in flavonoid biosynthesis between PCNA and PCA persimmon fruit
Yiru Wang, Yujing Suo, Weijuan Han, Huawei Li, Zhenxu Wang, Songfeng Diao, Peng Sun and Jianmin Fu

21 Metabolomic and transcriptomic analyses of rice plant interaction with invasive weed *Leptochloa chinensis*
Liang Zhang, Ke Chen, Tianrui Li, Shuren Yuan, Chenyang Li, Lianyang Bai and Lifeng Wang

33 Response of bacterial community metabolites to bacterial wilt caused by *Ralstonia solanacearum*: a multi-omics analysis
Chengjian Wei, Jinchang Liang, Rui Wang, Luping Chi, Wenjing Wang, Jun Tan, Heli Shi, Xueru Song, Zhenzhen Cui, Qiang Xie, Dejie Cheng and Xiaoqiang Wang

47 Untargeted metabolomics profiling of oat (*Avena sativa* L.) and wheat (*Triticum aestivum* L.) infested with wheat stem sawfly (*Cephus cinctus* Norton) reveals differences associated with plant defense and insect nutrition
Megan S. Hager, Megan L. Hofland, Andrea C. Varella, Brian Bothner, Hikmet Budak and David K. Weaver

67 Multiple omics revealed the growth-promoting mechanism of *Bacillus velezensis* strains on ramie
Xin Wang, Yanzhou Wang, Yafen Fu, Yang Zhai, Xuehua Bai, Tongying Liu, Guang Li, Liangbin Zeng and Siyuan Zhu

82 Metabolomics and quantitative analysis to determine differences in the geographical origins and species of Chinese dragon's blood
Xiuting Sun, Qing Huang, Mingsong Wu, Liu He, Xiangsheng Zhao and Xinquan Yang

98 A multi-omics insight on the interplay between iron deficiency and N forms in tomato
Arianna Lodovici, Sara Buoso, Begoña Miras-Moreno, Luigi Lucini, Nicola Tomasi, Pascual García-Pérez, Roberto Pinton and Laura Zanin

116 Application of metabolomics in quality control of traditional Chinese medicines: a review
Peiran Ji, Xinquan Yang and Xiangsheng Zhao

130 Color-induced changes in *Chrysanthemum morifolium*: an integrative transcriptomic and metabolomic analysis of petals and non-petals
Jianhong Wei, Zhaoxiang Zeng, Chengwu Song, Qing Lv, Guangya Chen, Guoyan Mo, Ling Gong, Shuna Jin, Rongzeng Huang and Bisheng Huang

142 Sprayable solutions containing sticky rice oil droplets reduce western flower thrips damage and induce changes in *Chrysanthemum* leaf chemistry
Thijs V. Bierman, Hocelayne P. Fernandes, Young H. Choi, Sumin Seo, Klaas Vrieling, Mirka Macel, Bram Knegt, Thomas E. Kodger, Ralph van Zwieten, Peter G. L. Klinkhamer and T. Martijn Bezemer

153 Transcriptional and metabolic analysis of oleic acid synthesis in seedless and tenera oil palm species
Wen Xu, Jerome Jeyakumar John Martin, Xinyu Li, Xiaoyu Liu, Shunghong Cheng and Hongxing Cao

166 Microstructure observation and flavor substances excavation of Yunyan 87 tobacco leaves with different oil contents
Xianfeng Hu, Wei Xu, Yubo Zhang, Shouhui Pan, Yanlan Xie, Rui Liao, Shenggang Yang, Youxiang Wu and Daomao Deng

178 Joint analysis of transcriptional metabolism for flavonoid synthesis during different developmental periods in oil palm exocarp
Ruimin Zhang, Jerome Jeyakumar John Martin, Xiaoyu Liu, Xinyu Li, Lixia Zhou, Rui Li, Xiaopeng Fu, Wenrao Li and Hongxing Cao

frontiers | Frontiers in Plant Science

TYPE Editorial
PUBLISHED 02 June 2025
DOI 10.3389/fpls.2025.1627911

OPEN ACCESS

EDITED AND REVIEWED BY
Laigeng Li,
Chinese Academy of Sciences (CAS), China

*CORRESPONDENCE
Marta Sousa Silva
mfsilva@fc.ul.pt

RECEIVED 13 May 2025
ACCEPTED 20 May 2025
PUBLISHED 02 June 2025

CITATION
Sousa Silva M and Cordeiro C (2025) Editorial: Metabolomics in crop research – current and emerging methodologies, volume III. *Front. Plant Sci.* 16:1627911. doi: 10.3389/fpls.2025.1627911

Editorial: Metabolomics in crop research – current and emerging methodologies, volume III

Marta Sousa Silva* and Carlos Cordeiro

FT-ICR and Structural Mass Spectrometry Laboratory, Biosystems and Integrative Sciences Institute (BioISI), Faculdade de Ciências, Universidade de Lisboa, Lisboa, Portugal

KEYWORDS

metabolomics, agriculture, biomarkers, plant metabolism, defense mechanisms, plant-microbe interactions, quality control

Editorial on the Research Topic
Metabolomics in crop research – current and emerging methodologies, volume III

The potential of metabolomics in plant and crop research was the driving force for the Research Topic "Metabolomics in Crop Research - Current and Emerging Methodologies" 8 years ago. Since then, this area has significantly evolved due to advances in analytical technologies, particularly mass spectrometry (MS), data processing, and integration with other "omics" fields. At the same time, artificial intelligence has improved the interpretation of complex metabolomic datasets, enabling researchers to link specific metabolic profiles with traits like stress tolerance, disease resistance, and nutritional content more effectively. Integration with genomics, transcriptomics, and phenomics became more straightforward, making metabolomics a central part of systems biology approaches to crop research.

The Research Topic "Metabolomics in Crop Research - Current and Emerging Methodologies" reached its third edition with 13 articles from 102 authors, highlighting different applications of metabolomics to plant metabolism and development, crop defense mechanisms, plant-microbe interactions and soil nutrient dynamics.

Understanding plant metabolism and development at the molecular level is crucial for improving crop quality, productivity, and resilience. Different analytical methodologies and "omics" strategies, particularly transcriptomics and metabolomics, are often combined to uncover the regulatory networks driving important phenotypic and metabolic outcomes in plants. In this Research Topic, Hu et al. explored the oil content of *Nicotiana tabacum* L. 'Yunyan 87' leaves as a crucial quality indicator, by combining a sensory evaluation with scanning electron microscopy (SEM) and GC×GC-TOF mass spectrometry. The high-oil tobacco leaves contained more metabolites than the low-oil content ones, with an increased concentration of oil- and aroma-related compounds. The oil of the palm *Elaeis guineensis* Jacq. was analyzed by Xu et al. to understand the regulatory mechanisms and metabolic pathways responsible for changes in oleic acid biosynthesis during fruit development. The metabolites from two oil palm varieties' fruits ('Seedless' and 'Tenera') at three developmental stages were analyzed using a targeted metabolomics approach, by LC-MS^2, combined with gene expression analysis of genes related to oleic acid metabolism. Significant differences were observed in both varieties and at the different fruit

developmental stages and revealed the ley regulatory mechanisms underlying oleic acid biosynthesis. In another variety of the same crop plant, the green-fruited oil palm variety ('O×G Amazon'), Zhang et al. analyzed the flavonoid content in fruits at different developmental stages. Flavonoids are important polyphenolic compounds with antioxidant and antimicrobial properties. The authors used a combined metabolomic (using an LC-TripleTOF) and transcriptomic approach to identify the compounds and key genes of flavonoid metabolism during fruit development. These studies paved the way for the development of metabolic engineering strategies for improving oleic acid and flavonoid content in oil palm plants. A similar research was performed by Wang et al. with different varieties of persimmon (*Diospyros kaki*) fruits, known by their rich flavonoid content. The authors analyzed the accumulation of flavonoids and its biosynthesis related genes' expression in different developmental stages of two mature pollination-constant non-astringent varieties ('Jiro' and 'Yohou') and in two pollination-constant astringent ones ('Zhongshi5' and 'Huojing'), using a targeted metabolomics and transcriptomic approach, relating them to the astringency and flavor traits of these persimmons' fruits.

An integrative metabolomic and transcriptomic study by Wei et al. was also conducted in the flowers of *Chrysanthemum morifolium*, an important ornamental plant with culinary and medicinal value. Different colored petals (yellow, gold, and white) and as non-petal tissues were analyzed, revealing the key regulatory pathways responsible for color variation and providing a foundation for future quality control in breeding strategies. These *Chrysanthemum* plants are highly susceptible to pests, particularly to *Frankliniella occidentalis* (Pergande), a widely spread pest thrip affecting many ornamental plants and horticultural crops. Investigating the variety "Baltica White" from *C. morifolium*, Bierman et al. used metabolomics (1H NMR and headspace GC-MS) to study the effects of spraying of solutions containing sticky oil droplets, in reducing infection's efficiency, in plant growth and in the leaf's metabolome. The authors observed that these natural origin spraying solutions had a repellent or toxic effect for the thrips, leading to chemical changes in the plant leaves, thus playing a role in plant defense against these pests.

Cereals too are highly affected by pests, the wheat stem sawfly *Cephus cinctus* Norton being particularly harmful to wheat *Triticum aestivum* L. in North America. One of the most adopted strategies to prevent yield loss is the use of wheat varieties with solid stems, preventing the development of the larvae. Hager et al. studied the metabolome's changes in response to infestation by the wheat stem sawfly in 2 varieties of oat (*Avena sativa* 'Dane' and 'Otana', resistant) and 4 varieties of spring wheat (*Triticum aestivum* 'Choteau', 'Scholar', 'Conan', and 'Reeder', with different levels of resistance), using an untargeted metabolomics approach by liquid chromatography-mass spectrometry (LC-MS). The analysis identified several compounds (carbohydrates, lipids and plant defense molecules) differentially expressed between samples and associated with the oat's constitutive resistance to this sawfly, establishing the basis for the future development of new strategies to prevent wheat infection.

Besides the threats caused by insects, some crops must cope with invasive weeds, which compromise a significant percentage of the production yield. Rice (*Oryza sativa* L.) is one of these examples, largely affected by the invasive weed *Leptochloa chinensis*. Zhang et al. investigated the mutual inhibition of rice and this weed under mono- and co-culture conditions. A combined metabolomic (UHPLC-MS) and transcriptomic analysis revealed the metabolic and transcriptional regulatory networks behind the mutual suppression between rice and *L. chinensis*, with a more pronounced inhibition of root length in co-culture conditions. These results are highly relevant for developing new and more effective strategies for weed control and crop protection.

Crops are also affected by soil bacteria. These microorganisms can either cause damage, which is the case of the wilt causing agent *Ralstonia solanacearum*, or act as a community to provide natural defenses against pathogens and support healthy plant growth. In all these pathogenic or symbiotic networks, metabolites produced by plants and rhizosphere microorganisms play an important role. Wei et al. studied the metabolite composition of the rhizosphere of *Nicotiana tabacum* plants, cultivar 'Yunyan 87', grown in healthy and infected soils (by GC-TOF), the effect of bacterial communities, and the changes in soil properties. These results enlighten how rhizosphere bacteria confer resistance during the early stages of infection, thus contributing to a more sustainable control of soil pathogens. In another work, Wang et al. investigated the effect of the plant growth-promoting bacteria *Bacillus velezensis* in the growth of ramie (*Boehmeria nivea*), through the analysis of the soil microbial communities and the metabolic profile of the plant (by LC-MS). The yield and traits of ramie crop plants were improved after treatment with *B. velezensis*, revealing that these bacteria played an important role in regulating soil microbial structure and promoting plant metabolism, growth, and development, highlighting the importance of using these microorganisms as biological fertilizers and growth-promoting stimulants.

Plant growth is highly affected by the bioavailability of several nutrients, particularly nitrogen (N) and iron (Fe). Lodovici et al. studied the interplay between N and Fe nutritional pathways in tomato plants (*Solanum lycopersicum* L. cv 'Marmande') under both elements' deficiency and after their reintroduction in the soil, by combining a physiological characterization with untargeted metabolomics (using UHPLC-QTOF) and gene expression analysis. The results revealed treatment-specific changes in tomato metabolic pathways, with changes in nitrogen-containing metabolites in leaves and roots and modulation of the phytohormone profile by the nitrogen source. This study contributes to understanding the interplay between nitrogen and iron nutritional pathways in crops.

Finaly, an important application of metabolomics in crop research is quality control and geographic origin. Sun et al. used an untargeted metabolomics approach (LC-MS/MS), combined with a targeted analysis for phenolic compounds (UHPLC-PDA), to analyze the Chinese dragon's blood species *Dracaena cochinchinensis* and *Dracaena cambodiana* from distinct

geographical origins. This study highlights the differences in the plant quality from different geographical origins and between the two species. Ji et al. presented a comprehensive review of the use of metabolomics in quality control of traditional Chinese medicinal plants. Their metabolism and metabolic profile were influenced by the plant's geographical origin, developmental stage, harvesting cycle, and processing methods, thus strongly affecting the quality of different plant organs and their suitability for use in traditional Chinese medicine.

Author contributions

MS: Conceptualization, Writing – original draft, Writing – review & editing, Funding acquisition. CC: Writing – review & editing, Funding acquisition, Writing – original draft.

Funding

The author(s) declare that financial support was received for the research and/or publication of this article. The authors acknowledge the support from the Fundacao para a Ciencia e a Tecnologia, Portugal, through the project 2023.14744.PEX (DOI: 10.54499/2023.14744.PEX) and the research center BioISI (ref. UIDB/04046/2020 and UIDP/04046/2020). The authors also acknowledge the support from the Portuguese Mass Spectrometry Network (RNEM, LISBOA2030-FEDER-01319300) and the Research Infrastructure project European Network of Fourier-Transform Ion-Cyclotron-Resonance Mass Spectrometry Centers (EU FT-ICR-MS) funded by the European Union's Horizon 2020 research and innovation programme, Grant Agreement No 731077.

Acknowledgments

The editors of this topic would like to thank all the authors and reviewers, and support staff who contributed to the success of the third volume of this Frontiers Research Topic. We also acknowledge the Frontiers Editorial Office, the Chief Editors and the Frontiers Plant Science Production Office for their technical support.

Conflict of interest

The authors declare that the research was conducted in the absence of any commercial or financial relationships that could be construed as a potential conflict of interest.

The author(s) declared that they were an editorial board member of Frontiers, at the time of submission. This had no impact on the peer review process and the final decision.

Generative AI statement

The author(s) declare that no Generative AI was used in the creation of this manuscript.

Publisher's note

frontiers | Frontiers in Plant Science

TYPE Original Research
PUBLISHED 27 February 2023
DOI 10.3389/fpls.2023.1130047

OPEN ACCESS

EDITED BY
Sezai Ercisli,
Atatürk University, Türkiye

REVIEWED BY
Yu Wang,
Northeast Forestry University, China
Roberto Mattioli,
Sapienza University of Rome, Italy
Gülçe Ilhan,
Atatürk University, Türkiye

*CORRESPONDENCE
Weijuan Han
hanweijuan2013@163.com
Jianmin Fu
fjm371@163.com

†These authors have contributed equally to this work and share first authorship

SPECIALTY SECTION
This article was submitted to Plant Metabolism and Chemodiversity, a section of the journal Frontiers in Plant Science

RECEIVED 22 December 2022
ACCEPTED 16 February 2023
PUBLISHED 27 February 2023

CITATION
Wang Y, Suo Y, Han W, Li H, Wang Z, Diao S, Sun P and Fu J (2023) Comparative transcriptomic and metabolomic analyses reveal differences in flavonoid biosynthesis between PCNA and PCA persimmon fruit. *Front. Plant Sci.* 14:1130047. doi: 10.3389/fpls.2023.1130047

Comparative transcriptomic and metabolomic analyses reveal differences in flavonoid biosynthesis between PCNA and PCA persimmon fruit

Yiru Wang[1†], Yujing Suo[1†], Weijuan Han[1*], Huawei Li[1], Zhenxu Wang[2], Songfeng Diao[1], Peng Sun[1] and Jianmin Fu[1*]

[1]Research Institute of Non-Timber Forestry, Chinese Academy of Forestry, Zhengzhou, China, [2]Food Inspection Center, Henan Institute of Product Quality Technology, Zhengzhou, China

The fruit of the persimmon (*Diospyros kaki*.) has high economic and nutritional value and is rich in flavonoids. Flavonoids are essential secondary metabolisms in plants. The association between persimmon astringency and changes in the proanthocyanidins (a flavonoid subclass) content is well-known. However, information on the relationships between different astringency types and other flavonoid subclasses and biosynthetic genes is more limited. In this study, an initial correlation analysis between total flavonoids and fruit astringency type, and KEGG analysis of metabolites showed that flavonoid-related pathways were linked to differences between mature pollination-constant non-astringent (PCNA) varieties ('Jiro' and 'Yohou') and pollination-constant astringent (PCA) fruit varieties ('Zhongshi5' and 'Huojing'). Based on these findings, variations in the expression of genes and metabolites associated with flavonoid biosynthesis were investigated between typical PCNA ('Jiro') and PCA ('Huojing') persimmons during fruit development. The flavonoid concentration in 'Huojing' fruit was significantly higher than that of 'Jiro' fruit, especially, in levels of proanthocyanin precursor epicatechin and anthocyanin cyanidin derivatives. Combined WGCNA and KEGG analyses showed that genes such as *PAL*, *C4H*, *CHI*, *CHS*, *F3H*, *F3'5'H*, *FLS*, *DFR*, *ANR*, *ANS*, and *UF3GT* in the phenylpropanoid and flavonoid biosynthesis pathways may be significant factors impacting the proanthocyanin precursor and anthocyanin contents. Moreover, interactions between the *R2R3MYB* (*evm.TU.contig7272.598*) and *WD40* (*evm.TU.contig3208.5*) transcription factors were found to be associated with the above structural genes. These findings provide essential information on flavonoid biosynthesis and its regulation in the persimmon and lay a foundation for further investigation into how astringency types affect flavor components in PCNA and PCA persimmons.

KEYWORDS

persimmon, fruit, flavonoid biosynthesis, metabonomic, transcriptomic

1 Introduction

Flavonoids are essential secondary metabolites in plants and include more than 10 000 structural variants (Quideau et al., 2011; Mikhailova et al., 2022; Tahmaz and Soylemezoglu, 2022). Flavonoids are divided into six subclasses according to substitutions and B-ring attachments to the basic skeletal structure, namely, flavones, flavonols, anthocyanins, flavanols, flavanones, and isoflavones (Winkel-Shirley, 2001; Sasaki and Nakayama, 2015). These compounds have essential physiological and ecological functions in regulating plant growth and development, flower coloring, fruit flavor, physiological activities, and adaptation to abiotic stress in plants (Havsteen, 2002; Tohge et al., 2018). Flavonoids produced by plants have many health benefits for humans, including antibacterial, antiparasitic, anti-inflammatory, anticancer, and anti-aging properties (Dias et al., 2021). Flavonoids have various pharmaceutical activities and often act as antioxidants according to their free radical-scavenging abilities (Kumar and Pandey, 2013). Thus, flavonoids have gained increasing attention and are widely used in the food, cosmetic, and pharmaceutical industries.

The flavonoid synthesis pathway is relatively well understood in model plants (Routaboul et al., 2006; Tohge et al., 2017). The structural genes encoding enzymes in the pathway have been identified, including genes encoding phenylalanine lyase (*PAL*), anthocyanidin synthase (*ANS*), cinnamic acid hydroxylase (*C4H*), coumadin CoA ligase (*4CL*), chalcone synthase (*CHS*), flavonoid 3'-hydroxylase (*F3'H*), chalcone isomerase (*CHI*), flavonol synthase (*FLS*), flavonoid 3'5'-hydroxylase (*F3'5'H*), and the other key genes (Routaboul et al., 2006; Saito et al., 2013; Chen and Li, 2016). Studies on flavonoid biosynthesis have been conducted in many horticultural plants such as *Vitis vinifera* (Azuma et al., 2012), *Malus×domestica* (Henry-Kirk et al., 2012), *Ziziphus jujuba* (Zhang et al., 2020), and others. Furthermore, flavonoid biosynthesis is known to be influenced by the environment, developmental stage, plant variety, temperature, and tissue type (Azuma et al., 2012; Wen et al., 2020). Transcription factors (TFs) involved in the flavonoid biosynthesis pathway have also been identified, such as *R2R3MYB*, *bZIP*, *WD40*, and *bHLH* (Chen et al., 2022).

Persimmon (*Diospyros kaki* Thunb.) is a fruit tree that belongs to the family Ebenaceae and has a long history of cultivation (Saleem et al., 2022). As a major fruit variety with a unique flavor, the persimmon has become increasingly popular and has high commercial value in Asian countries (Han et al., 2022). Flavonoids produced by plants have many health benefits for humans and play crucial roles in both the fruit quality and its economic value (Dias et al., 2021; Xie et al., 2022). Persimmons are rich in phytochemicals such as flavonoids, carotenoids, triterpenoids, fatty acids, and vitamin C (Direito et al., 2021), with flavonoids being the main active antioxidants (Sun et al., 2011). The persimmon fruit has a variety of pharmacological poroperties, including antiadipogenic, hypocholesterolemic, antioxidant, anti-inflammatory, and antitumor poroperties, due to its flavonoid components such as hesperidin, naringin, and nobiletin (Direito et al., 2021). Besides, flavonoids such as proanthocyanidins are associated with the astringency and flavor of the persimmon fruits (Zheng et al., 2021).

Proanthocyanidins (PAs), also known as condensed tannins, are a subclass of flavonoids and consist of oligomers of catechins that are biosynthesized through the flavonoid branch of the phenylpropanoid pathway (Dixon et al., 2005; Zheng et al., 2021). High concentrations of insoluble PAs usually lead to astringency in persimmon fruit. Based on the fruit characteristics, persimmons can be classified into four astringency types, namely, the pollination-variant non-astringent (PVNA), PCNA, PCA, and pollination-variant astringent (PVA) types (Yonemori et al., 2000). In China, almost all persimmon cultivars belong to the PCA type, and no PVA and PVNA types are found (Du et al., 2009). The quality and flavor of the persimmon fruit vary greatly, with significant differences between PCNA and PCA persimmons. The fruit astringency type is not only affected the proanthocyanidins content but also the accumulation of total soluble solids, individual sugars, total phenolics, and total flavonoids (Novillo et al., 2016; Yildiz and Kaplankiran, 2018). The influence of the astringency types on variations in the proanthocyanidins concentration is well-known in persimmon fruit (Akagi et al., 2009). However, little is known about the impact of the fruit astringency type on flavonoid metabolic pathway and its associated enzymes, genes, and TFs in persimmon fruit.

This study conducted transcriptomic and quasi-targeted metabolomic analyses to elucidate both gene expression and metabolite accumulated profiles in different stages of PCNA and PCA persimmon fruit. Specifically, dynamic changes in the expression of genes and TFs in flavonoid biosynthesis and the accumulation of a set of flavonoids were analyzed to clarify and compare the secondary metabolism of the persimmon fruit and its complex effects on the astringency and flavor components between PCNA and PCA persimmons.

2 Material and methods

2.1 Plant materials

Well-cultivated PCNA ('Jiro' and 'Youhou') and PCA ('Zhongshi No.5' and 'Huojing') persimmons were planted in the forest planting base of the Research Institute of Non-timber Forestry (34°55′18″–34°56′27″N, 113°46′14″–113°47′35″E), Yuanyang County, Henan Province, China. The fruits of the 'Jiro' and 'Huojing' persimmon fruit were sampled at the young-fruit stage (when the fruit had reached about 40% of the final size, stage 1), the fruit expansion stage (when the fruit had reached approximately 70% of its final size, stage 2), the turning stage (the initial change in the skin color of the fruit, stage 3) and the mature

Abbreviations: PCNA, pollination-constant non-astringent; PCA, pollination-constant astringent; PVNA, pollination-variant non-astringent; PVA, pollination-variant astringent; DAFs, differentially accumulated flavonoids; DEGs, differentially expressed genes; WGCNA, weighted gene coexpression network analysis; PAs, proanthocyanidins.

stage (fully developed fruit color without astringency, stage 4). Persimmon fruit from the 'Zhongshi No.5' and 'Youhou' varieties were also harvested at stage 4 and termed PCA1 and PCNA2, respectively. The four development stages (from stage 1 to stage 4) of the 'Jiro' and 'Huojing' fruit were labeled as Jiro_S1, Jiro_S2, Jiro_S3, Jiro_S4 and Huojing_S1, Huojing_S2, Huojing_S3, and Huojing_S4, respectively. Furthermore, fruits of 141 persimmon germplasms were also harvested at the mature stage (stage 4), and these samples were used for total flavonoids content detection. The fresh fruit was frozen immediately in liquid nitrogen and stored at -80° until used for RNA extraction and metabolic analyses.

2.2 Extraction and determination of total flavonoids

The total flavonoids of persimmon fruit were extracted and detected according to Han et al. (Han et al., 2021) with a few modifications. Briefly, fruit powder (precise weight 5 g) was extracted with 60% (v/v) ethanol in an ultrasonic bath (30 min). Total flavonoid content was determined by $AlCl_3$-(HAc-NaAC) colorimetric method, and rutin with purity = 98% (Solarbio Science & Technology Co., Ltd.) were used as a standard. The absorbance was determined at 420 nm wavelength in a UV spectrophotometer. Total flavonoids content and astringency type of 141 persimmon germplasms are listed in Supplementary Table 1.

2.3 Metabolome data analysis process

The method used for metabolite identification was similar to that of Wang et al. (Wang et al., 2022). Samples of freeze-dried persimmon fruit (100 mg) were weighed into 1.0 mL of 70% aqueous methanol. Metabolite profiling was performed using an ExionLC™ AD system (SCIEX) coupled with a QTRAP®6500+ mass spectrometer (SCIEX) and equipped with Xselect HSS T3 column (2.1×150 mm, 2.5 μm) by Novogene Co., Ltd. (Beijing, China). The mobile phase included eluent A, consisting of 0.1% formic acid in water, and eluent B, consisting of 0.1% formic acid-acetonitrile. The analysis conditions were as follows: column temperature, 50°C; injection volume, 1.5 μL; flow rate, 0.4 mL/min. The mobile phases were water. The gradient program of phase A/phase B was 98:2 (v/v) at 0 min, 98:2 (v/v) at 2 min, 0:100 (v/v) at 15 min, 0:100 (v/v) at 17 min, 98:2 (v/v), at 17.1 min and 98:2 (v/v) at 20 min. The qualitative analysis of metabolites was conducted according to the secondary spectral information using Novogene's in-house database. Metabolite quantification was carried out using the triple quadrupole mass spectrometer's multiple reaction monitoring (MRM) mode. The KEGG (Kyoto Encyclopedia of Genes and Genome) database (http://www.genome.jp/kegg/) (Kanehisa et al., 2004) and HMDB (Human Metabolome Database) database (http://www.hmdb.ca/) (Wishart et al., 2007) were used for metabolite annotation. The metabolites with P-value < 0.05 and fold change≥ 2 were considered as differentially accumulated flavonoids (DAFs).

2.4 Transcriptome data analysis

Total RNA was extracted using the TRIzol Total RNA Isolation Kit (Sangon, Shanghai, China), and a library was established. Bioanalyzer 2100 was used to assess the RNA integrity. The NovaSeq platform (Illumina, San Diego, CA, USA) sequencing generates 150 bp paired-end readings. HISAT2 software (Zhang et al., 2021) was used to map the filtered reads to the *D. kaki* reference genome (unpublished). The prediction of new transcripts was performed using StringTie (Shumate et al., 2022). FeatureCounts (Liao et al., 2014) was used to count the read numbers mapped to each gene. The FPKM of each gene was calculated according to the length of the gene and the read count mapped to the gene. DEseq2 (Love et al., 2014) was used to detect the differentially expressed genes (DEGs) between the two groups, with a |log2-fold change| ≥ 1 and padj ≤ 0.05. ClusterProfiler 4.0 (Wu et al., 2021) was used for DEGs in Gene Ontology (GO) (Ashburner et al., 2000) and KEGG (Kanehisa et al., 2004) functional enrichment analyses. Heatmaps and K-means clustering were prepared using the online software Hiplot (Li et al., 2022). The weighted gene coexpression network analysis (WGCNA) were constructed using all genes and were analyzed using WGCNA R package (Langfelder and Horvath, 2008). The networks were visualized using Cytoscape v3.9.1 (Shannon et al., 2003).

2.5 Quantitative RT-PCR analysis

The cDNA was synthesized from the high-quality total RNA using TRUE-script First-Strand cDNA Synthesis Kit (Kemix, Beijing, China). Reactions were performed with LightCycler 480 II (Roche), and PCR conditions were 95°C for 3 min, 45 cycles of 95°C for 5 s, and 55-60°C for 30 s. All analyses were conducted with three biological replicates. The relative expression of each sample was calculated by the 2−ΔΔCt method. The persimmon *GAPDH* gene was used as a reference gene (Du et al., 2019). All gene primers are listed in Supplementary Table 2.

3 Results

3.1 Correlation analysis between total flavonoids content and astringency type

The correlation between flavonoids content and fruit astringency were detected in the mature fruit of a natural population with different persimmon cultivars (Supplementary Table 1). The Pearson correlation coefficient (r) between total flavonoids content of persimmon fruit and astringency types of 141 persimmon resources was 0.415**, indicating a significant correlation between total flavonoids content and fruit astringency type (P < 0.01). The above information indicated that total flavonoids were differences between PCNA and PCA fruit.

3.2 Comparison of metabolites between mature PCNA and PCA persimmon fruit

To comprehensively define and compare the metabolite profiles between the PCNA and PCA persimmons, we evaluated metabolite compositions using a Quasi-Targeted metabolome. Mature fruits from the 'Jiro', 'Youhou', 'Zhongshi No.5', and 'Huojing' persimmon varieties were labeled as PCNA1, PCNA2, PCA1, and PCA2, respectively. Principal component analysis based on the data for all compounds separated all samples into four distinct groups, with each sample and its replicates forming a separate group, indicating that there were good correlations within group replicates and differences among the different groups (Figure S1). A total of 889 metabolites were identified in PCNA and PCA fruit, including five metabolite categories, namely, amino acids and their derivatives (170), flavonoids (135), carbohydrates and their derivatives (76), nucleotides and their derivates (65), and organic acid and its derivatives (62) (Supplementary Table 3).

To systematically identify and compare the metabolic pathways between the fruit of the PCNA and PCA genotypes, KEGG enrichment analysis was conducted on the differential metabolites of the four groups (PCNA1 vs. PCA1, PCNA1 vs. PCA2, PCNA2 vs. PCA1, and PCNA2 vs. PCA2). Phenylpropanoid biosynthesis (ko00940), phenylalanine metabolism (ko00360), flavonoid biosynthesis (ko00941), flavone and flavonol biosynthesis (ko00944), and anthocyanin biosynthesis (ko00942) were found to be significantly enriched. The KEGG annotation results suggested that flavonoid metabolism-related pathways were involved in the nutritional value and taste differences between PCNA and PCA fruit (Figures 1A-D). Given the importance of flavonoids to human health, the subsequent investigation were focused on flavonoid synthesis during PCNA and PCA fruit development.

3.3 RNA-Seq of PCNA and PCA persimmon developing fruits

To evaluate flavonoid variations between PCNA and PCA persimmons, the typical PCNA type 'Jiro' and PCA type 'Huojing' were selected for investigation. The fruit was harvested at four stages (S1–S4), namely, the young fruit stage (S1), expansion stage (S2), turning stage (S3), and mature stage (S4). After the removal of low-quality, poly-N, and adaptor sequences, the RNA-seq of the 'Jiro' and 'Huojing' fruit at the four stages yielded 160.80 GB of clean data. The filtered samples contained nearly 6.70 GB of high-quality data with an average Q30 base percentage of 92.42%. Approximately 85.43% of the reads mapped to the reference *D. kaki* genome, and 4416 novel genes were also identified. The transcriptome sequencing data were confirmed through qRT-PCR. Seven DEGs were randomly selected from the flavonoid metabolism pathway for qRT-PCR verification (Figure S2). The expression profiles of these genes were consistent with their FPKM values.

The DEGs were compared using DESeq2 software, and selected DEGs were then analyzed. There were 5009, 4023, 6340, and 10 989 DEGs in the Jiro_S1 vs. Huojing_S1, Jiro_S2 vs. Huojing_S2, Jiro_S3 vs. Huojing_S3, and Jiro_S4 vs. Huojing_S4 groups, respectively (Figure 2A). Venn diagrams showed that 849 genes were differentially expressed in all the comparison groups, suggesting that these DEGs might perform critical functions in the regulation of flavonoids in PCNA and PCA fruit (Figure 2B). These DEGs were analyzed by the KEGG database to identify their associated pathways. This showed that the flavonoid biosynthesis (ko00941) and phenylpropanoid biosynthesis (ko00940) pathways were signicificantly enriched in the Jiro_S1 vs. Huojing_S1, Jiro_S2 vs. Huojing_S2, and Jiro_S3 vs. Huojing_S3 comparison groups. These results indicated that flavonoid biosynthesis-related pathways may play essential roles in different stages of PCNA and PCA fruit development (Figures 2C-F).

3.4 Differential gene analysis of flavonoid biosynthesis during the development of PCNA and PCA persimmon fruit

Six expression patterns were generated through trend and clustering analyses of the DEGs in the 'Jiro' and 'Huojing' varieties of the four developmental stages, termed Cluster 1-Cluster 6 (Figure 3A). The genes in these expression profiles were functionally analyzed by KEGG annotation (Figure 3B). The expression levels of genes in Cluster 3 were higher in the 'Huojing' fruit than in the 'Jiro' fruit. Furthermore, the expression levels of genes in Cluster 3 decreased gradually with fruit maturation. The KEGG pathway analysis showed that genes in Cluster 3 were mainly involved in several primary metabolic processes, such as photosynthesis (ko00196) and starch and sucrose metabolism (ko00500), and secondary metabolisc processes, such as phenylalanine biosynthesis (ko00400) and flavonoid biosynthesis (ko00941). These results indicated that flavonoid metabolism was involved in the development of 'Jiro' and 'Huojing' fruit.

Genes involved in flavonoid biosynthesis were then selected from Cluster III based on the results of the KEGG analysis. A total of 44 DEGs involved in flavonoid biosynthesis were identified, including *CS*, *DAHPS*, *DHQS*, *DHD/SDH*, *EPSPS*, *PAL*, *C4H*, *4CL*, *CHS*, *CHI*, *F3H*, *DFR*, *ANS*, *FLS*, *OMT*, *SGT*, *UF3GT*, *LAC*, *ANR*, *AHA10* (ATPase), and *MATE* (Supplementary Table 4). The flavonoid-associated DEGs were more enriched in the Jiro_S1 vs. Huojing_S1 group than in the other groups, and most of the DEGs were decreased (Figure 3C). The analysis of the gene expression levels found that the numbers of DEGs gradually decreased during the developmental process and were specifically highly expressed in Huojing_S1. These results indicated that flavonoid metabolism occurred predominantly during in the early stage (S1) of fruit development and the expression of flavonoid biosynthesis genes in 'Huojing' was significantly higher than in the 'Jiro'.

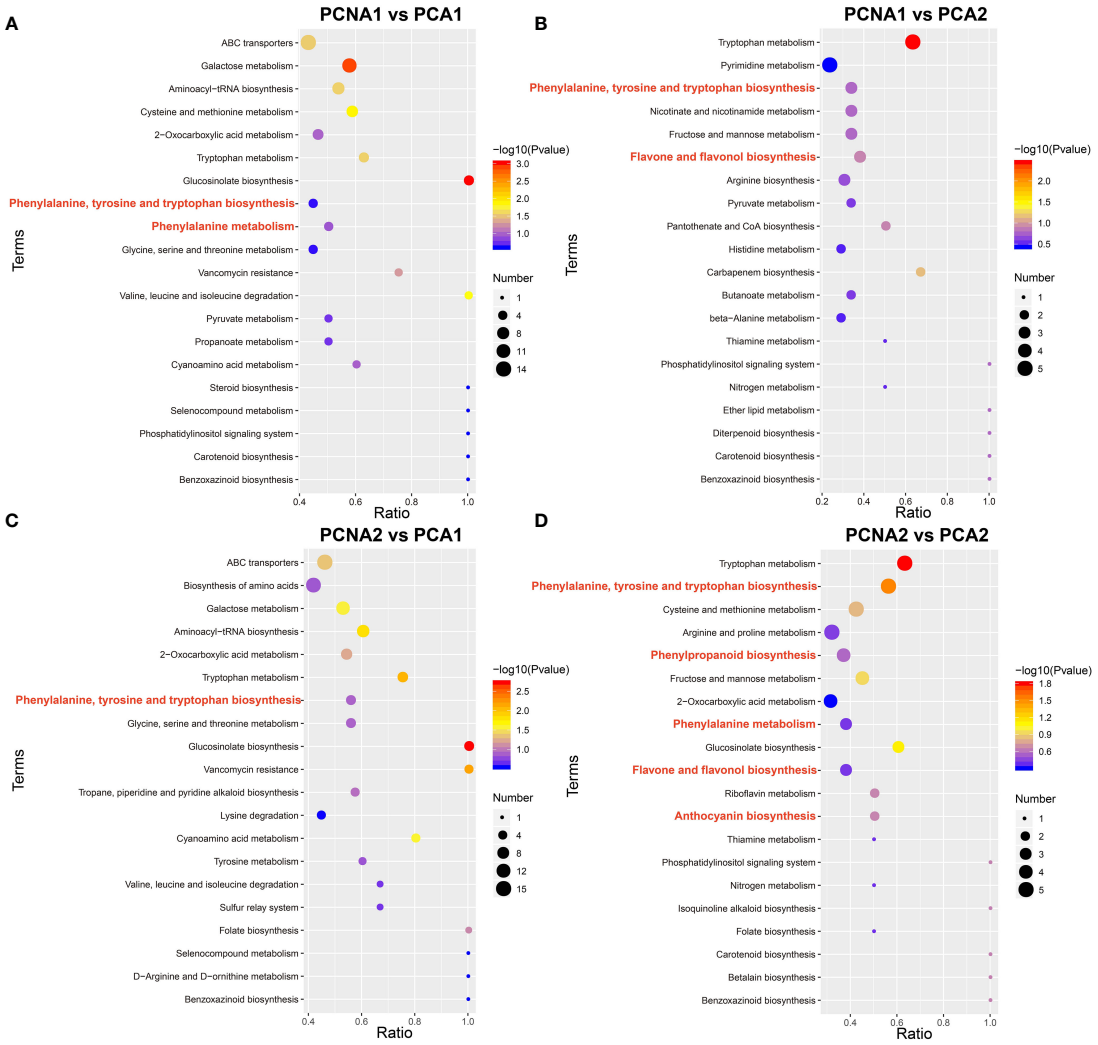

FIGURE 1
Comparison of metabolites between mature PCNA and PCA persimmon fruit. Scatter plot showing KEGG enrichment of DEGs between the PCNA and PCA groups. **(A)** PCNA1 vs. PCA1 group. **(B)** PCNA1 vs. PCA2 group. **(C)** PCNA2 vs. PCA1 group. **(D)** PCNA2 vs. PCA2 group.

3.5 Construction of a flavonoid co-expression module during PCNA and PCA fruit development

To further identify the specific genes involved in regulating flavonoid metabolism during the development of PCNA and PCA persimmon fruit, 29 057 genes were used in a WGCNA analysis (Figure S3). To ensure high-scale independence (near 0.9), the β-value was set at 5 (Figure S3A). The adjacency and topological overlap matrices were then constructed (Figures S3B, S3C). Based on average hierarchical clustering and dynamic tree clipping, a total of 42 modules were obtained (Figure S3D). The expression levels of the MEbrown transcripts were found to be significantly higher in S1 compared with S2, and gene expression was significantly higher in Huojing_S1 than in Jiro_S1 (Figure S3E). The MEblue module contains 3502 genes and KEGG analysis of genes in these modules showed that the genes in the MEblue module were associated with flavonoid biosynthesis during the fruit development, specifically, phenylalanine biosynthesis (ko00400) and flavonoid biosynthesis (ko00941) (Figure S3F).

The genes with high connectivity in the MEblue module were further investigated as candidate key genes related to flavonoid metabolism. The top 10% of genes in terms of connectivity were selected as potential hub genes. Of these, 12 hubs were identified as potential regulators of flavonoid metabolism, including the upstream chorismic acid pathway gene *DHD/SDH* (*evm.TU.contig8908.198*); phenylpropanoid biosynthesis *PAL* gene (*evm.TU.contig9504.51*) and *C4H* gene (*evm.TU.contig22.251*); isoflavonoid biosynthesis genes *CHI* (*evm.TU.contig3165.103* and *evm.TU.contig8036.16*), and *CHS* (*evm.TU.contig2115.175*); flavone and flavanonols biosynthesis genes *F3H* (*evm.TU.contig4466.49*), *F3'5'H* (*evm.TU.contig31.16*), and *FLS* (*evm.TU.contig4397.195*); anthocyanidin biosynthesis genes *DFR* (*evm.TU.contig1073.253*), *ANR* (*evm.TU.contig4466.754*), *ANS* (*evm.TU.contig5828.5*), and *UF3GT* (*evm.TU.contig6534.24*); And flavonoid transport *MATE* (*evm.TU.contig4078.12*) gene. We observed the transcription factors *R2R3MYB* (*evm.TU.contig7272.598*) and *WD40* (*evm.TU.contig3208.5*) also showed higher connectivity and were closely associated with the above structural genes. Therefore, these

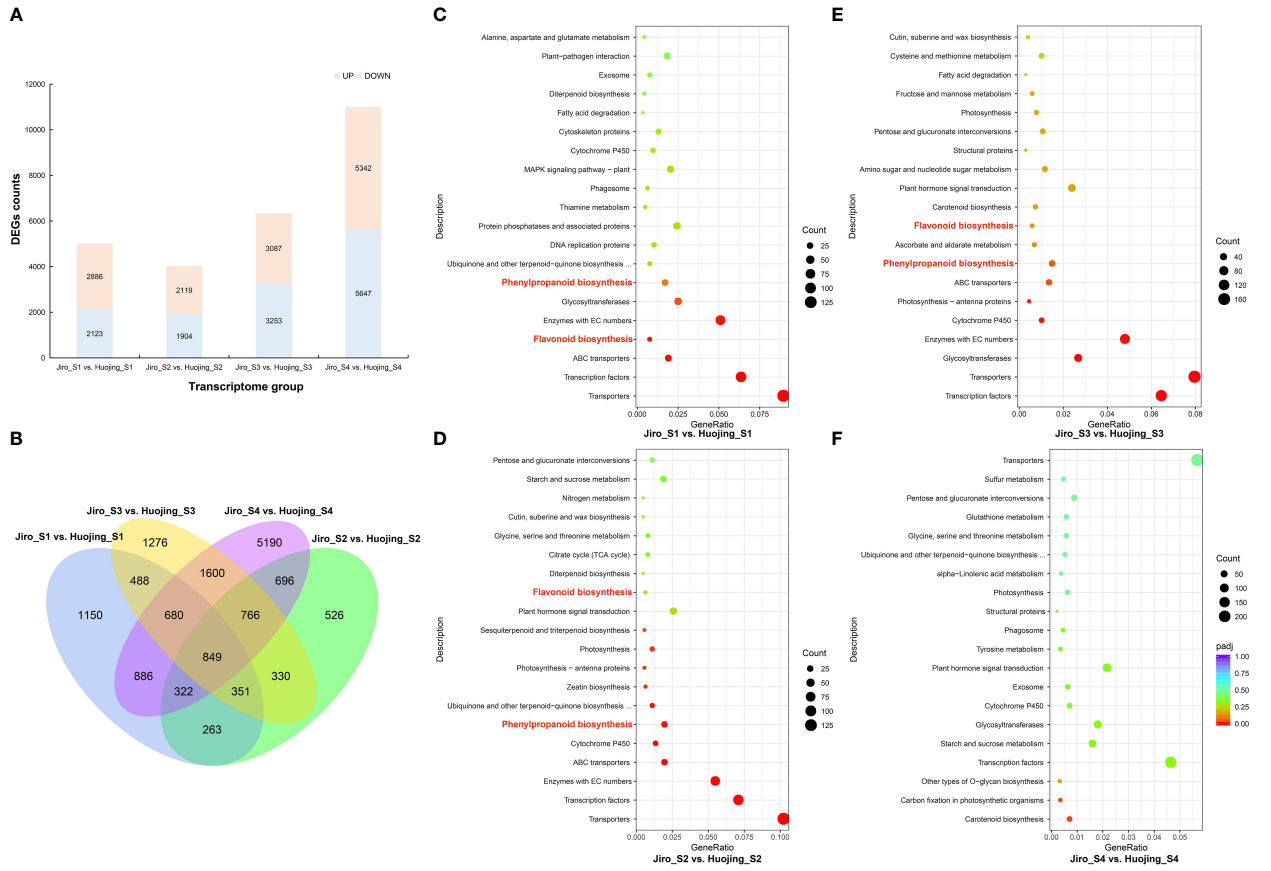

FIGURE 2
DEGs between 'Jiro' (PCNA type) and 'Huojing' (PCA type). **(A)** Summary of DEGs in different comparison groups of 'Jiro' and 'Huojing' fruit. **(B)** Venn diagram of DEGs. (c–f) Scatter plot showing KEGG enrichment of DEGs in four developmental stages in the 'Jiro' and 'Huojing' comparison groups. **(C)** Jiro_S1 vs. Huojing_S1 group. **(D)** Jiro_S2 vs. Huojing_S2 group. **(E)** Jiro_S3 vs. Huojing_S3 group. **(F)** Jiro_S4 vs. Huojing_S4 group.

TFs might participate in regulating the expression levels of the structural genes in flavonoid biosynthesis (Figure 4).

3.6 Analysis of flavonoid metabolites during the development of PCNA and PCA persimmon fruit

To further confirm flavonoid differences in the PCNA and PCA persimmon fruit during the developmental process, Quasi-Targeted metabolomic analysis of flavonoid compounds was used to evaluate the four developmental stages of PCNA and PCA persimmon fruit (Figure 5). In total, 135 flavonoids were identified in LS and JS fruit at different stages. These flavonoids included 75 flavonoids, 22 flavones and flavonols, 15 flavanones, 11 anthocyanins, four chalcones and dihydrochalcones, four isoflavonoids, and four tannins (Supplementary Table 5).

A total of 70 DAFs were identified among all the comparison groups, including 36 flavonoids, 13 flavones and flavonols, eight anthocyanins, six flavanones, four tannins, two chalcones, and dihydrochalcones, and one isoflavonoid, of which 28 flavonoids were glycosides. There were 27 DAFs in Jiro_S1 vs. Huojing_S1, 33 DAFs in Jiro_S1 vs. Huojing_S1, 41 DAFs in Jiro_S1 vs. Huojing_S1, and 27 DAFs in Jiro_S1 vs. Huojing_S1. Most of the DAFs were significantly higher in Huojing_S1 than in Jiro_S1, with only Procyanidin B2 and Procyanidin B3 were upregulated in at least two stages. The DAFs in the 'Huojing' variety were stronger than in the 'Jiro', which was consistent with the results of the RNA-seq analysis. Further analysis revealed that 8, 4, 12, and 10 flavonoid metabolites were stage-specific for S1, S2, S3, and S4, respectively (Figures 5A, B). In addition, six metabolites were differentially expressed at all developmental stages, including 3,7-dimethoxykaempferol-C-glucoside, corilagin, gallic acid, laricitrin, methyl gallate, and phlorizin. These results further confirmed that there were significant differences in the flavonoids between PCNA and PCA persimmons, and that flavonoid biosynthesis pathways play an essential role in PCNA and PCA fruit development.

3.7 Analysis of flavonoid biosynthesic genes and metabolies during the development of PCNA and PCA persimmon fruit

Based on the KEGG enrichment and WGCNA analyses, a flavonoid biosynthetic pathway was systematically constructed showing the expression levels of structural genes and the

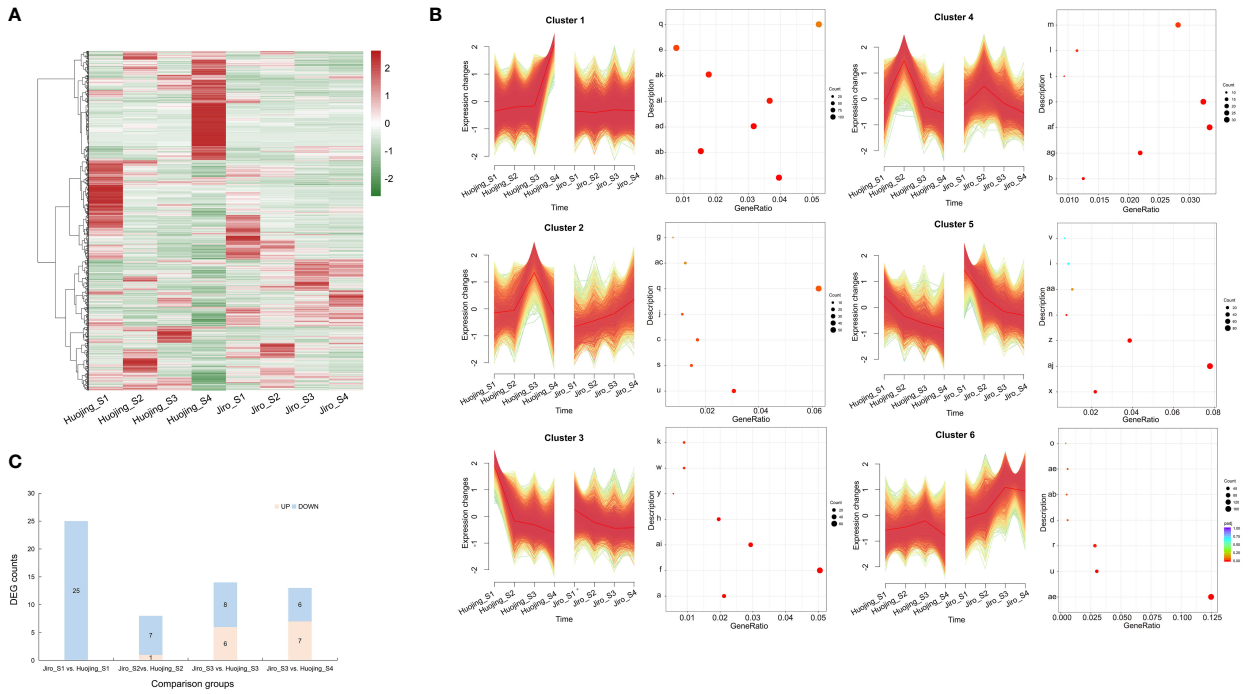

FIGURE 3
Expression patterns and KEGG analysis of genes in the transcriptomes of PCNA and PCA fruit. **(A)** Heatmap showing the overall common expression pattern. Heatmaps were constructed using the normalized gene expression values. **(B)** Expression profiles and KEGG annotations of six clusters. The y-axis of each cluster represents the KEGG categories, while the x-axis represents the rich factors. Red dots represent significantly overrepresented KEGG pathways. **(C)** Summary of flavonoid-associated DEGs in different comparison groups of 'Jiro' and 'Huojing'. a, ABC transporters; b, alpha-Linolenic acid metabolism; c, Amino sugar and nucleotide sugar metabolism; d, Arachidonic acid metabolism; e, Autophagy- other; f, Chromosome and associated protein; g, Circadian rhythm-plant; h, Cytoskeleton proteins; i, Exosome; j, Fatty acid biosynthesis; k, Flavonoid biosynthesis; l, Glycine, serine and threonine metabolism; m, Glycosyltransferases; n, Ion channels; o, Lipopolysaccharide biosynthesis proteins; p, MAPK signaling pathway-plant; q, Membrane trafficking; r, Mitochondrial biogenesis; s, N-Glycan biosynthesis; t, Nitrogen metabolism; u, Oxidative phosphorylation; v, Phagosome; w, Phenylalanine, tyrosine and tryptophan biosynthesis; x, Photosynthesis; y, Photosynthesis-antenna proteins; z, Plant hormone signal transduction; aa, Porphyrin metabolism; ab, Promasome; ac, Protein export; ad, Protein processing in endoplasmic reticulum; ae, Ribosome; af, Ribosome biogenesis; ag, Ribosome biogenesis in eukaryotes; ah, Spliceosome; ai, Starch and sucrose metabolism; aj, Transcription factors; ak, Transcription machinery; al, Ubiquitin system.

flavonoid contents during PCNA and PCA persimmon fruit development (Figure 6). Eleven structural genes and eight flavonoids were mapped to the pathway. Two structural genes (*PAL* and *C4H*) participated in the upstream phenylpropanoid pathway and nine structural genes (*CHS*, 2 *CHI*s, *F3'H*, *F3'5'H*, *DFR*, *ANS*, *ANR*, and *UF3GT*) participated in the flavonoid biosynthetic pathway. *PAL2* catalyzes the transformation of phenylalanine to cinnamic acid and as the expression of *C4H* was significantly higher in Huojing_S1 than in Jiro_S1, there was a upregulation of ρ-coumaroyl-CoA, with downregulation of cinnamic acid. Subsequently, a series of flavonoid structural genes, *CHS*, *CHI*s, *F3'5'H*, and *F3'H* showed significantly higher expression levels in Huojing_S1. Thus, some crucial intermediates such as dihydrokaempferol and dihydromyricetin, produced by the enzymes encoded by these structural genes, accumulated highly in Huojing_S1 than in Jiro_S1. All genes related to anthocyanin biosynthesis, such as *F3'5'H*, *DFR*, *ANS*, *ANR*, and *UF3GT*, were significantly downregulated in 'Jiro', resulting in lower accumulation of anthocyanins, such as pelargonidin chloride and cyanidin 3-O-glucoside in 'Jiro' than 'Huojing', which might be associated with the differences in flesh color between 'Jiro' and 'Huojing'. However, the levels of the colorless metabolites catechin (gallocatechin) and proanthocyanidin (procyanidin B2 and procyanidin B3) metabolites were significantly higher in Jiro_S4 than Huojing_S4. These findinge demonstrated the main contributions of these eight DAFs to the differences in flavonoid biosynthesis between PCNA ('Jiro') and PCA ('Huojing'), and the critical regulatory roles of 11 genes associated with flavonoid synthesis were hypothesized.

4 Discussion

As a fruit tree cultivated worldwide, the persimmon has essential ecological, economic, and social value. Presently, persimmon trees are mainly grown for their fruit, which can be eaten fresh or dried. Persimmon fruit varies greatly in terms of specific qualities, with significant variations observed between PCNA and non-PCNA persimmons (Novillo et al., 2016; Yildiz and Kaplankiran, 2018). Volatile compounds also vary significantly between PCNA and PCA fruit, especially in terms of aldehydes (Elhadi, 2017). In addition to soluble tannin, the astringency type also affected the contents of total phenolics, flavonoids, soluble solids, individual sugars, as well as antioxidant capacity

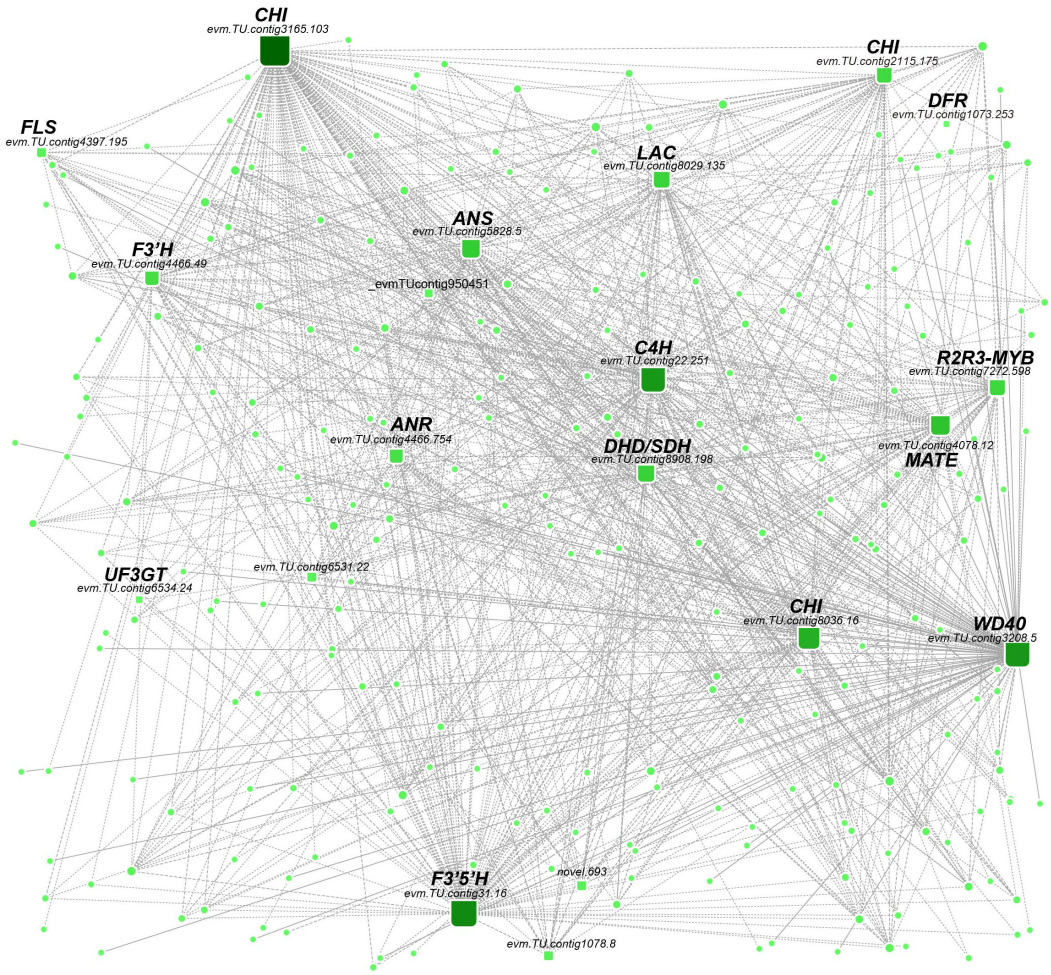

FIGURE 4
Weighted gene coexpression network analysis. The linkages between TFs and flavonoid-related structural genes in the MEblue module and the sizes of round rectangles were changed according to gene connectivity.

(Novillo et al., 2016; Yildiz and Kaplankiran, 2018). These studies provide a preliminary survey of how the astringency type affects the quality of the persimmon fruit; however, given the importance of flavonoids, the flavonoid composition and potential mechanisms involved in the regulation of flavonoid biosynthesis between the PCNA and PCA fruit varieties still require clarification.

With the rapid development of transcriptome sequencing, many studies have attempted to elucidate the molecular basis of flavonoid biosynthesis *via* RNA-seq. The key genes involved in flavonoid biosynthesis were identified by stage-specific transcriptomic analysis in the petals of *Camellia nitidissima* (Liu et al., 2023). Changes in the key genes and flavonoid metabolites were also investigated using metabolomics and transcriptomics in the developing exocarp and embryo of hickory (Chen et al., 2022). Metabolomics examines the overall metabolic profile of plant samples through high-throughput detection and data processing (Foito and Stewart, 2018) and can thus provide a reliable method for investigating compounds contributing to the flavor of the persimmon fruit. GC-MS has been used previously to identify volatile components in persimmon fruit (Besada et al., 2013; Elhadi, 2017). Nineteen polyhydroxyphenols were found to be reduced in CO2-treated fruit using untargeted metabolomics analysis, suggesting that persimmon browning might be caused by phenolic compounds (Han et al., 2022). Differences in metabolites between five Japanese persimmons were investigated using NMR (Ryu et al., 2019). In this study, a comprehensive transcriptomic and metabolite analysis was conducted to determine the differences in flavonoid composition between PCNA and PCA persimmons and identify genes related to flavonoid biosynthesis.

Flavonoid biosynthesis is complicated and diverse and requires the substrates derived from the phenylpropanoid pathway (Liu et al., 2021). Phenylpropanoid biosynthesis, flavonoid biosynthesis, flavone and flavonol biosynthesis, phenylalanine metabolism, isoflavone biosynthesis, and anthocyanin biosynthesis were observed to be enriched during the development of hickory fruit (Chen et al., 2022). In this study, a full-spectrum metabolomic determination of persimmon fruit was performed using liquid chromatography and triple quadrupole mass spectrometry in the MRM mode. This resulted in the identification of a total of 135 flavonoids, greatly broadening our

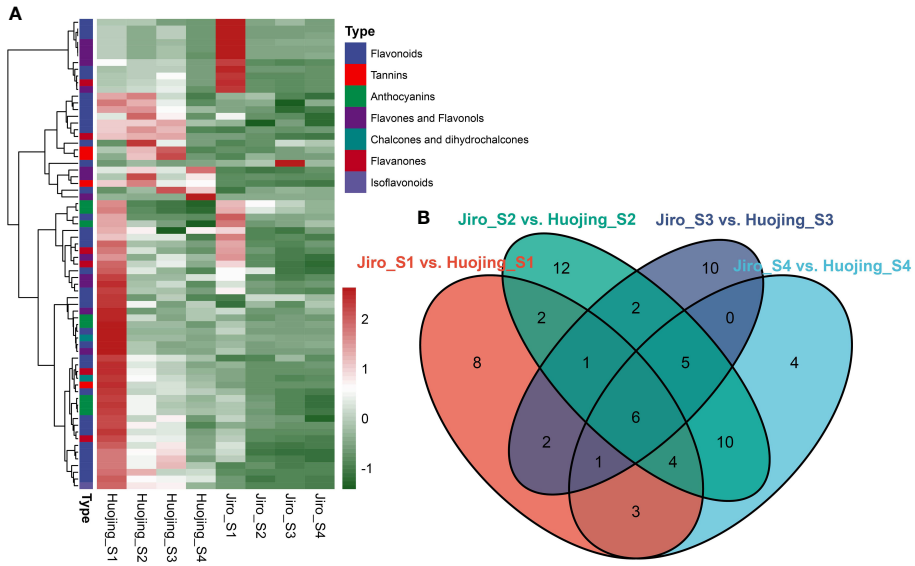

FIGURE 5
Differentially accumulated flavonoids (DAFs) in 'Jiro' (PCNA type) and 'Huojing' (PCA type). **(A)** Heatmap of the DAFs. The Heatmaps depict the normalized gene expression values, representing the mean value of three biological replicates. **(B)** Venn diagram of DAFs.

knowledge of flavonoids in ripening persimmon fruit. KEGG analysis of the differential accumulated metabolites in PCNA and PCA persimmons showed that pathways involved in phenylpropanoid biosynthesis, flavonoid biosynthesis, phenylalanine metabolism, anthocyanin biosynthesis, and flavone and flavonol biosynthesis were significantly enriched, indicating not only the high accumulation of flavonoids in persimmons but also that the flavonoids differed significantly between PCNA and PCA persimmons, which may be responsible for the differences in nutritional value and taste between the PCNA and PCA fruit.

In this study, a total of 70 differential accumulated flavonoids were identified between the fruit of the PCNA ('Jiro') and PCA ('Huojing') persimmon varieties at different developmental stages, of which the top three were flavonoids (36), flavones and flavonols (13), and anthocyanins (8). Twenty-eight DAFs were glycosides, which were mainly glycosylated derivatives of quercetin and cyanidin. Quercetin is mostly present in plants as glycosides and has been reported in foods such as onions, apples, broccoli, and tea, and it also has beneficial effects on health (Zheng et al., 2017). Glycoside modifications enhance the water solubility, structural

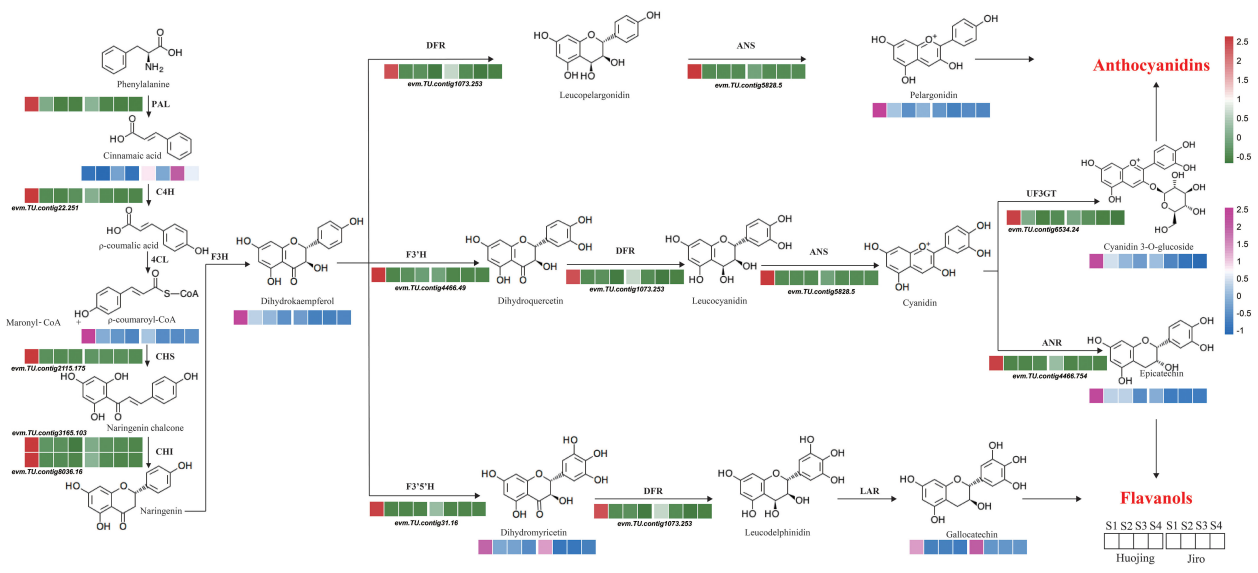

FIGURE 6
Diagram of phenylpropanoid and flavonoid biosynthetic pathways involving DEGs and DEMs. Heatmaps represent the normalized expression values.

complexity, and molecular stability of flavonoids (Bai et al., 2022). Thus, flavonoids with glycosides could play essential roles in plant growth, hormonal balance, and the elimination of toxic endogenous and exogenous substances (Wang et al., 2017; Bai et al., 2022); it has, for instance, been shown that delphinidin and its glycosides enhance plant resistance to a wide range of biotic and abiotic stresses (Silva et al., 2017).

In the early stages of flavonoid biosynthesis, the PCNA ('Jiro') and PCA ('Huojing') cultivars differed in the expression of the *C4H* (*evm.TU.contig22.251*), *PAL* (*evm.TU.contig9504.51*), *CHI* (*evm.TU.contig3165.103 and evm.TU.contig8036.16*), *and CHS* (*evm.TU.contig2115.175*) genes. L-phenylalanine is converted to cinnamic acid by *PAL*, the frist enzyme in the flavonoid biosynthetic pathway (Heldt and Piechulla, 2011). In addition to *PAL*, *C4H*, *CHS*, and *4CL* play critical roles in the synthesis of crucial secondary metabolites such as lignin, phenolic acids, coumarin, flavonoids, and anthocyanins (Chen et al., 2022; Xia et al., 2022). Subsequently, ρ-Coumaric-CoA produces naringenin, which is catalyzed by *CHS* and *CHI* (Yuan et al., 2022). *CHS* is a key initiating enzyme and forms part of a multi-gene family in most species (Niesbach-Klösgen et al., 1987). *CHS* (*evm.TU.contig2115.175*) expression was observed to be significantly lower in cultivar 'Jiro' compared with 'Huojing' at the early stage. Two DEGs that encode *CHI* (*evm.TU.contig3165.103* and *evm.TU.contig8036.16*) were also identified between PCNA and PCA persimmons; these two *CHI* genes were highly expressed in cultivar 'Huojing' at stage 1. The expression levels of these genes might influence flavonoid metabolism in PCNA and PCA persimmons.

At the late stage of flavonoid biosynthesis, the *F3H* (*evm.TU.contig4466.49*), *F3'5'H* (*evm.TU.contig31.16*), and *FLS* (*evm.TU.contig4397.195*), *DFR* (*evm.TU.contig1073.253*), *ANS* (*evm.TU.contig5828.5*), *ANR* (*evm.TU.contig4466.754*), and *UF3GT* (*evm.TU.contig6534.24*) genes showed differential expression between PCNA ('Jiro') and PCA ('Huojing') persimmon fruit. Two key enzymes, *F3'H* and *F3'5'H*, regulate the hydroxylation of naringenin and dihydrokaempferol at the 3' position or both the 3' and 5' locations in the B ring (Bailey et al., 2003), and the products are crucial intermediates in the biosynthesis of anthocyanins and proanthocyanidins (Jeong et al., 2006). Thus, the genes encoding the *F3'H* and *F3'5'H* enzymes have been extensively studied in horticultural plants such as cyclamen (Boase et al., 2010), tea (Guo et al., 2019) and grapes (Jeong et al., 2006). In this study, *F3'H* (*evm.TU.contig4466.49*) showed significantly lower expression in cultivar 'Jiro' compared with 'Huojing' at the early stage when it catalyzes dihydrokaempferol to produce dihydroquercetin, a substrate of cyanidin. *F3'5'H* (*evm.TU.contig31.16*) catalyzes the synthesis of dihydromyricetin, a substrate of leucodelphinidin. These results are consistent with those of similar studies of *Rhododendron pulchrums* (Xia et al., 2022).

LAR and *ANS* play essential roles in the synthesis of proanthocyanins and anthocyanins; both are downstream genes of the flavonoid biosynthetic pathway and catalyze leucocyanidin into catechins and cyanidins, respectively (Springob et al., 2003). *ANR* and *LAR* encode key enzymes involved in the production of 2,3-cis-flavan-3-ols [(-)-epigallocatechin (ECG), (-)-epicatechin (EC), and (-)-epi-gallocatechin 3-O-gallate (EGCG)] and 2,3-trans-flavan-3-ols [(+)-gallocatechin (GC) and (+)-catechin (CA)] respectively (Ikegami et al., 2007). Interestingly, there were no differences in the *LAR* expression level between the two cultivars but *ANR* (*evm.TU.contig4466.754*) was expressed at higher levels in cultivar 'Huojing', a finding similar to previous studies showing that the expression level of *DkANR* was much higher than that of *DkLAR* during proanthocyanin accumulation (Akagi et al., 2009). This resulted in a lower epicatechin content in the PCNA persimmon and was one of the main reasons for the reduction in the proanthocyanin contents in PCNA types. Cyanidin and pelargonidin usually provide the red pigment in fruit and flowers (Harborne and Williams, 2000). In this study, *UF3GT* (*evm.TU.contig6534.24*) catalyzed the formation of cyanidin 3-O-glucoside, and *ANS* (*evm.TU.contig5828.5*) also catalyzed naringin to produce pelargonidin chloride; both two genes were expressed at higher levels in 'Huojing' than in 'Jiro', which might result in the accumulation of less red pigmentation in PCNA persimmons.

Genes involved in flavonoid biosynthesis are mainly regulated by the *MYB*, *bHLH*, and *WD40* TFs and their *MBW* complex in plants (Hichri et al., 2011), such as rose (Shen et al., 2019) and pears (Premathilake et al., 2020). *R2R3MYB* TFs are core members of the *MBW* complex and are involved in the regulation of flavonoid biosynthesis through binding to the promoter regions of structural genes (Yoshida et al., 2015). In pears, *PpMYB17* has been shown to positively regulate flavonoid biosynthesis by activating the structural genes *PpCHS*, *PpCHI*, *PpF3H*, and *PpFLS* in fruit (Premathilake et al., 2020). In persimmon, the combined action of *DkMYB2*, *DkMYC1*, and *DkMYB4* (*MBW*) increases the expression levels of the *ANR* gene involved in the biosynthesis of the proanthocyanin precursor cis-flavan-3-ols (Gil-Muñoz et al., 2020), supporting the above findings on the structural gene *ANR* and the cis-flavan-3-ols epicatechin content. Besides, *DkMYB14* in the Chinese PCNA (C-PCNA) persimmon was found to suppress proanthocyanin biosynthesis and activate acetaldehyde biosynthesis, resulting in the deastringency of the C-PCNA persimmon fruit (Chen et al., 2021). *MYB82* is involved in trichome development (Liang et al., 2014) and has potential roles in anthocyanin biosynthesis in *Arabidopsis* (Yang et al., 2013). In this study, an *R2R3MYB* (*evm.TU.contig7272.598*) was identified by WGCNA, which was homologous to *AtMYB82* and *BrMYB82* (Yang et al., 2013), indicating a potential role of *MYB82* in anthocyanin biosynthesis regulation; however, the mechanism remains requires further investigation and confirmation.

In conclusion, a comprehensive metabolomic and transcriptomic analysis of PCNA ('Jiro') and PCA ('Huojing') persimmon fruit was conducted. The concentration of flavonoids in 'Huojing' was found to be significantly higher than in 'Jiro' fruit, especially the concentrations of the proanthocyanin precursor 2,3-cis-flavan-3-ols epicatechin and anthocyanin cyanidin derivatives. Combined WGCNA and KEGG analyses showed that genes such as *PAL*, *C4H*, *CHI*, *CHS*, *F3H*, *F3'5'H*, *FLS*, *DFR*, *ANR*, *ANS*, and *UF3GT* involved in the phenylpropanoid and flavonoid biosynthetic pathways might be the major factors impacting the proanthocyanin precursor flavan-3-ols and the anthocyanin

content. Moreover, the *R2R3MYB* (*evm.TU.contig7272.598*) and *WD40* (*evm.TU.contig3208.5*) TFs showed significant connections with the above structural genes. This study provides basic information on flavonoid biosynthesis and regulatory network in persimmon fruit and lays a foundation for ongoing investigations on the influence of astringency types on flavor components in PCNA and PCA persimmon.

Data availability statement

The datasets presented in this study can be found in online repositories. The names of the repository/repositories and accession number(s) can be found below: https://www.ncbi.nlm.nih.gov/, https://www.ncbi.nlm.nih.gov/bioproject/PRJNA910302.

Author contributions

YW and YS carried out the experiments and wrote this manuscript. YW and YS participated in the data analysis. HL, ZW, SD, and PS participated in the sampling and investigation; WH and JF conceived and designed the experiments and helped draft and review the manuscript. All authors contributed to the article and approved the submitted version. This article complies with ethical standards.

Funding

This work was supported by the National Natural Science Foundation of China (32071801) and the National Key R&D Program of China (2019YFD1000600 and 2018YFD1000606).

Conflict of interest

The authors declare that the research was conducted in the absence of any commercial or financial relationships that could be construed as a potential conflict of interest.

Publisher's note

Supplementary material

The Supplementary Material for this article can be found online at: https://www.frontiersin.org/articles/10.3389/fpls.2023.1130047/full#supplementary-material

SUPPLEMENTARY FIGURE 1
Principal component analysis score plot of all metabolites in mature PCNA and PCA persimmon fruit.

SUPPLEMENTARY FIGURE 2
Verification of transcriptomic data by qRT-PCR analysis of the expression of seven genes.

SUPPLEMENTARY FIGURE 3
WGCNA analysis. **(A)** Soft threshold selection; **(B)** Module hierarchical clustering tree; **(C)** The gene co-expression module; **(D)** The correlation between samples and modules; **(E)** Gene expression pattern of the MEblue module; and **(F)** KEGG enrichment analysis of the MEblue module.

References

Akagi, T., Ikegami, A., Suzuki, Y., Yoshida, J., Yamada, M., Sato, A., et al. (2009). Expression balances of structural genes in shikimate and flavonoid biosynthesis cause a difference in proanthocyanidin accumulation in persimmon (Diospyros kaki thunb.) fruit. *Planta.* 230, 899–915. doi: 10.1007/s00425-009-0991-6

Ashburner, M., Ball, C., Blake, J., Botstein, D., Butler, H., Cherry, J., et al. (2000). Gene ontology: Tool for the unification of biology. *Nat. Genet.* 25, 25–29. doi: 10.1038/75556

Azuma, A., Yakushiji, H., Koshita, Y., and Kobayashi, S. (2012). Flavonoid biosynthesis-related genes in grape skin are differentially regulated by temperature and light conditions. *Planta.* 236, 1067–1080. doi: 10.1007/s00425-012-1650-x

Bai, Y., Gu, Y., Liu, S., Jiang, L., Han, M., and Geng, D. (2022). Flavonoids metabolism and physiological response to ultraviolet treatments in tetrastigma hemsleyanum diels et gilg. *Front. Plant Science.* 13. doi: 10.3389/fpls.2022.926197

Bailey, P., Martin, C., Toledo-Ortiz, G., Quail, P., Huq, E., Heim, M., et al. (2003). Update on the basic helix-Loop-Helix transcription factor gene family in arabidopsis thaliana. *Plant Cell.* 15, 2497–2502. doi: 10.1105/tpc.151140

Besada, C., Sanchez, G., Salvador, A., and Granell, A. (2013). Volatile compounds associated to the loss of astringency in persimmon fruit revealed by untargeted GC–MS analysis. *Metabolomics.* 9, 157–172. doi: 10.1007/s11306-012-0436-2

Boase, M., Lewis, D., Davies, K., Marshall, G., Patel, D., Schwinn, K., et al. (2010). Isolation and antisense suppression of flavonoid 3', 5'-hydroxylasemodifies flower pigments and colour in cyclamen. *BMC Plant Biol.* 10, 107. doi: 10.1186/1471-2229-10-107

Chen, J., Hou, N., Xv, X., Zhang, D., Fan, T., Zhang, Q., et al. (2022). Flavonoid synthesis and metabolism during the fruit development in hickory (Carya cathayensis). *Front. Plant Science.* 13. doi: 10.3389/fpls.2022.896421

Chen, C., and Li, A. (2016). Transcriptome analysis of differentially expressed genes involved in proanthocyanidin accumulation in the rhizomes of fagopyrum dibotrys and an irradiation-induced mutant. *Front. Physiol.* 7. doi: 10.3389/fphys.2016.00100

Chen, W., Zheng, Q., Li, J., Liu, Y., Xu, L., Zhang, Q., et al. (2021). DkMYB14 is a bifunctional transcription factor that regulates the accumulation of proanthocyanidin in persimmon fruit. *Plant J.* 106, 1708–1727. doi: 10.1111/tpj.15266

Dias, M., Pinto, D., and Silva, A. (2021). Plant flavonoids: Chemical characteristics and biological activity. *Molecules.* 26, 5377. doi: 10.3390/molecules26175377

Direito, R., Rocha, J., Sepodes, B., and Eduardo-Figueira, M. (2021). From diospyros kaki l. (Persimmon) phytochemical profile and health impact to new product perspectives and waste valorization. *Nutrients.* 13, 3283. doi: 10.3390/nu13093283

Dixon, R., Xie, D., and Sharma, S. (2005). Proanthocyanidins – a final frontier in flavonoid research? *New Phytologist.* 165, 9–28. doi: 10.1111/j.1469-8137.2004.01217.x

Du, G., Wang, L., Li, H., Sun, P., Fu, J., Suo, Y., et al. (2019). Selection and validation of reference genes for quantitative gene expression analyses in persimmon (Diospyros kaki thunb.) using real-time quantitative PCR. *Biol. Futura.* 70, 261–267. doi: 10.1556/019.70.2019.24

Du, X., Zhang, Q., and Luo, Z. (2009). Comparison of four molecular markers for genetic analysis in diospyros l. (Ebenaceae). *Plant Systematics Evolution.* 281, 171. doi: 10.1007/s00606-009-0199-z

Elhadi, M. (2017). *Study of quality characteristics, aroma components and gene expression of alcohol acyltransferase (DkAAT1) of persimmon fruits. Ph.D. dissertation* (Yangzhou, China: Yangzhou University).

Foito, A., and Stewart, D. (2018). Metabolomics: A high-throughput screen for biochemical and bioactivity diversity in plants and crops. *Curr. Pharm. Design.* 24, 2043–2054. doi: 10.2174/1381612824666180515125926

Gil-Muñoz, F., Sánchez-Navarro, J., Besada, C., Salvador, A., Badenes, M., Naval, M., et al. (2020). MBW complexes impinge on anthocyanidin reductase gene regulation for proanthocyanidin biosynthesis in persimmon fruit. *Sci. Rep.* 10, 3543. doi: 10.1038/s41598-020-60635-w

Guo, L., Gao, L., Ma, X., Guo, F., Ruan, H., Bao, Y., et al. (2019). Functional analysis of flavonoid 3'-hydroxylase and flavonoid 3',5'-hydroxylases from tea plant (Camellia sinensis), involved in the b-ring hydroxylation of flavonoids. *Gene.* 717, 144046. doi: 10.1016/j.gene.2019.144046

Han, W., Cao, K., Diao, S., Sun, P., Li, H., Mai, Y., et al. (2022). Characterization of browning during CO_2 deastringency treatment in astringent persimmon fruit. *J. Food Measurement Characterization.* 16, 2273–2281. doi: 10.1007/s11694-022-01298-1

Han, W., Cao, K., Suo, Y., Diao, S., Sun, P., Li, H., et al. (2021). Effect of deastringency treatment with CO_2 on physiological quality of 'Hiratanenashi' persimmon fruit. *Food Science.* 42, 43–53. doi: 10.7506/spkx1002-6630-20200723-316

Harborne, J., and Williams, C. (2000). Advances in flavonoid research since 1992. *Phytochemistry.* 55, 481–504. doi: 10.1016/S0031-9422(00)00235-1

Havsteen, B. (2002). The biochemistry and medical significance of the flavonoids. *Pharmacol. Ther.* 96, 67–202. doi: 10.1016/S0163-7258(02)00298-X

Heldt, H., and Piechulla, B. (2011). "18 - phenylpropanoids comprise a multitude of plant secondary metabolites and cell wall components," in *Plant biochemistry, 4th ed.* Eds. H.-W. Heldt and B. Piechulla (San Diego: Academic Press), 431–449. doi: 10.1016/B978-0-12-384986-1.00018-1

Henry-Kirk, R., McGhie, T., Andre, C., Hellens, R., and Allan, A. (2012). Transcriptional analysis of apple fruit proanthocyanidin biosynthesis. *J. Exp. Botany.* 63, 5437–5450. doi: 10.1093/jxb/ers193

Hichri, I., Barrieu, F., Bogs, J., Kappel, C., Delrot, S., and Lauvergeat, V. (2011). Recent advances in the transcriptional regulation of the flavonoid biosynthetic pathway. *J. Exp. Botany.* 62, 465–2483. doi: 10.1093/jxb/erq442

Ikegami, A., Eguchi, S., Kitajima, A., Inoue, K., and Yonemori, K. (2007). Identification of genes involved in proanthocyanidin biosynthesis of persimmon (Diospyros kaki) fruit. *Plant Science.* 172, 1037–1047. doi: 10.1016/j.plantsci.2007.02.010

Jeong, S., Goto-Yamamoto, N., Hashizume, K., and Esaka, M. (2006). Expression of the flavonoid 3'-hydroxylase and flavonoid 3',5'-hydroxylase genes and flavonoid composition in grape (Vitis vinifera). *Plant Science.* 170, 61–69. doi: 10.1016/j.plantsci.2005.07.025

Kanehisa, M., Goto, S., Kawashima, S., Okuno, Y., and Hattori, M. (2004). The KEGG resource for deciphering the genome. *Nucleic Acids Res.* 32, D277–D280. doi: 10.1093/nar/gkh063

Kumar, S., and Pandey, A. (2013). Chemistry and biological activities of flavonoids: An overview. *Sci. World J.* 2013, 162750. doi: 10.1155/2013/162750

Langfelder, P., and Horvath, S. (2008). WGCNA: An r package for weighted correlation network analysis. *BMC Bioinf.* 9, 559. doi: 10.1186/1471-2105-9-559

Li, J., Miao, B., Wang, S., Dong, W., Xu, H., Si, C., et al. (2022). Hiplot: A comprehensive and easy-to-use web service for boosting publication-ready biomedical data visualization. *Briefings Bioinf.* 23, bbac261. doi: 10.1093/bib/bbac261

Liang, G., He, H., Li, Y., Ai, Q., and Yu, D. (2014). MYB82 functions in regulation of trichome development in arabidopsis. *J. Exp. Botany.* 65, 3215–3223. doi: 10.1093/jxb/eru179

Liao, Y., Smyth, G., and Shi, W. (2014). featureCounts: An efficient general purpose program for assigning sequence reads to genomic features. *Bioinformatics.* 30, 923–930. doi: 10.1093/bioinformatics/btt656

Liu, W., Feng, Y., Yu, S., Fan, Z., Li, X., Li, J., et al. (2021). The flavonoid biosynthesis network in plants. *Int. J. Mol. Sci.* 22, 12824. doi: 10.3390/ijms222312824

Liu, H., Liu, Q., Chen, Y., Zhu, Y., Zhou, X., and Li, B. (2023). Full-length transcriptome sequencing provides insights into flavonoid biosynthesis in camellia nitidissima petals. *Gene* 850, 146924. doi: 10.1016/j.gene.2022.146924

Love, M., Huber, W., and Anders, S. (2014). Moderated estimation of fold change and dispersion for RNA-seq data with DESeq2. *Genome Biol.* 15, 550. doi: 10.1186/s13059-014-0550-8

Mikhailova, A., Strygina, K., and Khlestkina, E. (2022). In silico analysis of the regulatory gene families for proanthocyanidins biosynthesis in the genus gossypium l. *Turkish J. Agric. Forestry.* 46, 743–761. doi: 10.55730/1300-011X.3039

Niesbach-Klösgen, U., Barzen, E., Bernhardt, J., Rohde, W., Schwarz-Sommer, Z., Reif, H., et al. (1987). Chalcone synthase genes in plants: A tool to study evolutionary relationships. *J. Mol. Evol.* 26 (3), 213–225. doi: 10.1007/BF02099854

Novillo, P., Salvador, A., Crisosto, C., and Besada, C. (2016). Influence of persimmon astringency type on physico-chemical changes from the green stage to commercial harvest. *Scientia Horticulturae.* 206, 7–14. doi: 10.1016/j.scienta.2016.04.030

Premathilake, A., Ni, J., Bai, S., Tao, R., Ahmad, M., and Teng, Y. (2020). R2R3-MYB transcription factor PpMYB17 positively regulates flavonoid biosynthesis in pear fruit. *Planta.* 252, 59. doi: 10.1007/s00425-020-03473-4

Quideau, S., Deffieux, D., Douat-Casassus, C., and Pouységu, L. (2011). Plant polyphenols: Chemical properties, biological activities, and synthesis. *Angewandte Chemie Int. Edition.* 50, 586–621. doi: 10.1002/anie.201000044

Routaboul, J., Kerhoas, L., Debeaujon, I., Pourcel, L., Caboche, M., Einhorn, J., et al. (2006). Flavonoid diversity and biosynthesis in seed of arabidopsis thaliana. *Planta.* 224, 96–107. doi: 10.1007/s00425-005-0197-5

Ryu, S., Muramatsu, T., Furihata, K., Wei, F., Koda, M., Miyakawa, T., et al. (2019). NMR-based metabolic profiling and comparison of Japanese persimmon cultivars. *Sci. Rep.* 9, 15011. doi: 10.1038/s41598-019-51489-y

Saito, K., Yonekura-Sakakibara, K., Nakabayashi, R., Higashi, Y., Yamazaki, M., Tohge, T., et al. (2013). The flavonoid biosynthetic pathway in arabidopsis: Structural and genetic diversity. *Plant Physiol. Biochem.* 72, 21–34. doi: 10.1016/j.plaphy.2013.02.001

Saleem, M. S., Ejaz, S., Anjum, M. A., Ali, S., Hussain, S., Ercisli, S., et al. (2022). Improvement of postharvest quality and bioactive compounds content of persimmon fruits after hydrocolloid-based edible coating application. *Horticulturae.* 8, 1045. doi: 10.3390/horticulturae8111045

Sasaki, N., and Nakayama, T. (2015). Achievements and perspectives in biochemistry concerning anthocyanin modification for blue flower coloration. *Plant Cell Physiol.* 56, 28–40. doi: 10.1093/pcp/pcu097

Shannon, P., Markiel, A., Ozier, O., Baliga, N., Wang, J., Ramage, D., et al. (2003). Cytoscape: a software environment for integrated models of biomolecular interaction networks. *Genome Res.* 13, 2498–2504. doi: 10.1101/gr.1239303

Shen, Y., Sun, T., Pan, Q., Anupol, N., Chen, H., Shi, J., et al. (2019). RrMYB5- and RrMYB10-regulated flavonoid biosynthesis plays a pivotal role in feedback loop responding to wounding and oxidation in Rosa rugosa. *Plant Biotechnol. J.* 17, 2078–2095. doi: 10.1111/pbi.13123

Shumate, A., Wong, B., Pertea, G., and Pertea, M. (2022). Improved transcriptome assembly using a hybrid of long and short reads with StringTie. *PloS Comput. Biol.* 18, e1009730. doi: 10.1371/journal.pcbi.1009730

Silva, S., Costa, E. M., Calhau, C., Morais, R. M., and Pintado, M. E. (2017). Anthocyanin extraction from plant tissues: A review. *Crit. Rev. Food Sci. Nutr.* 57, 3072–3083. doi: 10.1080/10408398.2015.1087963

Springob, K., Nakajima, J., Yamazaki, M., and Saito, K. (2003). Recent advances in the biosynthesis and accumulation of anthocyanins. *Natural product Rep.* 20, 288–303. doi: 10.1039/b109542k

Sun, L., Zhang, J., Lu, X., Zhang, L., and Zhang, Y. (2011). Evaluation to the antioxidant activity of total flavonoids extract from persimmon (Diospyros kaki l.) leaves. *Food Chem. Toxicology.* 49, 2689–2696. doi: 10.1016/j.fct.2011.07.042

Tahmaz, H., and Soylemezoglu, G. (2022). Selected phenolics and antioxidant capacities: From boğazkere (Vitis vinifera l.) grape to pomace and wine. *Turkish J. Agric. Forestry.* 46, 623–631. doi: 10.55730/1300-011X.3031

Tohge, T., de Souza, L., and Fernie, A. (2017). Current understanding of the pathways of flavonoid biosynthesis in model and crop plants. *J. Exp. Botany.* 68, 4013–4028. doi: 10.1093/jxb/erx177

Tohge, T., Perez de Souza, L., and Fernie, A. R. (2018). On the natural diversity of phenylacylated-flavonoid and their in planta function under conditions of stress. *Phytochem. Rev.* 17, 279–290. doi: 10.1007/s11101-017-9531-3

Wang, L., Li, H., Suo, Y., Han, W., Diao, S., Mai, Y., et al. (2022). Effects of different chemicals on sexual regulation in persimmon (Diospyros kaki thunb.) flowers. *Front. Plant Science.* 13. doi: 10.3389/fpls.2022.876086

Wang, X., Li, C., Zhou, C., Li, J., and Zhang, Y. (2017). Molecular characterization of the c-glucosylation for puerarin biosynthesis in pueraria lobata. *Plant J.* 90, 535–546. doi: 10.1111/tpj.13510

Wen, W., Alseekh, S., and Fernie, A. (2020). Conservation and diversification of flavonoid metabolism in the plant kingdom. *Curr. Opin. Plant Biol.* 55, 100–108. doi: 10.1016/j.pbi.2020.04.004

Winkel-Shirley, B. (2001). Flavonoid biosynthesis. a colorful model for genetics, biochemistry, cell biology, and biotechnology. *Plant Physiol.* 126, 485–493. doi: 10.1104/pp.126.2.485

Wishart, D., Tzur, D., Knox, C., Eisner, R., Guo, A., Young, N., et al. (2007). HMDB: The human metabolome database. *Nucleic Acids Res.* 35, D521–D526. doi: 10.1093/nar/gkl923

Wu, T., Hu, E., Xu, S., Chen, M., Guo, P., Dai, Z., et al. (2021). ClusterProfiler 4.0: A universal enrichment tool for interpreting omics data. *Innovation.* 2, 100141. doi: 10.1016/j.xinn.2021.100141

Xia, X., Gong, R., and Zhang, C. (2022). Integrative analysis of transcriptome and metabolome reveals flavonoid biosynthesis regulation in rhododendron pulchrum petals. *BMC Plant Biol.* 22, 401. doi: 10.1186/s12870-022-03762-y

Xie, L., Wang, J., Liu, F., Zhou, H., Chen, Y., Pan, L., et al. (2022). Integrated analysis of multi-omics and fine-mapping reveals a candidate gene regulating pericarp color and flavonoids accumulation in wax gourd (Benincasa hispida). *Front. Plant Science.* 13. doi: 10.3389/fpls.2022.1019787

Yang, F., Cai, J., Yang, Y., and Liu, Z. (2013). Overexpression of microRNA828 reduces anthocyanin accumulation in arabidopsis. *Plant Cell Tissue Organ Culture (PCTOC)*. 115, 159–167. doi: 10.1007/s11240-013-0349-4

Yildiz, E., and Kaplankiran, M. (2018). Changes in sugars content and some biochemical substances during fruit development in different persimmon cultivars. *J. Agric. Faculty Mustafa Kemal University*. 23, 12–23.

Yonemori, K., Sugiura, A., and Yamada, M. (2000). Persimmon genetics and breeding. *In: Plant Breed. Rev.* pp, 191–225. doi: 10.1002/9780470650172.ch6

Yoshida, K., Ma, D., and Constabel, C. (2015). The MYB182 protein down-regulates proanthocyanidin and anthocyanin biosynthesis in poplar by repressing both structural and regulatory flavonoid genes. *Plant Physiol.* 167, 693–710. doi: 10.1104/pp.114.253674

Yuan, Y., Zuo, J., Zhang, H., Li, R., Yu, M., and Liu, S. (2022). Integration of transcriptome and metabolome provides new insights to flavonoids biosynthesis in dendrobium huoshanense. *Front. Plant Science.* 13. doi: 10.3389/fpls.2022.850090

Zhang, Y., Park, C., Bennett, C., Thornton, M., and Kim, D. (2021). Rapid and accurate alignment of nucleotide conversion sequencing reads with HISAT-3N. *Genome Res.* 31, 1290–1295. doi: 10.1101/gr.275193.120

Zhang, Q., Wang, L., Liu, Z., Zhao, Z., Zhao, J., Wang, Z., et al. (2020). Transcriptome and metabolome profiling unveil the mechanisms of ziziphus jujuba mill. peel coloration. *Food Chem.* 312, 125903. doi: 10.1016/j.foodchem.2019.125903

Zheng, Q., Chen, W., Luo, M., Xu, L., Zhang, Q., and Luo, Z. (2021). Comparative transcriptome analysis reveals regulatory network and regulators associated with proanthocyanidin accumulation in persimmon. *BMC Plant Biol.* 21, 356. doi: 10.1186/s12870-021-03133-z

Zheng, Y., Deng, G., Liang, Q., Chen, D., Guo, R., and Lai, R. (2017). Antioxidant activity of quercetin and its glucosides from propolis: A theoretical study. *Sci. Rep.* 7, 7543. doi: 10.1038/s41598-017-08024-8

frontiers | Frontiers in Plant Science

TYPE Original Research
PUBLISHED 25 September 2023
DOI 10.3389/fpls.2023.1271303

OPEN ACCESS

EDITED BY
Zhentian Lei,
University of Missouri, United States

REVIEWED BY
Alice Raphael Karikachery,
University of Missouri, United States
Qijie Guan,
University of Mississippi, United States
Fang Chen,
Texas Tech University, United States

*CORRESPONDENCE
Lianyang Bai
lybai@hunaas.cn
Lifeng Wang
ifwang@hunaas.cn

†These authors have contributed equally to this work

RECEIVED 04 August 2023
ACCEPTED 08 September 2023
PUBLISHED 25 September 2023

CITATION
Zhang L, Chen K, Li T, Yuan S, Li C, Bai L and Wang L (2023) Metabolomic and transcriptomic analyses of rice plant interaction with invasive weed *Leptochloa chinensis*. *Front. Plant Sci.* 14:1271303. doi: 10.3389/fpls.2023.1271303

Metabolomic and transcriptomic analyses of rice plant interaction with invasive weed *Leptochloa chinensis*

Liang Zhang [1,2,3,4†], Ke Chen [1,2†], Tianrui Li [1,2], Shuren Yuan [1,2], Chenyang Li [3], Lianyang Bai [1,2,4*] and Lifeng Wang [1,2,4*]

[1]Longping Branch, College of Biology, Hunan University, Changsha, China, [2]Key Laboratory of Indica Rice Genetics and Breeding in the Middle and Lower Reaches of Yangtze River Valley, Ministry of Agriculture and Rural Affairs, Hunan Rice Research Institute, Hunan Academy of Agricultural Sciences, Changsha, China, [3]College of Biology, State Key Laboratory of Chemo/Biosensing and Chemometrics, and Hunan Province Key Laboratory of Plant Functional Genomics and Developmental Regulation, Hunan University, Changsha, China, [4]Huangpu Research Institute of Longping Agricultural Science and Technology, Guangzhou, China

Introduction: *Leptochloa chinensis* is an annual weed in paddy fields, which can engage in competition with rice, leading to a severe yield reduction. However, theunderlying mechanism governing this interaction remain unknown.

Methods: In this study, we investigated the mutual inhibition between rice and the weed undermono-culture and co-culture conditions. We found that the root exudates of both species played essential roles in mediating the mutual inhibition. Further metabolomic analysis identified a significant number of differential metabolites. These metabolites were predominantly enriched in the phenylpropanoid and flavonoid biosynthesis pathways in weed and rice. Transcriptomic analysis revealed that the differentially expressed genes responding to the interaction were also enriched in these pathways.

Results: Phenylpropanoid and flavonoid biosynthesis pathways are associated with allelopathy, indicating their pivotal role in the response of rice-weed mutual inhibition.

Discussion: Our findings shed light on the conserved molecular responses of rice and *L. chinensis* during theirinteraction, provide evidence to dissect the mechanisms underlying the allelopathic interaction and offer potential strategies for weed management in rice paddies.

KEYWORDS

rice, *Leptochloa chinensis*, metabolome, transcriptome, allelopathy

Introduction

Leptochloa chinensis, a highly invasive weed, represents a significant challenge in rice ecosystems (Wang et al., 2022). *L. chinensis* has recently become the major weed in direct seeded rice fields, encompassing approximately 21% of the total rice production area (Chakraborty et al., 2017). The combination of high seed production (Zheng and Huang, 1997) and the development of herbicide resistance (Yu et al., 2017; Zhang et al., 2021) in *L. chinensis* presents significant challenges for field management. The prolific seed production of this weed allows it to rapidly spread and establish itself in rice fields, exacerbating weed infestation and further reducing rice yields. Moreover, conventional chemical herbicides, which have long been used as the primary method for weed management, may no longer be as effective in controlling herbicide-resistant *L. chinensis* populations. Continued reliance on chemical herbicides in the presence of resistant weeds can lead to escalating herbicide use, posing serious risks to the soil environment and overall ecosystem health. Therefore, implementing environmentally friendly weed management strategies is important to address the challenges posed by herbicide-resistant weed *L. chinensis*.

During the course of their growth and development, plants release specific metabolites (also referred to as allelochemicals) into the surrounding environment (Kong et al., 2019). This phenomenon, known as allelopathy, leads to mutual exclusion or promotion among plants in close proximity (de Wit et al., 2012; Rice, 2012; Pierik et al., 2013; Karban, 2015). Allelopathy is a widespread occurrence in nature and holds significant implications for the competition dynamics between crops and weeds. The allelopathy exerted by weeds on crops often results in substantial losses in crop yield. Enhancing our understanding of the intricacies of allelopathy is crucial for devising effective strategies to mitigate its detrimental impact on crop production. Allelochemicals play a pivotal role in modulating and influencing interactions within plant communities and between plants and other organisms. Allelochemicals exert their influence through various mechanisms, including direct contact, release of volatile compounds, or secretion into the rhizosphere, resulting in a cascade of physiological and biochemical responses in target organisms (Farmer, 2001; Ma et al., 2016; Rasmann and Turlings, 2016). By modulating metabolic pathways, and signal transduction processes, allelochemicals regulate the growth, development, and physiological functions of target organisms (Heil and Ton, 2008; Broz et al., 2010; Inderjit et al., 2011).

The biosynthesis of phenylpropanoid biosynthesis and flavonoid is essential pathways in allelopathic interactions between plants. These pathways produce a variety of secondary metabolites, which act as allelochemicals and mediate the chemical signals involved in allelopathy. Phenylpropanoid biosynthesis produces a diverse group of phenolic compounds, such as coumarins, lignins, and tannins (Randhir et al., 2004). These phenolic compounds act as potent phytotoxins that can inhibit the germination and growth of neighboring plants and weeds (Lin et al., 2016; Yang et al., 2020). Flavonoids are phenylpropanoid metabolites, most of which are synthesized from p-coumaroyl-CoA and malonyl-CoA and share their precursors with the biosynthetic pathway for lignin biosynthesis (Hassan and Mathesius, 2012). Flavonoids can be released by plants into the surrounding soil or through root exudates, influencing the germination and growth of neighboring plants and weeds (Gressel et al., 2004; Hooper et al., 2010; Khan et al., 2010). They induce oxidative stress in weed cells, leading to the accumulation of reactive oxygen species (ROS) and causing cellular damage (Bais et al., 2003).

In this study, we conducted a combined metabolomics and transcriptomics approaches, identified a significant number of differentially expressed metabolites (DEMs) and differentially expressed genes (DEGs) associated with the mutual inhibition of rice and *L. chinensis* during their co-culture. Among the pathways implicated in this mutual inhibition, biosynthesis of phenylpropanoid and flavonoid stood out as potentially crucial players. This work provides a dataset of the potential metabolites and candidate genes that contribute to the mutual inhibition between rice and *L. chinensis*.

Results

A mutually inhibition between rice and *L. chinensis*

Competition between rice and weeds is often accompanied by allelopathy, particularly prominent during the seedling stage of plant growth, with profound implications for plant competition and establishment (Li et al., 2021). To investigate the interaction between rice (*Oryza sativa* L.) and *Leptochloa chinensis*, we generated a system consist of a cylindrical barrier composed of 0.45 μm nylon mesh positioned at the center of each pot (Figures 1A, B). The mesh was used: 1) to prevent the penetration of roots but to allow chemical and bacterial interactions; 2) to function as a barrier obstructing mycorrhizal linkages (Kong et al., 2018). Through co-culturing rice Nipponbare and *L. chinensis* and comparing them with their respective mono-cultures, we observed an obvious reduction in root growth of rice (31%) and *L. chinensis* (28%) (Figures 1A, C).

Metabolic profiling of rice and *L. chinensis* during their interaction

To determine the presence of root-mediated chemical signal communication that results in mutual root growth inhibition between rice and *L. chinensis*, we performed a widely used Liquid Chromatography Tandem Mass Spectrometry (LC-MS/MS) based metabolomics. Principal component analysis (PCA) of the metabolomic profiles indicated that the metabolites presented distinct variations at different conditions and high reproducibility among replicates (Figures 2A, B). A comprehensive analysis identified a total of 131 DEMs in rice and 143 DEMs in *L. chinensis* (Table S1). Subsequently, a correlation analysis was conducted to

10.3389/fpls.2023.1271303

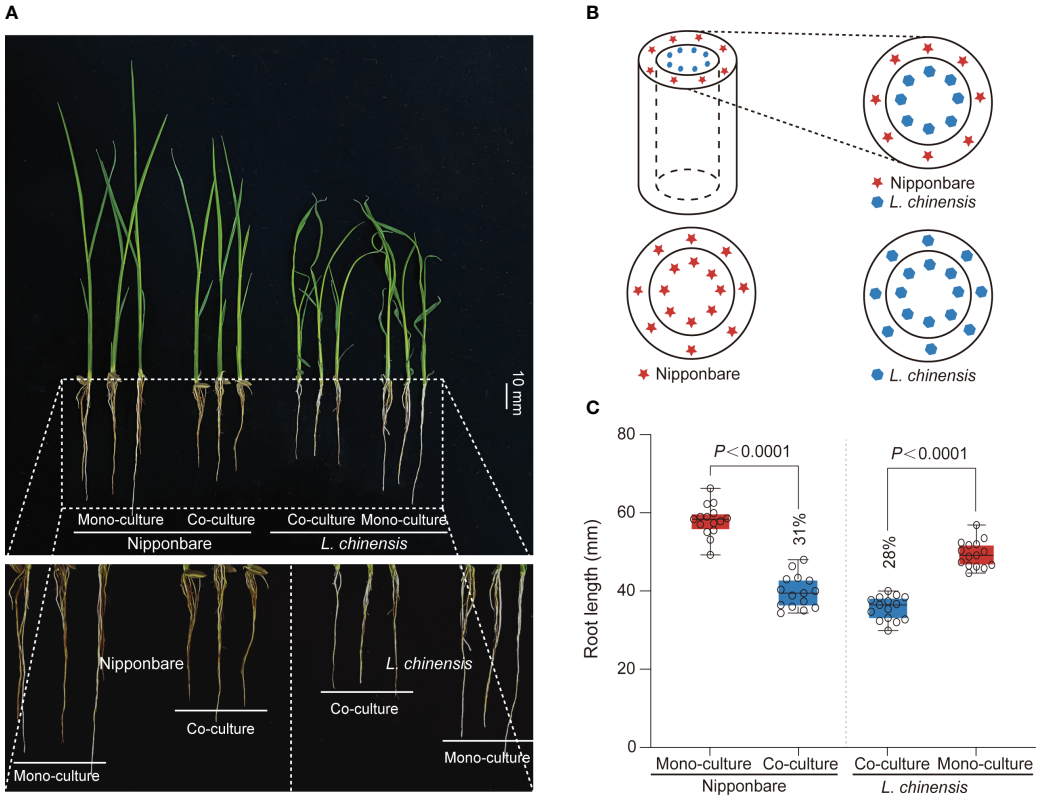

FIGURE 1
The mutual inhibition between rice and *L. chinensis*. **(A)** The co-cultured rice and *L. chinensis* results in a notable occurrence of mutual growth inhibition. The seedlings were grown in soil-filled cylindrical pots for 20 days. Bar=10 mm. **(B)** The pot experiment pattern diagram includes visual elements to illustrate key components. Specifically, a dashed cylindrical line is implemented to represent the 0.45 mm nylon mesh barrier. The red pentagram symbolizes rice nipponbare, while the blue hexagon represents *L. chinensis*. **(C)** Statistical analysis of root length in the pot experiment. The data shown are the means ± SDs (n = 15; n refers to the number of seedings per group). One-way ANOVA with Tukey's test.

investigate the relationships among the identified DEMs (Figures 2C, D). A heatmap with hierarchical clustering analysis of proportional content for all DEMs is shown in Figures 2E, F. Volcano plots show all differential metabolites for mono-cultured rice v.s. co-cultured rice (50 upregulated and 81 downregulated) and mono-cultured *L. chinensis* v.s. co-cultured *L. chinensis* (45 upregulated and 98 downregulated) (Figures 3A, B; Table S1). The accumulation of the majority of differential metabolites was lower in monoculture conditions than in co-culture environments for rice and *L. chinensis*. Compared to their respective monoculture conditions, obvious changes in the metabolic profiles of both rice and *L. chinensis* following their co-culture were detected, indicating a robust metabolic modification.

Kyoto Encyclopedia of Genes and Genomes (KEGG) analysis showed that the interaction between rice and *L. chinensis* influences multiple biological pathways (Figures 3C, D), such as the biosynthesis of isoquinoline alkaloid, phenylpropanoid and flavonoid. These identified pathways are intricately associated with allelopathy (Whittaker and Feeny, 1971), and the enrichment of these pathways in both rice and *L. chinensis* implies the adoption of highly similar coping strategies by both species in response to such interactions. The metabolites released by *L. chinensis* in response to allelopathy exhibited a higher degree of specific enrichment compared to rice in metabolite category phenylalanine metabolism. These findings suggest a convergence of molecular mechanisms underlying their respective responses, which provides a potential explanation for the observed inhibition of root length in co-cultures of rice and *L. chinensis*.

Transcriptomic dynamic profiling between rice and *L. chinensis* interaction

In order to validate the findings from the metabolomic analysis, we conducted transcriptome analysis to investigate the underlying genetic basis of the interaction between rice and *L. chinensis*. Root samples from four distinct treatments [rice mono-culture, co-culture samples (rice and *L. chinensis*) and *L. chinensis* mono-culture] were subjected to RNA-sequencing. Through a comparative analysis of gene expression between mono-cultured rice and co-cultured rice, we identified a total of 1,948 differentially expressed genes (DEGs, 1,026 upregulated and 922 downregulated) in rice (Figure 4A). We observed 2,598 differentially expressed genes in *L. chinensis*, with 1,734 genes showing significant up-regulation and 864 genes demonstrating significant down-regulation after co-cultured with rice (Figure 5A; Table S2). These results suggest that the interaction between rice and *L. chinensis* make substantial changes in the expression patterns of genes.

Gene Ontology (GO) enrichment analysis showed that the DEGs in rice were primarily associated with biological processes such as oxidation-reduction process, phenylpropanoid biosynthesis, and

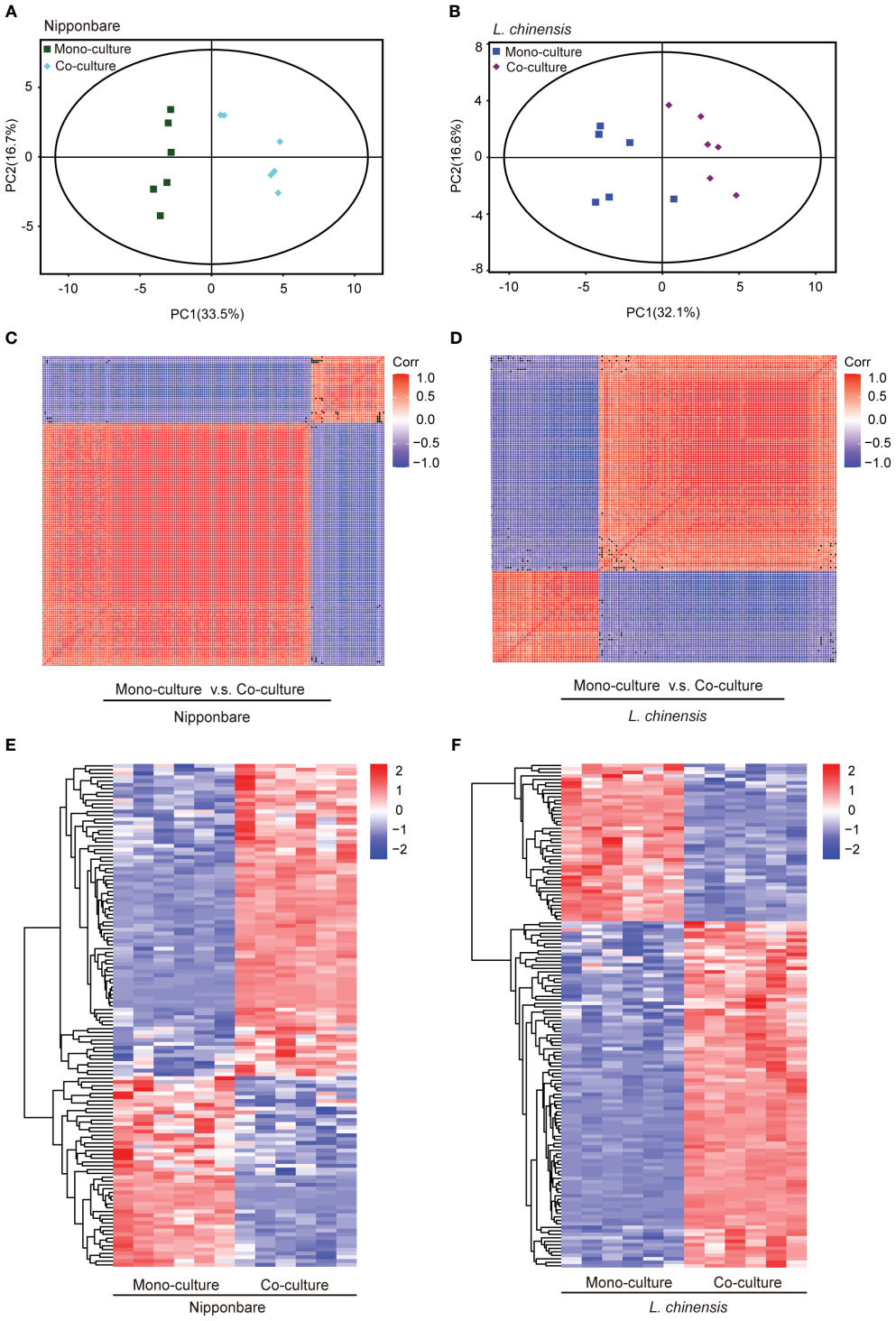

FIGURE 2
Dynamic metabolome of rice and *L. chinensis* in the reciprocal inhibition. **(A, B)** Principal component analysis (PCA) of metabolites identified in mono-cultures v.s. co-cultures (rice and *L. chinensis*). **(C, D)** Correlation analysis of metabolites identified in mono-cultures vs co-cultures (rice and *L. chinensis*). **(E, F)** Heatmap of all differentially expressed metabolites (DEMs) in rice and *L. chinensis*. Color indicates level of relative content of each DEM, from blue (low) to red (high).

secondary metabolic process. These genes were also enriched in molecular functions, such as iron ion binding, antioxidant activity, and oxidoreductase activity and enriched in cell components such extracellular region and apoplast (Figure 4B). Similarly, the DEGs in *L. chinensis* were associated with biological processes such as oxidation-reduction process, toxin metabolic process and secondary metabolic process. These DEGs were also enriched in molecular functions, such as heme binding, antioxidant activity, and oxidoreductase activity and enriched in cell components such as extracellular region and membrane (Figure 5B). Additional, KEGG analysis showed that

10.3389/fpls.2023.1271303

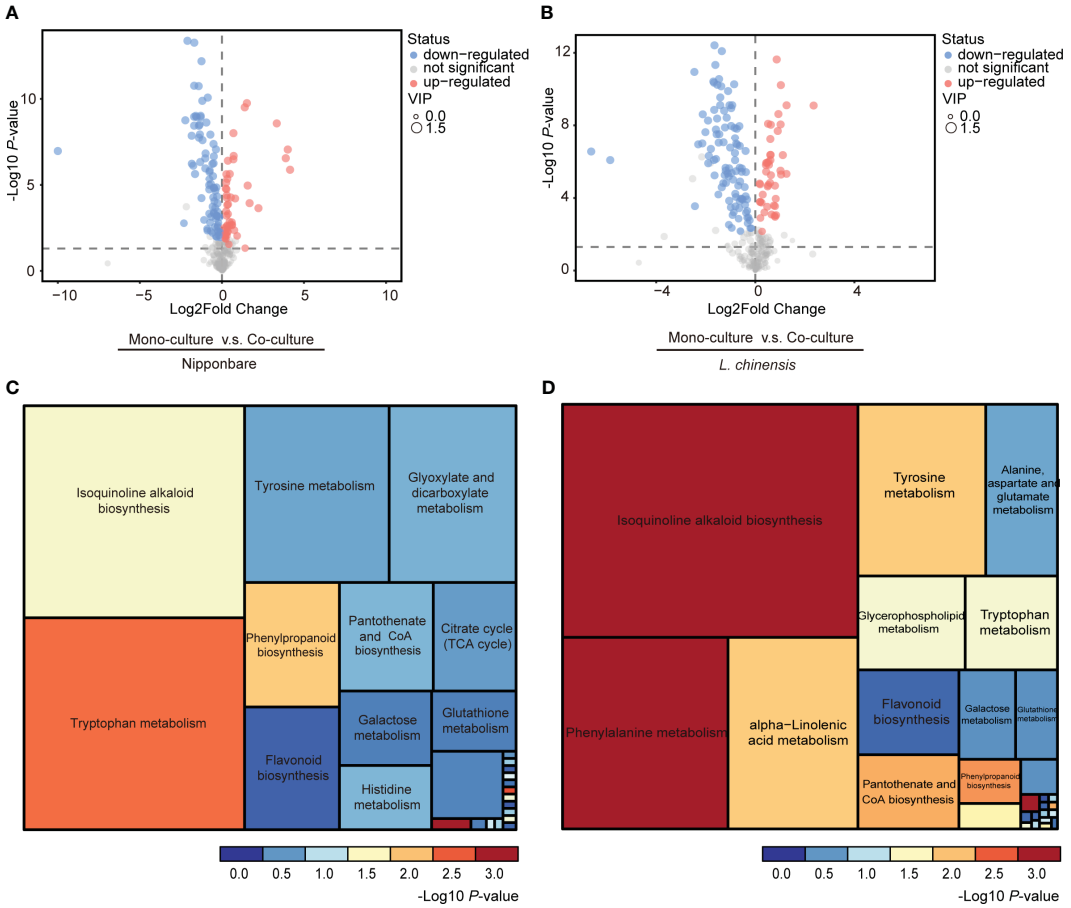

FIGURE 3
Changes in co-culture-induced metabolite are involved in various pathways. **(A, B)** Volcano plots of differential metabolites in mono-cultures vs co-cultures (rice and *L. chinensis*). **(C, D)** KEGG pathway enrichment analysis of DEMs in mono-cultures vs co-cultures (rice and *L. chinensis*).

interaction between rice and *L. chinensis* affect pathways in rice, including phenylpropanoid biosynthesis, flavonoid biosynthesis, and glutathione metabolism (Figure 4C). In *L. chinensis*, the pathways affected by this interaction also exhibit striking similarities to those observed in rice, including phenylpropanoid biosynthesis, flavonoid biosynthesis, and cysteine and methionine metabolism (Figure 5C). This parallelism suggests a conserved response mechanism across these two species. Results of the metabolomic and transcriptomic analyses together indicated that the interaction between rice and *L. chinensis* is likely attributed to allelopathy. The observed similarities in the affected pathways between *L. chinensis* and rice align with the parallel patterns identified in their metabolomic profiles. This congruence further supports the notion that *L. chinensis* and rice share common metabolic responses and employ similar strategies in response to their interaction.

Expression patterns associated with phenylpropanoid and flavonoid biosynthesis

To gain a more comprehensive understanding of the distribution of differential metabolites and differential genes within the biosynthesis pathways of phenylpropanoid and flavonoid, we performed an integrated analysis by combining transcriptomic and metabolomic data. This approach allowed us to map the expression patterns of these two pathways and identify key regulatory nodes that contribute to the allelopathic interaction between rice and *L. chinensis*.

Concerning phenylpropanoid biosynthesis, the accumulation of p-coumaric acid and coniferyl-aldehyde was higher in co-cultured rice than in mono-cultured rice, while the accumulation of metabolite tyrosine lower. The DEGs associated with the phenylpropanoid metabolism pathway in rice was predominantly up-regulated in the co-culture. In *L. chinensis*, major metabolites such as p-coumaric acid, tyrosine, and, phenylalanine were remarkably elevated in the co-culture. Similar to rice, DEGs associated with the phenylpropanoid metabolism pathway in *L. chinensis* was mainly up-regulated in the co-culture (Figure 6A). However, at the step from coniferyl-alcohol to guaiacyl lignin in this pathway, gene expression demonstrated a down-regulation trend in *L. chinensis*, which differed from the up-regulation observed in rice. These differences in gene expression patterns suggest that rice and *L. chinensis* respond differently to the allelopathic signals.

Concerning flavonoid biosynthesis, the observation of up-regulation of metabolite naringenin in both rice and *L. chinensis*

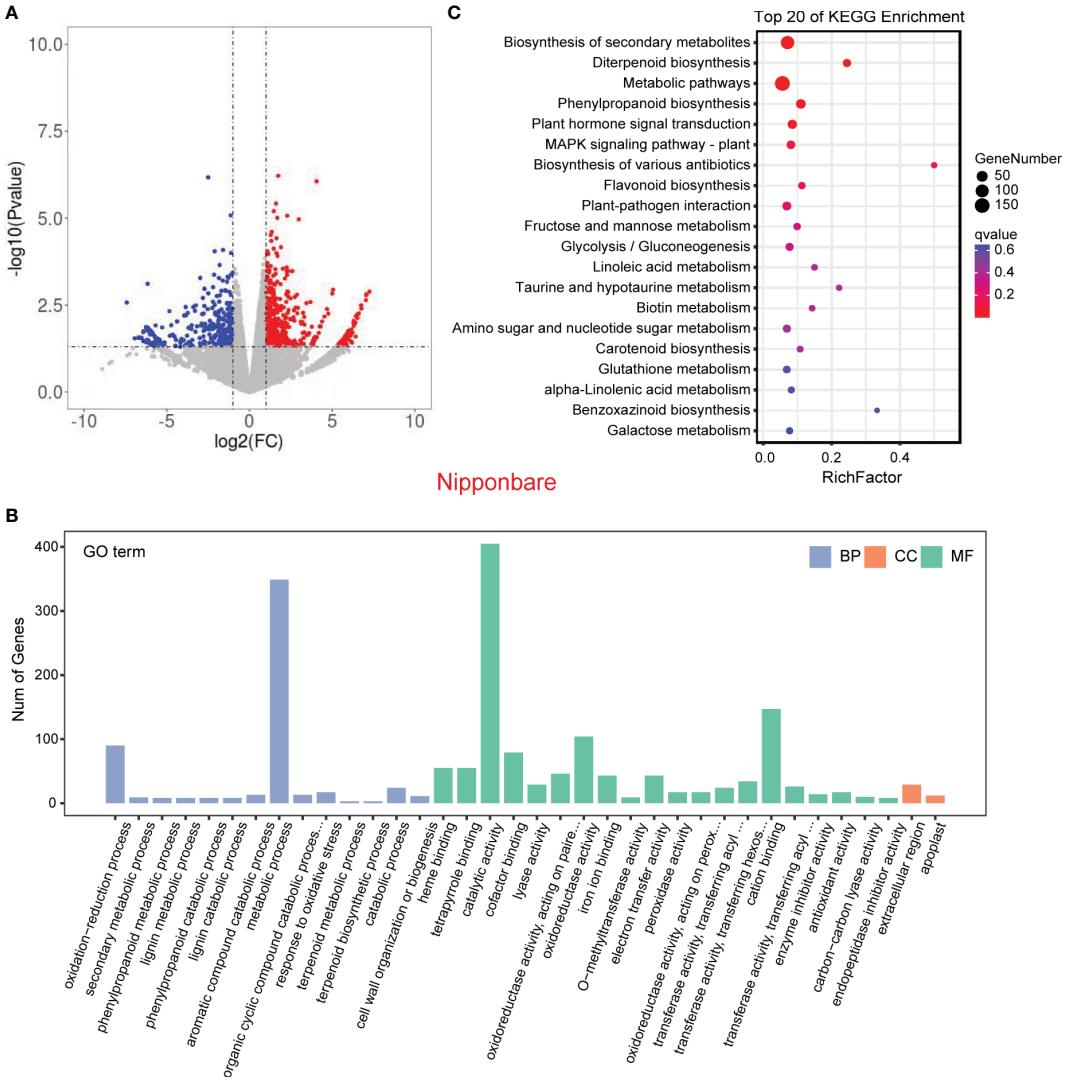

FIGURE 4
Transcriptome of rice in the reciprocal inhibition between rice and *L. chinensis*. **(A)** The volcano plot of differentially expressed genes (DEGs) in mono-cultures versus co-cultures (rice); **(B)** Gene ontology (GO) analysis of induced-DEGs in mono-cultures versus co-cultures. The DEGs were summarized in biological process (BP), cellular component (CC) and molecular function (MF). **(C)** KEGG annotation of induced-DEGs in mono-cultures versus co-cultures. The Rich factor is the ratio of the number of DEGs annotated in a pathway term to the total number of genes in that pathway.

in co-cultures compared to mono-cultures suggests a common response to the allelopathic interaction between these two plant species. This shared up-regulation of naringenin indicates that it may play a crucial role in mediating the allelopathic effects during their co-culture. Furthermore, the finding of highly similar differential gene expression patterns related to flavonoid metabolism in both rice and *L. chinensis* reinforces the notion of a conserved response to the allelopathic signals (Figure 6B). These results suggested that the flavonoid metabolism pathway is conserved in the two species and may be a critical component of their allelopathic response.

Discussion

Weed infestations pose a significant threat to rice crops, leading to substantial yield losses (Oerke, 2006). The escalating damage caused by *L. chinensis* in southern Chinese rice fields is a matter of particular concern (Peng et al., 2020). While chemical weed control has been widely adopted as an effective method, it brings about adverse environmental consequences and the emergence of herbicide-resistant superweeds. The exploration of allelopathy and allelochemicals holds promise for providing alternative and sustainable approaches to weed management in rice cultivation,

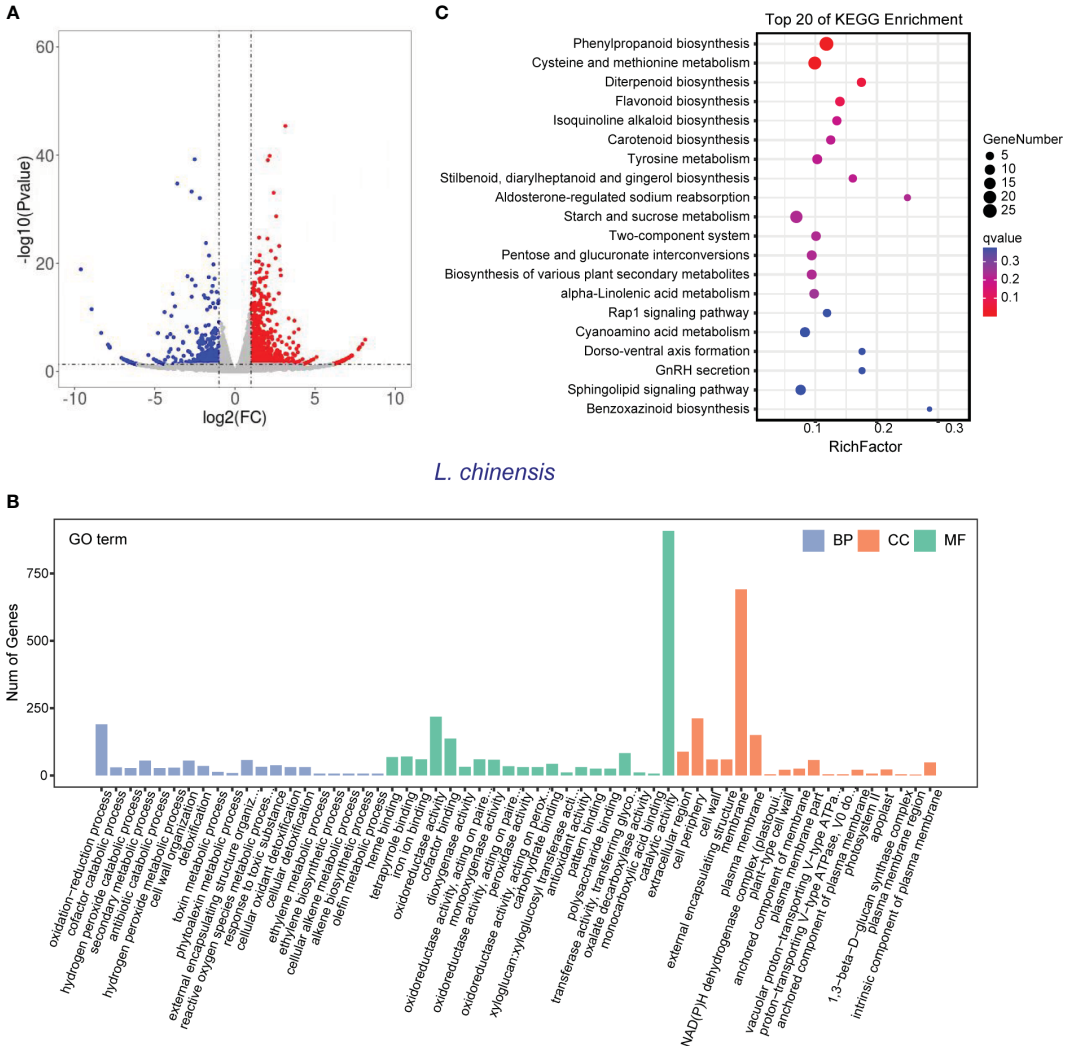

FIGURE 5
Transcriptome of *L. chinensis* in the reciprocal inhibition between rice and *L. chinensis*. **(A)** The volcano plot of differentially expressed genes (DEGs) in mono-cultures versus co-cultures (*L. chinensis*); **(B)** Gene ontology (GO) analysis of induced-DEGs in mono-cultures versus co-cultures. The DEGs were summarized in biological process (BP), cellular component (CC) and molecular function (MF). **(C)** KEGG annotation of induced-DEGs in mono-cultures versus co-cultures. The Rich factor is the ratio of the number of DEGs annotated in a pathway term to the total number of genes in that pathway.

with the potential to mitigate the reliance on chemical interventions and alleviate environmental hazards (Duke et al., 2002; de Albuquerque et al., 2011; Farooq et al., 2011).

In this study, we observed a notable mutual suppression between rice and *L. chinensis* through controlled potting experiments. Co-cultures of both plants exhibited a more pronounced inhibition of root length compared to separate cultures. We implemented a 0.45 μm nylon membrane in the soil, which allowed chemical and bacterial interactions but impeded the penetration of roots and common mycorrhizal hyphae (Kong et al., 2018). This membrane selectively permitted the passage of small molecules, indicating that the secretion of secondary metabolites into the environment likely contributes to the observed mutual inhibition phenomenon. To unravel the strategies employed by rice and *L. chinensis* in response to the mutual inhibition, we employed metabolomic and transcriptomic analyses to investigate their respective metabolic and transcriptional responses. We established a comprehensive network that incorporates differential gene and metabolite data, revealing the interaction between rice and *L. chinensis*. Notably, both plants exhibited a remarkable similarity at the transcriptional and metabolic levels in their responses to mutual inhibition. This finding suggests a conserved strategy in both rice and *L. chinensis* when confronted with allelopathic stress. Overall, our study provides evidence for the occurrence of allelopathic interactions between rice and *L. chinensis*. The utilization of metabolomic and transcriptomic approaches enhances our understanding of the mechanisms underlying their responses to allelopathy. These findings contribute to a broader comprehension of the conserved strategies adopted by both rice and *L. chinensis* in the face of allelopathic stress.

Phenylpropanoid biosynthesis and flavonoid biosynthesis pathways are intricately linked to allelopathy (Whittaker and

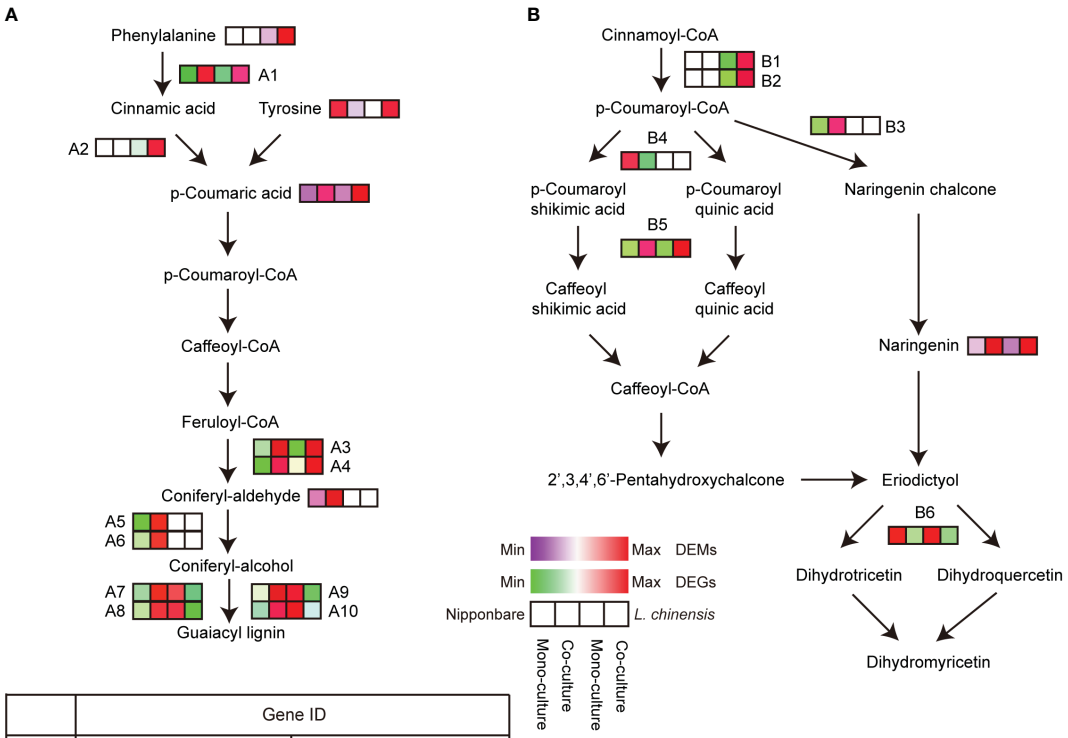

	Gene ID	
A1	LOC_Os12g33610	Chr7.g21917
A2		Chr4.g13272
A3	LOC_Os01g18120	Chr17.g45021
A4	LOC_Os09g04050	Chr18.g47164
A5	LOC_Os03g12270	
A6	LOC_Os11g40690	
A7	LOC_Os06g32990	Chr1.g00878
A8	LOC_Os01g73200	Chr1.g00961
A9	LOC_Os07g01380	Chr2.g04385
A10	LOC_Os12g02060	Chr4.g10809

	Gene ID	
B1		Chr10.g31650
B2		Chr9.g27608
B3	LOC_Os11g32650	
B4	LOC_Os08g10420	
B5	LOC_Os10g12050	Chr18.g47059
B6	LOC_Os04g56700	Chr8.g23334

FIGURE 6
Analysis of key metabolic pathways in the interaction between rice and *L. chinensis*. **(A)** Expression profiles of DEGs and DEMs associated with phenylpropanoid biosynthesis. **(B)** Expression profiles of DEGs and DEMs associated with flavonoid biosynthesis.

Feeny, 1971). The DEGs and DEMs in rice and *L. chinensis* revealed a significant enrichment of pathways associated with phenylpropanoid biosynthesis and flavonoid biosynthesis when compared to their respective monocultures. Implying that allelopathic interactions indeed occur between rice and *L. chinensis*. The observed enrichment suggested that both species respond to allelopathy by regulating key genes and metabolites involved in phenylpropanoid and flavonoid synthesis. Phenylpropanoid metabolism contributes to plant development and plant-environmental interplay (Dong and Lin, 2021). Phenylpropanes are a typical secondary metabolite, including, lignin, flavonoids, lignins, phenylpropanoid esters, hydroxycinnamicacid amides, and sporopollenin, are known for their inhibitory effects on the growth and development of neighboring plants (Boerjan et al., 2003; Yuan and Grotewold, 2020). Flavonoids, including flavones, flavonols, and flavanones, possess diverse allelopathic activities and contribute to the regulation of plant-plant interactions (Winkel-Shirley, 2001; Zhang et al., 2007; Wang et al., 2018). The production and release of phenylpropanoids and flavonoids by plants enable them to modulate the surrounding environment, influencing the physiology and growth of neighboring organisms. Indeed, exploring and developing natural herbicides derived from plant extracts or other organic sources can offer a promising eco-friendly alternative to chemical herbicides. By identifying and harnessing candidate metabolites from plant species, as demonstrated in our work, we contribute valuable insights into potential biogenic herbicides.

In summary, our study demonstrates mutually suppressive allelopathy between rice and *L. chinensis*. We constructed comprehensive metabolic and transcriptional regulatory networks, revealing a degree of conservation in their response strategies to

allelopathy. Our findings reveal the significant involvement of phenylpropanoid and flavonoid synthesis pathways in the response of both rice and *L. chinensis* to mutually inhibitory allelopathic interactions. These pathways are likely involved in the production of allelochemicals that contribute to the inhibitory effects observed during their interaction. Our data on candidate metabolites offer new perspectives and potential targets for the development of novel herbicides. These findings have significant implications for the development of effective strategies for weed management and crop protection in agricultural systems.

Materials and methods

Plant material and growth conditions

Rice Nipponbare and *L. chinensis* seeds were immersed in 0.3% gibberellin solution for 30 min. After rinsing thoroughly with distilled water, they were germinated in Petri dishes for 72 h. Germinating seedlings were grown under long-day conditions at 26-28°C.

Rice-neighbor interactions

The experiment for rice–neighbor interactions were carried out in plastic pots (11 cm diameter × 12 cm height) that contained a central cylinder (7.5 cm diameter, 12 cm height) where a barrier covered with 0.45 μm nylon mesh (prevented penetration of both roots and common mycorrhizal hyphae but allowed chemical and bacterial interactions) (Kong et al., 2018). Rice and *L. chinensis* at 8:8 proportions were sown simultaneously in the pots. Monocultures of rice or *L. chinensis* served as the controls. The experiments were conducted in a completely randomized design with three replicates for each treatment or control. All pots from the experiments described above were placed in a greenhouse with 20–30°C night and daytime temperatures and 65–90% relative humidity, watered daily and their positions randomized once a week. Seedlings were harvested after 3 weeks for subsequent metabolome and transcriptome analyses. To be better compare the metabolite and gene expression, we have employed a specific approach. In our co-culture experiment, we compare the outer rice plants exclusively to the outer rice plants in the mono-culture experiment. Similarly, the inner *L. chinensis* plants in the co-culture experiment are compared solely to the inner *L. chinensis* plants in the mono-culture *L. chinensis* experiments. A set of experimental pots was prepared using 800 g of soil sourced from the top layer (0-10 cm) of a rice field. This soil collection method ensured representation of the surface soil characteristics and facilitated the subsequent analyses conducted in the study.

Metabolite extraction

Metabolite extraction and profiling was performed as previously described (De Vos et al., 2007; Chen et al., 2013). The freeze-dried samples of root tissue were crushed with a mixer mill (Retsch, Germany) for 1 min at 60 Hz. 100 mg powder of each sample was transferred to 5 mL eppendorf tube, and extracted with 3000 μL methanol/water mixture (v:v=3:1). The samples were rotated for 30s, added with 2 small steel balls (MISUMI, China), ground at 35 Hz for 4 min, and ultrasonic in ice bath for 15 min. Then the samples were followed by overnighting shaking at 4°C. All the samples were centrifuged at 12000 rpm for 15 min at 4°C. 1800 μL of supernatant was transferred to a fresh 5 mL eppendorf tube and nitrogen blow dride. Here, the dried samples were reconstituted in 900 μL of 50% methanol for 15 min in ice-water bath. Then, all the samples were centrifuged at 12000 rpm for 15 min at 4°C. The resulting supernatants were through the 0.22 μm filter membrane. The resulting supernatants were diluted 10 times with methanol/water mixture (v:v=3:1) and vortexed for 30 s and transferred to 2 mL glass vials. The quality control (QC) sample was prepared by mixing of an equal aliquot of the supernatants from all of the samples. Then stored at -80°C until the UHPLC-MS/MS analysis.

UHPLC-MS analysis

The UHPLC separation utilized a Waters ACQUITY UPLC HSS T3 column (100 × 2.1 mm, 1.8 μm), following a previously described method (Yan et al., 2022). Mobile phase A consisted of 0.1% formic acid in water, while mobile phase B was acetonitrile. The gradient elution followed this protocol: 0–0.5 min, 98% A, 2% B; 0.5–10 min, 50% A, 50% B; 10–11 min, 5% A, 95% B; 11–13 min, 5% A, 95% B; 13–15 min, 98% A, 2% B. The column temperature was maintained at 40°C. The auto-sampler was set to 4°C, and injections of 2 μL were made.

An AB Sciex QTOF mass spectrometer was selected for its capability to perform MS/MS spectra acquisition using information-dependent acquisition (IDA) during LC/MS experiments. In this mode, the acquisition software (Analyst) continuously assessed full scan survey MS data and triggered MS/MS spectra acquisition based on predefined criteria. In each cycle, 5 precursor ions with intensities exceeding 100 were selected for fragmentation using collision energy. The acquired mass ranges were divided into 100–300, 300–450, 450–600, 600–750, and 750–1200 with 5 injections. ESI source conditions were set as follows: ion spray voltage at +5500/−4500 V, gas curtain at 35 psi, temperature at 600°C, Gases 1 and 2 at 60 psi for the ion source, and DP at ±100 V (Luo et al., 2016; Zha et al., 2018).

For assay development, an AB Sciex QTrap 6500 mass spectrometer was employed. The ion source parameters included ion spray voltage of +5000/−4500 V, curtain gas at 35 psi, temperature at 400°C, Gases 1 and 2 at 60 psi for the ion source, and DP at ±100 V.

Data preprocessing and annotation

The high resolution MS data were converted to the mzXML format using ProteoWizard, and processed by MAPS software (version 1.0) (A Mass Spectrometry Analysis and Processing

Software developed by Biotree Biotech Co., Ltd. Shanghai, China). The preprocessing results generated a data matrix that consisted of the retention time (RT), mass-to-charge ratio (m/z) values, and peak intensity. In-house MS2 database was applied in metabolites identification. And the MRM data were processed with Skyline software.

RNA extraction and quality determination for RNA-seq

For rice and *L. chinensis*, RNA-sequencing (RNA-seq) was performed using root tissues. The total RNA was extracted with the TransGen RNA extraction kit (TranGen, Beijing, China). RNA degradation and contamination were monitored on 1 % agarose gels. RNA purity was checked using the NanoPhotometer® spectrum photometer(IMPLEN, CA, USA), and RNA concentration was determined using the Qubit® RNA Assay Kit (Qubit®2.0Flurometer, Life Technologies, CA, USA). RNA integrity was assessed using the RNA Nano 6000 Assay Kit (Agilent Bioanalyzer 2100 system, Agilent Technologies, USA). The best quality RNA samples were chosen for cDNA library preparation.

Library preparation, and transcriptome sequencing

We used 3 μg of RNA per sample as input for RNA sample preparations. Sequencing libraries were created using the NEBNext® Ultra™ RNA Library Prep Kit for Illumina® (NEB, USA) following the manufacturer's instructions. Index-coded sample clustering was performed on a cBot Cluster Generation System using the TruSeq PE Cluster Kit v3-cBot-HS (Illumina). Following cluster generation, the Illumina NovaSeq 6000 was used for sequencing, producing 150 bp paired-end reads. Raw data containing over 10% poly-N and more than 50% low-quality reads ($Q \leq 20$) were removed using Trimmomatic v0.33 (Bolger et al., 2014). The quality metrics Q20 and Q30, GC content, and sequence duplication level were calculated for the clean data. All subsequent analyses were based on this clean, high-quality data. Clean reads were then aligned against the reference genome using Hisat2 (Kim et al., 2015).

Identification of differential expressed genes and functional annotation

In order to quantify the gene expression, the count based method, FeatureCounts (Liao et al., 2014) was used. Next, the transcript counts were used for pairwise differential gene expression analysis using the edgeR package. A cut-off value of $|\log2\ FC| > 1$ and P-value < 0.05 were used to filter out the significant transcripts in each case. Gene Ontology (GO, http://www.geneontology.org/) enrichment analysis of the DEGs was implemented using gOseq (v. 1.22) (Young et al., 2010) using Wallenius'noncentral hypergeometric distribution, which can adjust for gene length bias in DEGs. Affected pathways were determined using Kyoto Encyclopedia of Genes and Genomes (KEGG, http://www.kegg.jp) (Kanehisa et al., 2008).

Statistical analysis

The statistical significance of the populations was calculated with Tukey's test, and significance was indicated with different letters above the error bars. The heatmap was drawn by the tBtools software. Figures were drawn by Origin 8.0 (OriginLab Corp., Northampton, MA, USA).

Data availability statement

The datasets presented in this study can be found in online repositories. The names of the repository/repositories and accession number(s) can be found in the article/Supplementary Material.

Author contributions

LZ: Conceptualization, Writing – original draft, Writing – review and editing. KC: Writing – review and editing. TL: Conceptualization, Methodology, Writing – review and editing. SY: Conceptualization, Investigation, Writing – review and editing. CL: Data curation, Methodology, Writing – review and editing. LB: Funding acquisition, Resources, Writing – review and editing. LW: Funding acquisition, Investigation, Methodology, Resources, Writing – review and editing.

Funding

This research was supported by grants from the National Key R&D Program of China (No. 2021YFD1700101), the National Natural Science Foundation of China (No. 32272564 and No. 32001923), the Science and Technology Innovation Program of Hunan Province (2021RC3044, 2022RC1017, 2022WK2007, 2020WK2014), the Training Program for Excellent Young Innovators of Changsha (kq2106079), and the China Agriculture Research System of MOF and MARA (CARS-16-E19).

Conflict of interest

The authors declare that the research was conducted in the absence of any commercial or financial relationships that could be construed as a potential conflict of interest.

Publisher's note

All claims expressed in this article are solely those of the authors and do not necessarily represent those of their affiliated organizations, or those of the publisher, the editors and the reviewers. Any product that may be evaluated in this article, or claim that may be made by its manufacturer, is not guaranteed or endorsed by the publisher.

Supplementary material

The Supplementary Material for this article can be found online at: https://www.frontiersin.org/articles/10.3389/fpls.2023.1271303/full#supplementary-material

References

Bais, H. P., Vepachedu, R., Gilroy, S., Callaway, R. M., and Vivanco, J. M. (2003). Allelopathy and exotic plant invasion: from molecules and genes to species interactions. *Science* 301, 1377–1380. doi: 10.1126/science.1083245

Boerjan, W., Ralph, J., and Baucher, M. (2003). Lignin biosynthesis. *Annu. Rev. Plant Biol.* 54, 519–546. doi: 10.1146/annurev.arplant.54.031902.134938

Bolger, A. M., Lohse, M., and Usadel, B. (2014). Trimmomatic: a flexible trimmer for Illumina sequence data. *Bioinformatics* 15, 2114–2120. doi: 10.1093/bioinformatics/btu170

Broz, A. K., Broeckling, C. D., De-la-Peña, C., Lewis, M. R., Greene, E., Callaway, R. M., et al. (2010). Plant neighbor identity influences plant biochemistry and physiology related to defense. *BMC Plant Biol.* 10, 115. doi: 10.1186/1471-2229-10-115

Chakraborty, D., Ladha, J. K., Rana, D. S., Jat, M. L., Gathala, M. K., Yadav, S., et al. (2017). A global analysis of alternative tillage and crop establishment practices for economically and environmentally efficient rice production. *Sci. Rep.* 7, 9342. doi: 10.1038/s41598-017-09742-9

Chen, W., Gong, L., Guo, Z., Wang, W., Zhang, H., Liu, X., et al. (2013). A novel integrated method for large-scale detection, identification, and quantification of widely targeted metabolites: application in the study of rice metabolomics. *Mol. Plant* 6, 1769–1780. doi: 10.1093/mp/sst080

de Albuquerque, M. B., dos Santos, R. C., Lima, L. M., Mansur Custodio Nogueira, R. J., Câmara, C. A. G. D., de Rezende Ramos, A., et al. (2011). Allelopathy, an alternative tool to improve cropping systems. A review. *Agronomy Sust. Developm.* 31, 379–395. doi: 10.1051/agro/2010031

De Vos, R. C., Moco, S., Lommen, A., Keurentjes, J. J., Bino, R. J., and Hall, R. D. (2007). Untargeted large-scale plant metabolomics using liquid chromatography coupled to mass spectrometry. *Nat. Protoc.* 2, 778–791. doi: 10.1038/nprot.2007.95

de Wit, M., Kegge, W., Evers, J. B., Vergeer-van, E. M., Gankema, P., Voesenek, L. A., et al. (2012). Plant neighbor detection through touching leaf tips precedesphytochrome signals. *Proc. Natl. Acad. Sci. U.S.A.* 109, 14705–14710. doi: 10.1073/pnas.1205437109

Dong, N. Q., and Lin, H. X. (2021). Contribution of phenylpropanoid metabolism to plant development and plant-environment interactions. *J. Integr. Plant Biol.* 63, 180–209. doi: 10.1111/jipb.13054

Duke, S., Dayan, F., Rimando, A., Schrader, K., Aliotta, G., Oliva, A., et al. (2002). Chemicals from nature for weed management. *Weed Sci.* 50, 138–151. doi: 10.1614/0043-1745(2002)050[0138:IPCFNF]2.0.CO;2

Farmer, E. (2001). Surface-to-air signals. *Nature* 411, 854–856. doi: 10.1038/35081189

Farooq, M., Jabran, K., Cheema, Z. A., Wahid, A., and Siddique, K. H. (2011). The role of allelopathy in agricultural pest management. *Pest Manage. Sci.* 67, 493–506. doi: 10.1002/ps.2091

Gressel, J., Hanafi, A., Head, G., Marasas, W., Obilana, B., Ochanda, J., et al. (2004). Major heretofore intractable biotic constraints to African food security that may be amenable to novel biotechnological solutions. *Crop Prot.* 23, 661–689. doi: 10.1016/j.cropro.2003.11.014

Hassan, S., and Mathesius, U. (2012). The role of flavonoids in root-rhizosphere signalling: opportunities and challenges for improving plant-microbe interactions. *J. Exp. Bot.* 63, 3429–3444. doi: 10.1093/jxb/err430

Heil, M., and Ton, J. (2008). Long-distance signalling in plant defence. *Trends Plant Sci.* 13, 264–272. doi: 10.1016/j.tplants.2008.03.005

Hooper, A. M., Tsanuo, M. K., Chamberlain, K., Tittcomb, K., Scholes, J., Hassanali, A., et al. (2010). Isoschaftoside, a C-glycosylflavonoid from Desmodium uncinatum root exudate, is an allelochemical against the development of Striga. *Phytochemistry* 71, 904–908. doi: 10.1016/j.phytochem.2010.02.015

Inderjit,, Wardle, D. A., Karban, R., and Callaway, R. M. (2011). The ecosystem and evolutionary contexts of allelopathy. *Trends Ecol. Evol.* 26, 655–662. doi: 10.1016/j.tree.2011.08.003

Kanehisa, M., Araki, M., Goto, S., Hattori, M., Hirakawa, M., Itoh, M., et al. (2008). KEGG for linking genomes to life and the environment. *Nucleic Acids Res.* 36, D480–D484. doi: 10.1093/nar/gkm882

Karban, R. (2015). *Plant Sensing and Communication* (Chicago: University of Chicago Press).

Khan, Z. R., Midega, C. A., Bruce, T. J., Hooper, A. M., and Pickett, J. A. (2010). Exploiting phytochemicals for developing a 'push-pull' crop protection strategy for cereal farmers in Africa. *J. Exp. Bot.* 61, 4185–4196. doi: 10.1093/jxb/erq229

Kim, D., Langmead, B., and Salzberg, S. L. (2015). HISAT: a fast spliced aligner with low memory requirements. *Nat. Methods* 4, 357–360. doi: 10.1038/nmeth.3317

Kong, C. H., Xuan, T. D., Khanh, T. D., Tran, H. D., and Trung, N. T. (2019). Allelochemicals and signaling chemicals in plants. *Molecules* 24, 2737. doi: 10.3390/molecules24152737

Kong, C. H., Zhang, S. Z., Li, Y. H., Xia, Z. C., Yang, X. F., Meiners, S. J., et al. (2018). Plant neighbor detection and allelochemical response are driven by root-secreted signaling chemicals. *Nat. Commun.* 9, 3867. doi: 10.1038/s41467-018-06429-1

Li, J., Chen, L., Chen, Q., Miao, Y., Peng, Z., Huang, B., et al. (2021). Allelopathic effect of Artemisia argyi on the germination and growth of various weeds. *Sci. Rep.* 11, 4303. doi: 10.1038/s41598-021-83752-6

Liao, Y., Smyth, G. K., and Shi, W. (2014). featureCounts: an efficient general purpose program for assigning sequence reads to genomic features. *Bioinformatics* 30, 923–930. doi: 10.1093/bioinformatics/btt656

Lin, D., Xiao, M., Zhao, J., Li, Z., Xing, B., Li, X., et al. (2016). An overview of plant phenolic compounds and their importance in human nutrition and management of type 2 diabetes. *Molecules* 21, 1374. doi: 10.3390/molecules21101374

Luo, P., Yin, P., Zhang, W., Zhou, L., Lu, X., Lin, X., et al. (2016). Optimization of large-scale pseudotargeted metabolomics method based on liquid chromatography-mass spectrometry. *J. Chromatogr. A* 1437, 127–136. doi: 10.1016/j.chroma.2016.01.078

Ma, X., Xia, H., Liu, Y., Wei, H., Zheng, X., Song, C., et al. (2016). Transcriptomic and metabolomic studies disclose key metabolism pathways contributing to well-maintained photosynthesis under the drought and the consequent drought-tolerance in rice. *Front. Plant Sci.* 7, 1886. doi: 10.3389/fpls.2016.01886

Oerke, E. C. (2006). Crop losses to pests. *J. Agric. Sci.* 144, 31–43. doi: 10.1017/S0021859605005708

Peng, Y., Pan, L., Liu, D., Cheng, X., Ma, G., Li, S., et al. (2020). Confirmation and characterization of cyhalofop-butylresistant Chinese sprangletop (Leptochloa chinensis) populations from China. *Weed Sci.* 68, 253–259. doi: 10.1017/wsc.2020.15

Pierik, R., Mommer, L., Voesenek, L. A. C. J., and Robinson, D. (2013). Molecular mechanisms of plant competition: neighbour detection and response strategies. *Funct. Ecol.* 27, 841–853. doi: 10.1111/1365-2435.12010

Randhir, R., Lin, Y. T., and Shetty, K. (2004). Stimulation of phenolics, antioxidant and antimicrobial activities in dark germinated mung bean sprouts in response to peptide and phytochemical elicitors. *Process Biochem.* 39, 637–646. doi: 10.1016/S0032-9592(03)00197-3

Rasmann, S., and Turlings, T. C. J. (2016). Root signals that mediate mutualistic interactions in the rhizosphere. *Curr. Opin. Plant Biol.* 32, 62–68. doi: 10.1016/j.pbi.2016.06.017

Rice, E. L. (2012). *Allelopathy*, *2nd ed.* (New York: Elsevier Science).

Wang, W., Li, Y., Dang, P., Zhao, S., Lai, D., and Zhou, L. (2018). Rice secondary metabolites: structures, roles, biosynthesis, and metabolic regulation. *Molecules* 23, 3098. doi: 10.3390/molecules23123098

Wang, L., Sun, X., Peng, Y., Chen, K., Wu, S., Guo, Y., et al. (2022). Genomic insights into the origin, adaptive evolution, and herbicide resistance of Leptochloa chinensis, a devastating tetraploid weedy grass in rice fields. *Mol. Plant* 15, 1045–1058. doi: 10.1016/j.molp.2022.05.001

Whittaker, R. H., and Feeny, P. P. (1971). Allelochemics: chemical interactions between species. *Science* 171, 757–770. doi: 10.1126/science.171.3973.757

Winkel-Shirley, B. (2001). Flavonoid biosynthesis. A colorful model for genetics, biochemistry, cell biology, and biotechnology. *Plant Physiol.* 126, 485–493. doi: 10.1104/pp.126.2.485

Yan, H., Zheng, W., Ye, Z., Yu, J., and Wu, Y. (2022). Comparison of the main metabolites in different maturation stages of CamelliaVietnamensis Huang seeds. *Molecules* 20, 6817. doi: 10.3390/molecules27206817

Yang, Y., Zhang, Z., Li, R., Yi, Y., Yang, H., Wang, C., et al. (2020). RgC3H involves in the biosynthesis of allelopathic phenolic acids and alters their release amount in Rehmannia glutinosa roots. *Plants* 9, 567. doi: 10.3390/plants9050567

Young, M. D., Wakefield, M. J., Smyth, G. K., and Oshlack, A. (2010). Gene ontology analysis for RNA-seq: accounting for selection bias. *Genome Biol.* 11, R14. doi: 10.1186/gb-2010-11-2-r14

Yu, J., Gao, H., Pan, L., Yao, Z., and Dong, L. (2017). Mechanism of resistance to cyhalofop-butyl in Chinese sprangletop (Leptochloa chinensis (L.) Nees). *Pestic. Biochem. Physiol.* 143, 306–311. doi: 10.1016/j.pestbp.2016.11.001

Yuan, L., and Grotewold, E. (2020). Plant specialized metabolism. *Plant Sci.* 298, 110579. doi: 10.1016/j.plantsci.2020.110579

Zha, H., Cai, Y., Yin, Y., Wang, Z., Li, K., and Zhu, Z. J. (2018). SWATH to MRM: development of high-coverage targeted metabolomics method using SWATH technology for biomarker discovery. *Anal. Chem.* 90, 4062–4070. doi: 10.1021/acs.analchem.7b05318

Zhang, Y., Chen, L., Song, W., Cang, T., Xu, M., Zhou, G., et al. (2021). Reference genes for the study of herbicide stress responses in Leptochloa chinensis (L.) Nees and estimation of ACCase expression in cyhalofop-butyl resistant populations. *Pestic. Biochem. Physiol.* 171, 104739. doi: 10.1016/j.pestbp.2020.104739

Zhang, J., Subramanian, S., Zhang, Y., and Yu, O. (2007). Flavone synthases from Medicago truncatula are flavanone-2-hydroxylases and are important for nodulation. *Plant Physiol.* 144, 741–751. doi: 10.1104/pp.106.095018

Zheng, H., and Huang, G. (1997). Occurrence and control of Leptochloa chinensis in paddy field. *Plant Prot.* 23, 49–50.

frontiers | Frontiers in Plant Science

TYPE Original Research
PUBLISHED 22 January 2024
DOI 10.3389/fpls.2023.1339478

OPEN ACCESS

EDITED BY
Giovanni Bubici,
National Research Council (CNR), Italy

REVIEWED BY
Nagaraju Yalavarthi,
Central Silk Board, India
Abhijeet Shankar Kashyap,
National Bureau of Agriculturally Important Microorganisms (ICAR), India

*CORRESPONDENCE
Dejie Cheng
chengdejie@gxu.edu.cn
Xiaoqiang Wang
wangxiaoqiang@caas.cn

†These authors have contributed equally to this work

RECEIVED 16 November 2023
ACCEPTED 28 December 2023
PUBLISHED 22 January 2024

CITATION
Wei C, Liang J, Wang R, Chi L, Wang W, Tan J, Shi H, Song X, Cui Z, Xie Q, Cheng D and Wang X (2024) Response of bacterial community metabolites to bacterial wilt caused by *Ralstonia solanacearum*: a multi-omics analysis.
Front. Plant Sci. 14:1339478.
doi: 10.3389/fpls.2023.1339478

Response of bacterial community metabolites to bacterial wilt caused by *Ralstonia solanacearum*: a multi-omics analysis

Chengjian Wei[1,2†], Jinchang Liang[2†], Rui Wang[3†], Luping Chi[2], Wenjing Wang[2], Jun Tan[3], Heli Shi[3], Xueru Song[4], Zhenzhen Cui[2], Qiang Xie[5], Dejie Cheng[1*] and Xiaoqiang Wang[2*]

[1]College of Agriculture, Guangxi University, Nanning, China, [2]Key Laboratory of Tobacco Pest Monitoring & Integrated Management, Tobacco Research Institute of Chinese Academy of Agricultural Sciences, Qingdao, China, [3]Enshi Tobacco Science and Technology Center, Enshi, China, [4]Engineering Center for Biological Control of Diseases and Pests in Tobacco Industry, Yuxi, China, [5]Sichuan Tobacco Science and Technology Center, Chengdu, China

The soil microbial community plays a critical role in promoting robust plant growth and serves as an effective defence mechanism against root pathogens. Current research has focused on unravelling the compositions and functions of diverse microbial taxa in plant rhizospheres invaded by *Ralstonia solanacearum*, however, the specific mechanisms by which key microbial groups with distinct functions exert their effects remain unclear. In this study, we employed a combination of amplicon sequencing and metabolomics analysis to investigate the principal metabolic mechanisms of key microbial taxa in plant rhizosphere soil. Compared to the healthy tobacco rhizosphere samples, the bacterial diversity and co-occurrence network of the diseased tobacco rhizosphere soil were significantly reduced. Notably, certain genera, including *Gaiella*, *Rhodoplanes*, and MND1 (*Nitrosomonadaceae*), were found to be significantly more abundant in the rhizosphere of healthy plants than in that of diseased plants. Eight environmental factors, including exchangeable magnesium, available phosphorus, and pH, were found to be crucial factors influencing the composition of the microbial community. *Ralstonia* displayed negative correlations with pH, exchangeable magnesium, and cation exchange flux, but showed a positive correlation with available iron. Furthermore, metabolomic analysis revealed that the metabolic pathways related to the synthesis of various antibacterial compounds were significantly enriched in the healthy group. The correlation analysis results indicate that the bacterial genera *Polycyclovorans*, *Lysobacter*, *Pseudomonas*, and *Nitrosospira* may participate in the synthesis of antibacterial compounds. Collectively, our findings contribute to a more in-depth understanding of disease resistance mechanisms within healthy microbial communities and provide a theoretical foundation for the development of targeted strategies using beneficial microorganisms to suppress disease occurrence.

KEYWORDS

keystone taxa, metabolites, bacterial wilt, rhizosphere, microbiomes

Introduction

Bacterial wilt is a severely damaging vascular disease with a wide host range, including economically important crops, such as tomato, potato, eggplant, pepper, and tobacco (Hasegawa et al., 2019). The causal pathogen, *Ralstonia solanacearum*, infiltrates solanaceous plants through root wounds, establishes colonies, and eventually enters the xylem, resulting in necrosis and wilting of the infected plants. The resulting damage to crops leads to substantial economic losses annually (Prior et al., 2016). The results of numerous studies have confirmed the essential role of the rhizosphere microbial communities in plant health and growth (Besset-Manzoni et al., 2018; Kashyap et al., 2023). Plants adjust their rhizosphere microbial composition in response to pathogen infections by selectively recruiting a group of beneficial microorganisms that induce disease resistance and promote growth, thereby altering the structure of the microbial community (Berendsen et al., 2018). For example, *Streptomyces* has been found to promote plant growth, which helps to improve microbial community diversity in the rhizosphere. In addition, some bacterial genera such as *Bacillus* and *Pseudomonas* can improve the resistance of plants to diseases (Zheng et al., 2019; Gashaw et al., 2022). In agricultural ecosystems, rhizosphere microbial communities significantly affect the growth, development, and resistance of plants to soil-borne diseases (Mendes et al., 2018; Kashyap et al., 2021). Most studies have focused on the changes in bacterial community composition during pathogen invasion; however, the key bacterial taxon that may participate in the defence against pathogens remains unclear.

The keystone taxa within the rhizosphere microbial community play a crucial role in maintaining soil community structure stability and promoting plant health (Oberholster et al., 2018). For example, key soil microbial groups alter the flow of minerals between crops and soil, thereby improving crop production (Wang et al., 2022b). Certain keystone taxa play dominant roles in denitrification, which is a key driving factor in microbial nitrogen cycling. Additionally, some specific keystone taxa possess unique functions, such as nitrogen metabolism or phosphonate and phosphite metabolism, which are crucial for maintaining the stability of the soil microbial community (Xun et al., 2021). In recent years, network analysis has been widely applied to visualize the interrelationships within microbial communities and identify keystone taxa. Within microbial symbiotic networks, microbial taxa that are highly interconnected with other taxa are often considered keystone species that potentially exert a significant influence on the microbial community structure (Cardona et al., 2016; Herren and McMahon, 2018). Through network analysis, the soil bacterial networks and community structures of plots of healthy and diseased tomato plants were compared and bacterial strains with disease-suppressing activity were successfully identified (Zhang et al., 2020).

The metabolites produced by plants and rhizosphere microorganisms are crucial for regulating plant health (Bi et al., 2021). Plants interact with metabolites produced by their roots and rhizosphere microorganisms, and root exudates play a role in selectively influencing the rhizosphere environment through biological suppression and signaling activities (Pétriacq et al., 2017). For example, *Arabidopsis* plants selectively recruit *Bacillus* spp. by releasing malic acid from the roots, thereby improving disease resistance (Rudrappa et al., 2008). In the case of carnation (*Dianthus caryophyllus*) protection against pathogenic bacteria is a result of increased concentration of flavonol glycosides (Hassan and Mathesius, 2012). Microbial metabolites affect plant nutrient absorption, health, and soil biodiversity. For example, *Streptomyces* AN090126 produces various antibacterial secondary metabolites, including dimethyl sulfide and trimethyl sulfide, and exhibits broad-spectrum antagonistic activity against various plant pathogenic bacteria (Le et al., 2022). The secondary metabolites produced by *Trichoderma* can activate the disease resistance mechanism in plants and prevent pathogen invasion (Manzar et al., 2021; Manzar et al., 2022). *Bacillus cereus* has been shown to regulate salicylic acid and jasmonic acid signaling pathways in plants, promoting the aggregation of beneficial microorganisms in the rhizosphere, and thus controlling the growth of pathogenic bacteria (Yang et al., 2023a). However, relatively little research has been conducted on the metabolomics of plant rhizospheres during bacterial wilt infection. The rhizosphere keystone metabolites and associated metabolic pathways involved in regulating tobacco pathogen infection are not clear, and the potential keystone taxa that drive these essential metabolic functions have also not been identified.

In this study, we compared the community composition and metabolic profiles of the rhizosphere soil between tobacco plants infected with bacterial wilt and healthy plants. Variations in the rhizosphere soil microbial communities of tobacco plants under different health conditions were compared using amplicon sequencing, and the key environmental factors influencing soil microbial communities were identified. In addition, the keystone bacterial taxa in the rhizosphere soil of healthy plants that may contribute to bacterial wilt resistance were identified using co-occurrence network analysis. Furthermore, significantly enriched metabolic pathways in rhizosphere soil samples from healthy plants and their potential functions were investigated, and the relationships between different metabolites and keystone bacterial genera were established. The results of this study not only deepen our understanding of the roles of rhizosphere microbiomes in plant hosts, but also reveal the mechanisms of resisting pathogens of keystone microbes.

Materials and methods

Sample collection

Soil samples were collected in the tobacco-producing fields of Xuan'en County (29°59″1.932″N,109°35″2.976″E) in Hubei Province, China, where tobacco has been planted for decades. Bacterial wilt disease occurred beginning from 40 days after transplanting (about mid-June) every year, and the incidence rate of bacterial wilt was even more than 30% after the flowering stage, resulting in a 20-30% reduction in tobacco yield. Samples were collected from tobacco plants infected by the disease and from

healthy tobacco plants growing in the adjacent field on July 29, 2022 (80 days after transplanting), thus minimizing any geographical and environmental influences. Six plants (cultivar Yunyan 87) displaying light symptoms (grade 1 infection) (Standard, China, 2008) of tobacco bacterial wilt were selected, along with six healthy plants that exhibited similar growth as healthy controls. Rhizosphere soil was collected according to the method described by Yang et al. with some modifications (Yang et al., 2017). Specifically, the selected tobacco plants were carefully uprooted and the loosely adhered soil was shaken off. Fine roots collected from the same plant were combined as one sample and the soil on the surface (within approximately 1-2 mm) of the fine roots was brushed using a soft brush, which was defined as rhizosphere soil. Twelve rhizosphere soil samples were collected and stored at -80°C until used in the experiments.

Measurement of soil properties

The soil was dried in a 105°C constant temperature drying oven (Thermo Fisher Scientific Corp., USA) for 12 h, and the difference in mass was considered a measure of the soil water content. Soil bulk density was determined according to the method described by Al-Shammary A (Al-Shammary et al., 2018). Soil pH was measured in a mixture with a soil-water ratio of 1/2.5 (wt/vol) using a pH meter (Thermo Fisher Scientific Corp., USA). The available states of copper, manganese, zinc, iron, and boron were extracted using DPTA and determined using atomic absorption spectroscopy (PerkinElmer, USA). Soil porosity was determined using the method described by David et al. (Moret-FernÁNdez and Lopez, 2019). Exchangeable calcium, magnesium, quick-acting potassium, and cations were replaced with ammonium acetate solution and then determined by atomic absorption spectroscopy (PerkinElmer, USA) and ion chromatography (Shimadzu, Japan). The available phosphorus content was extracted using sodium bicarbonate, colored with molybdenum antimony, and measured and calculated using a spectrophotometer (Shimadzu, Japan). The hydrolyzable nitrogen content was determined by steam distillation using 10 M NaOH after Kjeldahl digested of the acid hydrolysate (Lin et al., 2023). Soil organic matter content was measured using a CHNS/O elemental analyzer (Thermo Fisher Scientific Corp., USA).

DNA sample extraction and Illumina sequencing

All DNA samples were extracted using the MP FastDNA spin kit according to the manufacturer's instructions. The purity and concentration of total DNA were measured using a NanoDrop 2000 spectrophotometer (Thermo Fisher Scientific Corp., USA). PCR was performed using primer 341F (5'-CCTAYGGGRBGCASCAG-3')/806R (5'-GGACTACNNGGGTATCTAAT-3') to target the V3-V4 region of the 16S rRNA gene. The PCR reaction was performed with 25 μL 2x Premix Taq (TaKaRa Premix Taq® Version 2.0), 3 μL dNTP, 2 μL primers (10 μM), and 10 ng template DNA in 50 μL reaction systems. The thermal cycle of the 16S rRNA gene consists of an initial denaturation at 94°C for 5 min, followed by 30 cycles at 94°C for 30 s, 55°C for 30 s, 72°C for 30 s, and an extension at 72°C for 10 min. The fragment lengths and concentrations of the PCR products were measured through 1% agarose gel electrophoresis. Library construction was performed according to the standard procedure of NEBNext® Ultra™ II DNA Library Prep Kit for Illumina® (New England Biolabs, USA). The constructed amplicon library was sequenced using a PE250 on an Illumina Nova 6000 platform at Novogene Co., Ltd. (Beijing, China).

Low-quality data and primers were removed using FASTP (version 0.14.1) and Cutadapt software to obtain clean reads. Through the use of DADA2, the raw sequences were denoised and merged into a single sequence based on the overlapping region. Subsequent analyses were performed using a standard pipeline of Quantitative Insights into Microbial Ecology (QIIME, version 2). The representative sequences were annotated against the SILVA database (release 138). The ASVs annotated as chloroplasts or mitochondria (16S amplicons) that could not be annotated at the boundary level were removed for further analysis. Alpha diversity indices, including Chao 1, Shannon index, ACE, and good's coverage were calculated. Differences in microbial community composition between the diseased and healthy samples were calculated using similarity analysis (ANOSIM). Non-metric multidimensional scaling (NMDS) analysis was performed using the Bray-Curtis distance algorithm. Significant differences between groups of species were analyzed using the Stamp software based on the relative abundance of ASVs. To determine the relationship between the environmental factors and microbial communities, redundancy analysis (RDA) was performed using Canoco (v5). Spearman's rank correlation analysis was performed to determine the correlation between the relative abundance of dominant species and environmental factors. All the above analyses were performed using R software (v.3.5.3).

For the network analysis, rare ASVs (<0.01% of the total sequences) and specific genera (present in <1/3 of the total samples) were removed to reduce noise. Spearman's correlation coefficients were calculated using a Molecular Ecological Network Analysis Pipeline (http://ieg2.ou.edu/MENA). Networks were constructed using random matrix theory-based methods. Network visualization and topological parameter analyses were performed using the Gephi software (v0.9.2).

Metabolite extraction and sequencing

To identify metabolites with the potential to drive microbiome assembly and improve pathogen resistance in healthy plants, metabolites in the rhizosphere of healthy and diseased soils were extracted and analyzed according to the methods described by Wen et al. with some modifications(Wen et al., 2020). The soil samples were extracted with methanol solutions (methanol: chloroform =3:1, v/v) containing 20 μL L-2-chlorophenylalanine. The extract was dried in a vacuum concentrator, and 40 μL methoxamine salt reagent (methoxamine hydrochloride, dissolved in pyridine 20 mg/mL) was added to the dried metabolites, followed by incubation at

80°C for 30 min. Then, 60 BSTFA (containing 1% TMCS, v/v) reagent was added to each sample and the mixture was incubated at 70°C for 1.5 h. After incubation, 5 µL FAMEs (soluble in chloroform) were added to the mixed samples before being analyzed in a gas chromatograph device (Agilent 7890) combined with a Pegasus HT time-of-flight mass spectrometer. Mass spectral data were obtained in full scan mode, and the *m*/*z* range was 50-500.

Metabolic data processing and analysis

Mass spectral data were analyzed using ChromaTOF software (V 4.3, LECO) for peak extraction, baseline correction, deconvolution, peak integration, and peak alignment. The LECO-Fiehn Rtx5 database was used for the qualitative analysis of substances. The peaks with a detection rate below 50% or RSD > 30% were excluded from further analysis. The collated data were logarithmically transformed and centrally formatted using SIMCA software (V15.0.2, Sartorius Stedim Data Analytics AB, Umea, Sweden), followed by automated modeling analysis and logarithmic transformation plus UV formatting. Differential metabolites were screened using a Student's *t*-test with a *P*-value of less than 0.05. To characterise differences in metabolic composition, principal coordinate analysis (PCA) plots were generated from Bray-Curtis similarity matrices. A correlation analysis of the differential metabolites was performed using correlation calculations of the quantitative values of the differential metabolites for each set of comparisons. All pathways associated with the identified differential metabolites in the respective species were compiled using the Kyoto Encyclopedia of Genes and Genomes (KEGG) database. In the comprehensive analysis of metabolites, enrichment metabolites were included as factors to further refine the key pathways. Spearman's rank correlation was performed using R (v. 3.5.3) to characterize the relationship between key metabolites and dominant genera.

Results

Soil properties

In total, 12 rhizosphere soil samples were collected to determine soil properties, including six samples from diseased plants and six samples from healthy plants. Exchangeable magnesium, pH, and cation exchange capacity were significantly higher in healthy soil samples than in diseased soil samples ($P < 0.05$, *t*-test). Specifically, compared to diseased samples, the pH value of healthy samples was 2.2 units greater (6.73 ± 0.64 vs 4.53 ± 0.39) and the exchange magnesium content was 0.43 units greater (Figures 1A, B and Supplementary Table 1). The cation exchange capacity of the healthy group was two-fold greater compared to that of the diseased groups. In contrast, in the soil samples of diseased plants, seven environmental factors, including available manganese, available zinc, available iron, available boron, quick-acting potassium, hydrolyzable nitrogen, and available phosphorus, were significantly higher than the corresponding measures in the healthy group ($P < 0.05$, *t*-test). For example, the level of available iron was three times greater in the soil of diseased plants compared to the level of iron in the soil of healthy plants; similarly, the amount of available manganese and phosphorus was more than two times greater in the soil of diseased plants (Figure 1C and Supplementary Table 1).

Diversity and composition of bacterial communities

Bacterial diversity was assessed via amplicon sequencing of the V3-V5 hypervariable regions of the 16S rRNA gene. A total of 5,143,167 sequences were obtained using 16S rRNA gene amplicon sequencing. To reduce the influence of sequencing depths on analysis results, the sequence numbers were rarefied according to the minimum sequences in the sample and 47,357 sequences remained in each sample. The total sequences clustering into 2,382 ASVs, ranging from 964 to 1294 in all samples (Supplementary Table 1). The good's coverage of each sample was above 99.8%, indicating good representativeness of the sequencing data (Supplementary Table 2). The Chao1 results showed that the richness of bacterial species in the healthy group was significantly higher than in the diseased group ($P < 0.05$, *t*-test; Figure 2A). Additionally, the Shannon index was higher in the healthy group, suggesting a significantly greater bacterial diversity in the healthy group ($P < 0.05$, *t*-test; Figure 2B). The Pielou index revealed that, compared to the soil bacteria in the diseased tobacco rhizosphere (Supplementary Table 2), the number of bacteria in the rhizosphere of healthy plants was distributed more evenly within the community ($P < 0.05$). NMDS analysis revealed that bacterial communities were clustered based on the health conditions of plants (Figure 2C), and a significant difference in bacterial community structure between the rhizosphere soil of healthy and diseased plants was confirmed through ANOSIM analysis ($P < 0.05$).

A significant variance in the bacterial community composition was observed between the soil samples from healthy and diseased plants. In the healthy group, *Gammaproteobacteria*, *Alphaproteobacteria*, *Bacteroidia*, *Gemmatimonadetes*, and *Vicinamibacteria* were the dominant groups, comprising 21%-26%, 17%-23%, 4%-8%, 7%-12%, and 4%-7% of the bacterial community, respectively, whereas *Gammaproteobacteria* (23%-38%), *Alphaproteobacteria* (15%-22%), *Acidobacteriae* (12%-28%), and *Bacteroidia* (6%-11%) dominated in soil samples from diseased plants (Figure 2D). Additionally, *Alphaproteobacteria*, *Gemmatimonadetes*, *Vicinamibacteria*, and *Blastocatellia* were more abundant in the rhizosphere soil of healthy plants than in the rhizosphere of diseased plants, whereas *Gammaproteobacteria*, *Acidobacteriae*, and *Bacteroidia* were less abundant.

At the genus level, marked differences were found between the diseased and healthy groups (Figure 3A). The relative abundance of the *Ralstonia* genus, which contains the pathogenic species of bacterial wilt disease, was significantly higher in the diseased group than in the healthy group ($P < 0.05$, *t*-test), which was consistent with the field phenotype. Compared with samples from healthy plants, there was a significant increase in the relative abundance of bacterial genera in the

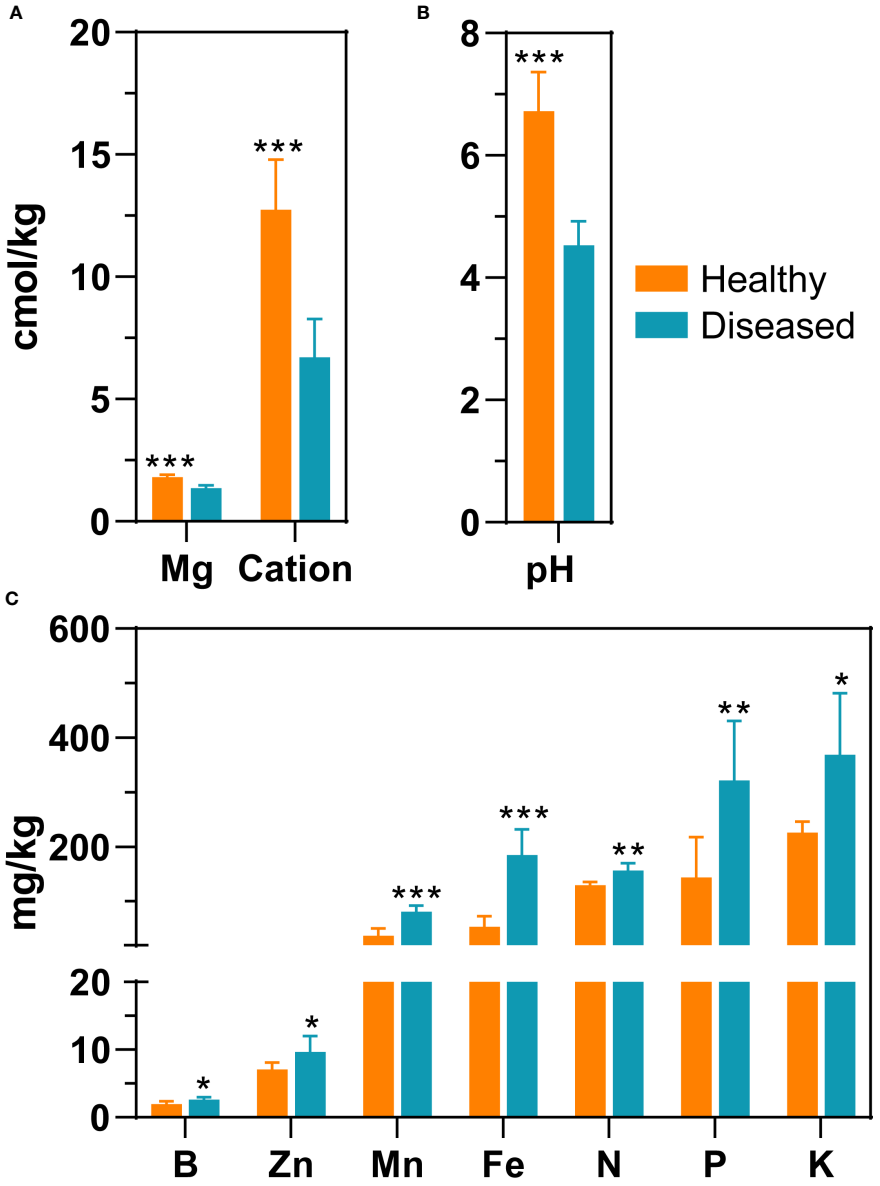

FIGURE 1
Differences in environmental parameters of rhizosphere soil samples from healthy plants and diseased plants. **(A)** Mg (exchangeable magnesium), cation (cation exchange capacity); **(B)** pH; **(C)** Zn (available zinc), B (available boron), Mn (available manganese), Fe (available iron), N (hydrolyzed nitrogen), P (available phosphorus), K (quick-acting potassium). The significance difference of soil properties between healthy plant and diseased plants was statistically analysed with a t-test (*, P<0.05; **, P<0.001; ***, P<0.0001).

diseased group, including *Burkholderia-Caballeronia-Paraburkholderia*, *Granulicella*, *Acidipila-Silvibacterium*, and *Chitinophagaceae*. Conversely, the genera RB41 (*Pyrinomonadaceae*), *Dongia*, MND1 (*Nitrosomonadaceae*), and *Nitrospia* were significantly enriched in healthy samples. To explore the marker bacterial genera in different groups, we conducted a Stamp analysis of the top 0.1% of the dominant genera. The results showed that 15 bacterial genera, including *Dongia*, *Nitrospia*, *Latescibacterota*, *Thiobacillus*, etc., were significantly more abundant in the healthy group than in the diseased group (P < 0.05, Figure 3B), whereas *Bryobater*, *Granulicella*, *Burkholderia-Caballeronia-Paraburkholderia*, *Dyella*, *Edaphobaculum*, *Bradyrhizobium*, and *Ralastonia* were significantly enriched in the disease groups.

Changes in microbial networks under pathogen invasions

To characterize the microbial networks in the rhizospheres of healthy and diseased plants, rare species at the genus level were removed from analysis (0.1‰ of the total sequences). Spearman's correlation analysis was conducted to assess the co-occurrence patterns among bacterial communities in the different samples. Significant differences in the structural and topological characteristics of the networks were observed between the diseased and healthy groups (Figure 4 and Supplementary Table 3). In the rhizosphere soil of healthy plants, the bacterial

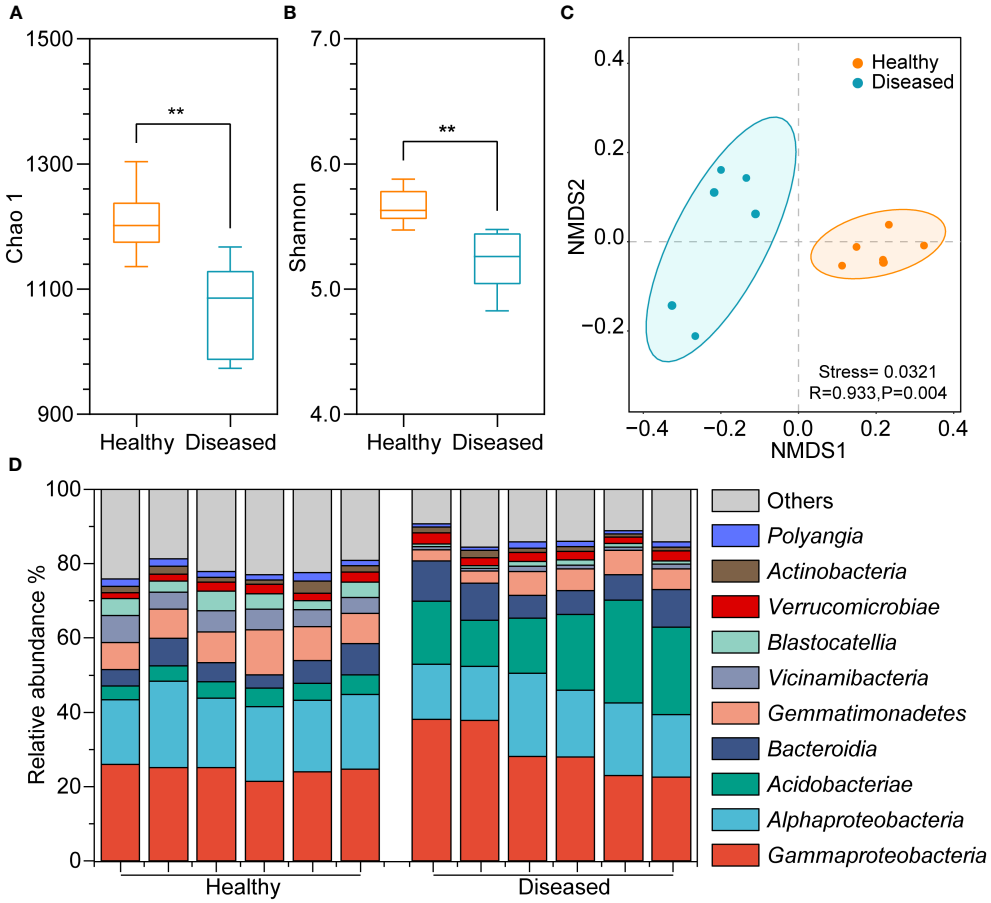

FIGURE 2
Diversity differences and community compositions of bacterial communities among different samples. **(A)** Chao 1 index; **(B)** Shannon index; **(C)** NMDS plot showing clustering relationship of bacterial communities between diseased and heathy groups, samples of different groups are color-coded; **(D)** Community composition of the top ten bacterial communities in different samples at the class level. (**, P <0.01; t-test).

community network consisted of 181 nodes, 2,742 connections, and an average degree of 30.298, which was greater than the corresponding results in the samples from diseased plants, which contained 154 nodes, 2,000 connections, and an average degree of 25.97. The number of positive connections was higher in the disease group than in the healthy group. Furthermore, the centralization of stress centrality (CS) in the healthy group was higher (0.458) than in the diseased rhizosphere soil (0.262). These results indicated that the bacterial community forms a more highly interactive and complex network in the rhizosphere soil of healthy plants than in that of diseased plants.

Based on the criteria of node degree and betweenness centrality, genera with the top 20% node degree and betweenness centrality values and the bottom 20% were regarded as keystone taxa. In the rhizosphere microbiome of healthy plants, seven genera, *Sphingomonas*, *Bryobacter*, *Micropepsis*, *Phenonobacterium*, *Acidipila*, *Silvibacterium*, and *Pseudomonas*, were the keystone taxa (Supplementary Table 4). These bacterial groups may be involved in maintaining community stability and in the prevention and control of bacterial wilt. In the rhizosphere microbiome of diseased plants, *Acidipila*, *Silvibacterium*, *Sphingomonas*, *Dechromonas*, *Chujaibacter*, *Bacillus*, and *Hyphomicrobium* were the keystone taxa.

Key environmental factors affecting bacterial communities

Redundancy analysis (RDA) was conducted to identify environmental factors affecting community structure. RDA1 explained 62.00% of the total variation, whereas RDA2 explained 19.58% (Supplementary Figure S1). Exchangeable magnesium, cation exchange capacity, and pH were found to be the key environmental factors affecting the bacterial community in diseased rhizosphere soils, whereas available phosphorus, available manganese, hydrolyzable nitrogen, available iron, and quick-acting potassium were the main factors affecting the bacterial community structure in the soils of healthy plants.

Spearman's correlation analysis was conducted between the dominant bacterial genera and environmental factors (Supplementary Figure S2), and it was found that *Ralstonia* genus showed a significant negative correlation with pH, exchangeable magnesium, and cation

10.3389/fpls.2023.1339478

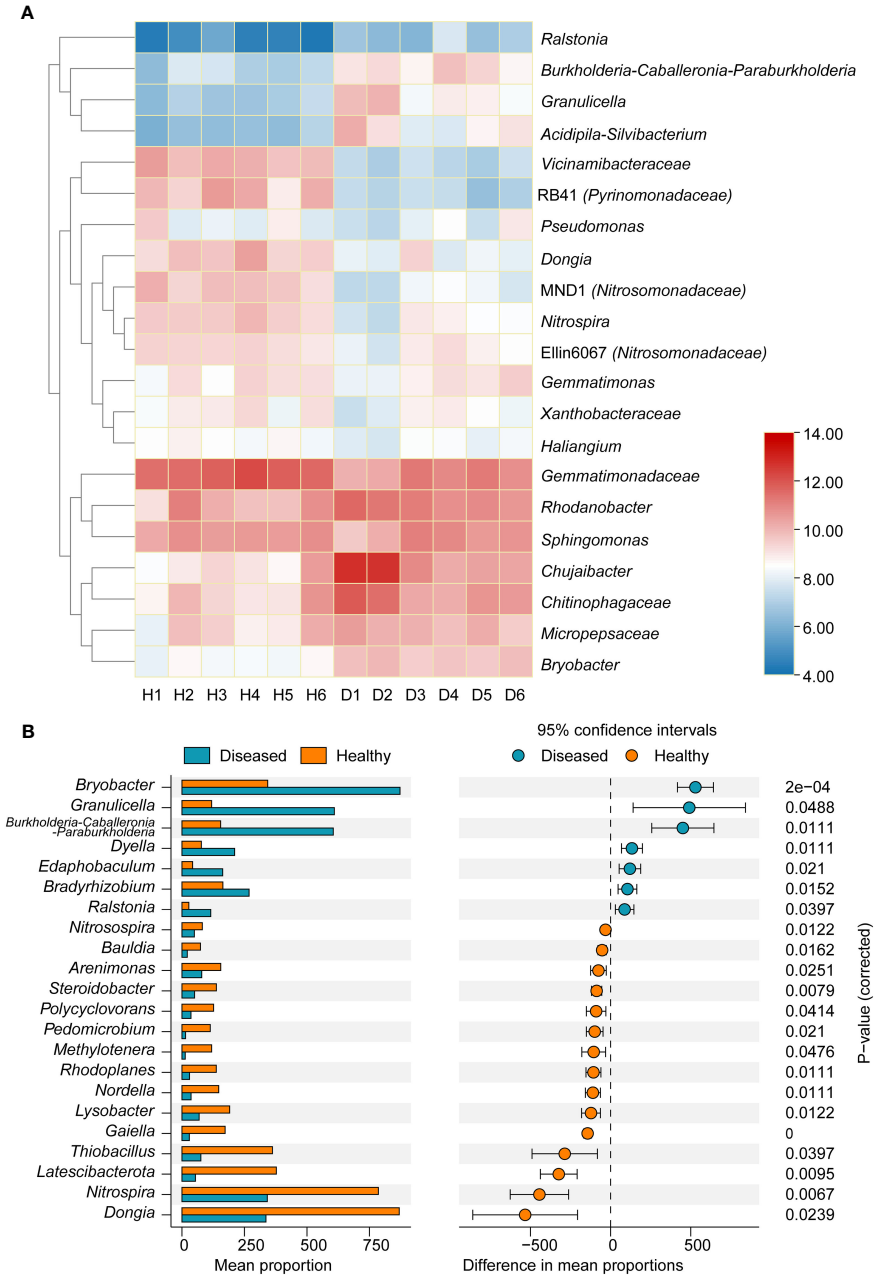

FIGURE 3
(A) Heatmap showing the relative abundance of dominant bacterial taxon (top 20) and *Ralstonia* genus at the genus level between two groups of samples. **(B)** Stamp analysis of the different of dominant bacterial genera between two groups. H, healthy plants; D, diseased plants.

exchange flux and a positive correlation with available iron. Furthermore, bacterial genera significantly enriched in the diseased group, namely *Burkholderia-Caballeronia-Paraburkholderia*, *Granulicella*, *Acidipila-Silvibacterium*, and *Chitinophagaceae*, also exhibited negative correlations with pH, exchangeable magnesium, and cation exchange flux, and positive correlations with available phosphorus, available manganese, hydrolyzable nitrogen, available iron, and quick-acting potassium levels. Conversely, bacterial genera that were significantly enriched in the healthy group, namely RB41, *Dongia*, MND1, and *Nitrospia*, were positively correlated with pH, exchangeable magnesium, and cation exchange flux, and negatively correlated with available phosphorus, available manganese, hydrolyzable nitrogen, available iron, and quick-acting potassium levels.

Changes in metabolites among different samples

The results of the PCA showed that all samples were clustered separately based on the healthy conditions of the plants, with two principal components explaining 62.12% of the overall variance (33.83% and 28.29% for PCA1 and PCA2, respectively; Figure 5A). In the healthy group, 352 metabolites showed significant changes: 165

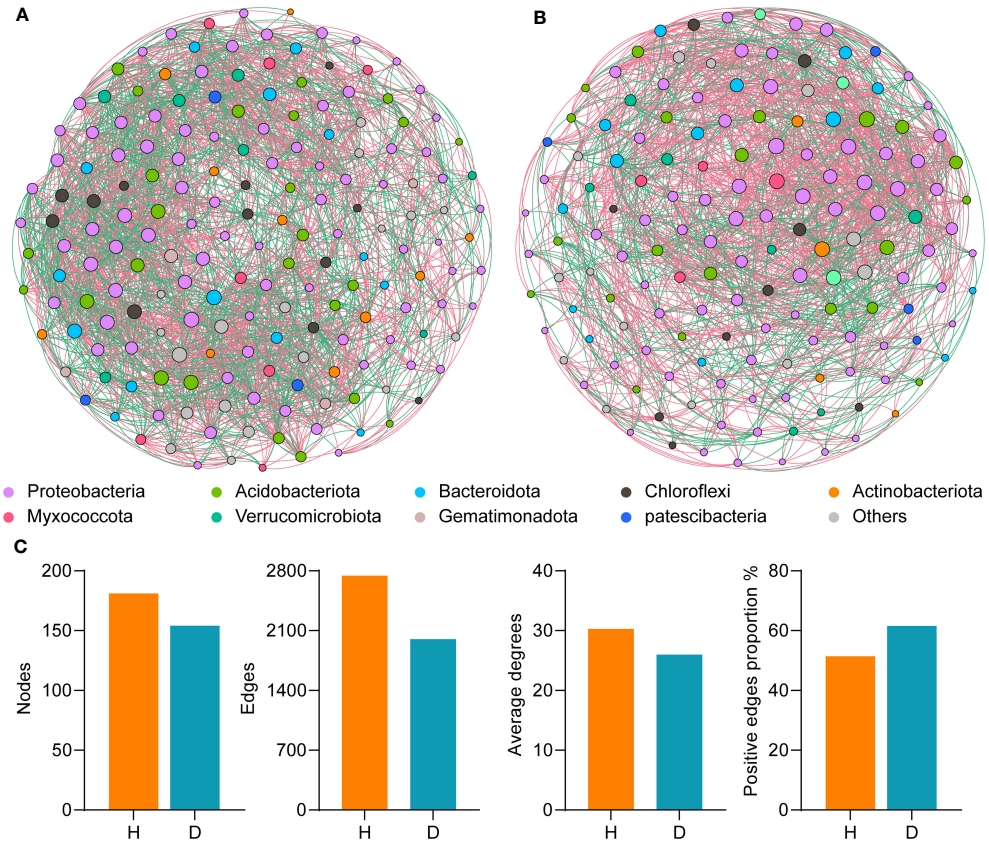

FIGURE 4
Co-occurrence network analysis of healthy and diseased tobacco plants. **(A)** The symbiotic network of microbial communities in healthy rhizosphere soil samples **(B)** The symbiotic network of microbial communities in diseased rhizosphere soil samples. The node is coloured at the class level, and the size of nodes represents the node degree of genera; **(C)**. Comparison of network topological parameters between healthy and diseased samples. H, healthy plants; D, diseased plants.

metabolites were significantly upregulated, and 197 metabolites were significantly downregulated (Figure 5B). To identify the key metabolites participating in the defense against pathogens, a KEGG pathway enrichment analysis was performed. The results showed that, compared to the rhizosphere metabolites of diseased plants, several pathways were significantly enriched in the rhizosphere samples of healthy plants, including ABC transporters, biosynthesis of antibiotics, phenylpropanoid biosynthesis, vitamin B6 metabolism, biosynthesis of alkaloids derived from shikimate pathway, pyrimidine metabolism, biosynthesis of phenylpropanoids, and isoquinoline alkaloid biosynthesis (Figure 5C). Seven genes were significantly enriched in pathways related to antibiotic biosynthesis (Figure 5C).

Spearman's analysis was performed using the top 35 genera with significant changes in relative abundance and nine differential metabolites associated with antimicrobial pathways. These nine metabolites were lauric acid, tetracycline, scopolin, eugenol, scopoletin, jervine, l-citrulline, 4-pyridoxate, and pyridoxine. The results showed that the *Ralstonia* genus was negatively correlated with seven metabolites, whereas *Polyclovorans* was positively correlated with all nine metabolites (Figure 6). Scopoletin was positively correlated with the bacterial genera RB41, *Gaiella*, Ellin6067, MND1, *Pseudomonas*, *Nitrosospira*, *Polycyclovorans*, and *Lysobacter*, indicating that scopoletin (known to have antibacterial activity) may be generated by these bacterial taxa. Moreover, tetracycline, which is used as a broad-spectrum antibiotic, was positively correlated with bacteria belonging to the genera RB41, *Gaiella*, *Ellin6067*, MND1, *Nitrosospira*, *Polycyclovorans*, and *Lysobacter*. The metabolites 4-pyridoxate and pyridoxine, which are related to vitamin B6 metabolism, were also positively correlated with these bacterial genera.

Discussion

The microbial community in plant rhizosphere soil is crucial for resisting pathogen invasion and maintaining plant health (Kashyap et al., 2022). At present, most research focuses on exploring the functions and effects of individual biocontrol strains; however, the mechanisms by which the microbial community exerts its effects in the field are still unclear. Here we analyzed the changes in soil properties, bacterial community responses, and metabolomics in the rhizosphere of tobacco plants infected with bacterial wilt. We found significant differences in the soil environmental parameters between the diseased and healthy samples. The occurrence of bacterial wilt significantly reduced the diversity of soil microbial communities and had a significant effect on the network structures

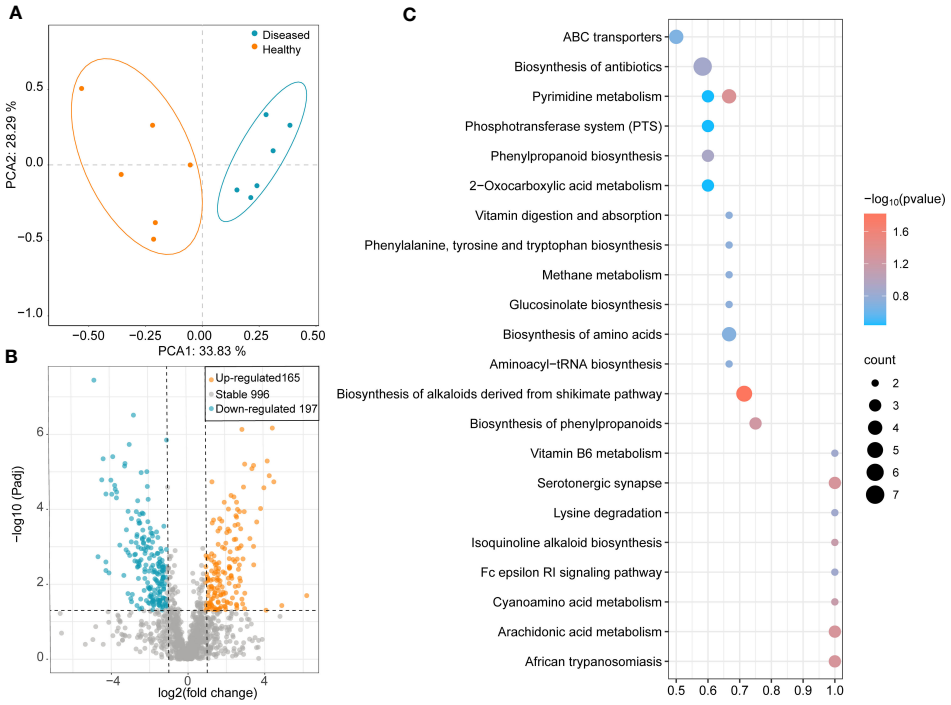

FIGURE 5
(A) PCA analysis of different samples based on bray-cutis-distance. **(B)** Volcano Plot shows the differential metabolites between healthy and diseased plant rhizosphere soil samples. **(C)** Heatmap shows functional differences in KEGG enrichment.

of the microbial communities. Metabolic pathways related to the synthesis of various antibacterial compounds that may participate in pathogen resistance were significantly enriched in the healthy group, and potential producers of these compounds were identified. Our findings provide a strong theoretical basis for the effective utilization of soil microbial communities for the biocontrol of crop diseases in the field.

Rhizosphere microbiomes were influenced by bacterial wilt

In the study, the relative abundance of *Ralstonia* genus in diseased plant samples significantly increased. The relative abundance of the *Ralstonia* genus from amplicon sequencing was been reported to be correlated positively with the density of pathogenic *R. solanacearum* determined (Zheng et al., 2021). The observed increase in *Ralstonia* genus abundance in the diseased group might confirm the occurrence of bacterial wilt. The diversity and community composition of rhizosphere microbiomes were influenced by the bacterial wilt. Soil microbial communities are closely associated with plant health, and high microbial diversity plays an important role in maintaining plant health (Berg et al., 2017). The more abundant bacterial genera and microbial diversity (Shannon index) were found in soil samples of healthy plants than in soil samples of diseased plants, which is consistent with previous findings (Niu et al., 2016). When tobacco plants are infected with bacterial wilt pathogens, they may cause the rapid growth of dominant species that outcompete other bacteria for survival space, thereby restricting the growth of other microbial groups. In addition, the evenness of the community (Pielou index) was higher in healthy samples than in diseased samples, indicating better diversity structure and a more stable community in healthy groups. Moreover, the NMDS and ANOSIM analysis confirmed the variation of bacterial assemblages by revealing a clear community separation according to plant health. This was consistent with previous reports which found bacterial and eukaryote communities were changed with invasion of pathogens (Gao et al., 2021).

In soil microbial system, the functionality of the microbial community is not merely the sum of the functions of individual microbial taxa. There are also frequent interactions between various microorganisms (Van der Heijden and Hartmann, 2016). Agler et al. (Agler et al., 2016) found that the plant host genotype can influence key microbial species, modulate interactions among microorganisms, and alter host adaptability, thereby affecting the entire microbial community. In this study, the number of nodes, connections, and average path lengths in the network were significantly higher in soil bacterial networks associated with healthy plants compared to those in soils from diseased plants, which is consistent with previous research results (Wei et al., 2018). The number of positive connections was higher in the disease group, indicating that there is more synergistic effect between microbial populations. In the diseased plant, there might be more microbiome with growth-promotive siderophores, causing a decrease in competition (Gu et al., 2020). Additionally, the microbial community in the rhizosphere of healthy plants exhibits a high degree of centralization of stress (CS), indicating

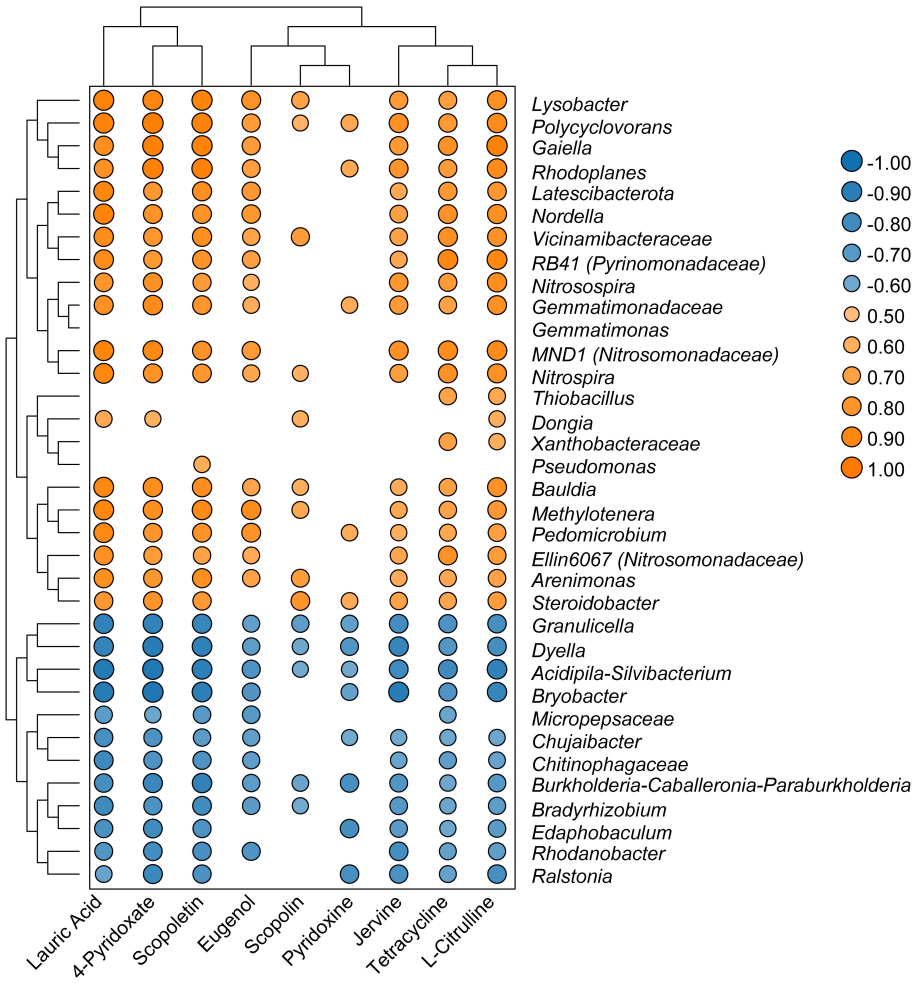

FIGURE 6
Heatmap showed that correlations between selected genera and significant changed metabolites.

more microbial hubs in the network may play a central role in responding to environmental stress and defending against the invasion of pathogens (Runge et al., 2023). Collectively, close interactions between different species may enhance effective defense against invading pathogens, and a more intricate microbial network might be pivotal for disease resistance in healthy root systems (Carrión et al., 2019).

Keystone taxa occupying central positions interact more closely with various community groups and play a crucial role in maintaining soil microenvironmental systems and regulating plant growth (Banerjee et al., 2018). As keystone taxon in the healthy tobacco rhizosphere soil, bacterial taxa such as *Sphingomonas*, *Silvibacterium*, and *Pseudomonas* are of great significance for the stability of bacterial co-occurrence network and the healthy growth of plants. For example, *Sphingomonas* significantly promotes plant growth and contributes to the degradation of persistent metabolites in the environment (Asaf et al., 2020). Previous studies have shown that *Pseudomonas* has a significant antagonistic ability against pathogenic bacteria and a significant inhibitory effect on bacterial wilt (Nadhira et al., 2021). However, *Acidipila*, *Silvibacterium*, *Sphingomonas*, and *Bacillus* were keystone taxons in the rhizosphere soil of diseased tobacco. *Acidipila* and *Silvibacterium* are both *Acidobacteria*, which have growth advantages under low pH conditions in diseased soil (Zhang et al., 2022). In addition, when plants are infected with pathogens, the structure and composition of the rhizosphere microbial community undergo significant changes (Diaz-Cruz and Cassone, 2022). Plants can recruit microbial communities during pathogen attacks and create a long-lasting protective soil microbial community (Goossens et al., 2023). *Sphingomonas* and *Bacillus*, as keystone taxon in the diseased rhizosphere soil, may play a role in responding to plant resistance to pathogen infection. The absence of these keystone taxa will make plants more vulnerable and difficult to adapt to external environmental changes and stress (Yin et al., 2022). Moreover, significant enrichment of bacteria such as MND1, *Gaiella*, *Rhodoplanes*, *Nitrospia*, *Latescibacterota*, and *Thiobacillus* was observed in healthy soil samples. These bacteria may be involved in functions related to plant-root symbiosis, nutrient cycling, and organic matter decomposition, thereby contributing positively to plant health (Ahmed et al., 2022). For example, MND1 is an ammonia-oxidizing bacterium that affects nutrient absorption in plants (Wang et al., 2022c) and inhibits pathogens (Yang et al.,

2023b). *Dongia* is considered to be involved in the soil nitrogen cycle, which may synergistically improve soil available nutrients and root uptake, promoting plant growth (Wang et al., 2022a; Sanka Loganathachetti and Mundra, 2023). *Nitrospira* was reported to be involved in the degradation and cycling of soil organic matter and increasing soil pH, thereby improving plant stress resistance of soil acidification and nutrient absorption (Hu et al., 2021). Although the specific functions of these genera and their interactions with plants may vary depending on the characteristics of the strains, plant species, and environmental conditions, these findings indicated that members of the rhizosphere microbiota have a significant impact on plant metabolism and resistance to pathogens (Le et al., 2022).

Soil physicochemical properties play a crucial role in the formation of soil microbial community structure (Liang et al., 2018). We found that pH, exchangeable magnesium, and cation exchange capacity are important environmental factors affecting the soil microbial community in the diseased plant rhizosphere. This is consistent with previous reports that a significant decrease in pH in the rhizosphere soil of diseased plants leads to weakened tobacco resistance, affecting microbial community structure (Qi et al., 2019). Higher soil pH directly influences plant disease infection by affecting the growth and reproduction of plant pathogens (Shen et al., 2018). In addition, lower soil pH can lead to a decrease in soil exchangeable magnesium content, significantly affecting the photosynthesis, enzyme activation, and metabolic reactions of tobacco (Farhat et al., 2016). The decrease in cation exchange capacity directly leads to a decrease in the ability of the soil to retain essential nutrients affecting the growth of plants and reducing their resistance to disease (Arthur, 2017). Therefore, pH and cation exchange capacity could be regarded as a potential environmental indicator for the onset of bacterial wilt disease. Furthermore, the amounts of available phosphorus, manganese, hydrolyzable nitrogen, iron, and quick-acting potassium significantly increase in diseased soil, which may indirectly affect plant health (Sun et al., 2022). For example, phosphorus availability has been found to increase the abundance of pathological biota, thereby increasing the infection by *Ralstonia* in the rhizosphere of plants (Li et al., 2021). A large amount of nitrogen and phosphorus in the soil may lead to a decrease in soil microbial biomass and changes in the structure of rhizosphere microbial communities (Wang et al., 2022e).

Specific rhizosphere metabolites in different plants

Metabolites in the soil play a crucial role in regulating plant-microbe interactions (Bi et al., 2021), and significant metabolite enrichment primarily occurs in the rhizosphere (Wong-Bajracharya et al., 2020). Similar to the results of Zhao et al., the results we report here indicated significant differences in the metabolites between the rhizospheres of diseased and healthy plants (Zhao et al., 2023). Compared to the metabolic profiles of rhizosphere soils from diseased plants, soils from healthy plants exhibited significant enrichment in metabolic pathways related to the synthesis of antimicrobial substances. These pathways include the biosynthesis of alkaloids derived from the shikimate pathway, phenylpropanoids, isoquinoline alkaloids, and antibiotics. This indicated that the synthesis of various antibiotics and alkaloids in the rhizosphere soil of healthy plants may effectively inhibit the growth of pathogenic microorganisms (Molina-Santiago et al., 2015). Furthermore, various metabolic pathways with important physiological functions in plants were significantly enriched in the rhizosphere of healthy plants (Figure 5C). For example, pyrimidine metabolism is closely associated with the synthesis of DNA, RNA, lipids, and carbohydrates (Garavito et al., 2015). ABC transporters participate in the active transport of intracellular substances, regulate the absorption, excretion, and distribution of substances, and participate in the biosynthesis of chlorophyll (Martinoia et al., 2014). Compounds produced in the phenylpropanoid and phenylalanine biosynthetic pathways have diverse physiological functions in plants, including antioxidation, defense, and signal transduction activities. The phosphotransferase system (PTS) in bacteria plays a crucial role in regulating sugar absorption and utilization, carbohydrate transport, and metabolism, thereby significantly impacting bacterial growth and metabolism (Wang et al., 2022d). These metabolic pathways are interconnected and collectively maintain the metabolic balance and physiological processes within organisms. Notably, while these metabolic pathways are primarily present in plants, similar biosynthetic pathways or related metabolic pathways may also exist in some microorganisms that synthesize similar compounds (Perry et al., 2022). Rhizosphere microorganisms and plants have been shown to interact and connect by producing corresponding secretions and hormones (De Vries et al., 2020). Although plants regulate the rhizosphere microbial ecosystem through corresponding metabolic and signaling pathways, rhizosphere microorganisms also influence plant growth through the production of metabolites.

The microbial community is an important factor driving the distribution of soil metabolites, and bacteria dominate the symbiotic network between microbial members and metabolites (Li et al., 2020). The *Ralstonia* genus exhibited negative correlations with seven active metabolites: lauric acid, jervine, scopoletin, tetracycline, 4-pyridoxate, l-citrulline, and pyridoxine. These antibiotic substances may directly participate in defense against pathogens. For example, tetracycline, lauric acid, and jervine can inhibit protein biosynthesis and block signal transduction in pathogens (Schäfer, 2017; Chen et al., 2020; Welch et al., 2020). Pyridoxine and 4-pyridoxate are directly related to vitamin B6 levels. Although vitamin B6 does not have a direct antibacterial effect, it can help plants cope with various environmental stresses such as drought, salt stress, and diseases. Pyridoxine acts as an antioxidant in plants and interferes with pathogen defense responses (Fudge et al., 2017). This indicate that secondary metabolites in the soil have many important ecological roles and can be used as bactericides to inhibit plant pathogens (Guo et al., 2022). In contrast, several genera that were significantly enriched in the healthy group samples, such as RB41 (*Pyrinomonadaceae*), *Gaiella*, Ellin6067 (*Nitrosomonadaceae)*, *Pseudomonas*, MND1 (*Nitrosomonadaceae*), *Polycyclovorans*, and *Lysobacter*, were significantly and positively correlated with these nine key

metabolites, suggesting their potential involvement in the synthesis of antibiotics and alkaloids. Therefore, these enriched bacterial taxa may be involved in maintaining soil health in tobacco fields. Rhizosphere antibacterial compounds can selectively promote the growth of specific microorganisms by restricting certain microorganisms, thus providing a mutually beneficial balance in the interaction between plants and microorganisms (Dastogeer et al., 2020). Therefore, the use of microbiomes with antibiotic abilities may reduce chemical pesticide use and lead to more sustainable control of soil-borne pathogens. In the future, the effects of keystone bacteria on pathogen invasion should be evaluated more comprehensively using physiological and biochemical analyses, greenhouse, and field experiments of a single isolate.

Conclusion

The occurrence of soil-borne plant diseases is closely related to the stability (and instability) of rhizosphere microbiota. In this study, we investigated the microbial community composition and metabolic profiles of the tobacco rhizosphere during the invasion of *R. solanacearum*, revealing the distinct microbial structures and potential defense strategies of plants. The high diversity and complex occurrence networks of tobacco rhizosphere microorganisms are important for plant rhizosphere health. In addition, environmental parameters, such as soil pH, cation exchange capacity, and exchangeable magnesium, are key factors influencing microbial community structure and pathogen growth. Lauric acid, tetracycline, eugenol, scopolin, jervine, L-citrulline, scopoletin, 4-pyridoxate, and pyridoxine are key metabolites involved in maintaining plant health. Potential bacterial groups involved in the synthesis of key metabolites were identified, namely *Pseudomonas*, *Gaiella*, *Nitrobacteria*, *Polycyclovorans*, and *Lysobacteria*. The symbiotic relationship between plants and microorganisms plays an important role in the formation and function of plant rhizosphere ecosystems, jointly resisting the invasion of bacterial wilt and promoting the healthy growth of plants. These findings may help understand the disease resistance mechanism of rhizosphere bacteria in the initial stage of disease infection, and samples of different disease incidence levels need to be investigated in the future to obtain the dynamic response mechanisms of rhizosphere microorganisms to whole infection stages.

Data availability statement

The datasets presented in this study can be found in online repositories. The names of the repository/repositories and accession number(s) can be found below: https://www.ncbi.nlm.nih.gov/, PRJNA1033381.

Author contributions

CW: Data curation, Investigation, Writing – original draft. JL: Data curation, Funding acquisition, Investigation, Writing – review & editing. RW: Conceptualization, Investigation, Writing – review & editing. LC: Data curation, Writing – review & editing. WW: Investigation, Writing – review & editing. JT: Investigation, Writing – review & editing. HS: Investigation, Writing – review & editing. XS: Data curation, Writing – review & editing. ZC: Data curation, Writing – review & editing. QX: Data curation, Writing – review & editing. DC: Funding acquisition, Writing – original draft. XW: Conceptualization, Funding acquisition, Writing – review & editing.

Funding

The author(s) declare financial support was received for the research, authorship, and/or publication of this article. This work was supported by the Major Tobacco Science and Technology Projects (110202101054(LS-14), YXYC2022008, SCYC202001), the Central Public-interest Scientific Institution Basal Research Fund (No. 1610232023018), the Key Laboratory of Tobacco Pest Monitoring & Integrated Management (KLTMMIMT2022-09), and the Agricultural Science and Technology Innovation Program of China (ASTIP- TRIC04).

Conflict of interest

The authors declare that the research was conducted in the absence of any commercial or financial relationships that could be construed as a potential conflict of interest.

Publisher's note

Supplementary material

The Supplementary Material for this article can be found online at: https://www.frontiersin.org/articles/10.3389/fpls.2023.1339478/full#supplementary-material

References

Agler, M. T., Ruhe, J., Kroll, S., Morhenn, C., Kim, S.-T., Weigel, D., et al. (2016). Microbial hub taxa link host and abiotic factors to plant microbiome variation. *PloS Biol.* 14 (1), e1002352. doi: 10.1371/journal.pbio.1002352

Ahmed, W., Dai, Z., Liu, Q., Munir, S., Yang, J., Karunarathna, S. C., et al. (2022). Microbial cross-talk: dissecting the core microbiota associated With flue-cured tobacco (*Nicotiana tabacum*) plants under healthy and diseased state. *Front. Microbiol.* 13, 845310. doi: 10.3389/fmicb.2022.845310

Al-Shammary, A. A. G., Kouzani, A. Z., Kaynak, A., Khoo, S. Y., Norton, M., and Gates, W. (2018). Soil bulk density estimation methods: a review. *Pedosphere* 28 (4), 581–596. doi: 10.1016/S1002-0160(18)60034-7

Arthur, E. (2017). Rapid estimation of cation exchange capacity from soil water content. *Eur. J. Soil Sci.* 68 (3), 365–373. doi: 10.1111/ejss.12418

Asaf, S., Numan, M., Khan, A. L., and Al-Harrasi, A. (2020). *Sphingomonas*: from diversity and genomics to functional role in environmental remediation and plant growth. *Crit. Rev. Biotechnol.* 40 (2), 138–152. doi: 10.1080/07388551.2019.1709793

Banerjee, S., Schlaeppi, K., and van der Heijden, M. G. A. (2018). Keystone taxa as drivers of microbiome structure and functioning. *Nat. Rev. Microbiol.* 16 (9), 567–576. doi: 10.1038/s41579-018-0024-1

Berendsen, R. L., Vismans, G., Yu, K., Yang, S., de Jonge, R., Burgman, W. P., et al. (2018). Disease-induced assemblage of a plant-beneficial bacterial consortium. *ISME J.* 12 (6), 1496–1507. doi: 10.1038/s41396-018-0093-1

Berg, G., Köberl, M., Rybakova, D. V., Müller, H., Grosch, R., and Smalla, K. (2017). Plant microbial diversity is suggested as the key to future biocontrol and health trends. *FEMS Microbiol. Ecol.* 93 (5), fix050. doi: 10.1093/femsec/fix050

Besset-Manzoni, Y., Rieusset, L., Joly, P., Comte, G., and Prigent-Combaret, C. (2018). Exploiting rhizosphere microbial cooperation for developing sustainable agriculture strategies. *Environ. Sci. pollut. Res. Int.* 25 (30), 29953–29970. doi: 10.1007/s11356-017-1152-2

Bi, B., Wang, K., Zhang, H., Wang, Y., Fei, H., Pan, R., et al. (2021). Plants use rhizosphere metabolites to regulate soil microbial diversity. *Land Degrad Dev.* 32, 5267–5280. doi: 10.1002/ldr.4107

Cardona, C., Weisenhorn, P., Henry, C., and Jack, G. (2016). Network-based metabolic analysis and microbial community modeling. *Curr. Opin. Microb.* 31, 124–131. doi: 10.1016/j.mib.2016.03.008

Carrión, V. J., Perez-Jaramillo, J., Cordovez, V., Tracanna, V., de Hollander, M., Ruiz-Buck, D., et al. (2019). Pathogen-induced activation of disease-suppressive functions in the endophytic root microbiome. *Science* 366 (6465), 606–612. doi: 10.1126/science.aaw9285

Chen, J., Wen, B., Wang, Y., Wu, S., Zhang, X., Gu, Y., et al. (2020). Jervine exhibits anticancer effects on nasopharyngeal carcinoma through promoting autophagic apoptosis via the blockage of Hedgehog signaling. *BioMed. Pharmacother.* 132, 110898. doi: 10.1016/j.biopha.2020.110898

Dastogeer, K. M. G., Tumpa, F. H., Sultana, A., Akter, M. A., and Chakraborty, A. (2020). Plant microbiome–an account of the factors that shape community composition and diversity. *Curr. Plant Biol.* 23, 100161. doi: 10.1016/j.cpb.2020.100161

De Vries, F. T., Griffiths, R. I., Knight, C. G., Nicolitch, O., and Williams, A. (2020). Harnessing rhizosphere microbiomes for drought-resilient crop production. *Science* 368 (6488), 270–274. doi: 10.1126/science.aaz5192

Diaz-Cruz, G. A., and Cassone, B. J. (2022). Changes in the phyllosphere and rhizosphere microbial communities of soybean in the presence of pathogens. *FEMS Microbiol. Ecol.* 98 (3), fiac022. doi: 10.1093/femsec/fiac022

Farhat, N., Elkhouni, A., Zorrig, W., Smaoui, A., Abdelly, C., and Rabhi, M. (2016). Effects of magnesium deficiency on photosynthesis and carbohydrate partitioning. *Acta Physiol. Plant* 38 (6), 145. doi: 10.1007/s11738-016-2165-z

Fudge, J., Mangel, N., Gruissem, W., Vanderschuren, H., and Fitzpatrick, T. B. (2017). Rationalising vitamin B6 biofortification in crop plants. *Curr. Opin. Biotech.* 44, 130–137. doi: 10.1016/j.copbio.2016.12.004

Gao, M., Xiong, C., Gao, C., Tsui, C. K. M., Wang, M.-M., Zhou, X., et al. (2021). Disease-induced changes in plant microbiome assembly and functional adaptation. *Microbiome* 9 (1), 1–187. doi: 10.1186/s40168-021-01138-2

Garavito, M. F., Narváez-Ortiz, H. Y., and Zimmermann, B. H. (2015). Pyrimidine metabolism: dynamic and versatile pathways in pathogens and cellular development. *J. Genet. Genomics* 42 (5), 195–205. doi: 10.1016/j.jgg.2015.04.004

Gashaw, T., Sitotaw, B., and Yilma, S. (2022). Evaluation of rhizosphere bacterial antagonists against *Ralstonia solanacearum* causing tomato (*Lycopersicon esculentum*) wilt in central Ethiopia. *Int. J. Agron.* 2022, 6341555. doi: 10.1155/2022/6341555

Goossens, P., Spooren, J., Baremans, K. C. M., Andel, A., Lapin, D., Echorbardo, D., et al (2023). Obligate biotroph downy mildew consistently induces near-identical protective microbiomes in *Arabidopsis thaliana*. *Nat. Microbiol.* 8 (12), 2349–2364. doi: 10.1038/s41564-023-01502-y

Gu, S., Wei, Z., Shao, Z., Friman, V.-P., Cao, K., Yang, T., et al. (2020). Competition for iron drives phytopathogen control by natural rhizosphere microbiomes. *Nat. Microbiol.* 5 (8), 1002–1010. doi: 10.1038/s41564-020-0719-8

Guo, S., Tao, C., Jousset, A., Xiong, W., Wang, Z., Shen, Z., et al. (2022). Trophic interactions between predatory protists and pathogen-suppressive bacteria impact plant health. *ISME J.* 16 (8), 1932–1943. doi: 10.1038/s41396-022-01244-5

Hasegawa, T., Kato, Y., Okabe, A., Itoi, C., Ooshiro, A., Kawaide, H., et al. (2019). Effect of secondary metabolites of tomato (*Solanum lycopersicum*) on chemotaxis of *Ralstonia solanacearum*, pathogen of bacterial wilt disease. *J. Agric. Food Chem.* 67 (7), 1807–1813. doi: 10.1021/acs.jafc.8b06245

Hassan, S., and Mathesius, U. (2012). The role of flavonoids in root–rhizosphere signalling: opportunities and challenges for improving plant–microbe interactions. *J. Exp. Bot.* 63 (9), 3429–3444. doi: 10.1093/jxb/err430

Herren, C. M., and McMahon, K. D. (2018). Keystone taxa predict compositional change in microbial communities. *Environ. Microbiol.* 20 (6), 2207–2217. doi: 10.1111/1462-2920.14257

Hu, J., Zhao, Y., Yao, X., Wang, J., Zheng, P., Xi, C., et al. (2021). Dominance of comammox Nitrospira in soil nitrification. *Sci. Total Environ.* 780, 146558. doi: 10.1016/j.scitotenv.2021.146558

Kashyap, A. S., Manzar, N., Meshram, S., and Sharma, P. K. (2023). Screening microbial inoculants and their interventions for cross-kingdom management of wilt disease of solanaceous crops- a step toward sustainable agriculture. *Front. Microbiol.* 14, 1174532–1174532. doi: 10.3389/fmicb.2023.1174532

Kashyap, A. S., Manzar, N., Nebapure, S. M., Rajawat, M. V. S., Deo, M. M., Singh, J. P., et al. (2022). Unraveling Microbial Volatile Elicitors Using a Transparent Methodology for Induction of Systemic Resistance and Regulation of Antioxidant Genes at Expression Levels in Chili against Bacterial Wilt Disease. *Antioxidants (Basel)* 11 (2), 404. doi: 10.3390/antiox11020404

Kashyap, A. S., Manzar, N., Rajawat, M. V. S., Kesharwani, A. K., Singh, R. P., Dubey, S. C., et al. (2021). Screening and biocontrol potential of rhizobacteria native to gangetic plains and hilly regions to induce systemic resistance and promote plant growth in chilli against bacterial wilt disease. *Plants (Basel)* 10 (10), 2125. doi: 10.3390/plants10102125

Le, K. D., Yu, N. H., Park, A. R., Park, D.-J., Kim, C.-J., and Kim, J.-C. (2022). *Streptomyces* sp. AN090126 as a biocontrol agent against bacterial and fungal plant diseases. *Microorganisms* 10 (4), 791. doi: 10.3390/microorganisms10040791

Li, P., Liu, M., Li, G., Liu, K., Liu, T., Wu, M., et al. (2021). Phosphorus availability increases pathobiome abundance and invasion of rhizosphere microbial networks by *Ralstonia*. *Environ. Microbiol.* 23 (10), 5992–6003. doi: 10.1111/1462-2920.15696

Li, X., Song, Y., Bian, Y., Gu, C., Yang, X., Wang, F., et al. (2020). Insights into the mechanisms underlying efficient rhizodegradation of PAHs in biochar-amended soil: from microbial communities to soil metabolomics. *Environ. Int.* 144, 105995. doi: 10.1016/j.envint.2020.105995

Liang, B., Ma, C., Fan, L., Wang, Y., and Yuan, Y. (2018). Soil amendment alters soil physicochemical properties and bacterial community structure of a replanted apple orchard. *Microbiol. Res.* 216, 1–11. doi: 10.1016/j.micres.2018.07.010

Lin, X., Yang, Y., Yang, P., Hong, Y., Zhang, L., Tong, C., et al. (2023). Soil organic nitrogen content and composition in different wetland habitat types along the south-east coast of China. *Catena* 232, 107457. doi: 10.1016/j.catena.2023.107457

Manzar, N., Kashyap, A. S., Goutam, R. S., Rajawat, M. V. S., Sharma, P. K., Sharma, S. K., et al. (2022). Trichoderma: advent of versatile biocontrol agent, its secrets and insights into mechanism of biocontrol potential. *Sustainability (Basel Switzerland)* 14 (19), 1278. doi: 10.3390/su141912786

Manzar, N., Singh, Y., Kashyap, A. S., Sahu, P. K., Rajawat, M. V. S., Bhowmik, A., et al. (2021). Biocontrol potential of native Trichoderma spp. against anthracnose of great millet (*Sorghum bicolour L.*) from Tarai and hill regions of India. *Biol. control* 152, 104474. doi: 10.1016/j.biocontrol.2020.104474

Martinoia, E., Klein, M., Geisler, M., Bovet, L., Forestier, C., Kolukisaoglu, Ü., et al. (2014). Multifunctionality of plant ABC transporters – more than just detoxifiers. *Planta* 214, 345–355. doi: 10.1007/s004250100661

Mendes, L. W., Raaijmakers, J. M., De Hollander, M., Mendes, R., and Tsai, S. M. (2018). Influence of resistance breeding in common bean on rhizosphere microbiome composition and function. *ISME J.* 12 (1), 212–224. doi: 10.1038/ismej.2017.158

Molina-Santiago, C., Udaondo, Z., and Ramos, J.-L. (2015). Draft whole-genome sequence of the antibiotic-producing soil isolate *Pseudomonas* sp. strain 250J. *Environ. Microbiol. Rep.* 7 (2), 288–292. doi: 10.1111/1758-2229.12245

Moret-FernÁNdez, D., and Lopez, M. V. (2019). Determination of soil aggregate porosity using the modified water saturation method. *Pedosphere* 29 (6), 794–800. doi: 10.1016/S1002-0160(17)60427-2

Nadhira, N. E., Wahyuni, I. D., and Addy, H. S. (2021). The potency of plant resistance inducers (PRIs) against bacterial wilt disease on tobacco caused by Ralstonia solanacearum. *IOP Conf. Series: Earth Environ. Sci.* 759 (1), 012067. doi: 10.1088/1755-1315/759/1/012067

Niu, J., Rang, Z., Zhang, C., Chen, W., Tian, F., Yin, H., et al. (2016). The succession pattern of soil microbial communities and its relationship with tobacco bacterial wilt. *BMC Microbiol.* 16 (1), 233. doi: 10.1186/s12866-016-0845-x

Oberholster, T., Vikram, S., Cowan, D., and Valverde, A. (2018). Key microbial taxa in the rhizosphere of sorghum and sunflower grown in crop rotation. *Sci. Total Environ.* 624, 530–539. doi: 10.1016/j.scitotenv.2017.12.170

Perry, E. K., Meirelles, L. A., and Newman, D. K. (2022). From the soil to the clinic: the impact of microbial secondary metabolites on antibiotic tolerance and resistance. *Nat. Rev. Microbiol.* 20 (3), 129–142. doi: 10.1038/s41579-021-00620-w

Pétriacq, P., Williams, A., Cotton, A., McFarlane, A. E., Rolfe, S. A., and Ton, J. (2017). Metabolite profiling of non-sterile rhizosphere soil. *Plant J.* 92 (1), 147–162. doi: 10.1111/tpj.13639

Prior, P., Ailloud, F., Dalsing, B. L., Remenant, B., Sanchez, B., and Allen, C. (2016). Genomic and proteomic evidence supporting the division of the plant pathogen *Ralstonia solanacearum* into three species. *BMC Genomics* 17 (1), 90. doi: 10.1186/s12864-016-2413-z

Qi, G., Ma, G., Chen, S., Lin, C., and Zhao, X. (2019). Microbial network and soil properties are changed in bacterial wilt-susceptible soil. *Appl. Environ. Microb.* 85 (13), e00162–e00119. doi: 10.1128/AEM.00162-19

Rudrappa, T., Czymmek, K. J., Paré, P. W., and Bais, H. P. (2008). Root-secreted Malic acid recruits beneficial soil bacteria. *Plant Physiol.* 148 (3), 1547–1556. doi: 10.1104/pp.108.127613

Runge, P., Ventura, F., Kemen, E., and Stam, R. (2023). Distinct phyllosphere microbiome of wild tomato species in central Peru upon dysbiosis. *Microb. Ecol.* 85 (1), 168–183. doi: 10.1007/s00248-021-01947-w

Sanka Loganathachetti, D., and Mundra, S. (2023). Water pH, not soil pH, alters bacterial community structural pattern and nitrogen cycling pathways in date palm (Phoenix dactylifera L.) roots and bulk soil under freshwater irrigation regime. *Front. Ecol. Evol.* 11. doi: 10.3389/fevo.2023.1142073

Schäfer, B. (2017). Tetracycline. *Chem. Unserer Zeit* 51 (4), 238–253. doi: 10.1002/ciuz.201700710

Shen, G., Zhang, S., Liu, X., Jiang, Q., and Ding, W. (2018). Soil acidification amendments change the rhizosphere bacterial community of tobacco in a bacterial wilt affected field. *Appl. Microbiol. Biotechnol.* 102 (22), 9781–9791. doi: 10.1007/s00253-018-9347-0

Standard, China (2008). *Grade and investigation method of tobacco diseases and insect pests*, GB/T 23222-2008. (Beijing: Standards Press of China).

Sun, M., Hou, E., Wu, J., Huang, J., Huang, X., and Xu, X. (2022). Spatial patterns and drivers of soil chemical properties in typical hickory plantations. *Forests* 13 (3), 457. doi: 10.3390/f13030457

Van der Heijden, M. G. A., and Hartmann, M. (2016). Networking in the plant microbiome. *PloS Biol.* 14 (2), e1002378. doi: 10.1371/journal.pbio.1002378

Wang, W., Liu, A., Fu, W., Peng, D., Wang, G., Ji, J., et al. (2022c). Tobacco-associated with Methylophilus sp. FP-6 enhances phytoremediation of benzophenone-3 through regulating soil microbial community, increasing photosynthetic capacity and maintaining redox homeostasis of plant. *J. Hazard Mater* 431, 128588. doi: 10.1016/j.jhazmat.2022.128588

Wang, J. L., Liu, K. L., Zhao, X. Q., Gao, G. F., Wu, Y. H., and Shen, R. F. (2022b). Microbial keystone taxa drive crop productivity through shifting aboveground-belowground mineral element flows. *Sci. Total Environ.* 811, 152342. doi: 10.1016/j.scitotenv.2021.152342

Wang, H., Wang, Y., Jiang, D., Xiang, Z., Wang, S., Kang, C., et al. (2022a). Soil microbe inoculation alters the bacterial communities and promotes root growth of Atractylodes lancea under heat stress. *Plant Soil* 478 (1-2), 371–389. doi: 10.1007/s11104-022-05369-6

Wang, Z., Wang, S., Liu, P., Yang, X., He, X., Xie, X., et al. (2022d). Molecular cloning and functional characterization of NtWRKY41a in the biosynthesis of phenylpropanoids in Nicotiana tabacum. *Plant Sci.* 315, 111154. doi: 10.1016/j.plantsci.2021.111154

Wang, Z., Zhang, Y., Bo, G., Zhang, Y., Chen, Y., Shen, M., et al. (2022e). *Ralstonia solanacearum* infection disturbed the microbiome structure throughout the whole tobacco crop niche as well as the nitrogen metabolism in soil. *Front. Bioeng Biotechnol.* 10, 903555. doi: 10.3389/fbioe.2022.903555

Wei, Z., Hu, J., Gu, Y., Yin, S., Xu, Y., Jousset, A., et al. (2018). *Ralstonia solanacearum* pathogen disrupts bacterial rhizosphere microbiome during an invasion. *Soil Biol. Biochem.* 118, 8–17. doi: 10.1016/j.soilbio.2017.11.012

Welch, J. L., Xiang, J., Okeoma, C. M., Schlievert, P. M., and Stapleton, J. T. (2020). Glycerol monolaurate, an Analogue to a Factor Secreted by Lactobacillus , is virucidal against enveloped viruses, including HIV-1. *mBio* 11 (3), e00686–00620. doi: 10.1128/mBio.00686-20

Wen, T., Zhao, M., Liu, T., Huang, Q., Yuan, J., and Shen, Q. (2020). High abundance of *Ralstonia solanacearum* changed tomato rhizosphere microbiome and metabolome. *BMC Plant Biol.* 20 (1), 166. doi: 10.1186/s12870-020-02365-9

Wong-Bajracharya, J., Castañeda-Gómez, L., Plett, K. L., Anderson, I. C., Carrillo, Y., and Plett, J. M. (2020). Untangling the effect of roots and mutualistic ectomycorrhizal fungi on soil metabolite profiles under ambient and elevated carbon dioxide. *Soil Biol. Biochem.* 151, 108021. doi: 10.1016/j.soilbio.2020.108021

Xun, W., Liu, Y., Li, W., Ren, Y., Xiong, W., Xu, Z., et al. (2021). Specialized metabolic functions of keystone taxa sustain soil microbiome stability. *Microbiome* 9 (1), 35. doi: 10.1186/s40168-020-00985-9

Yang, F., Jiang, H., Chang, G., Liang, S., Ma, K., Cai, Y., et al. (2023b). Effects of rhizosphere microbial communities on cucumber *Fusarium* wilt disease suppression. *Microorganisms* 11 (6), 1576. doi: 10.3390/microorganisms11061576

Yang, Y., Wang, N., Guo, X., Zhang, Y., and Ye, B. (2017). Comparative analysis of bacterial community structure in the rhizosphere of maize by high-throughput pyrosequencing. *PloS One* 12 (5), e0178425. doi: 10.1371/journal.pone.0178425

Yang, B., Zheng, M., Dong, W., Xu, P., Zheng, Y., Yang, W., et al. (2023a). Plant disease resistance-related pathways recruit beneficial bacteria by remodeling root exudates upon *Bacillus cereus* AR156 treatment. *Microbiol. Spectr.* 11 (2), e03611–e03622. doi: 10.1128/spectrum.03611-22

Yin, J., Zhang, Z., Zhu, C., Wang, T., Wang, R., and Ruan, L. (2022). Heritability of tomato rhizobacteria resistant to Ralstonia solanacearum. *Microbiome* 10 (1), 227–227. doi: 10.1186/s40168-022-01413-w

Zhang, Q.-M., Fu, J.-C., Chen, Z.-Q., and Qiu, L.-H. (2022). Paracidobacterium acidisoli gen. nov., sp. nov. and Alloacidobacterium dinghuense gen. nov., sp. nov., two acidobacteria isolated from forest soil, and reclassification of Acidobacterium ailaaui and Acidipila dinghuensis as Pseudacidobacterium ailaaui gen. nov., comb. nov. and Silvibacterium dinghuense comb. nov. *Int. J. Syst. Evol. Microbiol.* 72 (6), 5415. doi: 10.1099/ijsem.0.005415

Zhang, Y., Hu, A., Zhou, J., Zhang, W., and Li, P. (2020). Comparison of bacterial communities in soil samples with and without tomato bacterial wilt caused by *Ralstonia solanacearum* species complex. *BMC Microbiol.* 20 (1), 89. doi: 10.1186/s12866-020-01774-y

Zhao, W., Li, Y., Yang, C., Yang, Y., and Hu, Y. (2023). Rhizosphere microbial community and metabolites of susceptible and resistant tobacco cultivars to bacterial wilt. *J. Microbiol.* 61 (4), 389–402. doi: 10.1007/s12275-023-00012-0

Zheng, Y., Han, X., Zhao, D., Wei, K., Yuan, Y., Li, Y., et al. (2021). Exploring biocontrol agents from microbial keystone taxa associated to suppressive soil: a new attempt for a biocontrol strategy. *Front. Plant Sci.* 12, 655673–655673. doi: 10.3389/fpls.2021.655673

Zheng, X., Wang, J., Chen, Z., Zhang, H., Wang, Z., Zhu, Y., et al. (2019). A Streptomyces sp. strain: Isolation, identification, and potential as a biocontrol agent against soilborne diseases of tomato plants. *Biol. Control* 136, 104004. doi: 10.1016/j.biocontrol.2019.104004

frontiers | Frontiers in Plant Science

TYPE Original Research
PUBLISHED 24 January 2024
DOI 10.3389/fpls.2024.1327390

OPEN ACCESS

EDITED BY
Punya Nachappa,
Colorado State University, United States

REVIEWED BY
Sajjan Grover,
University of Nebraska-Lincoln, United States
Subhashree Subramanyam,
Agricultural Research Service (USDA), United States
Erika S. Peirce,
Colorado State University, United States

*CORRESPONDENCE
David K. Weaver
weaver@montana.edu

RECEIVED 24 October 2023
ACCEPTED 03 January 2024
PUBLISHED 24 January 2024

CITATION
Hager MS, Hofland ML, Varella AC, Bothner B, Budak H and Weaver DK (2024) Untargeted metabolomics profiling of oat (*Avena sativa* L.) and wheat (*Triticum aestivum* L.) infested with wheat stem sawfly (*Cephus cinctus* Norton) reveals differences associated with plant defense and insect nutrition.
Front. Plant Sci. 15:1327390.
doi: 10.3389/fpls.2024.1327390

Untargeted metabolomics profiling of oat (*Avena sativa* L.) and wheat (*Triticum aestivum* L.) infested with wheat stem sawfly (*Cephus cinctus* Norton) reveals differences associated with plant defense and insect nutrition

Megan S. Hager[1,2], Megan L. Hofland[2], Andrea C. Varella[3], Brian Bothner[4], Hikmet Budak[5] and David K. Weaver[2]*

[1]Department of Plant Sciences and Plant Pathology, Montana State University, Bozeman, MT, United States, [2]Wheat Stem Sawfly Laboratory, Department of Land Resources and Environmental Sciences, Montana State University, Bozeman, MT, United States, [3]Corteva Agriscience™, Woodstock Research and Development Centre, Tavistock, ON, Canada, [4]Department of Chemistry and Biochemistry, Montana State University, Bozeman, MT, United States, [5]Department of Agriculture, Arizona Western College, Yuma, AZ, United States

Introduction: Wheat stem sawfly (WSS), Cephus cinctus Norton, is a major pest of common bread wheat (Triticum aestivum L.) and other cultivated cereals in North America. Planting of cultivars with solid stems has been the primary management strategy to prevent yield loss due to WSS infestation, however expression of this phenotype can vary depending on environmental conditions and solid stems hinder biological control of WSS via braconid parasitoids Bracon cephi (Gahan) and Bracon lissogaster Muesebeck. In the hollow stems of oat (Avena sativa L.), WSS larvae experience 100% mortality before they reach late instars, but the mechanisms for this observed resistance have not been characterized.

Objective: The objective of this study was to explore additional sources of resistance outside of the historic solid stem phenotype.

Methods: Here, we use an untargeted metabolomics approach to examine the response of the metabolome of two cultivars of oat and four cultivars of spring wheat to infestation by WSS. Using liquid chromatography-mass spectrometry (LC-MS), differentially expressed metabolites were identified between oat and wheat which were associated with the phenylpropanoid pathway, phospholipid biosynthesis and signaling, the salicylic acid signaling pathway, indole-3-acetic acid (IAA) degradation, and biosynthesis of 1,4-benzoxazin-3-ones (Bxs). Several phospho- and galacto- lipids were found in higher abundance in oat, and with the exception of early stem solidness cultivar Conan, both species experienced a decrease in abundance once infested. In all wheat cultivars except Conan, an increase in abundance was observed for Bxs HMDBOA-glc and DIBOA-β-D-glucoside after infestation, indicating that this pathway is involved in wheat response to infestation in both solid and hollow stemmed cultivars. Differences

between species in compounds involved in IAA biosynthesis, degradation and inactivation suggest that wheat may respond to infestation by inactivating IAA or altering the IAA pool in stem tissue.

Conclusion: We propose that the species differences found here likely affect the survival of WSS larvae and may also be associated with differences in stem architecture at the molecular level. Our findings suggest pathways to focus on for future studies in elucidating plant response to WSS infestation.

KEYWORDS

metabolomics, wheat stem sawfly, host plant resistance, insect feeding, *Triticum aestivum*, *Avena sativa*

1 Introduction

The wheat stem sawfly (WSS), Hymenoptera *Cephus cinctus* Norton, is a major pest of grasses in the Great Plains of North America. Adult female WSS use their saw-like ovipositor to lay their eggs in the lumen of stems and once hatched, larvae begin consuming parenchyma tissue in the stem lining. As the larvae grows it breaches nodes, damaging vascular tissues, impacting photosynthetic ability and leading to decreased head weight (Macedo et al., 2005; Delaney et al., 2010). The stem girdling action of mature larvae to prepare overwintering chambers also weakens standing stems, which makes them prone to lodging and thus makes recovery of heads difficult during harvest (Ainslie, 1920; Morrill et al., 1998; Sherman et al., 2010). The stem-boring activity of the WSS larval stage causes devastating yield loss in cultivated grass hosts such as spring and winter wheat (*Triticum aestivum* L.). However, when eggs are laid in the stems of wild oat (*Avena fatua* L.) and cultivated oat (*Avena sativa* L.), larvae are unable to complete development (Criddle, 1917; Criddle, 1923; Farstad, 1940; Roemhild, 1954; Sing, 2002). Although cultivated oat exhibits total resistance to WSS, the mechanism behind this resistance remains unknown (Weaver et al., 2004).

In spring wheat, the solid stem phenotype is utilized by producers as the primary defense against WSS, but it does not prevent infestation or stem cutting completely and may decrease success of biological control efforts (Rand et al., 2012; Rand et al., 2020). Solid stems are filled with pith which appears to hinder oviposition, larval growth and maturation. Solid stems do not completely inhibit WSS and stem cutting as high as 30% has been reported for solid and semi-solid stemmed spring wheat cultivars (Sherman et al., 2010). While stem solidness is a relatively stable phenotype in some spring and winter wheat cultivars (Subedi et al., 2021), it is often negatively affected by light quality and sowing density (Roemhild, 1954; Nilsen et al., 2016; Beres et al., 2017; Nilsen et al., 2017). There is also evidence that braconid parasitoids *Bracon cephi* (Gahan) and *Bracon lissogaster* Muesebeck (Hymenoptera: Braconidae) cause less mortality to WSS larvae in solid stemmed cultivars compared to their hollow stemmed counterparts, indicating that continued use of solid stemmed cultivars may have a negative effect on populations of these parasitoids over time (Rand et al., 2012; Buteler et al., 2015; Rand et al., 2020). Host plant resistance against a specific pest can also promote secondary pest populations over time (Straub et al., 2020). It is important to support the tritrophic system of plant, WSS and parasitoid to increase success of control efforts, and it is therefore necessary to continue to explore sources of resistance in addition to the solid stem phenotype.

The stem solidness trait is highly heritable and is associated with the quantitative trait locus (QTL) *Qss.msub-3BL* (Cook et al., 2004). This QTL has been well studied, and several alleles conferring differing levels of stem solidness have been identified at this locus (Varella et al., 2017; Cook et al., 2019; Wong et al., 2022). The allele *Qss.msub-3BL.a* is associated with the hollow stemmed phenotype, while the allele *Qss.msub-3BL.b* confers stem solidness throughout plant development. A third allele, *Qss.msub-3BL.c* was identified in the cultivar 'Conan' (PI 607549), which has solid stems early in development with pith disappearing as the plant matures. WSS is known to target many grass species in addition to wheat including barley, oat and many native or introduced grasses, all of which have a hollow stemmed phenotype (Criddle, 1917; Wallace and McNeal, 1966; Cockrell et al., 2017; Achhami et al., 2020). Oat offers an opportunity to explore a source of complete resistance to WSS that appears unrelated to the stem solidness phenotype.

Female WSS will oviposit in wild oat as well as both small and large stemmed cultivated oat, but the larvae always die in the stem before reaching maturity (Criddle, 1917; Farstad, 1940; Holmes and Peterson, 1960; Holmes and Peterson, 1964; Wallace and McNeal, 1966; Sing, 2002; Weaver et al., 2004). This phenomenon has been discussed and documented for many years, and although research has explored the possibility of resistance due to physical differences between wheat and oat stems, the exact cause of larval mortality in oat remains unknown. In 1923, Criddle described "excessive sap" in oat stems as a possible cause of larval mortality, but this is likely due to environmental conditions as it was not replicable in dry

environments (Criddle, 1923; Farstad, 1940). Though the outcome is likely not caused by free moisture, there is some evidence that larvae in oat stems do not begin development as readily as larvae in wheat. In oat, larvae are less likely to form extensive, continuous tunnels throughout the stem and they molt less frequently than larvae developing in wheat (Farstad, 1940). Past research on oat plant responses to WSS infestation and injury has focused on the possibility of resistance due to physical differences between wheat and oat stems (Roemhild, 1954). Tissue surrounding vascular bundles in the nodes of oat stems is composed of tough sclerenchyma tissue, as opposed to the more pliable parenchyma tissue found in wheat nodes. However, this structural difference is not enough to explain the resistance observed in oat, since some larvae are still able to penetrate multiple nodes as they move throughout the stem (Roemhild, 1954). These observations on larvae feeding on oat stem tissues seem to suggest that there may be nutritional deficiencies or perhaps more likely, compounds present in oat which have antifeedant or insecticidal activities. WSS larvae are adapted to feeding within a plant stem, which prevents the use of conventional methods of insect rearing to test the effects of specific compounds in an artificial diet. This has resulted in limited knowledge of the nutritional requirements of WSS larvae. While little is known about the identity of compounds in oat which are detrimental to WSS development, it has been determined that stems of oat and wheat do not differ in moisture or nitrogen content at earlier growth stages when WSS larvae are susceptible to mortality (McGinnis and Kasting, 1961). Additionally, both oat and wild oat are known to produce several active phenolic compounds in roots, shoots and seeds (Schumacher et al., 1983; Kato-Noguchi et al., 1994). In early development these are exuded allelopathic compounds, preventing establishment of seedlings of other species, and can also be induced in response to pest or pathogen attack at any growth stage (Pérez and Ormeño-Nuñez, 1991; Kato-Noguchi et al., 1994). Overall, little mechanistic research has been done to explore oat resistance to WSS and defining the potential molecular mechanisms of WSS resistance in oat represents an important step towards developing wheat cultivars with new forms of resistance to WSS.

In this study we use liquid-chromatography mass spectrometry (LC-MS) to evaluate the metabolites that define the physiological response of spring wheat and oat to WSS infestation. Montana spring wheat cultivars 'Choteau' (PI 633974), 'Scholar' (PI 607557), Conan and Reeder (PI 613586) were chosen for comparison against the oat cultivars Dane and Otana. A susceptible cultivar of oat has not yet been found, and both Dane and Otana are considered to be resistant. The cultivars Choteau and Scholar both have the allele *Qss.msub-3BL.b* associated with the solid stem phenotype, though Choteau exhibits greater expression of stem solidness and is considered more resistant to WSS than Scholar as it experiences lower rates of stem cuttting. Reeder is a susceptible hollow stemmed cultivar with the allele *Qss.msub-3BL.a* and Conan shows a unique phenotypic expression of stem solidness, being solid at early growth stages and losing pith as the plant matures. Resistance due to the Conan allele is also conferred through antixenosis, which causes WSS females to reduce the number of ovipositor insertions and lay fewer eggs (Sherman et al., 2010; Talbert et al., 2014; Varella et al., 2016). While we expect to find differences in metabolites between species, the goal of this research is to discover how these differences may be involved in the resistance of oat to WSS through a comparison of the small molecule profiles of infested oat and wheat plants with varying degrees of resistance.

2 Materials and methods

2.1 Experimental conditions and plant collection

Seeds from the two cultivars of oat and four cultivars of spring wheat (Table 1) were planted in 20.32 cm circular pots in a mix of MSU mix and Sunshine mix #1 in a 50:50 by volume ratio. MSU mix contained a composite of mineral soils from the Gallatin Valley, Canadian sphagnum peat moss and washed concrete sand in a 1:1:1 by volume ratio as in Varella et al. (2017). Sunshine Mix #1 consisted of a soil-less blend of Canadian Sphagnum peat moss and horticultural grade Perlite. For each cultivar six pots containing four seeds were planted for infestation and four pots also containing four seeds were planted for controls. Once germinated, plants were culled to three per pot and maintained under greenhouse conditions (22° ± 2° during the day and 20° ± 2° during the night, and photoperiod of 15L:9D h) at the Plant Growth Center at Montana State University. Plants were exposed to both natural and artificial light (GE Multivapor lamps; model MVR1000/C/U, GE Lighting, General Electric Co., Cleveland, Ohio). All plants were watered daily and fertilized once a week with Peters Professional® General Purpose Fertilizer (J.R. Peters, Inc., Allentown, Pennsylvania, United States) at 100 ppm in aqueous solution. Common greenhouse pests were controlled using ladybugs (*Hippodamia convergens* Guérin-Méneville) and mechanical removal by hand or by using a water spray to dislodge them. Plant damage due to greenhouse pests was negligible.

Stubble containing overwintering wheat stem sawfly larvae in diapause were collected in a heavily infested field near Amsterdam, MT, USA. Stubs containing larvae were subjected to storage temperatures of 0-4 C for 3-6 months to ensure completion of diapause before transfer to ventilated plastic Tupperware boxes (70 x 35 x 20 cm) at approximately 20 C for 4-5 weeks to facilitate adult emergence. Adult sawflies used in this study were less than 48 hours old and were not prevented from mating prior to experimentation.

Plants were infested as soon as the first internode was detected to ensure elongating stem tissue was present for oviposition, at

TABLE 1 Stem solidness and resistance of oat and wheat cultivars.

Species	Cultivar	Stem solidness
Oat (*A. sativa*)	Dane	Hollow, complete resistance
Oat (*A. sativa*)	Otana	Hollow, complete resistance
Spring wheat (*T. aestivum*)	Choteau	Solid, resistant
Spring wheat (*T. aestivum*)	Scholar	Semi-solid, semi-resistant
Spring wheat (*T. aestivum*)	Conan	Early solid, resistant
Spring wheat (*T. aestivum*)	Reeder	Hollow, susceptible

approximately Zadoks growth stage 32 (Zadoks et al., 1974). This coincides with the earliest growth stage that sawfly females are likely to encounter and infest under field conditions. For each cultivar, three pots were randomly chosen for infestation and two pots were chosen for controls. Methods for infestation were adopted from Biyiklioglu et al., 2018. Briefly, a cage with 530 µM mesh openings was placed over the entire plant, including the main stem and any developing tillers and secured using a stake and wire. A 50/50 soil mix was added to the base of the chamber to prevent WSS escape. Supplementary lighting was placed approximately 45 cm on either side of the chamber to ensure that the sawflies were active (Supplementary Figure 1). Three WSS adult females were introduced to each chamber and oviposition was allowed for 72 hours, after which the chambers and sawflies were removed. Plant tissue was collected two weeks after the introduction of WSS to allow sufficient time for early instar larvae to cause damage to the lower internodes and maximize the likelihood that stem tissue in the upper internodes were free of frass. Specifically, the tissue was collected from upper internodes before more than one node could be bored by a small larva, so the upper internodes collected contained no frass. Sample tissue from upper internodes was not dissected in order to minimize damage to target plant tissues. To process samples, the main stem of the plant was cut at ground level and only the top two internodes were separated from the plant using a razor blade to ensure that stem tissue collected from infested plants was free of frass. The leaves were separated from the internodes, and internodes were wrapped in aluminum foil and immediately flash frozen in liquid nitrogen. Stems were considered infested if frass or larvae were observed in the lower internodes. Tillers were also checked for infestation, although most tillers had not reached the stem elongation stage during the infestation period. Three infested and three control samples were collected from individual plants for each cultivar and each sample was processed in 60 seconds or less. Samples were then stored in -80°C until metabolites were extracted.

2.2 Sample processing for metabolomics

Frozen wheat and oat stems were ground in liquid nitrogen with a mortar and pestle. Stem powder (approximately 150 mg per sample) was immersed in 100% methanol (MeOH) at 70°C for 15 min. Samples were vortexed for 1 min and then centrifuged (25,000 g, 10 min, 4°C). Proteins were separated from the metabolites by an acetone precipitation (two and a half parts acetone to one part tissue solution) at -80°C overnight, followed by centrifugation (25,000 g) at 4°C for 10 min. The resulting supernatant fraction was dried in a speed vacuum (low heat setting) and stored at -80°C. Prior to analyses by liquid chromatography-mass spectrometry (LC-MS), samples were resuspended in 20 µL of 50% HPLC grade water/50% MeOH.

2.3 LC-MS

Metabolite analysis was conducted at the Montana State Mass Spectrometry Facility using an Agilent 1290 ultra-performance liquid chromatography (UPLC) interface (Agilent Technologies, Santa Clara, CA, USA) fitted to an Agilent 6538 Accurate-Mass quadrupole time-of-flight mass spectrometer. Metabolites were separated by reversed-phase (RP) chromatography on a Kinetex 1.7 µm C18 150 x 2.1 mm column (Phenomenex, Torrance, CA) kept at 50°C with a flow rate of 600 µL min -1. The elution profile implemented started with a two-minute step of 98% solvent A (0.1% formic acid in H2O; waste) with 2% solvent B (0.1% formic acid in acetonitrile) followed by a 2% to 95% solvent B gradient over 24 min, a continued 95% solvent B for two min, and then a return to 2% solvent B over two min.

Mass detection was performed in positive mode, with a cone voltage of 3,500 V and a fragmentor voltage of 120 V. Drying gas temperature was 350°C (flow of 12 L per min -1) and the nebulizer was set at ~5.2 bar. Data was acquired with the following parameters: mass-to-charge ratio (m/z) range of 50-1,000 at 25,200 m/z-s. Mass analyzer resolution was 18,000 and post calibration tests had mass accuracy of approximately one ppm. For MS/MS acquisition, both standard compounds and ions of interest within a tolerance window of 1.7 m/z units were fragmented at 10 and 20 V.

2.4 LC-MS data preprocessing and analysis

Raw LC-MS data was converted to mzXML files using MSconvert from Proteowizard (Chambers et al., 2012). MZmine2 was used for preprocessing of spectral data (Pluskal et al., 2010). Raw data was acquired in centroid mode and was assigned m/z and retention time values using mass detection with noise level set at 1.0 E 3. Chromatograms were built using the chromatogram builder setting with minimum time span for peaks set to 0.1 min, minimum peak height set to 1.0 E 3 and m/z tolerance between 0.01 and 30 ppm. Resulting peaks were normalized using the same m/z tolerance, a retention time of 0.25 min and a minimum standard intensity of 2.0 E 4. Normalized peaks were then aligned, and the gap-filling feature was used to fill in missing peaks. Tentative identification of metabolites was completed using the online database metacyc.org (Katajamaa and Orešič, 2007; Pluskal et al., 2010; Caspi et al., 2014). Putatively identified metabolites were classified using the Chemical Entities of Biological Interest (ChEBI) database (http://www.ebi.ac.uk/chebi) (Hastings et al., 2016).

2.5 Statistical analysis

Data pre-processing and analysis was performed in R version 3.5.1 (Team, R. C 2022) using the R package MetaboAnalystR (Pang et al., 2020). Identified features were log transformed and range scaled to meet the assumption of normality. Normalized values were used to perform a principal component analysis (PCA) to identify which features contributed most to the variability of the dataset. To explore the response to infestation by each species as well as the effects of stem solidness, three related datasets were used: a complete dataset of all oat and wheat samples, an oat dataset containing infested and control samples from Dane and Otana, and

a wheat dataset containing infested and control samples from Choteau, Scholar, Conan and Reeder. These three datasets were used to perform PCA as well as two-way ANOVA. For the complete dataset, two-way ANOVA was performed with infestation status (infested, control) and cultivar (Dane, Otana, Choteau, Scholar, Conan and Reeder) as fixed effects. Two-way ANOVA was also performed using the oat dataset with infestation status (infested, control) and cultivar (Dane, Otana) as fixed effects. Finally, the wheat dataset was used to perform a two-way ANOVA with infestation status (infested, control) and cultivar (Choteau, Scholar, Conan, Reeder) as fixed effects. For all ANOVA testing, *post-hoc* pairwise testing was performed using Fishers Least Significant Difference (LSD) test and false discovery rate (FDR) correction of p-values was used to correct for multiple comparisons.

3 Results

3.1 Complete dataset – oat and wheat

Prior to transformation of data, the complete dataset was used to calculate log2 fold changes between infested and control samples for each cultivar (Supplementary Table 1). After transformation, PCA utilizing all metabolites from the oat and wheat dataset showed clear separation of the oat and wheat samples based on the first principal component (PC1) which explained 45.7% of the variability in the dataset. The second principal component (PC2) explained 9.1% of the variability and was able to clearly discriminate between the oat cultivars. Some separation of the infested and control wheat samples was also observed based on PC2, with the exception of Conan samples which showed high variability in infested and control samples (Figure 1). The first principal component was defined by low values for several carbohydrates as well as some lipids and amino acids, and high values for several glycosides. The second principal component was defined by low values for a different set of carbohydrates, as well as some lipids and high values for some terpenoids. The first and second principal components were both defined by variable groups of compounds and not strongly defined by a particular class or classes of compound (Supplementary Table 2).

Two-way ANOVA of all oat and wheat samples identified 159 metabolites that showed significant differences between oat and wheat cultivars (p-value<0.05) (Supplementary Table 3). Of these compounds, it was possible to classify 141 and match 126 to their respective biological pathways. The majority of compounds were found to be directly involved in plant defense, including several related to glucosinolate biosynthesis and degradation (Figure 2). Groups of terpenoids, phenols, alkaloids, glycerolipids and phospholipids were also significantly higher in oat samples compared to wheat in both infested and control groups (p-values<0.05) (Figure 3). Fishers Least Significant Difference (LSD) *post-hoc* pairwise testing identified significant differences in abundance of several groups of related compounds in oat and wheat which were part of the same biological pathway (Supplementary Table 4). Compounds of interest were also chosen based on those identified in previous 'omics studies of the WSS system and other studies of plant-insect interactions. Compounds O-sinapoylglucarolactone, O-sinapoylglucarate and 2-O-caffeoylglucarate, associated with the biosynthesis of hydroxycinnamate (HCA) esters were differentially expressed between oat and wheat cultivars, with O-sinapoylgluarate also showing significant differences among the wheat cultivars (Figure 4). Significantly higher abundance of oleate, 16-feruloyloxypalmitate and 5-hydroxyconiferyl alcohol, compounds

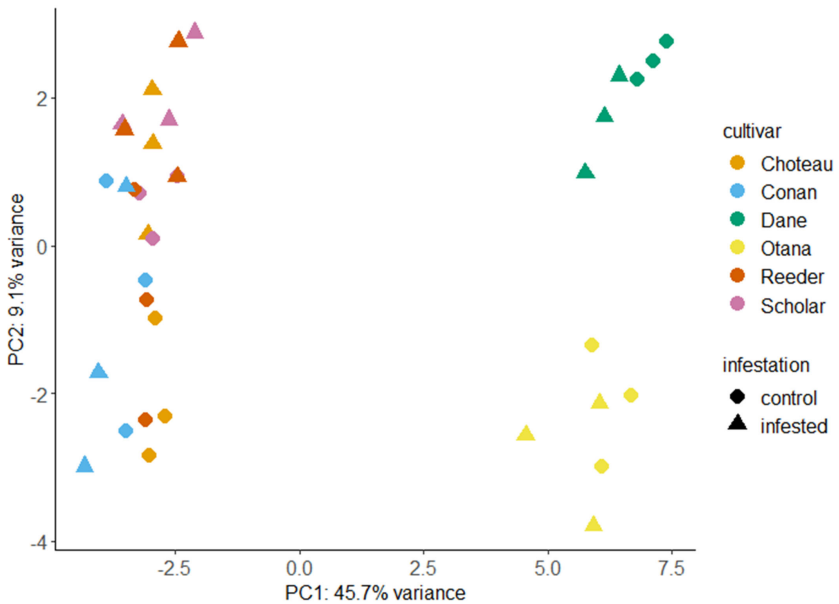

FIGURE 1
Principal component analysis (PCA) score plots for infested and control samples of all oat and wheat cultivars. PCA plots were created using LC-MS data from control and infested plants two weeks after caging with each point representing a stem sample. Choteau, orange; Conan, blue; Dane, green; Otana, yellow; Reeder, red; Scholar, Pink; Control, circle; Infested, triangle.

10.3389/fpls.2024.1327390

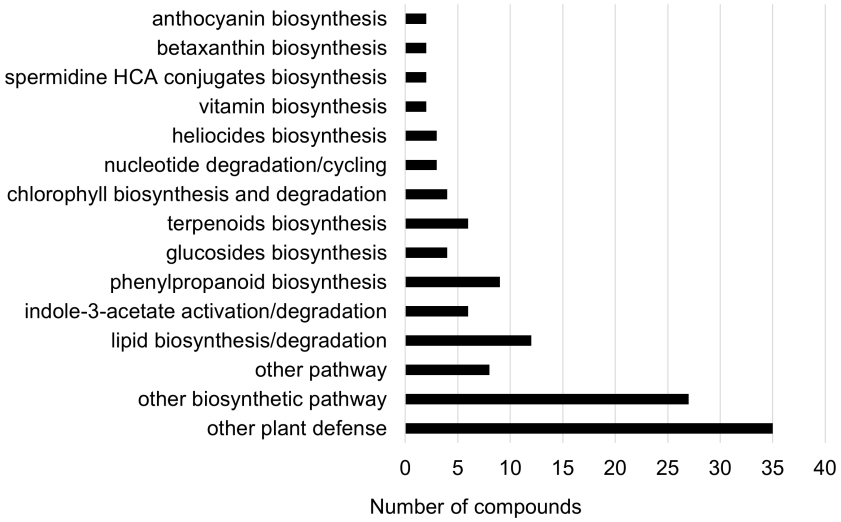

FIGURE 2
Biochemical pathway associations of significant compounds in the complete dataset which consisted of all oat and wheat samples from infested and control plants. Significant compounds (p-values<0.05) were identified using two-way ANOVA and Fishers LSD *post-hoc* test with FDR correction.

associated with lignin and suberin biosynthesis, was observed in oat compared to all wheat cultivars, with significant differences in 5-hydroxyconiferyl alcohol also observed between oat cultivars Dane and Otana (Figure 5). Phospho- and galactolipids were also generally found in higher abundance in oat, including 1-18:2-2-18:2-monogalactosyldiacylglycerol, 1-18:3-2-18:2-monogalactodiacylglycerol, 1-18:2-2-18:3-digalactosyldiacylglycerol, 1-18:0-2-18:1-phosphatidylethanolamine, 1-18:2-2-16:1-phosphatidate and 1-18:3-2-trans-16:1-phosphatidylglycerol, however some infested and control samples of a few wheat cultivars were not significantly different from the oat cultivars for several of these lipids (Figure 6). Two-way ANOVA identified significant effects of cultivar and infestation status on the abundance of salicylic acid-related compound salicylate 2-O-beta-D-glucoside, as well as significant effects of cultivar on salicyl-6-hydroxy-2-cyclohexene-on-oyl and salicin (Figure 7). Compounds associated with indole acetic acid degradation and inactivation 2-oxindole-3-acetyl-L-aspartate, indole-3-acetylgluatamate and indole-3-acetyl-leucine were significantly lower

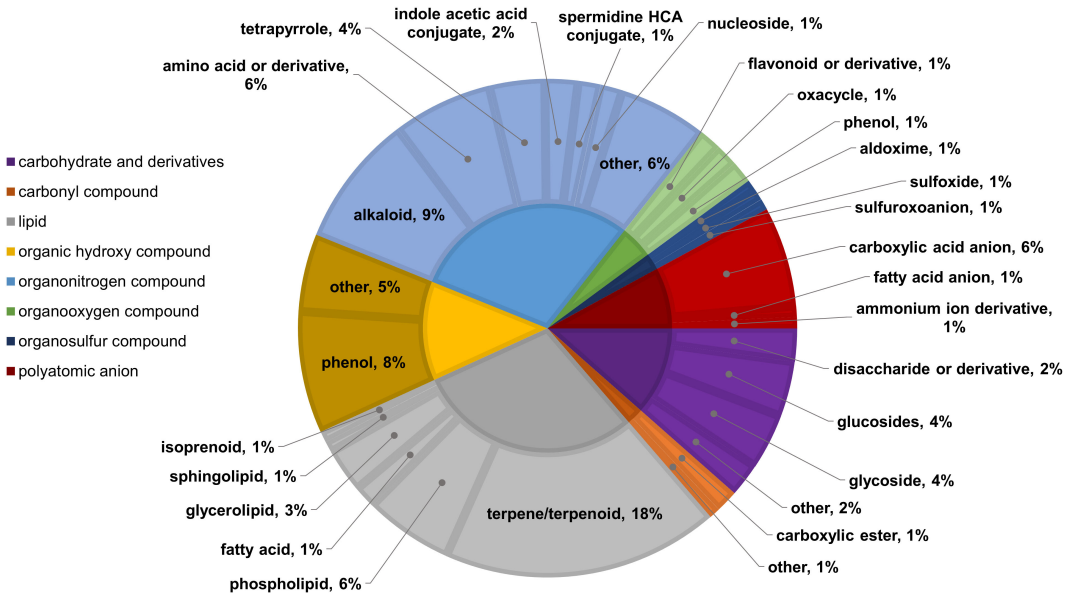

FIGURE 3
Classifications of significant putatively identified metabolites in the oat and wheat dataset. Significant compounds (p-values<0.05) were identified using two-way ANOVA and Fishers LSD *post-hoc* test with FDR correction. The innermost circle indicates the compound class with the outer ring representing compound subclass. Carbohydrate and derivatives, purple; carbonyl compound, orange; lipid, grey; organic hydroxy compound, yellow; organonitrogen compound, light blue; organooxygen compound, green; organosulfur compound, dark blue; polyatomic anion, red.

10.3389/fpls.2024.1327390

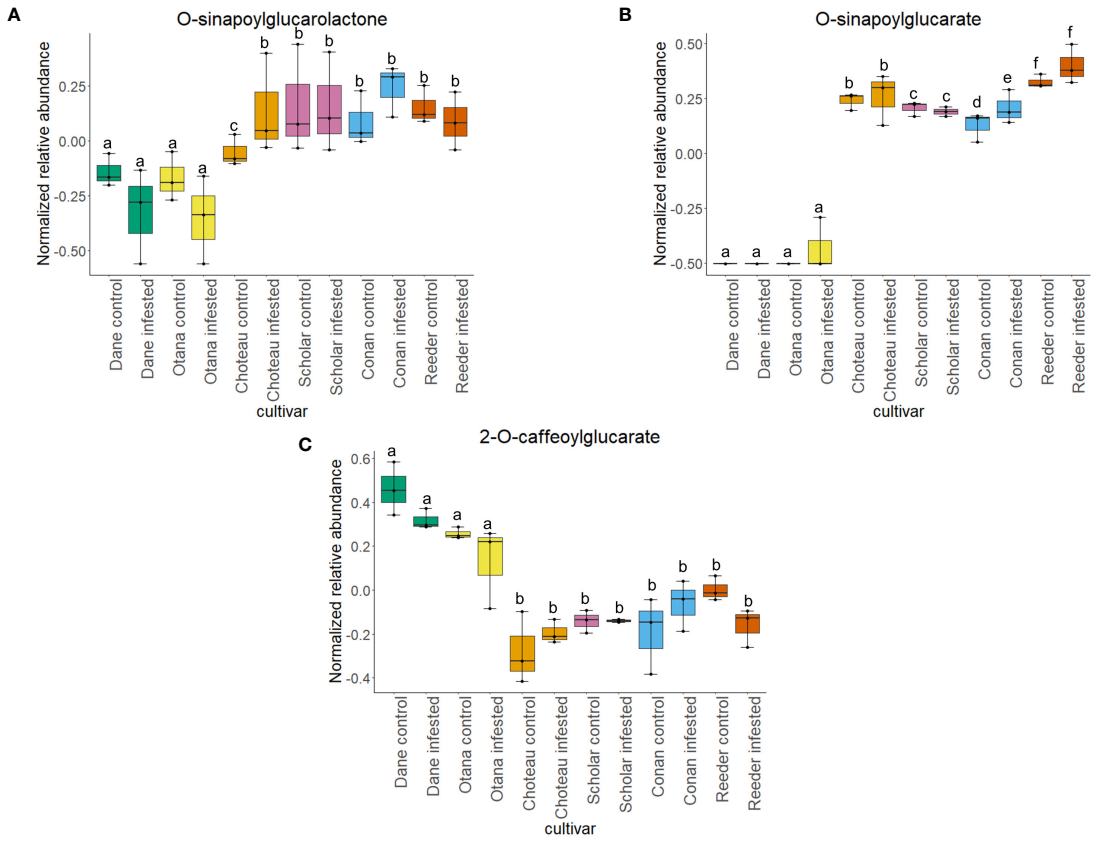

FIGURE 4
Boxplots showing differences in relative abundance of hydroxycinnamic acid conjugates in control and infested stem samples of oat and wheat. **(A)** O-sinapoylglucarolactone, **(B)** O-sinapoylglucarate, **(C)** 2-O-caffeoylglucarate. The box indicates the interquartile range (IQR) with the horizontal bar indicating the median. Lines extending from the box show the standard error for each sample group. Dane, green; Otana, yellow; Choteau, orange; Scholar, pink; Conan, blue; Reeder, red. Boxplots that do not share a letter have significantly different means.

in infested and control samples from oat cultivars compared to wheat, while 3-hydroxy-2-oxindole-3-acetyl-asp was significantly higher in oat cultivars, particularly in infested Dane samples (Figure 8). Benzoxazinoid-related glucoside DIBOA-beta-D-glucoside was found to be significantly higher in both Dane and Otana as well as in infested Choteau samples compared to other infested and control wheat samples (Figure 9).

3.2 Oat dataset

PCA using the oat dataset did not show any separation based on infestation status. The first principal component (PC1) explained 34.8% of the variability in the dataset and also allowed for discrimination of cultivars, while the second principal component (PC2) explained 15.7% of the variability in the dataset (Supplementary Figure 2). The first principal component was defined by low values for some amino acids and alkaloids and high values for some carbohydrate-related compounds. The second principal component was defined by low values for several lipids and high values for a different set of lipids as well as several carboxylic acids. The first and second principal components both were defined by a variable mix of compound classes (Supplementary Table 5).

Two-way ANOVA of all oat samples identified 96 metabolites that were significantly different between cultivars (p-value<0.05) (Supplementary Table 6). Of these, it was possible to classify 81 and match 79 to their respective biological pathway. The majority of these metabolites were involved in plant defense or biosynthetic pathways including nucleotide cycling and degradation, phosphatidylcholine biosynthesis and biosynthesis of secondary metabolites (Supplementary Figure 3). Compounds that were significantly different between the oat cultivars included several alkaloids, phenols, terpenes, flavonoids and carbohydrates (Supplementary Figure 4).

3.3 Wheat dataset

PCA with only the wheat dataset showed Choteau, Conan, Reeder and Scholar samples forming distinct clusters, but overlap between groups was observed due to the variability within sample groups (Supplementary Figure 5). The first principal component (PC1) explained 19.7% of the variability in the dataset and while the

10.3389/fpls.2024.1327390

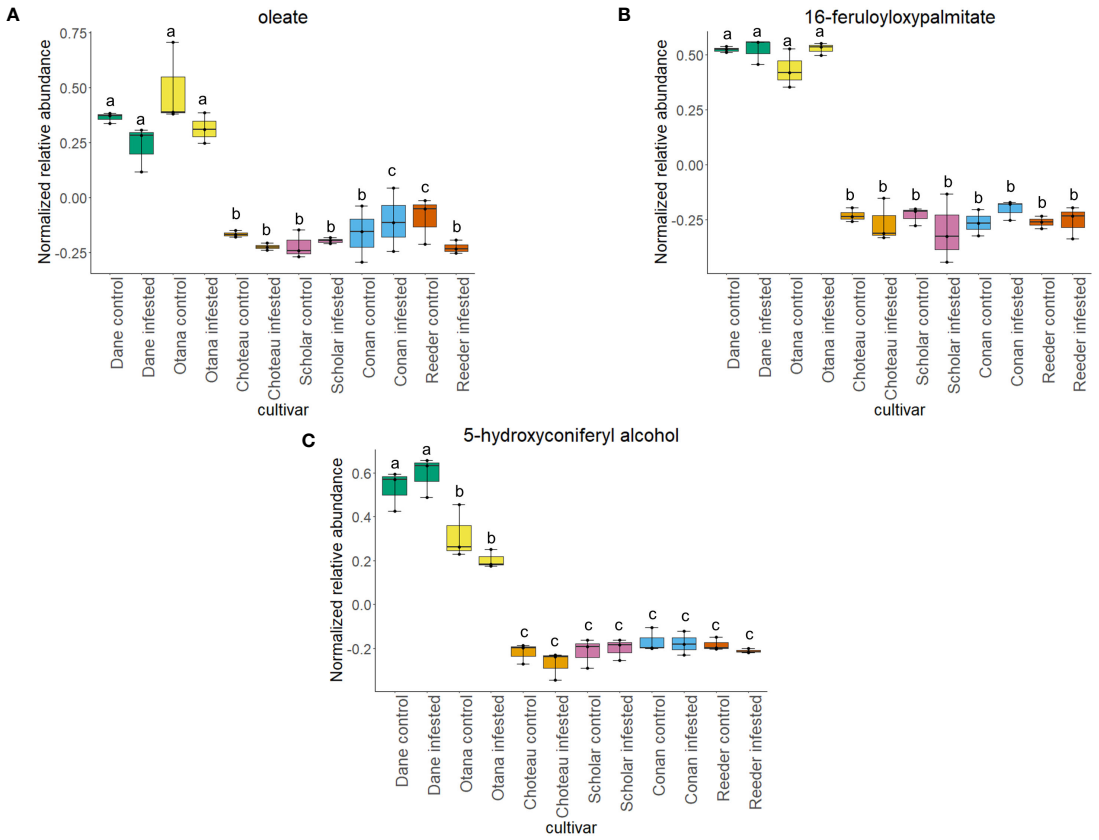

FIGURE 5
Boxplots showing relative abundance of compounds related to suberin and lignin biosynthesis in control and infested stem samples of oat and wheat. **(A)** oleate, **(B)** 16-feruloyloxypalmitate, **(C)** 5-hydroxyconiferyl alcohol. The box indicates the interquartile range (IQR) with the horizontal bar indicating the median. Lines extending from the box show the standard error for each sample group. Dane, green; Otana, yellow; Choteau, orange; Scholar, pink; Conan, blue; Reeder, red. Boxplots that do not share a letter have significantly different means.

second principal component (PC2) explained 16.3%. Overall, Scholar samples showed the tightest clustering, with lower variability observed in infested and control groups when compared with the other cultivars. The first principal component was defined by small values for some amino acids, lipids and polyatomic ions and large values for some carbohydrates and carbohydrate derivatives. The second principal component was defined by small values for some lipids, carbohydrates and organic hydroxy compounds and large values for a different set of lipids and some phenols. As with the complete dataset and oat dataset, neither principal component was strongly defined by any specific compound classes (Supplementary Table 7).

In the two-way ANOVA of wheat samples, a total of 58 metabolites showed significant differences. Cultivar had a significant effect on the abundance of 52 compounds and infestation status had a significant effect on 11 compounds, with evidence for an interaction between cultivar and infestation status for three compounds (p-value<0.05) (Supplementary Table 8). Of the 58 total compounds, it was possible to classify 52 and assign 39 to their respective pathway (Figures 10, 11). Metabolites that were significantly different between cultivars included several carbohydrate and carbohydrate derivatives, lipids and organonitrogen compounds, while infestation status had a significant effect on some lipids and carbohydrate related compounds.

3.4 Carbohydrates and derivatives

In the complete dataset, 17 carbohydrates, carbohydrate derivatives and carbonyl compounds were differentially expressed between cultivars, including salicin 6-phosphate, salicin, DIBOA β-D-glucoside and 2-O-caffeoylglucarate (p-values <0.05). In *post-hoc* tests, salicin showed significant differences between all samples from oat cultivars compared to all cultivars of wheat (Figure 7). 2-O-caffeoylglucarate and DIBOA beta-D-glucoside were both significantly higher in samples from oat cultivars compared to wheat, with significantly higher abundance of DIBOA beta-D-glucoside also observed in infested samples of Choteau compared to samples from other wheat cultivars (Figures 4, 9). There was also evidence for an interaction between cultivar and infestation status for four compounds: tetrahydropteroyltri-L-glutamate, vitexin 2”-O-β-D-glucoside, benzoyl-β-D-glucopyranose and phlorizin (p-values <0.05).

In the oat dataset, there was also a significant effect of cultivar on 11 carbohydrate-related compounds including salicortin, 2-O-

10.3389/fpls.2024.1327390

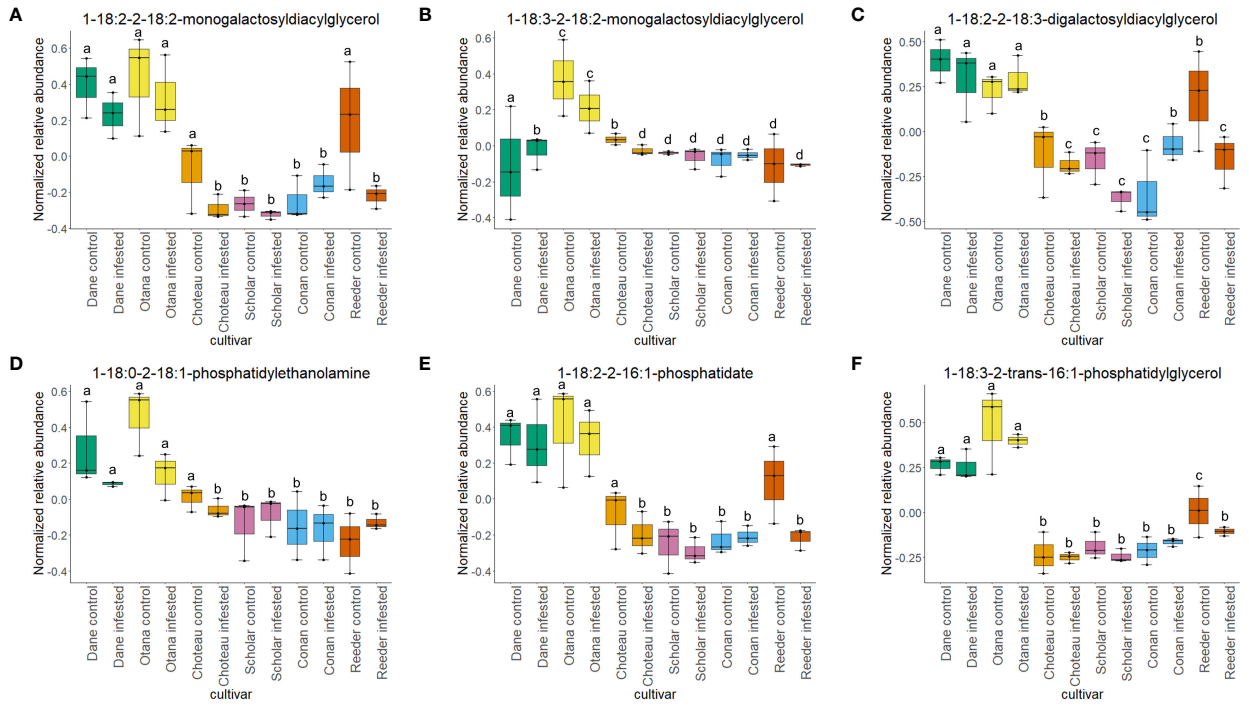

FIGURE 6
Boxplots showing relative abundance of phospho- and galactolipids in control and infested stem samples of oat and wheat. **(A)** 1-18:2-2-18:2-monogalactosyldiacylglycerol, **(B)** 1-18:3-2-18:2-monogalactosyldiacylglycerol, **(C)** 1-18:2-2-18:3-digalactosyldiacylglycerol, **(D)** 1-18:0-2-18:1-phosphatidylethanolamine, **(E)** 1-18:2-2-16:1-phosphatidate, **(F)** 1-18:3-2-trans-16:1-phosphatidylglycerol. The box indicates the interquartile range (IQR) with the horizontal bar indicating the median. Lines extending from the box show the standard error for each sample group. Dane, green; Otana, yellow; Choteau, orange; Scholar, pink; Conan, blue; Reeder, red. Boxplots that do not share a letter have significantly different means.

caffeoylglucarate, peonidin-3-(p-coumaroyl)-rutinoside-5-glucoside and 1,4-β-D glucan (p-values <0.05). Infestation status and cultivar both had significant effects on the relative abundance of glucosyl limonin and benzoyl-β-D-glucopyranose in the oat dataset, with evidence of an interaction between infestation status and cultivar for these compounds (p-values <0.05).

The wheat dataset contained 9 glucosides and carbonyl compounds which were differentially expressed between cultivars (p-value <0.05). Infestation status had a significant effect on bis(β-D-glucosyl) crocetin (p-value <0.05). Both cultivar and infestation status had a significant effect on the abundance of HMDBOA-glucoside, but there was no evidence of an interaction for this compound (p-value <0.05). Abundance of HMDBOA-glucoside was higher in all samples from oat cultivars compared with infested and control samples from wheat. Scholar infested and control samples were significantly higher than those from other wheat cultivars (Figure 9).

3.5 Lipids

In the complete dataset, 40 lipids were differentially expressed between cultivars, including several galactolipids, phospholipids and terpenoids (p-values<0.05). 1-18:2-2-18:2-monogalactosyldiacylglycerol, 1-18:3-2-18:2-monogalactodiacylglycerol, 1-18:2-2-18:3-digalactosyldiacylglycerol, 1-18:0-2-18:1-phosphatidylethanolamine and 1-18:2-2-16:1-phosphatidate and 1-18:3-2-trans-16:1-phosphatidylglycerol showed differential expression (Figure 6). Oleate was significantly higher in the oat samples compared to wheat, and was also significantly higher in infested Conan samples and control samples of Reeder compared to other samples from wheat (Figure 5). Infestation status also had a significant effect on the abundance of 2-omega-hydroxy- C22:0-LPA and hemigossypol, although there was no evidence of an interaction between cultivar and infestation status for these compounds (p-value<0.05).

There were 10 lipids in the oat dataset that were differentially expressed between cultivars, including oleate, the galactolipids 1-18:3-2-18:2-monogalactosyldiacylglycerol and 1-18:2-2-18:2-digalactosyldiacylglycerol and several terpenoids (p-value<0.05).

In the wheat dataset, cultivar had a significant effect on the abundance of 9 lipids, including the phospholipid 1-18:3-2-trans-16:1-phosphatidylglycerol. Infestation status had a significant effect on the abundance of 2-omega-hydroxy- C22:0-LPA (p-value<0.05). There was no evidence for an interaction between cultivar and infestation status for any lipids in the wheat dataset.

3.6 Other organic compounds

Cultivar had a significant effect on the abundance of 100 other organic compounds in the complete dataset, including 16-feruloyloxypalmitate, salicyl-6-hydroxy-2-cyclohexene-on-oyl, 2-

10.3389/fpls.2024.1327390

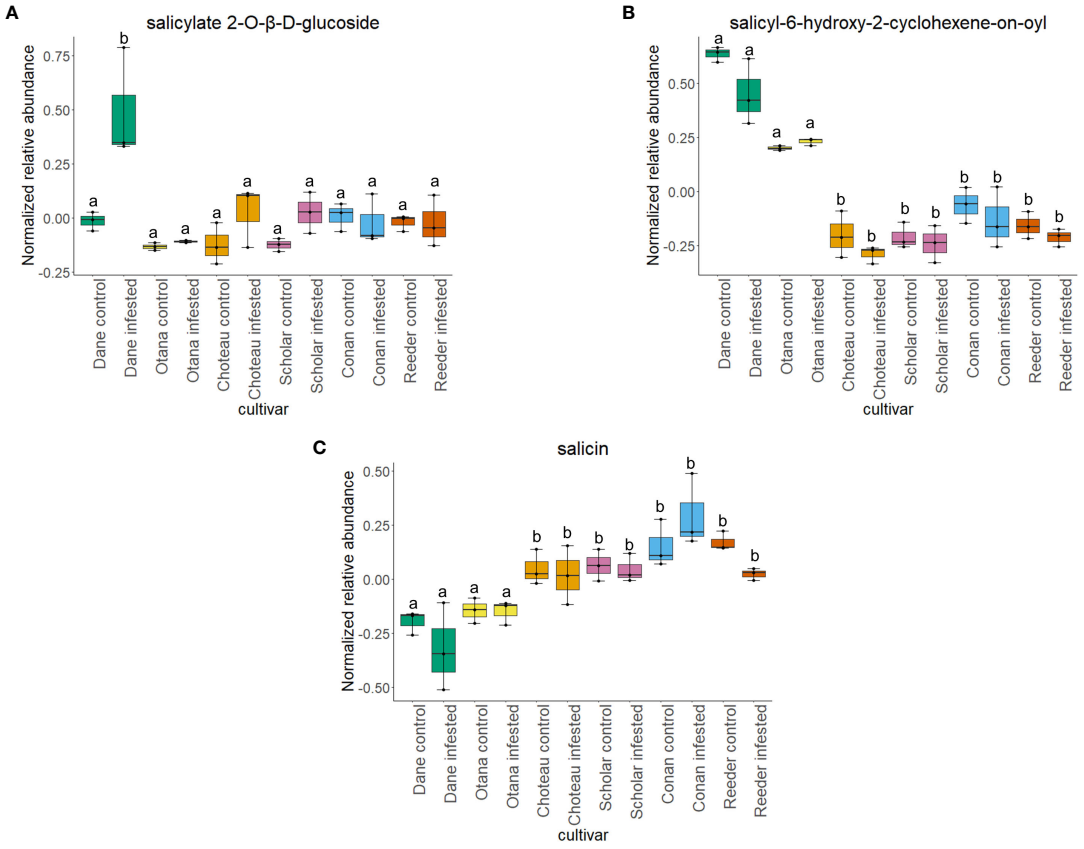

FIGURE 7
Boxplots showing relative abundance of salicylic acid related compounds in control and infested stem samples of oat and wheat. **(A)** salicylate 2-O-β-D-glucoside, **(B)** salicyl-6-hydroxy-2-cyclohexene-on-oyl, **(C)** salicin. The box indicates the interquartile range (IQR) with the horizontal bar indicating the median. Lines extending from the box show the standard error for each sample group. Dane, green; Otana, yellow; Choteau, orange; Scholar, pink; Conan, blue; Reeder, red. Boxplots that do not share a letter have significantly different means.

oxindole-3-acetyl-L-aspartate, 3-hydroxy-2-oxindole-3-acetyl-asp, phenols O-sinapoylglucarolactone and 5-hydroxyconiferyl alcohol, and amino acid derivatives oxindole-3-acetyl-L-aspartate, indole-3-acetyl-glutamate and indole-3-acetyl-leucine (p-value<0.05). Indole-3-acetylglutamate and indole-3-acetyl-leucine were both significantly lower in oat samples compared with all cultivars of wheat (Figure 8). Indole-3-acetylglutamate also showed differential expression between infested and control samples of Choteau and Scholar (Figure 8). 16-feruloyloxypalmitate and 5-hydroxyconiferyl alcohol were significantly higher in both oat cultivars compared with wheat (Figure 5). 2-oxindole-3-acetyl-L-aspartate and O-sinapoylglucarolactone were significantly lower in both Dane and Otana compared with the wheat cultivars (Figures 8, 4). 3-hydroxy-2-oxindole-3-acetyl-asp showed opposite expression, with significantly higher abundance in Dane infested samples, although all oat samples showed higher abundance than the wheat cultivars (Figure 8). Infestation status had a significant effect on the abundance of 4 organic compounds, including indole-3-acetyl isoleucine and salicylate 2-O-β-D-glucoside (p-value<0.05). Salicyl-6-hydroxy-2-cyclohexene-on-oyl was significantly higher in both oat cultivars compared with the wheat cultivars, however there were also differences observed between oat cultivars for this compound (Figure 7). Salicylate 2-O-β-D-glucoside was significantly higher in Dane infested samples compared with other oat samples and wheat samples from all cultivars (Figure 7). There was evidence for an interaction between cultivar and infestation status for tetrahydropteroyl-tri-L-glutamate, 10-deacetyl-2-debenzoylbaccatin III, hydroxyflavone and kamepferide triglycoside (p-value<0.05).

In the oat dataset, 62 organic compounds were differentially expressed between cultivars including DIMBOA, choline, cyanidin 3-(p-coumaroyl)-glucoside, indole-3-acetyl-isoleucine (p-value <0.05). Infestation status had a significant effect on the abundance of 6-hydroxy-allocryptopine and indole-3-acetohydroximoyl-glutathione (p-value <0.05), however there was evidence of an interaction between infestation status and cultivar for these compounds (p-value<0.05).

In the wheat dataset, 36 organic compounds were differentially expressed between cultivars including O-sinapoylglucarate and several phenols and alkaloids (p-value<0.05). Infestation status had a significant effect on the abundance of 4 compounds: serotonin, xanthine, dihydrocurcumin and 7-deoxyloganetate (p-value<0.05). There was evidence for an interaction between infestation status and cultivar for two compounds: laudanosine and luteolin 7-O-β-D-glucuronide (p-value<0.05).

10.3389/fpls.2024.1327390

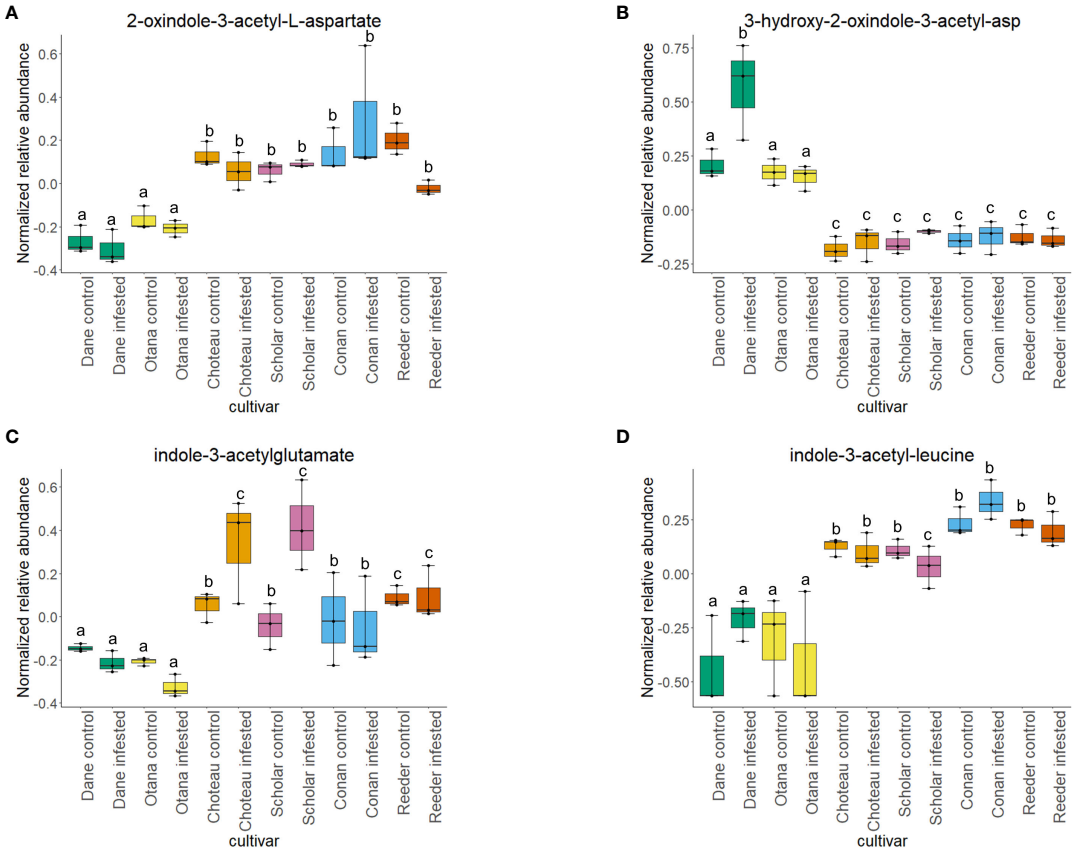

FIGURE 8
Boxplots showing relative abundance of indole-3-acetic acid (IAA) conjugates in control and infested stem samples of oat and wheat. **(A)** 2-oxindole-3-acetyl-L-aspartate, **(B)** 3-hydroxy-2-oxindole-3-acetyl-asp, **(C)** indole-3-acetylglutamate, **(D)** indole-3-acetyl-leucine. The box indicates the interquartile range (IQR) with the horizontal bar indicating the median. Lines extending from the box show the standard error for each sample group. Dane, green; Otana, yellow; Choteau, orange; Scholar, pink; Conan, blue; Reeder, red. Boxplots that do not share a letter have significantly different means.

4 Discussion

Here, we utilized comparisons of the metabolome of infested and uninfested stem tissue from two cultivars of oat, which exhibits complete resistance to stem cutting by WSS, and four cultivars of wheat with varying degrees of stem solidness to explore possible mechanisms of resistance to WSS. In our complete dataset, several carbohydrates, lipids and plant defense compounds were differentially expressed between samples from both oat cultivars and samples from wheat cultivars, indicating that these compounds may be responsible for the constitutive resistance to WSS observed in oat. In all datasets, cultivar had the greatest effect on most compounds, and although some did show change in response to WSS infestation, the effect of infestation status on relative abundance was rarely significant. Overall, constitutive and induced differences in lipids, plant defense compounds including HMDBOA glucoside, and compounds involved in the organization of cells or cell elongation within plant tissue such as O-sinapoylglucarate and indole-3-acetyl leucine appear to be related to WSS resistance and illustrate how the molecular environment of oat stems differ from wheat and may explain why oat is a poor host for developing larvae of WSS.

4.1 Phenylpropanoid pathway and species differences in lignin and suberin biosynthetic pathways

The phenylpropanoid pathway is extensive and complex, producing a wide range of compounds which are involved in plant defense in several ways including systemic signaling and providing chemical or physical barriers to insect or pathogen attack. This pathway is responsible for the biosynthesis of hydroxycinnamic acids, flavonoids, isoflavanones, anthocyanins, and sinapate esters (Strack et al., 1987). Several structural biopolymers are derived from the phenylpropanoid pathway as well, including lignin and suberin. Production of these compounds is highly variable depending on species and nearly every class of molecule produced by this superpathway has functions that are either directly or indirectly involved in plant defense (Dixon et al., 2002).

Biosynthesis of hydroxycinnamate (HCA) esters proceeds via three unique routes: one utilizing HCA-CoA thioesters, another uses HCA-glucosides from sinapate ester biosynthesis and the third utilizes HCA-quinate (Strack et al., 1987; Strack et al., 1988). O-sinapoylglucarate and O-sinapoylglucarolactone, both products of

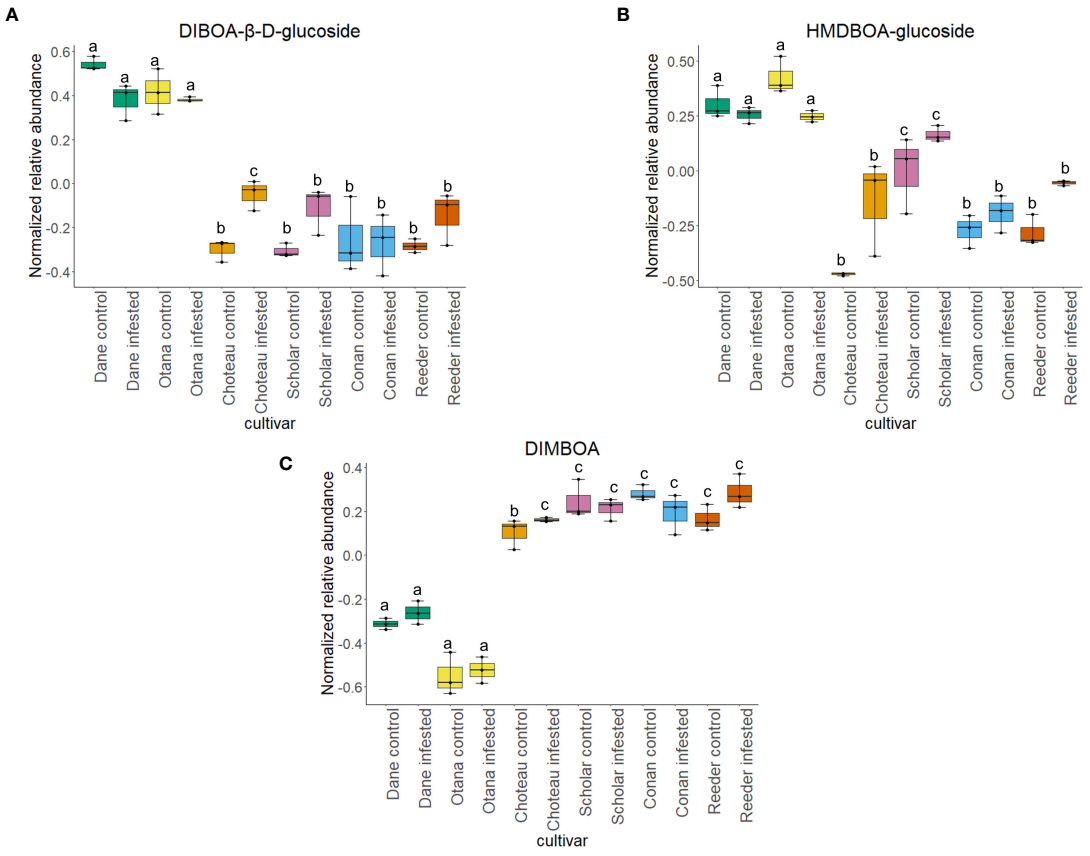

FIGURE 9
Boxplots showing relative abundance of benzoxazinoids in control and infested stem samples of oat and wheat. **(A)** DIBOA-β-D-glucoside, **(B)** HMDBOA-glucoside, **(C)** DIMBOA. The box indicates the interquartile range (IQR) with the horizontal bar indicating the median. Lines extending from the box show the standard error for each sample group. Dane, green; Otana, yellow; Choteau, orange; Scholar, pink; Conan, blue; Reeder, red. Boxplots that do not share a letter have significantly different means.

the second route of HCA ester biosynthesis, were found in lower abundance in oat samples when compared to wheat samples. In wheat, abundance of O-sinapoylglucarate and O-sinapoylglucarolactone increased or stayed the same when plants were infested, while infested oat plants had a significant decrease in O-sinapoylglucarolactone compared to uninfested oat plants (Figure 4). Overall, 2-O-caffeoylglucarate, a product of the third route of HCA ester biosynthesis, had increased abundance in oat samples compared to wheat and also had significantly lower abundance in infested oat plants compared to uninfested oat plants (Figure 4). These results indicate that oat may produce HCA esters primarily via the HCA-quinate route. It is not known whether the routes to HCA production differ in terms of efficiency or speed of response, so it is difficult to determine what role the HCA-quinate route plays in oat resistance to larval feeding.

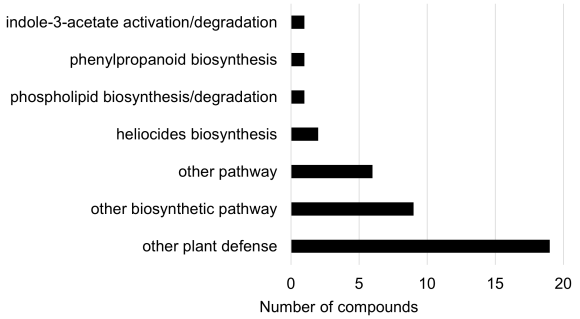

FIGURE 10
Biochemical pathway associations of significant compounds (p-value<0.05) in the wheat dataset. The wheat dataset consisted of all wheat samples from infested and control plants. Significant compounds (p-values<0.05) were identified using two-way ANOVA and Fishers LSD *post-hoc* test.

Hydroxycinnamic acid esters in plant tissues have a direct effect on plant resistance and can decrease oviposition and have a negative effect on larval mortality (Anyanga et al., 2021). They can also form polymers with polyamines to form hydroxycinnamic acid amines (HCAAs) which are deposited in the cell wall near regions of pathogen infection or wounding by boring insects, a process that is associated with strengthening of cell walls and increased resistance (Grandmaison et al., 1993; Facchini et al., 2002; Barros-Rios et al., 2011; Gunnaiah et al., 2012). HCAAs themselves can influence cell growth and lignin content as well as lignin subunit composition, which also affects plant resistance (Lima et al., 2013).

Suberin and lignin are structural polymers that are essential for plant protection from infection by fungal pathogens or infestation by insects (Wainhouse et al., 1990; Li et al., 2007; Kosma et al., 2010; Bakaze et al., 2020). Infection by some pathogens induces

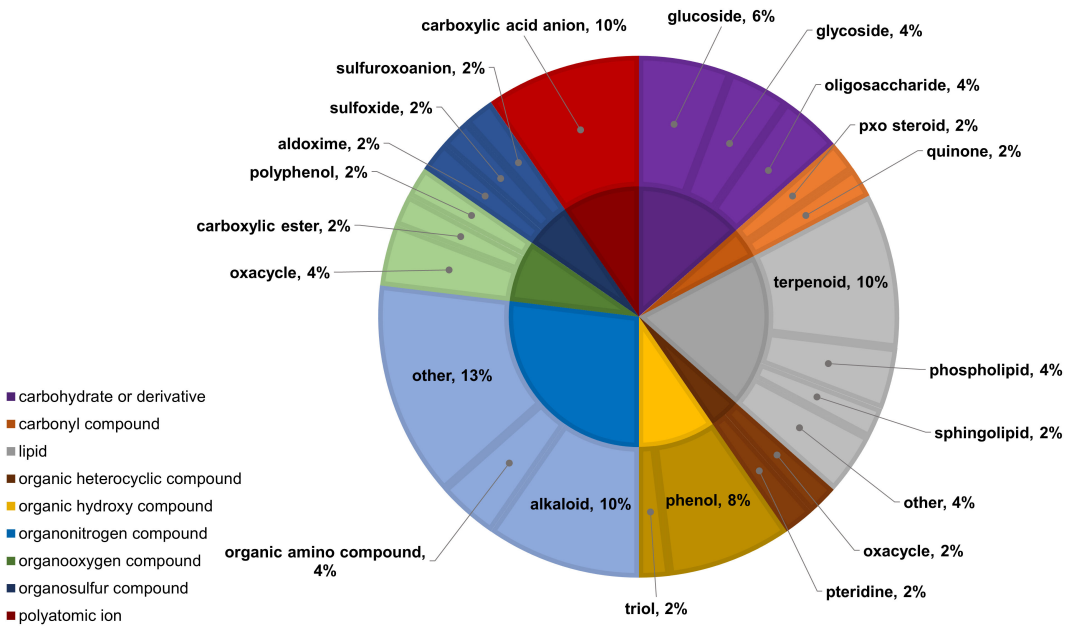

FIGURE 11
Classifications of significant, putatively identified metabolites in the wheat dataset. Significant compounds (p-values<0.05) were identified using two-way ANOVA and Fishers LSD *post-hoc* test with FDR correction. The innermost circle indicates the compound class with the outer ring representing compound subclass. Carbohydrate or derivative, purple; carbonyl compound, orange; lipid, grey; organic heterocyclic compound, brown; organic hydroxy compound, yellow; organonitrogen compound, light blue; organooxygen compound, light green; organosulfur compound, dark blue; polyatomic ion, red.

reinforcement of vascular cell walls with a ligno-suberin coating that strengthens the cell wall, preventing degradation and restricting the movement of the pathogen, conferring resistance (Kashyap et al., 2022). In wheat, lignin is present in the parenchyma of solid-stemmed cultivars, while lignification is not as extensive in barley or oat (Roemhild, 1954). In our complete dataset, abundance of 16-feruloyloxypalmitate, oleate, and 5-hydroxyconiferyl alcohol were significantly lower in wheat compared to all oat cultivars (Figure 5). 16-feruloyloxypalmitate and oleate are predicted to be involved in suberin biosynthesis, while 5-hydroxyconiferyl alcohol is incorporated into lignin via a dehydrogenation reaction, forming lignins that are linear in nature (Elder et al., 2016). While several studies have confirmed the positive impact of increased lignin on plant resistance to fungal pathogens and infestation by insects (Wainhouse et al., 1990; Bi et al., 2010), lignin content has not been found to have any effect on the amount of sawfly tunneling or stem cutting in the sawfly system (McNeal et al., 1965).

However, total lignin content is only one aspect of mechanical resistance to pests and pathogens. Lignin is a polymer composed of syringyl (S), guaiacyl (G) and p-hydroxyphenyl (H) subunits which may have an effect on resistance. In particular, some research has explored the influence of lignin subunit composition (S/G ratio) on palatability of plant tissue to insect herbivores, and there is evidence that resistant plants exhibit an altered S/G ratio depending on species (Sewalt et al., 1997; Poerschmann et al., 2005; Kärkönen et al., 2014). Lignin formed in response to bacterial infection or insect attack contains less G monolignin and more G and H monolignins, illustrating that biosynthesis of lignin can change depending on type of stress, though this does not always coincide with increased plant resistance (Zhang et al., 2007; Buhl et al., 2017). Further study is necessary to elucidate whether the lignin composition of oat differs from that of wheat and whether this has an effect on larval feeding or survival in oat.

4.2 Phospholipids in oat and wheat

Phospholipids such as phosphatidylcholine and phosphatidylethanalomine are important structural lipids found in plant cell membranes. These molecules can also be hydrolyzed by phospholipases and serve as co-factors, signaling molecules or precursors to signaling molecules that are necessary for plant defense responses (Munnik et al., 1998; Laxalt and Munnik, 2002). Phospholipids, galactolipids and related molecules found in this study have the potential for involvement in plant defense responses in some capacity and may be linked to the same putative pathway (Figure 6). Several phospholipid metabolizing enzymes have been identified and are thought to play an important role in plant defense signal transduction. A known product of phospholipases C (PLC; EC 3.1.4.3) and D (PLD; EC 3.1.4.4) is phosphatidic acid which is a conjugate acid of phosphatidate (Liscovitch et al., 2000). In many plants, levels of phosphatidic acid have been shown to increase in response to wounding, drought stress or treatment with a general synthetic elicitor (Lee et al., 1997; Frank et al., 2000; Van Der Luit et al., 2000). Phosphatidic acid is also a precursor to many complex lipids including digalactosyldiacylglycerol, which in turn contributes to salicylic acid biosynthesis and systemic acquired resistance (SAR) signal

azelaic acid (Gao et al., 2014). Phosphatidic acid can also activate the NADPH oxidase complex, indirectly triggering an oxidative burst in response to pathogen attack (Laxalt and Munnik, 2002).

In this study, both species experienced a decrease in phospholipid abundance in response to infestation, with the exception of Conan, which showed an increase in concentration for the majority of phospholipids observed. Lipid components of plant cellular membranes, 1-18:1-2-18:1-phosphatidylethanolamine, 1-18:0-2-18:1-phosphatidylethanolamine and 1-18:3-2-trans-16:1-phosphatidylglycerol, were significantly greater in oat compared with all cultivars of wheat. In the oat dataset, free galactolipids 1-18:2-2-18:2-digalactosyldiacylglycerol and 1-18:3-2-18:2-monogalactosyl diacylglycerol both decreased in response to infestation, but only cultivar had a significant effect on abundance. Lipids, including phospholipids, are nutritionally significant to many insects and are often required for normal growth and development (Turunen, 1979). Conversely, high concentrations of lipids in plant tissues can also cause larval mortality and decreased larval growth in some species (Li et al., 2014; Liao et al., 2021). WSS larvae are adapted to feeding inside the plant stem, making it difficult to test their dietary requirements with artificial diets, so little is known about their specific nutritional needs, but it is possible that higher levels of lipids in oat may have a negative effect on larval growth and development (Macedo et al., 2005).

Phospholipids have been well studied in relation to wheat resistance to Hessian fly, an insect that feeds within the exterior of the stem wall. In several studies using wheat lines resistant to Hessian fly, a decrease in membrane lipid concentration and increase in fatty acids and derivatives has often been observed in response to feeding by Hessian fly larvae (Zhu et al., 2012; Khajuria et al., 2013). In our results, infestation did not have a significant effect on the levels of phospho- or galactolipids in any of the datasets, although a decrease of abundance was observed in infested samples, indicating that phospholipid signaling is likely not a strong response to WSS infestation in either oat or wheat (Figure 6). The resistant cultivar Conan had similar levels of structural lipids to the other wheat cultivars but had increased abundance of free lipids 1-18:2-2-18:2-monogalactosyldiacylglycerol, 1-18:2-2-18:2-digalactosyldiacylglycerol, 1-18:2-2-18:3-digalactosyl diacylglycerol and 1-18:1-2-18:1-phosphatidate, though this increase was not significant in either the complete or wheat-only dataset (Figure 6). These results suggest that the increase in free lipids might be associated with the disappearance of pith observed as Conan matures and indicate that Conan may be more efficient than other wheat cultivars at re-mobilizing structural lipids after degradation to signaling lipids or precursors. The downstream effects of increased phosphatidic acid, including SAR and induction of an oxidative burst, may also partially explain the resistance of Conan to sawfly damage.

4.3 Other plant defense molecules

4.3.1 Salicylic acid and related metabolites

Salicylic acid (SA) and jasmonic acid (JA) hormone signaling pathways are the two most important and well-studied in relation to induced plant defense (Howe and Jander, 2008; Erb et al., 2012). The crosstalk between these pathways is complex, but SA can have a negative effect on JA-induced resistance, making plants more susceptible to damage from insect herbivores (Stotz et al., 2002; Bodenhausen and Reymond, 2007; Bruessow et al., 2010). Salicylates such as salicin and salicortin also play a role in direct plant defense against herbivory, negatively affecting larval performance by decreasing growth rates (Lindroth and Peterson, 1988; Lindroth and Bloomer, 1991; Hemming and Lindroth, 2000; Zhang et al., 2013). Additionally, there is evidence that activation of jasmonate and salicylic acid defenses can increase parasitism or predation of herbivores in many plant species (Dicke et al., 1990; Thaler, 1999; Van Poecke and Dicke, 2002).

In this study, there was a strong effect of cultivar on the abundance of the salicylic acid-related compounds salicylate 2-O-β-D-glucoside, salicin and salicyl-6-hydroxy-2-cyclohexene-on-oyl, while infestation status only had an effect on the levels of salicylate 2-O-β-D-glucoside in infested Dane samples. There was no significant effect of cultivar or infestation status on the abundance of salicortin, however, salicyl-6-hydroxy-2-cyclohexene-on-oyl, the final precursor in salicortin biosynthesis was significantly higher in both oat cultivars (Figure 7). Salicortin itself did decrease in all cultivars of oat and wheat in response to infestation, but this response was not found to be significant. Regardless, as salicyl-6-hydroxy-2-cyclohexene-on-oyl is likely more stable than salicortin *in vivo*, the increased abundance of salicyl-6-hydroxy-2-cyclohexene-on-oyl may indicate an upregulation of the salicortin biosynthesis pathway in oat. In a study of willow *Salix sericea* (Marsh.) subjected to damage by herbivory from various species of beetle, salicortin decreased in the affected leaves four days after the start of damage, possibly due to consumption of leaf tissue high in this compound (Fields and Orians, 2006). Since the tissue collected for our study was very likely to be undamaged by larval feeding, but was collected after larvae were able to feed within the stem for some time, the decrease in salicortin is more likely due to a systemic response or degradation as opposed to a short term induced defense response. Salicortin may be remobilized to damaged regions of the stem where it is rapidly degraded into salicin during larval feeding, which might explain the decrease in levels of salicortin in systemic stem tissue of infested samples.

In the complete dataset, cultivar had an effect on abundance of only one compound derived from the jasmonates biosynthesis pathway, 12-hydroxyjasmonic acid 12-O-β-D-glucoside (tuberonic acid glucoside, TAG), while infestation status had no measurable effect. Two additional jasmonate-related compounds, jasmonoyl-CoA and jasmonoyl-L-isoleucine, were identified in the complete dataset, but cultivar and infestation status had no effect on abundance (data not shown). While not a significant result, TAG decreased with infestation in Choteau and Conan with no change in infested Scholar or Reeder. Conversely, both cultivars of oat showed an increase in TAG abundance in infested samples, although this result was not significant in the complete or oat dataset. After JA is converted to TAG in damaged regions of the plant, it is translocated to undamaged plant tissue where it contributes to down-regulation of genes involved in JA biosynthesis, which may explain the insignificant effect of WSS infestation on JA-associated compounds identified in our analysis (Gidda et al., 2003; Seto et al., 2009).

4.3.2 DIMBOA pathway

2,4-dihydroxy-7-methoxy-1,4-benzoxazin-3-one (DIMBOA) and related 1,4-benzoxazin-3-ones (Bxs) are related to the resistance of cereal species to insects, fungi and bacteria (Niemeyer, 1988). These metabolites are present in plant cells as glucosides, which become available to hydrolyzing enzymes once plant tissues are damaged by insect feeding (Virtanen and Hietala, 1960). Bxs have recently been discovered to play a key role in the stem elongation phase in winter wheat (Xu et al., 2021). Much of the research conducted on this class of molecules has focused on increased levels of DIMBOA-Glc, 2-(2-hydroxy-7-methoxy-1,4-benzoxazin-3-one)-β-D-glucopyranose (HDMBOA-Glc) and 6-methoxy-2-benzoxazolinone (MBOA) in maize resistance to European corn borer, *Ostrinia nubilalis*, however Bxs have also been found to be involved in plant resistance to several species of aphids, as well as larvae from many species (Campos et al., 1989; Niemeyer et al., 1989; Houseman et al., 1992; Ortego et al., 1998). Evidence from previous untargeted proteomics and metabolomics experiments show that Bxs may also be involved in plant response to WSS in spring and winter wheat (Biyiklioglu et al., 2018; Lavergne et al., 2020).

A metabolite putatively identified as DIMBOA was included in our analysis, but abundance was only affected by cultivar in the oat dataset with no differences in the wheat or complete datasets. While all wheat cultivars experienced an increase in abundance of HDMBOA-Glc after infestation, the increase in Conan was insignificant compared to Choteau, Scholar and Reeder (Figure 9). HDMBOA-Glc can be induced during feeding by *O. nubilalis* or upon treatment with jasmonic acid (JA) or chitin derived saccharides in wheat and maize (Oikawa et al., 2001; Oikawa et al., 2002; Dafoe et al., 2011). After hydrolysis of HDMBOA-Glc, HDMBOA decomposes rapidly into MBOA at a faster rate than other known Bxs, and both HDMBOA and MBOA have negative effects on larval growth of Southwestern corn borer, *Diatraea grandiosella* Dyar (Grambow and Lückge, 1986; Hedin et al., 1993). This means that HDMBOA-Glc may be involved in the rapid defense response of wheat to WSS, although it appears that Conan may return to baseline levels more quickly than other cultivars.

In our complete dataset, DIBOA-β-D-glucoside had significantly higher abundance in both oat cultivars compared to all wheat cultivars. While not significant, wheat cultivars experienced an increase in DIBOA-β-D-glucoside upon infestation while both oat cultivars showed a decrease of this metabolite after infestation (Figure 1). The increased abundance of DIBOA-β-D-glucoside in infested wheat samples observed here matches the plant response observed in the hollow-stemmed partially tolerant cultivar Hatcher reported in figures of a previous study of plant metabolomic response to WSS (Lavergne et al., 2020). Conversely, we observed a decrease in DIBOA-β-D-glucoside upon infestation in all oat cultivars. In a separate study of the proteome of infested spring wheat cultivars, downregulation of DIMBOA glucoside β-D-glucosidase, a protein which hydrolyzes DIMBOA-glucoside to DIMBOA and D-glucose, was identified in infested stems of Scholar, but no change was observed in resistant cultivar Choteau (Biyiklioglu et al., 2018). These conflicting results illustrate the complex involvement of this pathway in WSS resistance and are not unexpected, since Bxs vary significantly based on cultivar, growth stage, plant part sampled and time after infestation (Niemeyer et al., 1989; Huang et al., 2006). Adding to the complexity of this response, there is some evidence that Bxs in the diet of cereal aphid species can have a positive effect on aphid predators, maximizing the tritrophic interaction between wheat, aphids and aphid predator *Eriopis connexa* Germar. (Martos et al., 1992). This means that Bxs in the diet of WSS larvae have the potential to impact the fitness of specialist braconid parasitoids that have WSS as their only known host. This possibility, along with the association of Bxs in plant response to WSS infestation and with the specific response of the resistant cultivar Conan show that further exploration of this pathway will be beneficial to understanding WSS resistance.

4.3.3 Indole-3-acetate degradation

Phytohormone indole-3-acetic acid (IAA), is the primary auxin found in plants, and is involved in many aspects of plant development and response including tropism, cell elongation and stem growth, cell division, phloem and xylem differentiation, root initiation, flowering, senescence and abscission (Davies, 2010). Concentrations of IAA in plant tissues is regulated by the plant in several ways, including biosynthesis, degradation, activation, transport in and out of cells, and inactivation via formation of IAA conjugates (Caruso, 1987; Bartel et al., 2001). Despite knowledge of the existence of these regulatory mechanisms, the exact pathways for many are still only partially elucidated (Ljung, 2013). IAA can also be produced by some species of insects in high concentrations, allowing them to form galls, increase nutritive value of plant tissue or overcome structural plant defenses (Tooker and De Moraes, 2010; Tooker and De Moraes, 2011; Dafoe et al., 2013).

In the complete dataset, cultivar had a strong effect on the abundance of several IAA-conjugates and IAA-derived compounds that are involved in indole-3-acetate degradation, while infestation status had no significant effect on the abundance of these compounds. Abundance of 2-oxindole-3-acetyl-L-aspartate, indole-3-acetylglutamate, and indole-3-acetyl-leucine had significantly lower abundance in oat samples compared to wheat, while 3-hydroxy-2-oxindole-3-acetyl-aspartate was significantly higher in oat samples (Figure 8). The function of IAA-leucine appears to be temporary storage to supply free IAA when needed by the cell (for IAA-activation), so the lower abundance observed in oat may indicate that free IAA can be readily provided by degradation of IAA-leucine or IAA-glutamate in wheat (Woodward and Bartel, 2005). IAA-glutamate is also involved in an indole-3-acetate conjugate degradation pathway and may serve as a temporary storage form of IAA since it is easily reconverted to IAA *in vivo* (Hayashi et al., 2021). IAA-glutamate can also be irreversibly oxidized to 2-oxindole-3-acetyl-L-aspartate and further hydrolyzed to 2-oxindole-3-acetic acid, an inactive form of IAA (Hayashi et al., 2021). 3-Hydroxy-2-oxindole-3-acetyl-aspartate was found in lower abundance in oat, with the exception of Dane infested samples. This compound may be involved in degradation of 2-oxindole-3-acetic acid aspartate to 3-O-β-glucosyl-2-oxindole-3-acetyl-aspartate, but it is unknown whether this mechanism can be reversed to provide free IAA (Caspi et al., 2014).

The significantly lower abundance of IAA-glutamate and the decrease that was observed in infested oat, while not significant, suggests that oat may not inactivate IAA to the same extent as in wheat, instead storing it in forms that can be re-activated. In fact, with the exception of Conan, all wheat cultivars experienced an increase in IAA-glutamate upon infestation and also had higher abundance of 2-oxindole-3-acetyl-L-aspartate, the product of the irreversible step of IAA inactivation in both infested and uninfested tissue samples. These results indicate that wheat may respond to WSS infestation by inactivating IAA in the stem, while fully irreversible inactivation of IAA is more variable depending on cultivar.

Free IAA, whether produced by the plant or by insect, can affect insect survival not only through physical consumption, but by altering plant host material for protection or increased nutrient availability. Hessian fly infestation causes elevated levels of IAA without a corresponding induction of jasmonic acid and salicylic acid, leading to increased nutrient availability while simultaneously lowering plant defense activation (Tooker and De Moraes, 2010). In maize, high levels of IAA are excreted in the frass of European corn borer, leading to increased protein accumulation in nearby tissues which provide larvae with more nutritional content, offsetting the decline in growth rates caused by the presence of increased plant defense compounds (Dafoe et al., 2013). IAA application to the larvae of lesser wax moth, *Achoria grisella* not only has an effect on lipid, protein and glycogen levels in the hemolymph of the pest, but also affects hemolymph content of its braconid natural enemy *Apanteles galleriae* (Uçkan et al., 2014). These changes can even have a negative effect on natural enemy populations, increasing adult emergence time after pupation and decreasing overall longevity of *A. galleriae* adults (Uçkan et al., 2011). These studies indicate that further exploration of IAA biosynthesis and degradation pathways may provide more information about the tritrophic interaction between wheat, WSS and their parasitoids.

5 Conclusion

The solid stem phenotype has historically been the most utilized defense against damage and yield loss from WSS infestation, but due to variability in solid stem expression under different growing conditions, and the negative effect of solid stems on braconid parasitoid populations, substantial stem cutting and yield loss can still occur. To support parasitoid populations and maximize the effectiveness of the tritrophic interaction between host, pest and parasitoid, it is necessary to explore new sources of resistance which are not associated with solid stems. Oat exhibits complete resistance to WSS, causing 100% larval mortality to early instar larvae, which makes it a prime candidate for investigating new mechanisms of host plant resistance.

Here, we identified differentially expressed metabolites between cultivars of oat and wheat which were associated with changes to the phenylpropanoid pathway and phospholipid biosynthesis and signaling. Compounds such as O-sinapoylglucarate, O-sinapoylglucarolactone, 2-O-caffeoylglucarate (all are HCAs) and 5-hydroxyconiferyl alcohol are ubiquitous in plants and are generally related to cellular organization and tissue structure. Due to their presence in stem tissue, HCAs as well as membrane and free lipids are directly encountered by foraging females during ovipositor insertions as well as by larvae feeding inside the stem. HCAs can also affect oviposition behavior and larval survival by strengthening the cell wall and inducing changes in overall lignin content and composition, while lipids can serve as signaling molecules, affecting a wide range of downstream defense responses. Additionally, increased abundance of 5-hydroxyconiferyl alcohol in oat suggests that there may be differences in lignin subunit composition that is related to WSS resistance. In oat, several phospho- and galacto- lipids were also found in greater abundance, and both species experienced a decrease in phospholipid abundance after infestation, with the exception of Conan, which has the early stem-solidness phenotype and loses pith as the plant develops. Other studies have also identified a role for the phenylpropanoid pathway in plant defense against wheat stem sawfly, and changes in lipid abundance have known associations with plant resistance in other systems, making these pathways good targets for further exploration (Zhu et al., 2012; Khajuria et al., 2013; Biyiklioglu et al., 2018; Lavergne et al., 2020). Further examination of lignin content and composition in hollow, solid, and early-solid cultivars may reveal differences in stem architecture that influence the behavior of both adult and larval WSS. Additionally, more reliable methods for observing larval behavior in laboratory conditions will also allow for rigorous testing of the dietary requirements of WSS larvae to determine how lipid content or lignin subunit composition might affect larval growth and development.

Differentially expressed metabolites in the response of oat and wheat to infestation by WSS were also found which were associated with the salicylic acid signaling pathway, IAA degradation, and biosynthesis of 1,4-benzoxazin-3-ones (Bxs). Some salicylic acid related compounds were found in higher abundance in oat samples of both cultivars, indicating that salicylic acid pathway defenses may be involved in the defense response to WSS in oat. Additional compounds related to plant defense that were identified in this study indicate the potential for defining the relationships between wheat, WSS and their parasitoids *B. cephi* and *B. lissogaster*. Bxs HDMBD-Glc and DIBOA-β-D-glucoside increased in all wheat cultivars after infestation with the exception of Conan, with oat expressing overall higher abundance of both compounds. Wheat also appears to respond to WSS infestation by inactivating IAA in stem tissues, while irreversible inactivation of IAA is dependent on cultivar. Further study of the effect of 1,4-benzoxazin-3-ones on sawfly development is necessary, especially since other studies of the sawfly system have identified changes in DIMBOA and related compounds in plants infested with WSS and the results have been highly variable (Biyiklioglu et al., 2018; Lavergne et al., 2020). There is evidence that both 1,4-benzoxazin-3-ones and IAA pathway-related compounds not only have an effect on larval pests but can either positively or negatively affect parasitoid populations so it is unclear what this means for braconid parasitoid populations in the WSS tritrophic system.

Ultimately, though solid stems do offer resistance to the plant, continued exploration of the tritrophic interaction between wheat, WSS and their parasitoids will help in mitigating negative effects on this system to maximize the success of control efforts. Additionally, increased abundance of metabolites in oat which are related to lignin biosynthesis and composition as well as increased abundance of several phospho- and galactolipids illustrate the need for further investigation of stem architecture at the molecular level as well as

examination of the developmental and behavioral effects these metabolites have on WSS at all stages of development.

Data availability statement

The original contributions presented in the study are included in the article/Supplementary Material. Further inquiries can be directed to the corresponding author.

Author contributions

MSH: Formal analysis, Writing – original draft. MLH: Data curation, Investigation, Writing – review & editing. AV: Data curation, Investigation, Writing – review & editing. BB: Data curation, Investigation, Writing – review & editing. HB: Conceptualization, Writing – review & editing. DW: Conceptualization, Supervision, Writing – review & editing.

Funding

The author(s) declare financial support was received for the research, authorship, and/or publication of this article. Funding for the Montana State Mass Spectrometry Facility used in this publication was made possible in part by the MJ Murdock Charitable Trust, the National Institute of General Medical Sciences of the National Institutes of Health under Award Numbers P20GM103474 and S10OD28650, and the MSU Office of Research and Economic Development. The content is solely the responsibility of the authors and does not necessarily represent the official views of the National Institutes of Health. This research was also supported by grants from the Montana Wheat and Barley Committee and by USDA National Institute of Food and Agriculture.

Acknowledgments

The authors would like to thank Dr. Fernando Guillen-Portal and Dr. Ani Akpinar for comments and advice during the preparation of an early version of this manuscript. This manuscript has been released as part of a dissertation (Hager, 2023).

Conflict of interest

Author AV was employed by company Corteva Agriscience™.

The remaining authors declare that the research was conducted in the absence of any commercial or financial relationships that could be construed as a potential conflict of interest.

Publisher's note

Supplementary material

The Supplementary Material for this article can be found online at: https://www.frontiersin.org/articles/10.3389/fpls.2024.1327390/full#supplementary-material

SUPPLEMENTARY FIGURE 1
Experimental setup for greenhouse infestation by WSS

SUPPLEMENTARY FIGURE 2
Principal component analysis (PCA) score plots for oat cultivars Dane and Otana. PCA plots were created using LC-MS data from control and infested plants two weeks after caging with each point representing a stem sample. Dane, green; Otana, yellow; Control, circle; Infested, triangle.

SUPPLEMENTARY FIGURE 3
Oat dataset - Biochemical pathway associations of significant compounds in the oat dataset. The oat dataset consisted of all oat samples from infested and control plants. Significant compounds (p-values<0.05) were identified using two-way ANOVA and Fishers LSD *post-hoc* test.

SUPPLEMENTARY FIGURE 4
Classifications of significant, putatively identified metabolites in the oat dataset. Significant compounds (p-values<0.05) were identified using two-way ANOVA and Fishers LSD *post-hoc* test with FDR correction. The innermost circle indicates the compound class with the outer ring representing compound subclass. Carbohydrate and derivatives, purple; carbonyl compound, orange; lipid, grey; organic heterocyclic compound, brown; organic hydroxy compound, yellow; organonitrogen compound, light blue; organooxygen compound, light green; organophosphorus compound, dark green; organosulfur compound, dark blue; polyatomic ion, red.

SUPPLEMENTARY FIGURE 5
Principal component analysis (PCA) score plots for wheat cultivars Choteau, Conan, Reeder and Scholar. PCA plots were created using LC-MS data from control and infested plants two weeks after caging with each point representing a stem sample. Choteau, orange; Conan, blue; Reeder, red; Scholar, pink; Control, circle; Infested, triangle.

SUPPLEMENTARY TABLE 1
Log2 fold changes between infested and control samples of oat and wheat.

SUPPLEMENTARY TABLE 2
PCA loadings for the oat and wheat complete dataset.

SUPPLEMENTARY TABLE 3
Significant compounds identified from the oat and wheat complete dataset. Significant compounds (p-values<0.05) were identified using two-way ANOVA and Fishers LSD *post-hoc* test with FDR correction.

SUPPLEMENTARY TABLE 4
Results from Fisher's LSD *post-hoc* test.

SUPPLEMENTARY TABLE 5
PCA loadings for the oat dataset.

SUPPLEMENTARY TABLE 6
Significant compounds identified from the oat dataset. Significant compounds (p-values<0.05) were identified using two-way ANOVA and Fishers LSD *post-hoc* test with FDR correction.

SUPPLEMENTARY TABLE 7
PCA loadings for the wheat dataset.

SUPPLEMENTARY TABLE 8
Significant compounds identified from the wheat dataset. Significant compounds (p-values<0.05) were identified using two-way ANOVA and Fishers LSD *post-hoc* test with FDR correction.

SUPPLEMENTARY TABLE 9
Complete oat and wheat dataset. Relative abundances of each compound for all oat and wheat stem samples, m/z ratio, retention time and predicted formula.

References

Achhami, B. B., Peterson, R. K. D., Sherman, J. D., Reddy, G. V. P., and Weaver, D. K. (2020). Multiple decrement life tables of *Cephus cinctus* Norton (Hymenoptera: Cephidae) across a set of barley cultivars: the importance of plant defense versus cannibalism. *PloS One* 15, 1–18. doi: 10.1371/journal.pone.0238527

Ainslie, C. N. (1920). *The Western Grass-Stem Sawfly. Bulletin no. 841* (Washington D. C.: United States Department of Agriculture).

Anyanga, M. O., Farman, D. I., Ssemakula, G. N., Mwanga, R. O. M., Stevenson,, and P., C. (2021). Effects of hydroxycinnamic acid esters on sweetpotato weevil feeding and oviposition and interactions with *Bacillus thuringiensis* proteins. *J. Pest Sci.* 94, 783–794. doi: 10.1007/s10340-020-01297-5

Bakaze, E., Dzomeku, B. M., and Wünsche, J.-N. (2020). Banana Defence Responses to *Cosmopolites sordidus* Feeding and Methyl Jasmonate application. *Ann. Appl. Biol.* 178, 98–108. doi: 10.1111/aab.12638

Barros-Rios, J., Malvar, R. A., Jung, H.-J. G., and Santiago, R. (2011). Cell wall composition as a maize defense mechanism against corn borers. *Phytochemistry* 72, 365–371. doi: 10.1016/j.phytochem.2011.01.004

Bartel, B., Leclere, S., Magidin, M., and Zolman, B. K. (2001). Inputs to the active indole-3-acetic acid pool: *de novo* synthesis, conjugate hydrolysis, and indole-3-butyric acid β-oxidation. *J. Plant Growth Regul.* 20, 198–216. doi: 10.1007/s003440010025

Beres, B. L., Hill, B. D., Carcamo, H., Knodel, J., Weaver, D., and Cuthbert, R. D. (2017). An artificial neural network model to predict wheat stem sawfly cutting in solid-stemmed wheat cultivars. *Can. J. Plant Sci.* 97, 329–336. doi: 10.1139/CJPS-2016-0364

Bi, C., Chen, F., Jackson, L., Gill, B. S., and Li, W. (2010). Expression of Lignin Biosynthetic Genes in Wheat during Development and upon Infection by Fungal Pathogens. *Plant Mol. Biol. Rep.* 29, 149–161. doi: 10.1007/s11105-010-0219-8

Biyiklioglu, S., Alptekin, B., Akpinar, B. A., Varella, A. C., Hofland, M. L., Weaver, D. K., et al. (2018). A large-scale multiomics analysis of wheat stem solidness and the wheat stem sawfly feeding response, and syntenic associations in barley, *Brachypodium*, and rice. *Funct. Integr. Genomics* 18, 241–259. doi: 10.1007/s10142-017-0585-5

Bodenhausen, N., and Reymond, P. (2007). Signaling pathways controlling induced resistance to insect herbivores in Arabidopsis. *MPMI* 20, 1406–1420. doi: 10.1094/MPMI-20-11-1406

Bruessow, F., Gouhier-Darimont, C., Buchala, A., Metraux, J.-P., and Reymond, P. (2010). Insect eggs suppress plant defence against chewing herbivores. *Plant J.* 62, 876–885. doi: 10.1111/j.1365-313X.2010.04200.x

Buhl, C., Meilan, R., and Lindroth, R. L. (2017). Genetic Modification of Lignin in Hybrid Poplar (*Populus alba* x *Populus tremula*) Does Not Substantially Alter Plant Defense or Arthropod Communities. *J. Insect Sci.* 17, 1–8. doi: 10.1093/jisesa/iex035

Buteler, M., Peterson, R. K. D., Hofland, M. L., Weaver,, and D., K. (2015). A multiple decrement life table reveals that host plant resistance and parasitism are major causes of mortality for the wheat stem sawfly. *Environ. Entomology* 44, 1571–1580. doi: 10.1093/ee/nvv128

Campos, F., Atkinson, J., Arnason, J. T., Philogene, B. J. R., Morand, P., Werstiuk, N. H., et al. (1989). Toxicokinetics of 2,4-dihydroxy-7-methoxy-1,4-benzoxazin-3-one (DIMBOA) in the European corn borer, *Ostrinia nubilalis* (Hübner). *J. Chem. Ecol.* 15, 1989–2001. doi: 10.1007/BF01207432

Caruso, J. L. (1987). The auxin conjugates. *HortScience* 22, 1201–1204. doi: 10.21273/HORTSCI.22.6.1201

Caspi, R., Altman, T., Billington, R., Dreher, K., Foerster, H., Fulcher, C. A., et al. (2014). The metaCyc database of metabolic pathways and enzymes and the bioCyc collection of pathway/genome databases. *Nucleic Acids Res.* 42, D459–D471. doi: 10.1093/nar/gkt1103

Chambers, M. C., Maclean, B., Burke, R., Amode, D., Ruderman, D. L., Neumann, S., et al. (2012). A cross-platform toolkit for mass spectrometry and proteomics. *Nat. Biotechnol.* 30, 918–920. doi: 10.1038/nbt.2377

Cockrell, D. M., Griffin-Nolan, R. J., Rand, T. A., Altilmisani, N., Ode, P. J., and Peairs, F. (2017). Host plants of the wheat stem sawfly (Hymenoptera: Cephidae). *Environ. Entomology* 46, 847–854. doi: 10.1093/ee/nvx104

Cook, J. P., Weaver, D. K., Varella, A. C., Sherman, J. D., Hofland, M. L., Heo, H. Y., et al. (2019). Comparison of three alleles at a major solid stem QTL for wheat stem sawfly resistance and agronomic performance in hexaploid wheat. *Crop Sci.* 59, 1639–1647. doi: 10.2135/cropsci2019.01.0009

Cook, J. P., Wichman, D. M., Martin, J. M., Bruckner, P. L., Talbert,, and L., E. (2004). Identification of microsatellite markers associated with a stem solidness locus in wheat. *Crop Sci.* 44, 1397–1402. doi: 10.2135/cropsci2004.1397

Criddle, N. (1917). Further observations upon the habits of the western wheat-stem sawfly in Manitoba and Saskatchewan. *Agric. Gazette* 4, 176–177.

Criddle, N. (1923). *Life Habits of Cephus cinctus Nort. in Manitoba* Vol. 55 (Ottawa, ON: The Canadian Entomologist), 1–4.

Dafoe, N. J., Huffaker, A., Vaughan, M. M., Duehl, A. J., Teal, P. E., Schmelz,, et al. (2011). Rapidly Induced Chemical defenses in maize stems and their effects on short-term growth of *Ostrinia nubilalis*. *J. Chem. Ecol.* 37, 984–991. doi: 10.1007/s10886-011-0002-9

Dafoe, N. J., Thomas, J. D., Shirk, P. D., Legaspi, M. E., Vaughan, M. M., Huffaker, A., et al. (2013). European corn borer (*Ostrinia nubilalis*) induced responses enhance susceptibility in maize. *PloS One* 8, 1–18. doi: 10.1371/journal.pone.0073394

Davies, P. J. (2010). *Plant Hormones: Biosynthesis, Signal Transduction, Action* (Boston, MA: Springer Science and Business Media).

Delaney, K. J., Weaver, D. K., and Peterson, R. K. D. (2010). Photosynthesis and yield reductions from wheat stem sawfly (Hymenoptera: Cephidae): interactions with wheat solidness, water stress, and phosphorus deficiency. *J. Economic Entomology* 103, 516–524. doi: 10.1603/EC09229

Dicke, M., Van Beek, T. A., Posthumus, M. A., Ben Dom, N., Van Bokhoven, H., and De Groot, A. (1990). Isolation and identification of volatile kairomone that affects acarine predator-prey interactions. *J. Chem. Ecol.* 16, 381–396. doi: 10.1007/BF01021772

Dixon, R. A., Achnine, L., Kota, P., Liu, C.-J., Srinivasa Reddy, ,. M. S., and Wang, L. (2002). The phenylpropanoid pathway and plant defence - a genomics perspective. *Mol. Plant Pathol.* 3, 371–390. doi: 10.1046/j.1364-3703.2002.00131.x

Elder, T., Berstis, L., Beckham, G. T., and Crowley, M. F. (2016). Coupling and reactions of 5-hydroxyconiferyl alcohol in lignin formation. *J. Agric. Food Chem.* 64, 4742–4750. doi: 10.1021/acs.jafc.6b02234

Erb, M., Meldau, S., and Howe, G. A. (2012). Role of phytohormones in insect-specific plant reactions. *Trends Plant Sci.* 17, 250–259. doi: 10.1016/j.tplants.2012.01.003

Facchini, P. J., Hagel, J., and Zulak, K. G. (2002). Hydroxycinnamic acid amide metabolism: physiology and biochemistry. *Can. J. Bot.* 80, 577–589. doi: 10.1139/b02-065

Farstad, C. (1940). *The development of Western Wheat stem Sawfly (Cephus cinctus Norton) in Various Host Plants as an Index of Resistance* (Ames, (IA: Iowa State College).

Fields, M. J., and Orians, C. M. (2006). Specificity of phenolic glycoside induction in willow seedlings (*Salix sericea*) in response to herbivory. *J. Chem. Ecol.* 32, 2647–2656. doi: 10.1007/s10886-006-9188-7

Frank, W., Munnik, T., Kerkmann, K., Salamini, F., and Bartels, D. (2000). Water deficit triggers phospholipase D activity in the resurrection plant *Craterostigma plantagineum*. *Plant Cell* 12, 11–123. doi: 10.1105/tpc.12.1.111

Gao, Q., Yu, K., Kachroo, A., and Kachroo, P. (2014). Mono- and digalactodiacylglycerol lipids function nonredundantly to regulate systemic acquired resistance in plants. *Cell Rep.* 9, 1681–1691. doi: 10.1016/j.celrep.2014.10.069

Gidda, S. K., Miersch, O., Levitin, A., Schmidt, J., Wasternack, C., and Varin, L. (2003). Biochemical and molecular characterization of a hydroxyjasmonate sulfotransferase from *Arabidopsis thaliana*. *J. Biol. Chem.* 278, 17895–17900. doi: 10.1074/jbc.M211943200

Grambow, H. J., and Lückge, J. (1986). Occurrence of 2-(2-Hydroxy-4,7-dimethoxy-2H-1,4,benzoxazin-3-one)-β-D-glucopyranoside in *Triticum aestivum* Leaves and Its Conversion into 6-Methoxy-benzoxazoline. *Z. für Naturforschung* 41c, 684–690. doi: 10.1515/znc-1986-7-804

Grandmaison, J., Olah, G. M., Van Calsteren, M.-R., and Furlan, V. (1993). Characterization and localization of plant phenolics likely involved in the pathogen resistance expressed by endomycorrhizal roots. *Mycorrhiza* 3, 155–164. doi: 10.1007/BF00203609

Gunnaiah, R., Kushalappa, A. C., Duggavathi, R., Fox, S., and Somers, D. J. (2012). Integrated metabolo-proteomic approach to decipher the mechanisms by which wheat QTL (*Fhb1*) contributes to resistance against *Fusarium graminearum*. *PloS One* 7, 1–15. doi: 10.1371/journal.pone.0040695

Hager, M. S. (2023). *Elucidation of Mechanisms of Host Plant Resistance to Wheat Stem Sawfly (Cephus cinctus Norton) in Relation to Antibiosis and the Early Stem Solidness Phenotype* (Bozeman, (MT: Montana State University).

Hastings, J., Owen, G., Dekker, A., Ennis, M., Kale, N., Muthukrishnan, V., et al. (2016). ChEBI in 2016: improved services and an expanding collection of metabolites. *Nucleic Acids Res.* 44, D1214–D1219. doi: 10.1093/nar/gkv1031

Hayashi, K., Arai, K., Aoi, Y., Tanaka, Y., Hira, H., Guo, R., et al. (2021). The main oxidative inactivation pathway of the plant hormone auxin. *Nat. Commun.* 12, 1–11. doi: 10.1038/s41467-021-27020-1

Hedin, P. A., Davis, F. M., and Williams, W. P. (1993). 2-Hydroxy-4,7-dimethoxy-1,4-benzoxazin-3-one (N-O-ME-DIMBOA), a possible toxic factor in corn to the southwestern corn borer. *J. Chem. Ecol.* 19, 531–542. doi: 10.1007/BF00994323

Hemming, J. D. C., and Lindroth, R. L. (2000). Effect of phenolic glycosides and protein on gypsy moth (Lepidoptera: Lymantriidae) and forest tent caterpillar (Lepidoptera: Lasiocampidae) performance and detoxification activities. *Environ. Entomology* 29, 1108–1115. doi: 10.1603/0046-225X-29.6.1108

Holmes, N. D., and Peterson, L. K. (1960). The influence of the host on oviposition by the wheat stem sawfly, *Cephus cinctus* nort. (Hymenoptera: Cephidae). *Can. J. Plant Sci.* 40, 29–46. doi: 10.4141/cjps60-004

Holmes, N. D., and Peterson, L. K. (1964). Resistance to the wheat stem sawfly, *Cephus cinctus* nort. *Can. Entomologist* 96, 120. doi: 10.4039/Ent96120-1

Houseman, J. G., Campos, F., Thie, N. M. R., Philogene, B. J. R., Atkinson, J., Morand, P., et al. (1992). Effect of the maize-derived compounds DIMBOA and MBOA on growth and digestive processes of European corn borer (Lepidoptera: Pyralidae). *J. Economic Entomology* 85, 669–674. doi: 10.1093/jee/85.3.669

Howe, G. A., and Jander, G. (2008). Plant immunity to insect herbivores. *Annu. Rev. Plant Biol.* 59, 41–66. doi: 10.1146/annurev.arplant.59.032607.092825

Huang, C., Wang, X., Wang, R., Xue, K., Yan, F., and Xu, C. (2006). Distribution and variations of three 1,4-benzoxazin-3-ones in maize induced by the Asian corn borer, *Ostrinia furnacalis* (Guenee). *Z. für Naturforsch.* 61c, 257–262. doi: 10.1515/znc-2006-3-417

Kärkönen, A., Tapanila, T., Laasko, T., Seppänen, M. M., Isolahti, M., Hyrkäs, M., et al. (2014). Effect of lignin content and subunit composition on digestibility in clones of timothy (*Phleum pratense* L.). *J. Agric. Food Chem.* 62, 6091–6099. doi: 10.1021/jf5016494

Kashyap, A., Jiménez-Jiménez, A. L., Zhang, W., Capellades, M., Srinivasan, S., Laromaine, A., et al. (2022). Induced ligno-suberin vascular coating and tyramine-derived hydroxycinnamic acid amides restrict *Ralstonia solanacearum* colonization in resistant tomato. *New Phytol.* 234, 1411–1429. doi: 10.1111/nph.17982

Katajamaa, M., and Orešič, M. (2007). Data processing for mass spectrometry-based metabolomics. *J. Chromatogr. A* 1158, 318–328. doi: 10.1016/j.chroma.2007.04.021

Kato-Noguchi, H., Kosemura, S., Yamamura, S., Mizutani, J., and Hasegawa, K. (1994). Allelopathy of oats. I. Assessment of allelopathic potential of extract of oat shoots and identification of an allelochemical. *J. Chem. Ecol.* 20, 309–314. doi: 10.1007/BF02064439

Khajuria, C., Wang, H., Liu, X., Wheeler, S., Reese, J. C., El Bouhssini, M., et al. (2013). Mobilization of lipids and fortification of cell wall and cuticle are important in host defense against Hessian fly. *BMC Genomics* 14, 1–16. doi: 10.1186/1471-2164-14-423

Kosma, D. K., Nemacheck, J. A., Jenks, M. A., and Williams, C. E. (2010). Changes in properties of wheat leaf cuticle during interactions with Hessian fly. *Plant J.* 63, 31–43. doi: 10.1111/j.1365-313X.2010.04229.x

Lavergne, F. D., Broeckling, C. D., Brown, K. J., Cockrell, D. M., Haley, S. D., Peairs, F. B., et al. (2020). Differential stem proteomics and metabolomics profiles for four wheat cultivars in response to the insect pest wheat stem sawfly. *J. Proteome Res.* 19, 1037–1051. doi: 10.1021/acs.jproteome.9b00561

Laxalt, A. M., and Munnik, T. (2002). Phospholipid signalling in plant defence. *Curr. Opin. Plant Biol.* 5, 1–7. doi: 10.1016/S1369-5266(02)00268-6

Lee, S., Suh, S., Kim, S., Crain, R. C., Kwak, J. M., Nam, H.-G., et al. (1997). Systemic elevation of phosphatidic acid and lysophospholipid levels in wounded plants. *Plant J.* 12, 547–556. doi: 10.1046/j.1365-313X.1997.00547.x

Li, Y., Beisson, F., Koo, A. J. K., Molina, I., Pollard, M., and Ohlrogge, J. (2007). Identification of acyltransferases required for cutin biosynthesis and production of cutin with suberin-like monomers. *PNAS* 104, 18339–18344. doi: 10.1073/pnas.0706984104

Li, X., Yang, Y., Li, G., Li, H., Wang, Q., and Wan, L. (2014). The effect of dietary fat levels on the size and development of *Chrysomya megacephala* (Diptera: Calliphoridae). *J. Insect Sci.* 14, 1–5. doi: 10.1093/jisesa/ieu036

Liao, S., Amcoff, M., and Nässel, D. R. (2021). Impact of high-fat diet on lifespan, metabolism, fecundity and behavioral senescence in *Drosophilia*. *Insect Biochem. Mol. Biol.* 133, 103495–103510. doi: 10.1016/j.ibmb.2020.103495

Lima, R. B., Salvador, V. H., Dos Santos, W. D., Bubna, G. A., Finger-Teixeira, A., Soares, A. R., et al. (2013). Enhanced lignin monomer production caused by cinnamic acid and its hydroxylated derivatives inhibits soybean root growth. *PloS One* 8, 1–8. doi: 10.1371/journal.pone.0080542

Lindroth, R. L., and Bloomer, M. S. (1991). Biochemical ecology of the forest tent caterpillar: responses to dietary protein and phenolic glycosides. *Oecologia* 86, 408–413. doi: 10.1007/BF00317609

Lindroth, R. L., and Peterson, S. S. (1988). Effects of plant phenols on performance of southern armyworm larvae. *Oecologia* 75, 185–189. doi: 10.1007/BF00378595

Liscovitch, M., Czarny, M., Fiucci, G., and Tang, X. (2000). Phospholipase D: molecular and cell biology of a novel gene family. *Biochem. J.* 345, 401–415. doi: 10.1042/bj3450401

Ljung, K. (2013). Auxin metabolism and homeostasis during plant development. *Development* 140, 943–950. doi: 10.1242/dev.086363

Macedo, T. B., Peterson, R. K. D., Weaver, D. K., and Morrill, W. L. (2005). Wheat stem sawfly, *Cephus cinctus* Norton, impact on wheat primary metabolism: an ecophysiological approach. *Environ. Entomology* 34, 719–726. doi: 10.1603/0046-225X-34.3.719

Martos, A., Givovich, A., and Niemeyer, H. M. (1992). Effect of DIMBOA, an aphid resistance factor in wheat, on the aphid predator *eriopis connexa* germar (Coleoptera: Coccinellidae). *J. Chem. Ecol.* 18, 469–479. doi: 10.1007/BF00994245

McGinnis, A. J., and Kasting, R. (1961). Comparison of tissues from solid- and hollow-stemmed spring wheats during growth. *Can. J. Plant Sci.* 41, 469–478. doi: 10.4141/cjps61-071

McNeal, F. H., Watson, C. A., Berg, M. A., and Wallace, L. E. (1965). Relationship of stem solidness to yield and lignin content in wheat selections. *Agron. J.* 57, 20–21. doi: 10.2134/agronj1965.00021962005700010007x

Morrill, W. L., Kushnak, G. D., and Gabor, J. W. (1998). Parasitism of the wheat stem sawfly (Hymenoptera: Cephidae) in montana. *Biol. Control* 12, 159–163. doi: 10.1006/bcon.1998.0629

Munnik, T., Irvine, R. F., and Musgrave, A. (1998). Phospholipid signalling in plants. *Biochim. Biophys. Acta* 1389, 222–272. doi: 10.1016/S0005-2760(97)00158-6

Niemeyer, H. M. (1988). Hydroxamic acids (4-hydroxy-1,4-benzoxazin-3-ones), defence chemicals in the gramineae. *Phytochemistry* 27, 3349–3358. doi: 10.1016/0031-9422(88)80731-3

Niemeyer, H. M., Pesel, E., Copaja, S. V., Bravo, H. R., Franke, S., and Francke, W. (1989). Changes in hydroxamic acid levels of wheat plants induced by aphid feeding. *Phytochemistry* 28, 447–449. doi: 10.1016/0031-9422(89)80029-9

Nilsen, K. T., Clarke, J. M., Beres, B. L., and Pozniak, C. J. (2016). Sowing density and cultivar effects on pith expression in solid-Stemmed durum wheat. *Agron. J.* 108, 219–228. doi: 10.2134/agronj2015.0298

Nilsen, K. T., N'diaye, A., Maclachlan, P. R., Clarke, J. M., Ruan, Y., Cuthbert, R. D., et al. (2017). High density mapping and haplotype analysis of the major stem-solidness locus *SSt1* in durum and common wheat. *PloS One* 12, e0175285. doi: 10.1371/journal.pone.0175285

Oikawa, A., Ishihara, A., Hasegawa, M., Kodama, O., and Iwamura, H. (2001). Induced accumulation of 2-hydroxy-4,7-dimethoxy-1,4,benzoxazin-3-one glucoside (HDMBOA-glc) in maize leaves. *Phytochemistry* 56, 669–675. doi: 10.1016/S0031-9422(00)00494-5

Oikawa, A., Ishihara, A., and Iwamura, H. (2002). Induction of HDMBOA-glc accumulation and DIMBOA-glc-4-O-methyltransferase by jasmonic acid in poaceous plants. *Phytochemistry* 61, 331–337. doi: 10.1016/S0031-9422(02)00225-X

Ortego, F., Ruiz, M., and Castanera, P. (1998). Effect of DIMBOA on growth and digestive physiology of *Sesamia nonagrioides* (Lepidoptera: Noctuidae) larvae. *J. Insect Physiol.* 44, 95–101. doi: 10.1016/S0022-1910(97)00103-0

Pang, Z., Chong, J., Li, S., and Xia, J. (2020). MetaboAnalystR 3.0: toward an optimized workflow for global metabolomics. *Metabolites* 10, 186. doi: 10.3390/metabo10050186

Pérez, F. J., and Ormeño-Nuñez, J. (1991). Root exudates of wild oats: alleleopathic effect on spring wheat. *Phytochemistry* 30, 2199–2202. doi: 10.1016/0031-9422(91)83614-Q

Pluskal, T., Castillo, S., Villar-Briones, A., and Orešič, M. (2010). MZmine 2: modular framework for processing, visualizing, and analyzing mass spectrometry-based molecular profile data. *BMC Bioinf.* 11, 395.

Poerschmann, J., Gathmann, A., Augustin, J., Langer, U., and Górecki, T. (2005). Molecular composition of leaves and stems of genetically modified Bt and near-isogenic non-bt maize - characterization of lignin patterns. *J. Environ. Qual.* 34, 1508–1518. doi: 10.2134/jeq2005.0070

Rand, T. A., Richmond, C. E., and Dougherty, E. T. (2020). Modeling the combined impacts of host plant resistance and biological control on the population dynamics of a major pest of wheat. *Pest Manage. Sci.* 76, 2818–2828. doi: 10.1002/ps.5830

Rand, T. A., Waters, D. K., Shanower, T. G., and Berzonsky, W. A. (2012). Effects of genotypic variation in stem solidity on parasitism of a grass-mining insect. *Basic Appl. Ecol.* 13, 250–259. doi: 10.1016/j.baae.2012.03.005

Roemhild, G. R. (1954). Morphological Resistance of Some of the Gramineae to the Wheat Stem Sawfly (*Cephus cinctus* Norton) (Bozeman (MT: Montana State College).

Schumacher, W. J., Thill, D. C., and Lee, G. A. (1983). Allelopathic Potential of Wild Oat (*Avena fatua*) on Spring Wheat (*Triticum aestivum*) Growth. *J. Chem. Ecol.* 9, 1235–1245. doi: 10.1007/BF00982225

Seto, Y., Hamada, S., Matsuura, H., Matsushige, M., Satou, C., Takahashi, K., et al. (2009). Purification and cDNA cloning of a wound inducible glucosyltransferase active toward 12-hydroxy jasmonic acid. *Phytochemistry* 70, 370–379. doi: 10.1016/j.phytochem.2009.01.004

Sewalt, V. J. H., Ni, W., Jung, H. G., and Dixon, R. A. (1997). Lignin impact on fiber degradation: increased enzymatic digestibility of genetically engineered tobacco (*Nicotiana tabacum*) stems reduced in lignin content. *J. Agric. Food Chem.* 45, 1977–1983. doi: 10.1021/jf9609690

Sherman, J. D., Weaver, D. K., Hofland, M. L., Sing, S. E., Buteler, M., Lanning, S. P., et al. (2010). Identification of novel QTL for sawfly resistance in wheat. *Crop Sci.* 50, 73–86. doi: 10.2135/cropsci2009.03.0145

Sing, S. E. (2002). *Spatial and Biotic Interactions of the Wheat Stem Sawfly with Wild oat and Montana Dryland Spring Wheat* (Bozeman (MT: Montana State University).

Stotz, H. U., Koch, T., Biedermann, A., Weniger, K., Boland, W., and Mitchell-Olds, T. (2002). Evidence for regulation of resistance in Arabidopsis to Egyptian cotton worm by salicylic and jasmonic acid signaling pathways. *Planta* 214, 648–652. doi: 10.1007/s004250100656

Strack, D., Gross, W., Heilemann, J., Keller, H., and Ohm, S. (1988). Enzymic synthesis of hydroxycinnamic acid esters of glucaric acid and hydroaromatic acids from the respective 1-O-hydroxycinnamoylglucoside and hydroxycinnamoyl-coenzyme A thioester as acyldonors with a protein preparation from *Cestrum elegans* leaves. *Z. für Naturforschung* 43c, 32–36. doi: 10.1515/znc-1988-1-209

Strack, D., Keller, H., and Weissenböck, G. (1987). Enzymatic synthesis of hydroxycinnamic acid esters of sugar acids and hydroaromatic acids by protein preparations from rye (*Secale cerale*) primary leaves. *J. Plant Physiol.* 131, 61–73. doi: 10.1016/S0176-1617(87)80268-7

Straub, C. S., Faselt, J. ,. A., Keyser, E. S., and Traugott, M. (2020). Host plant resistance promotes a secondary pest population. *Ecosphere* 11, 1–12. doi: 10.1002/ecs2.3073

Subedi, M., Cárcamo, H. A., Knodel, J. J., Weaver, D. K., Cuthbert, R. D., Pozniak, C. J., et al. (2021). Stability analysis of stem solidness, grain yield and grain protein

concentration in spring wheat. *Can. J. Plant Sci.* 101, 456–475. doi: 10.1139/cjps-2020-0089

Talbert, L. E., Sherman, J. D., Hofland, M. L., Lanning, S. P., Blake, N. K., Grabbe, R., et al. (2014). Resistance to *Cephus cinctus* Norton, the wheat stem sawfly, in a recombinant inbred line population of wheat derived from two resistance sources. *Plant Breed.* 133, 427–432. doi: 10.1111/pbr.12184

Team, R. C (2022) *R: A language and Environment for Statistical Computing*. Available at: https://www.R-project.org (Accessed August 1, 2023).

Thaler, J. S. (1999). Jasmonate-inducible plant defences cause increased parasitism of herbivores. *Nature* 399, 686–687. doi: 10.1038/21420

Tooker, J. F., and De Moraes, C. M. (2010). Feeding by Hessian Fly (*Mayetiola destructor* [Say]) Larvae on Wheat Increases Levels of Fatty Acids and Indole-3-Acetic Acid but not Hormones Involved in Plant-Defense Signaling. *J. Plant Growth Regul.* 30, 158–165. doi: 10.1007/s00344-010-9177-5

Tooker, J. F., and De Moraes, C. M. (2011). Feeding by a gall-inducing caterpillar species alters levels of indole-3-acetic and abscisic acid in *Solidago altissima* (Asteraceae) stems. *Arthropod-Plant Interact.* 5, 115–124. doi: 10.1007/s11829-010-9120-5

Turunen, S. (1979). Digestion and absorption of lipids in insects. *Comp. Biochem. Physiol.* 63A, 455–460. doi: 10.1016/0300-9629(79)90171-3

Uçkan, F., Haftaci, İ., and Ergın, E. (2011). Effects of indol-3-acetic acid on biological parameters of the larval endoparasitoid *Apanteles galleriae* (Hymenoptera: Braconidae). *Ann. Entomological Soc. America* 104, 77–82. doi: 10.1603/AN10098

Uçkan, F., Soydabaş, H. K., and Özbek, R. (2014). Effect of Indol-3-acetic Acid on the Biochemical Parameters of *Achoria grisella* hemolymph and *Apanteles galleriae* larva. *Pakistan J. Biotechnol.* 11, 163–171.

Van Der Luit, A. H., Piatti, T., Van Doorn, A., Musgrave, A., Felix, G., Boller, T., et al. (2000). Elicitation of suspension-cultured tomato cells triggers the formation of phosphatidic acid and diacylglycerol pyrophosphate. *Plant Physiol.* 123, 1507–1515. doi: 10.1104/pp.123.4.1507

Van Poecke, R. M. P., and Dicke, M. (2002). Induced parasitoid attraction by *Arabidopsis thaliana*: involvement of the octadecanoid and the salicylic acid pathway. *J. Exp. Bot.* 53, 1793–1799. doi: 10.1093/jxb/erf022

Varella, A. C., Talbert, L. E., Hofland, M. L., Buteler, M., Sherman, J. D., Blake, N. K., et al. (2016). Alleles at a quantitative trait locus for stem solidness in wheat affect temporal patterns of pith expression and level of resistance to the wheat stem sawfly. *Plant Breed.* 135, 546–551. doi: 10.1111/pbr.12398

Varella, A. C., Weaver, D. K., Peterson, R. K., Sherman, J. D., Hofland, M. L., Blake, N. K., et al. (2017). Host plant quantitative trait loci affect specific behavioral sequences in oviposition by a stem-mining insect. *Theor. Appl. Genet.* 130, 187–197. doi: 10.1007/s00122-016-2805-0

Virtanen, A. I., and Hietala, P. K. (1960). Precursors of benzoxazolinone in rye plants I. Precursor II, the aglucone. *Acta Chemica Scandinavica* 14, 499–502. doi: 10.3891/acta.chem.scand.14-0499

Wainhouse, D., Cross, D. J., and Howell, R. S. (1990). The Role of Lignin as a Defence against the Spruce Bark Beetle Dendroctonus micans: Effect on Larvae and Adults. *Oecologia* 85, 257–265. doi: 10.1007/BF00319411

Wallace, L. E., and McNeal, F. H. (1966). *Stem Sawflies of Economic Importance in Grain Crops in the United States* (Washington D.C.: Technical Bulletin United States Department of Agriculture), 1350.

Weaver, D. K., Sing, S. E., Runyon, J. B., and Morrill, W. L. (2004). Potential impact of cultural practices on wheat stem sawfly (Hymenoptera: Cephidae) and associated parasitoids. *J. Agric. Urban Entomology* 21, 271–287.

Wong, M. L., Bruckner, P. L., Berg, J. E., Lamb, P. F., Hofland, M. L., Caron, C. G., et al. (2022). Evaluation of Wheat Stem Sawfly-resistant Solid Stem *Qss.msub-3BL* alleles in hard red winter wheat. *Crop Sci.* 63, 556–567. doi: 10.1002/csc2.20866

Woodward, A. W., and Bartel, B. (2005). Auxin: regulation, action and interaction. *Ann. Bot.* 95, 707–735. doi: 10.1093/aob/mci083

Xu, D., Xie, Y., Guo, H., Zeng, W., Xiong, H., Zhao, L., et al. (2021). Transcriptome analysis reveals a potential role of benzoxazinoid in regulating stem elongation in the wheat mutant *qd*. *Front. Genet.* 12, 623861. doi: 10.3389/fgene.2021.623861

Zadoks, J. C., Chang, T. T., and Konzak, C. F. (1974). A decimal code for the growth stages of cereals. *Weed Res.* 14, 415–421. doi: 10.1111/j.1365-3180.1974.tb01084.x

Zhang, H.-J., Faucher, C. P., Anderson, A., Berna, A. Z., Trowell, S., Chen, Q.-M., et al. (2013). Comparisons of Contact Chemoreception and Food Acceptance by Larvae of Polyphagous *Helicoverpa armigera* and Oligophagous *Bombyx mori*. *J. Chem. Ecol.* 39, 1071–1080. doi: 10.1007/s10886-013-0303-2

Zhang, S.-H., Yang, Q., and Ma, R.-C. (2007). *Erwinia carotovora* ssp. carotovora Infection Induced "Defense Lignin" Accumulation and Lignin Biosynthetic Gene Expression in Chinese Cabbage (*Brassica rapa* L. ssp. *pekinensis*). *J. Integr. Plant Biol.* 49, 993–1002. doi: 10.1111/j.1672-9072.2007.00478.x

Zhu, L., Liu, X., Wang, H., Khajuria, C., Reese, J. C., Whitworth, R. J., et al. (2012). Rapid mobilization of membrane lipids in wheat leaf-sheaths during incompatible interactions with Hessian fly. *MPMI* 25, 920–930. doi: 10.1094/MPMI-01-12-0022-R

frontiers | Frontiers in Plant Science

TYPE Original Research
PUBLISHED 27 March 2024
DOI 10.3389/fpls.2024.1367862

OPEN ACCESS

EDITED BY
Qingfang He,
University of Arkansas at Little Rock,
United States

REVIEWED BY
Juan Song,
Huzhou University, China
Hong Li Wang,
University of Arkansas at Little Rock,
United States

*CORRESPONDENCE
Liangbin Zeng
Zengliangbin@caas.cn
Siyuan Zhu
zhusiyuan@caas.cn

†These authors have contributed equally to this work and share the first authorship

RECEIVED 09 January 2024
ACCEPTED 15 March 2024
PUBLISHED 27 March 2024

CITATION
Wang X, Wang Y, Fu Y, Zhai Y, Bai X, Liu T, Li G, Zeng L and Zhu S (2024) Multiple omics revealed the growth-promoting mechanism of *Bacillus velezensis* strains on ramie. *Front. Plant Sci.* 15:1367862. doi: 10.3389/fpls.2024.1367862

Multiple omics revealed the growth-promoting mechanism of *Bacillus velezensis* strains on ramie

Xin Wang†, Yanzhou Wang†, Yafen Fu†, Yang Zhai, Xuehua Bai, Tongying Liu, Guang Li, Liangbin Zeng* and Siyuan Zhu*

Institute of Bast Fiber Crops, Chinese Academy of Agricultural Sciences, Changsha, China

Beneficial bacteria that promote plant growth can shield plants from negative effects. Yet, the specific biological processes that drive the relationships between soil microbes and plant metabolism are still not fully understood. To investigate this further, we utilized a combination of microbiology and non-targeted metabolomics techniques to analyze the impact of plant growth-promoting bacteria on both the soil microbial communities and the metabolic functions within ramie (*Boehmeria nivea*) tissues. The findings indicated that the yield and traits of ramie plants are enhanced after treatment with *Bacillus velezensis* (*B. velezensis*). These *B. velezensis* strains exhibit a range of plant growth-promoting properties, including phosphate solubilization and ammonia production. Furthermore, strain YS1 also demonstrates characteristics of IAA production. The presence of *B. velezensis* resulted in a decrease in soil bacteria diversity, resulting in significant changes in the overall structure and composition of soil bacteria communities. Metabolomics showed that *B. velezensis* significantly altered the ramie metabolite spectrum, and the differential metabolites were notably enriched ($P < 0.05$) in five main metabolic pathways: lipid metabolism, nucleotide metabolism, amino acid metabolism, plant secondary metabolites biosynthesis, and plant hormones biosynthesis. Seven common differential metabolites were identified. Correlation analysis showed that the microorganisms were closely related to metabolite accumulation and yield index. In the *B. velezensis* YS1 and *B. velezensis* Y4-6-1 treatment groups, the relative abundances of *Blrii41* and *Bauldia* were significantly positively correlated with sphingosine, 9,10,13-TriHOME, fresh weight, and root weight, indicating that these microorganisms regulate the formation of various metabolites, promoting the growth and development of ramie. Conclusively, *B. velezensis* (particularly YS1) played an important role in regulating soil microbial structure and promoting plant metabolism, growth, and development. The application of the four types of bacteria in promoting ramie growth provides a good basis for future application of biological fertilizers and bio-accelerators.

KEYWORDS

plant growth-promoting rhizobacteria, microbial diversity, bacterial community, metabolomics correlation, ramie

1 Introduction

Ramie (*Boehmeria nivea*) is considered one of the most significant bast fiber crops in ancient China and is commonly known as "Chinese grass" (Ni et al., 2018). China is the leading country in terms of ramie production. It accounts for over 90% of the global production and has a significant advantage in terms of cultivation area and total output. Additionally, China possesses a vast array of germplasm resources and holds a dominant position in the international market (Rehman et al., 2020; Fu et al., 2023). Ramie is the second largest fiber crop in China after cotton (Liu et al., 2014). According to archaeological evidence, ramie has been used as a textile material for over 4,700 years owing to its strong natural fibers (Liao et al., 2014; Mu et al., 2022). At present, ramie fiber is commonly used in the textile sector due to its capacity to maintain form, minimize creases, and add a glossy sheen to the look of textiles (Kadolph and Langford, 2001). In recent years, ramie has also been used as an unconventional feed for livestock and poultry because of its high content of crude proteins and amino acids (Kipriotis et al., 2015). Therefore, ramie is an important commercial crop for both fiber and feed.

At present, farmers have applied chemical fertilizers and pesticides extensively to achieve higher agricultural yields. However, chemical fertilizers that are not absorbed and utilized by crops enter the soil easily (Gouda et al., 2018), resulting in the destruction of soil microbial community structure, soil degradation and consolidation, decreased productivity, and poor crop quality (Liu et al., 2015). Thus, the challenge in contemporary society lies in minimizing the reliance on artificial chemical pesticides and fertilizers. An effective approach to achieving this goal is by substituting a portion of synthetic fertilizers and pesticides with natural microbiological fertilizers. The most promising microbial biostimulants include arbuscular plant growth-promoting rhizobacteria (PGPR), mycorrhizal fungi (AMF), and *Trichoderma* spp (Ganugi et al., 2022). Inoculating beneficial microorganisms has shown to have biostimulant activity in plants, offering benefits such as stress alleviation (Sangiorgio et al., 2020), growth promotion (Nacoon et al., 2020), and etc.

PGPR are a class of beneficial bacteria that grow in plant rhizosphere soil, promote plant growth, and improve plant resistance (Bashan et al., 2014). Growth-promoting bacteria and their related growth-promoting factors are important for the research and development of biological bacterial fertilizers. The growth promotion of PGPR can be divided into direct and indirect effects (Arruda et al., 2013). The direct growth promotion mechanisms include improved nitrogen uptake (Taulé et al., 2012), improved root phosphorus solubilization (Wu et al., 2012), improved iron production carriers (Kurabachew and Wydra, 2013), and production of phytohormone-like substances (Piromyou et al., 2010). The indirect growth promotion mechanisms refer to the ability of certain microorganisms to inhibit the growth of pathogenic bacteria (Kheirandish and Harighi, 2015), which ultimately results in improved plant growth. This can be achieved through various means, such as suppressing the growth of harmful pathogens or stimulating the plant's defense mechanisms to fend off insect herbivores (Pineda et al., 2010; Gamalero and Glick, 2011). These mechanisms play a crucial role in biological control and can contribute to the overall health and productivity of plants. PGPR can not only promote plant growth and reduce the use of chemical fertilizers but also may reduce the application of pesticides to a certain extent (Helaly et al., 2022). Studies on plant rhizosphere growth-promoting bacteria have attracted increasing attention (Bhattacharyya and Jha, 2012).

There is a general agreement among researchers about the impact of PGPR on plants, however, there is a lack of in-depth understanding regarding the specific molecular and physiological mechanisms involved in this symbiosis, as well as how plants respond to PGPR in real-world field environments. However, the interrelationships among plant agronomic traits, microbiota, and metabolites remain largely unknown. In recent years, omics techniques have greatly developed, and the integration of multiple omics datasets has paved the way for a more profound comprehension of interactions between plants and microbes. Multi-omics joint analysis has been developed as a new technique. The application of rhizospheric growth-promoting bacteria in ramie production is almost nonexistent. In this study, strains related to ramie growth were identified using large number of screening procedures. Agronomic traits, metabolic mechanisms, and rhizosphere microbial changes in ramie plants treated with the four strains were comprehensively evaluated using a multi-omics analysis method, providing a basis for the development and application of these four strains in the future.

2 Matherials and methods

2.1 Screening and identification of PGPR

2.1.1 Screening of PGPR

Strain *B. velezensis* JIN4 was originally isolated from branch tissue of kiwifruit "Jintao" variety. *B. velezensis* LYM4-2 strains were isolated from the rhizosphere soil of lotus, and *B. velezensis* YS-1 and *B. velezensis* Y4-6-1 were isolated from the rhizosphere soil of purple yam. First, the soil sample and disinfected plant tissues were homogenized. Thereafter, each homogenate was serially diluted 10^{-1} to 10^{-5}, and 100 µl of each dilution was evenly spread on solid Luria-Bertani (LB) plates and incubated at 25°C for 72 h. After incubation, *Bacillus* isolates were randomly isolated from the plates based on colony morphology and identification was performed by stereomicroscopy. Purified single colonies of *Bacillus* spp. were co-cultured with *P. syringae pv. actinidiae* to screen for antagonistic *Bacillus* species. Briefly, freshly grown Pseudomonas cultures were spread on solid LB medium plates. Following adsorption, a 6 mm well was created using a metallic borer and then filled with 100 µl (108 CFU/ml) of the recently cultivated *Bacillus* culture in medium. The plates were then incubated at 25°C for 48 hours to facilitate bacterial culturing.

2.1.2 Identification and Validation of PGPR

To identify the bacteria at the molecular level, 16S rDNA was amplified by PCR using the standard method in the bacterial gene DNA advance kit (Tiangen) (Singh et al., 2015). Genomic DNA was

extracted from the strain for subsequent PCR amplification of 16S rDNA using the primers 27F and 1492R. Amplification products were directly sequenced and subjected to BLASTN analysis. Sequence alignment of isolated strains was performed using MEGA 10.0 software. The neighbor-joining algorithm was utilized for clustering, and the Kimura two-parameter model was employed to calculate evolutionary distances. Node support was determined through bootstrapping, with 1,000 replicates conducted for estimation.

2.1.3 Biochemical characterization of PGPR

Biochemical analyses such as Gram staining, starch agar, indole, methyl red, the Voges–Proskauer test, IMViC test for citrate utilization, and catalase activity were conducted as per the procedures outlined in Prescott and Harley (2002). A carbohydrate utilization test kit (KB 009; HiMedia, India) was employed to assess the bacteria's ability to use different carbon sources. For the evaluation of cellulose-degrading capabilities, bacterial isolates were streaked on Congo Red agar medium, as described by Gupta et al. (2012). The presence of zones of clearance surrounding and beneath the colonies indicated enzymatic breakdown of cellulose.

The test organism was cultivated in peptone water for 48 hours at 37°C before Nessler's reagent (0.5 ml) was added to each tube to detect the presence of ammonia production. A brown-to-yellow color indicated a positive result for ammonia production, as described by Cappuccino and Sherman, 1992. Indole-3-acetic acid (IAA) production was also evaluated using a colorimetric method outlined by Bric et al., 1991. To assess phosphate-solubilizing activity, the test isolate was grown on NBRIP medium with tricalcium phosphate, following the method by Mehta and Nautiyal, 2001. The presence of a halo zone around bacterial growth on NBRIP-agar plates, as explained by Frey-Klett et al. (2005), confirmed positive results for phosphate solubilization activity.

2.2 Experimental design and sample collection

Activated bacteria were suspended in sterile Nutrient Broth (NB) liquid medium and adjusted to the appropriate concentration. First, the soil for potting studies was autoclaved at 121°C for 1 h, and each plastic pot was filled with 300 g of sterilized soil. Thereafter, 4-weeks-old seedlings were sown in pots (one seedling per pot). Each seedling was irrigated with 15 mL of resuspended bacterial solution at an OD value of 2.5, and sterilized NB liquid medium was used as a control. The bacteria were used twice a week for a total of three weeks. The study utilized a fully randomized layout with six repetitions for each treatment: (i) sterilized LB broth control, (ii) JIN4, (iii) YS1, (iv) Y4-6-1, and (v) LYM4-2. Over a span of 4 weeks, plants were cultivated in a greenhouse under an average daytime and nighttime temperature of 25 and 18°C, respectively, with tap water supplementation as necessary. Throughout the experiment, each treatment was evaluated for its effects on the growth and development of the plants. The data collected was analyzed to determine any significant differences between the treatments. In this study, the ramie growing soil is a nutrition-growing seedling medium (Xiangzhneg Agriculture Technology, PH:5.5-7.0, organic matter ≥20%) purchased by the laboratory, which is very easy to cultivate ramie.

Following the completion of the experiment, a total of six pots from each experimental group were selected at random for analysis. The measurements taken included the length of their stems, the diameter of their stems, as well as their fresh weight and root weight. Additionally, samples of fresh leaves were collected to evaluate the levels of photosynthetic pigments and antioxidants present. The content of relative chlorophyll was determined utilizing a SPAD-502 device (KONICA MINOLTA SENSING, INC., JAPAN) chlorophyll meter (Yu et al., 2016). The activities of catalase (CAT), superoxide dismutase (SOD) and peroxidase (POD) were measured using the detection kit of Solarbio Ltd.

The rhizosphere soil of ramie (six pots for each strain) was sampled using the nomenclature of samples based on the name of the strain (e.g., for JIN4, samples were named JIN4-1, JIN4-2, JIN4-3, JIN4-4, JIN4-5, and JIN4-6), and root irrigation with sterilized NB liquid medium was used as a control (CK). Each sample was analyzed in 6 replicates, and 30 soil samples underwent sieving with a 2-mm sieve, homogenization and storage at −70°C for biological and biochemical analyses. To ensure make the experimental results were representative, six replicate samples of each treatment were measured separately. Similarly, the control and four bacteria-treated whole seedlings were sampled for metabolome analysis.

2.3 Microbial diversity analysis

Bacterial DNA was isolated from the 30 soil samples stored in −70°C refrigerator using a MagPure Soil DNA LQ Kit (Magen, Guangdong, China) following the manufacturer's instructions. The V3-V4 region of the bacterial 16S rRNA gene was amplified using the respective primer pairs 343F and 798R. Sequencing libraries were constructed using the TruSeq® DNA PCR-Free Sample Preparation Kit according to the manufacturer's instructions. Sequencing was performed on an Illumina NovaSeq6000 platform with two paired-end read cycles of 250 bases each. The 16S rRNA gene amplicon sequencing and analysis were conducted by OE Biotech Co., Ltd. (Shanghai, China). The raw data of 16SrRNA gene sequencing were analyzed using QIIME2 platform (v2020.2). The final effective labels were obtained by splicing, filtering, and removing chimeric sequences using FLASH (version 1.2.7), followed by cluster analysis. Microbial diversity and richness were assessed by calculating the number of OTUs and alpha diversity indexes like Shannon and Chao1. To identify soil microbial community structure and estimate beta diversity, principal component analysis (PCA) was utilized.

2.4 Metabolomic analysis and statistical analysis

Liquid chromatography-mass spectrometry (LC-MS) is an analytical instrument that integrates liquid chromatography with mass spectrometry, enabling the effective separation and analysis of intricate organic mixtures. The buds obtained by 2.2 were placed in liquid nitrogen for quick freezing and transferred to a refrigerator at − 70° C for storage.

Freeze-dried shoots of the CK, JIN4, YS1, Y4-6-1, and LYM4-2 plants were triturated in a mixer mill (MM 400, Retsch) with zirconia beads for 1.5 min at 30 Hz. Each approximately 100 mg sample was then sonicated for 30 minutes in 1 mL of pre-cooled solvent (methanol/water 1:1, v/v, containing L-2-chlorophenylalanine, 2 μg/mL). Subsequently, the samples were incubated at -20°C for 20 minutes, followed by centrifugation at 4°C and 13000 rpm for 10 minutes. After that, 150 μL of the resulting supernatant was extracted, passed through a 0.22 μm filter, and transferred to a vial for LC-MS analysis. Six biological replicates were analyzed for each sample. The LC-MS analysis was conducted by injecting a 10 μL sample into an HSS T3 C18 column (100 mm×2.1 mm×1.8 μm, Waters) that was maintained at 50°C. The gradient elution program consisted of the following steps: 0-2 min, 100% A; 2-11 min, 0%-100% B; 11-13 min, 100% B; 13-15 min, 0%-100% A. The Q-TOF mass spectrometer was used in both positive and negative ion modes, with specific parameters like the ESI source temperature set at 120°C and the desorption temperature at 450°C. The LC-MS metabolic profiles were generated through the combination of an ACQUITY UHPLC system (Waters Corporation, Milford, USA) and an AB SCIEX Triple TOF 5600 system (AB SCIEX, Framingham, MA, USA) in ESI positive and negative ion modes. Quality control (QC) samples were included at regular intervals to ensure reproducibility, and metabolites were identified using various databases and tandem mass spectrometry (MS/MS) spectra. Raw LC-MS data were provided by Luming (Shanghai, China). Metabolites were analyzed primarily using RT m/z and tandem mass spectrometry (MS/MS) pairs as well as HMDB and lipid mass spectrometry. The Excel file containing the data matrix, which includes 3D datasets of m/z, RT peaks, and intensities, was exported for additional analysis. PCA and OPLS-DA were performed to display metabolic shifts in the various groups. Metabolites that met the criteria of |log2 fold change|≥1.0 and VIP ≥1.0 were flagged as differentially regulated between the experimental and control groups. These metabolites were compared with the KEGG pathway database to investigate their involvement in distinct metabolic pathways.

2.5 Data availability

The datasets from this study have been made available in online repositories. The specific names of the repositories and the accession numbers can be accessed at https://www.ncbi.nlm.nih.gov/GenBank. The *B. velezensis* data set was deposited in the NCBI Sequence Read Archive under accession no. MZ277421.1(JIN4), OP493231.1(YS1), OP493232.1(Y4-6-1), and OP493233.1(LYM4-2).

3 Results

3.1 Isolation, biochemical trait, and identification

Based on colony morphology, *Bacillus* isolates were recovered from the soil and tissue, and an antagonism test was performed. The results showed that the test organism JIN4, YS1, Y4-6-1, and LYM4-2 inhibited the growth of *P. syringae* pv. *actinidiae*. Basic microbiological and biochemical tests of the four isolates indicated that they were Gram-positive bacteria, which showed positive results for methyl red, Voges–Proskauer, catalase, oxidase, lecithinase, gelatin liquefaction, and nitrate reductase, and negative results for indole and hydrogen sulfide. The four test strains were able to utilize various carbon sources, including malanate, citrate, glucose, D-mannose, D-xylose, and D-fructose (Table 1). The four test organisms formed clear colony zones on cellulose Congo Red agar media, indicating cellulose enzymatic degradation activity. To ascertain the taxonomic affiliation of the four strains at the molecular level, they were subjected to 16S rRNA gene sequence analysis, which revealed the closest match to the 16S rRNA gene sequence of *B. velezensis* (Figure 1). This indicated that all isolates were highly homologous to *B. velezensis*. The obtained sequences were submitted to NCBI GenBank under accession numbers MZ277421.1(JIN4), OP493231.1(YS1), OP493232.1(Y4-6-1), and OP493233.1(LYM4-2).

3.2 Plant growth-promoting traits

Four *B. velezensis* strains tested positive for ammonia production (Table 2). Regarding phytohormone production, strain YS1 was positive for IAA production, whereas the other three strains were negative. Furthermore, a distinct clear zone was observed on a solid agar medium enriched with an insoluble form of phosphate (tricalcium phosphate) by the four *B. velezensis* species, demonstrating their ability to solubilize mineral phosphate.

3.3 Plant growth promotion experiments in the glasshouse

The growth status of ramie after four different *B. velezensis* treatments is shown in Figure 2. To evaluate the effect of the four *B. velezensis*-treated plants, an analysis of variance was performed (ANOVA; $P < 0.05$), which demonstrated that the inoculation of the four *B. velezensis* resulted in a significant increase in ramie plant growth. Growth was assessed by measuring stem length, stem diameter, fresh weight, root weight, relative chlorophyll content, and antioxidant enzyme activities (POD, CAT, and SOD). After treatment with four bacteria, the stem length was significantly increased by 74%, 77%, 55% and 101%, respectively, compared with the uninoculated plants ($P < 0.01$). Stem diameter also increased significantly by 48%, 27%, 34% and 12%, respectively ($P < 0.01$). Similarly, fresh weight and root weight increased significantly ($P < 0.001$) by 67%, 141%, 229%, 50% and 52%, 115%, 143% and 45%, respectively. The relative chlorophyll content in the four bacterial treatment groups increased, but there was no significant difference compared to that in the control group ($P > 0.05$). The responses of plant antioxidant enzymes to the four *B. velezensis* strains are shown in Figure 2. Compared with the control group, the antioxidant enzyme activities of the four bacterial treatment groups significantly increased ($P < 0.01$), in addition to the SOD activity of the Y4-6-1 treatment.

10.3389/fpls.2024.1367862

TABLE 1 Biochemical and physiological characteristics of the four bacterial strains.

Characteristic(s)	JIN4	YS-1	Y4-6-1	LYM4-2
Gram test	+	+	+	+
Indole	–	–	–	–
MR	+	+	+	+
VP	+	+	+	+
Catalase	+	+	+	+
Oxidase	+	+	+	+
Lecithinase	+	+	+	+
Gelatin liquefaction	+	+	+	+
Nitrate reductase	+	+	+	+
Hydrogen sulfide	–	–	–	–
Malanate utilization	+	+	+	+
Citrate utilization	+	+	+	+
Glucose	+	+	+	+
D-galactose	–	–	–	–
D-arabinose	–	–	–	–
D-mannose	+	+	+	+
D-xylose	+	+	+	+
D-fructose	+	+	+	+
Cellulose-degrading	+	+	+	+

+, means that the characteristic reaction is positive; -, means that the characteristic reaction is negative. The same as below.

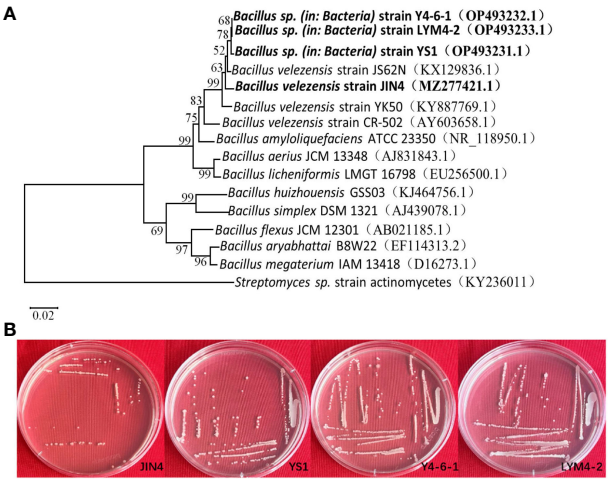

FIGURE 1
Phylogenetic tree showing the relationship of four *B. velezensis* strains with closely related bacteria **(A)**. The 16S rRNA gene sequences of closely related species were downloaded from the NCBI GenBank database. 16S rRNA gene of *Streptomyces* sp. strain actinomycetes was selected as an outgroup. The tree was obtained using neighbor joining method of software package Mega version 10.0 at the bootstrap value of n = 1000. Morphological picture of four *Bacillus velezensis* **(B)**.

3.4 Richness and diversity analysis of ramie soil microbial community

The results showed that alpha diversity and richness indices (Chao1, Shannon) were significantly decreased in the JIN4 and YS-1 groups compared to the (control) CK group, and the other groups showed no significant differences compared to the CK group (Figure 3A). In summary, the application of rhizosphere growth-promoting bacteria changed the diversity and richness indices of the microbial community in ramie soil.

3.5 Bacterial relative abundance and composition in the ramie soil

The bacterial sequences were distributed across 29 phyla, 315 families, and 612 genera (Supplementary Data 2). The dominant phyla in the bacterial communities across all soil samples were Proteobacteria (average per sample: 53.38%), *Bacterioidetes* (20.20%), *Myxococcota* (9.63%), *Actinobacteria* (4.36%), and *Firmicutes* (4.08%), which represented more than 80% of all sequences (Figure 3B). Compared with control (CK), among the top 10 phyla, the relative abundance of *Myxococcota* significantly

TABLE 2 Plant growth promoting traits of the four *B. velezensis* strains.

Activity	JIN4	YS1	Y4-6-1	LYM4-2
Ammonia Production	+	+	+	+
IAA	–	+	–	–
Phosphate solubilization	+	+	+	+

increased following treatment with the four *B. velezensis* strains, but Firmicutes were significantly lower in the YS1, Y4-6-1, and LYM4-2 treatment groups ($P < 0.01$). In addition, the relative abundance of Proteobacteria significantly increased following treatment with *Bacillus* Y4-6-1 ($P < 0.01$). However, the relative abundances of *Bacterioidetes* and *Actinobacteriota* significantly decreased following treatment with *Bacillus* YS1 ($P < 0.01$) and *Bacillus* JIN4 ($P < 0.05$), respectively. In summary, treatment with *B. velezensis* strains significantly changed the diversity and richness indices of the microbial community.

The top 10 genera of bacteria in all soil samples were *Flavobacterium* (7.20%), *BIrii41* (6.70%), *Asticcacaulis* (2.52%), *Bauldia* (2.31%), *Devosia* (2.09%), *Ramlibacter* (1.84%), *Caulobacter* (1.70%), *Steroidobacter* (1.61%), *Curvibacter* (1.43%), and *Gemmatimonas* (1.37%) (Figure 3C), which together represented less than 30% of all sequences. Compared with the control (CK), there were significant differences in the relative abundances of the top 10 genera ($P < 0.05$). The abundance of *Flavobacterium* in the YS1 and Y4-6-1 groups decreased significantly by 32.44% and 25.91% ($P < 0.01$), respectively. No significant changes were noted in the abundance of the *BIrii41* and *Bauldia* in the LYM4-2 group, whereas the abundance of *BIrii41* in the JIN4, YS1, and Y4-6-1 groups increased significantly ($P < 0.01$). In addition, the abundance of *Ramlibacter* showed differences among the different treatment groups; the YS1 group showed no significant changes, whereas the JIN4, Y4-6-1, and LYM4-2 groups

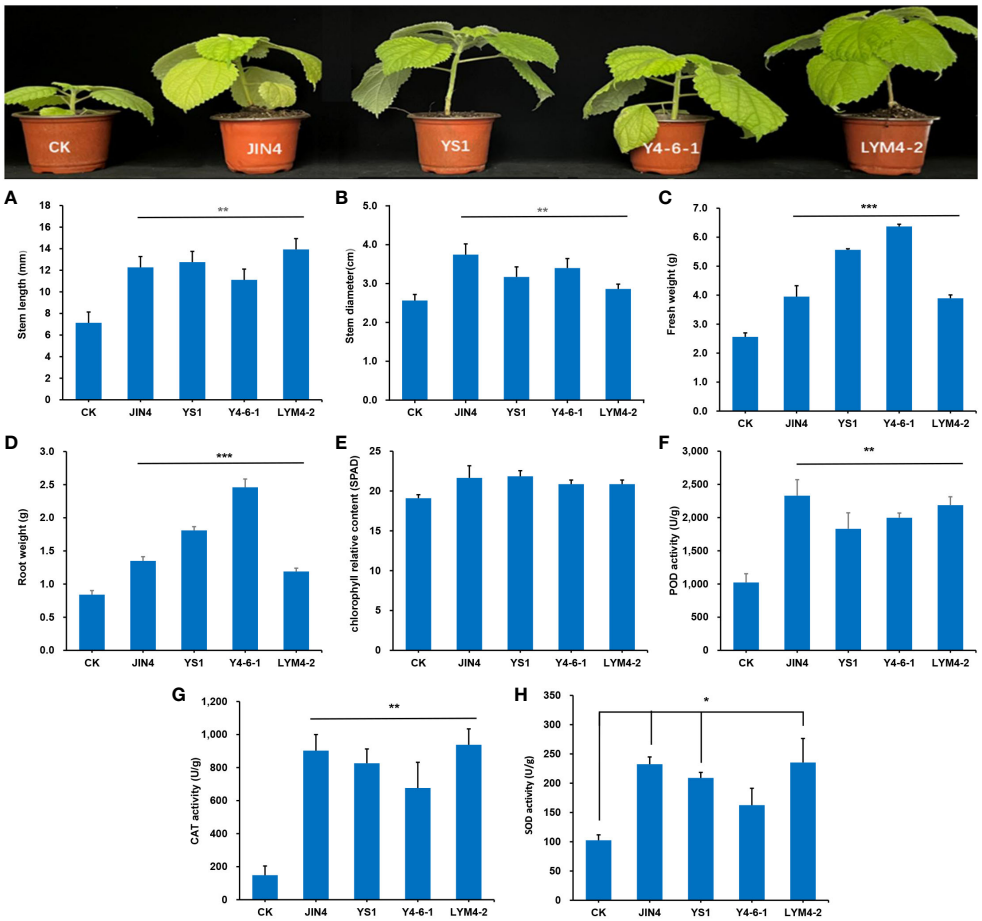

FIGURE 2
Effects of treatment with four *B. velezensis* strains. **(A)** Stem length, **(B)** stem diameter, **(C)** root weight, **(D)** fresh weight, **(E)** chlorophyll relative content, **(F)** POD activity, **(G)** CAT activity, **(H)** SOD activity. * $P < 0.05$, ** $P < 0.01$, *** $P < 0.001$.

10.3389/fpls.2024.1367862

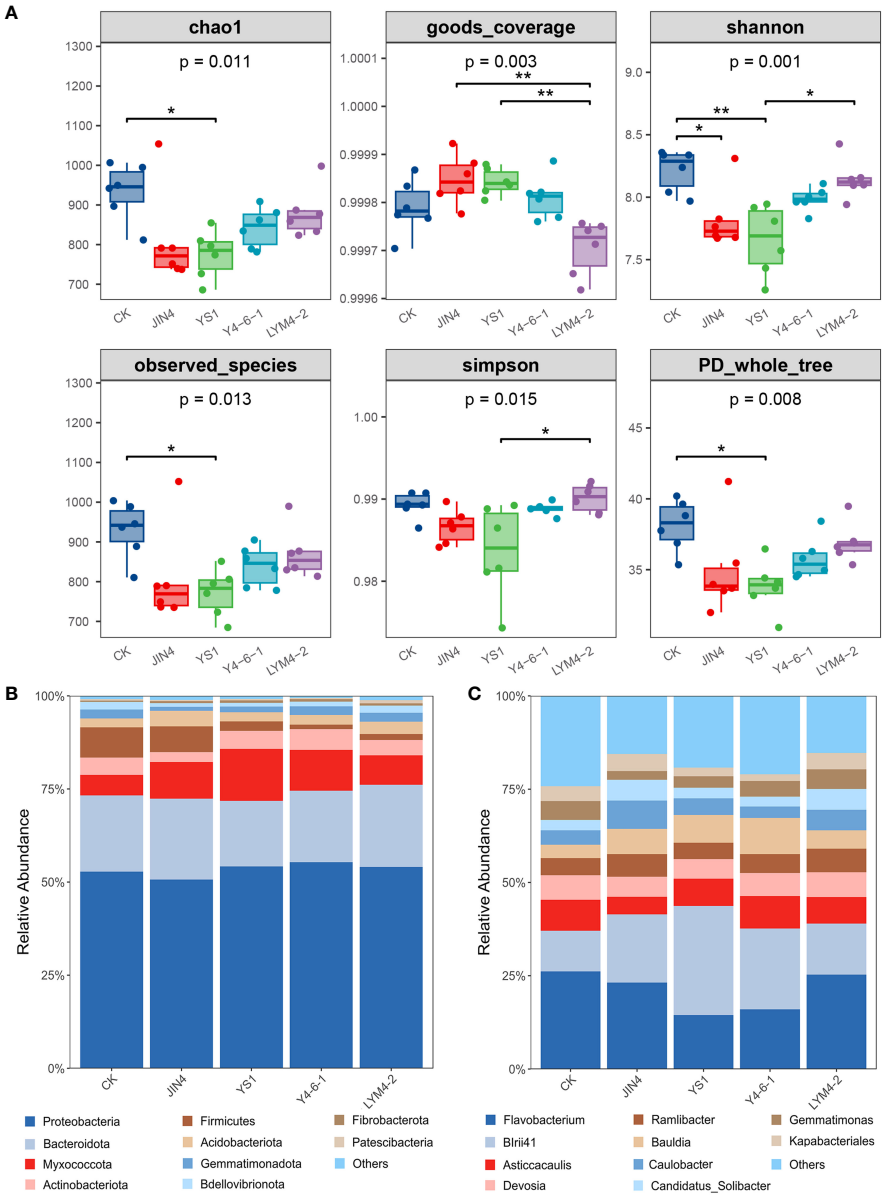

FIGURE 3
Richness and diversity analysis of ramie soil microbial community **(A)**; Relative abundances of dominant bacterial phyla **(B)** and genera **(C)** after treatment with the four *B. velezensis* strains. * $P < 0.05$, ** $P < 0.01$.

showed significant decreases of 50.30%, 35.45%, and 47.82%, respectively. These results indicate that the relative content and diversity of bacteria at the genus level in the ramie rhizosphere changed significantly after the application of *B. velezensis*.

Except for differences at the phylum and genus levels, certain bacteria showed increased abundance in the five treatments. A total of 32 biomarkers were detected at different taxonomic levels, including phylum, family, class, order, genus, or species, with a log10 LDA score greater than 4.0. These biomarkers reflected distinct species variations among the treatments (Supplementary Figure S1). In addition, enrichment of *B. velezensis* in each treatment group was identified at the species level. Compared with the control group, other groups had enrichment of *B. velezensis*; the LYM4-2 group was the most enriched (Supplementary Figure S1).

3.6 Metabolic differences in different ramie treatments

In order to assess how various *B. velezensis* strains affect the metabolic processes in ramie, metabolomics analysis was performed on differently treated ramie samples using an LC-MS platform. Following quality control (QC), PCA was utilized to compare the variations among the five experimental groups (Supplementary

10.3389/fpls.2024.1367862

Figure S2A). The QC samples exhibited close clustering, indicating the reliability and accuracy of the analysis method, resulting in high-quality data. In total, compared with the control, we detected 455 known differential metabolites (DMs) from 4 different treatments. These included lipids and lipid-like molecules (34.5%); organooxygen compounds (14.7%); organic oxygen compounds (14.1%); organoheterocyclic compounds (4.6%); phenylpropanoids and polyketides (13.0%); benzenoids (9.0%); nucleosides, pyrimidine nucleotides, nucleotides, and analogues (4.2%); organic nitrogen compounds (2.6%); alkaloids and derivatives (1.3%); lignans, neolignans and related compounds (1.1%); and other unclassified metabolites.

Multivariate statistical methods were employed to investigate the significant intergroup correlation present in the study. Through the application of supervised discriminant analysis (PLS-DA), differences within and between the control and treatment groups were thoroughly examined. This allowed for a comprehensive assessment of the impact of various *B. velezensis* strains on the metabolites present in ramie tissue. Based on the PLS-DA (Figures S2B–E), the metabolite compositions were comparable among the four bacterial treatments, but all differed from the control group. The PLS-DA model indicated that it was suitable for screening DMs ($R_2Y > 0.95$, $Q_2Y < 0.19$) (Supplementary Figure S3), which showed variations between the treatment and control groups. Volcano plots were employed to screen the discriminative metabolites (Supplementary Figure S4).

Hierarchical clustering analysis was carried out on all DMs within all pairs of comparisons. Various treatments of *B. velezensis* exerted distinct impacts on metabolites present in ramie tissues. As depicted in Figure 4A, the DMs generated by plant leaves subjected to different *B. velezensis* treatments predominantly comprised lipids and lipid-like compounds (34–45), with their atypical metabolism potentially influencing plant growth and development. Other metabolites produced included phenylpropanoids and polyketides (11–18), organic acids and derivatives (11–24), and organic oxygen compounds (13–18). Lipids and lipid-like molecules were further classified and analyzed using pie charts as follows: JIN4_CK (16 upregulated, 22 downregulated), YS1_CK (14 upregulated, 20 downregulated), Y4-6-1_CK (9 upregulated, 31 downregulated), and LYM4-2_CK (18 upregulated and 27 downregulated). The major DMs were prenol lipids (19–23), fatty acids (11–17), and steroids and steroid derivatives (2–2) (Figure 4B).

Enrichment analysis of KEGG pathways (top 20) indicated that all DMs were enriched in several key pathways including glucosinolate biosynthesis; pyrimidine metabolism; cyanoamino acid metabolism; tyrosine metabolism; zeatin biosynthesis; valine, leucine, and isoleucine biosynthesis; and aminoacyl-tRNA biosynthesis. This suggests that the treatment with *B. velezensis* had a significant impact on the synthesis of metabolites and their corresponding metabolic pathways, as shown in Figure 5A. A total of 7 common differentially expressed metabolites (DEMs) were identified by mapping to the KEGG metabolic pathway database,

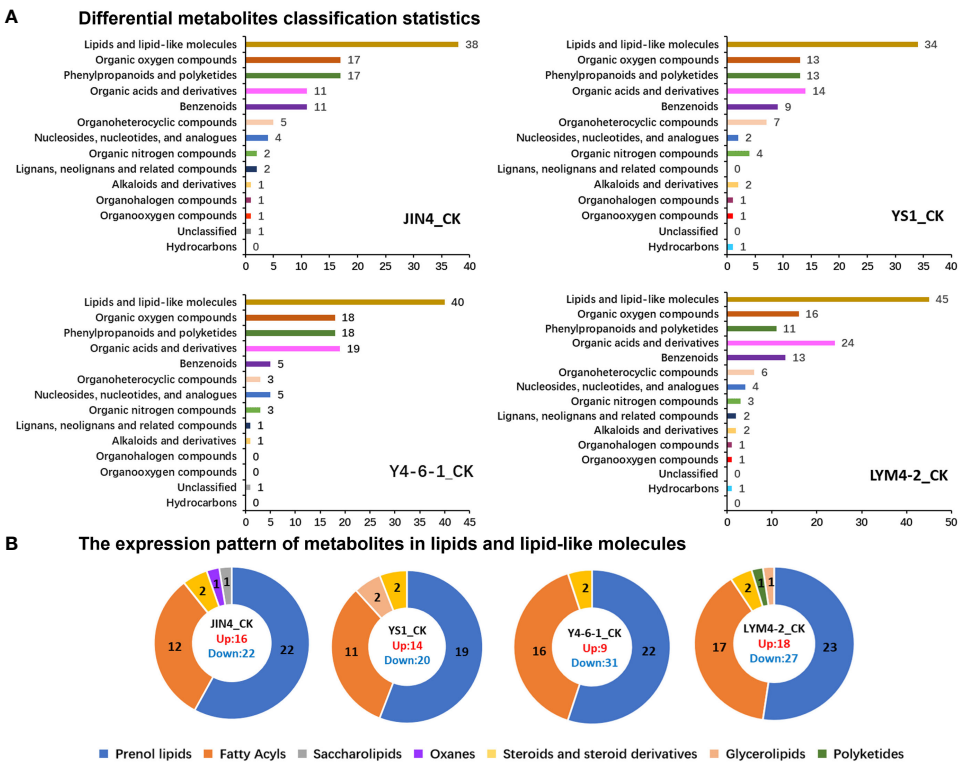

FIGURE 4
Analysis of the expression patterns of DMs. **(A)** DMs classification statistics. **(B)** The expression pattern of lipids and lipid-like molecules.

which could be used as potential biomarkers (Figure 5B). The DEMs involved in the metabolic pathways included 9,10,13-TriHOME ($C_{18}H_{34}O_5$), uridine diphosphate glucose ($C_{15}H_{22}N_2Na_2O_{17}P_2$), pseudouridine ($C_9H_{12}N_2O_6$), L-isoleucine ($C_6H_{13}NO_2$), trans-Ferulic acid ($C_{10}H_{10}O_4$), sphingosine ($C_{18}H_{37}NO_2$), and guanine ($C_5H_5N_5O$) (Figure 5C).

To gain a deeper understanding of how *B. velezensis* influences metabolism in ramie plants, we constructed a metabolic pathway consisting of 7 DEMs through research of the KEGG pathway database (Figure 6). These metabolites are involved in the metabolism of lipids, nucleotides, and amino acids, as well as the biosynthesis of plant secondary metabolites and plant hormones. In the four different *Bacillus* treatment groups, the trends for the seven metabolites were consistent. Compared with the control, the contents of the metabolites 9,10,13-TriHOME, pseudouridine, L-isoleucine, sphingosine, and guanine increased significantly in the four *B. velezensis* treatments. However, the levels of uridine diphosphate, glucose, and trans-Ferulic acid decreased significantly after the four different *B. velezensis* treatments. These findings suggest that *B. velezensis* has an indirect impact on the accumulation and makeup of plant metabolites. The irregular expression of these compounds could be a contributing factor to the enhanced growth of ramie following treatment with *B. velezensis*.

3.7 The relationship between soil microorganisms, plant metabolites, and ramie agronomic characters

Elucidating the relationships between microbes, metabolites, and yield indices is necessary to optimize PGPR for maximal plant growth. Therefore, the correlations between ramie yield indices, rhizosphere microorganisms, and metabolites were analyzed; their correlation coefficients (cor) were calculated, and the relationships were visualized, as shown in Table 3. Analysis of correlation revealed a circular relationship among the three variables ($P < 0.05$). Significantly strong correlations ($P < 0.05$) were evident among the top 10 bacterial genera, DEMs, and yield indices. The findings indicated that the relative abundances of three bacterial

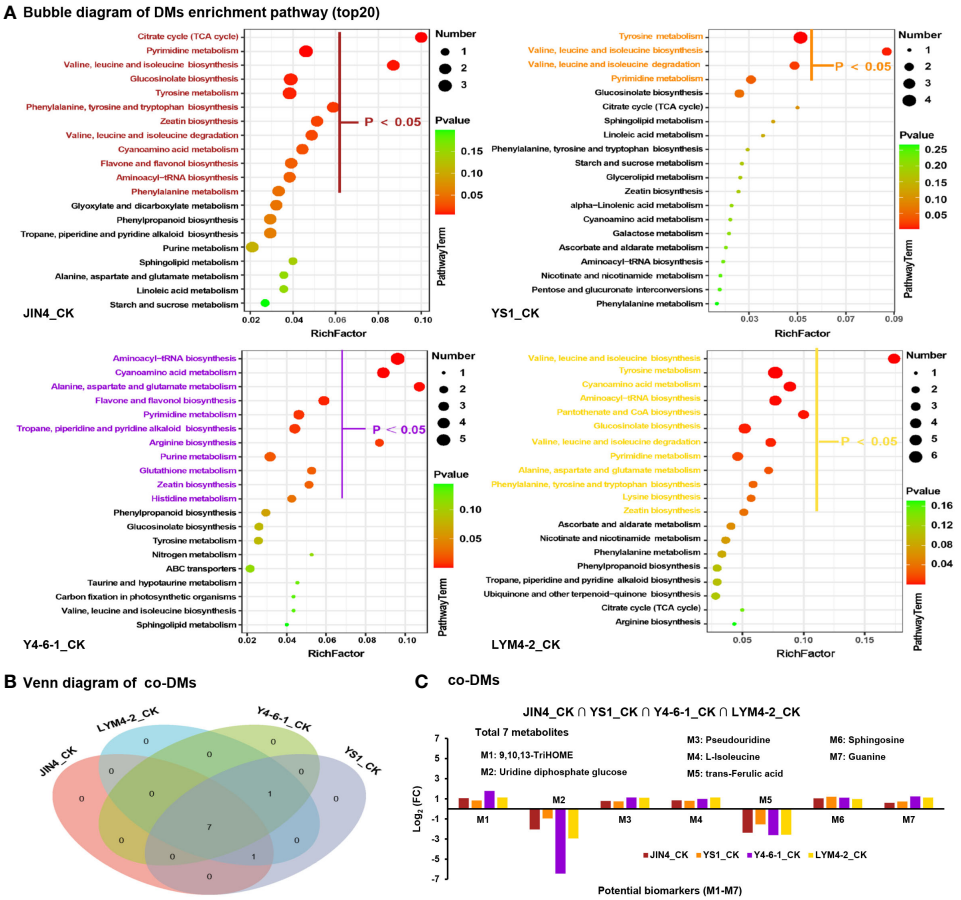

FIGURE 5
Analysis of metabolic pathways for DEMs. **(A)** Enrichment analysis of KEGG pathways of metabolites with significant differences in abundance among treatments. The X-axis displays the ratio of DEMs within the pathway to the total number of identified metabolites. Higher ratios indicate greater enrichment of DEMs in the pathway. Point color indicates the P-value from the hypergeometric test, with smaller values indicating higher reliability and statistical significance. Dot size corresponds to the number of DEMs within each pathway; larger dots represent more DEMs. **(B)** Evaluation of co-expressed DEMs across diverse treatment conditions. **(C)** Enrichment of co-expressed DEMs in metabolic pathways based on the average expression ratio between sample groups (Log2 FC). Positive values signify upregulation, while negative values indicate downregulation.

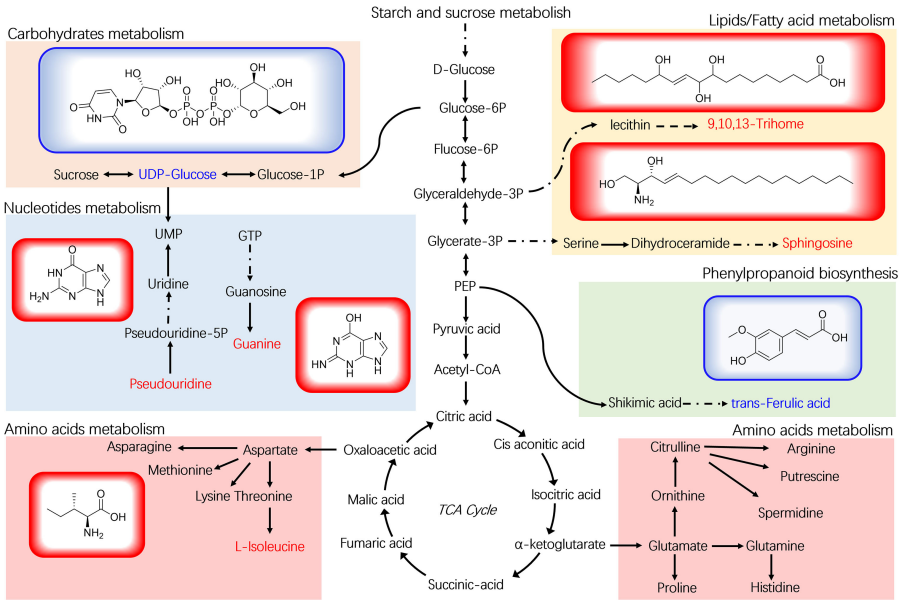

FIGURE 6
Plant metabolomic analysis of ramie treated with *B. velezensis*. The structural formulas of 7 DEMs are shown, along with the metabolic pathway map of differential marker metabolites. UDP-Glucose: uridine diphosphate glucose.

genera (*BIrii41*, *Bauldia*, and *Ramlibacter*) had the strongest correlations with certain metabolites (Sphingosine, 9,10,13-TriHOME, and trans-Ferulic acid) and yield indices (fresh weight, root weight, and stem length), indicating the role of these microbes in stimulating the growth and development of ramie through the regulation of metabolite production.

4 Discussion

In this study, NovaSeq sequencing and LC-MS were employed to analyze the variations in bacterial communities and metabolomics in ramie soil resulting from various treatments of *B. velezensis*. Soil microorganisms are essential components of microbial communities that have significant impacts on nutrient cycling, soil characteristics, plant development, and the overall sustainability of ecosystems (Zhang Z. et al., 2019). Different treatments with *B. velezensis* altered the diversity and abundance index of ramie rhizosphere soil and the metabolite composition and content of the ramie tissue. It was demonstrated that the four PGPR bacteria alter the rhizosphere microbiome, thereby regulating plant tissue metabolism and promoting plant growth by altering the abundance of other beneficial bacteria.

Soil microorganisms, particularly bacteria, are highly plentiful and varied, exerting significant influence in agricultural environments by aiding in nutrient cycling, upholding soil integrity, and enhancing plant development (Gans et al., 2005). Specific bacteria capable of promoting plant growth offer plants mechanisms to resist stress. Findings revealed that introducing *B. velezensis* altered the bacterial community diversity in soil ramie by reducing the alpha diversity (Chao1, Shannon) across all four treatment groups. This decrease could be attributed to the preferential growth of advantageous microorganisms driven by root secretions, resulting in the diminished presence of non-beneficial microbes. In the rhizosphere, plants attract soil microbes that are often plant-beneficial bacteria through the release of plant root exudates (Berendsen et al., 2012). The composition of soil bacterial communities is influenced by the application of *B. velezensis* (Sun et al., 2022) and the present results showed similar impacts. It was demonstrated that *B. velezensis* (JIN4, YS1, Y4-6-1, and LYM4-2) increased the abundance of various genera with documented beneficial roles, such as *BIrii41* (Jansen et al., 2008; Meiser, 2008), *Bauldia* (Yee et al., 2010), and *Ramlibacter* (Sun et al., 2019; Zhang L. N. et al., 2019). The promotion of advantageous bacteria in the rhizosphere seems to be a shared trait of *Bacillaceae*. Previous reports have indicated that *B. velezensis* can stimulate native soil Pseudomonas communities, which in turn enhance plant disease suppression (Sun et al., 2022). Furthermore, the secondary compounds generated by *B. velezensis* have the potential to induce systemic resistance in plants and support robust plant growth (Fan et al., 2018).

Plant growth-promoting properties also showed that the JIN4, YS1, Y4-6-1, and LYM4-2 groups produced ammonia and solubilized phosphate. Phosphate solubilization is a crucial characteristic of microorganisms in the rhizosphere, which plays a key role in providing plant growth with bioavailable phosphate (Liu et al., 2014; Dutta et al., 2015). The existence of bacteria that solubilize phosphate in soil can be viewed as a promising sign of using microbial biofertilizers to enhance crop yield and promote sustainable agriculture. Furthermore, apart from its ability to produce ammonia and solubilize phosphate, the isolated strain YS1 displayed additional characteristics that promote plant growth. These include the synthesis of plant hormones, specifically auxins, that support the enhancement of plant

10.3389/fpls.2024.1367862

TABLE 3 The correlation analysis between ramie yield indices, microorganisms and metabolites.

Var 1	Interraction	Var 2	Cor	*P* value
Fresh weight	Positive	*BIrii41*	0.8536	2.4E-05
Fresh weight	Positive	*Bauldia*	0.8250	0.0002
Root weight	Positive	*BIrii41*	0.8107	0.0004
Root weight	Positive	*Bauldia*	0.7893	0.0007
Root weight	Negative	*Flavobacterium*	-0.7893	0.0007
Fresh weight	Negative	*Flavobacterium*	-0.7679	0.0013
SOD	Positive	*Caulobacter*	0.6315	0.0116
SOD	Negative	*Asticcacaulis*	-0.6064	0.0165
Stem length	Positive	*Bauldia*	0.6036	0.0195
Stem length	Positive	*Ramlibacter*	0.6036	0.0195
SOD	Positive	*Ramlibacter*	0.5939	0.0196
CAT	Positive	*Caulobacter*	0.5714	0.0286
CAT	Negative	*Asticcacaulis*	-0.5357	0.0422
Ramlibacter	Positive	Pseudouridine	0.6979	0.0000
Ramlibacter	Positive	Guanine	0.6507	0.0001
Ramlibacter	Positive	9,10,13-TriHOME	0.6214	0.0003
Bauldia	Positive	9,10,13-TriHOME	0.6027	0.0004
Ramlibacter	Negative	Uridine diphosphate glucose	-0.5443	0.0019
Ramlibacter	Positive	L-Isoleucine	0.5506	0.0019
Ramlibacter	Negative	trans-Ferulic acid	-0.5395	0.0024
Bauldia	Positive	Pseudouridine	0.5284	0.0027
Bauldia	Positive	Guanine	0.5249	0.0029
Bauldia	Negative	Uridine diphosphate glucose	-0.4869	0.0064
Bauldia	Positive	Sphingosine	0.4761	0.0078
BIrii41	Positive	Sphingosine	0.4710	0.0093
Bauldia	Positive	L-Isoleucine	0.4332	0.0168
Bauldia	Negative	trans-Ferulic acid	-0.4136	0.0231
BIrii41	Positive	Guanine	0.4136	0.0239
BIrii41	Positive	Pseudouridine	0.3967	0.0308
BIrii41	Positive	9,10,13-TriHOME	0.3882	0.0348
BIrii41	Positive	L-Isoleucine	0.3740	0.0425
Sphingosine	Positive	Fresh weight	0.8000	0.0005
9,10,13-TriHOME	Positive	Stem length	0.7464	0.0021
trans-Ferulic acid	Negative	Stem length	-0.7214	0.0033
Sphingosine	Positive	Root weight	0.6857	0.0062
9,10,13-TriHOME	Positive	Root weight	0.6786	0.0069
9,10,13-TriHOME	Positive	Fresh weight	0.6643	0.0086
Uridine diphosphate glucose	Negative	Root weight	-0.5845	0.0221
L-Isoleucine	Positive	CAT	0.5786	0.0264

(Continued)

TABLE 3 Continued

Var 1	Interraction	Var 2	Cor	*P* value
L-Isoleucine	Positive	Stem length	0.5750	0.0275
trans-Ferulic acid	Negative	Root weight	-0.5750	0.0275
Guanine	Positive	Fresh weight	0.5714	0.0286
trans-Ferulic acid	Negative	Fresh weight	-0.5714	0.0286

productivity. Introducing bacteria that produce IAA stimulates root development through the augmentation of adventitious roots in terms of both quantity and length, along with modifications to root structure. This ultimately improves nutrient absorption and fosters plant growth (Chakraborty et al., 2006; Yang et al., 2009; Dutta et al., 2015).

Relative chlorophyll content can reflect changes in plant photosynthesis after bacterial treatment. In this study, the relative content of chlorophyll in ramie treated with the four bacteria increased to a certain extent, reflecting the health of plant leaves and an increase in photosynthesis. It has been speculated that these four bacterial species are involved in plant growth and metabolism.

The crucial role of the plant antioxidant enzyme system that fights off stress and eliminates free radicals cannot be overstated. Plants respond to adverse conditions by activating defense mechanisms. These mechanisms trigger the production of damaging substances like oxygen free radicals, peroxides, and membrane lipid peroxides, leading to the degradation of cell membrane structure and function (Singh and Jha, 2016). Four unique *B. velezensis* treatments led to a notable surge in antioxidant enzyme levels within plants, bolstering defense mechanisms and fostering unhindered plant development.

Metabolomics can reveal changes in endogenous substances and the molecular regulation mechanisms of organisms in different environments. The response strategies of the plants to the four growth-promoting bacteria were similar. The primary discrepancies found in metabolites were observed in lipids and lipid compounds, organic acids along with their variations, and organic oxygen substances. These variances showcase the enhancement of lipid and carbon metabolism within plants and could provide insights into potential pathways for stimulating plant development. A crucial metabolite, 9,10,13-TriHOME, is formed from linoleic acid oxidation, and is essential for plant defense mechanisms (Zeng et al., 2017). 9,10,13-TriHOME is associated with plant disease resistance and may induce plant root rot resistance by promoting linoleic acid and tyrosine metabolism (Zhang et al., 2022). Sphingolipids are essential components of the plasma membrane and other intramembrane systems, serving not just as structural elements but also as signaling molecules in response to various stresses. Recent research has highlighted the crucial involvement of sphingolipid metabolism in the regulation of plant growth and development (Ali et al., 2018). Among the diverse types of sphingolipids, sphingosine stands out as a key constituent of cellular membranes. In plants, sphingosine functions as a metabolic intermediate of sphingosine-1-phosphate, which in turn plays a pivotal role in enhancing plant resistance against diseases.

Uridine diphosphate glucose serves as a signaling molecule in plants and plays a crucial role in processes such as plant growth, development, and stress response. This molecule is involved in regulating various metabolic pathways including glucose metabolism, carbon metabolism, and phenylpropane metabolism. Furthermore, it impacts the signaling of plant hormones and the communications between plants and pathogens. For example, uridine diphosphate glucose is involved in zeaxanthin metabolism. Zeatin is a naturally occurring cytokinin that promotes cell division and differentiation and regulates plant growth and development. Pseudouridines are commonly present in evolutionarily conserved and functionally crucial sections of rRNA, tRNA, and additional noncoding RNA molecules. Pseuduridine modification helps stabilize RNA structure and ribosome biogenesis and activity and regulates rRNA processing, pre-mRNA splicing, and protein synthesis, thereby controlling growth, development, and response to stress in different organisms (Lu et al., 2017; Adachi et al., 2019; Sun et al., 2019; Wang et al., 2022). Ferulic acid and other phenolic acids have an inhibitory effect on plant growth, which can inhibit plant nutrient absorption, photosynthesis, respiration, the function and activity of various enzymes, endogenous hormone synthesis, and protein synthesis (Hussain and Reigosa, 2021; John and Sarada, 2012).

This study revealed the regulatory microbe–metabolite yield relationship between microorganisms, DEMs, and yield traits at the macro and micro levels, indicating that the rhizosphere microbial composition was dominated by drug-resistant bacteria, *Azotobacter* spp., and degrading bacteria, which had a strong correlation with the synthesis of organic acids and lipid metabolism, promoting an increase in plant fresh weight and root weight. The findings from this research indicated that the levels of *BIrii41* and *Bauldia* significantly rose in the YS1 group and Y4-6-1 group. In contrast, the relative abundance of *Flavobacterium* decreased significantly, corresponding to the significant increases of metabolites 9,10,13-TriHOME, sphingosine, uridine, guanine, and l-isoleucine along with the corresponding root weight and fresh weight of plants. In addition, the increased relative abundance of *Bauldia* significantly reduced uridine diphosphate, glucose, and trans-Ferulic acid contents. *Bauldia* is a nitrogen-fixing bacterium that inhibits plant diseases and promotes plant growth (Black et al., 2012; Kumar et al., 2012). *Myxobacteria*, for example BIrii41_norank, are found extensively throughout the environment and are plentiful in aerobic compost as well as vermicompost (Cai et al., 2018). The

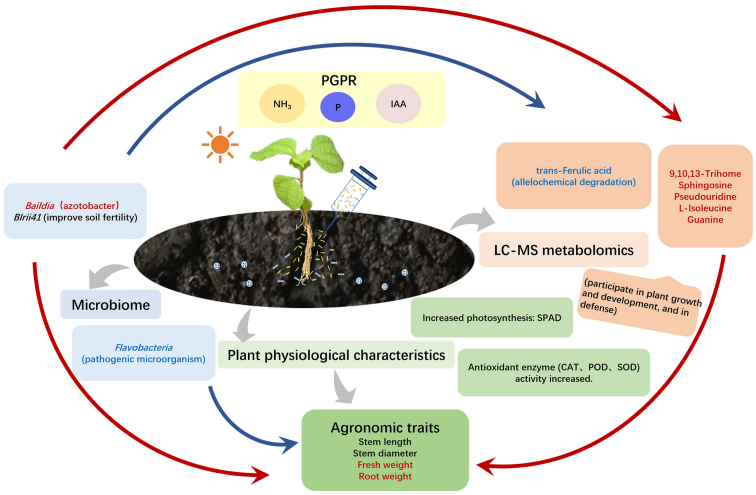

FIGURE 7
Mechanism diagram of *B. velezensis* promoting ramie growth. The red arrow shows a positive relationship, while the blue arrow represents a negative correlation. The red font signifies a noteworthy rise, and the blue font indicates a notable decline.

secondary metabolites of *Myxobacteria* exhibit antiviral and antifungal properties, capable of inhibiting eukaryotic RNA, DNA, and protein synthesis, as well as disrupting heavy metal ion transport, among other functions (Jansen et al., 2008; Meiser, 2008). *Flavobacterium* is the dominant bacterium in the rhizosphere soil that inhibits soil-borne bacterial wilt and is closely related to the inhibition ability of Verticillium wilt. However, some studies have found that certain *Flavobacterium* species can harm plant health as pathogenic microorganisms (Fu et al., 2018; Bao et al., 2022). Therefore, as shown in Figure 7, it is speculated that rhizosphere growth-promoting *B. velezensis* YS1 and Y4-6-1 may recruit beneficial bacteria *BIrii41* and *Bauldia* to reduce harmful *Flavobacterium*, promote plant lipid, carbon, amino acid, and nucleic acid metabolisms, as well as the production of phenolic acid auto-toxic substances, particularly in the YS1 strain, and also promote the production of IAA, thereby improving growth and development (Zhang et al., 2017).

5 Conclusion

The relationship between bacterial communities and metabolomics was investigated by utilizing NovaSeq sequencing and LC-MS for the analysis in ramie after different treatments with *B. velezensis*. Based on the diversity index, the four *B. velezensis* strains showed reduced bacterial diversity compared with the control. Furthermore, the four *B. velezensis* strains significantly changed bacterial community structures and compositions. Metabolomics studies showed that YS1 and Y4-6-1 caused significant changes in plant metabolic spectrum and affected metabolic pathways related to lipid metabolism, while *B.velezensis* enhanced the activity of lipid metabolism-related pathways. Additionally, these changes were closely linked to shifts in specific microbial taxa. Metabolites have strong connections with various rhizosphere microbes, which can significantly influence the composition of microbial communities in the rhizosphere of ramie. Through correlation analysis, it was evident that the abundance levels of *BIrii41* and *Bauldia* exhibited a positive relationship with sphingosine, 9,10,13-TriHOME, as well as the fresh weight and root weight. This suggests that these microorganisms play a crucial role in enhancing the growth and development of ramie by modulating the production of most ramie metabolites. The findings of this research validate the interconnectedness between soil microorganisms, plant metabolism, and yield indicators, indicating that the application of *B. velezensis* (particularly YS1) can yield more favorable outcomes. These insights may serve as a valuable guide for implementing microbial strategies to enhance soil quality and crop productivity sustainably.

Data availability statement

The original contributions presented in the study are included in the article/Supplementary Material. Further inquiries can be directed to the corresponding author.

Author contributions

XW: Writing – original draft, Data curation, Formal Analysis, Writing – review & editing. YW: Conceptualization, Methodology, Writing – review & editing. YF: Data curation, Writing – original draft. YZ: Investigation, Validation, Writing – review & editing. XB: Investigation, Validation, Writing – review & editing. TL: Investigation, Validation, Writing – review & editing. GL: Data

curation, Writing – review & editing. LZ: Supervision, Writing – review & editing. SZ: Funding acquisition, Project administration, Supervision, Writing – review & editing.

Funding

The author(s) declare financial support was received for the research, authorship, and/or publication of this article. This study was funded by the National Natural Science Foundation of China (31571618 and 31771734), the Agricultural Science and Technology Innovation Program (ASTIP-IBFC), China Agriculture Research System of MOF and MARA (CARS-16-E12) and Natural Science Foundation of Hunan Province (2022JJ30649).

Acknowledgments

We thank the Luming Biological Technology Co., Ltd (Shanghai, China) for their technical support.

Conflict of interest

The authors declare that the research was conducted in the absence of any commercial or financial relationships that could be construed as a potential conflict of interest.

Publisher's note

Supplementary material

The Supplementary Material for this article can be found online at: https://www.frontiersin.org/articles/10.3389/fpls.2024.1367862/full#supplementary-material

References

Adachi, H., De Zoysa, M. D., and Yu, Y. T. (2019). Post-transcriptional pseudouridylation in mRNA as well as in some major types of noncoding RNAs. *Biochim. Biophys. Acta Gene Regul. Mech.* 1862, 230–239. doi: 10.1016/j.bbagrm.2018.11.002

Ali, U., Li, H., Wang, X., and Guo, L. (2018). Emerging roles of Sphingolipid signaling in plant response to biotic and abiotic stresses. *Mol. Plant* 11, 1328–1343. doi: 10.1016/j.molp.2018.10.001

Arruda, L., Beneduzi, A., Martins, A., Lisboa, B., Lopes, C., Bertolo, F., et al. (2013). Screening of rhizobacteria isolated from maize (Zea mays L.) in Rio Grande do Sul State (South Brazil) and analysis of their potential to improve plant growth. *Appl. Soil Ecol.* 63, 15–22. doi: 10.1016/j.apsoil.2012.09.001

Bao, L., Liu, Y., Ding, Y., Shang, J., Wei, Y., Tan, Y., et al. (2022). Interactions between phenolic acids and microorganisms in rhizospheric soil from continuous cropping of Panax notoginseng. *Front. Microbiol.* 13. doi: 10.3389/fmicb.2022.791603

Bashan, Y., de-Bashan, L. E., Prabhu, S. R., and Hernandez, J. P. (2014). Advances in plant growth-promoting bacterial inoculant technology: formulations and practical perspectives, (1998-2013). *Plant Soil.* 378, 1–33. doi: 10.1007/s11104-013-1956-x

Berendsen, R. L., Pieterse, C. M., and Bakker, P. A. (2012). The rhizosphere microbiome and plant health. *Trends Plant Sci.* 17, 478–486. doi: 10.1016/j.tplants.2012.04.001

Bhattacharyya, P. N., and Jha, D. K. (2012). Plant growth-promoting rhizobacteria (PGPR): emergence in agriculture. *World J. Microbiol. Biotechnol.* 28, 1327–1350. doi: 10.1007/s11274-011-0979-9

Black, M., Moolhuijzen, P., Chapman, B., Barrero, R., Howieson, J., Hungria, M., et al. (2012). The Genetics of symbiotic nitrogen fixation: Comparative genomics of 14 rhizobia strains by resolution of Protein clusters. *Genes* 3, 138–166. doi: 10.3390/genes3010138

Bric, J. M., Bostock, R. M., and Silverstone, S. E. (1991). Rapid in *situ* assay for indoleacetic acid production by bacteria immobilized on a nitrocellulose membrane. *Appl. Environ. Microbiol.* 57, 535–538. doi: 10.1128/aem.57.2.535-538.1991

Cai, L., Gong, X., Sun, X., Li, S., and Yu, X. (2018). Comparison of chemical and microbiological changes during the aerobic composting and vermicomposting of green waste. *PloS One* 13, e0207494. doi: 10.1371/journal.pone.0207494

Cappuccino, J. G., and Sherman, N. (1992). "Biochemical activities of microorganisms," in *Microbiology, A Laboratory Manual* (The Benjamin/ Cummings Publishing Co, San Francisco, CA).

Chakraborty, U., Chakraborty, B., and Basnet, M. (2006). Plant growth promotion and induction of resistance in Camellia sinensis by Bacillus megaterium. *J. Basic Microbiol.* 46, 186–195. doi: 10.1002/jobm.200510050

Dutta, J., Handique, P. J., and Thakur, D. (2015). Assessment of culturable tea rhizobacteria isolated from tea estates of Assam, India for growth promotion in commercial tea cultivars. *Front. Microbiol.* 6. doi: 10.3389/fmicb.2015.01252

Fan, B., Wang, C., Song, X., Ding, X., Wu, L., Wu, H., et al. (2018). Bacillus velezensis FZB42 in 2018: the gram-positive model strain for plant growth promotion and biocontrol. *Front. Microbiol.* 16. doi: 10.3389/fmicb.2018.02491

Frey-Klett, P., Chavatte, M., Clausse, M. L., Courrier, S., Le Roux, C., Raaijmakers, J., et al. (2005). Ectomycorrhizal symbiosis affects functional diversity of rhizosphere fluorescent pseudomonads. *New Phytol.* 165, 317–328. doi: 10.1111/j.1469-8137.2004.01212.x

Fu, L., Wang, Y., Wang, X., Ji, G., and Wei, L. (2018). The study on microbial diversity of rhizosphere in continuous cropping system of Panax notoginseng. *J. Yunnan Agric. University.* 33, 198–207. doi: 10.12101/j.issn.1004-390X(n).201703036

Fu, Y., Liu, T., Wang, X., Wang, Y., Gong, Q., Li, G., et al. (2023). Untargeted metabolomics reveal rhizosphere metabolites mechanisms on continuous ramie cropping. *Front. Plant Sci.* 22. doi: 10.3389/fpls.2023.1217956

Gamalero, E., and Glick, B. R. (2011). "Mechanisms used by plant growth-promoting bacteria," in *Bacteria in Agrobiology: Plant Nutrient Management*. Ed. D. Maheshwari (Springer, Berlin, Heidelberg), 17–46. doi: 10.1007/978-3-642-21061-7_2

Gans, J., Wolinsky, M., and Dunbar, J. (2005). Computational improvements reveal great bacterial diversity and high metal toxicity in soil. *Science* 309, 1387–1390. doi: 10.1126/science.1112665

Ganugi, P., Fiorini, A., Ardenti, F., Caffi, T., Bonini, P., Taskin, E., et al. (2022). Nitrogen use efficiency, rhizosphere bacterial community, and root metabolome reprogramming due to maize seed treatment with microbial biostimulants. *Physiol. Plant* 174, e13679. doi: 10.1111/ppl.13679

Gouda, S., Kerry, R. G., Das, G., Paramithiotis, S., Shin, H. S., and Patra, J. K. (2018). Revitalization of plant growth promoting rhizobacteria for sustainable development in agriculture. *Microbiol. Res.* 206, 131–140. doi: 10.1016/j.micres.2017.08.016

Gupta, P., Samant, K., and Sahu, A. (2012). Isolation of cellulose-degrading bacteria and determination of their cellulolytic potential. *Int. J. Microbiol.* 2012, 578925. doi: 10.1155/2012/578925

Helaly, A. A., Mady, E., Salem, E. A., and Randhir, T. O. (2022). Stimulatory effects of growth-promoting bacteria on growth, nutritional composition, and yield of kale plants. *J. Plant Nutr.* 45, 2465–2477. doi: 10.1080/01904167.2022.2046084

Hussain, M. I., and Reigosa, M. J. (2021). Secondary Metabolites, Ferulic Acid and p-Hydroxybenzoic Acid Induced Toxic Effects on Photosynthetic Process in Rumex acetosa L. *Biomolecules* 11, 233. doi: 10.3390/biom11020233

Jansen, R., Steinmetz, H., Sasse, F., Schubert, W. D., Hagelüken, G., Albrecht, S. C., et al. (2008). Isolation and structure revision of the actin-binding macrolide rhizopodin from Myxococcus stipitatus (Myxobacteria). *Tetrahedron Lett.* 49, 5796–5799. doi: 10.1016/j.tetlet.2008.07.132

John, J., and Sarada, S. (2012). Role of phenolics in allelopathic interactions. *Allelopathy J.* 29, 215–229. doi: 10.1007/s11104-011-1042-1

Kadolph, S. J., and Langford, A. (2001). *Textiles. 9th ed* (Upper Saddle River, NJ: Prentice Hall).

Kheirandish, K., and Harighi, B. (2015). Evaluation of bacterial antagonists of Ralstonia solanacearum, causal agent of bacterial wilt of potato. *Biol. Control.* 86, 14–19. doi: 10.1016/j.biocontrol.2015.03.007

Kipriotis, E., Heping, X., Vafeiadakis, T., Kiprioti, M., and Alexopoulou, E. (2015). Ramie and kenaf as feed crops. *Ind. Crop Prod.* 68, 126–130. doi: 10.1016/j.indcrop.2014.10.002

Kumar, P. A., Srinivas, T. N. R., Manasa, P., Madhu, S., and Shivaji, S. (2012). Lutibaculum baratangense gen. nov., sp. nov., a proteobacterium isolated from a mud volcano. *Int. J. Syst. Evol. Microbiol.* 62, 2025–2031. doi: 10.1099/ijs.0.036350-0

Kurabachew, K., and Wydra, K. (2013). Characterization of plant growth promoting rhizobacteria and their potential as bioprotectant against tomato bacterial wilt caused by Ralstonia solanacearum. *Biol. Control.* 67, 75–83. doi: 10.1016/j.biocontrol.2013.07.004

Liao, L., Li, T., Zhang, J., Xu, L., Deng, H., and Han, X. (2014). The domestication and dispersal of the cultivated ramie (Boehmeria nivea (L.) Gaud. in Freyc.) determined by nuclear SSR marker analysis. *Genet. Resour Crop Evol.* 61, 55–67. doi: 10.1007/s10722-013-0014-0

Liu, F. P., Liu, H. Q., Zhou, H. L., Dong, Z. G., Bai, X. H., Bai, P., et al. (2014). Isolation and characterization of phosphate-solubilizing bacteria from betel nut (Areca catechu) and their effects on plant growth and phosphorus mobilization in tropical soils. *Biol. Fertil Soils* 50, 927–937. doi: 10.1007/s00374-014-0913-z

Liu, Y., Pan, X., and Li, J. (2015). A 1961-2010 record of fertilizer use, pesticide application and cereal yields: a review. *Agron. Sustain Dev.* 35, 83–93. doi: 10.1007/s13593-014-0259-9

Liu, T., Tang, S., Zhu, S., Tang, Q., and Zheng, X. (2014). Transcriptome comparison reveals the patterns of selection in domesticated and wild ramie (Boehmeria nivea L. Gaud). *Plant Mol. Biol.* 86, 85–92. doi: 10.1007/s11103-014-0214-9

Lu, S., Li, C., Zhang, Y., Zheng, Z., and Liu, D. (2017). Functional disruption of a chloroplast Pseudouridine synthase desensitizes Arabidopsis plants to phosphate starvation. *Front. Plant Sci.* 8. doi: 10.3389/fpls.2017.01421

Mehta, S., and Nautiyal, C. S. (2001). An efficient method for qualitative screening of phosphate-solubilizing bacteria. *Curr. Microbiol.* 43, 51–56. doi: 10.1007/s002840010259

Meiser, P. (2008). *Myxococcus xanthus-a myxobacterial model strain as multiproducer of secondary metabolites* (Universität des Saarlandes). Doctoral Dissertations.

Mu, L., Cai, M., Wang, Z., Liu, J., Liu, T., Wanapat, M., et al. (2022). Assessment of ramie leaf (Boehmeria nivea L. gaud) as an animal feed supplement in P.R. China. *Trop. Anim. Health Prod.* 52, 115–121. doi: 10.1007/s11250-019-01997-w

Nacoon, S., Jogloy, S., Riddech, N., Mongkolthanaruk, W., Kuyper, T. W., and Boonlue, S. (2020). Interaction between phosphate solubilizing bacteria and arbuscular mycorrhizal fungi on growth promotion and tuber inulin content of Helianthus tuberosus L. *Sci. Rep.* 10, 1–10. doi: 10.1038/s41598-020-61846-x

Ni, J. L., Zhu, A. G., Wang, X. F., Xu, Y., Sun, Z. M., Chen, H. J., et al. (2018). Genetic diversity and population structure of ramie (Boehmeria nivea L.). *Ind. Crops. Prod.* 115, 340–347. doi: 10.1016/j.indcrop.2018.01.038

Pineda, A., Zheng, S. J., van Loon, J. J., Pieterse, C. M., and Dicke, M. (2010). Helping plants to deal with insects: the role of beneficial soil-borne microbes. *Trends Plant Sci.* 15, 507–514. doi: 10.1016/j.tplants.2010.05.007

Piromyou, P., Buranabanyat, B., Tantasawat, P., Tittabutr, P., Boonkerd, N., and Teaumroong, N. (2010). Effect of plant growth promoting rhizobacteria (PGPR) inoculation on microbial community structure in rhizosphere of forage corn cultivated in Thailand. *Eur. J. Soil Biol.* 47, 44–54. doi: 10.1016/j.ejsobi.2010.11.004

Prescott, L. M., and Harley, J. P. (2002). *Laboratory Exercises in Microbiology. 5th Edn* (Boston, MA: McGraw-Hill).

Rehman, M., Fahad, S., Saleem, M., Hafeez, M., Rahman, M., and Deng, G. (2020). Red light optimized physiological traits and enhanced the growth of ramie (Boehmeria nivea L.). *Photosynthetica* (148131). doi: 10.32615/ps.2020.040

Sangiorgio, D., Cellini, A., Donati, I., Pastore, C., Onofrietti, C., and Spinelli, F. (2020). Facing climate change: application of microbial biostimulants to mitigate stress in horticultural crops. *Agronomy* 10, 794. doi: 10.3390/agronomy10060794

Singh, R. P., and Jha, P. N. (2016). A Halotolerant Bacterium Bacillus licheniformis HSW-16 Augments Induced Systemic Tolerance to Salt Stress in Wheat Plant (Triticum aestivum). *Front. Plant Sci.* 7. doi: 10.3389/fpls.2016.01890

Singh, R. P., Jha, P., and Jha, P. N. (2015). The plant growth promoting bacterium Klebsiella sp. SBP-8 confers induced systemic tolerance in wheat (Triticum aestivum) under salt stress. *J. Plant Physiol.* 184, 57–67. doi: 10.1016/j.jplph.2015.07.002

Sun, H., Narihiro, T., Ma, X., Zhang, X. X., Ren, H., and Ye, L. (2019). Diverse aromatic-degrading bacteria present in a highly enriched autotrophic nitrifying sludge. *Sci. Total Environ.* 666, 245–251. doi: 10.1016/j.scitotenv.2019.02.172

Sun, L., Xu, Y., Bai, S., Bai, X., Zhu, H., Dong, H., et al. (2019). Transcriptome-wide analysis of pseudouridylation of mRNA and non-coding RNAs in Arabidopsis. *J. Exp. Bot.* 70, 5089–5600. doi: 10.1093/jxb/erz273

Sun, X., Xu, Z., Xie, J., Hesselberg-Thomsen, V., Tan, T., Zheng, D., et al. (2022). Bacillus velezensis stimulates resident rhizosphere Pseudomonas stutzeri for plant health through metabolic interactions. *ISME J.* 16, 774–787. doi: 10.1038/s41396-021-01125-3

Taulé, C., Mareque, C., Barlocco, C., Hackembruch, F., Reis, V. M., Sicardi, M., et al. (2012). The contribution of nitrogen fixation to sugarcane (Saccharum officinarum L.), and the identification and characterization of part of the associated diazotrophic bacterial community. *Plant Soil.* 356, 35–49. doi: 10.1007/s11104-011-1023-4

Wang, Z., Sun, J., Zu, X., Gong, J., Deng, H., Hang, R., et al. (2022). Pseudouridylation of chloroplast ribosomal RNA contributes to low temperature acclimation in rice. *New Phytol.* 236, 1708–1720. doi: 10.1111/nph.18479

Wu, F. Y., Wan, J. H. C., Wu, S. C., and Wong, M. H. (2012). Effects of earthworms and plant growth-promoting rhizobacteria (PGPR) on availability of nitrogen, phosphorus, and potassium in soil. *J. Plant Nutr. Soil Sci.* 175, 423–433. doi: 10.1002/jpln.201100022

Yang, J., Kloepper, J. W., and Ryu, C. M. (2009). Rhizosphere bacteria help plants tolerate abiotic stress. *Trends Plant Sci.* 14, 1–4. doi: 10.1016/j.tplants.2008.10.004

Yee, B., Oertli, G. E., Fuerst, J. A., and Staley, J. T. (2010). Reclassification of the polyphyletic genus Prosthecomicrobium to form two novel genera, Vasilyevaea gen. nov. and Bauldia gen. nov. with four new combinations: Vasilyevaea enhydra comb. nov., Vasilyevaea mishustinii comb. nov., Bauldia consociata comb. nov. and Bauldia litoralis comb. nov. *Int. J. Syst. Evol. Microbiol.* 60, 2960–2966. doi: 10.1099/ijs.0.018234-0

Yu, J., Zhang, Y., Di, C., Zhang, Q., Zhang, K., Wang, C., et al. (2016). JAZ7 negatively regulates dark-induced leaf senescence in Arabidopsis. *J. Exp. Bot.* 67, 751–762. doi: 10.1093/jxb/erv487

Zeng, W., Sun, Z., Cai, Z., Chen, H., Lai, Z., Yang, S., et al. (2017). Proteomic analysis by iTRAQ-MRM of soybean resistance to Lamprosema Indicate. *BMC Genomics* 18, 444. doi: 10.1186/s12864-017-3825-0

Zhang, Z., Bi, X., Du, X., Liu, H., An, T., Zhao, Y., et al. (2022). Comparative metabolomics reveal the participation of soybean unique rhizosphere metabolites in susceptibility and resistance of host soybean to phytophthora sojae. *Plant Soil.* 480, 185–199. doi: 10.1007/s11104-022-05571-6

Zhang, R., Vivanco, J. M., and Shen, Q. (2017). The unseen rhizosphere root–soil–microbe interactions for crop production. *Curr. Opin. Microbiol.* 37, 8–14. doi: 10.1016/j.mib.2017.03.008

Zhang, L. N., Wang, D. C., Hu, Q., Dai, X. Q., Xie, Y. S., Li, Q., et al. (2019). Consortium of plant growth-promoting rhizobacteria strains suppresses sweet pepper disease by altering the rhizosphere microbiota. *Front. Microbiol.* 10. doi: 10.3389/fmicb.2019.01668

Zhang, Z., Zhang, P., Lin, Q., Cha, Z., and Luo, W. (2019). Response of bacterial communities in rubber plantations to different fertilizer treatments. *3 Biotech.* 9, 293. doi: 10.1007/s13205-019-1821-6

frontiers | Frontiers in Plant Science

TYPE Original Research
PUBLISHED 18 September 2024
DOI 10.3389/fpls.2024.1427731

OPEN ACCESS

EDITED BY
Marta Sousa Silva,
University of Lisbon, Portugal

REVIEWED BY
Shouchuang Wang,
Hainan University, China
Bo Tian,
Chinese Academy of Sciences (CAS), China

*CORRESPONDENCE
Xiangsheng Zhao
xiangshengzhao@hotmail.com
Xinquan Yang
xqyang@implad.ac.cn

RECEIVED 04 May 2024
ACCEPTED 29 August 2024
PUBLISHED 18 September 2024

CITATION
Sun X, Huang Q, Wu M, He L, Zhao X and Yang X (2024) Metabolomics and quantitative analysis to determine differences in the geographical origins and species of Chinese dragon's blood.
Front. Plant Sci. 15:1427731.
doi: 10.3389/fpls.2024.1427731

Metabolomics and quantitative analysis to determine differences in the geographical origins and species of Chinese dragon's blood

Xiuting Sun[1,2], Qing Huang[1], Mingsong Wu[3], Liu He[1], Xiangsheng Zhao[1*] and Xinquan Yang[1*]

[1]Hainan Provincial Key Laboratory of Resources Conservation and Development of Southern Medicine, Hainan Branch of the Institute of Medicinal Plant Development, Chinese Academy of Medical Sciences and Peking Union Medical College, Haikou, China, [2]Institute of Medicinal Plant Development, Chinese Academy of Medical Sciences and Peking Union Medical College, Beijing, China, [3]College of Life Science, Sichuan University, Chengdu, China

Objective: The aim of this study was to comprehensively analyze the differences in Chinese dragon's blood (CDB), specifically *Dracaena cochinchinensis* and *Dracaena cambodiana*, from different geographical origins.

Methods: Metabolomic analysis of CDB was performed by liquid chromatography-tandem mass spectrometry (LC–MS/MS). A reliable ultrahigh-performance liquid chromatography method with a photodiode array detector (UHPLC-PDA) was developed and applied for the quantitative analysis of 12 phenolic compounds in 51 batches of samples.

Results: A total of 1394 metabolites were detected, of which 467 were identified as differentially accumulated metabolites. Multivariate analysis revealed that both origin and species had an effect on the composition of CDB, with greater variation between species. 19 phenolic compounds were selected as quality markers to distinguish *D. cochinchinensis* (Hdsp) from *D. cambodiana* (Hdca), and oppositin and spinoflavanone a were identified as quality markers to discriminate *D. cochinchinensis* samples from Hainan (Hdsp) and Guangxi Provinces (Gdc). Quantitative analysis indicated that four phenolic compounds, including loureirin D, 4H-1-benzopyran-4-one,2,3-dihydro-3,5,7-trihydroxy-3-[(4-methoxyphenyl)methyl]-,(R)-, loureirin B, and pterostilbene, showed significant differences between Gdc and Hdsp. Additionally, five phenolic compounds, namely resveratrol, loureirin D, pinostilbene, 4H-1-benzopyran-4-one,2,3-dihydro-3,5,7-trihydroxy-3-[(4-methoxyphenyl)methyl]-, (R)-, and loureirin B, exhibited significant differences between Hdsp and Hdca.

Conclusion: There are significant differences in the quality of CDB from different geographical origins and species, which lays the foundation for the in-depth development and utilization of different sources of CDB.

KEYWORDS

Chinese dragon's blood, geographical origins, species, metabolomics, UHPLC-PDA, quality control

1 Introduction

Chinese dragon's blood (CDB, *Longxuejie* in Chinese) is a rare and valuable traditional Chinese medicine (TCM) with a long history of medical use and is known as a "holy medicine for promoting blood circulation". Previous phytochemical investigations have revealed that polyphenols, terpenes, steroids and steroidal saponins are major chemical constituents of this herb (Xu et al., 2010; Sun et al., 2017; Pang et al., 2018; Sun et al., 2019; Chen P. Q. et al., 2023). Among these constituents, phenolic constituents are considered the primary pharmacologically active constituents (Lang et al., 2020; Xu et al., 2022). At present, the Chinese Pharmacopoeia does not include CDB, and loureirin B are chosen as marker compounds to assess the quality (>0.4%, *m/m*) in the National Drug Standard [WS3-082(Z-016)-99(Z)] (Zheng et al., 2021). In recent years, the metabolites extracted from the resin have received increased attention for their extensive and promising bioactivities, such as antifungal (Niu et al., 2020), antibacterial (Wang et al., 2017; He et al., 2021), anticerebral ischemia (Krishnaraj et al., 2019; Liu T. et al., 2023), antithrombotic (Sun et al., 2019), antidiabetic (Liu Y. et al., 2021), anti-inflammatory and analgesic (Kuo et al., 2017; Sun et al., 2017; Pang et al., 2018) effects and the ability to promote epidermal repair (Chen et al., 2021; Sun et al., 2017).

The quality of TCMs is closely related to their metabolites (Wang et al., 2015; Lu and Cui, 2019). During production, these metabolites are susceptible to not only interference and changes caused by genetic factors but also various physiological and environmental factors, which may lead to differences in the pharmacological effects and activities of TCMs (Yang et al., 2020; Chen X. B. et al., 2023; Sha et al., 2023). Therefore, the study of variations in the metabolites of TCM has been a consistent focus. As a multiorigin TCM, CDB is derived from the resin of *Dracaena cochinchinensis* and *Dracaena cambodiana* in China. *D. cochinchinensis* is cultivated mainly in Guangxi and Hainan Provinces of China (Cai and Xu, 1979), whereas *D. cambodiana* is found primarily in Hainan Province, China (Yuan, 1991). To date, research on the influence of the plant species and geographical factors on the chemical components of CDB is relatively limited and has focused mainly on determining the differences in the contents of a few specific classes of metabolites (Qin et al., 2013; Wan, 2017; Chen et al., 2018). The chemical composition of TCMs is complex, and the current TCM quality evaluation model relies mainly on the determination of a few compounds, which makes accurate evaluate of the quality of TCMs difficult. Thus, there is an urgent need to identify additional metabolites of CDB to evaluate the overall chemical features of samples collected from different geographical origins and of different species.

Plant metabolomics, a branch of metabolomics, is a powerful tool designed to study the overall changes in many metabolites in plant samples and then perform deep data mining and bioinformatics to identify differences between samples (Abraham and Kellogg, 2021; Xiao et al., 2022). Liquid chromatography-tandem mass spectrometry (LC–MS/MS) is one of the most frequently used techniques for plant metabolomics analysis of TCMs because of its short analysis time, exact mass identification, and high selectivity and sensitivity (Alseekh et al., 2021; Waris et al., 2022). Plant metabolomics has been widely applied for source identification, authenticity identification, processing method evaluation and other quality control applications of TCM (Liang et al., 2018; Abraham and Kellogg, 2021; Yoon et al., 2022; Liu X. et al., 2023; Rivera-Pérez et al., 2023). This finding offers a valuable opportunity to understand the metabolite differences that influence the medicinal quality of CDB from different geographical origins and species. However, there are no studies on plant metabolomics for CDB. In addition, quantitative analysis based on ultrahigh-performance liquid chromatography-photodiode array detector (UHPLC-PDA) technology has become a widely used method for TCM quality control and quality standard improvement (Lee et al., 2010; Liao et al., 2021).

In this study, a total of 51 samples were collected, including samples of *D. cochinchinensis* from Guangxi Province (Gdc) and Hainan Province (Hdsp), and *D. cambodiana* from Hainan Province (Hdca). A plant metabolomic strategy based on LC–MS/MS was established to identify the differentially abundant metabolites (DAMs) in 21 samples. A UHPLC-PDA method was developed to quantitatively assess the variation of 12 phenolic compounds in 51 samples. This study enhances the understanding of the differences between the geographical origins and species of the CDB. The results will contribute to effective quality control measures and provide a theoretical basis for the rational and effective use of CDB.

2 Materials and methods

2.1 Samples

Fifty-one batches of wild *D. cochinchinensis* and *D. cambodiana* samples were collected from natural habitats in Hainan and Guangxi Provinces, China (Supplementary Table S1). The samples were identified by associate researcher Rongtao Li (Hainan Branch of the Institute of Medicinal Plant Development, Chinese Academy of Medicinal Sciences), and voucher specimens (No. Gdc-24, Hdsp-8, Hdca-2) were deposited in the herbarium of the Hainan Branch Institute of Medicinal Plant Development, Chinese Academy of Medical Sciences, Hainan, China. All the samples were utilized for content determination, and 21 samples were selected from the three groups for plant metabolomics analysis.

2.2 Solvents and chemicals

The reference material for CDB (*D. cochinchinensis*, collected from Guangxi Province) was purchased from the National Institutes of Food and Drug Control (Beijing, China). Reference standards of *p*-hydroxybenzyl alcohol (LOT: 6100) were purchased from Shanghai Shidande Standard Technical Service Co., Ltd. (Shanghai, China). Loureirin D (LOT: RFS-L02801907025) and

loureirin C (LOT: RFS-L05901907025) were purchased from Chengdu Herbpurify Co., Ltd. (Chengdu, China). 4H-1-benzopyran-4-one,2,3-dihydro-5-hydroxy-3-[(4-hydroxyphenyl) methyl]-7-methoxy (LOT: CHB210112), liquiritigenin (LOT: CHB180609), pinostilbene (LOT: CHB210104) and 4H-1-benzopyran-4-one,2,3-dihydro-3,5,7-trihydroxy-3-[(4-methoxyphenyl) methyl]-,(R)- (LOT: CHB210113) were purchased from Chroma-Biotechnology Co., Ltd. (Chengdu, China). Resveratrol (LOT: 137-12-47), (3R)-5,7-dihydroxy-3-(4-hydroxybenzyl)-2,3-dihydro-4H-chromen-4-one (LOT: CHB210113), loureirin A (LOT: 0817-RB-0015), loureirin B (LOT: 0817-RB-0016) and pterostilbene (LOT: 0817-RB-0036) were purchased from Hainan Lead and Change Technology Co., Ltd. (Haikou, China). The purities of all standards were above 98%. HPLC-grade acetonitrile and acetic acid were purchased from Fisher Co., Ltd. (Emerson, IA, USA). Analytical-grade ethanol was purchased from Beijing Chemical Works (Beijing, China). Pure water was obtained from Wahaha (Hangzhou, China).

2.3 Plant metabolomic analysis

2.3.1 Metabolite extraction

A total of 20 mg of sample was weighed into an eppendorf tube, and 1000 µL of extraction solution (methanol:water = 3:1, with an isotopically labeled internal standard mixture) was added. The sample was subsequently homogenized at 35 Hz for 4 min and sonicated for 5 min in an ice-water bath. The homogenization and sonication cycles were conducted in triplicate. The samples were subsequently tincubated for 1 h at -40°C and centrifuged at 12000 rpm for 15 min at 4°C. The supernatant was filtered through a 0.22 µm microporous membrane and transferred to a fresh glass vial for analysis. The quality control (QC) sample was prepared by mixing equal aliquots of the supernatants from all of the samples to evaluate the reproducibility and stability of the LC-MS/MS method.

2.3.2 LC–MS/MS analysis

Sample analyses were performed on a UHPLC system (Vanquish, Thermo Fisher Scientific) with a UPLC HSS T3 column (2.1 mm × 100 mm, 1.8 µm) coupled to an Orbitrap Exploris 120 mass spectrometer (Orbitrap MS, Thermo), and the column temperature was 40°C. The mobile phase consisted of 5 mmol/L ammonium acetate and 5 mmol/L acetic acid in water (A) and acetonitrile (B) with flow 0.35 ml/min. The following gradient program was used: 0-0.7 min, 1% B; 0.7-9.5 min, 1%-99% B; 9.5-11.8 min, 99% B; 11.8-12 min, 99%-1% B; 12-14.6 min, 1% B; 14.6-14.8 min, 1% B; 14.8-15 min, 1% B. The autosampler temperature was 4°C, and the injection volume was 2 µL. An Orbitrap Exploris 120 mass spectrometer was used for its ability to acquire MS/MS spectra in information-dependent acquisition (IDA) mode via acquisition software (Xcalibur, Thermo). In this mode, the acquisition software continuously evaluates the full-scan MS spectrum. The electrospray ionization (ESI) source conditions were set as follows: sheath gas flow rate, 50 Arb; aux gas flow rate, 15 Arb; capillary temperature, 320°C; full MS resolution, 60000; MS/MS resolution, 15000; collision energy, 10/30/60 NCE; and spray voltages, 3.8 kV (positive) and -3.4 kV (negative).

2.4 Data processing and metabolite characterization

The raw data were converted to the mzXML format via ProteoWizard and processed with an in-house program, which was developed using R and based on XCMS, for peak detection, extraction, alignment, and integration. The criteria for the structural identification of metabolites are categorized into three levels. Level 1 is achieved by comparing information such as MS, MS/MS, and retention times of standards. Level 2 is achieved by comparing information such as MS and MS/MS from public databases, which include HMDB (https://hmdb.ca/), PubChem (https://pubchem.ncbi.nlm.nih.gov/), and KEGG (https://www.kegg.jp/). Finally, level 3 is achieved by comparing information such as MS, MS/MS, and retention time using a matching algorithm based on MetDNA2 (BiotreeDB) (Zhou et al., 2022). The cutoff for annotation was set at 0.3. Furthermore, principal component analysis (PCA) and orthogonal partial least squares discriminant analysis (OPLS-DA) were performed with SIMCA 16.0.2 software (Sartorius Stedim Data Analytics AB, Umea, Sweden). To evaluate the OPLS-DA model, 7-fold cross-validation was performed to calculate the R^2 (model fitness) and Q^2 (predictive ability) values, and a permutation test (200 times) was subsequently conducted.

2.5 Potential biomarker identification and metabolic pathway analysis

In this study, the metabolites with variable importance in the projection (VIP) > 1 and a P value < 0.05 (Student's t test) were screened as potential differentially abundant metabolites. After the metabolites were identified, the metabolic enrichment pathways of potential DAMs were analyzed via MetaboAnalyst (http://metpa.metabolomics.ca) and the Kyoto Encyclopedia of Genes and Genomes (KEGG) pathway database (http://www.genome.jp/kegg/) with a map of the same plant family, *Asparagus officinalis*. Through comprehensive analysis of the pathways in which the DAMs were located, the most important pathways that correlated with the metabolite differences were screened.

2.6 UHPLC-PDA analysis

2.6.1 Preparation of stock and mixed standards

Each standard was accurately weighed and dissolved in 70% aqueous ethanol (*v/v*) to obtain a stock solution. An initial stock solution was prepared as a mixture of the above stock solutions. A series of working solutions of the analytes were obtained by diluting

the mixed stock solution with 70% aqueous ethanol to the appropriate concentration.

2.6.2 Sample preparation

A total of 0.2 g of the sample was extracted with 10 mL of 70% ethanol (*v/v*) in an ultrasonic water bath for 30 min and then centrifuged at 13000 rpm for 10 min. The supernatant solution was filtered through a 0.22 μm micropore membrane before injection into the UHPLC system. Each sample was analyzed in triplicate.

2.6.3 UHPLC-PDA conditions

The quantitative analysis of 12 phenolic compounds was performed on a UHPLC system (Waters Corporation, USA) coupled with a photodiode array detector (PDA). The analytes were separated on a Waters Acquity HSS T3 column (2.1 mm × 100 mm, 1.8 μm), and the column temperature was maintained at 40°C. The mobile phase consisted of acetonitrile (A) and water containing 0.3% acetic acid (B) with a flow rate of 0.3 mL/min. The following gradient program was used: 0-5 min, 20-25% A; 5-30 min, 25-30% A; 30-62 min, 30-38% A; 62-75 min, 38-95% A; and 75-76 min, 95-20% A. The PDA detector was set to monitor the signal at 278 nm. The sample injection volume was 5.0 μL.

2.6.4 Method validation

The developed UHPLC-PDA method was validated by determining its linearity, limit of detection (LOD), limit of quantification (LOQ), precision (intra- and interday), repeatability, stability and accuracy. The mixed standard containing 12 analytes was diluted with 70% aqueous ethanol to obtain a range of appropriate concentrations for calibration curves, which were constructed by plotting the peak area (y) versus the corresponding concentration (x, μg/ml). The LODs and LOQs were determined at signal-to-noise (S/N) ratios of 3 and 10, respectively. The precision of the intra- and inter-day was tested by performing six replicates of a mixed standard solution within a single day and repeating the experiment on three consecutive days. Repeatability was tested by preparing six replicates of *D. cochinchinensis*. The stability of all analytes was evaluated by injecting samples at 0, 2, 4, 8, 12 and 24 h. The relative standard deviation (RSD) value was used to assess precision, repeatability and stability. The accuracy of the method was determined via a recovery test by spiking an equal amount of standard mixture to a known amount of sample (0.1 g) of *D. cochinchinensis* (n=6). The spiked samples were subsequently extracted and analyzed via the proposed method.

2.7 Statistical analysis

The data were analyzed via SPSS 26.0 (SPSS Inc., Chicago, IL, USA). All values are expressed as the means ± SDs of at least three independently performed experiments. The results were considered statistically significant when $p<0.05$. Figure processing was performed with GraphPad Prism 8.0 software(GraphPad Software, Inc., San Diego, CA, USA).

3 Results

3.1 Metabolomic analysis

3.1.1 Identification and analysis of differentially abundant metabolites

To better understand the metabolic differences between geographical origins and species, LC–MS/MS was employed to detect CDB metabolites in three different groups: Gdc, Hdsp and Hdca. Mass spectral data were processed by alignment of all data sets from the samples in the CDB group. Metabolite annotation was performed by comparing accurate *m/z* values (Supplementary Figure S1). A total of 1237 metabolites were annotated (Supplementary Table S2), the most abundant of which were shikimates and phenylpropanoids (49.475%), followed by terpenoids (16.168%), fatty acids (8.892%), polyketides (5.74%) and alkaloids (5.416%) (Supplementary Figure S2).

PCA was used as an unsupervised method to study the differences in metabolic profiles between two geographical origins and two species of CDB. The PCA results revealed significant separation of three different groups of samples, which reflected significant differences in metabolite levels in different sources, with 43.5% of the differences explained by the first two principal components (32.7% for PC1 and 10.8% for PC2). In addition, Hdca samples were significantly separated from Hdsp samples in the PCA, whereas the Gdc and Hdsp samples partially overlapped (Figure 1A). A correlation analysis of the multisource metabolome revealed strong correlations between the biorepeats within the same group. In different groups of samples, Hdca and Hdsp samples could be distinguished from each other, but this was not true for some Gdc and Hdsp samples, similar to the PCA results (Supplementary Figure S3). The heatmap of the hierarchical clustering analysis (HCA) results illustrate the differences in metabolite accumulation among the three groups of samples. These samples were divided into two large clusters, with significant differences between Hdca and Hdsp and Gdc (Figure 1B), preliminarily revealing that the difference in metabolites between the two species was greater than the difference between the two geographical origins.

To investigate the differences in metabolites between different species and different geographical origins of CDB, OPLS-DA was performed. The Hdsp and Gdc groups were significantly separated on the first principal component, with P1 values of 15.3% and 9.7%, respectively (Figure 1C). Hdsp and Hdca were also significantly separated on the first principal component, with P1 values of 27.7% and 14.0%, respectively (Figure 1D). The R^2Y and Q^2 values of CDB from different origins were 0.96 and 0.59, respectively (Supplementary Figure S4A), whereas the R^2Y and Q^2 values of the samples from different species were 0.84 and 0.94, respectively (Supplementary Figure S4B), both of which did not exceed the true value (horizontal line), implying that there was no overfitting. DAMs were identified via Student's t test and variable importance in projection ($P<0.05$; VIP>1). Volcano plots revealed 214 DAMs in samples from different geographical origins (Figure 2A), and 366 DAMs in samples from different species (Figure 2B), which also

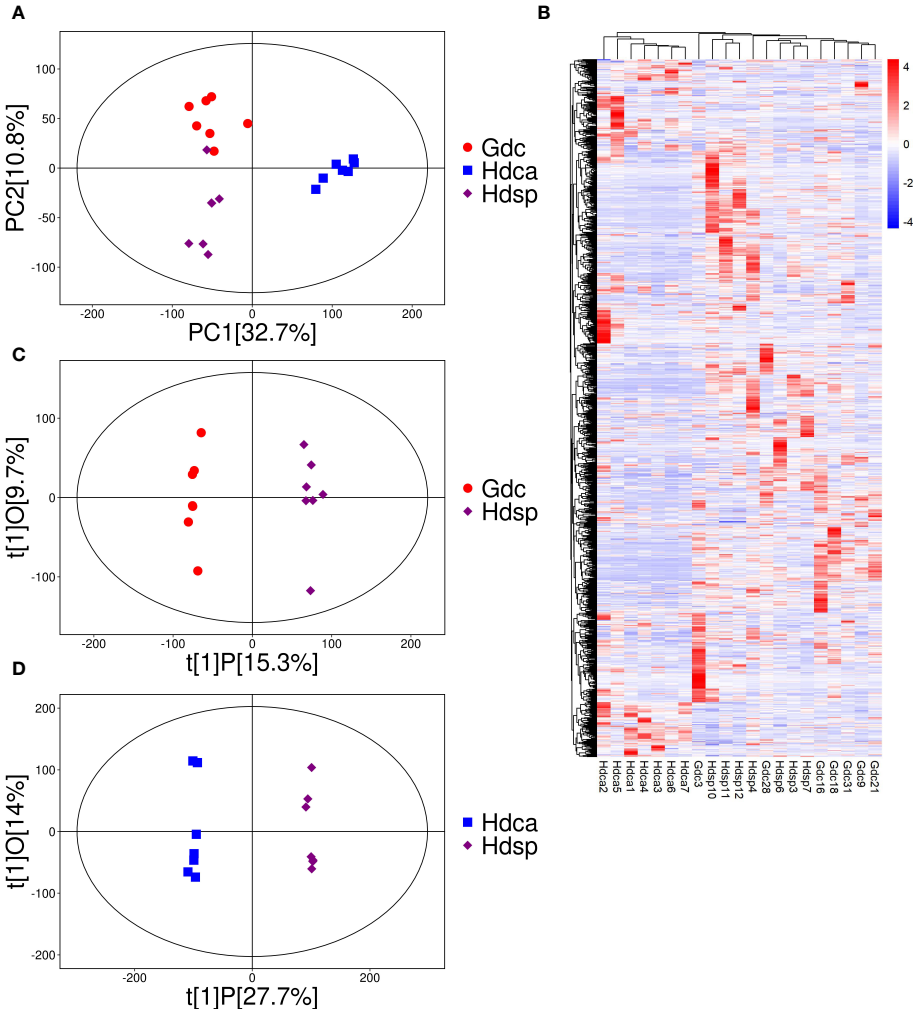

FIGURE 1
Principal component analysis (PCA) **(A)**, heatmap of hierarchical clustering analysis (HCA) **(B)**, OPLS-DA loading plots **(C, D)** of metabolites detected in different geographical origins and species.

suggested that the differences in the metabolome between the two species were greater than the differences between the two geographical origins.

3.1.2 Metabolite biomarkers differentiating geographical origins and species of CDB

When the DAMs between different species and different geographical origins were compared, 113 DAMs were common to the two comparison groups, and 253 and 101 DAMs were specific to Hdsp *vs* Hdca and Gdc *vs* Hdsp, respectively (Figure 2C).

The 113 shared compounds could be divided into 31 categories (Figure 2D), including 25 flavonoids. For binary logistic regression, the top 10 DAMs from the 113 DAMs ($P < 0.05$, VIP > 1) were selected as candidate combined biomarkers for receiver operating characteristic (ROC) curve analysis. The ROC curve results revealed that these combined biomarkers had excellent sensitivity and high specificity (AUC = 1) (Supplementary Figure S5), effectively distinguishing CDB from different geographical origins and species. Therefore, these 10 DAMs can discriminate *D. cochinchinensis* from the Guangxi and Hainan origins and different species of *D. cochinchinensis* and *D. cambodiana*. Additionally, individual ROC analyses of these 10 DAMs also demonstrated high sensitivity and specificity (AUC > 0.96) (Supplementary Figure S5), allowing them to be used as biomarkers alone to screen for different geographical origins and species.

The differences in metabolites between *D. cochinchinensis* collected from Guangxi and Hainan Provinces were compared (Gdc *vs* Hdsp). The volcano plot (Figure 2A) and HCA (Figure 3A) revealed that among 214 DAMs between Gdc and Hdsp, 111 were upregulated, with a greater relative abundance in Gdc, and 103 were downregulated, with a greater relative abundance in Hdsp. These findings indicate the promising potential of these metabolites to distinguish CDB from different geographical origins. These DAMs can be broadly classified into 8 categories: shikimates and phenylpropanoids (57.01%), terpenoids (13.55%), fatty acids (5.61%), polyketides (5.14%), alkaloids (4.21%), amino acids and peptides (2.8%), carbohydrates (3.27%)

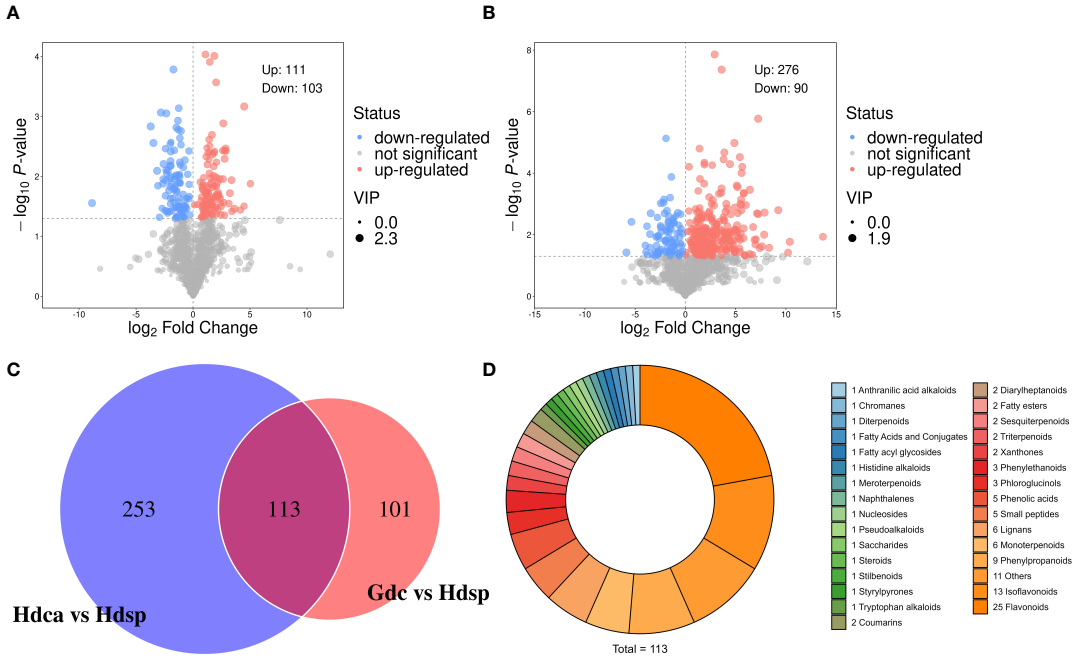

FIGURE 2
Volcano plots (red, blue and grey dots mean the metabolites were thought to be up-, down-regulated and inapparent.) of differentially accumulated metabolites in different geographical origins **(A)** and different species **(B)**. Venn diagram built to discriminate CDB samples from two geographical origins (Gdc vs Hdsp) and two species (Hdsp vs Hdca) **(C)**. Pie chart illustrating the classification of the 113 potential biomarkers **(D)**.

and others (8.41%) (Figure 3B). Phenolic compounds, particularly flavonoids and stilbenoids, which are abundant and primary pharmacological components, are the active ingredients in CDB. Therefore, these metabolites were selected for the significance analysis of relative abundance and significance between different geographical origins. A total of 101 unique compounds were identified in the comparative groups. Further screening revealed no unique stilbenoid compounds, whereas there were 22 unique flavonoid compounds. Among these 22 flavonoids, 15 had a relatively high relative abundance in the Gdc samples, whereas 7 had a relatively high relative abundance in the Hdsp samples, indicating that the relative abundance of flavonoids in the Gdc samples was greater than that in Hdsp samples (Supplementary Table S3). Additionally, oppositin and spinoflavanone a showed more than a 10-fold difference in relative abundance between the two groups, confirming their role as crucial biomarkers for tracking CDB from different origins.

Two species of *D. cochinchinensis* and *D. cambodiana* growing in Hainan Province were compared to identify differences. A total of 366 compounds were identified as potentially DAMs between Hdca and Hdsp. The volcano plot (Figure 2B) and HCA (Figure 3C) illustrate that among these metabolites, 276 were upregulated, with a greater relative abundance in Hdsp. Additionally, 90 metabolites were downregulated, exhibiting a greater relative abundance in Hdca. These findings indicate the promising potential of these metabolites in distinguishing CDB from *D. cochinchinensis* and *D. cambodiana*. These DAMs can be broadly classified into 8 categories: shikimates and phenylpropanoids (57.65%), terpenoids (14.21%), fatty acids (6.01%), polyketides (5.46%), alkaloids (5.46%), amino acids and peptides (1.37%), carbohydrates (1.37%) and others (8.47%) (Figure 3D). Additionally, because flavonoids and stilbenoids are the main active ingredients of CDB, these metabolites were selected for the analysis of their relative abundance and significance between the different species. In the comparisons between the different CDB species, there were 253 unique compounds, including 53 flavonoids and 9 stilbenoids. Among these 53 flavonoids, 28 had greater relative abundance in Hdsp, and another 15 in Hdca; of the 10 stilbenoids, 8 were more abundant in Hdsp and 1 was more abundant in Hdca, indicating higher relative abundance of these two main compound classes in Hdsp samples (Supplementary Table S4). In addition, the relative abundance of 19 DAMs, including naringin, sanggenol l, 6-hydroxy-2-(4-methoxyphenyl)-4h-chromen-4-one, artonol c, (2s)-4'-hydroxy-5,7,3'-trimethoxyflavan, 7-methoxyflavonol, brosimacutin i, farrerol, 5,7-dihydroxy-2-(4-hydroxyphenyl)-8-[3,4,5-trihydroxy-6-(hydroxymethyl)oxan-2-yl]-6-(3,4,5-trihydroxyoxan-2-yl)chromen-4-one, 7-hydroxy-2-(4-hydroxy-3,5-dimethoxyphenyl)-5-[(2s,3r,4s,5s,6r)-3,4,5-trihydroxy-6-(hydroxymethyl)oxan-2-yl]oxychromen-4-one, sempervirenoside b, robinin, didymin, 2'-methoxyflavone, cardamonin, angoletin, trans-resveratrol, pinosylvin and 3,4,5-trihydroxystilbene, exhibited more than a 10-fold difference between the two groups, and these metabolites were identified as important biomarkers for tracking different species of CDB.

3.1.3 Metabolic pathway analysis

To elucidate the metabolic activities in CDB obtained from different geographical origins and species, we mapped the DAMs to

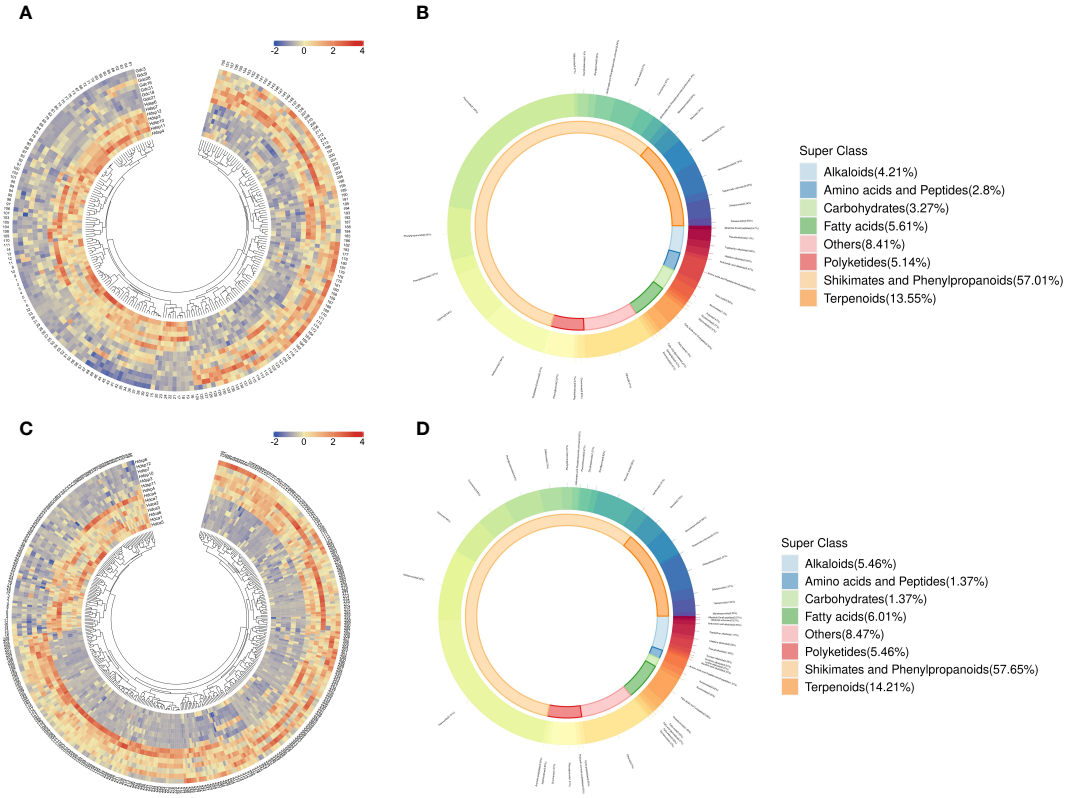

FIGURE 3
Hierarchical clustering analysis **(A)** (red colors show high abundance, whereas low abundance is presented by blue) and donut plot **(B)** for CDB samples from different geographical origins. Hierarchical clustering analysis **(C)** and donut plot **(D)** for CDB samples from different species. The names of the compounds represented by each number in Figures 2A, C are listed in Supplementary Table S7.

KEGG pathways. After comprehensive consideration, the significant pathways were marked with large bubbles and dark colors. Phenylpropanoid biosynthesis, arginine and proline metabolism, histidine metabolism, flavonoid biosynthesis, and glycerophospholipid metabolism were the main pathways enriched between Gdc and Hdsp, and the results are shown in Figure 4A. In addition, pathways such as histidine metabolism; phenylpropanoid biosynthesis; linoleic acid metabolism; alanine, aspartate and glutamate metabolism and galactose metabolism were enriched predominantly between Hdsp and Hdca (Figure 4B). Among these major enrichment pathways, histidine metabolism and phenylpropanoid biosynthesis were two pathways common to both comparison groups. It can be inferred that the aforementioned biosynthetic pathways act as critical pathways and play a significant role in the quality variation in CDB from different geographical origins and species.

To explore how geographical origins and species quantitatively affect the chemical components of CDB, 12 phenolic compounds, namely, p-hydroxybenzyl alcohol, resveratrol, 4H-1-benzopyran-4-one,2,3-dihydro-5-hydroxy-3-[(4-hydroxyphenyl)methyl]-7-methoxy-, liquiritigenin, pinostilbene, (3R)-5,7-dihydroxy-3-(4-hydroxybenzyl)-2,3-dihydro-4H-chromen-4-one, 4H-1-benzopyran-4-one,2,3-dihydro-3,5,7-trihydroxy-3-[(4-methoxyphenyl)methyl]-,(R)-, loureirin A, loureirin B, loureirin D, loureirin C, and pterostilbene, were selected as the analytes for UHPLC-PDA analysis. These chemicals were not only identified as major chemical components but also reported to be the major bioactive chemical components in CDB.

3.2 UHPLC-PDA analysis

3.2.1 UHPLC-PDA conditions

In this study, the extraction conditions (extraction solvent, extraction time) and chromatographic conditions (mobile phase, gradient program) were optimized for the 12 phenolic compounds because of their different chemical properties.

To achieve the optimal extraction conditions, the extraction solvent (50%, 70% and 100% ethanol, *v/v*) and extraction time (15, 30, 60, and 90 min) were investigated. Aqueous ethanol was found to be more suitable for the samples since it provided the highest amounts of the target analytes. The extraction efficiency did not significantly increase with ethanol concentrations above 70%. Furthermore, the extraction time was also investigated, and the extraction efficiency did not significantly increase when the extraction time exceeded 60 min (Supplementary Figure S6).

To separate the compounds and improve the sensitivity, the chromatographic and detector conditions were systemically optimized. First, gradient elution was chosen because of the wide polarity range of the 12 analytes selected. The most suitable elution

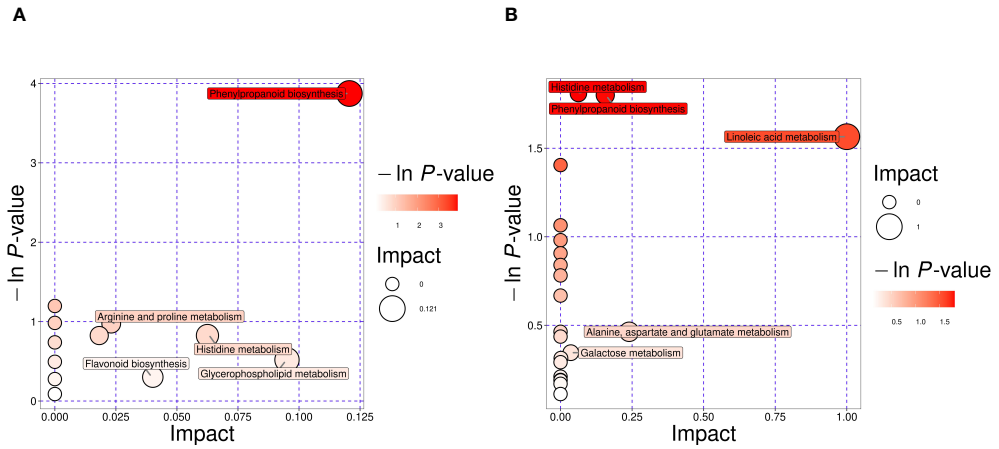

FIGURE 4
Pathway analysis of differential metabolites. Gdc vs Hdsp **(A)**. Hdsp vs. Hdca **(B)**. Each bubble represents one pathway, the abscissa and the size of the bubble reflect the influencing factors of the pathway.

solvents were acetonitrile (A) and 0.3% acetic acid. The proportions of acetonitrile and acetic acid, as well as the gradient elution time, were carefully adjusted based on the various schemes outlined in Supplementary Table S5. Remarkably, Scheme 4 demonstrated exceptional separation results in a relatively short timeframe. Consequently, under the established optimal conditions, a representative chromatogram (Supplementary Figure S7) was obtained, effectively illustrating the successful separation and elution of the target compounds.

3.2.2 Method validation

The optimized UHPLC-PDA method was validated by evaluating its linearity, LOD, LOQ, precision, repeatability, stability and accuracy. The results are summarized in Table 1. Notably, excellent linearity was observed in the regression equations of all analytes, with a coefficient of determination (R^2) ≥ 0.9983. The LODs and LOQs of the 12 analytes ranged from 0.021 to 0.031 μg/mL and 0.069 to 0.089 μg/mL, respectively. The overall RSDs of the intraday and interday variations were not greater than 3.47% and 4.92%, respectively. The repeatability and stability did not exceed 2.99% and 2.82%, respectively. The recovery of the method was determined to be between 93.70% and 104.91%, with RSDs (%) ranging from 1.06 to 5.16 (Table 2). All these results showed that the established method has good linearity, precision, stability, reproducibility and accuracy and can be used for the quantification of 12 phenolic compounds in CDB.

3.2.3 Quantitative results

The developed UHPLC-PDA method was applied to simultaneously determine the amount of 12 phenolic compounds in 51 batches of CDB samples collected from different sources (Supplementary Table S6).

Among the 51 batches of CDB samples, the contents of the 12 analytes ranged from 0.01 to 21.05 mg/g. Notably, loureirin B, loureirin C, p-hydroxybenzyl alcohol and resveratrol had the highest average contents of 3.63, 3.48, 3.21 and 3.12 mg/g, respectively, suggesting a potentially crucial role for these four phenolic compounds in CDB. Furthermore, loureirin B has been used as a chemical marker for quality control with CDB. Among the 51 samples tested, only 13 batches of loureirin B met the 0.4% limit. More precisely, only 5 of 31 batches of Gdc samples were qualified, 8 of 12 batches of Hdsp samples were qualified, and none of the Hdca samples met the criteria. In other words, almost 75% of the samples did not meet the expected quality standards, and the Hdca samples have a particularly prominent quality issue, highlighting the need for further investigation into the reasons and implementation of appropriate measures to ensure product quality and safety.

3.2.4 Quantitative analysis of CDB from differentiating geographical origins and species

Notable variations were observed in the comparative analysis of 12 phenolic compounds in the CDB samples obtained from different geographical origins. The Hdsp samples presented relatively high contents of loureirin D, pinostilbene, 4H-1-benzopyran-4-one,2,3-dihydro-3,5,7-trihydroxy-3-[(4-methoxyphenyl) methyl]-, (R)-, and loureirin B. Conversely, the Gdc samples presented higher contents of the remaining eight components. Statistical analysis ($P < 0.05$) revealed significant difference between the two geographical origins in China for loureirin D, 4H-1-benzopyran-4-one,2,3-dihydro-3,5,7-trihydroxy-3-[(4-methoxyphenyl) methyl]-, (R)-, loureirin B, and pterostilbene (Figure 5).

Furthermore, when comparing the CDB samples from the different species, significant differences were observed in the average contents of the 12 phenolic compounds. Specifically, the contents of all 12 compounds were greater in Hdsp than in Hdca. In addition, the analytical results (Figure 5) revealed that the contents of components such as resveratrol, loureirin D, pinostilbene, 4H-1-benzopyran-4-one,2,3-dihydro-3,5,7-trihydroxy-3-[(4-methoxyphenyl) methyl]-, (R)- and loureirin B significantly differed ($P < 0.05$).

TABLE 1 Calibration curves,testrange,LOD,LOQ,precision,stability and repeatability for the 12 analytes.

Analytes	Linearrange ($\mu g \cdot mL^{-1}$)	Calibration curves	R^2	LOQ ($\mu g \cdot mL^{-1}$)	LOD ($\mu g \cdot mL^{-1}$)	Precision(RSD, %)		Stability (RSD,%)	Reproducibility (RSD,%,n=6)
						intraday (n=6)	Interday (n=6)		
p-hydroxybenzyl alcohol	0.67~33.33	y=16859x+2199.4	0.9983	0.083	0.027	2.04	4.92	1.73	2.99
resveratrol	0.6~30.00	y=109,961x-14,874.5	1.0000	0.072	0.024	0.21	0.98	1.15	2.17
liquiritigenin	0.53~26.67	y=99799x+4093.5	1.0000	0.070	0.021	0.45	3.11	0.50	2.17
4H-1-benzopyran-4-one,2,3-dihydro-5-hydroxy-3-[(4-hydroxyphenyl) methyl]-7-methoxy-	0.78~39.00	y=121263x+4635.3	1.0000	0.087	0.031	3.01	4.50	0.62	2.60
loureirin D	0.70~35.00	y=81439x+1910.8	0.9999	0.088	0.028	0.22	0.86	2.70	1.19
loureirin C	0.66~33.00	y=88,723x+939.6	1.0000	0.081	0.026	0.19	1.46	2.45	1.68
(3R)-5,7-Dihydroxy-3-(4-hydroxybenzyl)-2,3-dihydro-4H-chromen-4-one	0.62~31.00	y=97163x+2408.9	0.9999	0.073	0.025	0.52	3.81	2.62	2.25
pinostilbene	0.64~32.00	y=105306x-25996.7	0.9999	0.074	0.026	0.57	2.84	1.06	2.98
4H-1-benzopyran-4-one,2,3-dihydro-3,5,7-trihydroxy-3-[(4-methoxyphenyl) methyl]-,(R)-	0.59~29.33	y=88730x+2171.2	1.0000	0.069	0.023	3.47	4.27	2.49	2.08
loureirin A	0.77~38.33	y=110474x+2046.7	1.0000	0.089	0.031	2.44	4.16	2.82	2.44
loureirin B	0.77~38.33	y=95,204x-220.9	1.0000	0.086	0.031	1.09	3.12	2.75	2.46
pterostilbene	0.64~32.00	y=96782x-35754.5	0.9998	0.079	0.026	2.58	2.51	2.65	2.13

10.3389/fpls.2024.1427731

10.3389/fpls.2024.1427731

TABLE 2 Experimental results of sample addition recovery rate (n=6).

Analytes	Original (mg)	Added (mg)	Found (mg)	Recovery (%)	Recovery (%)	RSD (%,n=6)
p-hydroxybenzyl alcohol	0.0034	0.0169	0.0211	104.60	104.91	1.85
	0.0034	0.0169	0.0210	103.90		
	0.0034	0.0169	0.0206	101.74		
	0.0034	0.0169	0.0213	106.02		
	0.0034	0.0169	0.0215	107.21		
	0.0034	0.0169	0.0213	106.01		
resveratrol	0.0366	0.0160	0.0533	104.62	104.85	1.69
	0.0366	0.0160	0.0532	104.16		
	0.0366	0.0160	0.0532	103.83		
	0.0366	0.0160	0.0532	103.91		
	0.0366	0.0160	0.0532	104.13		
	0.0366	0.0160	0.0539	108.42		
liquiritigenin	0.0016	0.0136	0.0155	101.91	100.58	1.26
	0.0016	0.0136	0.0151	99.03		
	0.0016	0.0136	0.0154	101.04		
	0.0016	0.0136	0.0153	100.37		
	0.0016	0.0136	0.0151	99.23		
	0.0016	0.0136	0.0155	101.90		
4H-1-benzopyran-4-one,2,3-dihydro-5-hydroxy-3-[(4-hydroxyphenyl)methyl]-7-methoxy-	0.0022	0.0218	0.0230	95.23	93.70	1.34
	0.0022	0.0218	0.0225	93.00		
	0.0022	0.0218	0.0227	93.75		
	0.0022	0.0218	0.0226	93.30		
	0.0022	0.0218	0.0223	91.93		
	0.0022	0.0218	0.0230	95.01		
loureirin D	0.0094	0.0152	0.0250	102.57	101.59	1.61
	0.0094	0.0152	0.0247	100.30		
	0.0094	0.0152	0.0249	101.52		
	0.0094	0.0152	0.0247	100.32		
	0.0094	0.0152	0.0247	100.44		
	0.0094	0.0152	0.0253	104.38		
loureirin C	0.0170	0.0170	0.0337	98.31	97.87	1.49
	0.0170	0.0170	0.0335	96.77		
	0.0170	0.0170	0.0338	98.48		
	0.0170	0.0170	0.0334	96.41		
	0.0170	0.0170	0.0335	96.96		
	0.0170	0.0170	0.0341	100.31		
(3R)-5,7-Dihydroxy-3-(4-hydroxybenzyl)-2,3-dihydro-4H-chromen-4-one	0.0151	0.0156	0.0310	101.63	97.79	2.44
	0.0151	0.0156	0.0301	96.26		

(Continued)

TABLE 2 Continued

Analytes	Original (mg)	Added (mg)	Found (mg)	Recovery (%)	Recovery (%)	RSD (%,n=6)
	0.0151	0.0156	0.0303	97.09		
	0.0151	0.0156	0.0300	95.55		
	0.0151	0.0156	0.0302	96.45		
	0.0151	0.0156	0.0307	99.79		
pinostilbene	0.0115	0.0172	0.0282	97.05	101.43	2.77
	0.0115	0.0172	0.0286	99.49		
	0.0115	0.0172	0.0295	104.19		
	0.0115	0.0172	0.0291	102.31		
	0.0115	0.0172	0.0289	101.25		
	0.0115	0.0172	0.0295	104.26		
4H-1-benzopyran-4-one,2,3-dihydro-3,5,7-trihydroxy-3-[(4-methoxyphenyl)methyl]-,(R)-	0.0022	0.0143	0.0159	95.47	93.72	1.24
	0.0022	0.0143	0.0156	93.53		
	0.0022	0.0143	0.0156	93.90		
	0.0022	0.0143	0.0155	93.02		
	0.0022	0.0143	0.0154	92.06		
	0.0022	0.0143	0.0157	94.34		
loureirin A	0.0042	0.0228	0.0265	97.59	98.14	1.06
	0.0042	0.0228	0.0264	97.11		
	0.0042	0.0228	0.0268	98.88		
	0.0042	0.0228	0.0266	98.10		
	0.0042	0.0228	0.0265	97.33		
	0.0042	0.0228	0.0270	99.84		
loureirin B	0.0505	0.0196	0.0702	100.74	102.42	2.21
	0.0505	0.0196	0.0706	102.40		
	0.0505	0.0196	0.0707	103.27		
	0.0505	0.0196	0.0702	100.28		
	0.0505	0.0196	0.0704	101.36		
	0.0505	0.0196	0.0714	106.47		
pterostilbene	0.0084	0.0160	0.0235	94.08	103.80	5.16
	0.0084	0.0160	0.0249	103.18		
	0.0084	0.0160	0.0250	103.35		
	0.0084	0.0160	0.0253	105.31		
	0.0084	0.0160	0.0256	107.31		
	0.0084	0.0160	0.0260	109.60		

4 Discussion

CDB is a rare and valuable traditional medicine that is found mainly in Hainan and Guangxi, China, and is extracted from the fat-containing wood of *D. cochinchinensis* and *D. cambodiana*. Previous studies have shown that the main components of CDB are phenolic compounds with antibacterial, anti-inflammatory, analgesic, antiplatelet aggregation, blood circulation and epidermal repair properties (Zheng et al., 2021). The intrinsic quality of TCM is closely associated with its secondary metabolites. The types, quantities and activities of these secondary metabolites are in turn affected by factors such as the growth

10.3389/fpls.2024.1427731

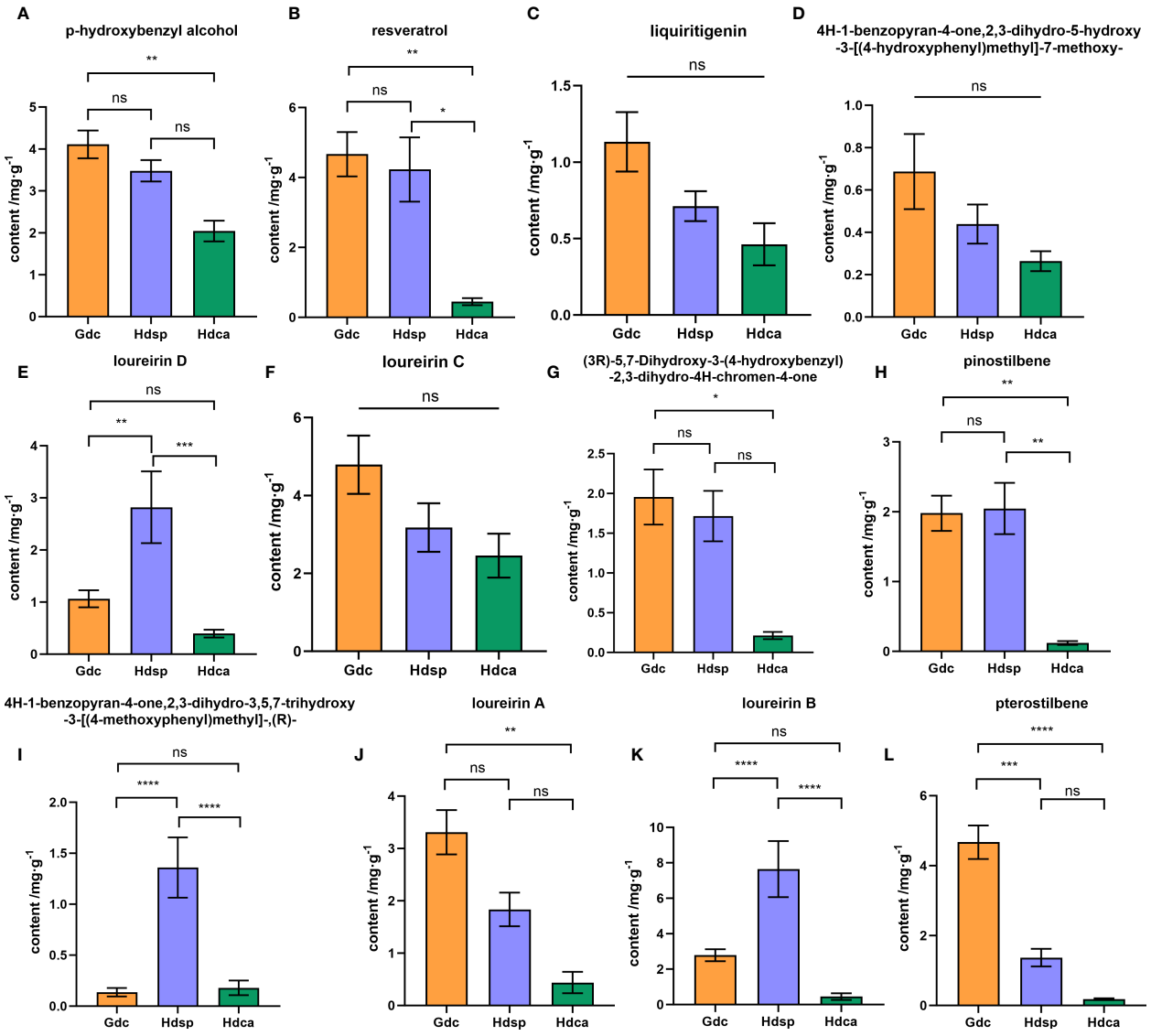

FIGURE 5
Results of quantitative analysis of 12 phenolic components **(A-L)** in Chinese dragon's blood samples from Gdc (D. cochinchinensis from Guangxi Province), Hdsp (D. cochinchinensis from Hainan Province) and Hdca (D. cambodiana from Hainan Province). *P < 0.05, **P < 0.01, ***P < 0.001, ****P < 0.0001, ns means no significance. p-hydroxybenzyl alcohol **(A)**, resveratrol **(B)**, liquiritigenin **(C)**, 4H-1-benzopyran-4-one,2,3-dihydro-5-hydroxy-3-[(4-hydroxyphenyl) methyl]-7-methoxy- **(D)**, loureirin D **(E)**, loureirin C **(F)**, (3R)-5,7-dihydroxy-3-(4-hydroxybenzyl)-2,3-dihydro-4H-chromen-4-one **(G)**, pinostilbene **(H)**, 4H-1-benzopyran-4-one,2,3-dihydro-3,5,7-trihydroxy-3-[(4-methoxyphenyl)methyl]-,(R)- **(I)**, loureirin A **(J)**, loureirin B **(K)**, and pterostilbene **(L)**.

environment, climatic conditions and species of medicinal materials (Guo et al., 2023). Therefore, it is highly important to study and elucidate the influence of these external factors on the secondary metabolites of TCM to ensure and improve its quality. In this study, LC–MS/MS technology combined with UHPLC–PDA quantitative analysis was used to conduct in-depth metabolomics analysis to systematically study the differences in the metabolite composition and content of CDB from different geographical origins and species.

In-depth analyses of the compounds shared by the two comparison groups of CDB from different origins and species were performed via Venn diagrams, and we identified 10 metabolites with significant differences in abundance. Furthermore, these 10 shared metabolites were analyzed via ROC curve analysis, and they exhibited very high AUC values (>0.96) in distinguishing between different groups of samples, whether analyzed in combination or individually, which fully demonstrated their excellent performance in identifying and distinguishing between different samples. The results of the available pharmacological studies indicate that coniferyl alcohol has significant anti-inflammatory and analgesic activities and can act as a signaling agent to modulate the phenylpropane pathway in several ways (Wang et al., 2021; Guan et al., 2022). 4-acetamidobutanoate is a product of the urea cycle, and its levels increase with renal dysfunction and are altered in inflammatory disorders such as rheumatoid arthritis. In addition, it is involved in several key metabolic pathways including arginine and proline metabolism, histidine metabolism, lysine degradation, and phenylalanine metabolism (Zhang K. et al., 2023; Kui et al., 2022). Artoindonessianin a exhibited cytotoxic activity against murine leukemia (Jamil et al., 2014). The compound (1E,4Z,6E)5-hydroxy-1-7-bis(4-hydroxy-3-methoxyphenyl)hepta-1,4,6-trien-3-one, which is commonly known

as curcumin (enol form), possesses antioxidant, anti-inflammatory, antiviral, antibacterial, antihypertensive, and insulin sensitizer activities; is cytotoxic to cancer cell lines; and can modulate apoptosis (Arenaza-Corona et al., 2023). The unique properties and wide range of biological activities of these compounds reveal their great potential and broad prospects for the future medical research and clinical applications of CDB.

4.1 Influence of different origins on *D. cochinchinensis*

Flavonoids are the major components of CDB and are associated with the phenylpropanoid biosynthetic pathway (Nabavi et al., 2020; Liu W. et al., 2021; Xu et al., 2022). Through metabolomics analyses, 2 significantly different flavonoid metabolites were identified as ideal chemomarkers for distinguishing CDB from different origins, with spinoflavanone a showing higher relative abundance in Gdc and oppositin showing higher relative abundance in Hdsp. These two DAMs may serve as useful quality markers for the identification of Gdc and Hdsp.

Among several pathways associated with DAMs enrichment between Gdc and Hdsp, the phenylpropanoid pathway and flavonoid biosynthesis are vital pathways for the production of important secondary metabolites (Petrussa et al., 2013; Du et al., 2022). During the formation of CDB, enzymes in the phenylpropanoid pathway are induced to metabolize phenylalanine to loureirin A and loureirin B, which are the main active ingredients in CDB (Su et al., 2020). Histidine metabolism is not only involved in the plant response to environmental stress and signal transduction but also acts as a chelator and transporter of metal ions, helping plants maintain metal ion homeostasis in different environments (Stepansky and Leustek, 2006). Arginine metabolism helps balance N availability for anabolic processes in a fluctuating environment (Kiss et al., 2023). Proline biosynthesis and accumulation are common responses to unfavorable environments in many plants (Yan et al., 2021). The increased metabolism of arginine and proline promotes root development, increases plant tolerance to osmotic stress, and improves crop resistance to salt stress. These findings suggest that under different geographic environments *D. cochinchinensis* may adapt to environmental changes by fine-tuning these key metabolic pathways to maintain a balance between their growth and survival.

Secondary metabolites are more affected by external stressors, and their metabolic profiles can vary depending on their growth environment even in genetically identical plants (Erb and Kliebenstein, 2020; Yoon et al., 2022). Quantitative analysis revealed that 8 of the 12 phenolic compounds were more abundant in Gdc group than in Hdsp, and the other 4 were more abundant in Hdsp. The difference in phenolic compound content is considered important because each compound has different biological activities (Zhao et al., 2018; Gu et al., 2019). When CDB is used for pharmacological purposes, its purpose may vary depending on the content of phenolic compounds. The main phenolic compounds have been extensively studied for their biological activity. According to the literature, *p*-hydroxybenzyl alcohol, resveratrol, loureirin A, loureirin B, loureirin D, pinostilbene, 4H-1-benzopyran-4-one,2,3-dihydro-3,5,7-trihydroxy-3-[(4-methoxyphenyl)methyl], (R)- and pterostilbene have antibacterial (Zheng et al., 2021), ischemic stroke (Jiang et al., 2020), antioxidant (Hu et al., 2020; Liu Y. S. et al., 2023), analgesic (Wan et al., 2019), antiaging (Allen et al., 2018) and anticancer (Chen et al., 2020) activities. These findings indicate that the different components have multiple biological activities and are source dependent. Changes in these components result in differences in nutritional or pharmacological functions that are related to quality. Therefore, these data can be used to select the origin most suitable for the expected activity.

4.2 Differences between the species of *D. cochinchinensis* and *D. cambodiana*

Species genetically determine the differences in the types and contents of plant metabolites, resulting in differences in clinical effects (Xiao et al., 2019). Using metabolomics approaches, 16 flavonoid metabolites were found to exhibit significant differences in abundance between the Hdca and Hdsp groups, among which only naringin showed higher relative abundance in Hdca. Naringin possesses antioxidant, neuroprotective, anti-inflammatory, antiapoptotic, antiulcer, antiosteoporotic, and anticancer properties (Ravetti et al., 2023). The remaining 15 flavonoids presented higher relative abundances in Hdsp, among them, didymin has anticancer, antioxidant, anti-inflammatory, and neuroprotective, hepatoprotective, and cardiovascular effects (Yang et al., 2023). Farrerol has therapeutic effects on pathological conditions such as cancer, muscular dystrophy, inflammation, microbial infections, and oxidative stress (He et al., 2023). Cardamonin has significant anticancer, anti-inflammatory, and antioxidant activities and neuroprotective effects and can attenuate cerebral ischemia/reperfusion injury through activation of the HIF-1α/VEGFA pathway (Ni et al., 2022). Robinin has significant anti-inflammatory, analgesic and antitumor effects (Zhang W. et al., 2023). Sanggenol l possesses a wide range of biological activities such as neuroprotective, anti-inflammatory, and antitumor effects (Fu et al., 2024). Combretastatin A4 is a potent mitotic inhibitor of a variety of tumor cells that inhibits mitosis in a variety of tumor cells, including multidrug-resistant cancer cell lines. It also acts on proliferative endothelial cells and ruptures tumor blood vessels (Yang et al., 2022). Natural stilbenoids are secondary metabolites produced by plants to protect themselves against stressful conditions such as UV irradiation, overheating and fungal or bacterial infections (Medrano-Padial et al., 2021). Compared with the Hdca and Hdsp groups, three significantly different stilbenoid metabolites, trans-resveratrol, pinosylvin, and 3,4,5-trihydroxystilbene, presented greater relative abundances. Among these metabolites, resveratrol, often found in its trans form, possesses pharmacological activities, such as anticancer,

anti-inflammatory, cardiovascular protection, and antioxidant effects, and inhibits platelet aggregation (Basholli-Salihu et al., 2016). Pinosylvin possesses a variety of biological properties, such as antimicrobial, anti-inflammatory, anticancer, antioxidant, neuroprotective and antiallergenic effects (Bakrim et al., 2022). Thus, our results suggest that differences in both the composition and abundance of flavonoids and stilbenoids may explain the variation in therapeutic effects observed in herbs from different species. These discriminating metabolites may be useful quality markers for differentiating *D. cochinchinensis* and *D. cambodiana*.

Among the several pathways associated with DAMs enrichment between Hdsp and Hdca, amino acid metabolism is crucial for plant growth and stress resistance (Huang and Jander, 2017). Among them, alanine, aspartate and glutamate metabolism are resistant to pathogens and provide nitrogen for growth when exposed to external stresses, reducing the toxic effects of nitrate in crops (Martinelli et al., 2007). In addition, alanine metabolism plays an important role in the synthesis and defense of the cell wall (Qiao et al., 2018). Furthermore, galactose metabolism plays a coordinating role in cellular metabolism. These differences in metabolic pathways reflect the diversity of genetic backgrounds, environmental adaptations and metabolic requirements of different species, providing an important basis for understanding the uniqueness of different species of CDB.

Quantitative analysis based on UHPLC-PDA revealed that the content of 12 phenolic compounds in the Hdca samples was consistently lower than that in the Hdsp samples. Owing to the differences in pharmacological activities corresponding to different metabolite types and contents, it is inferred that CDB extracts from Hdsp possesses more potent pharmacological activities. Therefore, it is highly important to distinguish CDB samples from different sources in practical applications to ensure the consistency of efficacy and batch reproducibility.

However, importantly, relying solely on component concentrations is insufficient to draw definitive conclusions regarding the quality of medicinal materials such as CDB. Pharmacological experiments are essential to further validate the analytical findings and provide a more comprehensive understanding of the therapeutic.

5 Conclusion

In this study, plant metabolomics approaches (LC-MS/MS) combined with a developed UHPLC-PDA method were used to systematically investigate the differences of CDB from different geographical origins and species. The results revealed that origin and species had significant effects on the chemical composition and content of CDB, with species showing particularly pronounced differences. Comprehensive metabolite analysis and quantitative assessment revealed that *D. cochinchinensis* exhibits outstanding performance in compound diversity, relative abundance, and content of phenolic compounds, making it an ideal source of CDB. Furthermore, considering the significant potential of *D. cambodiana*, additional research is necessary to fully explore its considerable potential.

Data availability statement

The original contributions presented in the study are included in the article/Supplementary Material. Further inquiries can be directed to the corresponding authors.

Author contributions

XS: Data curation, Formal analysis, Investigation, Methodology, Visualization, Writing – original draft, Writing – review & editing. QH: Formal analysis, Investigation, Visualization, Writing – review & editing. MW: Resources, Writing – review & editing. LH: Resources, Writing – review & editing. XZ: Conceptualization, Methodology, Project administration, Writing – review & editing. XY: Funding acquisition, Project administration, Resources, Supervision, Writing – review & editing.

Funding

The author(s) declare financial support was received for the research, authorship, and/or publication of this article. This work was supported by the International Science & Technology Cooperation Program of Hainan Province (No. GHYF2024018), Hainan Province Science and Technology Special Fund, China (ZDYF2024XDNY159; ZDYF2023SHFZ141), and the Innovation Fund for Medical Sciences of Chinese Academy of Medical Sciences, China (Grant No. 2021-I2M-1-032).

Acknowledgments

We thank Shanghai Biotree Biotech Co. Ltd. for the LC-MS/MS analysis and metabolomics data processing.

Conflict of interest

The authors declare that the research was conducted in the absence of any commercial or financial relationships that could be construed as a potential conflict of interest.

Publisher's note

Supplementary material

The Supplementary Material for this article can be found online at: https://www.frontiersin.org/articles/10.3389/fpls.2024.1427731/full#supplementary-material

References

Abraham, E. J., and Kellogg, J. J. (2021). Chemometric-guided approaches for profiling and authenticating botanical materials. *Front. Nutr.* 8. doi: 10.3389/fnut.2021.780228

Allen, E. N., Potdar, S., Tapias, V., Parmar, M., Mizuno, C. S., Rimando, A., et al. (2018). Resveratrol and pinostilbene confer neuroprotection against aging-related deficits through an ERK1/2-dependent mechanism. *J. Nutr. Biochem.* 54, 77–86. doi: 10.1016/j.jnutbio.2017.10.015

Alseekh, S., Aharoni, A., Brotman, Y., Contrepois, K., D'Auria, J., Ewald, J., et al. (2021). Mass spectrometry-based metabolomics: a guide for annotation, quantification and best reporting practices. *Nat. Methods* 18, 747–756. doi: 10.1038/s41592-021-01197-1

Arenaza-Corona, A., Obregón-Mendoza, M. A., Meza-Morales, W., Ramírez-Apan, M. T., Nieto-Camacho, A., Toscano, R. A., et al. (2023). The homoleptic curcumin–copper single crystal (ML2): A long awaited breakthrough in the field of curcumin metal complexes. *Molecules* 28, 6033. doi: 10.3390/molecules28166033

Bakrim, S., Machate, H., Benali, T., Sahib, N., Jaouadi, I., Omari, N. E., et al. (2022). Natural sources and pharmacological properties of pinosylvin. *Plants* 11, 1541. doi: 10.3390/plants11121541

Basholli-Salihu, M., Schuster, R., Mulla, D., Praznik, W., Viernstein, H., and Mueller, M. (2016). Bioconversion of piceid to resveratrol by selected probiotic cell extracts. *Bioprocess Biosyst. Eng.* 39, 1879–1885. doi: 10.1007/s00449-016-1662-1

Cai, X. T., and Xu, Z. F. (1979). A study on the resource of Chinese dragon's blood. *Acta Bot. Yunnanica* 1, 1–10. Available at: http://ir.xtbg.org.cn/handle/353005/2190.

Chen, P. Q., Ban, W. K., Wang, W. Y., Lu, J., Chen, X., and Yang, Z. H. (2023). Research progress of pharmacological effects and mechanism of Resina Draconis and its active constituents on cerebral ischemia. Chin. Tradit. Herb. *Drugs* 54, 6172–6184. doi: 10.7501/j.issn.0253-2670.2023.18.034

Chen, S., Ma, M. J., Wang, L. N., Du, P., and Lin, X. G. (2021). Modulation of total flavonoids of Dragon's blood on acid-sensing ion channels and its analgesic effect. *J. South-Cent. Univ. Natl. Nat. Sci. Ed.* 40, 158–164. doi: 10.12130/znmdzk.20210208

Chen, Q. P., Tang, C. F., Long, H. R., and He, L. L. (2018). Determination of loureirin a and loureirin b in artificially induced dragon's blood of dracaena cochinchinensis. *Contemp. Chem. Ind.* 47, 434–436 + 440. doi: 10.13840/j.cnki.cn21-1457/tq.2018.02.058

Chen, X. B., Yao, C. L., Hou, J. R., Nie, M., Li, Y., Wei, W. L., et al. (2023). Systematical characterization of gypenosides in Gynostemma pentaphyllum and the chemical composition variation of different origins. *J. Pharm. Biomed. Anal.* 232, 115328. doi: 10.1016/j.jpba.2023.115328

Chen, X., Zhao, Y., Yang, A., Tian, Y., Pang, D., Sun, J., et al. (2020). Chinese dragon's blood etOAc extract inhibits liver cancer growth through downregulation of smad3. *Front. Pharmacol.* 11. doi: 10.3389/fphar.2020.00669

Du, J., Lu, X., Geng, Z., Yuan, Y., Liu, Y., Li, J., et al. (2022). Metabolites changes of Eucommia ulmoides Olive samaras from different regions and cultivars. *Ind. Crops Prod.* 189, 115824. doi: 10.1016/j.indcrop.2022.115824

Erb, M., and Kliebenstein, D. J. (2020). Plant secondary metabolites as defenses, regulators, and primary metabolites: the blurred functional trichotomy. *Plant Physiol.* 184, 39–52. doi: 10.1104/pp.20.00433

Fu, R., You, Y., Wang, Y., Wang, J., Lu, Y., Gao, R., et al. (2024). Sanggenol L induces ferroptosis in non-small cell lung cancer cells via regulating the miR-26a-1-3p/MDM2/p53 signaling pathway. *Biochem. Pharmacol.* 226, 116345. doi: 10.1016/j.bcp.2024.116345

Gu, S., Li, L., Huang, H., Wang, B., and Zhang, T. (2019). Antitumor, antiviral, and anti-inflammatory efficacy of essential oils from atractylodes macrocephala koidz. Produced with different processing methods. *Molecules* 24, 2956. doi: 10.3390/molecules24162956

Guan, M., Li, C., Shan, X., Chen, F., Wang, S., Dixon, R. A., et al. (2022). Dual mechanisms of coniferyl alcohol in phenylpropanoid pathway regulation. *Front. Plant Sci.* 13. doi: 10.3389/fpls.2022.896540

Guo, J., Wang, X., and Ma, H. (2023). Research progress of blockchain -based integrated information sharingmodel for production, research and use of Chinese medicinal materials. *China J. Mod. Med.* 30, 27–30 + 36. doi: 10.3969/j.issn.1674-4721.2023.36.007

He, T. C., Wang, D. W., Zheng, S. M., Yan, Y. M., Jiao, Y. B., Cheng, Y. X., et al. (2021). Antifungal and wound healing promotive compounds from the resins of Dracaena cochinchinensis. *Fitoterapia* 151, 104904. doi: 10.1016/j.fitote.2021.104904

He, J., Xu, D., Wang, L., and Yu, X. (2023). Farrerol prevents Angiotensin II-induced cardiac remodeling in *vivo* and in *vitro*. *Front. Pharmacol.* 13. doi: 10.3389/fphar.2022.1079251

Hu, S. L., Wang, K., Shi, Y. F., Shao, Z. X., Zhang, C. X., Sheng, K. W., et al. (2020). Downregulating Akt/NF-κB signaling and its antioxidant activity with Loureirin A for alleviating the progression of osteoarthritis: *In vitro* and vivo studies. *Int. Immunopharmacol.* 78, 105953. doi: 10.1016/j.intimp.2019.105953

Huang, T., and Jander, G. (2017). Abscisic acid-regulated protein degradation causes osmotic stress-induced accumulation of branchedchain amino acids in Arabidopsis thaliana. *Planta* 246, 737–747. doi: 10.1007/s00425-017-2727-3

Jamil, S., Abdullah, S. A., Lathiff, S. M. A., and Sirat, H. M. (2014). Tyrosinase inhibitory activity of flavonoids from Artocarpus lowii King. *J. Teknol.* 71, 55–58. doi: 10.11113/jt.v71.2711

Jiang, M., Su, X., Liu, J., Zheng, C., and Li, X. (2020). Systems pharmacology-dissection of the molecular mechanisms of dragon's blood in improving ischemic stroke prognosis. *Evidence-Based Complementary Altern. Med.* 2020, 4858201. doi: 10.1155/2020/4858201

Kiss, É., Talbot, J., Adams, N. B. P., Opekar, S., Moos, M., Pilný, J., et al. (2023). Chlorophyll biosynthesis under the control of arginine metabolism. *Cell Rep.* 42, 113265. doi: 10.1016/j.celrep.2023.113265

Krishnaraj, P., Chang, Y., Ho, T. J., Lu, N. C., Lin, M. D., and Chen, H. P. (2019). *In vivo* pro-angiogenic effects of dracorhodin perchlorate in zebrafish embryos: A novel bioactivity evaluation platform for commercial dragon blood samples. *J. Food Drug Anal.* 27, 259–265. doi: 10.1016/j.jfda.2018.08.005

Kui, H., Su, H., Wang, Q., Liu, C., Li, Y., Tian, Y., et al. (2022). Serum metabolomics study of anxiety disorder patients based on LC-MS. *Clin. Chim. Acta* 533, 131–143. doi: 10.1016/j.cca.2022.06.022

Kuo, P. C., Hung, H. Y., Hwang, T. L., Du, W. K., Ku, H. C., Lee, E. J., et al. (2017). Anti-inflammatory flavan-3-ol-dihydroretrochalcones from daemonorops draco. *J. Nat. Prod.* 80, 783–789. doi: 10.1021/acs.jnatprod.7b00039

Lang, G. Z., Li, C. J., Gaohu, T. Y., Li, C., Ma, J., Yang, J. Z., et al. (2020). Bioactive flavonoid dimers from Chinese dragon's blood, the red resin of Dracaena cochinchinensis. *Bioorg. Chem.* 97, 103659. doi: 10.1016/j.bioorg.2020.103659

Lee, S. M., Lee, H. B., and Lee, C. G. (2010). A convenience UPLC/PDA method for the quantitative analysis of panaxfuraynes A and B from Panax ginseng. *Food Chem.* 123, 955–958. doi: 10.1016/j.foodchem.2010.05.002

Liang, L., Xu, J., Zhou, W. W., Brand, E., Chen, H. B., and Zhao, Z. Z. (2018). Integrating targeted and untargeted metabolomics to investigate the processing chemistry of polygoni multiflori radix. *Front. Pharmacol.* 9. doi: 10.3389/fphar.2018.00934

Liao, J. C., Wu, Y. S., Xu, F. F., Chen, W. Y., Zheng, Z. L., Han, X. D., et al. (2021). Comprehensive evaluation of NAODESHENG by combining UPLC quantitative fingerprint and antioxidant activity. *J. Pharm. Biomed. Anal.* 193, 113636. doi: 10.1016/j.jpba.2020.113636

Liu, T., Bai, M., Liu, M., Li, T., Liao, Y., Zhao, C., et al. (2023). Novel synergistic mechanism of 11-keto-β-boswellic acid and Z-Guggulsterone on ischemic stroke revealed by single-cell transcriptomics. *Pharmacol. Res.* 193, 106803. doi: 10.1016/j.phrs.2023.106803

Liu, W., Feng, Y., Yu, S., Fan, Z., Li, X., Li, J., et al. (2021). The flavonoid biosynthesis network in plants. *Int. J. Mol. Sci.* 22, 12824. doi: 10.3390/ijms222312824

Liu, Y. S., Zhang, G. Y., and Hou, Y. (2023). Theoretical and experimental investigation of the antioxidation mechanism of loureirin C by radical scavenging for treatment of stroke. *Molecules* 28, 380. doi: 10.3390/molecules28010380

Liu, Y., Zhao, X., Yao, R., Li, C., Zhang, Z., Xu, Y., et al. (2021). Dragon's blood from dracaena worldwide: species, traditional uses, phytochemistry and pharmacology. *Am. J. Chin. Med.* 49, 1315–1367. doi: 10.1142/S0192415X21500634

Liu, X., Zhong, C., Xie, J., Liu, H., Xie, Z., Zhang, S., et al. (2023). Geographical region traceability of Poria cocos and correlation between environmental factors and biomarkers based on a metabolomic approach. *Food Chem.* 417, 135817. doi: 10.1016/j.foodchem.2023.135817

Lu, C. M., and Cui, X. M. (2019). Research progress in TCM quality control and toxicity evaluation based on metabolomics technology. *Chin. J. Inf. Tradit. Chin. Med.* 26, 141–144. doi: 10.3969/j.issn.1005-5304.2019.01.034

Martinelli, T., Whittaker, A., Bochicchio, A., Vazzana, C., Suzuki, A., and Masclaux-Daubresse, C. (2007). Amino acid pattern and glutamate metabolism during dehydration stress in the 'resurrection' plant ASporobolus stapfianus: a comparison between desiccation-sensitive and desiccation-tolerant leaves. *J. Exp. Bot.* 58, 3037–3046. doi: 10.1093/jxb/erm161

Medrano-Padial, C., Prieto, A. I., Puerto, M., and S Pichardo, S. (2021). Toxicological evaluation of piceatannol, pterostilbene, and ε-viniferin for their potential use in the food industry: A review. *Foods* 10, 592. doi: 10.3390/foods10030592

Nabavi, S. M., Šamec, D., Tomczyk, M., Milella, L., Russo, D., Habtemariam, S., et al. (2020). Flavonoid biosynthetic pathways in plants: Versatile targets for metabolic engineering. *Biotechnol. Adv.* 38, 107316. doi: 10.1016/j.bioteChadv.2018.11.005

Ni, H., Li, J., Zheng, J., and Zhou, B. (2022). Cardamonin attenuates cerebral ischemia/reperfusion injury by activating the HIF-1α/VEGFA pathway. *Phytother. Res.* 36, 1736–1747. doi: 10.1002/ptr.7409

Niu, S., Liu, T., Deng, Y., Wang, W., Zhang, Y., Hong, W., et al. (2020). Production and evaluation of antifungal stilbenoids in Dracaena cochinchinensis elicited by fungal inoculation. *Ind. Crops Prod.* 145, 112148. doi: 10.1016/j.indcrop.2020.112148

Pang, D. R., Pan, B., Sun, J., Sun, H., Yao, H. N., Song, Y. L., et al. (2018). Homoisoflavonoid derivatives from the red resin of Dracaena cochinchinensis. *Fitoterapia* 131, 105–111. doi: 10.1016/j.fitote.2018.10.017

Petrussa, E., Braidot, E., Zancani, M., Peresson, C., Bertolini, A., Patui, S., et al. (2013). Plant flavonoids–biosynthesis, transport and involvement in stress responses. *Int. J. Mol. Sci.* 14, 14950–14973. doi: 10.3390/ijms140714950

Qiao, Y., Liu, G., Leng, C., Zhang, Y., Lv, X., Chen, H., et al. (2018). Metabolic profiles of cysteine, methionine, glutamate, glutamine, arginine, aspartate, asparagine, alanine and glutathione in Streptococcus thermophilus during pH-controlled batch fermentations. *Sci. Rep.* 8, 12441. doi: 10.1038/s41598-018-30272-5

Qin, J., Wu, J., Li, J., Bi, Y., Wang, Z., and Xiao, W. (2013). Determination of five components in Draconis Resina from different habitats by HPLC. *Drugs Clin.* 28, 547–549. doi: 10.7501/j.issn.1674-5515.2013.04.019

Ravetti, S., Garro, A. G., Gaitán, A., Murature, M., Galiano, M., Brignone, S. G., et al. (2023). Naringin: nanotechnological strategies for potential pharmaceutical applications. *Pharmaceutics* 15, 863. doi: 10.3390/pharmaceutics15030863

Rivera-Pérez, A., García-Pérez, P., Romero-González, R., Frenich, A. G., and Lucini, L. (2023). UHPLC-QTOF-HRMS metabolomics insight on the origin and processing authentication of thyme by comprehensive fingerprinting and chemometrics. *Food Chem.* 407, 135123. doi: 10.1016/j.foodchem.2022.135123

Sha, M., Li, X., Liu, Y., Tian, H., Liang, X., Li, X., et al. (2023). Comparative chemical characters of Pseudostellaria heterophylla from geographical origins of China. *Chin. Herb. Med.* 15, 439–446. doi: 10.1016/j.chmed.2022.10.005

Stepansky, A., and Leustek, T. (2006). Histidine biosynthesis in plant. *Amino Acids* 30, 127–142. doi: 10.1007/s00726-005-0247-0

Su, J., Li, Y. H., Zhou, L. J., Qin, T. D., Liu, S. F., Chen, X., et al. (2020). Comparative study on differences of resin-containing drugs in Dracaena from different appearance based on HS-GC-MS and chemometrics. *China J. Chin. Mater. Med.* 45, 3467–3474. doi: 10.19540/j.cnki.cjcmm.20200424.201

Sun, J., Liu, J. N., Fan, B., Chen, X. N., Pang, D. R., Zheng, J., et al. (2019). Phenolic constituents, pharmacological activities, quality control, and metabolism of Dracaena species: A review. *J. Ethnopharmacol.* 244, 112138. doi: 10.1016/j.jep.2019.112138

Sun, J., Song, Y., Sun, H., Liu, W., Zhang, Y., Zheng, J., et al. (2017). Characterization and quantitative analysis of phenolic derivatives in Longxuetongluo Capsule by HPLC-DAD-IT-TOF-MS. *J. Pharm. Biomed. Anal.* 145, 462–472. doi: 10.1016/j.jpba.2017.07.012

Wan, Q. (2017). Determination of five active components in Draconis Resina by qams method. *Chin. Tradit. Herb. Drugs* 48, 4541–4545. doi: 10.7501/j.issn.0253-2670.2017.21.028

Wan, Y., Yu, Y., Pan, X., Mo, X., Gong, W., Liu, X., et al. (2019). Inhibition on acid-sensing ion channels and analgesic activities of flavonoids isolated from dragon's blood resin. *Phytother. Res.* 33, 718–727. doi: 10.1002/ptr.6262

Wang, C., Bai, Y., Yang, Y., and He, R. (2021). Chemical synthesis and anti-inflammatory andanalgesic activities studies of coniferyl alcohol. *J.Zunyi Med. Univ.* 44, 594–599 + 606. doi: 10.14169/j.cnki.zunyixuebao.2021.0094

Wang, H., Jiang, H. M., Li, F. X., Chen, H. Q., Liu, W. C., Ren, S. Z., et al. (2017). Flavonoids from artificially induced dragon's blood of Dracaena Cambodiana. *Fitoterapia* 121, 1–5. doi: 10.1016/j.fitote.2017.06.019

Wang, P., Wang, Q., Yang, B., Zhao, S., and Kuang, H. (2015). The progress of metabolomics study in traditional Chinese medicine research. *Am. J. Chin. Med.* 43, 1281–1310. doi: 10.1142/S0192415X15500731

Waris, M., Kocak, E., Gonulalan, E. M., Demirezer, L. O., Kır, S., and Nemutlu, E. (2022). Metabolomics analysis insight into medicinal plant science. *Trends Anal. Chem.* 157, 116795. doi: 10.1016/j.trac.2022.116795

Xiao, Q., Mu, X., Liu, J., Li, B., Liu, H., Zhang, B., et al. (2022). Plant metabolomics: a new strategy and tool for quality evaluation of Chinese medicinal materials. *Chin. Med.* 17, 45. doi: 10.1186/s13020-022-00601-y

Xiao, J. M., Yang, Y., Zhou, J., He, F. Y., Zeng, H. J., and Yang, Y. T. (2019). Research strategy of quality markers of Chinese materia medica based on total quantum statistical moment theory. *Chin. Tradit. Herb. Drugs* 50, 4589–4594. doi: 10.7501/j.issn.0253-2670.2019.19.010

Xu, M., Zhang, Y. J., Li, X. C., Jacob, M. R., and Yang, C. R. (2010). Steroidal saponins from fresh stems of Dracaena angustifolia. *J. Nat. Prod.* 73, 1524–1528. doi: 10.1021/np100351p

Xu, Y., Zhang, K., Zhang, Z., Liu, Y., Lv, F., Sun, P., et al. (2022). A chromosome-level genome assembly for Dracaena cochinchinensis reveals the molecular basis of its longevity and formation of dragon's blood. *Plant Commun.* 3, 100456. doi: 10.1016/j.xplc.2022.100456

Yan, L., Li, S., Riaz, M., and Jiang, C. (2021). Proline metabolism and biosynthesis behave differently in response to boron-deficiency and toxicity in Brassica napus. *Plant Physiol. Biochem.* 167, 529–540. doi: 10.1016/j.plaphy.2021.08.029

Yang, F., Chu, T., Zhang, Y., Liu, X., Sun, G., and Chen, Z. (2020). Quality assessment of licorice (Glycyrrhiza glabra L.) from different sources by multiple fingerprint profiles combined with quantitative analysis, antioxidant activity and chemometric methods. *Food Chem.* 324, 126854. doi: 10.1016/j.foodchem.2020.126854

Yang, L., Ma, X., Guo, K., Li, J., Zhang, C., and Wu, L. (2022). Dual-functional antitumor conjugates improving the anti-metastasis effect of combretastatin A4 by targeting tubulin polymerization and matrix metalloproteinases. *Eur. J. Med. Chem.* 238, 114439. doi: 10.1016/j.ejmech.2022.114439

Yang, J., Zou, Y., Chen, J., Cui, C., Song, J., Yang, M., et al. (2023). Didymin alleviates metabolic dysfunction-associated fatty liver disease (MAFLD) via the stimulation of Sirt1-mediated lipophagy and mitochondrial biogenesis. *J. Transl. Med.* 21, 921. doi: 10.1186/s12967-023-04790-4

Yoon, D., Shin, W. C., Oh, S. M., Choi, B. R., and Lee, D. Y. (2022). Integration of multiplatform metabolomics and multivariate analysis for geographical origin discrimination of Panax ginseng. *Food Res. Int.* 159, 111610. doi: 10.1016/j.foodres.2022.111610

Yuan, S. H. (1991). Hainan pharmaceutical factory developed and produced "Nandao Brand Dragon's blood. *J. Chin. Med. Mater.* 14, 54. doi: 10.13863/j.issn1001-4454.1991.12.032

Zhang, W., Liu, W., and Hu, X. (2023). Robinin inhibits pancreatic cancer cell proliferation, EMT and inflammation via regulating TLR2-PI3k-AKT signaling pathway. *Cancer Cell Int.* 23, 328. doi: 10.1186/s12935-023-03167-3

Zhang, K., Liu, Y., Liu, L., Bai, B., Shi, L., and Zhang, Q. (2023). Untargeted metabolomics analysis using UHPLC-Q-TOF/MS reveals metabolic changes associated with hypertension in children. *Nutrients* 15, 836. doi: 10.3390/nu15040836

Zhao, Y., Liang, G., Gong, W., Tian, J., and Qin, X. (2018). Quantitative analysis of multi-components by single marker for determination of three atractylenolides in atractylodis macrocephalae rhizoma. *Chin. Pharm. J.* 53, 499–503. doi: 10.11669/cpj.2018.07.004

Zheng, X., Chen, L., Zeng, W., Liao, W., Wang, Z., Tian, X., et al. (2021). Antibacterial and Anti-biofilm Efficacy of Chinese Dragon's blood Against Staphylococcus aureus Isolated from Infected Wounds. *Front. Microbiol.* 12. doi: 10.3389/fmicb.2021.672943

Zhou, Z., Luo, M., Zhang, H., Yin, Y., and Zhu, Z. (2022). Metabolite annotation from knowns to unknowns through knowledge-guided multi-layer metabolic networking. *Nat. Commun.* 13, 6656. doi: 10.1038/s41467-022-34537-6

frontiers | Frontiers in Plant Science

TYPE Original Research
PUBLISHED 16 October 2024
DOI 10.3389/fpls.2024.1408141

OPEN ACCESS

EDITED BY
Miroslav Nikolic,
University of Belgrade, Serbia

REVIEWED BY
Francisco Javier Romera,
University of Cordoba, Spain
Soichi Kojima,
Tohoku University, Japan

*CORRESPONDENCE
Nicola Tomasi
nicola.tomasi@uniud.it

RECEIVED 27 March 2024
ACCEPTED 04 September 2024
PUBLISHED 16 October 2024

CITATION
Lodovici A, Buoso S, Miras-Moreno B, Lucini L, Tomasi N, García-Pérez P, Pinton R and Zanin L (2024) A multi-omics insight on the interplay between iron deficiency and N forms in tomato.
Front. Plant Sci. 15:1408141.
doi: 10.3389/fpls.2024.1408141

A multi-omics insight on the interplay between iron deficiency and N forms in tomato

Arianna Lodovici[1], Sara Buoso[1], Begoña Miras-Moreno[2,3], Luigi Lucini[2], Nicola Tomasi[1]*, Pascual García-Pérez[2], Roberto Pinton[1] and Laura Zanin[1]

[1]Department of Agricultural. Food, Environmental and Animal Sciences, University of Udine, Udine, Italy, [2]Department for Sustainable Food Process, Università Cattolica del Sacro Cuore, Piacenza, Italy, [3]Department of Plant Biology, University of Murcia, Murcia, Spain

Introduction: Nitrogen (N) and iron (Fe) are involved in several biochemical processes in living organisms, and their limited bioavailability is a strong constraint for plant growth and yield. This work investigated the interplay between Fe and N nutritional pathways in tomato plants kept under N and Fe deficiency and then resupplied with Fe and N (as nitrate, ammonium, or urea) through a physiological, metabolomics and gene expression study.

Results: After 24 hours of Fe resupply, the Fe concentration in Fe-deficient roots was dependent on the applied N form (following the pattern: nitrate > urea > ammonium > Fe-deficient control), and whereas in leaves of urea treated plants the Fe concentration was lower in comparison to the other N forms. Untargeted metabolomics pointed out distinctive modulations of plant metabolism in a treatment-dependent manner. Overall, N-containing metabolites were affected by the treatments in both leaves and roots, while N form significantly shaped the phytohormone profile. Moreover, the simultaneous application of Fe with N to Fe-deficient plants elicited secondary metabolites' accumulation, such as phenylpropanoids, depending on the applied N form (mainly by urea, followed by nitrate and ammonium). After 4 hours of treatment, ammonium- and urea-treated roots showed a reduction of enzymatic activity of Fe(III)-chelate reductase (FCR), compared to nitrate or N-depleted plants (maintained in Fe deficiency, where FCR was maintained at high levels). The response of nitrate-treated plants leads to the improvement of Fe concentration in tomato roots and the increase of Fe(II) transporter (IRT1) gene expression in tomato roots.

Conclusions: Our results strengthen and improve the understanding about the interaction between N and Fe nutritional pathways, thinning the current knowledge gap.

KEYWORDS

ammonium, metabolomic, multi-omic, nitrate, nutrient interplay, root uptake, Strategy I, urea

Introduction

Despite being abundant on the Earth's crust, Fe bioavailability under well-aerated and calcareous soil is strongly limited by a scarce solubility of ferric and ferrous forms in solution. It has been estimated that this unfavorable condition affects more than 30% of cultivated soils (Marastoni et al., 2020). Fe is acquired by crops with two distinct strategies based upon type of plant family (Strategy I used by all higher plants such as tomato except graminaceous, Strategy II used by graminaceous plants, Kobayashi et al., 2019; Mori, 1999). Strategy I, consist primarily in proton extrusion by activation of protonic pumps (H+-ATPase family; *AHA2* in Arabidopsis, *SlHA4* in tomato; Harper et al., 1990; Liu et al., 2016), followed by Fe(III) reduction to Fe(II) by FCR at the root surface level and then adsorbed into the root by iron regulated transporter (IRT; IRT1 in Arabidopsis; *SlIRT* 1 in tomato; Eide et al., 1996; Eckhardt et al., 2001).

Under Fe deficiency, crops exhibit leaf chlorosis and decreased photosynthesis, resulting in adverse consequences for yield and quality (Mahender et al., 2019; Zhang et al., 2019; Zuo and Zhang, 2011). In tomato roots, Zamboni et al. (2012) provided evidence that Fe deficiency induced the modulation of 97 genes in comparison to Fe sufficiency and, at the transcriptional level, this response is similar to the response activated by Arabidopsis (the so-called "Ferrome" by Schmidt and Buckhout, 2011).

Nowadays, one solution involves providing Fe to the soil in the form of synthetic chelates, causing a significant environmental and economic impact (Piccinelli et al., 2022). To move towards a more precise 4.0 agriculture, which is more restrained in the use of synthetic inputs, it is urgent to identify new agricultural practices aimed at the preservation of the environment and optimizing the already available soil resources (Anas et al., 2020; Congreves et al., 2021).

To identify new environmentally friendly solutions aimed at improving the efficiency of applied fertilizers and natural resources in the soil, the study of the Fe acquisition process in plants should consider the interplay of Fe with other nutrients (Fan et al., 2021). Among these, nitrogen (N) is the nutrient most used as fertilizer, mainly applied as urea, nitrate, or ammonium. More than 110 million tons of N fertilizers are used globally (FAOSTAT, 2021). Still, only a small quantity is effectively taken up by crops (30–40%), whereas the remaining fraction is lost in the environment (Eickhout et al., 2006; Gao et al., 2022; Sainju et al., 2019).

The influence of an N form on Fe acquisition is linked to changes occurring at the molecular and physiological levels in plants and the rhizosphere. Being nitrate and ammonium the ions with higher uptake (accounting for more than 70% of the total), their role in the control of cations and anions uptake, dry matter production, carbon assimilation rate, root apoplastic pH, and rhizosphere pH is significant (Arnozis and Findenegg, 1986; Marschner, 1995; Mengel, 1994). In particular, changes in the pH within the rhizosphere (e.g. alkalinization by nitrate or overall acidification by ammonium) and the plant apoplast largely modulate the uptake, remobilization and allocation of metals such as Fe and the acquisition of other nutrients (such as phosphorous, P; Thomson et al., 1993; Zou et al., 2001; Sarasketa et al., 2016; De la Peña et al., 2022). In addition to rhizospheric acidification and changes in plant metabolism, Zou et al. (2001) highlighted that ammonium even triggers nitric oxide production in *Arabidopsis*. This signaling molecule induces FCR activity and also the Fe release from the cell wall (especially from hemicellulose). Moreover, ammonium upregulates genes involved in Fe translocation from roots to shoots, such as *FRD3* and *NAS1* (*NA SYNTHASE1*), increasing the amount of soluble Fe in shoots and thus alleviating Fe deficiency symptoms in *Arabidopsis* (a reduction in interveinal leaf chlorosis; Zhu et al., 2019).

On the other hand, nitrate can lead to the alkalinization of the rhizosphere decreasing Fe solubility and of the root apoplast inhibiting the activity of FCR (Nikolic and Römheld, 2003), similar results were also shown at the leaf apoplast (Kosegarten et al., 1999). Moreover, Fe is a cofactor of several enzymes involved in the reductive assimilatory pathway of nitrate, such as nitrate reductase (NR), nitrite reductase (NiR) and glutamate synthase (GOGAT; Marschner, 1995). Thus, under Fe deficiency, nitrate assimilation is slowed down in plants (Alcaraz et al., 1986; Borlotti et al., 2012) and triggers a limitation in net nitrate uptake into roots at the same time (Iacuzzo et al., 2011). In apple, Sun et al. (2021) provided evidence that Fe deficiency symptoms were alleviated by a low nitrate nutrition, which in roots induced the accumulation of citrate and abscisic acid and activated their biosynthetic pathways, maintaining Fe homeostasis. This aspect is highly relevant for crop nutrition, especially in aerobic soils, where oxidation reactions convert N into nitrate, making this latter the main N-form available for plant nutrition.

Another important form of N in agriculture is urea, the most used fertilizer. In the last decade, the molecular mechanisms underlying urea uptake in cultivated plants started to be revealed (Wang et al., 2012a; Zanin et al., 2014, 2015); however, no information regarding the interaction between urea and the response to plant Fe deficiency is currently available.

Based on these considerations, there is still a gap in knowledge about the interplay between N and Fe nutritional pathways in plants (Nikolic et al., 2007; Borlotti et al., 2012; Liu et al., 2015; Chen et al., 2021), especially regarding the effects of different N forms in overcoming low Fe-bioavailability (Zou et al., 2001). Given the key role played by Fe in N assimilation and *vice versa*, strong cross-connections between the N and Fe nutritional pathways and the close relationships in the regulation and activation of their reciprocal acquisition mechanisms are likely (Liu et al., 2015; Chen et al., 2021). Studying the relationship between Fe and N in crop production is crucial as these two nutrients are fundamental to plant growth and productivity. A proper balance between Fe and N supply ensures that plants can efficiently gather energy and develop properly, leading to higher yields and better yield quality. Understanding this relationship helps in optimizing fertilizer use, preventing nutrient imbalances, and also improving soil fertility management, all of which are key to sustainable agricultural practices.

The present study aimed to evaluate the interplay between Fe and N nutritional pathway in tomato depending on the N-form applied: nitrate, urea or ammonium (the three most applied forms as N fertilizers). The characterization of plant responses to the Fe and N interplay will greatly advance our understanding of the role

played by known and unknown components involved in Fe and N nutritional responses.

Materials and methods

Plant growth

Solanum lycopersicum L. cv "Marmande" (DOTTO Spa. Italy) were germinated for 7 days on filter paper moistened with 0.5 mM $CaSO_4$ and then 180 seedlings were grown under hydroponic conditions as previously described by Tomasi et al. (2009). Twenty-one-day-old plants were then transferred to a Fe-free nutrient solution containing (mM): 0.70 K_2SO_4, 0.1 KCl, 2.00 $Ca(NO_3)_2$, 0.50 $MgSO_4$, 0.10 KH_2PO_4; (μM): 10.00 H_3BO_3, 0.50 $MnSO_4$, 0.50 $ZnSO_4$, 0.20 $CuSO_4$, 0.07 Na_2MoO_4 adjusted to pH 6.0 with KOH 1 M. After 14 days some tomato plants (35-day-old plants) were transferred to a N-free and Fe-free nutrient solution (-N-Fe NS, mM: 0.7 K_2SO_4, 0.1 KCl, 1.0 $CaSO_4$, 0.5 $MgSO_4$, 0.1 KH_2PO_4; μM: 10.00 H_3BO_3, 0.50 $MnSO_4$, 0.50 $ZnSO_4$, 0.20 $CuSO_4$, 0.07 Na_2MoO_4). Under these nutritional conditions, plants were grown for 7 days, and the pH was buffered using 1.5 mM MES-BTP (pH 6.0). The nutrient solutions were renewed every 3 days. At the end of the growing period (42-day-old), plants were treated for 24 hours with different N-forms and Fe-resupply, resulting in a total of four experimental conditions: plants were transferred to -N-Fe NS with addition of 2 mM total N (in the form of nitrate, KNO_3; urea, $CO(NH_2)_2$; or ammonium, $(NH_4)_2SO_4$) and 5μM Fe-EDTA (*-Fe/+Fe+Nit*; *-Fe/+Fe+U*; *-Fe/+Fe+A* plants, respectively), or control plants were maintained in -N-Fe NS (without adding N and without Fe, *-Fe/-Fe-N* plants). As an additional control, 36 plants (35-day-old plants) were transferred to -N-Fe NS where was added 0.1 mM Fe-EDTA and maintained under this condition up to the end of the experiment (43-day-old; *+Fe/+Fe-N* plants; see Supplementary Table S1). The characterization of the early response of tomato plants to the 24-hour application of the same three N forms under Fe sufficiency has been previously studied and reported in Lodovici et al. (2024).

At the end of the experiment, tomato plants (43-day-old) were washed in deionized water and then roots, young leaves (YL, at 43 days were considered as YL the last fully expanded leaves) or old leaves (OL, at 43 days were considered as OL the first leaves above the cotyledons) were sampled for transcriptional, elemental content and metabolomic analyses.

During the whole growing period, the controlled climatic conditions were the following: 16/8 (day/night) photoperiod; 220 μmol m^{-2} s^{-1} light intensity; 25/20°C (day/night) temperature and 70-80% relative humidity. The light transmittance of leaves was monitored using the SPAD instrument (SPAD-502, Minolta, Osaka, Japan).

Elemental analyses

The element concentrations of macro- and micro-nutrients in tomato samples were determined by Inductively Coupled Plasma–Optical Emission Spectroscopy (ICP-OES 5800, Agilent Technologies, Santa Clara, USA) and CHN analyzer (CHN IRMS Isoprime 100 Stable Isotope Ratio Mass Spectrometer, Elementar, Como, Italy).

For ICP-OES analyses, plant samples were oven-dried for 72 hours (at 60-80°C) and ground. For each sample, around 100 mg of ground powder was digested with concentrated ultrapure HNO_3 using a microwave oven (ETHOS EASY, Milestone Srl, Sorisole (BG), Italy) accordingly to the USEPA 3052 method "Plant Xpress" (USEPA, 1995). Element quantifications were carried out using certified multi-element standards.

Regarding CHN analyses, plant shoots and roots were dried, and their total N and C contents were determined by CHN-IRMS (CHN IRMS Isoprime 100 Stable Isotope Ratio Mass Spectrometer, Elementar, Como, Italy).

Metabolomic analysis

Roots, YL, and OL (four samples of each plant material per treatment) were ground in liquid nitrogen using a pestle and mortar. Briefly, 1.0 g of each plant sample was extracted in 10 mL of a hydroalcoholic solution (80:20 *v/v* methanol: water) acidified with 0.1% (*v/v*) formic acid, using an Ultra Turrax (Polytron PT, Switzerland). The extracts were then centrifuged (6000 × *g* for 10 min at 4°C) and the supernatants filtered through 0.22 μm cellulose syringe filters in UHPLC vials for analysis. The untargeted metabolomic analysis was performed using a quadrupole-time-of-flight mass spectrometer (6550 iFunnel, Agilent Technologies, Santa Clara, USA), coupled to an ultra-high-performance liquid chromatograph (UHPLC, 1290 series, Agilent Technologies, Santa Clara, USA) *via* a JetStream Electrospray ionization system, under previously optimized analytical conditions. Briefly, 6 μL of each sample were injected and a reverse-phase chromatographic separation was achieved by using a C18 column (Agilent Zorbax eclipse plus; 50 mm × 2.1 mm, 1.8 μm) and a water-acetonitrile binary gradient (from 6 to 94% organic in 32 min). The mass spectrometer worked in positive FULL SCAN mode (range 100 – 1200 *m/z*, 0.8 spectra/s, 30.000 FWHM). Compound identification was achieved through the 'find-by-formula' algorithm using the software Profinder B.07 (from Agilent Technologies) and the PlantCyc 9.6 database (Plant Metabolic Network, Filiz and Akbudak, 2020). The whole isotope pattern (i.e., monoisotopic mass, isotopic spacing, and isotopic ratio) was considered, considering 5 ppm for mass accuracy, resulting in a level 2 of confidence in annotation (Salek et al., 2013). The raw metabolomic dataset was extrapolated from the software Mass Profiler Professional B.12.06 (from Agilent Technologies) after post-acquisition data filtering (compounds do not present in 100% of the replications within at least one treatment were discarded), baselining and normalization.

Ferric-chelate reductase activity

The FCR activity by tomato roots was determined according to Pinton et al., 1999. Briefly, the roots of single intact plants were

incubated in the dark at 25°C for 30 min in 25 mL of an assay solution containing 0.5 mM $CaSO_4$, 10 mM MES-KOH, 0.25 mM Fe(III)-EDTA, 0.5 mM Na_2-bathophenanthrolinedisulfunic acid (BPDS). Every 15 min, the absorbance of the assay solution was measured at 535 nm. The amount of the Fe(III) reduced, as Fe(II)-$BPDS_3$ complex, was calculated using an extinction coefficient of 22 mM^{-1} cm^{-1} and expressed as: µmol Fe(II) g^{-1} root FW h^{-1} (FW, Fresh Weight).

Gene expression analysis

Tomato roots were ground in liquid nitrogen. Total RNA was extracted from approximately 60-70 mg of powder using the Spectrum Plant Total RNA Kit (Sigma Aldrich, St. Louis, MO, USA) according to the manufacturer's instructions (protocol A). RNA quantity and quality were inspected through a NanoDrop device (NanoDrop Technologies, Wilmington, Delaware, USA) and by migration in agarose gel, respectively. Afterwards, 1 µg of extracted RNA was retrotranscribed into cDNA, adding: 1 µL of Oligo-d (T) 70 µM, 1 µl dNTP (10 mM), 20 U Rnase inhibitors, 200 U M-MLV Reverse Transcriptase (M-MLV Reverse Transcriptase Sigma Aldrich, St. Louis, MO, USA) according to the manufacturer's instruction.

Using primer3 software (version 4.0.1) primers were designed and then synthesized by Merck (MERCK KGAA Darmstadt, Germany; Supplementary Table S2). RT-PCR analysis was performed with CFX96 Touch Real-Time PCR Detection System (Bio-Rad, Hercules, CA, USA). Data were referred to the averaged expression of two housekeeping genes *SlEF1* and *SlUbi* (Supplementary Table S2). Data were normalized using the $2^{-\Delta\Delta CT}$ according to Livak and Schmittgen (2001). The efficiency of each set of primer was estimated using the qPCR package for statistical analysis by R software (R version 2.9.1. www.dr-spiess.de/qpcR.html) as indicated by Ritz and Spiess (2008; R Core Team, 2021).

Statistical analysis

Three independent experiments were performed and a pool of roots of young leaves or old leaves from three tomato plants was used for each sample (Roots, YL and OL, respectively).

Statistical analyses were performed by SigmaPlot 14.0 (SigmaPlot Software, CA, USA), using one-way ANOVA with a Holm-Sidak's test as *post hoc* test for multiple comparisons (p-value <0.05, N = 3).

The metabolomic dataset was processed as previously reported (García-Pérez et al., 2021). Outliers were detected and removed, and the remaining samples were employed for multivariate statistics and post-acquisition analyses. Hierarchical cluster analysis (HCA) (Euclidean distance, Ward's linkage), one-way ANOVA and the subsequent fold-change (FC) analysis ($p < 0.01$, Bonferroni multiple testing correction; FC ≥ 2) were obtained from the Mass Profiler Professional B.12.06 software tool. The differential compounds were then interpreted using the PlantCyc Pathway Tool (Karp et al., 2010).

Moreover, the raw metabolomic dataset was exported into SIMCA 16 (Umetrics, Malmo, Sweden) for orthogonal projection to latent structures discriminant analysis (OPLS-DA) supervised modelling. Each model was cross-validated, inspected for outliers and overfitting, and then R^2Y (goodness-of-fit) and Q^2Y (goodness-of-prediction) parameters were recorded. Finally, the variables importance in projection (VIP) method allowed identifying discriminant compounds (VIP markers) with a VIP score > 1.3.

Regarding gene expression analysis and elemental content analyses the heatmap and principal component analyses (PCAs) were generated using ClustVis (https://biit.cs.ut.ee/clustvis/; Metsalu and Vilo, 2015) webtool using the fold parameters. The significance of the clustering observed in PCAs was assessed by PERMANOVA test using 5000 permutations performed with R version 4.3.0 (vegan package, Oksanen et al., 2014).

Results

Morphological observations

Morphometric measures were performed in all the considered plant organs (YL, OL, roots, and whole shoots (S)) under our experimental conditions. At the end of the growing period and after the 24-hour treatment, Fe-deficient tomato plants (-Fe/-Fe-N, -Fe/+Fe +Nit, -Fe/+Fe+U, -Fe/+Fe+A) resulted in being homogeneous at whole plants and foliar cover level (Supplementary Figures S1, S2). As expected, the SPAD values in YL were highly responsive to Fe nutritional status, as Fe-deficient plants displayed the lowest values, whereas the highest values were observed under Fe-sufficiency. After 24 hours, the resupply of nitrogen to Fe-deficient plants increased the SPAD values compared to the Fe-deficient control (-Fe/-Fe-N), increasing significantly under nitrate or ammonium nutrition. The SPAD values measured in old leaves were significantly lower in -Fe/-Fe-N, -Fe/+Fe+Nit and -Fe/+Fe+A if compared to +Fe/+Fe-N plants (Supplementary Figure S3). No significant changes in the dry biomass were detected in shoots and roots among treatments (Supplementary Figure S3). The height of shoots of +Fe/+Fe-N plants was significantly higher than those detected in plants grown under Fe deficiency (Supplementary Figure S3).

Elemental content

After 24 hours of N and Fe resupply, the concentration of macro- and micro-nutrients in OL, YL and roots were determined (Table 1, Supplementary Table S3, Figure 1).

The principal component analysis (PCA) showed that +Fe/+Fe-N was separated from the other treatments (-Fe/-Fe-N, -Fe/+Fe +Nit, -Fe/+Fe+U or -Fe/+Fe+A, which generally clustered together; PERMANOVA p-value<0.001 for YL and OL, p-value<0.05 for roots, Figure 1). Supplementary Figure S4 reports the PCA of plants grown only under nitrogen and Fe deficiency.

The results mentioned above are reflected in the specific elemental concentration. The supply of nitrate or ammonium to N and Fe-deficient plants induced an increase of N concentration in

10.3389/fpls.2024.1408141

TABLE 1 Elemental concentration in tomato plants.

µg g^{-1} DW	Cu	Fe	Mn	Na	Zn
Young leaves					
+Fe/+Fe-N	12.6 ± 1^{b}	196.2 ± 33.2^{a}	32.7 ± 2.1^{c}	208 ± 41.2^{a}	31.5 ± 1.4^{c}
-Fe/-Fe-N	20.7 ± 3^{a}	69.6 ± 12^{c}	49.8 ± 4.2^{b}	98.1 ± 20.6^{b}	42.4 ± 3.4^{b}
-Fe/+Fe+Nit	22 ± 4.4^{a}	115.5 ± 23.4^{b}	68.3 ± 8.1^{a}	137 ± 21.2^{b}	54 ± 3.6^{a}
-Fe/+Fe+U	19.8 ± 1^{ab}	70.2 ± 4^{c}	51.2 ± 4^{b}	120 ± 16.3^{b}	42.8 ± 1.1^{b}
-Fe/+Fe+A	23.2 ± 2.2^{a}	119.8 ± 17.8^{b}	51.2 ± 5^{bc}	150 ± 10.9^{ab}	42.9 ± 5.3^{b}
Old leaves					
+Fe/+Fe-N	8.4 ± 0.9^{b}	253 ± 10.2^{a}	33.1 ± 2^{c}	458.1 ± 22.4^{a}	26.7 ± 1.2^{c}
-Fe/-Fe-N	20.4 ± 4.2^{a}	65 ± 3^{c}	67 ± 11.6^{b}	304.2 ± 11.7^{c}	51.4 ± 8.4^{b}
-Fe/+Fe+Nit	20.6 ± 5^{a}	94.1 ± 15.8^{b}	108 ± 7.9^{a}	359.1 ± 23.7^{b}	83 ± 10.1^{a}
-Fe/+Fe+U	18.4 ± 2.9^{a}	63.8 ± 7.8^{c}	70.5 ± 12.3^{b}	339 ± 9.6^{bc}	47.2 ± 5.5^{b}
-Fe/+Fe+A	25.2 ± 3.2^{a}	106 ± 14.1^{b}	86 ± 9^{ab}	341 ± 8.8^{bc}	59.7 ± 11.2^{b}
Roots					
+Fe/+Fe-N	121 ± 5.1^{c}	1182 ± 110^{a}	117 ± 10.6^{b}	4339 ± 1333^{a}	144 ± 5.21^{c}
-Fe/-Fe-N	451 ± 108^{ab}	58.9 ± 10.7^{e}	130 ± 19.2^{ab}	545 ± 184^{b}	416 ± 116^{a}
-Fe/+Fe+Nit	618 ± 97.7^{a}	427 ± 104^{b}	177 ± 35.7^{a}	806 ± 154^{b}	522 ± 60.7^{a}
-Fe/+Fe+U	327 ± 41.4^{b}	271 ± 42.5^{c}	81.8 ± 9.5^{b}	524 ± 20.8^{b}	283 ± 61.0^{b}
-Fe/+Fe+A	310 ± 50.2^{b}	130 ± 28.8^{d}	98.9 ± 9^{b}	529 ± 33^{b}	341 ± 77.1^{abc}
mg g^{-1} DW	Ca	K	Mg	P	S
Young leaves					
+Fe/+Fe-N	11.1 ± 0.2^{b}	40 ± 0.1^{ab}	4.7 ± 0.2^{b}	5.6 ± 0.2^{b}	17.5 ± 1.8^{ab}
-Fe/-Fe-N	14.1 ± 1^{ab}	36.8 ± 4^{b}	7.1 ± 0.3^{a}	6 ± 0.5^{ab}	16.1 ± 2.3^{abc}
-Fe/+Fe+Nit	17 ± 2^{a}	47.2 ± 3.8^{a}	7.5 ± 0.5^{a}	7.1 ± 0.9^{a}	11.4 ± 2.3^{c}
-Fe/+Fe+U	15.1 ± 2^{ab}	35.3 ± 1.3^{b}	7.2 ± 0.2^{a}	5.9 ± 0.2^{ab}	13.9 ± 1.4^{c}
-Fe/+Fe+A	14.6 ± 2.7^{ab}	43.4 ± 3.2^{a}	7.1 ± 0.7^{a}	6.7 ± 0.2^{ab}	20.9 ± 1.1^{a}
Old leaves					
+Fe/+Fe-N	16.9 ± 0.3^{b}	39.8 ± 2.1^{ab}	4.6 ± 0.2^{b}	4.5 ± 0.5^{c}	38.1 ± 0.8^{ab}
-Fe/-Fe-N	25.4 ± 4.5^{ab}	33.8 ± 2.9^{b}	8 ± 1.2^{a}	5.3 ± 0.5^{c}	37.4 ± 6.9^{ab}
-Fe/+Fe+Nit	34.7 ± 1.9^{a}	46.8 ± 5.4^{a}	8.2 ± 0.5^{a}	7.8 ± 0.4^{a}	35.6 ± 4.8^{b}
-Fe/+Fe+U	26.7 ± 1.5^{ab}	33 ± 1.9^{b}	8 ± 0.3^{a}	5.4 ± 0.2^{c}	37 ± 4.2^{ab}
-Fe/+Fe+A	32 ± 6.8^{a}	41.5 ± 6.6^{a}	8.6 ± 1.5^{a}	6.6 ± 0.3^{b}	49.6 ± 3.1^{a}
Roots					
+Fe/+Fe-N	3.7 ± 0.5	62.5 ± 11.9^{ab}	2.3 ± 0.4^{b}	5.7 ± 0.8^{b}	10.9 ± 1.6
-Fe/-Fe-N	5.7 ± 1.2	72.9 ± 9.8^{a}	4.7 ± 1.2^{b}	8.2 ± 1.3^{a}	12.8 ± 1.8
-Fe/+Fe+Nit	5.2 ± 1	54.1 ± 5.4^{ab}	10 ± 2.9^{a}	7 ± 0.2^{ab}	10 ± 0.5
-Fe/+Fe+U	5.5 ± 0.6	47.5 ± 0.7^{b}	5.4 ± 1.3^{b}	6.3 ± 0.2^{ab}	9.4 ± 0.3
-Fe/+Fe+A	5.2 ± 1.5	51.9 ± 10.1^{ab}	2.7 ± 0.5^{b}	6.5 ± 0.8^{ab}	10 ± 1.7
mg g^{-1} DW	C	N			

(Continued)

10.3389/fpls.2024.1408141

TABLE 1 Continued

mg g^{-1} DW	C	N
Shoots		
+Fe/+Fe-N	368 ± 8.2^{a}	25.4 ± 1.0^{ab}
-Fe/-Fe-N	324 ± 13.9^{ab}	20.4 ± 1.6^{b}
-Fe/+Fe+Nit	335 ± 11.8^{ab}	30.6 ± 1.9^{a}
-Fe/+Fe+U	337 ± 5.8^{ab}	22.2 ± 2.3^{b}
-Fe/+Fe+A	307 ± 36.2^{b}	22.1 ± 4.2^{b}
Roots		
+Fe/+Fe-N	415 ± 2.8^{a}	30.4 ± 1.8^{b}
-Fe/-Fe-N	407 ± 9.3^{a}	31.8 ± 0.8^{b}
-Fe/+Fe+Nit	385.8 ± 3^{b}	38.6 ± 1.0^{a}
-Fe/+Fe+U	399.4 ± 6.8^{ab}	30.8 ± 1.5^{b}
-Fe/+Fe+A	401 ± 7.4^{ab}	40.1 ± 0.4^{a}

Plants were maintained in N-free nutrient solution and Fe sufficiency (control +Fe/+Fe-N) or Fe deficiency (control -Fe/-Fe-N) or exposed to three different N sources and Fe-resupply (nitrate and Fe-EDTA, -Fe/+Fe+Nit; urea and Fe-EDTA, -Fe/+Fe+U; or ammonium and Fe-EDTA, -Fe/+Fe+A) for 24 hours. Data refers to the analyses performed on three plant organs: young leaves, old leaves and roots. Data refers to mean values ± SD; letters refer to statistical significance for each element and plant organ among experimental conditions (Holm–Sidak test ANOVA. N =3. p-value < 0.05). Data are expressed in µg g^{-1} or mg g^{-1} dry weight (DW).

shoots and roots, respectively, in comparison to the controls and urea-treated plants (-Fe/-Fe-N, +Fe/+Fe-N, -Fe/+Fe+U). It is interesting to highlight that Fe concentration is significantly and differentially concentrated considering each applied experimental condition. As expected, +Fe/+Fe-N has the highest Fe concentration, whereas the other conditions followed the pattern: -Fe/+Fe+Nit > -Fe/+Fe+U > -Fe/+Fe+A > -Fe/-Fe-N.

Regarding the other analyzed elements, in YL, the application of Nit as N-form resulted in a significant increase of Mn and Zn in comparison to +Fe/+Fe-N, -Fe/-Fe-N, -Fe/+Fe+U or -Fe/+Fe+A treatments. Besides, Fe concentration resulted in being higher in YL treated with Nit and A in comparison to -Fe/-Fe-N and -Fe/+Fe+U, while A supply led to a higher concentration of S in comparison to -Fe/+Fe+Nit and -Fe/+Fe+A treatment.

The elemental analysis in OL showed an increase in the concentration of Zn and P when Nit was supplied as N-form in comparison to +Fe/+Fe-N, -Fe/-Fe-N, -Fe/+Fe+U or -Fe/+Fe+A treatment. Moreover, as in YL, Fe concentration increased when Nit and A were supplied to the nutrient solution compared to -Fe/-Fe-N and U treatment.

In roots, the supply of Nit led to a higher concentration of Mn and Mg compared to the other treatments.

Metabolomic analysis

The application of untargeted metabolomics provided the annotation of 3320 chemical entities among the extracts derived from YL, OL, and roots of tomato plants. Supplementary Table S4 shows the provides the list of annotated compounds in tomato samples, their abundance, molecular formula, composite mass spectra, and retention time. To decipher the influence of each factor involved in the metabolic profile of tomato plants, an unsupervised multivariate hierarchical cluster analysis (HCA) was first performed (Supplementary Figure S5). According to the similarity of metabolic profiles, the fold change-based heatmap showed that tissue played a clear role in clustering samples, grouping the profile associated with roots apart from that derived from leaves, suggesting a tissue-dependent response towards different N sources in tomato plants (Supplementary Figure S5). Consequently, further analyses were applied individually to each organ to provide insight into the impact of different N forms. Thus, the results from HCA of YL, OL, and roots are displayed in Figure 2 (A, B, and C, respectively). In all cases, the same trend was observed for each tissue: according to their metabolic profile, Fe-deficient tomato plants treated with nitrate (-Fe/+Fe+Nit) showed a clear similarity with those cultured under the combined deficiency of nitrogen and iron (-Fe/-Fe-N), as they clustered together (Figure 2). Concerning the other subcluster, Fe-supplied plants (+Fe/+Fe-N) exhibited a distinctive profile, whereas those Fe-deficient plants treated with ammonium (-Fe/+Fe+A) and urea (-Fe/+Fe+U) showed a similar profile between them (Figure 2). These results suggest that 1) Fe deficiency shows a coordinated whole-plant impact; and 2) A and U supply may counter the effects of iron deficiency in tomato plants at a metabolic level.

Afterwards, to provide a distinctive perspective due to the application of different N sources under Fe deficiency, a supervised multivariate orthogonal projection to latent structures discriminant analysis (OPLS-DA) was performed for each tissue, and the obtained models for young and old leaves, and roots are shown in Figure 2 (D, E, F, respectively). All models presented high-quality parameters in terms of goodness-of-fit (R^2Y) and goodness-of-prediction (Q^2Y): $R^2Y = 0.991$ and $Q^2Y = 0.875$ for the model of young leaves; $R^2Y = 0.985$ and $Q^2Y = 0.865$ for the model of old leaves; and $R^2Y = 0.979$ and $Q^2Y = 0.894$ for the model of roots. All models were also proved statistically significant at $p < 0.001$ (CV-

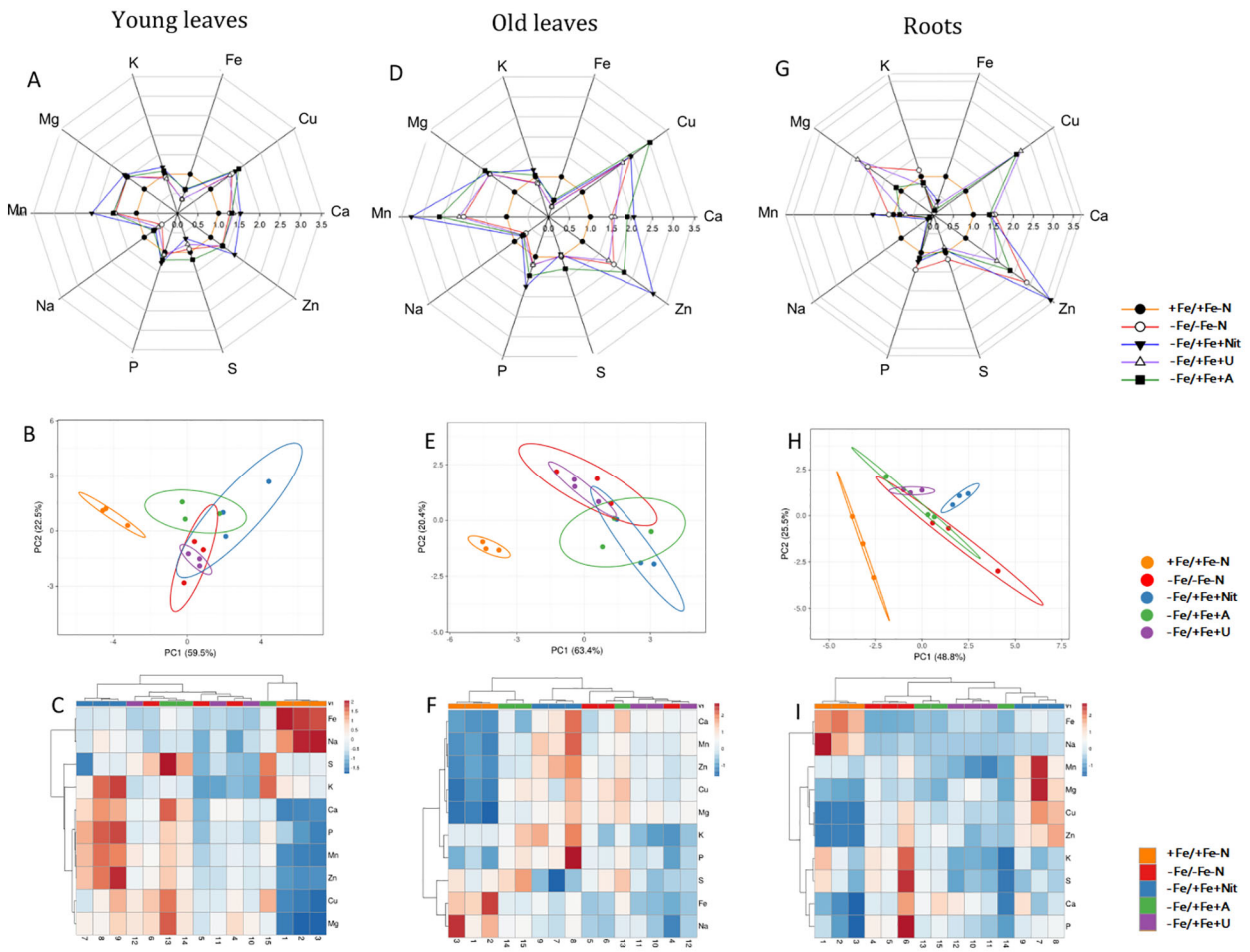

FIGURE 1
Elemental content of tomato plants after 24 hours of treatment with different N sources in old leaves, young leaves and roots. In radar plots, the concentration of considered elements in young leaves **(A)**, old leaves **(D)** and roots **(G)** was scaled to average value of +Fe/+Fe-N samples (value 1.0). PCA analyses show principal component 1 and principal component 2 that explain: 63.4% and 20.4% of the total variance in old leaves **(B)**, 59.5% and 22.5% of the total variance in young leaves **(E)** and 48.8% and 25.5% of the total variance in roots **(H)**. In heatmaps, a clustering of elemental concentration and samples in old leaves **(C)**, young leaves **(F)** and roots **(I)**.

ANOVA). Focusing on the discrimination between treatments, Fe-supplied plants exhibited an exclusive profile in all tissues as +Fe/+Fe-N was found apart from the rest of the treatments (Figures 2D–F). Considering the profiles of Fe-deficient plants, a high dependence on N sources was observed, following a tissue-dependent behavior. For young leaves, -Fe/+Fe+U promoted a similar profile to -Fe/-Fe-N, whereas -Fe/+Fe+Nit and -Fe/+Fe+A promoted distinctive profiles (Figure 2D). In the case of old leaves and roots, the profile from Nit-treated plants promoted a negligible difference with respect to those from -Fe/-Fe-N, whereas –Fe/+Fe+A drove the most differential profile compared to -Fe/-Fe-N in old leaves (Figure 2E). In comparison, -Fe/+Fe+U triggered the most distinctive profile in roots (Figure 2F).

The obtained OPLS models were combined with variable importance in projection (VIP) analysis to detect the metabolites with the highest discriminant power, the so-called VIP markers, which were determined by their VIP score. The full list of VIP markers is provided in Supplementary Table S5. In addition, a Venn diagram is provided in Supplementary Figure S6 to graphically indicate the different and/or coincident VIP markers between tissues. The high number of metabolites exclusively associated with each tissue (a total of 78, 89 and 162 for young and old leaves and roots, respectively) confirms a clear tissue-dependent effect of N sources under Fe deficiency (Supplementary Figure S6). Moreover, YL and OL shared a total of 27 metabolites, suggesting a slightly similar modulation of their metabolic profiles, being mostly represented by stress-related metabolites, as shown for abscisic acid (ABA) derivatives and glucosinolates, as well as a wide range of metabolites closely related to N metabolism, i.e.: amino acids like Pro, and Ser and Glu derivatives, adenosine derivatives, and triferuloyl spermidine. Furthermore, both leaf tissues and roots also shared a series of discriminant N-containing compounds, represented by amino acid derivatives, such as histidinol and ornithine; nucleotide-derived metabolites, like those from adenine, uridine, cytidine, hypoxanthine and guanine; as well as some metabolites related to oxidative stress management, including glutathione derivatives and polyphenols, like daidzein, (-)-epicatechin, and cyanidin glycosides (Supplementary Figure S6).

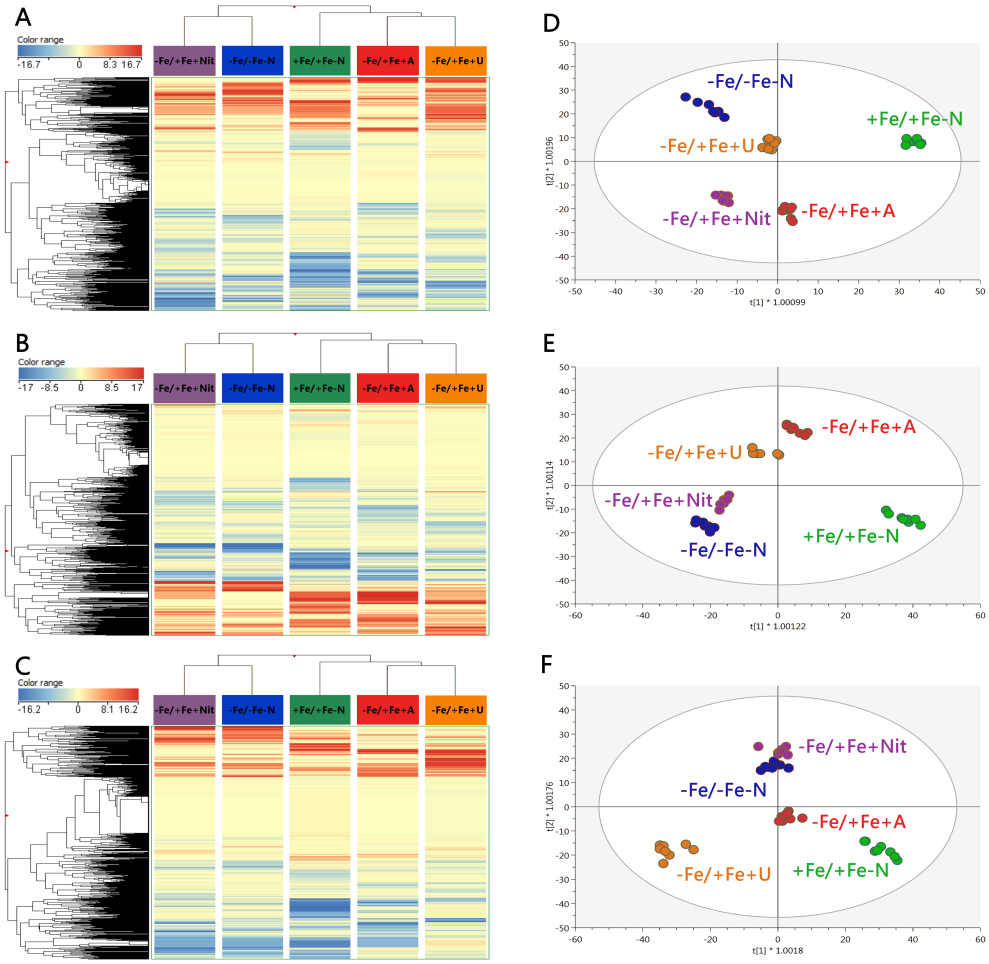

FIGURE 2
Unsupervised hierarchical cluster analysis carried out from ultra-performance liquid chromatography electrospray-ionization quadrupole time-of-flight mass spectrometry (UPLC ESI/QTOF-MS) metabolomic analysis of young **(A)** and old leaves **(B)** and roots **(C)** after N supply. The fold-change-based heat map was used to build hierarchical clusters (linkage rule: Ward; distance: Euclidean). Score plot of orthogonal projection to latent structure discriminant analysis (OPLS-DA) supervised modelling carried out on untargeted metabolomic profiles of young **(D)** and old leaves **(E)** and roots **(F)** after N supply. +Fe/+Fe-N, control with N deficiency; -Fe/-Fe-N, control with Fe and N deficiency; -Fe/+Fe+Nit, nitrate; -Fe/+Fe+A, ammonium; -Fe/+Fe+U, urea.

Finally, to get insight into the effect of N source on the biosynthetic metabolic pathways of Fe-depleted tomato plants, the significant compounds ($p < 0.01$, FC ≥ 2) with respect to +Fe/+Fe-N (under N deficiency) were subjected to the PlantCyc Pathway Tools, and independently processed for young and old leaves and roots. Figure 3 shows the modulation of biosynthetic metabolism for young and old leaves and roots of Fe-deficient tomato plants concerning Fe-supplied plants (+Fe/+Fe-N, Figures 3A–C, respectively). In general, Fe-deficient tomato plants exhibited an intense up-regulation of secondary metabolism, which was more evident in the case of urea supply, followed by a moderate induction of phytohormone biosynthesis (Figure 3). Given the importance of phytohormones and secondary metabolism in the response towards different N sources under Fe-deficient conditions, Figure 4 includes the modulation of hormone biosynthesis and secondary metabolism in tomato plants.

Concerning young leaves, a general decrease in amino acid biosynthesis was observed, thus suggesting an impairment of N metabolism (Figure 3A). The induction of hormone biosynthesis under Fe deficiency in young leaves (Figure 3A) was mostly due to the increase of jasmonates and brassinosteroids biosynthesis (Figure 4A). In the case of jasmonates, all treatments strongly induced their biosynthesis, as observed for (-)-jasmonate (logFC = 15.88 – 21.86 for all treatments) and its precursor 3-oxo-2-(cis-2'-pentenyl)-cyclopentane-1-(3-oxooctanoyl)-CoA (Figure 4A). In the case of brassinosteroids, although A supply caused a decrease in their biosynthesis, the rest of the treatments (-Fe/-Fe-N > -Fe/+Fe +Nit > -Fe/+Fe+U) promoted their induction, being represented by brassinolide, 6-hydroxytaphasterol, and cathasterone derivatives (Figure 4A). Interestingly, young leaves from plants grown under the combined N and Fe deficiency (-Fe/-Fe-N) exhibited a sharp increase in abscisic acid accumulation (ABA, as shown for 2-trans-

10.3389/fpls.2024.1408141

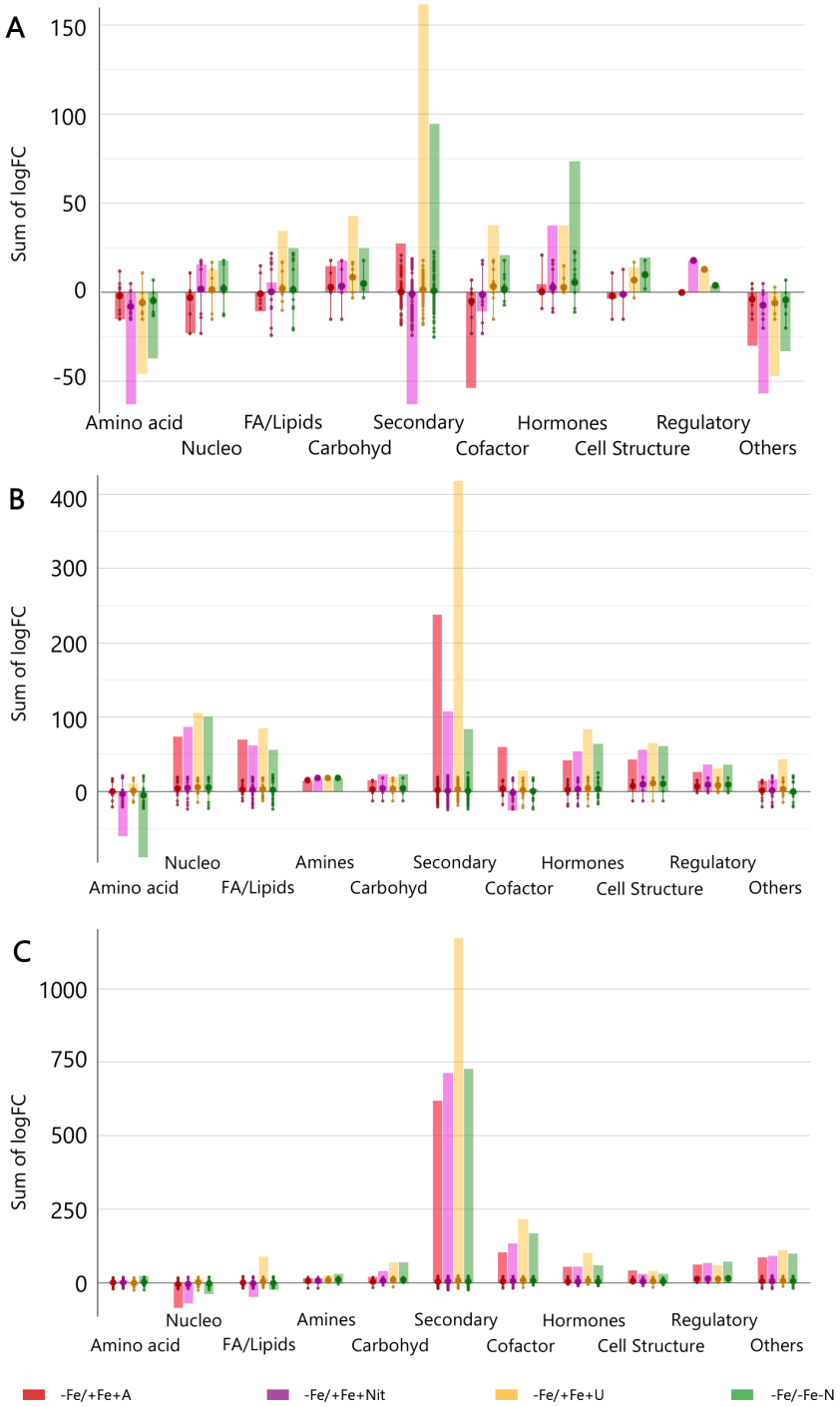

FIGURE 3
Biosynthetic pathways modulated by ammonium, nitrate, and urea in young leaves **(A)**, old leaves **(B)**, and roots **(C)** of Fe-deficient tomato plants. Significant metabolites ($p < 0.01$) and with fold-change (FC) values ≥ 2 for each treatment with respect to +Fe/+Fe-N were subjected to Pathway Analysis and visualized by the Omics Viewer Dashboard of the PlantCyc pathway Tool software (www.pmn.plantcyc.com). Large dots represent the average (mean) of all logFC for metabolites within the same subcategory, and the small dots represent the individual logFC values for each metabolite. The x-axis represents each set of subcategories. while the y-axis corresponds to the cumulative logFC. Amino acid, amino acids; Nucleo, nucleosides and nucleotides; FA/Lipids, fatty acids and lipids; Amines, amines and polyamines; Carbohyd, carbohydrates; Secondary, secondary metabolites; Cofactors, cofactors, prosthetic groups, electron carriers, and vitamins; Cell structure, cell structure-related metabolites; Regulatory, regulatory metabolites; Others: other metabolites. +Fe/+Fe-N, control with N deficiency; -Fe/-Fe-N, control with Fe and N deficiency; -Fe/+Fe+Nit, nitrate; -Fe/+Fe+A, ammonium; -Fe/+Fe+U, urea.

FIGURE 4
Hormone and secondary metabolite biosynthetic pathways modulated by ammonium, nitrate, and urea in young leaves **(A, B)**, old leaves **(C, D)**, and roots **(E, F)** of Fe-deficient tomato plants. Significant metabolites ($p < 0.01$) and with fold-change (FC) values ≥ 2 for each treatment with respect to +Fe/+Fe-N were subjected to Pathway Analysis and visualized by the Omics Viewer Dashboard of the PlantCyc pathway Tool software (www.pmn.plantcyc.com). Large dots represent the average (mean) of all logFC for metabolites within the same subcategory, and the small dots represent the individual logFC values for each metabolite. The x-axis represents each set of subcategories; while the y-axis corresponds to the cumulative logFC. STR, strigolactones; ABA, abscisic acid; AUX, auxins; BR, brassinosteroids; CK, cytokinins; GB, gibberellins and precursors; Jas, jasmonates; ETH, ethylene; JHI, juvenile hormone I; JHIII, juvenile hormone III; N-containing, N-containing secondary metabolites; Phenylprop, phenylpropanoids derivatives; S-containing, sulfur-containing secondary metabolites. +Fe/+Fe-N, control with N deficiency; -Fe/-Fe-N, control with Fe and N deficiency; -Fe/+Fe+Nit, nitrate; -Fe/+Fe+A, ammonium; -Fe/+Fe+U, urea.

abscisate, logFC = 23.97) coupled with a decrease in gibberellins biosynthesis (gibberellin A_{13}, GA_{13}, logFC = -11.84), whose effects were similar in Nit-supplied plants (logFC = 5.39 for ABA and logFC = -11.84 for GA_{13}). Regarding secondary metabolism (Figure 4B), all treatments under Fe-deficiency promoted the biosynthesis of phenylpropanoids, mostly represented by flavonoid and anthocyanin glycosides, following the trend (-Fe/-Fe-N > -Fe/+Fe+U > -Fe/+Fe+Nit > -Fe/+Fe+A). In contrast, the

10.3389/fpls.2024.1408141

biosynthesis of N-containing compounds (NCCs) was found increased by the treatments -Fe/+Fe+U and -Fe/+Fe+A (average logFC = 2.56 and 0.56, respectively), which essentially involved alkaloids and glucosinolates, whereas a decrease was recorded by -Fe/+Fe+Nit and -Fe/-Fe-N (sum of logFC < -25.00 for both treatments; Figure 4B). Accordingly, -Fe/+Fe+Nit and -Fe/-Fe-N showed a similar effect by causing a pronounced decrease in terpenoid biosynthesis (average logFC = -4.70 and -3.45, respectively), thus reinforcing the parallel metabolic modulation driven by both treatments.

With respect to old leaves, the modulation of biosynthetic metabolism followed a similar trend to that observed in young leaves, exhibiting a clear induction of secondary metabolism and phytohormone biosynthesis by all treatments (Figure 3B). Regarding phytohormones, the biosynthesis of jasmonates was found increased by all treatments (Figure 4C), affecting a wide range of metabolites, such as 3-oxo-2-(cis-2'-pentenyl)-cyclopentane-1-(E-buta-2-enoyl)-CoA, 3-oxo-2-(cis-2'-pentenyl)-cyclopentane-1-(3R-hydroxybutanoyl)-CoA and related compounds (respectively: logFC = 4.27 and 4.29 for A, 13.77 and 13.94 for N, 17.92 and 18.14 for U, and 18.84 and 19.15 for -Fe/-Fe-N). In parallel, the biosynthesis of the cytokinin isopentenyladenine-7-N-glucoside was found to be strongly decreased by all treatments (logFC = -20.28 – -8.48; Figure 4C). Again, as observed for young leaves, Nit-supplied and -Fe/-Fe-N plants showed a similar influence on the phytohormonal profile of tomato plants under Fe deficiency (Figure 4C), since both drove the induction of 2-trans-abscisate biosynthesis (logFC = 12.41 and 25.44, respectively) and the repression of brassinosteroids (such as 3-epi-6-deoxycathasterone, logFC = -17.09 for both treatments) and gibberellins biosynthesis, as reported by gibberellins A_3 (logFC = -9.08 and -9.07, respectively) and A_{36} (logFC = -20.06 and -14.86, respectively). Focusing on secondary metabolism, the same results were observed with respect to young leaves (Figure 4D) since all Fe-deficient plants exhibited an increase in phenylpropanoid biosynthesis, essentially represented by flavonoid glycosides and stilbenes. Furthermore, the biosynthesis of NCCs and terpenes was increased by -Fe/+Fe+A and -Fe/+Fe+U, whereas -Fe/-Fe-N and -Fe/+Fe+Nit treatments provoked the repression of both pathways.

Considering roots, the impact of Fe deficiency again caused significant induction of secondary metabolism and phytohormone biosynthesis, as reported for leaves (Figure 3C). In the case of phytohormones, all Fe-deficient treatments increased cytokinins biosynthesis, especially kinetin-7-*N*-glucoside, which exhibited logFC = 15.23 – 17.18 in all treatments (Figure 4E). Again, a parallel behavior

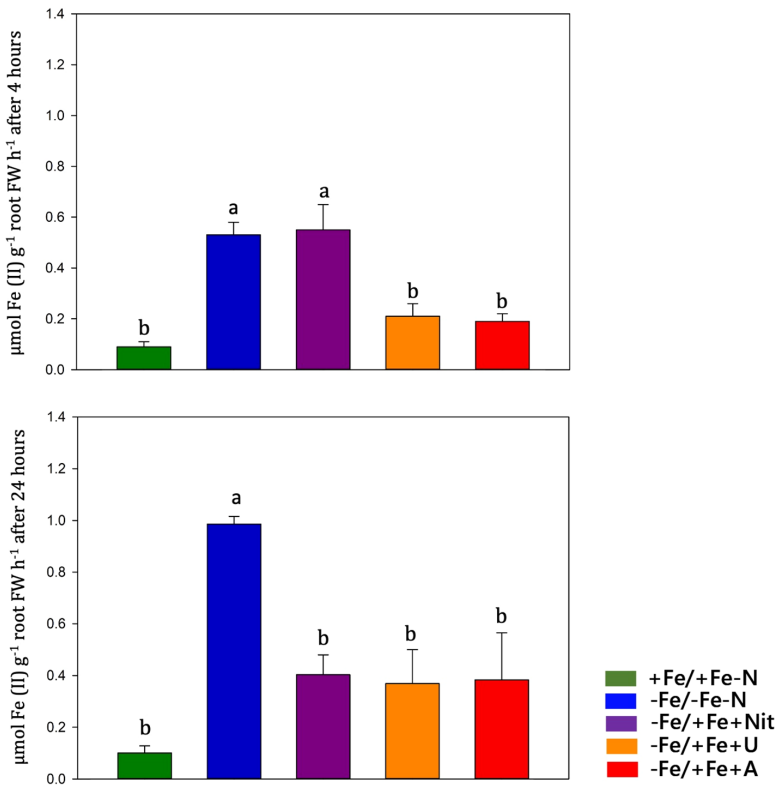

FIGURE 5
Ferric chelate reductase (FCR) activity quantification (expressed in µmol Fe (II) g^{-1} root FW h^{-1}) in tomato roots measured at 4 and 24 hours after treatment (+Fe/+Fe-N, green; -Fe/+Fe-N, blue; -Fe/+Fe+Nit, purple; -Fe/+Fe+U, orange; -Fe/+Fe+A, red).

was reported to roots from Nit-supplied plants and those grown under Fe and nitrogen combined deficiency (-Fe/-Fe-N). Both treatments, -Fe/+Fe+Nit and -Fe/-Fe-N, elicited the biosynthesis of 2-trans-abscisate (logFC = 13.78 and 8.87, respectively), gibberellins A_{36} (logFC = 14.58 and 19.89, respectively) and A_{37} (logFC = 9.64 and 7.25, respectively), and the jasmonate precursor 3-oxo-2-(cis-2'-pentenyl)-cyclopentane-1-(3-oxooctanoyl)-CoA (logFC = 2.31 and 6.76, respectively), whereas they strongly inhibited brassinosteroids biosynthesis, mostly represented by campesterol derivatives, such as (6α)-hydroxycampestanol and campest-5-en-3-one (logFC = -11.93 and -5.25 for both treatments for each compound, respectively). U and A supply countered those effects since these treatments (-Fe/+Fe+U and -Fe/+Fe+A) promoted a decrease in the biosynthesis of 2-trans-abscisate (logFC < -6.22 for both treatments), meanwhile they boosted the biosynthesis of brassinosteroids, especially in U-supplied roots, logFC = 10.79, 15.14, and 10.79 for (6α)-hydroxycampestanol, campest-5-en-3-one, and 3-epi-6-oxocathasterone, respectively (Figure 4F). Considering secondary metabolism, roots from Fe-deficient tomato plants showed a similar effect among all treatments, boosting the biosynthesis of phenylpropanoids, mainly flavonoid glycosides, and NCCs, represented by alkaloids and glucosinolates and their derivatives, where U-treated roots exhibited the highest cumulative logFC values (Figure 4F).

Overall, Fe deprivation promoted a general induction of plant stress, reported by the strong biosynthetic induction of stress-related phytohormones, such as jasmonates and abscisic acid derivatives, as well as important secondary metabolites implicated in plant stress management, as is the case of phenylpropanoids, glucosinolates, and alkaloids. In leaves, the stress associated with Fe-deficiency was partially reverted by U and A as N sources, whereas Nit supply play a negligible effect, showing an impairment of phytohormone biosynthesis and nitrogen metabolism comparable to that of Fe and N-deficient plants. The same behavior could be attributed to roots, where Nit supply promoted the accumulation of stress-derived phytohormones, such as ABA and jasmonates derivatives in Fe-deficient tomato plants. Such a stress-inducing fingerprint was also countered by the supply of both U and A, which also boosted the biosynthesis of brassinosteroids, phenylpropanoids, and NCCs compared to Fe-supplied, nitrogen-deficient tomato plants.

Ferric-chelate reductase activity

Fe(III)-chelate reductase activity was measured on intact tomato roots at 4 and 24 hours after treatment (Figure 5). Under Fe-sufficient condition (+Fe/+Fe-N), tomato roots displayed low FCR activity values, whereas high FCR activity values were observed under Fe deficiency. Under Fe resupply, Fe deficient plants (-Fe/-Fe-N) operated a feedback regulation on previously activated mechanisms, such as FCR activity. The timing of these feedback regulations was dependent on the N form applied: under urea (-Fe/+Fe+U) and ammonium (-Fe/+Fe+A), the FCR activity was slowed down already after 4 hours from the Fe-resupply, whereas under nitrate (-Fe/+Fe+Nit) the FCR activity was reduced after 24 hours.

Gene expression analyses

Gene expression analysis was performed at 24 hours after treatments on tomato roots by real-time RT-PCR and showed differences among treatments in the expression of key genes involved in Fe and N acquisition and utilization that can be well visualized by PCA (PERMANOVA $p<0.001$) and by heatmap clustering analysis (Figures 6A–C). These analyses were performed on twenty-two genes coding for: Fe and heavy metal transporters (*SlIRT1, SlIRT2, SlNRMAP1, SlCDF-type)*, proteins involved in Fe assimilation (*SlLHA4, SlOPT3*), a ferric reductase oxidase (*SlFRO1*), nitrate transporters with one of their accessory proteins (*SlNRT2.2, SlNRT1.5, NPF6.3, SlNAR2.1*), ammonium transporters (*SlAMT1-1, SL AMT1-2)*, urea transporter (*SlDUR3*) and N assimilatory enzymes (*SlNii1, SlNiR, SlGS2, SlGS1, SlNR, SlGOGAT, SlAS*).

Nitrate (-Fe/+Fe+Nit) treatment led to an increase of relative gene expression level of *SlIRT1, SlIRT2, SlNii1,SlNPF6.3, SlNiR, SlGS2cp, SlNRT2.2* in comparison to other N-treatment and controls (+Fe/+Fe-N, -Fe/-Fe-N), while was observed a downregulation of *SlNRAMP1, SlOPT3, SlLFER(bHLH), SlFRO1* if compared with -Fe/-Fe-N and downregulation of *SlGS1, SlAS1, SlAMT1-1, SlDUR3, SlNRT1.5* if compared with +Fe/+Fe-N.

Regarding the effect of ammonium treatment (-Fe/+Fe+A), the genes *SlAS1 and AMT 1-2* were significantly upregulated compared to the controls (+Fe/+Fe-N, -Fe/-Fe-N). On the other hand, the supply of A led to a downregulation of *SlGS1, SlGS2cp* and *SlNRT1.5* genes compared to +Fe/+Fe-N.

Urea treatment (-Fe/+Fe+U) resulted in a significant upregulation of *SlGOGAT, SlNR, SlCDF-type* and *SlFER(bHLH)* in comparison to other N-treatment, +Fe/+Fe-N and -Fe/-Fe-N. Moreover, a similar pattern to -Fe/-Fe-N was observed concerning *SlNRMAP1, SlOPT3* and *SlFRO1* genes that resulted in being upregulated in -Fe/-Fe-N and -Fe/+Fe+U treatment in comparison to +Fe/+Fe-N, -Fe/+Fe+Nit or -Fe/+Fe+A.

Discussion

Iron deficiency response

Before starting the treatment of N and Fe resupply, 42-day-old plants displayed visible symptoms and molecular evidence of Fe shortage and N limitation in agreement with literature (Zamboni et al., 2012; Sainju et al., 2003; Zamboni et al., 2016).

After 24 hours, the Fe resupplied plants (-Fe/+Fe+A, -Fe/+Fe +U, -Fe/+Fe+Nit) displayed an increase in Fe content and a decreased FCR activity compared to the control plants (-Fe/-Fe-N). These results suggest that Fe-deficient plants could use the resupplied Fe and indicate the occurrence of a feedback regulation of Fe responsive genes by Fe resupplied along with nitrate or ammonium.

In roots, nitrate and ammonium treatments exhibited similar gene expression patterns except for *IRT1* and *IRT2*, which were

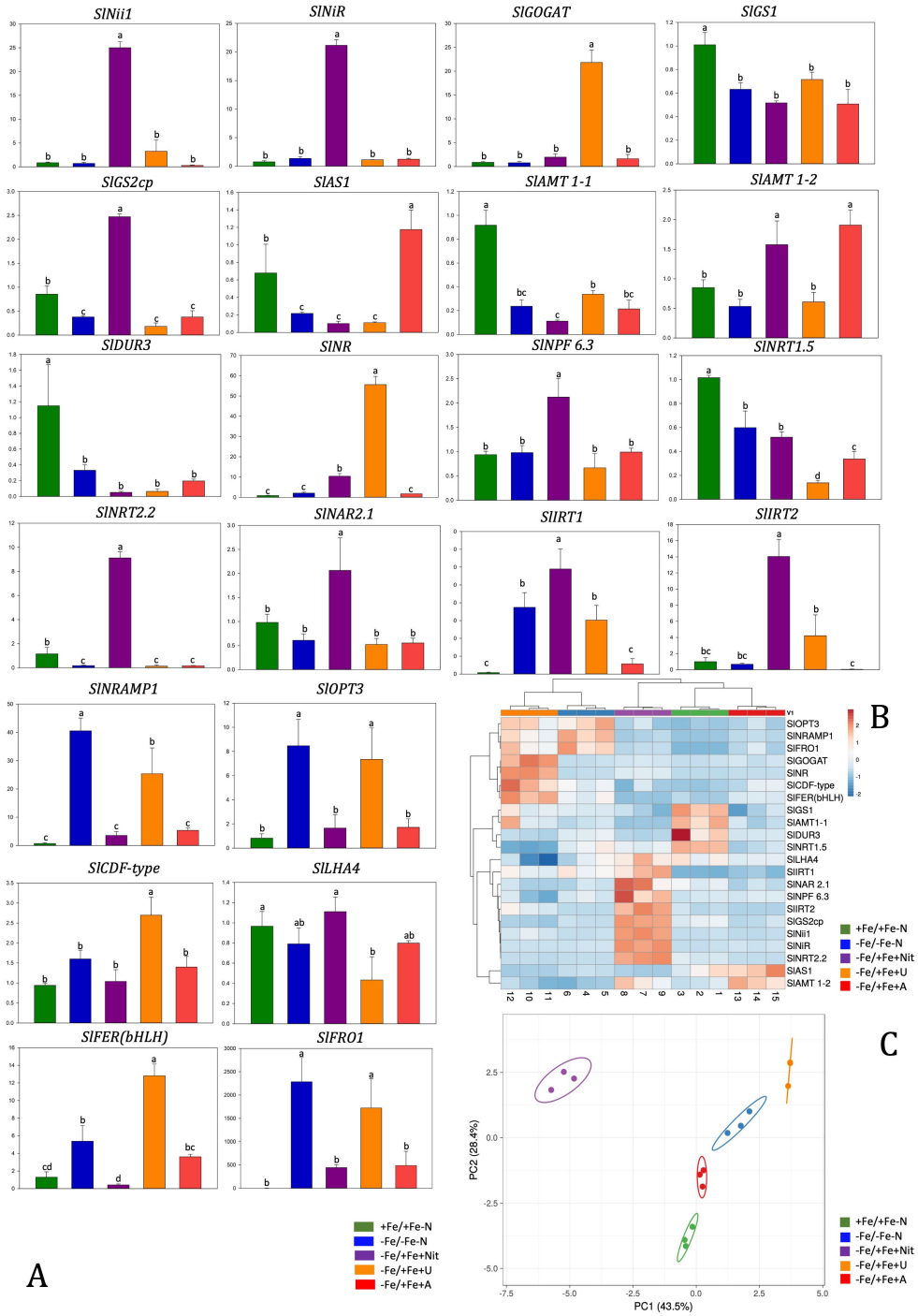

FIGURE 6
Relative gene expression level of tomato roots after 24 hours of treatment with different N sources and with Fe resupply **(A)**. Data were referred to the averaged expression of two housekeeping genes *SlEF1* and *SlUbi*. Relative changes in gene transcript levels were referred to the average transcript level of housekeeping genes in +Fe/+Fe-N roots (relative gene expression = 1). Letters refer to statistical significance (Holm-Sidak ANOVA, N= 3, p-value< 0.05). In the heatmap, a clustering of relative gene expression and samples in tomato roots **(B)**. PCA analyses show principal component 1 and principal component 2 that explain: 43.5% and 28.4% of the total variance in root **(C)**.

found both upregulated by nitrate compared to the other treatments. The upregulation of *IRTs* by nitrate agrees with evidence from the literature (Liu et al., 2015) and explains the high concentration of Fe measured in plants. In contrast to the reduced N forms (urea or ammonium), nitrate seems to delay the activation of the retro regulation on FCR activity (which was still high after 4 hours). This longer activation maybe due to the higher pH of the apoplast in nitrate-fed plants therefore to an inhibition of

FCR activity (Nikolic and Römheld, 2003). Regarding urea, even after 24 hours of Fe resupply, root maintained upregulated several genes involved in *Strategy I*, such as *FRO1, IRT1, NRAMP1, OPT3*, and *FER*. In *Arabidopsis*, Mérigout et al. (2008) observed that *FRO* and *IRT* genes were positively regulated by urea treatment compared to the inorganic N forms (ammonium, nitrate). Thus, urea might have a *per se* effect at the transcriptional level on some components of *Strategy I*. Considering the high Fe concentration in roots, this transcriptional pattern suggests that the urea acquisition pathway interacts with the one of Fe, promoting the acquisition of the micronutrient and its use by plants. The unalike response of *SlFRO1* expression and FCR activity could be ascribable to the contribution of other *SlFRO* isoforms to the enzymatic activity or to a post-transcriptional modulation (Connolly et al., 2003; Jeong and Connolly, 2009). It is interesting how FER is upregulated by urea and Fe supply, as its expression level was even higher than those recorded in -Fe/-Fe-N (Fe-deficient plants). This transcription factor plays a key role in activating the Fe-deficiency response by inducing the expression of genes involved in the Fe-uptake system (i.e. *FRO* and *IRT*; Ling et al., 2002; Brumbarova and Bauer, 2005). Thus, its upregulation only by urea (and not by other N forms) might explain the absence of feedback regulation on *Strategy I* components after 24 hours from the Fe resupply. Based on these observations, we can suppose that the effect of the three N forms depends on the gene expression, orchestration and timing of the feedback regulation on the Strategy I components.

The form of N also affects the accumulation of other nutrients

Being Fe an essential co-factor for N assimilation is plausible to state that Fe-nutritional status influences N uptake and content in plants. Parveen et al. (2018) observed that the Fe supply improved the N uptake and accumulation in roots. Under our experimental conditions, a higher N content was measured in nitrate and ammonium Fe-resupplied roots (-Fe/+Fe+Nit, -Fe/+Fe+A), suggesting a different acquisition rate linked to the N-form supplied and/or a different promptness of reaction to Fe presence in the nutrient solution.

Significant interactions between S and Fe homeostasis have been widely studied and described in several crops, together with the one between S and N, in both grasses and dicots (Varin et al., 2010; Ciaffi et al., 2013; Paolacci et al., 2014; Wu et al., 2015; Zuchi et al., 2015; Coppa et al., 2018). Ammonium induced a higher S concentration in leaves than other N treatments in our conditions. This behavior might result from a competition effect between nitrate and sulphate anions for reducing equivalents needed for their assimilation (De Bona et al., 2011; Kruse et al., 2007).

Under Fe deficiency, plants display changes in the composition of other micronutrients, such as Cu, Mn and Zn (Rai et al., 2021), probably due to the capability of FRO and IRT to mediates also the acquisition of other metals (Korshunova et al., 1999; Connolly et al., 2002). Indeed, several studies reported that these metals influence each other's fate inside the plant, and they also compete for metal transporters' a specific activities, such as IRT1 and NRAMPs (Bashir et al., 2016; Grotz and Guerinot, 2006; Rai et al., 2021).

Regarding Cu, its concentration increased under Fe deficiency in comparison to Fe sufficient ones in all organs (roots, OL, YL). In leaves this response was previously observed in several plant species both grasses and dicots (Waters and Troupe, 2012; Waters et al., 2006; Welch et al., 1993; Valdés-López et al., 2010; Suzuki et al., 2006; Chaignon et al., 2002). It has been reported that a high level of Fe availability reduces the acquisition of Zn while Fe-shortage determines Zn, Mn and Cu accumulation due to the induction of bivalent metal transporters, such as *SlIRT1* and *SlNRAMP1* (Arrivault et al., 2006; Eckhardt et al., 2001; Waters and Armbrust, 2013; Ray et al., 2014; Saenchai et al., 2016; Vert et al., 2002; Zhang et al., 1991). In agreement with the cited literature, overall, all Fe-deficient plants showed higher Zn concentration in leaves (as well as Mn) in comparison to +Fe/+Fe-N, especially Nit-treated plants (-Fe/+Fe+Nit). Previous work performed on tomato plants grown under Fe sufficient conditions highlighted that the application of urea led to high concentrations of these micronutrients in plants (Lodovici et al., 2024). These findings suggest that an interplay between N-form and Fe-availability concurs to shape these nutrient profiles.

N forms interact with the primary metabolism in the Fe resupply response

Regarding the effect of Fe nutritional status on N acquisition in plants, only fragmented information is available, especially referring to the changes in N metabolism that occurs under Fe-deficiency conditions. Rellán-Álvarez et al. (2011) stated that the main changes in the metabolite profile of Fe-deficient leaves include a consistent increase in amino acid (AA) and N-related metabolite content. In agreement with literature (Holley and Cain, 1955), the Fe deficiency response determined an overall increase of some amino acid concentrations in comparison to Fe-sufficient plants depending on the available N-form. In particular, results indicate an increase of glutamine- and glutamate-related compounds in roots. The high concentration of glutamine in urea or ammonium treated roots suggests a fast assimilation of N in this organ that could occur by a cytosolic N assimilatory pathway (cytosolic GS1 and ASN, Buoso et al., 2021a, b) rather than by the plastidial one.

In agreement with our results (arginine);, Another amino acid is known to be responsive to Fe deficiency is arginine (Holley and Cain, 1955), which was found more concentrated in -Fe/-Fe-N, -Fe/+Fe+Nit and -Fe/+Fe+A and less in -Fe/+Fe+U. Interestingly, the arginine concentration under Fe sufficiency condition was found to be responsive only to urea occurrence in nutrient solution and not to the presence of other inorganic N forms (Lodovici et al., 2024). The higher concentration of arginine can be related to the catabolic processes and in particular to the arginine cycle that mediates the degradation of arginine to produce L-ornithine and urea (Girard-Thernier et al., 2015). This hydrolytic reaction is mediated by

arginase, which activity is dependent to divalent cation as cofactor (ferrous ion in yeast arginase, Middelhoven et al., 1969). We can speculate that the higher arginine concentration in Fe-deficient plants are the consequence of a reduction in the arginase activity, and this effect is less present in urea-treated plants due to a redistribution of the metal with a positive effect on arginase activity and maybe a inhibition of the arginase due to the accumulation of its product, urea.

Interplay between Fe and N on secondary metabolism phytohormones

It is well known that phytohormones have a role in plant stress responses to both biotic and abiotic stresses (Checker et al., 2018; Divte et al., 2021; Banerjee and Roychoudhury, 2022). In general, the plant response to Fe-limiting conditions are positively regulated by auxins, ethylene, gibberellins, and nitric oxide and negatively controlled by cytokinins, abscisic acid, brassinosteroids (BRs) and jasmonic acid (Rai et al., 2021). Auxin and ethylene are involved in root hair proliferation (Hindt and Guerinot, 2012) and in the control of root growth by nitric oxide and auxins (Ramírez et al., 2008). Wang et al. (2012b) reported that BRs are involved in inhibiting Fe uptake as it can be observed in -Fe/+Fe+A plants showing a lower Fe concentration in roots in comparison to other N forms. In fact, the application of BRs to cucumber seedlings resulted in a substantial limited increase in FRO activity under Fe deficiency (Wang et al., 2012b). A different modulation in the BRs biosynthetic pathway has been observed across treatments (Nit, U, A) and tissues confirming their role in the Fe-deficient response. In Fe-sufficient condition all three N-forms led to the same modulation on that biosynthetic pathway (Lodovici et al., 2024) suggesting that Fe availability influences how N forms affect the biosynthesis of BRs in plants. On the other hand, gibberellins (GA) positively regulate Fe uptake by promoting the induction of *FRO2* and *IRT1* in *Arabidopsis* (Matsuoka et al., 2014). Moreover, ethylene and nitric oxide positively induce the expression of *IRT1* and *FRO2*, suggesting that these two signals increase the sensitivity of plants towards Fe uptake (García et al., 2010; Graziano and Lamattina, 2007; Lucena et al., 2006; Waters et al., 2007). Cytokinins led to a down-regulation of the two genes (Séguéla et al., 2008). Hormonal influence on Fe acquisition gene expression may serve to coordinate physiology and stress responses with necessary adaptations for altered root growth and Fe uptake (Schikora and Schmidt, 2001; Schmidt, 1999; Schmidt et al., 2000). In our experimental conditions, changes in the accumulation of phytohormones and phytohormone-related compounds were observed suggesting a different timing of plant responses to Fe-deficiency conditions.

Both biotic and abiotic stresses, such as nutritional stresses, often lead to phenylpropanoid accumulation (Mai and Bauer, 2016). According to the literature, plants under Fe-deficiency promoted the biosynthesis of phenylpropanoids (e.g. lignin and suberin precursors, flavonoids and anthocyanin glycosides) in all the analyzed plant organs, especially those treated with urea (-Fe/+Fe+U) that showed the highest accumulation, especially in roots followed by A (-Fe/+Fe+A), Nit (-Fe/+Fe+Nit) and then -Fe/-Fe-N.

Conclusions

The obtained results coupled with the information available in the literature, suggesting different promptness and regulation of tomato plants adaptation mechanisms to the Fe-deficiency conditions strictly related to a specific plant organ and to the applied N-forms. During the Fe supply, the N forms alter differently the primary metabolism (particularly amino acids), secondary metabolisms, and hormones, leading to changes in the morphology, physiology, and exudation. These processes are relevant to define rhizosphere conditions and hence they contribute to define the Fe bioavailability for the root uptake.

Data availability statement

The original contributions presented in the study are included in the article/Supplementary Material. Further inquiries can be directed to the corresponding author.

Author contributions

AL: Writing – original draft, Writing – review & editing. SB: Writing – original draft, Writing – review & editing. BM: Writing – review & editing. LL: Writing – review & editing. NT: Writing – original draft, Writing – review & editing. PG: Writing – review & editing. RP: Writing – review & editing. LZ: Writing – original draft, Writing – review & editing.

Funding

The author(s) declare that financial support was received for the research, authorship, and/or publication of this article. This study was supported by the Departmental Strategic Plan (PSD) of the University of Udine - Interdepartmental Project on Artificial Intelligence (2020-25) and within the Agritech National Research Center and received funding from the European Union Next-GenerationEU (PIANO NAZIONALE DI RIPRESA E RESILIENZA (PNRR) – MISSIONE 4 COMPONENTE 2, INVESTIMENTO 1.4 – D.D. 1032 17/06/2022, CN00000022). This manuscript reflects only the authors' views and opinions, neither the European Union nor the European Commission can be considered responsible for them.

Conflict of interest

The authors declare that the research was conducted in the absence of any commercial or financial relationships that could be construed as a potential conflict of interest.

The author(s) declared that they were an editorial board member of Frontiers, at the time of submission. This had no impact on the peer review process and the final decision.

Publisher's note

Supplementary material

The Supplementary Material for this article can be found online at: https://www.frontiersin.org/articles/10.3389/fpls.2024.1408141/full#supplementary-material

SUPPLEMENTARY TABLE 4
Dataset from untargeted metabolomics of leaves and roots after nitrogen supply. Compounds are presented with individual intensities, molecular formulas, retention time, and composite mass spectra.

SUPPLEMENTARY TABLE 5
Discriminant metabolites identified by the VIP analysis in leaves and roots after nitrogen supply. Compounds were selected as discriminant by possessing a VIP score > 1.3.

SUPPLEMENTARY TABLE 6
VIP markers associated with Venn diagram regions from leaves and roots after nitrogen supply.

SUPPLEMENTARY TABLE 7
Significant compounds (p-$value$ < 0.01, FC ≥ 2) with respect to +Fe/+Fe-N (under nitrogen deficiency) subjected to the Plantcyc Pathway Tools for young and old leaves and roots from Fe-deficient tomato plants.

References

Alcaraz, C. F., Martínez-Sánchez, F., Sevilla, F., and Hellln, E. (1986). Influence of ferredoxin levels on nitrate reductase activity in iron deficient lemon leaves. *J. Plant Nutr.* 9, 1405–1413. doi: 10.1080/01904168609363537

Anas, M., Liao, F., Verma, K. K., Sarwar, M. A., Mahmood, A., Chen, Z. L., et al. (2020). Fate of nitrogen in agriculture and environment: agronomic, eco-physiological and molecular approaches to improve nitrogen use efficiency. *Biol. Res.* 53, 1–20. doi: 10.1186/s40659-020-00312-4

Arnozis, P. A., and Findenegg, G. R. (1986). Electrical charge balance in the xylem sap of beet and Sorghum plants grown with either NO^{3-} or NH^{4+} nitrogen. *J.Plant Physiol.* 125, 441–449. doi: 10.1016/S0176-1617(86)80007-4

Arrivault, S., Senger, T., and Krämer, U. (2006). The Arabidopsis metal tolerance protein AtMTP3 maintains metal homeostasis by mediating Zn exclusion from the shoot under Fe deficiency and Zn oversupply. *Plant J.* 46, 861–879. doi: 10.1111/j.1365-313X.2006.02746.x

Banerjee, A., and Roychoudhury, A. (2022). Dissecting the phytohormonal, genomic and proteomic regulation of micronutrient deficiency during abiotic stresses in plants. *Biologia* 77, 3037–3058. doi: 10.1007/s11756-022-01099-3

Bashir, K., Rasheed, S., Kobayashi, T., Seki, M., and Nishizawa, N. K. (2016). Regulating subcellular metal homeostasis: the key to crop improvement. *Front. Plant Sci.* 7. doi: 10.3389/fpls.2016.01192

Borlotti, A., Vigani, G., and Zocchi, G. (2012). Iron deficiency affects nitrogen metabolism in cucumber (*Cucumis sativus* L.) plants. *BMC Plant Biol.* 12, 1–15. doi: 10.1186/1471-2229-12-189

Brumbarova, T., and Bauer, P. (2005). Iron-mediated control of the basic helix-loop-helix protein FER, a regulator of iron uptake in tomato. *Plant Physiol.* 137, 1018–1026. doi: 10.1104/pp.104.054270

Buoso, S., Tomasi, N., Arkoun, M., Maillard, A., Jing, L., Marroni, F., et al. (2021b). Transcriptomic and metabolomic profiles of Zea mays fed with urea and ammonium. *Physiol. Plant* 173, 935–953. doi: 10.1111/ppl.13493

Buoso, S., Tomasi, N., Said-Pullicino, D., Arkoun, M., Yvin, J. C., Pinton, R., et al. (2021a). Characterization of physiological and molecular responses of *Zea mays* seedlings to different urea-ammonium ratios. *Plant Physiol. Biochem.* 162, 613–623. doi: 10.1016/j.plaphy.2021.03.037

Chaignon, V., Di Malta, D., and Hinsinger, P. (2002). Fe-deficiency increases Cu acquisition by wheat cropped in a Cu-contaminated vineyard soil. *New Phytol.* 154, 121–130. doi: 10.1046/j.1469-8137.2002.00349.x

Checker, V. G., Kushwaha, H. R., Kumari, P., and Yadav, S. (2018). Role of phytohormones in plant defense: signaling and cross talk. *Mol. aspects plant-pathogen interaction*, 159–184. doi: 10.1007/978-981-10-7371-7_7

Chen, S. Y., Gu, T. Y., Qi, Z. A., Yan, J., Fang, Z. J., Lu, Y. T., et al. (2021). Two NPF transporters mediate iron long-distance transport and homeostasis in Arabidopsis. *Plant Commun.* 2, 100244. doi: 10.1016/j.xplc.2021.100244

Ciaffi, M., Paolacci, A. R., Celletti, S., Catarcione, G., Kopriva, S., and Astolfi, S. (2013). Transcriptional and physiological changes in the S assimilation pathway due to single or combined S and Fe deprivation in durum wheat (*Triticum durum* L.) seedlings. *J. Exp. Bot.* 64, 1663–1675. doi: 10.1093/jxb/ert027

Congreves, K. A., Otchere, O., Ferland, D., Farzadfar, S., Williams, S., and Arcand, M. M. (2021). Nitrogen use efficiency definitions of today and tomorrow. *Front. Plant Sci.* 12. doi: 10.3389/fpls.2021.637108

Connolly, E. L., Campbell, N. H., Grotz, N., Prichard, C. L., and Guerinot, M. L. (2003). Overexpression of the FRO2 ferric chelate reductase confers tolerance to growth on low iron and uncovers posttranscriptional control. *Plant Physiol.* 133, 1102–1110. doi: 10.1104/pp.103.025122

Connolly, E. L., Fett, J. P., and Guerinot, M. L. (2002). Expression of the IRT1 metal transporter is controlled by metals at the levels of transcript and protein accumulation. *Plant Cell* 14, 1347–1357. doi: 10.1105/tpc.001263

Coppa, E., Celletti, S., Pii, Y., Mimmo, T., Cesco, S., and Astolfi, S. (2018). Revisiting Fe/S interplay in tomato: a split-root approach to study the systemic and local responses. *Plant Sci.* 276, 134–142. doi: 10.1016/j.plantsci.2018.08.015

De Bona, F. D., Fedoseyenko, D., von Wirén, N., and Monteiro, F. A. (2011). Nitrogen utilization by sulfur-deficient barley plants depends on the nitrogen form. *Environ. Exp. Bot.* 74, 237–244. doi: 10.1016/j.envexpbot.2011.06.005

De la Peña, M., Marín-Peña, A. J., Urmeneta, L., Coleto, I., Castillo-González, J., van Liempd, S. M., et al. (2022). Ammonium nutrition interacts with iron homeostasis in Brachypodium distachyon. *J. Exp. Bot.* 73, 263–274. doi: 10.1093/jxb/erab427

Divte, P. R., Yadav, P., Pawar, A. B., Sharma, V., Anand, A., Pandey, R., et al. (2021). Crop response to iron deficiency is guided by cross-talk between phytohormones and their regulation of the root system architecture. *Agric. Res.* 10, 347–360. doi: 10.1007/s40003-020-00532-w

Eckhardt, U., Mas Marques, A., and Buckhout, T. J. (2001). Two iron-regulated cation transporters from tomato complement metal uptake-deficient yeast mutants. *Plant Mol. Biol.* 45, 437–448. doi: 10.1023/A:1010620012803

Eickhout, B., Bouwman, A. F., and van Zeijts, H. (2006). The role of nitrogen in world food production and environmental sustainability. *Agric. Ecosyst. Environ.* 116, 4–14. doi: 10.1016/j.agee.2006.03.009

Eide, D., Broderius, M., Fett, J., and Guerinot, M. L. (1996). A novel iron-regulated metal transporter from plants identified by functional expression in yeast. *Proc. Natl. Acad. Sci.* 93, 5624–5628. doi: 10.1073/pnas.93.11.5624

Fan, X., Zhou, X., Chen, H., Tang, M., and Xie, X. (2021). Cross-talks between macro-and micronutrient uptake and signaling in plants. *Front. Plant Sci.* 12. doi: 10.3389/fpls.2021.663477

FAOSTAT (2021). *Inorganic fertilizers 1961–2019* (Rome: FAOSTAT Analytical Brief Series No 27).

Filiz, E., and Akbudak, M. A. (2020). Ammonium transporter 1 (AMT1) gene family in tomato (*Solanum lycopersicum* L.): Bioinformatics, physiological and expression analyses under drought and salt stresses. *Genom.* 112, 3773–3782. doi: 10.1016/j.ygeno.2020.04.009

Gao, Y., Qi, S., and Wang, Y. (2022). Nitrate signaling and use efficiency in crops. *Plant Commun.* 3, 100353. doi: 10.1016/j.xplc.2022.100353

García, M. J., Lucena, C., Romera, F. J., Alcantara, E., and Pérez-Vicente, R. (2010). Ethylene and nitric oxide involvement in the up-regulation of key genes related to iron acquisition and homeostasis in Arabidopsis. *J. Exp. Bot.* 61, 3885–3899. doi: 10.1093/jxb/erq203

García-Pérez, P., Miras-Moreno, B., Lucini, L., and Gallego, P. P. (2021). The metabolomics reveals intraspecies variability of bioactive compounds in elicited suspension cell cultures of three *Bryophyllum* species. *Ind. Crops Prod.* 163, 113322. doi: 10.1016/j.indcrop.2021.113322

Girard-Thernier, C., Pham, T. N., and Demougeot, C. (2015). The promise of plant-derived substances as inhibitors of arginase. *Mini Rev. Med. Chem.* 15, 798–808. doi: 10.2174/1389557515666150511153852

Graziano, M., and Lamattina, L. (2007). Nitric oxide accumulation is required for molecular and physiological responses to iron deficiency in tomato roots. *Plant J.* 52, 949–960. doi: 10.1111/j.1365-313X.2007.03283.x

Grotz, N., and Guerinot, M. L. (2006). Molecular aspects of Cu, Fe and Zn homeostasis in plants. *Biochim. Biophys. Acta Mol. Cell Res.* 1763, 595–608. doi: 10.1016/j.bbamcr.2006.05.014

Harper, J. F., Manney, L., DeWitt, N. D., Yoo, M. H., and Sussman, M. R. (1990). The Arabidopsis thaliana plasma membrane H (+)-ATPase multigene family. Genomic sequence and expression of a third isoform. *J. Biol. Chem.* 265, 13601–13608. doi: 10.1016/S0021-9258(18)77391-2

Hindt, M. N., and Guerinot, M. L. (2012). Getting a sense for signals: regulation of the plant iron deficiency response. *Biochim. Biophys. Acta Mol. Cell Res.* 1823, 1521–1530. doi: 10.1016/j.bbamcr.2012.03.010

Holley, R. W., and Cain, J. C. (1955). Accumulation of arginine in plants afflicted with iron-deficiency type chlorosis. *Science* 121, 172–173. doi: 10.1126/science.121.3136.172

Iacuzzo, F., Gottardi, S., Tomasi, N., Savoia, E., Tommasi, R., Cortella, G., et al. (2011). Corn salad (*Valerianella locusta* (L.) Laterr.) growth in a water-saving floating system as affected by iron and sulfate availability. *J. Sci. Food Agric.* 91, 344–354. doi: 10.1002/jsfa.4192

Jeong, J., and Connolly, E. L. (2009). Iron uptake mechanisms in plants: functions of the FRO family of ferric reductases. *Plant Sci.* 176, 709–714. doi: 10.1016/j.plantsci.2009.02.011

Karp, P. D., Paley, S. M., Krummenacker, M., Latendresse, M., Dale, J. M., Lee, T. J., et al. (2010). Pathway Tools version 13.0: integrated software for pathway/genome informatics and systems biology. *Brief. Bioinform.* 11, 40–79. doi: 10.1093/bib/bbp043

Kobayashi, T., Nozoye, T., and Nishizawa, N. K. (2019). Iron transport and its regulation in plants. *Free Radic. Biol. Med.* 133, 11–20. doi: 10.1016/j.freeradbiomed.2018.10.439

Korshunova, Y. O., Eide, D., Gregg Clark, W., Lou Guerinot, M., and Pakrasi, H. B. (1999). The IRT1 protein from Arabidopsis thaliana is a metal transporter with a broad substrate range. *Plant Mol. Biol.* 40, 37–44. doi: 10.1023/A:1026438615520

Kosegarten, H. U., Hoffmann, B., and Mengel, K. (1999). Apoplastic pH and Fe^{3+} reduction in intact sunflower leaves. *Plant Physiol.* 121, 1069–1079. doi: 10.1104/pp.121.4.1069

Kruse, J., Kopriva, S., Hänsch, R., Krauss, G. J., Mendel, R. R., and Rennenberg, H. (2007). Interaction of sulfur and nitrogen nutrition in tobacco (*Nicotiana tabacum*) plants: significance of nitrogen source and root nitrate reductase. *Plant Biol.* 9, 638–646. doi: 10.1055/s-2007-965434

Ling, H. Q., Bauer, P., Bereczky, Z., Keller, B., and Ganal, M. (2002). The tomato fer gene encoding a bHLH protein controls iron-uptake responses in roots. *Proc. Natl. Acad. Sci.* 99, 13938–13943. doi: 10.1073/pnas.212448699

Liu, X., Cui, H., Li, A., Zhang, M., and Teng, Y. (2015). The nitrate transporter NRT1.1 is involved in iron deficiency responses in Arabidopsis. *J. Plant Nutr. Soil Sc.* 178, 601–608. doi: 10.1002/jpln.201400480

Liu, J., Liu, J., Chen, A., Ji, M., Chen, J., Yang, X., et al. (2016). Analysis of tomato plasma membrane H+-ATPase gene family suggests a mycorrhiza-mediated regulatory mechanism conserved in diverse plant species. *Mycorrhiza* 26, 645–656. doi: 10.1007/s00572-016-0700-9

Livak, K. J., and Schmittgen, T. D. (2001). Analysis of relative gene expression data using Real-Time quantitative PCR and the 2-ΔΔCT Method. *Methods* 25, 402–408. doi: 10.1006/meth.2001.1262

Lodovici, A., Buoso, S., Miras-Moreno, B., Lucini, L., Garcia-Perez, P., Tomasi, N., et al. (2024). Peculiarity of the early metabolomic response in tomato after urea, ammonium or nitrate supply. *Plant Physiol. Biochem.* 211, 108666. doi: 10.1016/j.plaphy.2024.108666

Lucena, C., Waters, B. M., Romera, F. J., García, M. J., Morales, M., Alcántara, E., et al. (2006). Ethylene could influence ferric reductase, iron transporter, and H^+-ATPase gene expression by affecting FER (or FER-like) gene activity. *J. Exp. Bot.* 57, 4145–4154. doi: 10.1093/jxb/erl189

Mahender, A., Swamy, B. M., Anandan, A., and Ali, J. (2019). Tolerance of iron-deficient and-toxic soil conditions in rice. *Plants* 8, 31. doi: 10.3390/plants8020031

Mai, H. J., and Bauer, P. (2016). From the proteomic point of view: Integration of adaptive changes to iron deficiency in plants. *Curr. Plant Biol.* 5, 45–56. doi: 10.1016/j.cpb.2016.02.001

Marastoni, L., Lucini, L., Miras-Moreno, B., Trevisan, M., Sega, D., Zamboni, A., et al. (2020). Changes in physiological activities and root exudation profile of two grapevine rootstocks reveal common and specific strategies for Fe acquisition. *Sci. Rep.* 10, 18839. doi: 10.1038/s41598-020-75317-w

Marschner, H. (1995). *Mineral nutrition of higher plants. 2nd Edition* (London: Academic Press).

Matsuoka, K., Furukawa, J., Bidadi, H., Asahina, M., Yamaguchi, S., and Satoh, S. (2014). Gibberellin-induced expression of Fe uptake-related genes in Arabidopsis. *Plant Cell Physiol.* 55, 87–98. doi: 10.1093/pcp/pct160

Mengel, K. (1994). Iron availability in plant tissues-iron chlorosis on calcareous soils. *Plant Soil* 165, 275–283. doi: 10.1007/BF00008070

Metsalu, T., and Vilo, J. (2015). Clustvis: a web tool for visualizing clustering of multivariate data using Principal Component Analysis and heatmap. *Nucleic Acids Research* 43(W1), W566–W570. doi: 10.1093/nar/gkv468

Mérigout, P., Lelandais, M., Bitton, F., Renou, J. P., Briand, X., Meyer, C., et al. (2008). Physiological and transcriptomic aspects of urea uptake and assimilation in Arabidopsis plants. *Plant Physiol.* 147, 1225–1238. doi: 10.1104/pp.108.119339

Middelhoven, W. J., De Waard, M. A., and Mulder, E. G. (1969). The ferrous ion as the cofactor of arginase in *vivo*: II. Experiments on the replacement of ferrous ions in native yeast arginase by other cations in *vivo*. *Biochim. Biophys. Acta-Enzymology* 191, 122–129. doi: 10.1016/0005-2744(69)90321-0

Mori, S. (1999). Iron acquisition by plants. *Curr. Opin. Plant Biol.* 2, 250–253. doi: 10.1016/S1369-5266(99)80043-0

Nikolic, M., Cesco, S., Römheld, V., Varanini, Z., and Pinton, R. (2007). Short-term interactions between nitrate and iron nutrition in cucumber. *Funct. Plant Biol.* 34, 402–408. doi: 10.1071/FP07022

Nikolic, M., and Römheld, V. (2003). Nitrate does not result in iron inactivation in the apoplast of sunflower leaves. *Plant Physiol.* 132, 1303–1314. doi: 10.1104/pp.102.017889

Oksanen, J., Blanchet, F. G., Kindt, R., Legendre, P., Minchin, P. R., O'Hara, R. B., et al. (2014). Vegan: community ecology package. R Package Version 2.2-0. Available online at: http://CRAN.Rproject.org/package=veganlo (accessed May 21, 2023).

Paolacci, A. R., Celletti, S., Catarcione, G., Hawkesford, M. J., Astolfi, S., and Ciaffi, M. (2014). Iron deprivation results in a rapid but not sustained increase of the expression of genes involved in iron metabolism and sulfate uptake in tomato (*Solanum lycopersicum* L.) seedlings. *J. Integr. Plant Biol.* 56, 88–100. doi: 10.1111/jipb.12110

Parveen, S., Ranjan, R. K., Anand, A., and Singh, B. (2018). Combined deficiency of nitrogen and iron increases senescence induced remobilization of plant immobile iron in wheat. *Acta Physiol. Plant* 40, 1–12. doi: 10.1007/s11738-018-2782-9

Piccinelli, F., Sega, D., Melchior, A., Ruggieri, S., Sanadar, M., Varanini, Z., et al. (2022). Regreening properties of the soil slow-mobile H2bpcd/Fe3+ complex: Steps forward to the development of a new environmentally friendly Fe fertilizer. *Front. Plant Sci.* 13. doi: 10.3389/fpls.2022.964088

Pinton, R., Cesco, S., Santi, S., Agnolon, F., and Varanini, Z. (1999). Water-extractable humic substances enhance iron deficiency responses by Fe-deficient cucumber plants. *Plant Soil* 210, 145–157. doi: 10.1023/A:1004329513498

Rai, S., Singh, P. K., Mankotia, S., Swain, J., and Satbhai, S. B. (2021). Iron homeostasis in plants and its crosstalk with copper, zinc, and manganese. *Plant Stress* 1, 100008. doi: 10.1016/j.stress.2021.100008

Ramírez, L., Graziano, M., and Lamattina, L. (2008). Decoding plant responses to iron deficiency: is nitric oxide a central player? *Plant Signal. Behav.* 3, 795–797. doi: 10.4161/psb.3.10.5874

Ray, H., Bett, K., Vandenberg, A., Thavarajah, D., and Warkentin, T. (2014). Mineral micronutrient content of cultivars of field pea, chickpea, common bean, and lentil grown in Saskatchewan, Canada. *Crop Sci.* 54, 1698–1708. doi: 10.2135/cropsci2013.08.0568

R Core Team (2021). *R: A language and environment for statistical computing* (Vienna. Austria: R Foundation for Statistical Computing). Available at: https://www.R-project.org/.

Rellán-Álvarez, R., El-Jendoubi, H., Wohlgemuth, G., Abadía, A., Fiehn, O., Abadía, J., et al. (2011). Metabolite profile changes in xylem sap and leaf extracts of strategy I plants in response to iron deficiency and resupply. *Front. Plant Sci.* 2. doi: 10.3389/fpls.2011.00066

Ritz, C., and Spiess, A.-N. (2008). qpcR: an R pacjage for sigmoidal model selection in quantitative real-time polymerase chain reaction analysis. *Bioinformatics* 24, 1549–1551. doi: 10.1093/bioinformatics/btn227

Saenchai, C., Bouain, N., Kisko, M., Prom-u-thai, C., Doumas, P., and Rouached, H. (2016). the involvement of ospho1;1 in the regulation of iron transport through integration of phosphate and zinc deficiency signaling. *Front. Plant Sci.* 7. doi: 10.3389/fpls.2016.00396

Sainju, U. M., Dris, R., and Singh, B. (2003). Mineral nutrition of tomato. *Food Agric. Environ.* 1, 176–183.

Sainju, U. M., Ghimire, R., and Pradhan, G. P. (2019). Nitrogen fertilization I: Impact on crop, soil, and environment. *Nitrogen Fixation* 9, 1–9. doi: 10.5772/intechopen.86028

Salek, R. M., Haug, K., and Steinbeck, C. (2013). Dissemination of metabolomics results: role of MetaboLights and COSMOS. *GigaScience* 2, 2047–217X. doi: 10.1186/2047-217X-2-8

Sarasketa, A., González-Moro, M. B., González-Murua, C., and Marino, D. (2016). Nitrogen source and external medium pH interaction differentially affects root and shoot metabolism in Arabidopsis. *Front. Plant Sci.* 7. doi: 10.3389/fpls.2016.00029

Schikora, A., and Schmidt, W. (2001). Acclimative changes in root epidermal cell fate in response to Fe and P deficiency: a specific role for auxin? . *Protoplasma* 218, 67–75. doi: 10.1007/BF01288362

Schmidt, W. (1999). Mechanisms and regulation of reduction-based iron uptake in plants. *New Phytol.* 141, 1–26. doi: 10.1046/j.1469-8137.1999.00331.x

Schmidt, W., and Buckhout, T. J. (2011). A hitchhiker's guide to the Arabidopsis ferrome. *Plant Physiol. Biochem.* 49, 462–470. doi: 10.1016/j.plaphy.2010.12.001

Schmidt, W., Tittel, J., and Schikora, A. (2000). Role of hormones in the induction of iron deficiency responses in Arabidopsis roots. *Plant Physiol.* 122, 1109–1118. doi: 10.1104/pp.122.4.1109

Séguéla, M., Briat, J.-F., Vert, G., and Curie, C. (2008). Cytokinins negatively regulate the root iron uptake machinery in Arabidopsis through a growth-dependent pathway. *Plant J.* 55, 289–300. doi: 10.1111/j.1365-313X.2008.03502.x

Sun, W. J., Zhang, J. C., Ji, X. L., Feng, Z. Q., Wang, X., Huang, W. J., et al. (2021). Low nitrate alleviates iron deficiency by regulating iron homeostasis in apple. *Plant Cell Environ.* 44, 1869–1884. doi: 10.1111/pce.13998

Suzuki, M., Takahashi, M., Tsukamoto, T., Watanabe, S., Matsuhashi, S., Yazaki, J., et al. (2006). Biosynthesis and secretion of mugineic acid family phytosiderophores in zinc-deficient barley. *Plant J.* 48, 85–97. doi: 10.1111/j.1365-313X.2006.02853.x

Thomson, C. J., Marschner, H., and Römheld, V. (1993). Effect of nitrogen fertilizer form on pH of the bulk soil and rhizosphere, and on the growth, phosphorus, and micronutrient uptake of bean. *J. @ Plant Nutr.* 16, 493–506. doi: 10.1080/01904169309364548

Tomasi, N., Rizzardo, C., Monte, R., Gottardi, S., Jelali, N., Terzano, R., et al. (2009). Micro-analytical, physiological and molecular aspects of Fe acquisition in leaves of Fe-deficient tomato plants re-supplied with natural Fe-complexes in nutrient solution. *Plant Soil* 325, 25–38. doi: 10.1007/s11104-009-0069-z

USEPA (1995). "EPA Method 3052: Microwave assisted acid digestion of siliceous and organically based matrices," in *Test Methods for Evaluating Solid Waste*, *3rd edn* (U.S. Environmental Protection Agency: Washington. DC).

Valdés-López, O., Yang, S. S., Aparicio-Fabre, R., Graham, P. H., Reyes, J. L., Vance, C. P., et al. (2010). MicroRNA expression profile in common bean (Phaseolus vulgaris) under nutrient deficiency stresses and manganese toxicity. *New Phytol.* 187, 805–818. doi: 10.1111/j.1469-8137.2010.03320.x

Varin, S., Cliquet, J. B., Personeni, E., Avice, J. C., and Lemauviel-Lavenant, S. (2010). How does sulphur availability modify N acquisition of white clover (Trifolium repens L.)? *J. Exp. Bot.* 61, 225–234. doi: 10.1093/jxb/erp303

Vert, G., Grotz, N., Dédaldéchamp, F., Gaymard, F., Guerinot, M. L., Briat, J. F., et al. (2002). IRT1, an Arabidopsis transporter essential for iron uptake from the soil and for plant growth. *Plant Cell* 14, 1223–1233. doi: 10.1105/tpc.001388

Wang, W. H., Köhler, B., Cao, F. Q., Liu, G. W., Gong, Y. Y., Sheng, S., et al. (2012a). Rice DUR3 mediates high-affinity urea transport and plays an effective role in improvement of urea acquisition and utilization when expressed in Arabidopsis. *New Phytol.* 193, 432–444. doi: 10.1111/j.1469-8137.2011.03929.x

Wang, B., Li, Y., and Zhang, W. H. (2012b). Brassinosteroids are involved in response of cucumber (Cucumis sativus) to iron deficiency. *Ann. Bot.* 110, 681–688. doi: 10.1093/aob/mcs126

Waters, B. M., and Armbrust, L. C. (2013). Optimal copper supply is required for normal plant iron deficiency responses. *Plant Signal. Behav* 8, e26611. doi: 10.4161/psb.26611

Waters, B. M., Chu, H. H., DiDonato, R. J., Roberts, L. A., Eisley, R. B., Lahner, B., et al. (2006). Mutations in Arabidopsis yellow stripe-like1 and yellow stripe-like3 reveal their roles in metal ion homeostasis and loading of metal ions in seeds. *Plant Physiol.* 141, 1446–1458. doi: 10.1104/pp.106.082586

Waters, B. M., Lucena, C., Romera, F. J., Jester, G. G., Wynn, A. N., Rojas, C. L., et al. (2007). Ethylene involvement in the regulation of the H+-ATPase CsHA1 gene and of the new isolated ferric reductase CsFRO1 and iron transporter CsIRT1 genes in cucumber plants. *Plant Physiol. Biochem.* 45, 293–301. doi: 10.1016/j.plaphy.2007.03.011

Waters, B. M., and Troupe, G. C. (2012). Natural variation in iron use efficiency and mineral remobilization in cucumber (Cucumis sativus). *Plant Soil* 352, 185–197. doi: 10.1007/s11104-011-0988-3

Welch, R. M., Norvell, W. A., Schaefer, S. C., Shaff, J. E., and Kochian, L. V. (1993). Induction of iron (III) and copper (II) reduction in pea (Pisum sativum L.) roots by Fe and Cu status: Does the root-cell plasmalemma Fe (III)-chelate reductase perform a general role in regulating cation uptake? *Planta* 190, 555–561. doi: 10.1007/BF00224795

Wu, Z., Zhang, C., Dai, C., and Ge, Y. (2015). Sufficient sulfur supply promotes seedling growth, alleviates oxidation stress, and regulates iron uptake and translocation in rice. *Biol. Plant* 59, 788–792. doi: 10.1007/s10535-015-0554-6

Zamboni, A., Zanin, L., Tomasi, N., Avesani, L., Pinton, R., Varanini, Z., et al. (2016). Early transcriptomic response to Fe supply in Fe-deficient tomato plants is strongly influenced by the nature of the chelating agent. *BMC Genom.* 17, 1–17. doi: 10.1186/s12864-015-2331-5

Zamboni, A., Zanin, L., Tomasi, N., Pezzotti, M., Pinton, R., Varanini, Z., et al. (2012). Genome-wide microarray analysis of tomato roots showed defined responses to iron deficiency. *BMC Genom.* 13, 1–14. doi: 10.1186/1471-2164-13-101

Zanin, L., Tomasi, N., Wirdnam, C., Meier, S., Komarova, N. Y., Mimmo, T., et al. (2014). Isolation and functional characterization of a high affinity urea transporter from roots of Zea mays. *BMC Plant Biol.* 14, 1–15. doi: 10.1186/s12870-014-0222-6

Zanin, L., Zamboni, A., Monte, R., Tomasi, N., Varanini, Z., Cesco, S., et al. (2015). Transcriptomic analysis highlights reciprocal interactions of urea and nitrate for nitrogen acquisition by maize roots. *Plant Cell Physiol.* 56, 532–548. doi: 10.1093/pcp/pcu202

Zhang, F. S., Römheld, V., and Marschner, H. (1991). Diurnal rhythm of release of phytosiderophores and uptake rate of zinc in iron-deficient wheat. *Soil Sci. Plant Nutr.* 37, 671–678. doi: 10.1080/00380768.1991.10416935

Zhang, X., Zhang, D., Sun, W., and Wang, T. (2019). The adaptive mechanism of plants to iron deficiency via iron uptake, transport, and homeostasis. *Int. J. Mol. Sci.* 20, 2424. doi: 10.3390/ijms20102424

Zhu, X. F., Dong, X. Y., Wu, Q., and Shen, R. F. (2019). Ammonium regulates Fe deficiency responses by enhancing nitric oxide signaling in *Arabidopsis thaliana*. *Planta* 250, 1089–1102. doi: 10.1007/s00425-019-03202-6

Zou, C., Shen, J., Zhang, F., Guo, S., Rengel, Z., and Tang, C. (2001). Impact of nitrogen form on iron uptake and distribution in maize seedlings in solution culture. *Plant Soil* 235, 143–149. doi: 10.1023/A:1011902320662

Zuchi, S., Watanabe, M., Hubberten, H. M. H.-M., Bromke, M., Osorio, S., Fernie, A. R., et al. (2015). The interplay between sulfur and iron nutrition in tomato. *Plant Physiol.* 169, 2624–2639. doi: 10.1104/pp.15.00995

Zuo, Y., and Zhang, F. (2011). Soil and crop management strategies to prevent iron deficiency in crops. *Plant Soil* 339, 83–95. doi: 10.1007/s11104-010-0566-0

frontiers | Frontiers in Plant Science

TYPE Review
PUBLISHED 15 November 2024
DOI 10.3389/fpls.2024.1463666

OPEN ACCESS

EDITED BY
Marta Sousa Silva,
University of Lisbon, Portugal

REVIEWED BY
Shouchuang Wang,
Hainan University, China
Jiang Hai,
Heilongjiang University of Chinese Medicine, China

*CORRESPONDENCE
Xinquan Yang
yangxinquan@sina.com
Xiangsheng Zhao
xiangshengzhao@hotmail.com

RECEIVED 12 July 2024
ACCEPTED 29 October 2024
PUBLISHED 15 November 2024

CITATION
Ji P, Yang X and Zhao X (2024) Application of metabolomics in quality control of traditional Chinese medicines: a review.
Front. Plant Sci. 15:1463666.
doi: 10.3389/fpls.2024.1463666

Application of metabolomics in quality control of traditional Chinese medicines: a review

Peiran Ji[1,2], Xinquan Yang[2]* and Xiangsheng Zhao[2]*

[1]Institute of Medicinal Plant Development, Chinese Academy of Medical Sciences and Peking Union Medical College, Beijing, China, [2]Hainan Branch of the Institute of Medicinal Plant Development, Chinese Academy of Medical Sciences & Peking Union Medical College, Haikou, China

Plant metabolites are the components endowing traditional Chinese medicine (TCM) with therapeutic effects, and, simultaneously, they are the primary targets for quality control. From germplasm selection and origin determination to field management, growth duration, harvesting and processing, and, finally, storage and transportation, each step profoundly influences TCM quality. The complexity of these plant or herb metabolites poses numerous quality control challenges. Metabolomics, as a comprehensive and systematic approach, has demonstrated value in this field. This technique not only meets the requirements for studying the complex mechanisms of TCM but also has significant advantages in identifying the TCM components, including active components. Therefore, in this article, several key factors affecting the chemical characteristics and quality traits of TCM, including their origin, harvesting period, medicinal parts, and processing methods, are researched. Additionally, the current challenges of integrating metabolomics with other omics technologies (transcriptomics, spatial metabolomics, etc.) are discussed. Furthermore, a future development trends and prospects are highlighted. With the continuous deepening of research and ongoing updates in technological capabilities, metabolomics will play an increasingly important role in the quality control of TCM, providing more scientific and robust support for quality assurance and safety evaluation.

KEYWORDS

Traditional Chinese medicine, metabolomics, quality, safety, multiomics

1 Introduction

Traditional Chinese medicine (TCM) has a thousand-year history in China and is widely employed for the treatment and prevention of diseases. Moreover, TCM is playing an increasingly crucial role in modern healthcare. With the gradual global recognition of TCM in recent years, the TCM industry has experienced rapid development in various countries. Compared with chemically synthesized drugs, Chinese herbal formulations consist of multiple natural herbs, each potentially containing hundreds or even thousands of active components. The variations in the combinations of different herbs and their sources further

increase the chemical complexity. However, the quality control system for Chinese medicinal materials, which is the foundation of the TCM industry, still has some limitations. Although comprehensive monographs and standards, including definitions, characteristics, identification, testing, determination, and storage information, for TCM have been established worldwide and documented in publications such as pharmacopeias and directives, this information is insufficient for exerting comprehensive and effective control over factors influencing the quality of TCM (including germplasm, origin, field management, growth duration, harvesting, processing, storage, and transportation) (Commisso et al., 2013; Li, 2019). The subsequent pharmaceutical processes, involving extraction, purification, separation, concentration, and drying, significantly impact the quality of TCM. Currently, the regulatory framework for TCM quality control is meticulously structured around key elements. Firstly, it is firmly rooted in a comprehensive legal foundation, encompassing laws, regulations, and normative documents such as the Pharmaceutical Administration Law, the Law on Traditional Chinese Medicine, and related implementing regulations and measures. Building on this, the National Medical Products Administration (NMPA) has formulated Specialized Provisions for TCM Standards, providing strong legal backing. Secondly, the framework establishes a TCM-specific standard management system that covers various areas like medicinal materials, decoction pieces, formula granules, extracts, and proprietary medicines. This system ensures comprehensive management across national, registration, and provincial standards. Lastly, while preserving traditional knowledge and techniques, the framework actively integrates modern science and technology. It focuses on developing practical and economically reasonable TCM standards, thereby ensuring the scientific and feasible nature of the quality control system. At present, the quality control paradigm for TCM predominantly relies on the quantitation of active (or marker) ingredients and fingerprint technology. While these methodologies offer valuable insights into the content of bioactive compounds present in TCM, they often exhibit a certain degree of specificity, rendering a comprehensive and precise evaluation of the holistic quality of the herbs challenging. Consequently, they prove inadequate in providing an exhaustive and comprehensive depiction of key metabolites and their metabolic pathways (Li et al., 2018b; Munekata et al., 2022). In addition to existing national or multinational legal frameworks, ensuring the quality of TCM relies on powerful analytical tools to determine their chemical composition and active principles. These tools help identify potentially harmful substances and adulterants, ensuring the efficacy and safety of TCM and enhancing the quality standards and regulatory levels of TCM products.

Metabolomics appears to be highly suitable for this purpose. As metabolism occurs, metabolites, which are small molecules involved in energy conversion and biosynthesis, are generated. External disturbances and developmental stimuli can impact the accumulation of intermediate or end products in plant cells or tissues over time and space. With the aim of capturing these changes, metabolomics technology monitors metabolites and their quantities in cells or tissues at a given state over time and space (Goodacre et al., 2004; Alawiye and Babalola, 2021). Furthermore, as the ultimate products of cellular regulation processes, metabolites serve as a bridge connecting the genotype and phenotype of plants. They provide crucial information about the phenotypic characteristics and biological functional changes in target organisms (Patti et al., 2012). For the quality control of TCM, metabolomics, leveraging its distinctive advantages of comprehensiveness and systematicness, enables a global analysis of small-molecule metabolites within TCM. It employs a variety of advanced separation and analysis technology platforms to precisely identify and accurately quantify characteristic metabolites, while integrating diversified data processing methods. This approach effectively avoids the limitation of relying solely on partial chemical components as quality control indicators, ensuring the comprehensiveness and accuracy of the evaluation. In recent years, beyond applications in clinical and biomedical fields, metabolomics research has been applied to various disciplines in food and nutritional science (Kang and Suh, 2022). Regarding research related to TCM, a literature survey based on the Web of Science core collection showed that in the last five years (from 2019 to the present of October 16, 2024), there have been 1998 publications on the theme of “traditional Chinese medicine” and “metabolites”, including 257 review papers (Figure 1). The core focus of these review papers is the practical application of the bioactive components of TCM in disease treatment (Zhang et al., 2021; Yang et al., 2020; Su et al., 2022; Zheng et al., 2020). Furthermore, several studies have investigated specific Chinese medicinal species (such as *Patriniae* (Gong et al., 2021), *Kaempferia galanga* L (Wang et al., 2021), and *Bufo bufo gargarizans* Cantor (Zhan et al., 2020)), genera (such as *Panax* L (Liu et al., 2020b), *Aconitum* [(Kakkar et al., 2023), and *Asarum* (Liu and Wang, 2022)), and active ingredients (such as scoparone (Hui et al., 2020), rhaponticin (Chen et al., 2020a), and gentiopicroside (Liu et al., 2023a)), comprehensively elucidating their phytochemical, pharmacological, and pharmacokinetic characteristics. Moreover, advancements in the application of high-resolution mass spectrometry (HRMS) technology have been introduced (Yin et al., 2021; Huang et al., 2022), which holds significant importance in elucidating the efficacy and toxicity mechanisms of TCM (Bai et al., 2022). Some reviews have also assessed and analyzed the potential of secondary metabolites from medicinal plants for the treatment of the 2019 coronavirus (Jamal, 2022; Harwansh and Bahadur, 2022; Murck, 2020; Al-Kuraishy et al., 2022). However, a comprehensive review of the application of metabolomics technology in the quality control of TCM and the combined use of metabolomics with other omics methods to analyze various factors affecting the quality of TCM is still lacking. It is noteworthy that TCM, as an extensive and complex system, encompasses plant-based medicines, animal-based medicines, mineral-based medicines, as well as certain chemical and biological products. Among these, plant-based medicines undoubtedly occupy a pivotal position in the field of TCM, with a prominent proportion exceeding 80%. Therefore, the main content of this article primarily focuses on the application of metabolomics in the realm of plant-based medicines.

Currently, out of the millions of potential metabolites in the plant kingdom, only approximately 14,000 can be practically quantified,

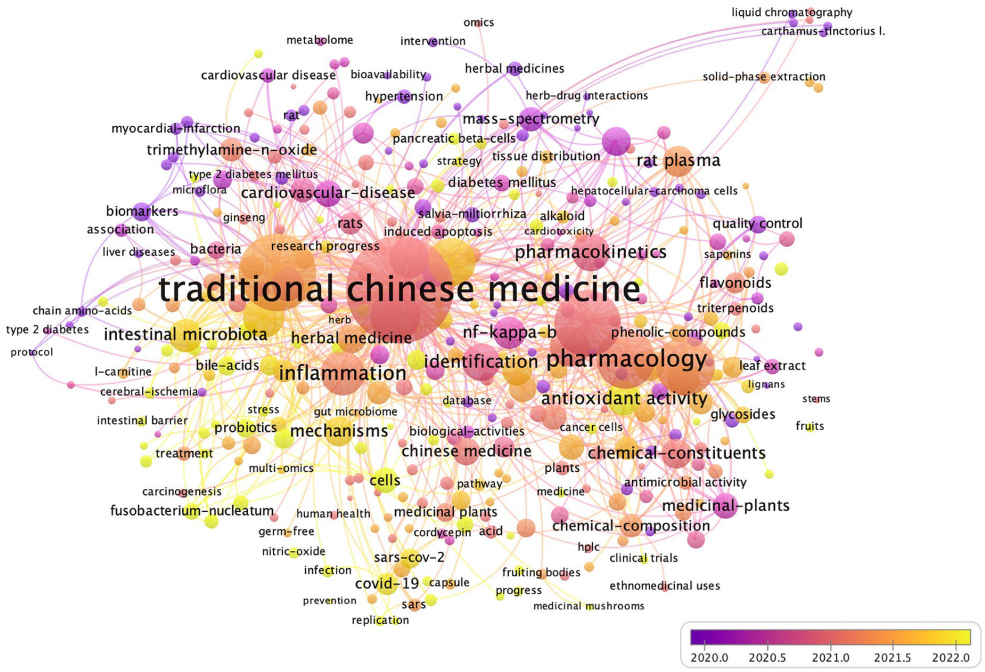

FIGURE 1
Analysis of research hotspots in the perspective of time (keyword co-occurrence frequency ≥2).

which unequivocally underscores the pressing need for more advanced analytical techniques (Alseekh and Fernie, 2018). The hybrid approach that integrates both non-targeted and targeted metabolomics has demonstrated its efficacy in significantly enhancing the scope and depth of metabolome detection (Figure 2). In general, metabolomics can be divided into targeted metabolomics and untargeted metabolomics. Targeted metabolomics focuses on the identification and quantification of expected metabolites, requiring higher levels of purification and selective extraction of metabolites. In contrast, untargeted metabolomics aims to capture as many metabolites as possible without necessarily identifying or quantifying specific compounds (Sun et al., 2021; Schrimpe-Rutledge et al., 2016). In recent years, the novel metabolomic detection technique of widely targeted metabolomics, which integrates the advantages of the comprehensive nature of untargeted and the accuracy of targeted metabolomics, has been extensively applied, achieving high precision, sensitivity, rapid separation, and broad coverage (Wang et al., 2023a; Ren et al., 2023). The choice of separation and analytical platform varies depending on the sample type and research direction. Currently, commonly used platforms fall into two major categories: MS-based and nuclear magnetic resonance (NMR)-based platforms. The advantages and disadvantages of each platform are summarized in Table 1. Gas chromatography–mass spectrometry (GC–MS) is the most developed hybrid chromatography–MS technology widely applied in metabolomics research. The coupling of GC and MS offers several advantages, such as both instruments operating in the gas phase, direct connection, and a straightforward interface (Alawiye and Babalola, 2021; Fiehn, 2016; Xu and Feng, 2023; Liu and Locasale, 2017). Liquid chromatography–mass spectrometry (LC–MS) is also a

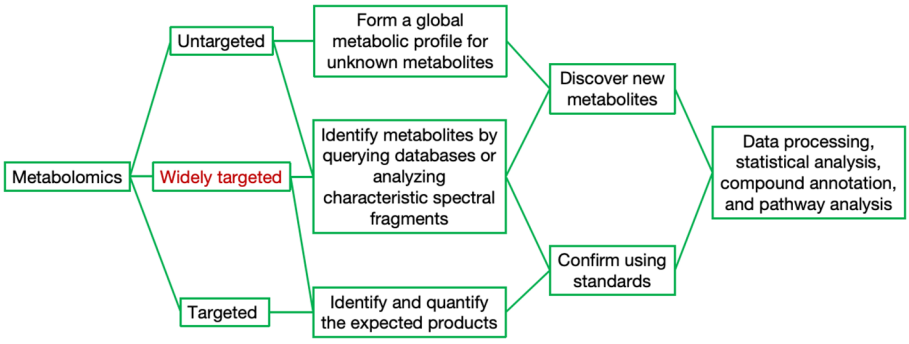

FIGURE 2
Targeted, widely-targeted, and untargeted approaches for metabolomic analysis.

TABLE 1 Metabolomics platforms.

	Pros	cons
GC-MS	• High sensitivity and resolution • Suitable for natural volatile compounds and small molecule metabolites • Large-scale open-source database	• Thermally sensitive, non-volatile polar metabolites require derivatization • The molecular weight of the target analyte is limited • Low capacity • Destructive to the sample
LC-MS	• High sensitivity and resolution • Suitable for non-volatile, thermally unstable, and high-molecular-weight compounds • Broad detection range • Simple sample preparation • Superior flexibility in compound separation and detection, including the selection of LC columns, mobile phases, and MS method settings. • Large-scale open-source database	• Organic compounds that do not form molecular ion adducts (such as hydrocarbons) cannot be measured • Destructive to the sample • Matrix effect • Narrow linear range of response
NMR	• Simple sample preparation • Low sample consumption • Non-destructive • High-throughput, unbiased detection system • High reproducibility • Highly automated • Easy to perform real-time metabolite identification • Able to provide deeper structural information	• Narrow detection range • Low sensitivity • High equipment and maintenance costs

commonly used analytical platform. In addition to having powerful separation capabilities, high sensitivity, and high resolution, LC–MS can overcome the limitations of GC–MS by effectively detecting nonvolatile, heat-sensitive, highly polar, and large-molecular-weight substances (Alawiye and Babalola, 2021; Liu and Locasale, 2017; Zhou and Yin, 2016; Yu et al., 2018). NMR has a limited dynamic range and lacks methods for determining the structures of unknown metabolites at low concentrations; hence, its application in plant metabolomics research is relatively limited (Alawiye and Babalola, 2021; Liu and Locasale, 2017; Emwas et al., 2019).

In recent years, metabolomics has undergone rapid development. Among its various techniques, Metabolic Flux Analysis (MFA) stands as a traditional yet potent method, utilizing stable isotope labeling experiments to delve into the metabolic pathways within biological systems. However, MFA encounters multiple constraints in practical applications, such as cellular heterogeneity, indirect analysis of energy and reducing power supplies, and the intricacies of experimental and analytical procedures. To circumvent these limitations, Flux Balance Analysis based on constraints (FBA) has emerged. FBA predicts flux distributions within metabolic networks under specified conditions through optimization techniques, offering a more flexible and robust alternative for exploring the metabolic capacity of plant metabolic networks (Kruger and Ratcliffe, 2021). Furthermore, single-cell metabolomics represents an emerging field that studies the composition and dynamic changes of metabolites within individual cells, encompassing advanced technologies like Laser Capture Microdissection, Laser Ablation Electrospray Ionization Mass Spectrometry (LAESI-MS), and pico Pressure Probe Electrospray Ionization Mass Spectrometry (picoPPESI-MS) (Katam et al., 2022). These techniques not only enhance our understanding of intercellular heterogeneity but also provide profound insights into metabolic pathways and cellular functions. For instance, by investigating the impact of UV-C radiation and melatonin treatment on secondary metabolite synthesis in *Lepidium sativum* L (Ullah et al., 2019), as well as exploring the effects of dolomite [$CaMg(CO_3)_2$] treatment on the growth, secondary metabolite production, and anti-malarial activity of *Sonchus arvensis* L. callus (Wahyuni et al., 2021), single-cell metabolomics offers a rich perspective and deep understanding of plant metabolism. Recently, researchers have developed a Widely Targeted Metabolite modificomics (WTMM) strategy. This strategy combines UHPLC-Q-Trap and UHPLC-QE-Orbitrap technologies, conducting systematic studies on metabolite modifications using tomato as a model. The WTMM strategy not only enables large-scale detection and quantitative analysis of modified metabolites in plants but also provides robust support for the development of plant biomarkers. This innovative research approach not only broadens the application scope of metabolomics but also furnishes new perspectives and tools for a deeper understanding of plant metabolic mechanisms (Yang et al., 2024). The represent cutting-edge technologies in the field of metabolomics. Regrettably, these advanced techniques have not yet been applied in the realm of quality control for TCM. Nevertheless, with the continuous deepening and expansion of research in these related fields, there is reason to believe that these sophisticated technologies will play a significant role in the quality control of TCM in the future.

Therefore, the focus of this review is to compile the latest advancements in metabolomics methods for assessing the quality and safety of TCM components. In this article, several key factors influencing the chemical profile and quality traits of TCM, including their origin, harvesting, and processing methods, are described. The current challenges of integrating metabolomics with other omics technologies, such as transcriptomics, have been actively explored in this field. Furthermore, future development trends and prospects are discussed.

2 Metabolomics for enhancing TCM quality

The quality of TCM is a crucial factor in determining its effectiveness and safety, and it has a direct impact on all subsequent steps of pharmaceutical production. The visual characteristics and active components of TCM are essential criteria for assessing their quality and are subject to various internal and external factors. From the selection of germplasm origins to the precision of field management, the application of harvesting and processing techniques, environmental conditions during storage and transportation, and the judicious selection of processing methods, each step can have an impact on the quality of TCM. Subsequently, various factors influencing the quality of TCM were detailed in this review, and the specific applications of metabolomics technology in controlling these factors to enhance the quality of TCM are discussed. Factors related to the quality of TCM are illustrated in Figure 3.

2.1 Origin

The origin of TCM is directly related to their quality, efficacy, and safety. The growth of plants in different environments and under different cultivation methods can result in variations in growth rate, yield, and active ingredients, leading to the unique regional characteristics of TCM. Although genuine medicinal materials have superior quality, their high price and demand have led to the presence of substitutes and adulterants on the market. Therefore, accurate identification is crucial for the quality control of TCM. Traditional identification methods are time-consuming and lack accuracy. Metabolomic techniques can be applied to the identification of TCM of different geographical origins, ensuring the quality and safety of the herbs and preventing their confusion and substitution (Tang et al., 2021).

In-depth research on the differences in the quality of Goji (*Lycium chinense* Miller) plants from different climatic regions was conducted by Yao et al (Yao et al., 2018). By observing morphological characteristics, they found that Goji plants cultivated in the monsoon region are lighter in weight, smaller in size, and shinier than those cultivated in other regions. On the other hand, Goji plants cultivated in the plateau region of Ningxia are the largest and brightest. However, despite the ability of ^{1}H NMR technology to distinguish between the two species, there were no significant differences in the quality of Goji plants from different cultivation regions. Based on differences in origin and variety, *Fritillariae Bulbus* is classified into three major categories: Chuan-Beimu, Zhe-Beimu, and Ping-Beimu. Among them, Chuan-Beimu

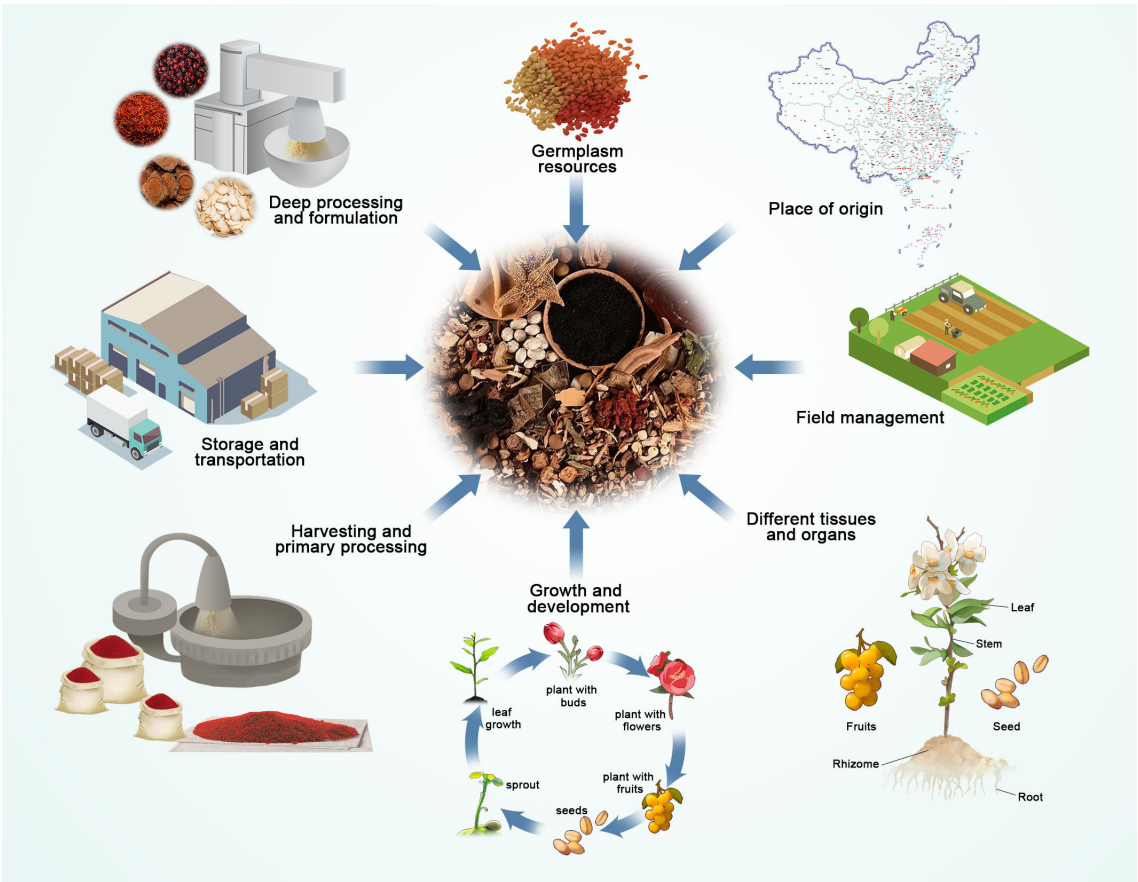

FIGURE 3
Factors affecting the quality and safety of TCM.

stands out for its outstanding therapeutic effects and low toxicity, resulting in a price several times higher than that of Zhe-Beimu and Ping-Beimu (Li et al., 2009). However, due to the complexity of the market, some businesses, in pursuit of profits, use low-priced varieties to impersonate Chuan-Beimu, severely impacting the quality of TCM and consumer rights (Luo et al., 2018). Liu et al., (2020a) successfully collected eight medicinal species of Chuan-Beimu (*Fritillariae Bulbus*), conducted comprehensive metabolic fingerprint analysis of Chuan-Beimu and its counterfeits using nontargeted metabolomics methods, and further applied chemometric methods to determine the characteristic substances of Chuan-Beimu and its counterfeits.

Gao et al. (2012) conducted a metabolomic analysis of the flower buds of seven species of Lonicera using LC-QTOF MS technology. By optimizing extraction conditions, chromatographic separation parameters, and mass spectrometry detection protocols, they achieved comprehensive detection of metabolites in the flower buds of these Lonicera species. Leveraging molecular feature extraction algorithms and multivariate statistical analysis methods, the researchers identified 82 statistically significant metabolite markers that exhibited notable distribution differences across the various Lonicera species. Through subsequent analysis of these markers' chemical classes and fragment ion information, they successfully established a rapid and accurate method for discriminating among the flower buds of the seven Lonicera species. The metabolomics-based approach to the identification of TCM facilitates the prompt distinction between substitutes and adulterants, thereby not only contributing to the protection of consumer rights but also promoting the healthy development of the TCM market.

Although research on heavy metal and microbial contamination in the field of TCM currently appears to be relatively weak, and the main focus of studies has largely centered on areas related to staple crops, such as exploring how *Fusarium graminearum* affects the quality degradation of stored wheat (Niu et al., 2024), as well as the absorption characteristics and interaction mechanisms of sweet potato (*Ipomoea batatas* L.) with uranium (U) and cadmium (Cd) (Lai et al., 2020), with the continuous deepening and expansion of research in these related fields, these findings will undoubtedly inject new vitality into the quality control of TCM in the future and provide valuable references and insights.

Apart from the medicinal materials mentioned above, metabolomics technology is also widely applied in studying the quality differences of TCM from various sources and varieties. For instance, researchers have conducted in-depth studies on *Codonopsis lanceolata* from different production areas using metabolomics methods to explore quality differences and potential impacting factors (Nam et al., 2023). Furthermore, studies have focused on different varieties of Dandelions (Zhang et al., 2021), *Pulsatilla Adans* (Zhang et al., 2019), *Eucommia ulmoides* Oliv (Wu et al., 2018), and other TCM, exploring quality differences using metabolomics technology. These studies provide methods and perspectives for in-depth understanding of the metabolic differences and bioactivity of medicinal plants from different sources, contributing to better quality control and standardization of medicinal plants.

2.2 Growth and development

The medicinal components of TCM usually reach their optimal therapeutic efficacy and contain the highest levels of active ingredients during specific growth stages. Moreover, at certain growth stages, the plants exhibit the best visual qualities, including color, shape, and size. Selecting the appropriate harvest time is crucial for obtaining relatively high-quality TCM. Currently, there is a shortage of wild medicinal resources, and in the case of cultivated herbs, inadequate understanding of ecological environments, regional differences, human activities, and the growth patterns of medicinal herbs during actual harvesting leads to a decline in the quality of TCM (Chen et al., 2021; Liu et al., 2022). Metabolomic methods utilizing technologies such as MS and NMR can be used to thoroughly analyze small-molecule metabolites during the growth and development of TCM, revealing changes in their composition and content. This provides a powerful basis for scientifically determining the maturity of TCM.

Eucommia ulmoides, which is widely distributed in China, has significant applications in the medical field due to its high content of chlorogenic acid (CGA), flavonoids, lignans, and other compounds in its leaves and bark. In a recent study, Li et al. (2019) employed nontargeted metabolomics and chemometrics to analyze the metabolic fingerprint patterns of *Eucommia ulmoides* leaves at different growth stages and identified characteristic substances that can be used to accurately distinguish between different growth stages. Most flavonoid compounds reached their peak accumulation in growing leaves, followed by mature leaves. The present study also revealed a stable increase in the large accumulation of CGA during leaf growth and development, while rutin exhibited higher accumulation levels in leaf buds and growing leaves. Additionally, this study investigated the transcriptome of leaves at different growth stages and revealed dynamic changes in gene expression. In addition to leaves, floral medicinal materials exhibit significant diversity due to the synthesis and accumulation of pigments. During the growth of safflower (*Carthamus tinctorius* L.), the color of the flowers gradually transitions from yellow to red. Researchers such as Ren et al. (2022) conducted a comprehensive analysis of flavonoid biosynthesis in safflower flowers through metabolomics and transcriptomics, detecting changes in flavonoid compound biosynthesis on the 2nd day (yellow stage) and 4th day (red stage) of flowering. The authors identified a total of 212 different flavonoid metabolites, with the levels of hydroxysafflor yellow A and carthamin significantly increasing during the color transition, indicating their crucial role in changing flower color from yellow to red. Xia et al. (2021) conducted a metabolomic and transcriptomic analysis of *Lonicera japonica* flower petals at different developmental stages, employing nontargeted and targeted metabolomics to analyze metabolite changes during the green, white, and yellow stages. By combining these data with transcriptomic data, they extensively investigated gene expression changes involved in pigment accumulation. The results showed that flavonoid and carotenoid synthesis and accumulation played a critical role in the color transition of *Lonicera japonica* flower petals. By applying metabolomics techniques or integrating them with other omics approaches, researchers have investigated the differences in quality during

different growth and development stages of TCM, such as *Scutellaria baicalensis* (Sun et al., 2023), *Fritillaria hupehensis* (Duan et al., 2023), and *Ganoderma lingzhi* (Satria et al., 2019; Xie et al., 2020). These research findings provide a scientific basis for optimizing the cultivation, harvesting, and subsequent development and utilization of TCM.

2.3 Medicinal parts

Medicinal herbs typically consist of multiple medicinal parts, such as roots, stems, leaves, flowers, fruits, and seeds. Each part may contain different medicinal components, allowing for the selection of the appropriate medicinal part based on the desired pharmacological effect. On the other hand, due to differences in the growth period and the content of medicinal components in different parts of medicinal herbs, utilizing the characteristics of various medicinal parts can maximize the resource utilization efficiency of these herbs. Liu et al (Liu et al., 2017), using nontargeted metabolomics methods, conducted a comprehensive analysis of the metabolite profiles in different tissues, including roots, stems and leaves of *P. ginseng* and *P. quinquefolius*. By comparing the metabolite compositions of different tissues, researchers identified several significantly different metabolites, mainly amino acids, organic acids, sugars, and other primary metabolites. Furthermore, researchers have performed correlation analyses between the metabolite profiles of different tissues and the accumulation of saponin components. The results showed a close association between the changes in primary metabolites and the accumulation of saponin components in different tissue parts. For example, in the roots and leaves of *P. ginseng*, the contents of amino acid metabolites such as glycine and serine were positively correlated with the accumulation of ginsenosides. In the roots and stems of *P. quinquefolius*, the contents of organic acid metabolites such as malic acid and citric acid were negatively correlated with the accumulation of *P. quinquefolius* saponins. Chen et al. (2020b) reported that the content of saponins in the stems and leaves of *P. ginseng* and *P. quinquefolius* was significantly greater than that in the roots and flowers. In a combined metabolomics and glycomic analysis of the xylem and cortex of *Morinda officinalis* Radix (MOR), researchers found that, compared to the cortex, the xylem contained more potentially toxic components, such as vernolic acid, physcion and linoleic acid. However, the xylem has relatively few bioactive components, such as rubiadin-1-methyl ether (Yip et al., 2019). Cui et al. (2018), using GC–MS technology, conducted an in-depth analysis of the metabolites in the rhizomes, flowers, leaves, and stems of *Fritillaria thunbergii* Miq. Through multivariate data analysis, the authors found significant differences in primary metabolites in the rhizomes compared to the other three plant parts. Metabolites in the rhizomes formed one cluster, while those in the flowers, leaves, and stems formed another cluster. Li et al. (2022) also conducted a nontargeted metabolomics study on the rhizomes and flowers of *Fritillaria thunbergii* Miq., and their results indicated substantial chemical composition differences between the two plant parts. Some alkaloids and flavonoids were found to be more abundant in the flowers than in the rhizomes. Molecular network analysis categorized the obtained metabolites into two main groups, with one group mainly present in the rhizomes and the other enriched in the flowers. The chemical differences among different plant parts may affect the efficacy and mechanisms of action of *Fritillaria thunbergii* Miq. Therefore, in drug development and clinical applications, it is essential to consider the chemical composition differences among different plant parts to maximize the pharmacological effects of medicinal herbs. Metabolomic techniques have also been applied to study quality differences among different medicinal plant parts, such as *Codonopsis pilosula* (Zeng et al., 2021), *Lonicera japonica* Thunb (Wang et al., 2023c), and velvet antler (Tseng et al., 2014).

Plant medicines are typically complex systems composed of multiple organs and tissues (Dong et al., 2020). In traditional metabolomic studies, researchers often crush and homogenize plant samples, but this approach can lead to the loss of valuable spatial information (Li et al., 2023; Dai et al., 2020). Spatial information is crucial for understanding metabolic processes, as various metabolites continuously interact in complex and delicate ways within plant tissues. Fortunately, the emergence of spatial metabolomics has provided an effective solution to this problem. Spatial metabolomics is a new field that integrates mass spectrometry imaging (MSI) technology with metabolomics. It can simultaneously analyze the spatial distribution characteristics of hundreds of metabolites on the same tissue section and utilize high-resolution mass spectrometry to deeply analyze differential components in the region, thereby closely linking dynamic changes in metabolites with spatial distribution (Heyman and Dubery, 2016). MALDI-MSI currently stands as the most extensively utilized MSI technique. The process begins with the placement of the sample within a carrier gas chamber, where a laser serves as a dependable ionization source. Following this, the sample is subjected to raster scanning, a methodical procedure that systematically captures mass spectrum data from various locations. By integrating the intensity of ion signals with the XY coordinates of the sample's surface, it is possible to generate detailed ion maps or mass spectrometry images (Lange et al., 2017). These high-resolution maps not only afford precise determination of the molecular weights and structural attributes of compounds but also offer valuable insights into their distribution patterns and concentration gradients within the sample. These high-resolution maps not only afford precise determination of the molecular weights and structural attributes of compounds but also offer valuable insights into their distribution patterns and concentration gradients within the sample (Norris and Caprioli, 2013; Lange et al., 2017). In contrast, DESI-MSI employs charged fine droplet beams that are rapidly sprayed onto the sample surface. These droplets efficiently extract and dissolve the analytes. As the solvent evaporates swiftly, charges are transferred from the droplets to the analyte molecules, facilitating the desorption and ionization of the molecules on the sample surface. Concurrently, with the aid of gases such as nitrogen, the charged sample droplets undergo desolvation and are directed along the ion transfer tube into the mass spectrometry detector for analysis. A significant advantage of DESI technology lies in its elimination of the need for sample pretreatment, enabling analysis to be conducted at atmospheric pressure (Yuan et al., 2024; Wang et al., 2023b). Lastly, SIMS-MSI holds the distinction of being the MSI

technique with the highest spatial resolution. It utilizes a focused primary ion beam to strike the sample surface, resulting in the sputtering of positive and negative secondary ions (Heyman and Dubery, 2016). Through spatial metabolomics technology, we can intuitively observe the distribution of specific plant metabolites at different growth stages and in various organs, revealing the patterns of metabolite changes over time and space. This makes the intricate secondary metabolic pathways of plants clear and greatly advances our understanding and research on the complex system of plant medicines (Li et al., 2013; Sun et al., 2020). Studies indicated that metabolites that accumulate in the roots of *Tripterygium wilfordii* exhibit considerable toxicity, necessitating spatial isolation to prevent adverse effects (Brinker et al., 2007). Using MALDI-MSI, researchers have assessed the localization of metabolites. The results revealed that two major quinone methide triterpenoids, celastrol and demethylzeylasteral, predominantly accumulated in the periderm tissue. Researchers speculated that this accumulation pattern might be related to *Tripterygium wilfordii*'s defense against bacteria and/or fungal soil pathogens. Additionally, they found via MSI that triptophenolide, a diterpenoid, accumulated significantly more in the woody roots of *Tripterygium wilfordii* and was slightly enriched in the periderm. Conversely, sesquiterpene alkaloids showed a more even distribution, primarily concentrated in the root cortex (Dai et al., 2020). Leveraging MALDI-MSI, Kuo et al. (2019) successfully obtained mass spectral images of agarwood samples, revealing the distribution of chemical components in different regions and providing an intuitive visual reference for subsequent studies. By associating MSI data with known compounds and utilizing molecular network analysis and machine learning algorithms, they successfully inferred the possible structures of new compounds. After experimental verification and structural elucidation, the structures and properties of the new compounds were ultimately confirmed. Furthermore, researchers have used MALDI-MSI technology to conduct metabolomic studies on the roots of two plants in the genus *Paeonia*, *Paeonia suffruticosa* and *Paeonia lactiflora*. The results showed significant spatial heterogeneity in the distribution of metabolites in these plant roots, indicating differences in metabolic activities in different regions of the roots (Li et al., 2021). Tong et al. (2022) and other researchers have studied the distribution and compositional characteristics of metabolites in different tissue parts of *Salvia miltiorrhiza* by combining metabolomics with DESI-MSI. The authors inferred the biosynthetic pathways of *S. miltiorrhiza* through data analysis and corresponding studies. The results demonstrated a close correlation between the distribution and composition of metabolites in different tissues of *S. miltiorrhiza* and the associated biosynthetic pathways.

Spatial metabolomics has addressed the limitations of traditional metabolomics in *in-situ* visualization analysis, thus introducing a fresh perspective and dynamism to the field of quality control in TCM. Nonetheless, several challenges persist in its practical application. Specifically, there is a lack of standardized operational procedures and quantitative methodologies, necessitating the establishment of unified guidelines. Furthermore, there is an urgent demand for novel, high-sensitivity mass spectrometry imaging devices capable of balancing high resolution with rapid imaging speeds.

2.4 Processing and formulation

Processing refers to a series of procedures, including drying, frying, steaming, and roasting, etc., applied to TCM, and this process is a distinctive feature of TCM. Through processing, the efficacy of medicinal materials can be enhanced, toxicity can be reduced, and taste and aroma can be improved. Chemical components in TCM inevitably undergo changes during these processes. In terms of quality control, the assessment of processed product quality often relies on the quantitative analysis of a few active ingredients. However, since TCM comprise complex components, evaluating its overall quality based on the analysis of a few components alone is challenging (Kui et al., 2022). By employing metabolomic approaches to comprehensively analyze substances undergoing changes during processing, detect trends in the alteration of medicinal components, and understand the biological transformation pathways under different processing conditions, it is possible to optimize the processing techniques regarding their impact on the medicinal components of TCM.

Cymbopogon citratus (citronella grass), a plant use for fragrance development and as a traditional herbal medicine, can be more easily stored and transported after drying than when fresh (Oladeji et al., 2019). However, the differences in medicinal components between dried and fresh citronella grass are currently unclear. To address this issue, Xiong et al. (2023) conducted chemical component identification and determination of fresh and dried citronella grass and explored the changes in metabolite concentrations before and after drying. Citronella grass is rich in volatile and nonvolatile components, including flavonoids, amino acids, organic acids, and vitamins. The contents of flavonoids and certain amino acids increased, while the contents of organic acids, other amino acids, and vitamins decreased during the drying process. Notably, flavonoids have beneficial effects, such as antioxidant properties (Figueirinha et al., 2008) and cardiovascular protection (Formica and Regelson, 1995), and positively influence human health. Additionally, drying altered the astringency of citronella grass, making it more suitable for medicinal use. Kang et al. (2021), utilizing UHPLC-Q/TOF-MS/MS, conducted a study on the overall chemical composition and differences between *Morinda officinalis* Radix (MOR) and processed *Morinda officinalis* Radix (PMOR). In this study, they successfully analyzed 41 batches of MOR samples and 32 batches of PMOR samples, identifying a total of 110 common components. The results indicated significant differences in the contents of 55 compounds between MOR and PMOR. Specifically, 29 components, including fructooligosaccharides, monotropein, deacetylasperulosidic acid, geniposide, and anthraquinone glycosides, had relatively high concentrations in MOR. On the other hand, PMOR had higher concentrations of 26 components than MOR, with difructose anhydrides and iridoid glycoside derivatives being discovered in PMOR for the first time. In a study investigating the chemical composition changes of processed Moutan Cortex, Li et al. (2018a) analyzed 30 samples using ESI-Q/TOF-MS/MS. These samples included 11 batches of raw Moutan Cortex (RMC), 9 batches of Moutan Cortex Tostus (MCT), and 10 batches of Moutan Cortex Carbonisatus (MCC). Through screening in

negative ion mode, 14 chemical markers were successfully identified. These markers included monoterpene glycosides, acetophenones, gallic derivatives, flavonoids and carbohydrates. Importantly, most chemical markers exhibited a significant decrease after frying of MCC. Specifically, the levels of monoterpenoid glycosides, such as oxypaeoniflorin, decreased markedly after processing, potentially leading to a decrease in its antithrombotic effect. Moreover, the content of dissociated gallic acid increased after frying, suggesting that gallic acid may enhance the anti-inflammatory and hemostatic functions of Moutan Cortex. These research findings provide a deeper understanding of the compounds and therapeutic changes that occur during the processing of TCM, offering robust support for the modernization and standardization of these materials.

In addition to the abovementioned TCM, differences between raw and processed Radix Rehmanniae (Li et al., 2010) and *Atractylodes macrocephala* Koidz (Shan et al., 2014) have also been investigated. Metabolomic techniques have been used to study the overall components changes during processing, such as the effect of boiling time on the overall quality of White Paeony Root (Ming et al., 2017), screening differentially abundant metabolites in *Polygoni Multiflora* Radix with varying processing times (Yu et al., 2017) and revealing the overall chemical changes and the correlation of key markers during the distillation process of *Ligustri Lucidi* Fructus (Li et al., 2020). Furthermore, exploring the synergistic effects and detoxification of processing products, such as raw *Pinelliae Rhizoma* and processed *Pinelliae Rhizoma* with alum (Sun et al., 2019), could constitute another avenue for further investigations.

3 Multiomics technologies in TCM quality and safety

Metabolomics analysis has demonstrated high accuracy and reliability in assessing the quality and safety of TCM. The advantage of this method lies in the fact that metabolites, as the end products of cell signaling, can directly reflect the organism's immediate state and functional changes. This opens a window for observing and evaluating the condition of the organism (or product). However, relying solely on metabolomics cannot provide a complete understanding of the root causes of TCM quality, especially for botanical drugs. Their metabolic networks involve complex and diverse regulatory mechanisms that exist not only on the surface of metabolism (such as various tissue forms formed through protein-protein interactions) but also throughout the multi-gene, multi-level regulatory networks of the transcriptome and even epigenetics (Muthamilarasan et al., 2019; Ideker et al., 2001) Therefore, current metabolomics research is gradually trending towards integration with other omics fields (such as genomics, transcriptomics, and proteomics), aiming to comprehensively depict various functions from the genome to the metabolome, and then to phenotypic characteristics. This forms a more complete and in-depth understanding framework (Sheth and Thaker, 2014; Yang et al., 2021). The specific technical flowchart is shown in Figure 4.

As mentioned above, the combined analysis of metabolomics and transcriptomics (Li et al., 2019; Ren et al., 2022; Xia et al., 2021) is currently one of the most developed techniques in multiomics studies. This involves separately conducting transcriptome sequencing and metabolite detection of specific samples during a particular period. The data obtained from the transcriptome, which reveals numerous differentially expressed genes, is then correlated with the differentially abundant metabolites identified through metabolomic analysis. This correlation analysis aims to analyze the intrinsic changes in the organism at both the causative and resultant levels, identifying pathways enriched with genes and metabolites. The two omics disciplines mutually validate each other, providing a comprehensive explanation of biological questions (Gahlan et al., 2012; Hao et al., 2011, 2012; Desgagné-Penix et al., 2012; Hagel et al., 2015). For instance, to delve into the alkaloid biosynthesis pathway of *Veratrum mengtzeanum*, researchers have employed transcriptomics and metabolomics to systematically analyze its various tissues (roots, stems, and leaves). Transcriptomic analysis revealed genes expressed in different tissues, including key genes closely related to alkaloid synthesis. Metabolomics identified various alkaloid components in different tissues. The results indicated that alkaloid biosynthesis in *V. mengtzeanum* mainly occurs in the roots and is closely related to specific transcript expression patterns. Despite earlier findings that only the roots were the most abundant source of alkaloid

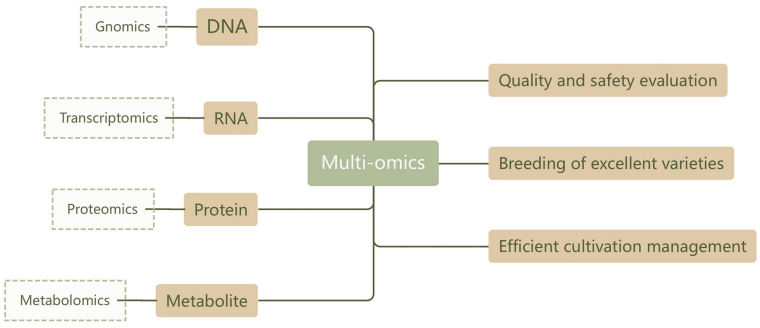

FIGURE 4
Technical route of multi-omics research.

biosynthesis, this study revealed that both leaves and roots play crucial roles in alkaloid biosynthesis. This finding expands the medicinal efficacy of different *V. mengtzeanum* parts, providing important evidence for further exploration of its medicinal value (Liu et al., 2023b). Tanshinones in *Salvia miltiorrhiza* (Danshen) are important active components, which mainly accumulate in the periderm, giving the roots of Danshen their characteristic red color. However, during long-term cultivation, researchers have observed a variation in which the roots of Danshen turn orange. A comparative analysis of metabolites in orange and red Danshen roots revealed a total of 40 lipophilic components, among which 7 were significantly reduced in the orange variant, including the abundant active compounds tanshinone IIA and tanshinone I. Further gene expression studies showed that dehydrogenase-related gene expression was not downregulated, but genes related to stress resistance and endoplasmic reticulum (ER)-associated protein degradation were upregulated. This suggests that the dehydrogenase enzymes may not have decreased, but their functionality might be compromised. Investigations uncovered that these changes could potentially lead to misfolding of the catalytic C_{15}-C_{16} dehydrogenase, which subsequently undergoes ER-associated degradation, resulting in a decrease of dehydrogenated furan ring tanshinones. This decrease is not solely caused by reduced gene expression. This reduction further affects the dehydrogenation conversion of other tanshinones, negatively impacting the overall quality of cultivated Danshen and causing the root color to shift from red to orange. Thus, this series of complex biochemical processes, rather than a single reduction in gene expression, is the key factor contributing to the decline in the quality of Danshen (Zhan et al., 2019). Genome-wide association study (GWAS) is a method to analyze genetic markers in large-scale population DNA samples at the genome-wide level, aiming to explore genetic factors associated with specific phenotypes, such as metabolite abundance. When GWAS is combined with metabolomics technology (i.e., mGWAS), it can deeply analyze the genetic mechanism of metabolite synthesis, thereby locking the gene loci that control metabolic synthesis and regulation (Duan et al., 2016). Through in-depth research on *Salvia miltiorrhiza*, scholars have compared the gene expression patterns of different diterpene synthesis pathways and their corresponding metabolites, thereby clarifying the importance of diterpene synthases (diTPSs). In their investigation of five Copalyl Diphosphate Synthases (SmCPSs), they observed that SmCPS3 may not be active, while the other SmCPSs correspond to different diterpene synthesis pathways. Interestingly, despite their biochemical similarity, SmCPS1 and SmCPS2 play distinctly different roles in the biosynthesis of tanshinones. This similarity is not meaningless but rather reflects their unique functions in different plant tissues (roots and aerial tissues). This novel discovery provides insights into increasing the yield of tanshinones in aerial parts, implying that we can sustainably and environmentally friendly obtain tanshinones by selectively cultivating and harvesting only the aerial tissues of the plant, without the need to destroy the entire plant (Cui et al., 2015). Regarding the joint analysis of metabolome and proteome, in the study of *S. baicalensis* mentioned in Section 2.2 (Growth and Development), researchers conducted an in-depth analysis of metabolite accumulation and protein expression changes in *S. baicalensis* at different growth years (i.e., "Zi Qin" and "Ku Qin") through the combined application of untargeted metabolomics technology and label-free proteomics methods (Sun et al., 2023). The results have shown that there are differences in metabolite and protein expression of *S. baicalensis* at different growth stages, and these differences mainly focus on the biosynthetic pathways of phenylalanine, tyrosine, tryptophan, and their related compounds. These findings reveal the variation pattern of metabolism and protein expression of *S. baicalensis* with growth time, providing a strong basis for scientifically determining the optimal harvest time. Given the diversity and dynamic changes of secondary metabolites during the development of *Lonicera japonica* flowers (honeysuckle) (Jiang et al., 2009), coupled with the diversification of gene families involved in the phenylpropanoid synthesis pathway in honeysuckle and its closely related species, this uncertainty has a profound impact on the medicinal value of honeysuckle and its related species (Yuan et al., 2014; Fraser and Chapple, 2011). To delve deeper into this issue, Yang et al. integrated transcriptomics, proteomics, and metabolomics approaches to systematically dissect the tight relationship between molecular changes and the regulation of secondary metabolites during the development of honeysuckle flowers (Yang et al., 2019). After a comprehensive analysis of omics data, the research team found that the metabolic changes of honeysuckle during its developmental stages mainly focus on core pathways such as sugar metabolism, lipopolysaccharide synthesis, carbon conversion, and secondary metabolism. Interestingly, as the flower develops, the number of genes associated with cellular and secondary metabolism decreases, revealing dynamic gene expression during the development of honeysuckle. In-depth proteomics research indicates significant differences in protein expression between the early and late stages of flower development. In the early stages, proteins related to glycolysis and phenylpropanoid metabolism are predominantly active, whereas in the later stages, proteins related to the citric acid cycle and terpenoid backbone pathway dominate. Epigenomics focuses on mapping various epigenetic regulators across the entire genome, exploring chemical modifications of the genome (such as DNA methylation, histone modifications, etc.) and changes in spatial structure without altering the DNA sequence. It is worth noting that the various physiological processes experienced by medicinal plants during growth and development are profoundly influenced by epigenetic marks, which directly or indirectly regulate various life activities of plants (He et al., 2011; Guo et al., 2021). Given the important role of DNA methylation and secondary metabolism in medicinal plants' response to cold stress, researchers have explored the effects of cold exposure time on American ginseng (Hao et al., 2020). They observed American ginseng at different growth stages and under various durations of cold treatment, examining the accumulation of ginsenosides, DNA methylation levels, and gene expression. The study revealed that DNA methylation and demethylation in perennial American ginseng dynamically adjust in response to seasonal temperature changes. Adequate cold exposure during winter can facilitate sufficient DNA demethylation in early spring tender leaves, subsequently promoting the high expression of

specific genes during flowering and fruiting stages, and ultimately leading to the maximum accumulation of ginsenosides in the roots of American ginseng. Ginsenosides are the core medicinal components of American ginseng, and their content directly affects the efficacy and quality of the medicinal material. This study not only provides a scientific basis for the quality control of American ginseng but also suggests that environmental factors should be fully considered in the quality control of TCM to ensure the optimal quality.

Despite the significant potential demonstrated by multi-omics approaches in the field of quality control of TCM, their application still faces multiple challenges and limitations. The primary difficulty lies in the complexity and analytical challenges of data processing, which stem from both the mismatch between the high-efficiency processing demands of massive data and current technological capabilities, as well as the complexity of integrating and analyzing data from different omics. This poses higher requirements for researchers' interdisciplinary knowledge and the application of bioinformatics tools. Furthermore, there are limitations in sensitivity and resolution at the technological application level, particularly in the detection of low-abundance metabolites and proteins. Coupled with the challenge of ensuring the representativeness of TCM samples, this further exacerbates the uncertainty of the research. Additionally, the high research costs and time-consuming experimental processes constitute economic and temporal barriers to practical application. Nevertheless, with the continuous development of the combined application of metabolomics and other omics, we have been able to construct a panoramic multi-dimensional information platform through the organic integration of various omics technologies, including genomics, epigenomics, transcriptomics, proteomics, metabolomics, and phenomics. This platform is dedicated to deeply mining functional genes and comprehensively and systematically elucidating the synthesis and metabolic mechanisms of active components in TCM, thereby providing a more scientific basis for research on the quality control of TCM.

4 Conclusion and perspectives for the future

This review provides a thorough exploration of the utilization of metabolomics for ensuring the quality of TCM, delving into the essential elements that shape its overall superiority. These factors encompass various aspects, such as geographical origins, growth and developmental stages, medicinal parts, and processing methods, providing comprehensive theoretical support for the quality control of TCM. Furthermore, this review briefly introduces the application of spatial metabolomics visualization techniques in the study of metabolite distribution in medicinal plants, revealing the specific distribution of metabolites in different spatial contexts within plants. Although multiomics applications in this field are still in their early stages, their potential and prospects in the quality control of TCM have garnered widespread attention and discussion.

Although the application of metabolomics technologies in the field of TCM quality control is gradually expanding, the limitations and challenges it faces are becoming apparent, given the current technological landscape. First, the processing, interpretation, and validation of metabolomics data pose challenges. Due to the high-dimensional and multifaceted nature of metabolomics data, complex methods are required for statistical and bioinformatics analyses. However, different statistical methods and hypothesis settings may lead to disparate results, making the interpretation and validation of results challenging. Second, the identification of metabolite markers, especially unknown metabolites, requires further analysis. Many substances found in metabolomics lack standard spectra in current mass spectrometry databases, and acquiring corresponding standard substances is difficult, making substance identification a formidable task. Finally, metabolomics research faces issues of data reproducibility. Due to various interferences, such as differences in sample preparation and environmental factors, metabolomics data from the same sample may exhibit considerable variations across different laboratories and time points. Therefore, while metabolomics technologies hold immense potential in the quality control of TCM, overcoming these difficulties and challenges is essential. Continuous improvement and refinement of technology are necessary to enhance the accuracy of data analysis and the reliability of results.

In the future, the application of metabolomics research in the quality control of TCM may move forward in three key directions. Firstly, with the continuous improvement of separation and detection technology, metabolomics techniques will be able to detect and quantify more metabolites more accurately, including those present at low concentrations. Metabolomics research will tend towards automation, standardization, and integrity to improve data reliability and reproducibility. Secondly, metabolomics will be more tightly integrated with other omics data such as genomics, transcriptomics, proteomics, etc., to comprehensively elaborate the metabolic pathways and genetic structures of medicinal plants. This integration will help discover new biomarkers and understand the regulatory mechanisms of complex metabolic networks in medicinal plants. Finally, an important development direction will be to build and improve metabolite databases, especially for unique metabolites of TCM. This will assist researchers in more rapidly identifying unknown metabolites and understanding their functions and mechanisms of action in TCM.

With the continuous advancement of research technologies, the refinement of platforms, ongoing progress in genomics and transcriptomics, and the efficient application of artificial intelligence (AI) algorithms, particularly machine learning for handling large datasets, we believe that methods based on metabolomics will play an increasingly important role in research on the quality and safety assessment of TCM.

Author contributions

PJ: Conceptualization, Visualization, Writing – original draft. XY: Funding acquisition, Resources, Supervision, Writing – review

& editing. XZ: Funding acquisition, Resources, Supervision, Writing – review & editing.

Funding

The author(s) declare financial support was received for the research, authorship, and/or publication of this article. This work was supported by the Hainan Province Science and Technology Special Fund, China (ZDYF2023SHFZ141, ZDYF2024XDNY159), the CAMS Innovation Fund for Medical Sciences (2021-I2M-1-032), National Natural Science Foundation of China (82074130), International Science & Technology Cooperation Program of Hainan Province (GHYF2024018), Hainan Academician Innovation Platform Scientific Research Project (SQ2021PTZ0052).

Conflict of interest

The authors declare that the research was conducted in the absence of any commercial or financial relationships that could be construed as a potential conflict of interest.

Publisher's note

References

Alawiye, T. T., and Babalola, O. O. (2021). Metabolomics: current application and prospects in crop production. *Biol. (Bratisl.)* 76, 227–239. doi: 10.2478/s11756-020-00574-z

Al-Kuraishy, H. M., Al-Fakhrany, O. M., Elekhnawy, E., Al-Gareeb, A. I., Alorabi, M., De Waard, M., et al. (2022). Traditional herbs against COVID-19: back to old weapons to combat the new pandemic. *Eur. J. Med. Res.* 27, 186. doi: 10.1186/s40001-022-00818-5

Alseekh, S., and Fernie, A. R. (2018). Metabolomics 20 years on: what have we learned and what hurdles remain? *Plant J. Cell Mol. Biol.* 94, 933–942. doi: 10.1111/tpj.13950

Bai, X., Zhu, C., Chen, J., Jiang, X., Jin, Y., Shen, R., et al. (2022). Recent progress on mass spectrum based approaches for absorption, distribution, metabolism, and excretion characterization of traditional Chinese medicine. *Curr. Drug Metab.* 23, 99–112. doi: 10.2174/1389200223666220211093548

Brinker, A. M., Ma, J., Lipsky, P. E., and Raskin, I. (2007). Medicinal chemistry and pharmacology of genus Tripterygium (Celastraceae). *Phytochemistry* 68, 732–766. doi: 10.1016/j.phytochem.2006.11.029

Chen, W., Balan, P., and Popovich, D. G. (2020b). Comparison of ginsenoside components of various tissues of New Zealand forest-grown Asian ginseng (Panax ginseng) and American ginseng (Panax quinquefolium L.). *Biomolecules* 10, 372. doi: 10.3390/biom10030372

Chen, Z., Lai, C., Wei, X., Gong, L., and Que, Z. (2021). [amp]]#xFF32;esearch progress on identification methods of growth years of traditional Chinese medicinal materials. *China J. Chin. Mater. Med.* 46, 1357–1367. doi: 10.19540/j.cnki.cjcmm.20201223.102

Chen, D., Liu, J.-R., Cheng, Y., Cheng, H., He, P., and Sun, Y. (2020a). Metabolism of rhaponticin and activities of its metabolite, rhapontigenin: A review. *Curr. Med. Chem.* 27, 3168–3186. doi: 10.2174/0929867326666190121143252

Commisso, M., Strazzer, P., Toffali, K., Stocchero, M., and Guzzo, F. (2013). Untargeted metabolomics: an emerging approach to determine the composition of herbal products. *Comput. Struct. Biotechnol. J.* 4, e201301007. doi: 10.5936/csbj.201301007

Cui, M.-C., Chen, S.-J., Wang, H.-H., Li, Z.-H., Chen, H.-J., Chen, Y., et al. (2018). Metabolic profiling investigation of Fritillaria thunbergii Miq. by gas chromatography–mass spectrometry. *J. Food Drug Anal.* 26, 337–347. doi: 10.1016/j.jfda.2016.10.003

Cui, G., Duan, L., Jin, B., Qian, J., Xue, Z., Shen, G., et al. (2015). Functional divergence of diterpene syntheses in the medicinal plant salvia miltiorrhiza. *Plant Physiol.* 169, 1607–1618. doi: 10.1104/pp.15.00695

Dai, W., Hu, Z., Xie, D., Tan, J., and Lin, Z. (2020). A novel spatial-resolution targeted metabolomics method in a single leaf of the tea plant (Camellia sinensis). *Food Chem.* 311, 126007. doi: 10.1016/j.foodchem.2019.126007

Desgagné-Penix, I., Farrow, S. C., Cram, D., Nowak, J., and Facchini, P. J. (2012). Integration of deep transcript and targeted metabolite profiles for eight cultivars of opium poppy. *Plant Mol. Biol.* 79, 295–313. doi: 10.1007/s11103-012-9913-2

Dong, Y., Sonawane, P., Cohen, H., Polturak, G., Feldberg, L., Avivi, S. H., et al. (2020). High mass resolution, spatial metabolite mapping enhances the current plant gene and pathway discovery toolbox. *New Phytol.* 228, 1986–2002. doi: 10.1111/nph.16809

Duan, L., Dai, Y., Sun, C., and Chen, S. (2016). Metabolomics research of medicinal plants. *China J. Chin. Mater. Med.* 41, 4090–4095. doi: 10.4268/cjcmm20162202

Duan, Y., Wu, J., Wang, F., Zhang, K., Guo, X., Tang, T., et al. (2023). Transcriptomic and metabolomic analyses provide new insights into the appropriate harvest period in regenerated bulbs of Fritillaria hupehensis. *Front. Plant Sci.* 14. doi: 10.3389/fpls.2023.1132936

Emwas, A.-H., Roy, R., McKay, R. T., Tenori, L., Saccenti, E., Gowda, G. A. N., et al. (2019). NMR spectroscopy for metabolomics research. *Metabolites* 9, 123. doi: 10.3390/metabo9070123

Fiehn, O. (2016). Metabolomics by gas chromatography-mass spectrometry: combined targeted and untargeted profiling. *Curr. Protoc. Mol. Biol.* 114, 30.4.1–30.4.32. doi: 10.1002/0471142727.mb3004s114

Figueirinha, A., Paranhos, A., Pérez-Alonso, J. J., Santos-Buelga, C., and Batista, M. T. (2008). Cymbopogon citratus leaves: Characterization of flavonoids by HPLC–PDA–ESI/MS/MS and an approach to their potential as a source of bioactive polyphenols. *Food Chem.* 110, 718–728. doi: 10.1016/j.foodchem.2008.02.045

Formica, J. V., and Regelson, W. (1995). Review of the biology of quercetin and related bioflavonoids. *Food Chem. Toxicol.* 33, 1061–1080. doi: 10.1016/0278-6915(95)00077-1

Fraser, C. M., and Chapple, C. (2011). The phenylpropanoid pathway in Arabidopsis. *Arab. Book* 9, e0152. doi: 10.1199/tab.0152

Gahlan, P., Singh, H. R., Shankar, R., Sharma, N., Kumari, A., Chawla, V., et al. (2012). *De novo* sequencing and characterization of Picrorhiza kurrooa transcriptome at two temperatures showed major transcriptome adjustments. *BMC Genomics* 13, 126. doi: 10.1186/1471-2164-13-126

Gao, W., Yang, H., Qi, Lw, Liu, Eh, Ren, Mt, Yan, Yt, et al. (2012). Unbiased metabolite profiling by liquid chromatography-quadrupole time-of-flight mass spectrometry and multivariate data analysis for herbal authentication: classification of seven Lonicera species flower buds. *J. Chromatogr. A* 1245, 109–116. doi: 10.1016/j.chroma.2012.05.027

Gong, L., Zou, W., Zheng, K., Shi, B., and Liu, M. (2021). The Herba Patriniae (Caprifoliaceae): A review on traditional uses, phytochemistry, pharmacology and quality control. *J. Ethnopharmacol.* 265, 113264. doi: 10.1016/j.jep.2020.113264

Goodacre, R., Vaidyanathan, S., Dunn, W. B., Harrigan, G. G., and Kell, D. B. (2004). Metabolomics by numbers: acquiring and understanding global metabolite data. *Trends Biotechnol.* 22, 245–252. doi: 10.1016/j.tibtech.2004.03.007

Guo, W., Ma, H., Wang, C.-Z., Wan, J.-Y., Yao, H., and Yuan, C.-S. (2021). Epigenetic studies of chinese herbal medicine: pleiotropic role of DNA methylation. *Front. Pharmacol.* 12. doi: 10.3389/fphar.2021.790321

Hagel, J. M., Mandal, R., Han, B., Han, J., Dinsmore, D. R., Borchers, C. H., et al. (2015). Metabolome analysis of 20 taxonomically related benzylisoquinoline alkaloid-producing plants. *BMC Plant Biol.* 15, 220. doi: 10.1186/s12870-015-0594-2

Hao, D. C., Ge, G., Xiao, P., Zhang, Y., and Yang, L. (2011). The first insight into the tissue specific taxus transcriptome via Illumina second generation sequencing. *PloS One* 6, e21220. doi: 10.1371/journal.pone.0021220

Hao, D., Ma, P., Mu, J., Chen, S., Xiao, P., Peng, Y., et al. (2012). *De novo* characterization of the root transcriptome of a traditional Chinese medicinal plant Polygonum cuspidatum. *Sci. China Life Sci.* 55, 452–466. doi: 10.1007/s11427-012-4319-6

Hao, M., Zhou, Y., Zhou, J., Zhang, M., Yan, K., Jiang, S., et al. (2020). Cold-induced ginsenosides accumulation is associated with the alteration in DNA methylation and relative gene expression in perennial American ginseng (Panax quinquefolius L.) along

with its plant growth and development process. *J. Ginseng Res.* 44, 747–755. doi: 10.1016/j.jgr.2019.06.006

Harwansh, R. K., and Bahadur, S. (2022). Herbal medicines to fight against COVID-19: new battle with an old weapon. *Curr. Pharm. Biotechnol.* 23, 235–260. doi: 10.2174/1389201022666210322124348

He, G., Elling, A. A., and Deng, X. W. (2011). The epigenome and plant development. *Annu. Rev. Plant Biol.* 62, 411–435. doi: 10.1146/annurev-arplant-042110-103806

Heyman, H. M., and Dubery, I. A. (2016). The potential of mass spectrometry imaging in plant metabolomics: a review. *Phytochem. Rev.* 15, 297–316. doi: 10.1007/s11101-015-9416-2

Huang, L., Nie, L., Dai, Z., Dong, J., Jia, X., Yang, X., et al. (2022). The application of mass spectrometry imaging in traditional Chinese medicine: a review. *Chin. Med.* 17 (1), 35. doi: 10.1186/s13020-022-00586-8

Hui, Y., Wang, X., Yu, Z., Fan, X., Cui, B., Zhao, T., et al. (2020). Scoparone as a therapeutic drug in liver diseases: Pharmacology, pharmacokinetics and molecular mechanisms of action. *Pharmacol. Res.* 160, 105170. doi: 10.1016/j.phrs.2020.105170

Ideker, T., Galitski, T., and Hood, L. (2001). A new approach to decoding life: systems biology. *Annu. Rev. Genomics Hum. Genet.* 2, 343–372. doi: 10.1146/annurev.genom.2.1.343

Jamal, Q. M. S. (2022). Antiviral Potential of Plants against COVID-19 during Outbreaks-An Update. *Int. J. Mol. Sci.* 23, 13564. doi: 10.3390/ijms232113564

Jiang, K., Pi, Y., Hou, R., Zeng, H., Huang, Z., Zhang, Z., et al. (2009). Molecular cloning and expression profiling of the first specific jasmonate biosynthetic pathway gene allene oxide synthase from Lonicera japonica. *Mol. Biol. Rep.* 36, 487–493. doi: 10.1007/s11033-007-9205-0

Kakkar, R. A., Haneen, M. A., Parida, A. C., and Sharma, G. (2023). The known, unknown, and the intriguing about members of a critically endangered traditional medicinal plant genus Aconitum. *Front. Plant Sci.* 14. doi: 10.3389/fpls.2023.1139215

Kang, M. J., and Suh, J. H. (2022). Metabolomics as a tool to evaluate nut quality and safety. *Trends Food Sci. Technol.* 129, 528–543. doi: 10.1016/j.tifs.2022.11.002

Kang, L., Zhang, Y., Zhou, L., Yang, J., He, Y., Yang, S., et al. (2021). Structural Characterization and Discrimination of Morinda officinalis and Processing Morinda officinalis Based on Metabolite Profiling Analysis. *Front. Chem.* 9. doi: 10.3389/fchem.2021.803550

Katam, R., Lin, C., Grant, K., Katam, C. S., and Chen, S. (2022). Advances in plant metabolomics and its applications in stress and single-cell biology. *Int. J. Mol. Sci.* 23, 6985. doi: 10.3390/ijms23136985

Kruger, N. J., and Ratcliffe, R. G. (2021). Whither metabolic flux analysis in plants? *J. Exp. Bot.* 72, 7653. doi: 10.1093/jxb/erab389

Kui, X., Wang, J., Chen, W., Wei, Y., Lv, Y., Zu, X., et al. (2022). Metabonomics and its application in Chinese medicine processing. *China J. Chin. Mater. Med.* 47, 593–602. doi: 10.19540/j.cnki.cjcmm.20210927.601

Kuo, T.-H., Huang, H.-C., and Hsu, C.-C. (2019). Mass spectrometry imaging guided molecular networking to expedite discovery and structural analysis of agarwood natural products. *Anal. Chim. Acta* 1080, 95–103. doi: 10.1016/j.aca.2019.05.070

Lai, J., Zhang-xuan, D., Xiao-hui, J., and Xue-gang, L. (2020). Absorption and interaction mechanisms of uranium & cadmium in purple sweet potato(Ipomoea batatas L.). *J. Hazard. Mater.* 400, 123264. doi: 10.1016/j.jhazmat.2020.123264

Lange, B. M., Fischedick, J. T., Lange, M. F., Srividya, N., Šamec, D., and Poirier, B. C. (2017). Integrative approaches for the identification and localization of specialized metabolites in tripterygium roots. *Plant Physiol.* 173, 456–469. doi: 10.1104/pp.15.01593

Li, Y. (2019). Quality markers of traditional Chinese medicine: concept, progress, and perspective. *Engineering* 5 (5), 888–894. doi: 10.1016/j.eng.2019.01.015

Li, Z., Cui, Y., and Qin, X. (2018b). Challenge of quality evaluation of traditional Chinese medicinal materials and application progress on metabolomic approach in its quality valuation. *Chin. Tradit. Herb. Drugs* 49, 2221–2229. doi: 10.7501/j.issn.0253-2670.2018.10.001

Li, B., Ge, J., Liu, W., Hu, D., and Li, P. (2021). Unveiling spatial metabolome of Paeonia suffruticosa and Paeonia lactiflora roots using MALDI MS imaging. *New Phytol.* 231, 892–902. doi: 10.1111/nph.17393

Li, H.-J., Jiang, Y., and Li, P. (2009). Characterizing distribution of steroidal alkaloids in Fritillaria spp. and related compound formulas by liquid chromatography-mass spectrometry combined with hierarchial cluster analysis. *J. Chromatogr. A* 1216, 2142–2149. doi: 10.1016/j.chroma.2008.03.093

Li, B., Knudsen, C., Hansen, N. K., Jørgensen, K., Kannangara, R., Bak, S., et al. (2013). Visualizing metabolite distribution and enzymatic conversion in plant tissues by desorption electrospray ionization mass spectrometry imaging. *Plant J. Cell Mol. Biol.* 74, 1059–1071. doi: 10.1111/tpj.12183

Li, C.-R., Li, M.-N., Yang, H., Li, P., and Gao, W. (2018a). Rapid characterization of chemical markers for discrimination of Moutan Cortex and its processed products by direct injection-based mass spectrometry profiling and metabolomic method. *Phytomedicine* 45, 76–83. doi: 10.1016/j.phymed.2018.04.003

Li, S., Lin, P., Xing, H., Li, X., Yao, Z., Zhang, X., et al. (2023). Unveiling the spatial metabolome and anti-atherosclerosis effects of Allium macrostemon Bunge and Allium chinense G. Don. *Arab. J. Chem.* 16, 104772. doi: 10.1016/j.arabjc.2023.104772

Li, L., Liu, M., Shi, K., Yu, Z., Zhou, Y., Fan, R., et al. (2019). Dynamic Changes in Metabolite Accumulation and the Transcriptome during Leaf Growth and Development in Eucommia ulmoides. *Int. J. Mol. Sci.* 20, 4030. doi: 10.3390/ijms20164030

Li, S.-L., Song, J.-Z., Qiao, C.-F., Zhou, Y., Qian, K., Lee, K.-H., et al. (2010). A novel strategy to rapidly explore potential chemical markers for the discrimination between raw and processed Radix Rehmanniae by UHPLC-TOFMS with multivariate statistical analysis. *J. Pharm. Biomed. Anal.* 51, 812–823. doi: 10.1016/j.jpba.2009.10.002

Li, M., Wang, X., Han, L., Jia, L., Liu, E., Li, Z., et al. (2020). Integration of multicomponent characterization, untargeted metabolomics and mass spectrometry imaging to unveil the holistic chemical transformations and key markers associated with wine steaming of Ligustri Lucidi Fructus. *J. Chromatogr. A* 1624, 461228. doi: 10.1016/j.chroma.2020.461228

Li, X., Wang, P., Tong, Y., Liu, J., and Shu, G. (2022). UHPLC-Q-exactive orbitrap MS/MS-based untargeted metabolomics and molecular networking reveal the differential chemical constituents of the bulbs and flowers of fritillaria thunbergii. *Mol. Basel Switz.* 27, 6944. doi: 10.3390/molecules27206944

Liu, J., Han, L., Li, G., Zhang, A., Liu, X., and Zhao, M. (2023b). Transcriptome and metabolome profiling of the medicinal plant Veratrum mengtzeanum reveal key components of the alkaloid biosynthesis. *Front. Genet.* 14. doi: 10.3389/fgene.2023.1023433

Liu, F.-J., Jiang, Y., Li, P., Liu, Y.-D., Yao, Z.-P., Xin, G.-Z., et al. (2020a). Untargeted metabolomics coupled with chemometric analysis reveals species-specific steroidal alkaloids for the authentication of medicinal Fritillariae Bulbus and relevant products. *J. Chromatogr. A* 1612, 460630. doi: 10.1016/j.chroma.2019.460630

Liu, J., Lai, C., Liang, X., Mei, N., and Zhang, Y. (2022). Research progress on the mechanism and control methods of traditional Chinese medicine harvesting period. *J. Chin. Med. Mater.* 45, 2019–2025. doi: 10.13863/j.issn1001-4454.2022.08.044

Liu, J., Liu, Y., Wang, Y., Abozeid, A., Zu, Y.-G., and Tang, Z.-H. (2017). The integration of GC-MS and LC-MS to assay the metabolomics profiling in Panax ginseng and Panax quinquefolius reveals a tissue- and species-specific connectivity of primary metabolites and ginsenosides accumulation. *J. Pharm. Biomed. Anal.* 135, 176–185. doi: 10.1016/j.jpba.2016.12.026

Liu, X., and Locasale, J. W. (2017). Metabolomics: A primer. *Trends Biochem. Sci.* 42, 274–284. doi: 10.1016/j.tibs.2017.01.004

Liu, B., Pang, F., Bi, H., and Guo, D. (2023a). Regulatory mechanisms of Gentiopicroside on human diseases: a brief review. *Naunyn. Schmiedebergs Arch. Pharmacol.* 397 (2), 725-750. doi: 10.1007/s00210-023-02672-6

Liu, H., and Wang, C. (2022). The genus Asarum: A review on phytochemistry, ethnopharmacology, toxicology and pharmacokinetics. *J. Ethnopharmacol.* 282, 114642. doi: 10.1016/j.jep.2021.114642

Liu, L., Xu, F.-R., and Wang, Y.-Z. (2020b). Traditional uses, chemical diversity and biological activities of Panax L. (Araliaceae): A review. *J. Ethnopharmacol.* 263, 112792. doi: 10.1016/j.jep.2020.112792

Luo, D., Liu, Y., Wang, Y., Zhang, X., Huang, L., and Duan, B. (2018). Rapid identification of Fritillariae Cirrhosae Bulbus and its adulterants by UPLC-ELSD fingerprint combined with chemometrics methods. *Biochem. Syst. Ecol.* 76, 46–51. doi: 10.1016/j.bse.2017.12.007

Ming, K., Xu, J., Liu, H.-H., Xu, J.-D., Li, X.-Y., Lu, M., et al. (2017). Effects of boiling duration in processing of White Paeony Root on its overall quality evaluated by ultra-high performance liquid chromatography quadrupole/time-of-flight mass spectrometry based metabolomics analysis and high performance liquid chromatography quantification. *Chin. J. Nat. Med.* 15, 62–70. doi: 10.1016/S1875-5364(17)30009-2

Munekata, P. E. S., Pateiro, M., Rocchetti, G., Domínguez, R., Rocha, J. M., and Lorenzo, J. M. (2022). Application of metabolomics to decipher the role of bioactive compounds in plant and animal foods. *Curr. Opin. Food Sci.* 46, 100851. doi: 10.1016/j.cofs.2022.100851

Murck, H. (2020). Symptomatic protective action of glycyrrhizin (Licorice) in COVID-19 infection? *Front. Immunol.* 11. doi: 10.3389/fimmu.2020.01239

Muthamilarasan, M., Singh, Nk, and Prasad, M. (2019). Multi-omics approaches for strategic improvement of stress tolerance in underutilized crop species: A climate change perspective. *Adv. Genet.* 103, 1–38. doi: 10.1016/bs.adgen.2019.01.001

Nam, M., Jo, S. R., Kim, Y.-C., and Kim, M.-S. (2023). UPLC-QTOF-MS-based metabolomics and antioxidant capacity of codonopsis lanceolata from different geographical origins. *Foods Basel Switz.* 12, 267. doi: 10.3390/foods12020267

Niu, H., Li, J., Wang, Y., Yang, W., and Zhang, M. (2024). Non▪Targeted metabolomics reveals the effect of fusarium graminearum on quality deterioration of wheat in storage. *Food Res. Dev.* 45, 23–30. doi: 10.12161/j.issn.1005-6521.2024.18.004

Norris, J. L., and Caprioli, R. M. (2013). Analysis of tissue specimens by matrix-assisted laser desorption/ionization imaging mass spectrometry in biological and clinical research. *Chem. Rev.* 113, 2309–2342. doi: 10.1021/cr3004295

Oladeji, O. S., Adelowo, F. E., Ayodele, D. T., and Odelade, K. A. (2019). Phytochemistry and pharmacological activities of Cymbopogon citratus: A review. *Sci. Afr.* 6, e00137. doi: 10.1016/j.sciaf.2019.e00137

Patti, G. J., Yanes, O., and Siuzdak, G. (2012). Metabolomics: the apogee of the omics trilogy. *Nat. Rev. Mol. Cell Biol.* 13, 263–269. doi: 10.1038/nrm3314

Ren, C., Chen, C., Dong, S., Wang, R., Xian, B., Liu, T., et al. (2022). Integrated metabolomics and transcriptome analysis on flavonoid biosynthesis in flowers of safflower (Carthamus tinctorius L.) during colour-transition. *PeerJ* 10, e13591. doi: 10.7717/peerj.13591

Ren, X., Wang, S., Wang, J., Xu, D., Ye, Y., and Song, Y. (2023). Widely targeted metabolome profiling of different plateau raspberries and berry parts provides innovative insight into their antioxidant activities. *Front. Plant Sci.* 14. doi: 10.3389/fpls.2023.1143439

Satria, D., Tamrakar, S., Suhara, H., Kaneko, S., and Shimizu, K. (2019). Mass spectrometry-based untargeted metabolomics and α-glucosidase inhibitory activity of lingzhi (Ganoderma lingzhi) during the developmental stages. *Mol. Basel Switz.* 24, 2044. doi: 10.3390/molecules24112044

Schrimpe-Rutledge, A. C., Codreanu, S. G., Sherrod, S. D., and McLean, J. A. (2016). Untargeted metabolomics strategies-challenges and emerging directions. *J. Am. Soc Mass Spectrom.* 27, 1897–1905. doi: 10.1007/s13361-016-1469-y

Shan, G.-S., Zhang, L.-X., Zhao, Q.-M., Xiao, H.-B., Zhuo, R.-J., Xu, G., et al. (2014). Metabolomic study of raw and processed Atractylodes macrocephala Koidz by LC–MS. *J. Pharm. Biomed. Anal.* 98, 74–84. doi: 10.1016/j.jpba.2014.05.010

Sheth, B. P., and Thaker, V. S. (2014). Plant systems biology: insights, advances and challenges. *Planta* 240, 33–54. doi: 10.1007/s00425-014-2059-5

Su, M., Hu, R., Tang, T., Tang, W., and Huang, C. (2022). Review of the correlation between Chinese medicine and intestinal microbiota on the efficacy of diabetes mellitus. *Front. Endocrinol.* 13. doi: 10.3389/fendo.2022.1085092

Sun, J., Du, L., Qu, Z., Wang, H., Dong, S., Li, X., et al. (2023). Integrated metabolomics and proteomics analysis to study the changes in Scutellaria baicalensis at different growth stages. *Food Chem.* 419, 136043. doi: 10.1016/j.foodchem.2023.136043

Sun, C., Zhang, M., Dong, H., Liu, W., Guo, L., and Wang, X. (2020). A spatially-resolved approach to visualize the distribution and biosynthesis of flavones in Scutellaria baicalensis Georgi. *J. Pharm. Biomed. Anal.* 179, 113014. doi: 10.1016/j.jpba.2019.113014

Sun, X., Zhang, M., Kong, L., and Gao, H. (2021). Research progress of metabolomics in food science and engineering. *China Food Addit.* 32, 175–181. doi: 10.19804/j.issn1006-2513.2021.09.024

Sun, L.-M., Zhang, B., Wang, Y.-C., He, H.-K., Chen, X.-G., and Wang, S.-J. (2019). Metabolomic analysis of raw Pinelliae Rhizoma and its alum-processed products via UPLC-MS and their cytotoxicity. *Biomed. Chromatogr. BMC* 33, e4411. doi: 10.1002/bmc.4411

Tang, C., Zhou, Y., Zhang, R., Wei, P., Xie, P., Liao, X., et al. (2021). Metabolomics application in quality evaluation of Chinese medicine and research on mechanism of antibacterial and anti-inflammatory effects. *Mod Chin. Med.* 23, 1664–1670. doi: 10.13313/j.issn.1673-4890.20200701004

Tong, Q., Zhang, C., Tu, Y., Chen, J., Li, Q., Zeng, Z., et al. (2022). Biosynthesis-based spatial metabolome of Salvia miltiorrhiza Bunge by combining metabolomics approaches with mass spectrometry-imaging. *Talanta* 238, 123045. doi: 10.1016/j.talanta.2021.123045

Tseng, S.-H., Sung, C.-H., Chen, L.-G., Lai, Y.-J., Chang, W.-S., Sung, H.-C., et al. (2014). Comparison of chemical compositions and osteoprotective effects of different sections of velvet antler. *J. Ethnopharmacol.* 151, 352–360. doi: 10.1016/j.jep.2013.10.060

Ullah, M. A., Tungmunnithum, D., Garros, L., Drouet, S., Hano, C., and Abbasi, B. H. (2019). Effect of ultraviolet-C radiation and melatonin stress on biosynthesis of antioxidant and antidiabetic metabolites produced in *in vitro* callus cultures of lepidium sativum L. *Int. J. Mol. Sci.* 20, 1787. doi: 10.3390/ijms20071787

Wahyuni, D. K., Rahayu, S., Zaidan, A. H., Ekasari, W., Prasongsuk, S., and Purnobasuki, H. (2021). Growth, secondary metabolite production, and in *vitro* antiplasmodial activity of Sonchus arvensis L. callus under dolomite [CaMg(CO3)2] treatment. *PloS One* 16, e0254804. doi: 10.1371/journal.pone.0254804

Wang, Q., Ban, J., Cai, R., Zhang, X., Lai, C., Chen, Y., et al. (2023a). Metabolic composition and quality traits of polygonatum cyrtonema hua from different germplasms and age sections based on widely targeted metabolomics analysis. *Int. J. Mol. Sci.* 24, 6077. doi: 10.3390/ijms24076077

Wang, Y., Li, L., Ji, W., Liu, S., Fan, J., Lu, H., et al. (2023c). Metabolomics analysis of different tissues of lonicera japonica thunb. Based on liquid chromatography with mass spectrometry. *Metabolites* 13, 186. doi: 10.3390/metabo13020186

Wang, S.-Y., Zhao, H., Xu, H.-T., Han, X.-D., Wu, Y.-S., Xu, F.-F., et al. (2021). Kaempferia galanga L.: progresses in phytochemistry, pharmacology, toxicology and ethnomedicinal uses. *Front. Pharmacol.* 12. doi: 10.3389/fphar.2021.675350

Wang, S., Zou, Y., Sun, S., Yan, Z., Tang, W., Li, P., et al. (2023b). Recent advances in mass spectrometry imaging and its application in drug research. *J. China Pharm. Univ.* 54, 653–661. doi: 10.11665/j.issn.1000-5048.2023091901

Wu, D., Yu, D., Zhang, Y., Dong, J., Li, D., and Wang, D. (2018). Metabolite profiles, bioactivity, and HPLC fingerprint of different varieties of eucommia ulmoides oliv.: towards the utilization of medicinal and commercial Chinese endemic tree. *Mol. Basel Switz.* 23, 1898. doi: 10.3390/molecules23081898

Xia, Y., Chen, W., Xiang, W., Wang, D., Xue, B., Liu, X., et al. (2021). Integrated metabolic profiling and transcriptome analysis of pigment accumulation in Lonicera japonica flower petals during colour-transition. *BMC Plant Biol.* 21, 98. doi: 10.1186/s12870-021-02877-y

Xie, C., Yan, S., Zhang, Z., Gong, W., Zhu, Z., Zhou, Y., et al. (2020). Mapping the metabolic signatures of fermentation broth, mycelium, fruiting body and spores powder from Ganoderma lucidum by untargeted metabolomics. *LWT* 129, 109494. doi: 10.1016/j.lwt.2020.109494

Xiong, Y., Ma, P., Yan, Y., Huang, L., Li, Y., and Wang, X. (2023). Widely targeted metabolomics analysis reveals the differences in nonvolatile compounds of citronella before and after drying. Biomed. Chromatogr. *BMC* 37, e5620. doi: 10.1002/bmc.5620

Xu, B., and Feng, T. (2023). Advances in metabolomics of peach fruit flavor. *China Fruit Veg.* 43, 10–16. doi: 10.19590/j.cnki.1008-1038.2023.01.002

Yang, F., Chen, H., Gao, Y., An, N., Li, X., Pan, X., et al. (2020). Gut microbiota-derived short-chain fatty acids and hypertension: Mechanism and treatment. *Biomed. Pharmacother. Biomedecine Pharmacother.* 130, 110503. doi: 10.1016/j.biopha.2020.110503

Yang, J., Chen, R., Wang, C., Li, C., Ye, W., Zhang, Z., et al. (2024). A widely targeted metabolite modificomics strategy for modified metabolites identification in tomato. *J. Integr. Plant Biol.* 66, 810–823. doi: 10.1111/jipb.13629

Yang, Y., Saand, M. A., Huang, L., Abdelaal, W. B., Zhang, J., Wu, Y., et al. (2021). Applications of multi-omics technologies for crop improvement. *Front. Plant Sci.* 12. doi: 10.3389/fpls.2021.563953

Yang, B., Zhong, Z., Wang, T., Ou, Y., Tian, J., Komatsu, S., et al. (2019). Integrative omics of Lonicera japonica Thunb. Flower development unravels molecular changes regulating secondary metabolites. *J. Proteomics* 208, 103470. doi: 10.1016/j.jprot.2019.103470

Yao, R., Heinrich, M., Zou, Y., Reich, E., Zhang, X., Chen, Y., et al. (2018). Quality variation of goji (Fruits of lycium spp.) in China: A comparative morphological and metabolomic analysis. *Front. Pharmacol.* 9. doi: 10.3389/fphar.2018.00151

Yin, J., Wu, M., Lin, R., Li, X., Ding, H., Han, L., et al. (2021). Application and development trends of gas chromatography–ion mobility spectrometry for traditional Chinese medicine, clinical, food and environmental analysis. *Microchem. J.* 168, 106527. doi: 10.1016/j.microc.2021.106527

Yip, K.-M., Xu, J., Zhou, S.-S., Lau, Y.-M., Chen, Q.-L., Tang, Y.-C., et al. (2019). Characterization of chemical component variations in different growth years and tissues of morindae officinalis radix by integrating metabolomics and glycomics. *J. Agric. Food Chem.* 67 (26), 7304–7314. doi: 10.1021/acs.jafc.9b01910

Yu, X.-A., Ge, A.-H., Zhang, L., Li, J., An, M., Cao, J., et al. (2017). Influence of different processing times on the quality of Polygoni Multiflora Radix by metabolomics based on ultra high performance liquid chromatography with quadrupole time-of-flight mass spectrometry. *J. Sep. Sci.* 40, 1928–1941. doi: 10.1002/jssc.201600913

Yu, Z., Zhang, M., Zhao, X., Zhang, Q., and Luan, J. (2018). Advances in metabolomics of malting barley and malt. *J. Dalian Polytech. Univ.* 37, 326–331. doi: 10.19670/j.cnki.dlgydxxb.2018.0503

Yuan, j., Ma, Y., and Guo, Q. (2024). Application of mass spectrometry imaging technology in medicinal plants research. *Plant Physiol. J.* 60, 56–62. doi: 10.13592/j.cnki.ppj.300154

Yuan, Y., Wang, Z., Jiang, C., Wang, X., and Huang, L. (2014). Exploiting genes and functional diversity of chlorogenic acid and luteolin biosyntheses in Lonicera japonica and their substitutes. *Gene* 534, 408–416. doi: 10.1016/j.gene.2012.09.051

Zeng, X., Li, J., Lyu, X., Chen, J., Chen, X., and Guo, S. (2021). Untargeted metabolomics reveals multiple phytometabolites in the agricultural waste materials and medicinal materials of codonopsis pilosula. *Front. Plant Sci.* 12. doi: 10.3389/fpls.2021.814011

Zhan, Z., Fang, W., Ma, X., Chen, T., Cui, G., Ma, Y., et al. (2019). Metabolome and transcriptome analyses reveal quality change in the orange-rooted Salvia miltiorrhiza (Danshen) from cultivated field. *Chin. Med.* 14, 42. doi: 10.1186/s13020-019-0265-6

Zhan, X., Wu, H., Wu, H., Wang, R., Luo, C., Gao, B., et al. (2020). Metabolites from bufo gargarizans (Cantor 1842): A review of traditional uses, pharmacological activity, toxicity and quality control. *J. Ethnopharmacol.* 246, 112178. doi: 10.1016/j.jep.2019.112178

Zhang, W., Jiang, H., Yang, J., Song, G., Wen, D., Liu, W., et al. (2019). A high-throughput metabolomics approach for the comprehensive differentiation of four Pulsatilla Adans herbs combined with a nontargeted bidirectional screen for rapid identification of triterpenoid saponins. *Anal. Bioanal. Chem.* 411, 2071–2088. doi: 10.1007/s00216-019-01631-6

Zhang, Gx, Jin, L., Jin, H., and Zheng, Gs (2021). Influence of dietary components and traditional Chinese medicine on hypertension: A potential role for gut microbiota. *Evid.-Based Complement. Altern. Med. ECAM* 2021, 5563073. doi: 10.1155/2021/5563073

Zhang, S., Li, C., Gu, W., Qiu, R., Chao, J., Pei, L., et al. (2021). Metabolomics analysis of dandelions from different geographical regions in China. *Phytochem. Anal. PCA* 32, 899–906. doi: 10.1002/pca.3033

Zheng, Y., Ding, Q., Zhang, L., Gou, X., Wei, Y., Li, M., et al. (2020). The effect of traditional Chinese medicine on gut microbiota in adults with type 2 diabetes: A protocol for systematic review and meta-analysis. *Med. (Baltimore)* 99, e22233. doi: 10.1097/MD.0000000000022233

Zhou, J., and Yin, Y. (2016). Strategies for large-scale targeted metabolomics quantification by liquid chromatography-mass spectrometry. *Analyst* 141, 6362–6373. doi: 10.1039/c6an01753c

frontiers | Frontiers in Plant Science

TYPE Original Research
PUBLISHED 20 December 2024
DOI 10.3389/fpls.2024.1498577

OPEN ACCESS

EDITED BY
Marta Sousa Silva,
University of Lisbon, Portugal

REVIEWED BY
Jonathan R. Cumming,
University of Maryland Eastern Shore, United States
Rasmieh Hamid,
Education and Extension Organization (AREEO), Iran

*CORRESPONDENCE
Rongzeng Huang
hrz0909@163.com
Bisheng Huang
hbsh1963@163.com

†These authors have contributed equally to this work and share first authorship

RECEIVED 19 September 2024
ACCEPTED 06 December 2024
PUBLISHED 20 December 2024

CITATION
Wei J, Zeng Z, Song C, Lv Q, Chen G, Mo G, Gong L, Jin S, Huang R and Huang B (2024) Color-induced changes in *Chrysanthemum morifolium*: an integrative transcriptomic and metabolomic analysis of petals and non-petals. *Front. Plant Sci.* 15:1498577. doi: 10.3389/fpls.2024.1498577

Color-induced changes in *Chrysanthemum morifolium*: an integrative transcriptomic and metabolomic analysis of petals and non-petals

Jianhong Wei[1†], Zhaoxiang Zeng[1†], Chengwu Song[1,2†], Qing Lv[1], Guangya Chen[3], Guoyan Mo[1,4], Ling Gong[1], Shuna Jin[2,5], Rongzeng Huang[1,2*] and Bisheng Huang[1,2*]

[1]School of Pharmacy, Hubei University of Chinese Medicine, Wuhan, Hubei, China, [2]Hubei Shizhen Laboratory, Wuhan, Hubei, China, [3]Department of Pharmacy, Ezhou Central Hospital, Ezhou, Hubei, China, [4]Key Laboratory of Traditional Chinese Medicine Resource and Prescription, Ministry of Education, Wuhan, Hubei, China, [5]School of Basic Medical Sciences, Hubei University of Chinese Medicine, Wuhan, Hubei, China

Chrysanthemum morifolium (CM), renowned for its diverse and vibrant varieties, holds significant ornamental and medicinal value. Despite this, the core regulatory mechanisms underlying its coloration, especially in non-petal tissues (i.e., the parts of CM that do not include petals, such as the reproductive tissues, receptacle and calyx), have been insufficiently studied. In this study, we performed transcriptomic and metabolomic analyses on yellow, gold, and white CM petals, as well as non-petal tissues, to investigate the molecular processes driving color variation. A total of 90 differential metabolites were identified, with flavonoids, their derivatives, and lipids emerging as the predominant components of the metabolic profile. At the transcriptional level, 38 pathways were significantly enriched based on the expression of differential genes. The combined metabolomic and transcriptomic analyses revealed that glycerophospholipid metabolism, primarily involving lipids, served as a key regulatory pathway for both petal and non-petal parts across different tissue colors. Notably, white CM exhibited marked differences from their gold and yellow counterparts at both the metabolic and transcriptional levels. These findings offer critical insights into the molecular mechanisms governing CM coloration and provide a foundation for optimizing future breeding efforts.

KEYWORDS

***Chrysanthemum morifolium*, transcriptomics, metabolomics, integrative omics, color regulation mechanism**

1 Introduction

Chrysanthemum morifolium (CM) is a globally significant ornamental plant, extensively used for culinary and medicinal purposes, with a history spanning three thousand years (Sharma et al., 2023; Liu et al., 2024b). Evidence suggests that CM comprises a multitude of chemical constituents, including flavonoids, phenolic acids, and lipids (Chen et al., 2021; Zhou et al., 2022b). This diverse chemical composition endows CM with numerous pharmacological effects, such as anti-inflammatory, antioxidant, and chronic disease prevention properties (Li et al., 2022b, 2023c; Chen et al., 2023). Over time, and with its long history of cultivation, CM has been diversified into various varieties through hybridization with wild relatives and artificial breeding (Song et al., 2023). In addition to its medicinal value, the ornamental characteristics of CM, particularly its wide range of colors and shapes, have contributed to its commercial and cultural significance.

Significant differences exist in the composition and content of nutrients and bioactive substances among various plant varieties and their parts (Lebaka et al., 2021; Lu et al., 2021b). CM encompasses a wide range of varieties, each exhibiting distinct variations in color, shape, and functional properties (Han et al., 2019). Among these, flower color is a critical ornamental trait, significantly influencing the commercial value of CM varieties (Zhang et al., 2019; Wu et al., 2023). Understanding the mechanisms that regulate flower color in CM is helpful for advancing breeding strategies and optimizing the ornamental and medical applications of these varieties. While existing studies predominantly focus on the differences in petal color among CM varieties, the non-petal parts—such as the reproductive tissues, receptacle, and calyx—have received far less attention (Sawada et al., 2019; Zou et al., 2021). Although these non-petal parts may not exhibit visible differences across various CM colors, significant variations could exist at the molecular or metabolic level (Zhou et al., 2022a). Given that both petal and non-petal parts contribute to the ornamental and medicinal uses of CM, expanding research beyond petals offer helpful insights into the broader utility of this species. Thus, further investigation into the non-petal parts is warranted to uncover potential differences and their implications.

The advent of high-throughput technologies, including genomics, transcriptomics, and metabolomics, has greatly advanced the exploration of the intricate molecular foundations of plant biology (Guo et al., 2021; Tsugawa et al., 2021; Sun et al., 2022). These technologies have become particularly valuable in understanding the genetic and metabolic basis of traits such as flower color in CM. Metabolic profiling serves as a direct link between plant phenotypes and genotypes, identifying stage-specific metabolites and revealing the metabolic mechanisms underlying a wide variety of traits (Shen et al., 2023). Recent advancements in omics technologies have led to the increasing integration of metabolomics with other disciplines, such as transcriptomics. This synergy facilitates a systematic understanding of complex plant biological networks and fosters a more comprehensive biological knowledge base (Liu et al., 2024a; Yang et al., 2024). Investigating the alterations in plant genes and metabolites will help elucidate the molecular mechanisms underlying the non-petal and petal parts of CM exhibiting various colors.

To investigate the distinct characteristics of non-petal and petal parts in CM of varying colors and uncover potential regulatory mechanisms, white, yellow, and gold CM were subjected to transcriptomic and metabolomic analyses. Metabolomic profiling, conducted using ultra-high pressure liquid chromatography coupled with quadrupole time-of-flight mass spectrometry (UPLC-QTOF-MS/MS), revealed substantial differences between the non-petal and petal components of these differently colored CM. To further elucidate the molecular basis of coloration, RNA sequencing was performed. By integrating transcriptomic and metabolomic data, the study aimed to identify key regulatory mechanisms underlying the color-dependent differences in non-petal and petal parts. This research provides new insights into the genetic basis of CM, supporting efforts to diversify CM varieties through informed breeding strategies.

2 Materials and methods

2.1 Materials and reagents

The CM samples gathered from the medicinal botanical garden at Hubei University of Chinese Medicine were identified and authenticated by Professor Gong Ling of Hubei University of Chinese Medicine. Fresh CM samples were immediately imaged after collection and separated into petal and non-petal tissues for subsequent analysis, as shown in Figure 1. Non-petal samples were collected from white, yellow, and gold CM, and were designated as groups WCNP, YCNP, and GCNP, respectively. The petal samples from these colors were designated as groups WCP, YCP, and GCP. Fresh samples were stored at -80°C prior to metabolomics analysis and RNA extraction. High-performance liquid chromatography-grade acetonitrile and methanol were acquired from Merck Chemicals, Darmstadt, Germany.

2.2 Sample extraction for untargeted metabolomic analysis

The samples were first freeze-dried to a constant weight and then ground into a fine, uniform powder. To begin the extraction process, 100 mg of the powdered sample was weighed and extracted with 3 mL of an 80% methanol solution using ultrasonic extraction for 10 minutes. This extraction step was repeated twice: first with 3 mL of a 50% methanol solution and then with 3 mL of a 95% methanol solution. The three resulting extracts were combined, and the mixture was centrifuged at 12,000 rpm for 10 minutes. After centrifugation, the supernatant was carefully filtered and prepared for further analysis. Curcumin was employed as an internal standard in the samples at a final concentration of 200 ng mL^{-1}. After filtration, the quality control (QC) sample was prepared by combining equal aliquots from all individual samples.

FIGURE 1
Chrysanthemum morifolium (CM) from three different colors-gold, yellow, and white. Non-petal tissues of CM included the reproductive tissues, receptacle, and calyx, excluding the petals.

2.3 UPLC-QTOF-MS/MS-based untargeted metabolomic analysis

For the analysis of the extracts, an ACQUITY UPLC H-Class system from Waters (Milford, MA, USA) was utilized, featuring a Waters ACQUITY UPLC BEH C18 column (2.1 × 100 mm, 1.7 µm). The injection volume was 2.0 µL, the flow rate was maintained at 0.3 mL min^{-1}, and the column temperature was set to 40°C. The mobile phase consisted of two solvents: mobile phase A, a solution of water and formic acid in a 1000:1 (v/v) ratio, and mobile phase B, acetonitrile. The chromatographic gradient was programmed as follows: 0 min, 5% (B); 12 min, 35% (B); 18 min, 80% (B); 22 min, 95% (B); 25 min, 95% (B); 26 min, 5% (B); and 30 min, 95% (A) and 5% (B).

Mass spectrometry analysis was carried out using a Waters Xevo G2-XS QTOF system equipped with an electrospray ionization source. The parameters were set according to our previously published reports (Zeng et al., 2023, 2024). The optimal parameters were as follows: desolvation temperature of 500°C, cone voltage of 20 V, capillary voltage of 3 KV, source temperature of 100°C, desolvation gas flow rate of 1000 L h^{-1}, collision energy range of 30 to 40 eV, and cone gas flow rate of 50 L h^{-1}. The mass range for full scans was set from *m/z* 50 to 1500 Da, with a scan duration of 1.0 s. Data acquisition was conducted in MS^E mode, employing both positive and negative ion electrospray modes. Metabolomics analysis predominantly utilized positive ion mode, while structural determination of metabolites was achieved with both ion modes.

2.4 RNA extraction and Illumina sequencing

RNA extraction and Illumina sequencing of the samples were primarily conducted by MetWare Biotechnology Co., Ltd. (Wuhan, Hubei, China). Total RNA was extracted from plant samples using ethanol precipitation and the CTAB-PBIOZOL method, then dissolved in DEPC-treated water. RNA integrity and concentration were assessed using a Qubit fluorescence quantifier and Qsep400 biofragment analyzer (Bioptic Inc., Taiwan, China). PolyA-tailed mRNAs were enriched with Oligo (dT) magnetic beads, fragmented, and reverse-transcribed into first-strand cDNA using random hexamer primers. Strand-specific second-strand cDNA synthesis was performed with dUTPs to ensure strand specificity, followed by end repair, A-tailing, and sequencing adapter ligation. The cDNA was size-selected (250-350 bp), PCR-amplified, purified, and quantified using Qubit 4.0 (Thermo Fisher Scientific, Massachusetts, USA) and Q-PCR (Bio-rad, California, USA). Libraries were pooled based on effective concentrations and sequenced on an Illumina platform, generating 150 bp paired-end reads via sequencing-by-synthesis. Raw sequencing data were filtered with fastp, and clean reads were assembled using Trinity. Corset was then used to remove redundant isoforms from the assembled transcripts. CDS prediction was conducted with TransDecoder, and gene function annotation was performed using DIAMOND and HMMER across databases. The fragments per kilobase of transcript per million mapped reads (FPKM) for each gene were subsequently calculated based on the gene length and the number of reads mapped to it. Transcript expression levels were quantified using RSEM, with differential expression analysis conducted using DESeq2 and edgeR, followed by Kyoto Encyclopedia of Genes and Genomes (KEGG) enrichment analyses.

2.5 Data analysis

The raw data from UPLC-QTOF-MS/MS were acquired using MassLynx v4.1 (Waters, Milford, MA, USA). Following data acquisition, the open-access software MS-DIAL (Version 4.9) was utilized for comprehensive data processing, encompassing peak detection, alignment, spectral deconvolution, identification, and

normalization (Tsugawa et al., 2015). The retention time for the collected peaks was set between 1 and 30 minutes. Peaks with a minimum height of 3000 and *m/z* values ranging from 100 to 1500 Da were selectively retained, guided by the expected component range, while the *m/z* value for fragment ions was set between 50 and 1500 Da. Mass tolerance parameters were established at 0.015 Da for MS and 0.02 Da for MS/MS. To determine the elemental composition of the peaks, common positive ion adducts such as $[M+H]^+$, $[M+Na]^+$, $[M+K]^+$, $[M+H-H_2O]^+$, and $[2M+H]^+$ were employed. In negative ion mode, adducts like $[M-H]^-$, $[M+HCOOH-H]^-$, and $[M-H_2O-H]^-$ were used to assist in adduct correction alongside the positive ion adducts. Feature alignment across all samples was performed with a retention time tolerance of 0.1 and an MS tolerance of 0.015. Furthermore, the deconvolution value and MS/MS abundance cutoff were set at 0.6 and 100, respectively, to facilitate peak deconvolution. The response values of the peaks were normalized using internal standards and the LOWESS method. Finally, to ensure that the screened metabolites accurately represented each group, peaks were required to be present in at least one group, with every sample within that group exhibiting the corresponding peak.

In the search for characteristic differentially accumulated metabolites (DAMs) between two groups, we utilized variable importance in projection (VIP) values exceeding 1.25 and fold change (FC) thresholds greater than 1.5 or less than 0.67 to identify potential distinctive peaks. In the transcriptome analysis, to ensure the genes were both representative and meaningful, we applied the following criteria to eliminate false positives: (1) the average FPKM value of the gene in at least one group exceeds 1; (2) the gene's detection rate across all samples is greater than 0.167; (3) the gene's detection rate in any individual group is above 0.667. For the differentially expressed genes (DEGs) identified in the comparison between the two groups, the initial requirement was that genes had an FPKM > 1 in at least one group and were detected in at least two samples within any group. Subsequently, based on FPKM quantitative data, the fold change (FC) for the DEGs had to exceed 2 or fall below 0.5, with a *q*-value between the two groups required to be < 0.05. In the co-enrichment analysis, to identify pathways that represent both metabolomics and transcriptomics, we selected pathways containing at least two DAMs and conducted a comprehensive analysis of the DEGs upstream and downstream of the DAMs within these pathways.

The SIMCA 14.1 software (Umetrics AB, Umeå, Sweden) was employed for principal component analysis (PCA) and orthogonal partial least squares-discriminant analysis (OPLS-DA). Data visualization was carried out using Origin 2021 (OriginLab Corporation, Northampton, MA, USA) and R version 4.3.2 (R Foundation for Statistical Computing, Vienna, Austria). Statistical analyses were performed with SPSS version 26.0 (SPSS, Inc., Chicago, IL, USA). The significance of DAMs was assessed with a *P*-value < 0.05 using the Mann-Whitney *U* test, while DEGs were evaluated with a *q*-value < 0.05 using the Benjamini-Hochberg test. Qualitative analysis of DAMs was conducted by comparing fragment ions using literature references (Chen et al., 2017), MS-FINDER version 3.60 (Tsugawa et al., 2016), and public databases such as the Human Metabolome Database (https://www.hmdb.ca) and MassBank (https://massbank.eu/MassBank/). Quantitative determination of metabolites was achieved using Quanlynx software version 4.1 (Waters, Milford, MA, USA). For the co-enrichment analysis of metabolomics and transcriptomics, metabolic pathways of DAMs and DEGs were primarily constructed with reference to KEGG.

3 Results

3.1 Untargeted metabolomic analysis

In this study, a total of 6704 features were acquired for all samples using MS-DIAL based on UPLC-QTOF-MS/MS. As shown in Figure 2A, the PCA model was applied for unsupervised analysis of all samples, including quality controls. The first two principal components accounted for 63.30% and 9.74% of the variance among the samples, respectively. The results revealed clear intra-group clustering, demonstrating strong reproducibility within each sample group. Additionally, the WCNP and YCNP groups displayed a higher degree of global similarity to each other. The clustering of the QC sample further confirmed the robust stability of instrument throughout the analysis.

Furthermore, supervised OPLS-DA was employed to identify DAMs between the two groups in both petal or non-petal areas (see Supplementary Figures S1 and S2). The scatter plots derived from OPLS-DA revealed clear segregation between each pair of groups. All pairwise comparisons yielded R2Y and Q2 scores consistently exceeding 0.9. Additionally, the results of the 999 permutation tests showed that the blue regression line of Q2 intersected the vertical axis below zero, confirming the absence of overfitting in the original OPLS-DA model. Ultimately, 90 DAMs ($P < 0.05$) were characterized, with a higher number identified in the petals than in the non-petal areas. The qualitative information of these metabolites, including retention time, actual *m/z* mass of the quasi-molecular ion peak, tentative identification, molecular formula, secondary fragments, and classification details, was provided in Supplementary Table S1. The FC and VIP values of DAMs across different comparison groups were listed in Supplementary Table S2. When comparing various petal groups, WCP *vs.* YCP had the fewest number of DAMs, while WCP *vs.* GCP had the most (Figure 2B). Meanwhile, WCNP *vs.* GCNP had the highest number of DAMs among the various non-petal groups. As illustrated in Figure 2C, the identified DAMs were mainly categorized into 6 categories: amino acids, flavonoid glycosides, flavonoids, lipids, other glycosides, and others. Among these, flavonoid glycosides, lipids, and flavonoids were predominantly classified in the petal parts, whereas flavonoid glycosides and lipids were primarily classified in the non-petal parts.

3.2 DAMs in CMs with different colors

To elucidate variations in the expression levels of these DAMs across different morphologies of CM, we conducted a relative

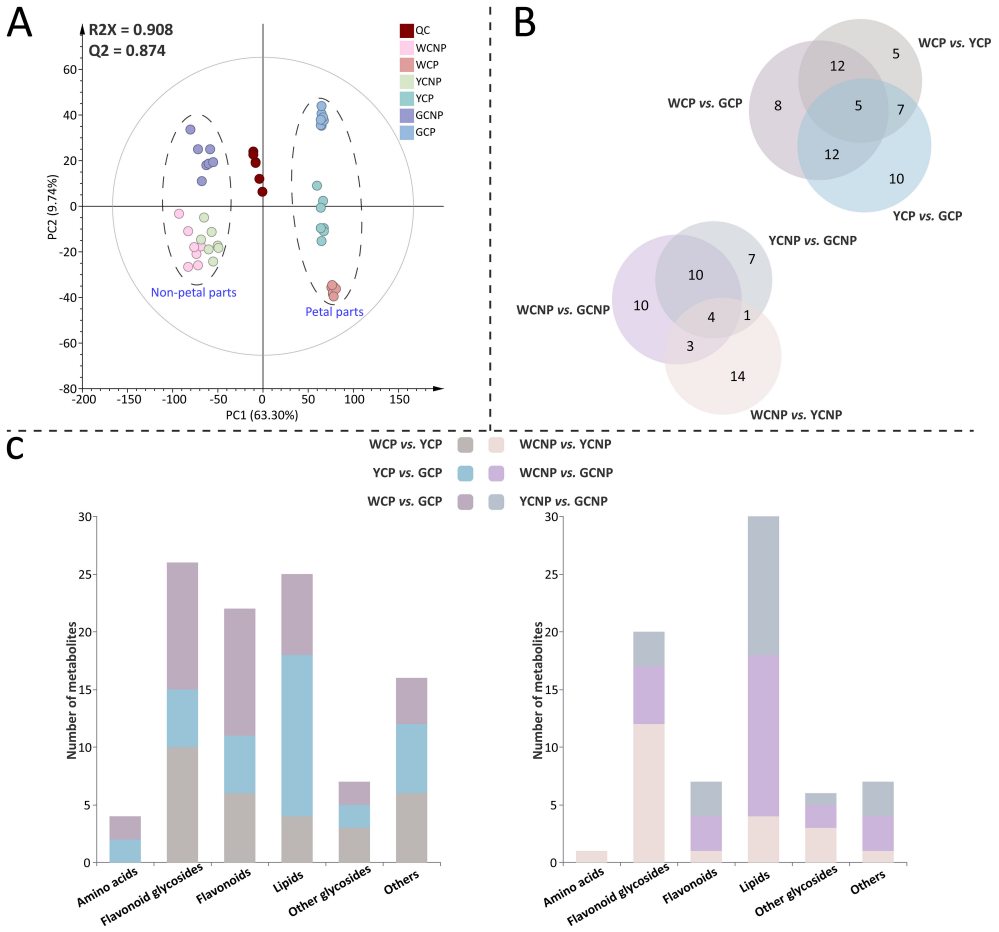

FIGURE 2
(A) Principal component analysis of metabolomic data from petals and non-petals of *Chrysanthemum morifolium* (CM) in three distinct colors. **(B)** Venn diagram of differentially accumulated metabolites across comparative groups. **(C)** Primary chemical classification of differentially accumulated metabolites in various comparisons. Non-petal samples from white, yellow, and gold CM were classified as WCNP, YCNP, and GCNP, respectively, while petal samples from these colors were designated as WCP, YCP, and GCP. "QC" represented the quality control group prepared from all samples.

quantitative analysis of the corresponding groups with the ratio of peak area between DAMs and internal standards, as shown in Figure 3. In the petals of CM, the following metabolite changes were observed: 8 up-regulated and 21 down-regulated in the WCP *vs.* YCP, 14 up-regulated and 20 down-regulated in YCP *vs.* GCP, and 12 up-regulated and 25 down-regulated in WCP *vs.* GCP. Similarly, in the non-petals of CM, 16 up-regulated and 6 down-regulated metabolites were identified in the WCNP *vs.* YCNP, 5 up-regulated and 17 down-regulated in YCNP *vs.* GCNP, and 11 up-regulated and 16 down-regulated in WCNP *vs.* GCNP.

As highlighted in Figure 3, most flavonoid glycosides showed higher concentrations in white CM, both in non-petal and petal parts. However, within the flavonoids, the petal part of white CM exhibited lower contents, while the non-petal part showed higher contents. Additionally, most lipids within DAMs were found at lower concentrations in both WCP and WCNP compared to the other two groups. Conversely, in the petals, most lipids were more abundant in YCP, whereas in the non-petal parts, they were predominantly higher in GCNP.

3.3 Transcriptomic analysis

To gain a more comprehensive understanding of the non-petal and petal parts across different phenotypes, transcriptomic sequencing and variance analysis of DEGs were employed to investigate the underlying molecular mechanisms. After data acquisition and transcript assembly, a total of 231670 raw sequencing reads were retained. To reduce false positives while preserving valid data, 181404 reads were selected for further transcriptomic analysis. The PCA results revealed that both yellow and gold CM showed similar trends in non-petal and petal parts compared to white CM (Figure 4A). Moreover, each sample displayed a distinct clustering pattern within its respective group. The first two principal components accounted for 23.16% and 13.49% of the total variance among the samples, respectively. DEGs between the two groups were identified using criteria of a FC greater than 2 or less than 0.5, and a *q*-value less than 0.05. As illustrated in Figure 4B, the comparisons between WCP and GCP, and WCNP and GCNP, revealed the highest number of DEGs in the

10.3389/fpls.2024.1498577

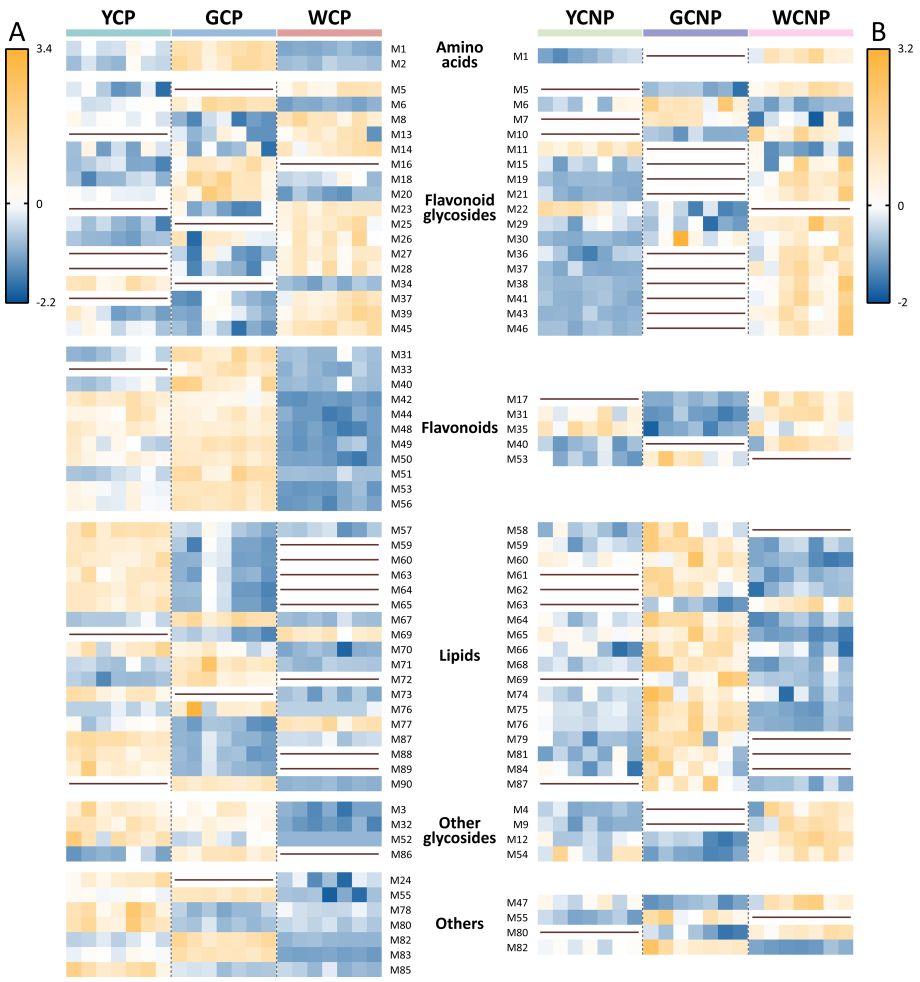

FIGURE 3
Heatmaps of differentially accumulated metabolites in petals **(A)** and non-petals **(B)** of *Chrysanthemum morifolium* (CM) across various colors. Non-petal samples from white, yellow, and gold CM were classified as WCNP, YCNP, and GCNP, respectively, while petal samples from these colors were designated as WCP, YCP, and GCP. The brown horizontal line in the figure indicated that the compound was not differentially accumulated metabolite between this group and the other groups.

petal and non-petal groups, respectively. Additionally, fewer transcriptional differences were observed between yellow and gold CM.

To further illustrate the differences between the groups, a heat map was generated from the quantitative data of DEGs, as detailed in Supplementary Figure S3. Statistical analysis of DEG expression trends between the two groups, presented in Figure 4C, revealed that most DEGs exhibited a decreasing trend, particularly in comparisons between WCNP *vs.* YCNP and WCNP *vs.* GCNP.

These pathways fall into several categories, including cellular processes, environmental information processing, genetic information processing, metabolism, and organismal systems, with metabolism representing the largest portion (78.95%). Within the metabolism category, pathways related to carbohydrate and lipid metabolism were the most prevalent. Moreover, the three metabolic pathways with the highest number of DEGs were phenylpropanoid biosynthesis, pentose and glucuronate interconversions, and glycerophospholipid metabolism.

3.4 DEGs in CMs with different colors

To systematically explore the biological functions of DEGs in petal and non-petal parts across different flower colors, we performed KEGG pathway enrichment analysis on the DEGs from each group separately. As shown in Figure 5, the top fifteen pathways enriched by DEGs in each comparison group were selected and visualized in a bubble chart.

3.5 Integrative analysis of CMs with different colors based on metabolomics and transcriptomics

To investigate the genetic regulation of CM flower color, this study conducted a comprehensive analysis of pathways involving DEGs and DAMs, building on prior metabolomic and transcriptomic data. In order to identify pathways representing

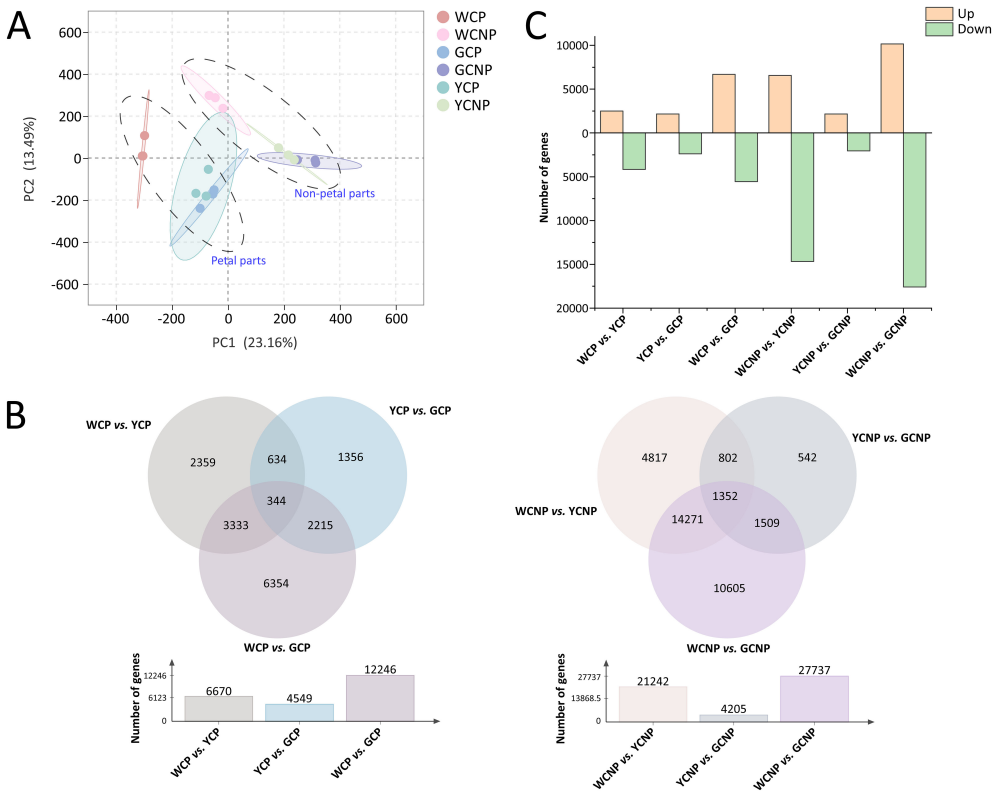

FIGURE 4
(A) Principal component analysis of transcription data from petals and non-petals of *Chrysanthemum morifolium* (CM) in three distinct colors. **(B)** Venn diagram of differentially expressed genes across comparative groups. **(C)** Statistics on the variation trends of differentially expressed genes. Non-petal samples from white, yellow, and gold CM were classified as WCNP, YCNP, and GCNP, respectively, while petal samples from these colors were designated as WCP, YCP, and GCP.

both the transcriptome and metabolome, only metabolic pathways containing at least two DAMs were retained for further analysis, with DEGs included only if located upstream or downstream of the DAMs. The KEGG codes and pathways, along with the numbers and lengths of the DEGs involved in the core pathways, were displayed in Supplementary Table S3.

As shown in Figure 6, glycerophospholipid metabolism and glycerolipid metabolism, both primarily involving lipids, were the primary pathways associated with CM flower color. In petal tissues, the majority of DEGs in WCP exhibited the lowest expression compared to other groups, particularly EPT1, DAD1, MGD, and psd (Figure 6A). However, at the metabolite level, only MGDG, MGMG, and LysoPC (*sn*-1) showed reduced levels in WCP. Additionally, compared to YCP, a greater number of DAMs in GCP displayed a downward trend, including LysoPC (*sn*-2), PC, PE, and LysoPE (*sn*-2).

Likely, in non-petal tissues, a significant number of DEGs, including MGLL, EPT1, LPCAT1_2, and DAD1, showed reduced expression in WCNP (Figure 6B). Unlike the DAMs in petal tissues, the majority of DAMs in WCNPs exhibited significantly lower levels, particularly LysoPC (*sn*-1), LysoPC (*sn*-2), LysoPA (*sn*-1), and LysoPE (*sn*-2). Moreover, a substantial number of DAMs in GCP showed an upward trend compared to YCP, which contrasts with the pattern observed in the petal tissues.

4 Discussion

This study investigated the impact of three distinct colors (white, gold, and yellow) on both petal and non-petal tissues of CM, utilizing an integrated approach combining transcriptomics and metabolomics to uncover the molecular mechanisms and metabolic processes associated with CM coloration. At the metabolic level, 90 DAMs were identified, predominantly flavonoids, flavonoid glycosides, and lipids. Concurrently, 38 significant metabolic pathways were enriched through transcriptomics, primarily related to metabolism, which provided potential mechanistic insights into CM coloration. By integrating metabolomic and transcriptomic data, we identified two central pathways—glycerophospholipid metabolism and glycerolipid metabolism—encompassing various lipid compounds. These pathways emerged as the primary mechanisms through which flower color influenced metabolism and gene expression in CM.

As a plant with a rich cultivation history, CM has evolved a diverse range of flower colors, including white and yellow (Lu et al., 2021a). Flower color plays a pivotal role in shaping the aesthetic appeal and market demand for CM (Wan et al., 2024). Prior research on CM predominantly focused on the differential analysis of petals with notable color variations (Zou et al., 2021; Wu et al., 2023). However, our study expanded this scope, showing

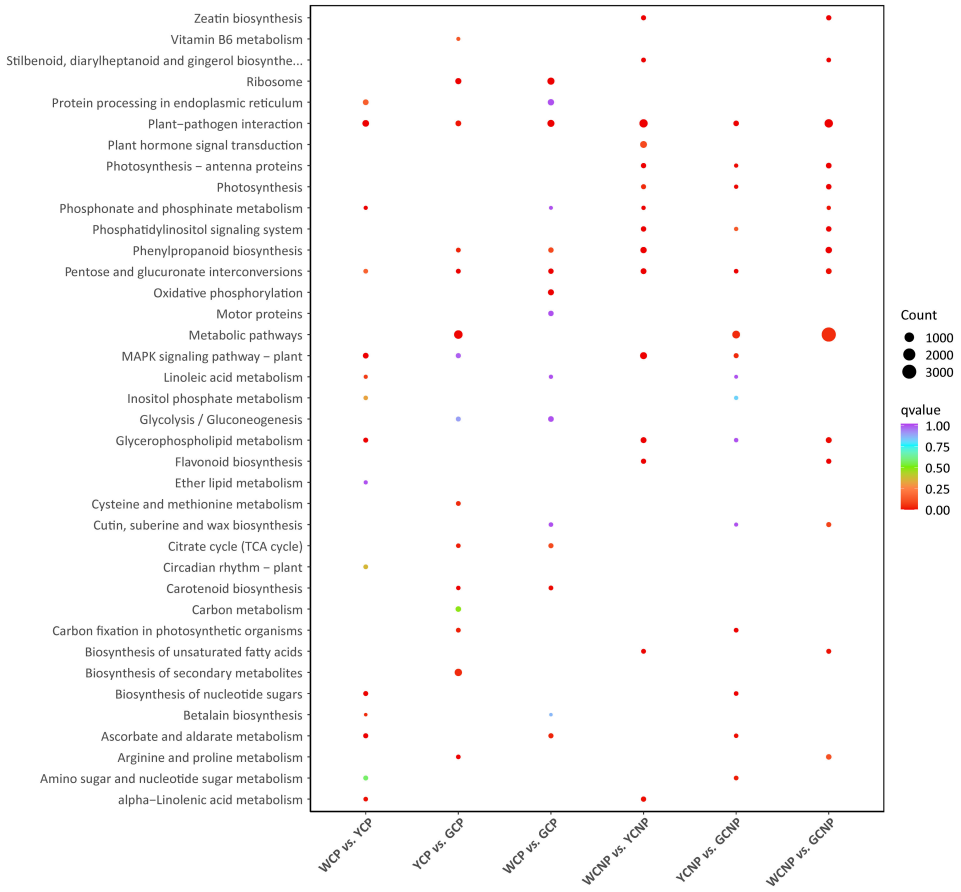

FIGURE 5
Analysis of KEGG pathway enrichment of differentially expressed genes in different comparative groups. Non-petal samples from white, yellow, and gold CM were classified as WCNP, YCNP, and GCNP, respectively, while petal samples from these colors were designated as WCP, YCP, and GCP. Only the top fifteen pathways identified through the enrichment of differentially expressed genes between the two groups were shown.

that varietal differences extend beyond petals to non-petal regions as well. While color variations in non-petal tissues are subtler, our results clearly demonstrated these differences.

Metabolomics, which studies metabolites as the bridge between genotype and phenotype, plays a critical role in revealing plant-environment interactions (Le et al., 2023; Shen et al., 2023). Our analysis revealed that DAMs in different CM color variants were mainly flavonoids, their derivatives, and lipids. Flavonoids and their derivatives are known functional compounds and key pharmacological constituents of CM (Chen et al., 2023; Wu et al., 2024). WCP exhibited higher levels of flavonoid glycosylation compared to YCP and GCP, with a reduction in free flavonoids and an increase in flavonoid glycosides. The decrease in flavonoids and increase in glycosylation were consistent with previous research results on white CM and yellow CM (Ouyang et al., 2022). This is likely because flavonoids contribute to vibrant coloration, offering protection against microorganisms and insects (Zhu et al., 2012; Wan et al., 2019). Lipid components, essential to plant cell composition, regulate environmental adaptability (Li et al., 2023a; Sharma et al., 2023). These distinctions were evident not only in petals but also in non-petal regions, suggesting that flower color may influence the physiological and functional properties of CM beyond the petals. Transcriptomics is a valuable tool in studying the genetic basis of plant diversity and addressing variations within species (Tyagi et al., 2022; Li et al., 2023b). Our transcriptomic analysis indicated that WCP and WCNP tissues exhibited significant differences from gold and yellow CM, with many DEGs showing a downward trend. This supported the findings of our metabolomics analysis.

The integration of transcriptomics and metabolomics provided a robust approach to identifying key pathways across plant species (Bai et al., 2021; Yuan et al., 2022). Our findings revealed that a significant number of DAMs and DEGs were co-enriched within the glycerophospholipid metabolism pathway, predominantly involving lipids. Glycerophospholipids, as essential components of cell membranes, played crucial roles in plant growth, development, and responses to environmental stimuli (Colin and Jaillais, 2020). Prior studies have noted significant differences in lipid composition among color variants, suggesting that lipid accumulation might play a key role in the coloration process (Middleton et al., 2020; Huang et al., 2024). Notably, white CM showed clear differences from yellow and gold CM. Previous studies have also highlighted significant variations in the lipid composition of CM across different varieties (Zhou et al., 2022b).

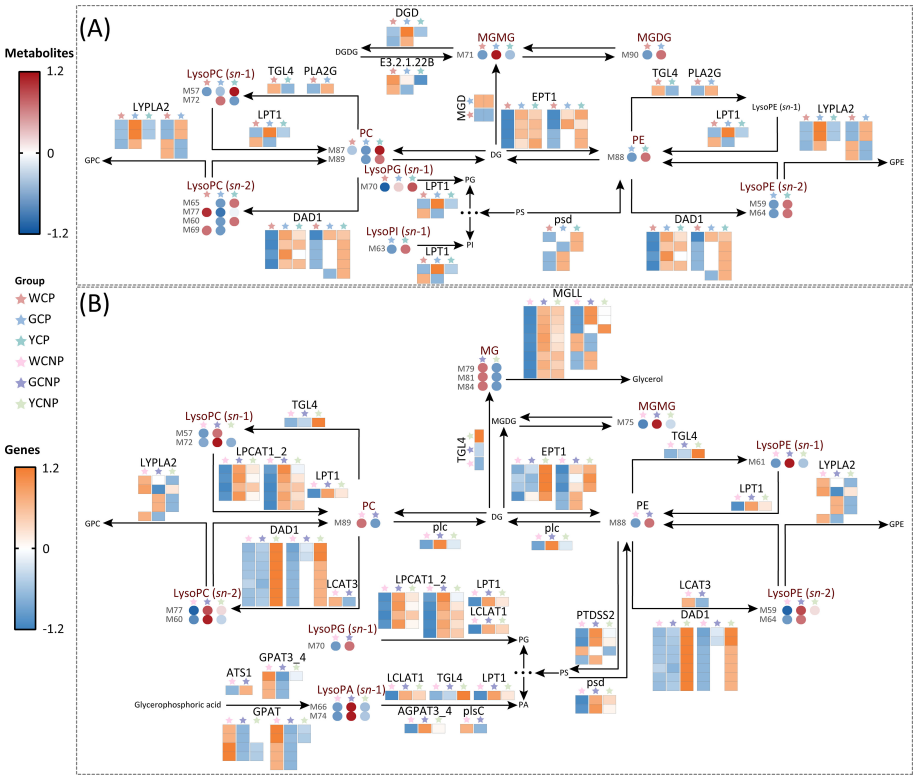

FIGURE 6
(A) Key metabolic pathways in the petals of *Chrysanthemum morifolium* (CM) across three distinct colors. **(B)** Key metabolic pathways in the non-petal tissues of CM from the same three colors. Non-petal samples from white, yellow, and gold CM were classified as WCNP, YCNP, and GCNP, respectively, while petal samples from these colors were designated as WCP, YCP, and GCP. The data used in the drawing were all converted by z-score normalization.

Our analysis further revealed that the expression levels of most DAMs and DEGs in white CM were lower than in yellow and gold CM. This suggests that the yellow and gold coloration of CM was closely associated with the synthesis of lipid metabolites and the expression of related genes. The upregulation of genes related to glycerophospholipid metabolism enhances lipid levels and increases the plant's resilience to environmental stress (Liu et al., 2022). Other studies have shown that environmental changes can alter glycerophospholipid composition, modulating plant responses and potentially leading to color variation (Zhou et al., 2022c; Li et al., 2024). Importantly. phospholipase A1 (DAD1) and acylglycerol lipase (MGLL) were identified as critical enzymes in mediating plant responses to both biotic and abiotic stress (Zhang et al., 2021; Zhao et al., 2024). Additionally, lysophospholipids accumulate in plants under stress conditions, such as freezing, injury, and pathogen infection (Hou et al., 2016). Since carotenoids are synthesized in plant chloroplasts and glycerophospholipid transport also occurred within these organelles, flower color might be regulated through this indirect pathway (Vishnevetsky et al., 1999; Benning, 2008). Therefore, the environmental adaptability of CM likely regulates metabolites and genes involved in glycerophospholipid metabolism, leading to color changes. Furthermore, earlier research indicated that yellow CM exhibited superior adaptability compared to white CM, further supporting our findings (Chumber and Jhanji, 2022).

As early as the Tang Dynasty in China, only yellow varieties of CM were cultivated (Song et al., 2023). Due to their high ornamental value, years of cultivation and refinement expanded their colors to include yellow, gold, white, pink, and more (Su et al., 2019). Understanding the mechanisms behind this coloration had proven highly beneficial in enhancing their economic value. If the identified DAMs and DEGs were validated through further experimental verification, the expression of plant DEGs could be modulated by altering environmental conditions, introducing exogenous stimuli, or applying advanced genetic technologies based on the results. Relevant literature has reported the modification of plant color through methods such as environmental changes, introduction of exogenous interference, and gene silencing (Li et al., 2022a; Yangyang et al., 2022; Zhou et al., 2022c). This modulation would then regulate DAM expression, leading to the desired color. This strategy also represents a key direction for us to further explore through experiments in the future. While the most apparent differences in color lay in the petals, identifying distinctions across the entire plant, including both petals and non-petal parts, provided deeper insights into the coloration process. The integration of transcriptomics and metabolomics in this study allowed us to reveal how metabolic and genetic pathways affect non-petal tissues. These findings suggested that metabolic and genetic changes in response to flower color variation were not limited to

petals, where phenotypes varied more, but may also have affected non-petal tissues. For instance, metabolic pathways involved in lipid metabolism, such as glycerophospholipid and glycerolipid biosynthesis, were found to be active in both petals and non-petal tissues, indicating that flower color regulation not only had a significant impact on the metabolic processes in petal tissues, but also on non-petal tissues.

5 Conclusion

This study employed transcriptomic and metabolomic analyses to elucidate the underlying mechanisms influencing color both in petal and non-petal tissues of CM. Pairwise comparisons of gene expression and metabolite levels across different colors revealed that lipids, flavonoids, and their derivatives were the principal metabolites affected. The glycerophospholipid metabolism, predominantly composed of lipids, and its associated gene variations emerged as crucial factors contributing to color differences in CM. Notably, significant metabolic and genetic distinctions were observed between white CM and their yellow and gold counterparts, extending beyond the petals to the non-petal tissues. Understanding the role of glycerophospholipid metabolism in flower coloration can provide a scientific basis for developing strategies to modulate flower color through environmental or genetic interventions. Furthermore, glycerophospholipids, which play a role in plant stress response and environmental adaptability, could be leveraged to breed CM varieties with improved resilience to abiotic stresses, thus contributing to sustainable cultivation practices. This research establishes a foundation for further exploration of CM coloration pathways and provides a scientific basis for quality control, cultivation, and enhancement strategies for CM.

Data availability statement

The datasets presented in this study can be found in online repositories. The names of the repository/repositories and accession number(s) can be found below: https://www.ncbi.nlm.nih.gov/, https://www.ncbi.nlm.nih.gov/bioproject/PRJNA1162299.

Author contributions

JW: Data curation, Investigation, Writing – original draft, Writing – review & editing. ZZ: Methodology, Supervision, Validation, Writing – review & editing. CS: Data curation, Formal analysis, Writing – review & editing, Writing – original draft. QL: Data curation, Validation, Writing – review & editing. GC: Methodology, Software, Writing – review & editing. GM: Investigation, Validation, Writing – review & editing. LG: Investigation, Software, Writing – original draft. SJ: Data curation, Software, Writing – review & editing. RH: Conceptualization, Resources, Writing – original draft. BH: Conceptualization, Funding acquisition, Investigation, Project administration, Writing – review & editing.

Funding

The author(s) declare financial support was received for the research, authorship, and/or publication of this article. This research was supported by the Joint Fund Project of Hubei Provincial Natural Science Foundation (No. 2023AFD163) and the Traditional Chinese Medicine Research Project of Hubei Provincial Administration of Traditional Chinese Medicine (No. ZY2023M068).

Conflict of interest

The authors declare that the research was conducted in the absence of any commercial or financial relationships that could be construed as a potential conflict of interest.

Publisher's note

Supplementary material

The Supplementary Material for this article can be found online at: https://www.frontiersin.org/articles/10.3389/fpls.2024.1498577/full#supplementary-material

References

Bai, Y., Liu, H., Pan, J., Zhang, S., Guo, Y., Xian, Y., et al. (2021). Transcriptomics and metabolomics changes triggered by inflorescence removal in *Panax notoginseng* (burk.). *Front. Plant Sci.* 12. doi: 10.3389/fpls.2021.761821

Benning, C. (2008). A role for lipid trafficking in chloroplast biogenesis. *Prog. Lipid Res.* 47, 381–389. doi: 10.1016/j.plipres.2008.04.001

Chen, S., Liu, J., Dong, G., Zhang, X., Liu, Y., Sun, W., et al. (2021). Flavonoids and caffeoylquinic acids in *Chrysanthemum morifolium* Ramat flowers: A potentially rich source of bioactive compounds. *Food Chem.* 344, 128733. doi: 10.1016/j.foodchem.2020.128733

Chen, G., Song, C., Jin, S., Li, S., Zhang, Y., Huang, R., et al. (2017). An integrated strategy for establishment of metabolite profile of endogenous lysoglycerophospholipids by two LC-MS/MS platforms. *Talanta* 162, 530–539. doi: 10.1016/j.talanta.2016.10.045

Chen, L., Sun, J., Pan, Z., Lu, Y., Wang, Z., Yang, L., et al. (2023). Analysis of chemical constituents of *Chrysanthemum morifolium* extract and its effect on postprandial lipid metabolism in healthy adults. *Molecules* 28, 579. doi: 10.3390/molecules28020579

Chumber, M., and Jhanji, S. (2022). Morpho-physiological and biochemical characterization of chrysanthemum varieties for early flowering under heat stress. *S. Afr. J. Bot.* 146, 603–613. doi: 10.1016/j.sajb.2021.11.035

Colin, L. A., and Jaillais, Y. (2020). Phospholipids across scales: Lipid patterns and plant development. *Curr. Opin. Plant Biol.* 53, 1–9. doi: 10.1016/j.pbi.2019.08.007

Guo, J., Huang, Z., Sun, J., Cui, X., and Liu, Y. (2021). Research progress and future development trends in medicinal plant transcriptomics. *Front. Plant Sci.* 12. doi: 10.3389/fpls.2021.691838

Han, A.-R., Nam, B., Kim, B.-R., Lee, K.-C., Song, B.-S., Kim, S. H., et al. (2019). Phytochemical composition and antioxidant activities of two different color chrysanthemum flower teas. *Molecules* 24, 329. doi: 10.3390/molecules24020329

Hou, Q., Ufer, G., and Bartels, D. (2016). Lipid signalling in plant responses to abiotic stress. *Plant Cell Environ.* 39, 1029–1048. doi: 10.1111/pce.12666

Huang, F., Yang, P., Bai, S., Liu, Z., Li, J., Huang, J., et al. (2024). Lipids: A noteworthy role in better tea quality. *Food Chem.* 431, 137071. doi: 10.1016/j.foodchem.2023.137071

Le, Q. T. N., Sugi, N., Yamaguchi, M., Hirayama, T., Kobayashi, M., Suzuki, Y., et al. (2023). Morphological and metabolomics profiling of intraspecific *Arabidopsis* hybrids in relation to biomass heterosis. *Sci. Rep.* 13, 9529. doi: 10.1038/s41598-023-36618-y

Lebaka, V. R., Wee, Y.-J., Ye, W., and Korivi, M. (2021). Nutritional composition and bioactive compounds in three different parts of mango fruit. *Int. J. Environ. Res. Public Health* 18, 741. doi: 10.3390/ijerph18020741

Li, X., Cao, J., Zhao, H., Jiang, G., Liu, J., and Yu, Y. (2022a). Ph5GT silencing alters flower color and flavonoids metabolome profile in petunia. *Physiol. Plant* 174, e13795. doi: 10.1111/ppl.13795

Li, X., Li, R., Wang, X., Zhang, X., Xiao, Z., Wang, H., et al. (2023c). Effects and mechanism of action of *Chrysanthemum morifolium* (jinsi huangju) on hyperlipidemia and non-alcoholic fatty liver disease. *Eur. J. Med. Chem.* 255, 115391. doi: 10.1016/j.ejmech.2023.115391

Li, Y., Liu, X., Su, S., Yan, H., Guo, S., Qian, D., et al. (2022b). Evaluation of anti-inflammatory and antioxidant effects of chrysanthemum stem and leaf extract on zebrafish inflammatory bowel disease model. *Molecules* 27, 2114. doi: 10.3390/molecules27072114

Li, S., Nakayama, H., and Sinha, N. R. (2023b). How to utilize comparative transcriptomics to dissect morphological diversity in plants. *Curr. Opin. Plant Biol.* 76, 102474. doi: 10.1016/j.pbi.2023.102474

Li, M., Yu, A., Sun, Y., Hu, Q., Kang, J., Chen, L., et al. (2023a). Lipid composition remodeling and storage lipid conversion play a critical role in salt tolerance in alfalfa (*Medicago sativa* L.) leaves. *Environ. Exp. Bot.* 205, 105144. doi: 10.1016/j.envexpbot.2022.105144

Li, T., Zheng, C., Wu, J., Xu, W., Yan, T., Liu, J., et al. (2024). Comparative lipidomics analysis provides new insights into the metabolic basis of color formation in green cotton fiber. *Plants* 13, 3063. doi: 10.3390/plants13213063

Liu, Y., Lu, C., Zhou, J., Zhou, F., Gui, A., Chu, H., et al. (2024b). *Chrysanthemum morifolium* as a traditional herb: A review of historical development, classification, phytochemistry, pharmacology and application. *J. Ethnopharmacol.* 330, 118198. doi: 10.1016/j.jep.2024.118198

Liu, H., Xin, W., Wang, Y., Zhang, D., Wang, J., Zheng, H., et al. (2022). An integrated analysis of the rice transcriptome and lipidome reveals lipid metabolism plays a central role in rice cold tolerance. *BMC Plant Biol.* 22, 91. doi: 10.1186/s12870-022-03468-1

Liu, C., Zhou, G., Qin, H., Guan, Y., Wang, T., Ni, W., et al. (2024a). Metabolomics combined with physiology and transcriptomics reveal key metabolic pathway responses in apple plants exposure to different selenium concentrations. *J. Hazard. Mater.* 464, 132953. doi: 10.1016/j.jhazmat.2023.132953

Lu, C., Li, Y., Wang, J., Qu, J., Chen, Y., Chen, X., et al. (2021a). Flower color classification and correlation between color space values with pigments in potted multiflora chrysanthemum. *Sci. Hortic.* 283, 110082. doi: 10.1016/j.scienta.2021.110082

Lu, X., Zhao, C., Shi, H., Liao, Y., Xu, F., Du, H., et al. (2021b). Nutrients and bioactives in citrus fruits: Different citrus varieties, fruit parts, and growth stages. *Crit. Rev. Food Sci. Nutr.* 63, 2018–2041. doi: 10.1080/10408398.2021.1969891

Middleton, R., Sinnott-Armstrong, M., Ogawa, Y., Jacucci, G., Moyroud, E., Rudall, P. J., et al. (2020). *Viburnum tinus* fruits use lipids to produce metallic blue structural color. *Curr. Biol.* 30, 3804–3810. doi: 10.1016/j.cub.2020.07.005

Ouyang, H., Fan, Y., Wei, S., Chang, Y., and He, J. (2022). Study on the chemical profile of chrysanthemum (*Chrysanthemum morifolium*) and the evaluation of the similarities and differences between different cultivars. *Chem. Biodivers.* 19, e202200252. doi: 10.1002/cbdv.202200252

Sawada, Y., Sato, M., Okamoto, M., Masuda, J., Yamaki, S., Tamari, M., et al. (2019). Metabolome-based discrimination of chrysanthemum cultivars for the efficient generation of flower color variations in mutation breeding. *Metabolomics* 15, 118. doi: 10.1007/s11306-019-1573-7

Sharma, N., Radha, Kumar, M., Kumari, N., Puri, S., Rais, N., et al. (2023). Phytochemicals, therapeutic benefits and applications of chrysanthemum flower: A review. *Heliyon* 9, e20232. doi: 10.1016/j.heliyon.2023.e20232

Shen, S., Zhan, C., Yang, C., Fernie, A. R., and Luo, J. (2023). Metabolomics-centered mining of plant metabolic diversity and function: Past decade and future perspectives. *Mol. Plant* 16, 43–63. doi: 10.1016/j.molp.2022.09.007

Song, A., Su, J., Wang, H., Zhang, Z., Zhang, X., Van de Peer, Y., et al. (2023). Analyses of a chromosome-scale genome assembly reveal the origin and evolution of cultivated chrysanthemum. *Nat. Commun.* 14, 2021. doi: 10.1038/s41467-023-37730-3

Su, J., Jiang, J., Zhang, F., Liu, Y., Ding, L., Chen, S., et al. (2019). Current achievements and future prospects in the genetic breeding of chrysanthemum: A review. *Hortic. Res.* 6, 109. doi: 10.1038/s41438-019-0193-8

Sun, Y., Shang, L., Zhu, Q.-H., Fan, L., and Guo, L. (2022). Twenty years of plant genome sequencing: Achievements and challenges. *Trends Plant Sci.* 27, 391–401. doi: 10.1016/j.tplants.2021.10.006

Tsugawa, H., Cajka, T., Kind, T., Ma, Y., Higgins, B., Ikeda, K., et al. (2015). MS-DIAL: Data-independent MS/MS deconvolution for comprehensive metabolome analysis. *Nat. Methods* 12, 523–526. doi: 10.1038/nmeth.3393

Tsugawa, H., Kind, T., Nakabayashi, R., Yukihira, D., Tanaka, W., Cajka, T., et al. (2016). Hydrogen rearrangement rules: Computational MS/MS fragmentation and structure elucidation using MS-FINDER software. *Anal. Chem.* 88, 7946–7958. doi: 10.1021/acs.analchem.6b00770

Tsugawa, H., Rai, A., Saito, K., and Nakabayashi, R. (2021). Metabolomics and complementary techniques to investigate the plant phytochemical cosmos. *Nat. Prod. Rep.* 38, 1729–1759. doi: 10.1039/d1np00014d

Tyagi, P., Singh, D., Mathur, S., Singh, A., and Ranjan, R. (2022). Upcoming progress of transcriptomics studies on plants: An overview. *Front. Plant Sci.* 13. doi: 10.3389/fpls.2022.1030890

Vishnevetsky, M., Ovadis, M., and Vainstein, A. (1999). Carotenoid sequestration in plants: The role of carotenoid-associated proteins. *Trends Plant Sci.* 4, 232–235. doi: 10.1016/S1360-1385(99)01414-4

Wan, W., Jia, F., Liu, Z., Sun, W., Zhang, X., Su, J., et al. (2024). Quantitative evaluation and genome-wide association studies of chrysanthemum flower color. *Sci. Hortic.* 338, 113561. doi: 10.1016/j.scienta.2024.113561

Wan, H., Yu, C., Han, Y., Guo, X., Luo, L., Pan, H., et al. (2019). Determination of flavonoids and carotenoids and their contributions to various colors of rose cultivars (*Rosa* spp.). *Front. Plant Sci.* 10. doi: 10.3389/fpls.2019.00123

Wu, D., Wu, Y., Gao, R., Zhang, Y., Zheng, R., Fang, M., et al. (2024). Integrated metabolomics and transcriptomics reveal the key role of flavonoids in the cold tolerance of chrysanthemum. *Int. J. Mol. Sci.* 25, 7589. doi: 10.3390/ijms25147589

Wu, D., Zhuang, F., Wang, J., Gao, R., Zhang, Q., Wang, X., et al. (2023). Metabolomics and transcriptomics revealed a comprehensive understanding of the biochemical and genetic mechanisms underlying the color variations in chrysanthemums. *Metabolites* 13, 742. doi: 10.3390/metabo13060742

Yang, X., Chen, Y., Liu, W., Huang, T., Yang, Y., Mao, Y., et al. (2024). Combined transcriptomics and metabolomics to analyse the response of *Cuminum cyminum* L. under pb stress. *Sci. Total Environ.* 923, 171497. doi: 10.1016/j.scitotenv.2024.171497

Yangyang, Y., Qin, L., Kun, Y., Xiaoyi, W., and Pei, X. (2022). Transcriptomic and metabolomic analyses reveal how girdling promotes leaf color expression in *Acer rubrum* L. *BMC Plant Biol.* 22, 498. doi: 10.1186/s12870-022-03776-6

Yuan, Z., Dong, F., Pang, Z., Fallah, N., Zhou, Y., Li, Z., et al. (2022). Integrated metabolomics and transcriptome analyses unveil pathways involved in sugar content and rind color of two sugarcane varieties. *Front. Plant Sci.* 13. doi: 10.3389/fpls.2022.921536

Zeng, Z., Jin, S., Xiang, X., Yuan, H., Jin, Y., Shi, Q., et al. (2023). Dynamical changes of tea metabolites fermented by *Aspergillus cristatus*, *Aspergillus neoniger* and mixed fungi: A temporal clustering strategy for untargeted metabolomics. *Food Res. Int.* 170, 112992. doi: 10.1016/j.foodres.2023.112992

Zeng, Z., Song, C., Hu, X., Zhu, X., Li, Y., Ren, J., et al. (2024). Constituent-taste relationship of Kuding tea fermented by *Aspergillus neoniger* and *Aspergillus cristatus*: Unveiling taste characteristics through untargeted metabolomics. *Food Bioscience* 62, 105027. doi: 10.1016/j.fbio.2024.105027

Zhang, X., Xu, Z., Yu, X., Zhao, L., Zhao, M., Han, X., et al. (2019). Identification of Two Novel R2R3-MYB Transcription factors, PsMYB114L and PsMYB12L, Related to Anthocyanin Biosynthesis in Paeonia suffruticosa. *Int. J. Mol. Sci.* 20, 1055. doi: 10.3390/ijms20051055

Zhang, H., Zhang, Y., Xu, N., Rui, C., Fan, Y., Wang, J., et al. (2021). Genome-wide expression analysis of phospholipase A1 (PLA1) gene family suggests phospholipase A1-32 gene responding to abiotic stresses in cotton. *Int. J. Biol. Macromol.* 192, 1058–1074. doi: 10.1016/j.ijbiomac.2021.10.038

Zhao, Y., Li, S., Wu, J., Liu, H., Wang, P., and Xu, L. (2024). Insights into membrane lipids modification in barley leaves as an adaptation mechanism to cold stress. *Plant Growth Regul.* 103, 369–388. doi: 10.1007/s10725-023-01114-w

Zhou, L., Cai, Y., Yang, L., Zou, Z., Zhu, J., and Zhang, Y. (2022a). Comparative metabolomics analysis of stigmas and petals in Chinese saffron (*Crocus sativus*) by widely targeted metabolomics. *Plants* 11, 2427. doi: 10.3390/plants11182427

Zhou, Z., Chen, M., Wu, Q., Zeng, W., Chen, Z., and Sun, W. (2022c). Combined analysis of lipidomics and transcriptomics revealed the key pathways and genes of lipids in light-sensitive albino tea plant (*Camellia sinensis* cv. *Baijiguan*). *Front. Plant Sci.* 13. doi: 10.3389/fpls.2022.1035119

Zhou, L., Ma, Y., Yao, J., Zhang, M., Fu, H., Yang, J., et al. (2022b). Discrimination of chrysanthemum varieties using lipidomics based on UHPLC-HR-AM/MS/MS. *J. Sci. Food Agric.* 103, 837–845. doi: 10.1002/jsfa.12195

Zhu, M., Zheng, X., Shu, Q., Li, H., Zhong, P., Zhang, H., et al. (2012). Relationship between the composition of flavonoids and flower colors variation in tropical water lily (nymphaea) cultivars. *PloS One* 7, e34335. doi: 10.1371/journal.pone.0034335

Zou, Q., Wang, T., Guo, Q., Yang, F., Chen, J., and Zhang, W. (2021). Combined metabolomic and transcriptomic analysis reveals redirection of the phenylpropanoid metabolic flux in different colored medicinal *Chrysanthemum morifolium*. *Ind. Crops Prod.* 164, 113343. doi: 10.1016/j.indcrop.2021.113343

frontiers | Frontiers in Plant Science

TYPE Original Research
PUBLISHED 28 January 2025
DOI 10.3389/fpls.2025.1509126

OPEN ACCESS

EDITED BY
Marta Sousa Silva,
University of Lisbon, Portugal

REVIEWED BY
Jiaping Zhao,
Chinese Academy of Forestry, China
Andrey Stoyanov Marchev,
Bulgarian Academy of Sciences, Bulgaria

*CORRESPONDENCE
Thijs V. Bierman
t.v.bierman@biology.leidenuniv.nl

RECEIVED 10 October 2024
ACCEPTED 10 January 2025
PUBLISHED 28 January 2025

CITATION
Bierman TV, Fernandes HP, Choi YH, Seo S, Vrieling K, Macel M, Knegt B, Kodger TE, van Zwieten R, Klinkhamer PGL and Bezemer TM (2025) Sprayable solutions containing sticky rice oil droplets reduce western flower thrips damage and induce changes in *Chrysanthemum* leaf chemistry. *Front. Plant Sci.* 16:1509126. doi: 10.3389/fpls.2025.1509126

Sprayable solutions containing sticky rice oil droplets reduce western flower thrips damage and induce changes in *Chrysanthemum* leaf chemistry

Thijs V. Bierman[1*], Hocelayne P. Fernandes[1,2], Young H. Choi[2], Sumin Seo[2], Klaas Vrieling[1], Mirka Macel[3], Bram Knegt[3], Thomas E. Kodger[4], Ralph van Zwieten[4], Peter G. L. Klinkhamer[2] and T. Martijn Bezemer[1]

[1]Above-Belowground Interactions, Institute of Biology Leiden, Leiden, Netherlands, [2]Natural Products Laboratory, Institute of Biology Leiden, Leiden, Netherlands, [3]Weerbare Planten, Aeres University of Applied Sciences, Almere, Netherlands, [4]Physical Chemistry and Soft Matter, Agrotechnology & Food Sciences Group, Wageningen University & Research, Wageningen, Netherlands

Thrips are one of the most challenging pests in agricultural crops, including *Chrysanthemum*. In this study we tested via two plant assays whether solutions containing sticky rice germ oil (RGO) droplets could effectively trap thrips and lower thrips damage on *Chrysanthemum*. In the first assay, we additionally assessed the metabolomic effects of these RGO droplet sprays and thrips presence on plant chemistry via ^{1}H NMR and headspace GC-MS on multiple timepoints to investigate which plant metabolites were affected by spraying and their potential relation to plant resistance against thrips. In the second assay, we tested the individual RGO solution constituents against thrips. Our results suggested that the adhesive RGO droplets were not effective as a physical trap as only three out of 600 adult thrips were caught at the achieved coverage. However, average thrips damage was still reduced up to 50% and no negative effects on plant growth were observed up to 25 days. Results from the second plant assay indicated that the individual constituents of the solution containing RGO droplets may have direct effects against thrips. Metabolomics analysis of sprayed leaves via headspace GC-MS and ^{1}H NMR indicated that fatty acids and several volatile compounds such as 4(10)-thujene (sabinene), eucalyptol, *cis*-4-thujanol, and isocaryophyllene were highest on day 10, while sucrose, malic acid, *o*-Cymene, and 3-Methyl-2-butenoic acid were highest on day 25. Plants with thrips showed higher flavonoid, carbohydrate and glutamine acetic acid levels, and lower fatty acids and malic acid levels. RGO application increased the levels of fatty acids and alcohols present on top of and inside the *Chrysanthemum* leaves, while decreasing the concentrations of volatile compounds such as eucalyptol, chrysanthenone and eugenol in the *Chrysanthemum* leaves. Most interestingly, the thrips effect on the plant metabolome was no longer visible in RGO treated plants at the later harvesttime, suggesting that RGO application may

10.3389/fpls.2025.1509126

overrule or prevent the metabolomic effects of thrips infestation. In conclusion, our study provides new information on how the application of a new plant-based plant protection product affects insect herbivores and alters crop phytochemistry for improved herbivore resistance.

KEYWORDS

thrips, *Chrysanthemum*, integrated pest management, rice oil, metabolomics, GC-MS, 1H NMR

Introduction

Frankliniella occidentalis (Pergande), or western flower thrips, is a globally occurring pest of many horticultural crops and ornamentals (Reitz and Funderburk, 2012), including *Chrysanthemum* (*Chrysanthemum* × *morifolium*). Thrips cause damage directly by sucking the contents of plant cells, which can lead to stunted growth and overall reduced biomass, and cause damage indirectly via the transmission of plant viruses (De Jager et al., 1995). Due to their small size, thigmotactic behavior, rapid reproduction, and resistance to pesticides, thrips are a difficult pest to manage (Reitz, 2009). Billions of dollars' worth of yield are lost annually to thrips and plant viruses in the USA alone (Nilon et al., 2021; Reitz et al., 2008). Although chemical pesticides have been vital to manage thrips and other pests (Reitz and Funderburk, 2012), their environmental impact and the increasing ability of pests to resist them has led to the consensus that pesticide use is unsustainable (Cloyd, 2016). As such, alternative pest control methods are urgently needed to expand the arsenal that growers use to control thrips and other pests.

Recently, we introduced a new way to utilize plant-derived oils for pest control: sprayable solutions containing adhesive droplets made from oxidized plant oils for trapping small arthropods (Bierman et al., 2024; van Zwieten et al., 2024). These sticky droplets can be made from different oils, including rice germ oil (RGO) which is often seen as a waste material. By spraying plants with sticky oil droplets, we may provide them with a mechanical defensive function, similar to how glandular trichomes that secrete sticky substances help to protect a large variety of vascular plants against herbivore attackers (LoPresti et al., 2015). So far, we only tested in Petri-dish assays if the sticky droplets could catch thrips and reduce their damage. In this study, we took the next logical step and investigated whether spraying *Chrysanthemum* plants with the sticky rice germ oil droplets could be an effective way to trap thrips and reduce thrips damage to full plants.

In addition to acting against pests directly, the application of plant-derived oils may affect the physiology of the plants that are sprayed. Plant-derived oils can cause phytotoxic responses, can affect plant growth, nutrient content, expression of plant compounds that are toxic to herbivores, and can induce the emission of herbivore repellent or predator attractive volatiles (De Almeida et al., 2010; Kesraoui et al., 2022; Verdeguer et al., 2020). The precise effects of plant-derived oils on plant physiology may depend on several factors, including the type of compound, its dose, the time after application, and the physiological age of the plant (Leiss et al., 2011; Razzaq et al., 2019).

Herbivores, including thrips, can also affect plant physiology, for example via the induction of chemical plant defense pathways such as the jasmonic acid and salicylic acid pathways (Escobar-Bravo et al., 2017). Metabolites induced by these pathways may be toxic or repellent to herbivores, or attract herbivore predators, which both may affect the feeding behavior and fitness of the herbivores (Dicke and Baldwin, 2010; Kessler and Baldwin, 2002; Walling, 2000). Combined with resistance screening, metabolomics approaches (advanced chemical profiling techniques) provide a useful tool to understand the relationship between plant chemistry and insect performance (Kim et al., 2011). For example, Mežaka et al. (2023) used GC-MS to investigate the phytotoxic effects of aqueous extracts of *Carum carvi* (caraway) seed distillation by-products and found that application of these compounds decreased certain green-leaf volatiles emitted by *Cucumis sativus* (cucumber) up to ten days after application. Using UHPLC-MS, Macel et al. (2019) found that monomeric and dimeric acyclic diterpene glycosides were linked to thrips resistance in *Capsicum* spp. (pepper). Leiss et al. (2009b) identified the phenylpropanoids chlorogenic acid and feruloylquinic acid as a thrips resistance factor in *Chrysanthemum* leaves via ^{1}H NMR.

For many crops, it is still unknown which metabolites are related to increased herbivore resistance and in what way the application of pest control products and the presence of pests may interact to alter the concentrations of these metabolites over time. Therefore, in addition to assessing direct effects on thrips, we also investigated the effects of the application of our solutions containing sticky droplets on the plant metabolome, both in absence and presence of thrips at multiple timepoints. Two full-plant assays were performed with *Chrysanthemum* where plants were sprayed with solutions containing adhesive droplets or other control solutions and infested with thrips or not. In the first assay, thrips damage and plant growth were measured after ten and twenty-five days. The metabolomes of RGO sprayed plants and of control plants (sprayed with water) were analyzed using ^{1}H NMR and headspace GC-MS. In the second assay measurements were done after twenty-five days and all plants were infested with thrips. Our main research questions were: (1) Do solutions that contain adhesive droplets made from plant-based oils

that are sprayed on plants catch thrips and reduce thrips damage? (2) Does spraying of solutions containing sticky oil droplets affect plant growth? (3) In what way do the solutions containing sticky droplets affect the metabolome of *Chrysanthemum* and (4) Are there interactions between RGO spraying, harvesttime, and thrips presence to shape the plant metabolome? Before new crop protection products are applied on a large scale, knowledge on their effects on target pests, plant growth, and plant chemistry are essential to understand their mode of action and infer whether these products are suitable for commercial use.

Materials and methods

RGO solution

A sprayable solution containing adhesive RGO droplets was produced at Wageningen University & Research as described by van Zwieten et al. (2024). The solution contained 95.75 wt% tap water, 1.25 wt% oxidized RGO (type: R360) droplets, 1 wt% F-108 (a surfactant), and 2 wt% alginate. This RGO solution and a water control were tested in plant assay 1. The RGO solution and four control solutions: a 1% F-108 solution, 2% alginate solution, and a solution containing both 1% F-108 and 2% alginate, and a water control, were tested in plant assay 2.

Insects

A colony of *Frankliniella occidentalis* (obtained from a greenhouse in the Netherlands) was maintained in plastic cages (60×60×40 cm) at Leiden University for over 15 years on *Chrysanthemum* cut flowers (cv. Baltica Yellow) as described by Bierman et al. (2024). Climate room conditions were 25°C, 60% RH (70% inside cages) and 16-8 light-dark photoperiod (fluorescent TL-light).

Plants and growth conditions

Ten-day old *Chrysanthemum* × *morifolium* (cv. Baltica White) cuttings, rooted in small peat blocks (source: Deliflor B.V., Maasdijk, The Netherlands) were transplanted to 2.2 liter plastic pots filled with a mixture of 3:1 (v/v) autoclaved potting soil to vermiculite, with 2.5 g/l osmocote fertilizer pellets. Plants were grown in a climate room at 25°C day, 23°C night temperature, 70% RH and a 8-16 light-dark photoperiod (6:00am-10:00pm, fluorescent TL-light, 15,340 lm m^{-2}). When plants were 25 days old, plant assays were performed at Leiden University under the same climate conditions as during the plant growth phase.

Plant assay 1

Eighty *Chrysanthemum* plants of similar size (25 days old, 10 unfolded leaves, 14.3 cm [SD: 0.99] shoot length) were selected and divided into eight groups of ten plants. 40 plants were sprayed with 10 ml water per plant and 40 plants were sprayed with 10 ml solution containing RGO droplets using a paint spray gun (Einhell, Art. No. 41.330.00). Spraying was done from 20 cm above each plant under 1.4 bar airflow pressure. The spray pattern control valve was opened a quarter rotation. The flow control valve was opened two full rotations. Plant coverage was estimated from pictures of several leaves of five randomly chosen plants using ImageJ-Fiji V2.9.0 by counting adhesive droplets and by estimating the percentage leaf area covered (Supplementary Figure S1). After 30 minutes of drying, plants were placed on felt circles located on plastic dishes (25cm diameter) and covered with thrips-proof cages made of transparent plastic cylinders (50 cm height, 22.5 cm diameter) that were closed off at the top with lids made of plastic rings with 120 µm thrips-proof nylon mesh (Leiss et al., 2009a). Felt circles were kept moist during the experiment to water the plants and to prevent thrips from escaping. Per spray treatment, 20 plants were infested with 20 female adult *F. occidentalis* at the base of each plant. One group of ten plants of each combination of spray treatment and thrips was harvested after 10 days, the other ten plants after 25 days. The cages with plants were placed in the climate room in ten blocks containing one plant of each treatment and harvesttime (Supplementary Figures S2A, B).

At harvest, the number of thrips caught in adhesive droplets, total thrips damage and necrosis damage (brown spots) on all leaves were scored in mm^2 and the shoot length (cm) and number of leaves were recorded. Then, for each plant a stack of sprayed leaves, leaf number 2 to 9 (counted from the bottom and up) was sampled in aluminum foil, flash frozen between 7 to 9 pm and stored at -80°C until freeze drying. After freeze drying, samples were ground into a fine powder using 2 ml Eppendorf tubes with 5 tiny iron balls and a Tissuelizer II Bead Mill (Qiagen, Hilden, Germany). The leaf powder would be used for ^{1}H NMR and headspace (HS)- GC-MS analysis. The remainder of the shoot of each plant was oven-dried at 60°C to obtain the dry weight (g).

Plant assay 2

Five groups of ten plants (25 days old, 11 [SD: 0.83] unfolded leaves, 15.5 cm [SD: 1.57] shoot length) were sprayed with 10 ml of one of five treatments: (1) water, (2) 1% F-108 solution, (3) 2% alginate solution, (4) 1% F-108 + 2% alginate solution, or (5) the full solution containing adhesive RGO droplets. Coverage (no. droplets and % leaf area covered) was estimated as before. Each plant was placed in a thrips cage, infested with 20 female adult thrips, and placed in the climate room in ten blocks with one plant per treatment. After 25 days, the number of thrips caught in adhesive droplets, total thrips damage (both on the adaxial and abaxial leaf side) (Supplementary Figures S3A, B) and necrosis damage (adaxial and abaxial), shoot length, number of leaves, and shoot total dry weight were recorded.

Analysis of plant growth and thrips performance

RStudio (v. 4.3.1) was used for data analysis. p values < 0.05 were considered significant. Assumptions for normality and

homogeneity of variance were tested using Shapiro-Wilk tests and Levene's tests. For plant assay 1: Total thrips damage was ln-transformed to meet normality assumptions, and a two-way ANOVA was used with spraying treatment and harvesttime as factors. Shoot length and dry weight were analyzed using three-way ANOVAs with spraying treatment, thrips presence (thrips or no thrips) and harvesttime as factors. Significant interactions of two-way and three-way ANOVAs were followed by simple effects analysis via pairwise comparison of marginal means, corrected for family wise error using Bonferroni adjustment. For plant assay 2, total thrips damage, the proportion of total adaxial leaf damage to total leaf damage per plant, shoot length, and shoot dry weight were analyzed using one-way ANOVAs, followed by pairwise comparison using Tukey tests.

^{1}H NMR analysis

The samples were prepared for ^{1}H NMR analysis following the protocol described by Kim et al. (2010) with some modifications as follows. Per sample (five replicates), thirty mg of freeze-dried and ground leaf material was extracted by 15 minutes of ultrasonication in 1 ml of CD_3OD-KH_2PO_4 buffer in D_2O (pH 6.0, 1:1, v/v) containing 0.29 mM TMSP-d_4) as an internal standard. The resulting extracts were centrifuged at 13,000 rpm and 300 µl of the supernatant was transferred to 3 mm NMR tubes. ^{1}H NMR measurements were performed on a Bruker Avance-III 600 MHz standard bore liquid-state NMR spectrometer with operating frequency of ^{1}H resonating at 600.13 MHz. A cryoprobe of type TCI H&F/C/N-D with Z gradient was used. The temperature was kept constant at 298 K. For internal locking, CD_3OD was used. For each proton measurement, a 30-degree pulse of 2.64 msec at 5.5 W power with a fid resolution of 0.36 Hz, 64 scans with a relaxation delay of 1.5 secs, and acquisition time of 2.7 sec, in total taking 5 min to complete the measurement. The water signal was suppressed using a pre-saturation method and low-power selective irradiation at 0.3 Hz H_2O at 4.87 ppm. Time domain data was transformed to the frequency domain by Fourier transformation with a window function of exponential function and a line broadening parameter set to 0.3 Hz for smoothening. The generated spectrums were manually phased, baseline corrected and calibrated to TMSP-d_4 at 0.00 ppm or HMDSO at 0.06 ppm using TOPSPIN V. 3.2 software (Bruker). The NMR spectra were bucketed using AMIX 3.9.12 (Bruker Biospin GmbH Rheinstetten, Germany). The bucketed data was obtained by integration of the spectra at 0.04 ppm intervals. The peak intensity of individual peaks was scaled to the total intensity recorded from δ 0.30 to δ 10.02. Due to the residual signals of HMDSO and CH_3OH-d_4, the regions δ 4.7 – δ 5.0 and δ 3.28 – δ 3.34 were excluded from the analysis.

Headspace GC-MS analysis

Headspace-GC-MS measurements (five replicates) were performed using a 7890A gas chromatograph equipped with a 7693 automatic sampler and a 5975C single-quadrupole mass detector (Agilent, Folsom, CA, USA). Volatile compounds were separated on a DB-5 column: 30 m × 0.25 mm, 0.25 µm film (J&W Scientific, Folsom, CS, USA), using helium (99.9% purity) as a carrier gas at a flow rate of 1.6 ml/min. Freeze-dried, ground and homogenized leaf material (100 mg per sample) was placed into 20 ml glass headspace vials. Each vial was incubated at 100°C for 30 minutes, then 500 µl headspace was sampled and injected (split mode 5:1, 8 ml/min flow) into the gas chromatograph. The oven temperature was programmed starting at 70°C, held for 1 minute, then increased at 3°C/min to 100°C, re-increased to 220°C at 7°C/min, and finally increased at 14°C/min to 300°C, held for 3 min. The ionization energy in EI mode was 70 eV, and the mass scan range was set to 50-550 m/z. Tridecane (500 ng/ml) was used as an internal standard. The obtained HS-GC-MS data files of the samples were converted to.mzml format using the MSConvert tool from the Proteowizard software suite. The auto-deconvolution of GC-MS data and multivariate analysis were executed according to the workflow outlined by the Global Natural Product Social Molecular Networking (GNPS) platform (Global Natural Product Social Molecular Networking, 2024). The detected peaks were identified by comparison of their retention times and ion spectra with those listed in Atomic Spectra Database, NIST 14 (libscore cutoff value of 70). The data was then processed using MassHunter (B.07, Agilent). The obtained GC-MS data were processed by GNPS.

Multivariate data analysis of HS-GC-MS and ^{1}H NMR data

Principal component analysis (PCA) and orthogonal projection to latent structures discriminant analysis (OPLS-DA) were performed using SIMCA P (version 18.1, Sartorius). PCA was used to analyze the inherent variation within the datasets, with all data subjected to Pareto-scaling. OPLS-DA models were then used to assess variation in metabolite profiles between spray treatments and to discern distinct chemical compounds. The quality of the OPLS-DA models was estimated by R^2X and Q^2 values. Q^2 values were obtained from permutation tests (100 permutations). R^2X indicated the model's fitness and was defined as the proportional variance, whereas Q^2 was defined as the predictable variance (Villa-Ruano et al., 2019). S-plots were used to identify possible biomarkers.

Results

Effect of RGO application on thrips performance and plant growth over time

Plant assay 1: RGO sprayed plants showed lower mean thrips damage than water sprayed plants, both after ten days ($F_{1,\ 36}$ = 11.97, $p < 0.01$) and 25 days ($F_{1,\ 36}$ = 49.12, $p < 0.01$; Figure 1A). Furthermore, thrips damage on water sprayed plants increased faster over time than on RGO sprayed plants ($F_{1,\ 36}$ = 6.30, p = 0.02). However, only one adult thrips was observed to be stuck in an adhesive droplet. Coverage with adhesive droplets was also rather low with on average 159 (SD: 13) droplets per leaf (108 with area

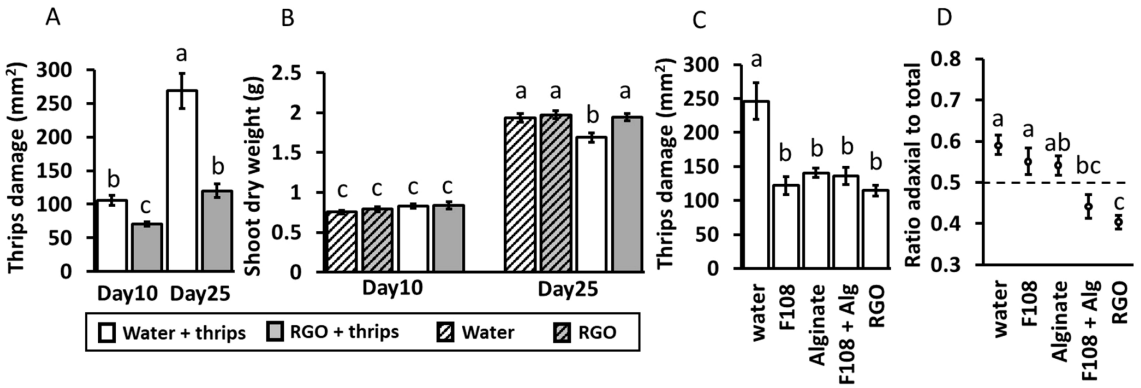

FIGURE 1
Plant assay 1 (n = 10): mean (± 1SE) total thrips damage (mm^2) per plant **(A)**, and mean shoot dry weight (g) **(B)** of *Chrysanthemum* plants sprayed with water or solution containing adhesive RGO droplets. Plants were harvested after 10 or 25 days and were infested with thrips or not infested. Plant assay 2: mean (± 1SE) total thrips damage (mm^2) **(C)**, and proportion of adaxial leaf damage to total leaf damage **(D)** after 25 days with thrips on leaves of *Chrysanthemum* plants sprayed with: water, 1% F-108 solution, 2% alginate solution, 1% F-108 + 2% alginate (F108 + Alg) solution, or an F-108 + alginate solution containing adhesive RGO droplets (RGO). Different letters indicate significant differences at $p < 0.05$ between treatment groups as found by two-way ANOVA (for **A**), three-way ANOVA (for **B**), both followed by comparison of marginal means or one-way ANOVAs followed by Tukey tests (for **C, D**).

0.1-0.5 mm^2, 44 of 0.5-1 mm^2, 7 of 1 mm^2 or above) or 1.74% (SD: 0.1) of the total leaf area. The leaf surface also shimmered slightly and small white flakes were visible, indicating that some of the other compounds in the sprayable solution were also present on the leaf surface (Supplementary Figures S4A, B). Observation via a binocular confirmed droplets of presumably less oxidized rice germ oil were also present in the sprayable RGO solutions, likely being responsible for the shimmer (Supplementary Figures S5A, B).

As expected, shoot length (Supplementary Figure S6) was higher on day 25 than on day 10 ($F_{1, 72} = 1601.64$, $p < 0.01$). Spray treatment did not affect mean shoot length ($F_{1, 72} = 2.26$, $p = 0.14$). In general, plants with thrips had a lower shoot length ($F_{1, 72} = 44.67$, $p < 0.01$) and thrips presence reduced shoot length more on day 25 than on day 10 (thrips × day interaction: $F_{1, 72} = 9.60$, $p < 0.01$). Other two-way interactions and three-way interactions were not significant for shoot length. Dry weight (Figure 1B) was also higher for plants on day 25 than on day 10 ($F_{1, 72} = 1266.26$, $p < 0.01$). However, significant interactions were detected between thrips presence and harvesttime ($F_{1, 72} = 10.74$, $p < 0.01$) and between spray treatment and harvesttime ($F_{1, 72} = 4.09$, $p = 0.047$). Pairwise comparisons of marginal means indicated that, only for day 25, for plants infested with thrips, dry weight was less in water-treated plants compared to plants treated with solution containing RGO droplets ($F_{1, 72} = 17.77$, $p < 0.01$). For plants without thrips, no difference in treatments was visible on day 25 ($F_{1, 72} = 0.42$, $p = 0.52$) and the dry weight of these plants was similar to that of plants treated with RGO solution and infested with thrips.

Plant assay 2: Only two thrips were found stuck in adhesive droplets. Coverage with adhesive droplets was estimated at around 199 (SD: 15) droplets per leaf (141 with area 0.1-0.5 mm^2, 46 of 0.5-1 mm^2, 12 of 1 mm^2 or above) or 3.3% (SD: 0.2) of the total leaf area. Thrips damage was higher in the water treatment than in all other treatments ($F_{4, 45} = 12.23$, $p < 0.01$; Figure 1C). The proportion of adaxial to total damage was highest in the water treatment, intermediate in the F-108, alginate and F-108 + alginate treatments, and lowest in the RGO treatment ($F_{4, 45} = 9.95$, $p < 0.01$; Figure 1D). No differences in mean shoot length ($F_{4, 45} = 0.66$, $p = 0.62$, Supplementary Figure S7A) or shoot dry weight ($F_{4, 45} = 1.10$, $p = 0.37$, Supplementary Figure S7B) were found between treatments.

Effect of RGO droplets, harvesttime, and thrips on the metabolome of *Chrysanthemum* leaves as detected by ^{1}H NMR

In this study, we used ^{1}H NMR to examine the metabolite profiles of *Chrysanthemum* leaves of RGO sprayed and control plants. As shown in Supplementary Figure S8, major detected compounds included flavonoids (such as apigenin glycosides, 5',7',3',4'-tetrahydroxy flavanone glycosides, epi- or gallocatechin gallate), carbohydrates (glucose, fructose, stachyose, and sucrose), organic acids (including formic-, fumaric-, malic-, and acetic acid), amines (choline, betaine), amino acids (alanine, glutamine), triterpenoids, and steroids.

After initial visual inspection of the ^{1}H NMR spectra, multivariate data analysis was conducted. The spectra were binned at intervals of 0.04 ppm, yielding 243 variables. Principal component analysis (PCA) was initially applied to the binned data to assess the primary factors influencing the *Chrysanthemum* leaf metabolome. As depicted in Figure 2A, the rice germ oil (RGO) treatment had the most significant impact on the metabolome, while other factors, such as harvesttime (10 vs. 25 days) and thrips infestation, were less prominent in the major principal components (PC1 and PC2).

To further investigate these minor factors, orthogonal partial least squares-discriminant analysis (OPLS-DA) was applied. The data were classified into three groups: (1) water vs. RGO treatment (Figure 2B), (2) control vs. thrips infestation (Figure 2C), and (3) harvesttime (10 vs. 25 days) (Figure 2D). The OPLS-DA results confirmed that the RGO treatment had a distinct impact on the metabolome, with a high Q^2 value of 0.97, while harvesttime also had a significant effect ($Q^2 = 0.45$).

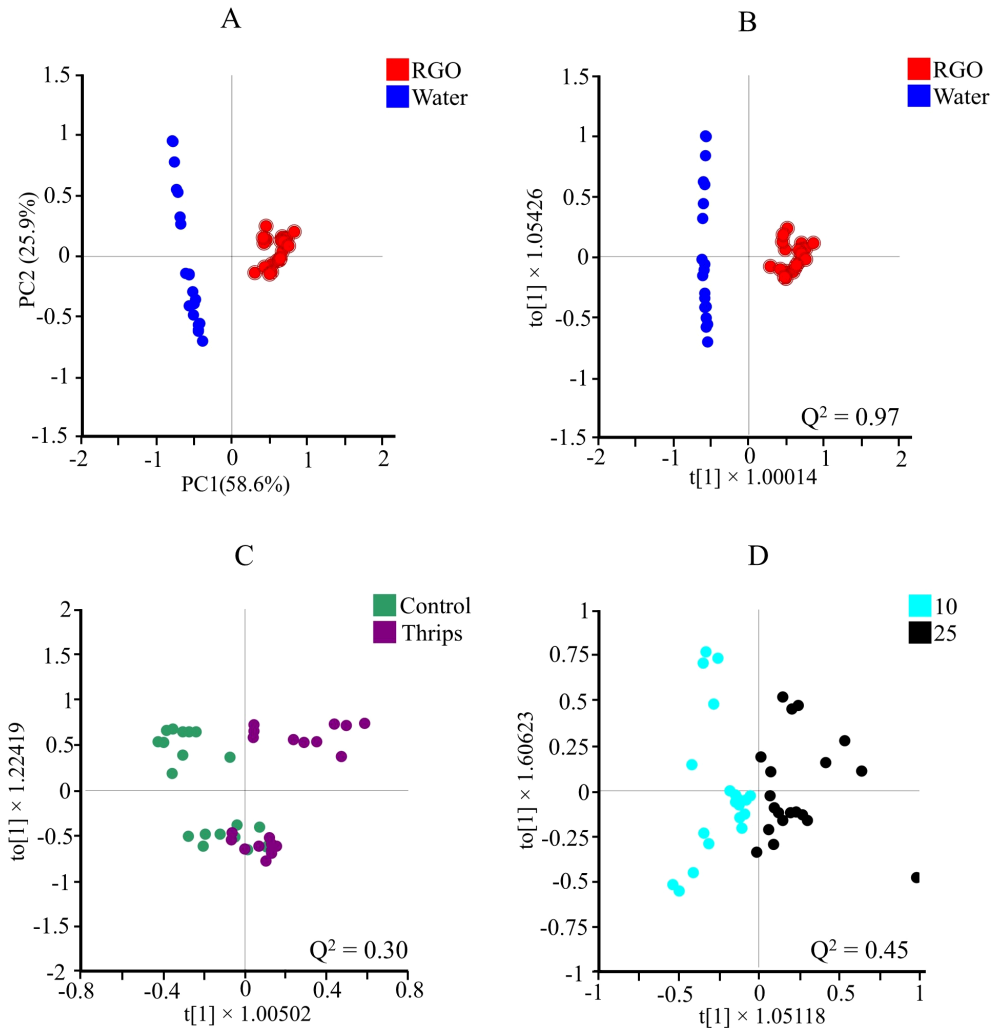

FIGURE 2
Score plots of principal component analysis (PCA, n = 10) **(A)**, and orthogonal partial least squares discriminant analysis (OPLS-DA) obtained from ^{1}H NMR data using two classes of: RGO and water treated **(B)**, control and thrips treated **(C)**, and two different harvesting days after treatment (10 and 25 days after treatment) **(D)** of *Chrysanthemum* leaves. For each of OPLS-DA, Q^2 values are depicted for each score plot.

In contrast, thrips infestation showed only a marginal separation with a Q^2 value of 0.30 (Figure 2C).

To identify the specific metabolic changes associated with each factor, S-plots from the OPLS-DA models were examined (Figure 3). The RGO treatment was associated with higher levels of sugar alcohols assumed by the increase signal in the range of δ 3.5 – 3.7 and oxygenated fatty alcohols and acids likely present on top or inside of the leaves (Figure 3A). Thrips infestation led to increased levels of flavonoids, sucrose, glucose, glutamine, and acetic acid, but decreased levels of fatty acids and malic acid (Figure 3B). Regarding the harvesttime, older leaves (25 days) exhibited higher levels of sucrose and malic acid, while fatty acid levels were lower (Figure 3C).

Finally, to assess the potential interactions between RGO treatment and other factors, separate OPLS-DA models were constructed for water-treated and RGO-treated samples (Supplementary Figure S9). In RGO-treated leaves, the separation by harvesttime was more pronounced, while the effect of thrips infestation on the metabolome was reduced with a Q^2 value of 0.14 (Supplementary Figure S9).

Effect of RGO droplets, harvesttime, and thrips on the volatile headspace of *Chrysanthemum* leaves as detected by headspace GC-MS

The use of ^{1}H NMR with CD_3OD-KH^2PO^4 buffer extraction effectively identified a variety of metabolite groups influenced by different factors. However, some volatile compounds were not detected. To address this, headspace GC-MS was applied to the same set of *Chrysanthemum* leaves. A typical headspace GC-MS chromatogram is shown in Supplementary Figure 10. The resulting data, processed through GNPS for multivariate analysis, yielded 853 variables. The separation between groups in the GC-MS data (Figures 4A–C) was consistent with the results from ^{1}H NMR analysis. A notable difference, however, was that in the GC-MS analysis, the primary factor influencing the metabolome was harvesttime, whereas in ^{1}H NMR, RGO treatment was the dominant factor. Both methods revealed that thrips infestation

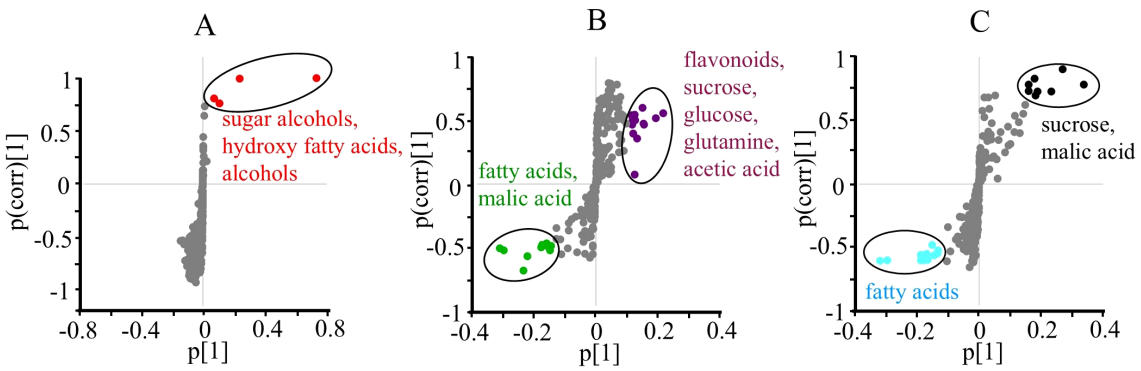

FIGURE 3
S-plots of orthogonal partial least squares discriminant analysis (OPLS-DA, n = 10) obtained from ^{1}H NMR data using two classes of RGO and water treated **(A)**, control and thrips treated **(B)**, and two different harvesting days after treatment (10 and 25 days after treatment) **(C)** of *Chrysanthemum* leaves. Potential biomarkers are indicated with an oval outline and descriptive text.

had only a marginal impact, with a Q^2 value of less than 0.30 (Figure 4B).

Further analysis of the GC-MS data using S-plots of OPLS-DA allowed for the identification of characteristic metabolites associated with each factor. RGO treated leaf samples were generally found to have higher levels of octanal (most likely a component of the RGO) and lower levels of eucalyptol, chrysanthenone, and eugenol than those in water sprayed leaves. In terms of harvesttime, samples collected 10 days post-treatment exhibited higher levels of compounds such as 4(10)-thujene, *cis*-4-thujanol, eucalyptol, and isocaryophyllene, whereas samples collected after 25 days showed elevated levels of *o*-Cymene and 3-Methyl-2-butenoic acid.

Additional OPLS-DA analysis of GC-MS data, conducted separately for water- and RGO-treated samples, aimed to explore the relationship between RGO treatment, thrips infestation, and harvesttime (Figures 4D, E; Supplementary Figure 11). Similar to the ^{1}H NMR findings, RGO-treated *Chrysanthemum* leaves exhibited reduced differences between control and thrips-infested samples. The Q^2 value for control and thrips-infested RGO-treated samples was 0.30, compared to 0.79 in water-treated samples. The lower Q^2 value in the RGO-treated samples may indicate that the separation between control and thrips-infested samples diminishes over time, particularly after 25 days. This suggests that the RGO treatment becomes more effective later, around 25 days post-treatment (Figure 4D).

Discussion

Natural materials hold a currently underutilized potential for use in crop protection. In previous work (Bierman et al., 2024), we showed that adhesive droplets made from oxidized rice germ oil (RGO) or other plant oils can catch western flower thrips and that the application of solutions containing these droplets may lead to lower damage and reproduction on detached *Chrysanthemum* leaves. In this study, we performed two full-plant assays to further investigate the effectiveness of the solutions containing RGO droplets to trap thrips and prevent thrips damage. Furthermore, we used ^{1}H NMR and headspace GC-MS to study the effects of the RGO sprays on plant growth and the plant metabolome in presence and absence of thrips at different timepoints and tested the effects on thrips of the individual RGO constituents. The results of our study provide new insights into how plant-derived oils can be used directly for pest control, their effects on the metabolite content of plants, and how such metabolomic changes relate to levels of herbivory by thrips.

In nature, adhesive trichomes provide plants with a form of physical and chemical defense against herbivores and other insects (LoPresti et al., 2015). In line with our expectations, we were able to catch some thrips on plants covered with adhesive droplets, however, the number of caught thrips (three out of 600 adults that were released in RGO treatments) was very low, suggesting that the current RGO droplets are not effective for trapping thrips. Several factors in our experiment may explain these low thrips catch rates: the low density of 20 thrips per plant, a low coverage with (sufficiently sized) sticky droplets which were also only sprayed on the upper side of leaves, a potential decrease in adhesion of the RGO droplets over time, the ability of thrips to hide and feed on unsprayed and newly grown plant parts, and the potential ability of thrips to easily escape from the adhesive droplets once caught. Subsequent experiments with increased density of droplets on the plant, e.g., via increasing the concentration of droplets in the sprayable solutions or by performing multiple coatings with higher thrips densities and measurements at specific time intervals, are needed to determine to what extent a higher coverage of the droplets improves catch rate and for how long droplets remain effective. Since thrips may be repelled or attracted by plant-derived oils and their individual constituents (Koschier, 2008), experiments focusing on investigation of thrips behavior in the presence of the adhesive RGO droplets and their released volatiles may provide further insights into whether thrips actively avoid the droplets and to what extent volatile cues play a role in the trapping process.

Despite the low number of thrips caught, observed thrips damage was up to 50% lower and plant biomass loss was better prevented in plants sprayed with RGO solutions than in plants

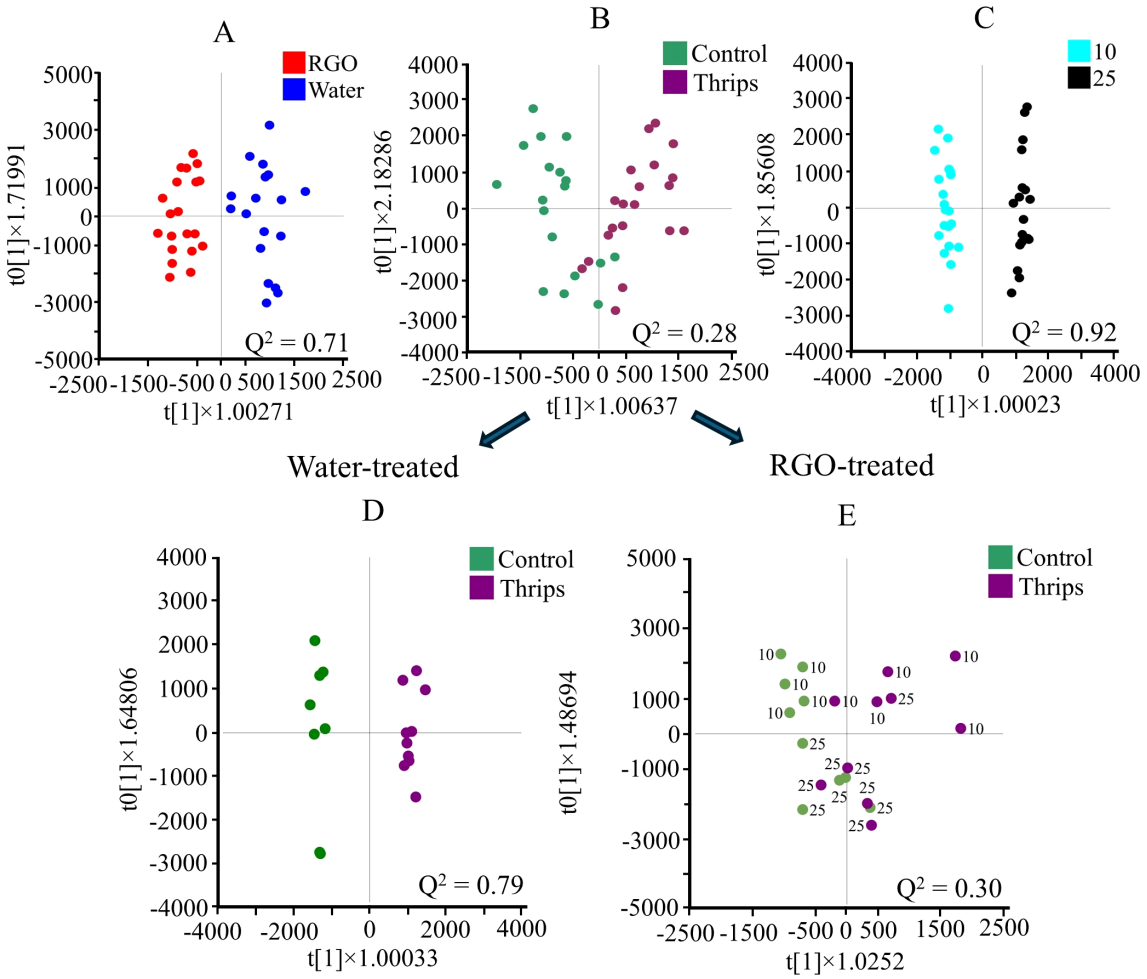

FIGURE 4
Orthogonal partial least squares discriminant analysis (OPLS-DA, n = 20) score plots obtained from headspace GC-MS data using two classes of RGO and water treated **(A)**, control and thrips treated **(B)**, and two different harvesting days after treatment (10 and 25 days after treatment) **(C)** of *Chrysanthemum* leaves. Additional OPLS-DA, n =10) analysis of the thrips factor for plants sprayed treated with water **(D)** and RGO **(E)**, separately. Numbers are used to indicate the harvesttime.

sprayed with water. The observed reduction in thrips performance suggests that, instead of the adhesive droplets acting as a physical trap, other mechanisms were likely involved, e.g., repellent or toxic effects of the droplets or other compounds in the sprayable solution, or chemical alterations in the plant or its surrounding headspace. Results from plant assay 2 support this hypothesis as the application of 1% F-108, 2% alginate, and F-108 + alginate solutions, and the full RGO sample were all found to reduce thrips feeding and cause a shift in feeding preference to the underside of the leaf. Results from prior leaf assays (Bierman et al., 2024) and earlier studies on effects of F-108 (Affeld et al., 2004), alginate (Saberi Riseh et al., 2022), rice germ oil (Rajput et al., 2017), and other plant-derived oils (Koschier, 2008) against arthropods also provide support that compounds in the spraying solution may have acted against thrips.

Upon stress, herbivore attack, or the application of natural compounds, plants commonly synthesize or release chemicals that may help to defend the plant (Kesraoui et al., 2022). The ^{1}H NMR and HS-GC-MS analyses performed on the leaf material of plant assay 1 were a valuable approach to further investigate the effects of RGO application on the plant metabolome and headspace in relation to thrips performance over time. Many of the major ^{1}H NMR and HS-GC-MS detected signals correspond to compounds such as flavonoids, carbohydrates, organic acids, amines, amino acids, triterpenoids, and steroids, which are commonly found in different *Chrysanthemum* cultivars and related species (Chae, 2016; Jiang et al., 2021; Kumar et al., 2005). The PCA and OPLS-DA plots showed clear effects on plant metabolism of RGO application, harvesttime, and to some extent thrips presence. RGO application increased hydroxy fatty acids and alcohols, while volatile compounds such as eucalyptol, chrysanthenone, and eugenol were decreased. Thrips presence was associated with increased flavonoid, carbohydrate, glutamine acetic acid levels, and lower fatty acids and malic acid levels. Sucrose, malic acid, *o*-Cymene, and 3-Methyl-2-butenoic acid, were highest after 25 days, while fatty acids and several volatile compounds such as 4(10)-thujene (sabinene), eucalyptol, *cis*-4-thujanol (an alcohol), and isocaryophyllene were highest after 10 days.

While the effect of harvesttime on metabolome content stayed consistent regardless of RGO application, more in depth analysis

revealed that the thrips effect was more pronounced in water-treated plants than in RGO-treated plants. In the plants sprayed with RGO there was a considerable overlap in the multivariate plots at 25 days post infestation. A first explanation for this overlap may be that the RGO application induced a more general stress response that was unaffected by further stress from thrips as indicated by the increased levels of fatty acids, which are known to play a key role in general plant defense (He and Ding, 2020). A second explanation may be that the effect of thrips on RGO-treated plants diminished over time, perhaps as a result of decreased feeding which is known to be a factor in the severity of plant chemical responses to herbivores (Pan et al., 2021).

The altered concentrations of several of the compounds found on or inside the leaves of RGO-and water-sprayed plants and how the levels of these compounds changed over time and in presence of thrips, raises the question about their role in plant defense against arthropod pests. Flavonoids, such as kaempferol glucoside, are known to confer resistance to herbivory (Bennett and Wallsgrove, 1994; Chen et al., 2020; Leiss et al., 2009a). Carbohydrates have been reported to play a role in plant defenses as signaling molecules (Trouvelot et al., 2014) or as carbon resources for the sequestration of phenolic compounds (Arnold et al., 2004). Although some carbohydrates are used by herbivores for their own nutrition (Roeder and Behmer, 2014), an increase in general carbohydrate content may have deterred herbivory of thrips. Acetic acid has been shown to be involved in the jasmonic acid pathway and its application may induce plant herbivore and abiotic stress tolerance (Chen et al., 2019; Rahman et al., 2024). Fatty acids and malic acids have also been found in earlier work to be indicators of *F. occidentalis* resistance in tomato (Mirnezhad et al., 2010). Eucalyptol (1,8-cineole), a monoterpene, is a major constituent of *Chrysanthemum* (Chae, 2016) and is also found in eucalyptus tree leaves and other plant species like *Rosmarinus officinalis* (Koschier et al., 2002) or *Lavandula latifolia* (Erland et al., 2015). Eucalyptol has been found to have toxic activity against several arthropods such as the red flour beetle (Tripathi et al., 2001), house fly (Rice and Coats, 1994; Kumar et al., 2013), lesser grain borer (Ebadollahi et al., 2022), *Thrips palmi* (Kim et al., 2015) and *F. occidentalis* (Gharbi and Tay, 2022), although reports have also been made of 1,8-cineole acting as an attractant for *F. occidentalis* (Chermenskaya et al., 2001; Katerinopoulos et al., 2005; Koschier et al., 2000) and being negatively correlated with *F. occidentalis* mortality (Durr et al., 2022). Chrysanthenone, another major volatile constituent of *Chrysanthemum* (Chae, 2016), is suggested to have broader insecticidal activity (Kherroubi et al., 2021; Negahban et al., 2007). Eugenol, a fenylpropanoid, was found to attract *F. occidentalis* (Koschier et al., 2000), while also being an oviposition and feeding deterrent for *Thrips tabaci* (Riefler and Koschier, 2009) and deterrent of other insects such as mosquitoes (Nerio et al., 2010). α-Thujene (a monoterpene), of which 4(10)thujene (sabinene) and β-thujene are isomers, γ-terpinene, an isomer of β-terpinene, terpinolene, and δ-cadinene (a sesquiterpene) have all been found to be correlated with increased mortality of *F. occidentalis* (Durr et al., 2022). (E)-β-caryophyllene (an isomer of isocaryophyllene) is well known from studies in maize to be involved in resistance against some herbivore species, or as an attractant for other herbivores, nematodes, and for predatory insects (Degenhardt, 2009). The fact that we found decreased levels of eucalyptol, chrysanthenone, and eugenol in the leaves of RGO sprayed plants, and the fact that these compounds can be attractive to *F. occidentalis* seems to suggest that eucalyptol, chrysanthenone and eugenol are not the main drivers for conveying resistance to *F. occidentalis*. Instead, non-volatile constituents such as the presence of fatty acids on the leaves, carbohydrate content, malic acid, flavonoids and others may have contributed to the observed decrease in thrips damage. Further studies into the pathways and herbivore-antagonistic properties of the detected (volatile) compounds will be needed to gain deeper insight in their role in plant defense and to assess their potential for use in integrated pest management.

Conclusion

New natural materials are being discovered and implemented in crop protection at a fast pace to replace synthetic pesticides. In this paper, we investigated whether sprayable solutions containing sticky droplets made from rice germ oil could be used for physical trapping of small arthropods such as thrips on plant surfaces and to what extent plant metabolomic changes induced by application of such oils may be related to increased crop resilience against thrips. While the solutions containing adhesive droplets did not act as an efficient trap, their application did reduce thrips damage substantially and caused altered levels of some metabolites such as flavonoids that are generally considered to be related to herbivore resistance. However, before spraying of solutions with sticky oil droplets is broadly implemented, further trials will first be needed to properly assess the droplet densities needed where spraying plants with solutions with adhesive droplets provides a reliable advantage, whether the droplets are compatible with natural enemies and pollinators, and to what extent their application affects photosynthesis, plant respiration and long-term growth, all of which may ultimately affect yield. The successful implementation of sprayable sticky plant oil droplets for arthropod trapping on crops will furthermore depend on the opinions of farmers and consumers about this method. Finally, NMR and GC-MS proved to be valuable tools in this study and will likely continue to prove their usefulness in the coming decades as a way to advance our knowledge of plant-insect interactions and to allow for this knowledge to be applied in agriculture e.g., via priming of plant defenses or breeding for arthropod resistance.

Data availability statement

The datasets presented in this study can be found in online repositories. The names of the repository/repositories and accession number(s) can be found below: https://zenodo.org/records/14604988.

Ethics statement

The manuscript presents research on animals that do not require ethical approval for their study.

Author contributions

TVB: Conceptualization, Data curation, Formal analysis, Investigation, Methodology, Validation, Visualization, Writing – original draft, Writing – review & editing. HF: Conceptualization, Data curation, Formal analysis, Investigation, Methodology, Visualization, Writing – original draft, Writing – review & editing. YC: Conceptualization, Data curation, Formal analysis, Investigation, Methodology, Resources, Software, Supervision, Validation, Visualization, Writing – original draft, Writing – review & editing. SS: Data curation, Formal analysis, Methodology, Visualization, Writing – original draft, Writing – review & editing. KV: Conceptualization, Formal analysis, Methodology, Supervision, Visualization, Writing – review & editing. MM: Conceptualization, Methodology, Writing – review & editing. BK: Conceptualization, Methodology, Writing – review & editing. TK: Methodology, Resources, Writing – review & editing. RV: Methodology, Resources, Writing – review & editing. PK: Conceptualization, Funding acquisition, Project administration, Writing – review & editing. TB: Formal analysis, Supervision, Validation, Visualization, Writing – original draft, Writing – review & editing.

Funding

The author(s) declare financial support was received for the research, authorship, and/or publication of this article. This work was funded by the Dutch Research Council (NWA-ORC Grant Number 1160.18.071).

Acknowledgments

The authors would like to acknowledge Christiana Papadaki and Karin van Veen for practical assistance, and Peter Kuijvenhoven and Deliflor B.V. as a whole, for kindly providing plants for this study.

Conflict of interest

A patent for the method to fabricate solutions with adhesive plant-derived oil droplets has been filed with the European Patent Office, application no. 22202752.6; EP4356732A1, by Wageningen University.

The authors declare that the research was conducted in the absence of any commercial or financial relationships that could be construed as a potential conflict of interest.

The author(s) declared that they were an editorial board member of Frontiers, at the time of submission. This had no impact on the peer review process and the final decision.

Generative AI statement

The author(s) declare that no Generative AI was used in the creation of this manuscript.

Publisher's note

Supplementary material

The Supplementary Material for this article can be found online at: https://www.frontiersin.org/articles/10.3389/fpls.2025.1509126/full#supplementary-material

References

Affeld, K., Hill, K., Smith, L. A., and Syrett, P. (2004). "Toxicity of herbicides and surfactants to three insect biological control agents for *Cytisus scoparius*," in *XI international symposium on biological control of weeds*. Eds. J. M. Cullen, D. T. Briese, D. J. Kriticos, W. M. Lonsdale, L. Morin and J. K. Scott (CSIRO Entomology, Canberra), 375–380.

Arnold, T., Appel, H., Patel, V., Stocum, E., Kavalier, A., and Schultz, J. (2004). Carbohydrate translocation determines the phenolic content of *Populus* foliage: a test of the sink–source model of plant defense. *New Phytol.* 164, 157–164. doi: 10.1111/j.1469-8137.2004.01157.x

(2024). Global natural product social molecular networking. Available online at: https://gnps.ucsd.edu (Accessed September 30, 2024).

Bennett, R. N., and Wallsgrove, R. M. (1994). Secondary metabolites in plant defense mechanisms. *New Phytol.* 127, 617–633. doi: 10.1111/j.1469-8137.1994.tb02968.x

Bierman, T. V., Vrieling, K., van Zwieten, R., Kodger, T. E., Macel, M., and Bezemer, T. M. (2024). Adhesive droplets made from plant-derived oils for control of western flower thrips. *J. Pest Sci.* 97, 2175–2186. doi: 10.1007/s10340-024-01755-4

Chae, S. C. (2016). An up-to-date review of phytochemicals and biological activities in chrysanthemum spp. *Biosci. Biotech. Res. Asia* 13, 615–623. doi: 10.13005/bbra/2077

Chen, G., Kim, H. K., Klinkhamer, P. G., and Escobar-Bravo, R. (2020). Site-dependent induction of jasmonic acid-associated chemical defenses against western flower thrips in *Chrysanthemum*. *Planta* 251, 1–14. doi: 10.1007/s00425-019-03292-2

Chen, D., Shao, M., Sun, S., Liu, T., Zhang, H., Qin, N., et al. (2019). Enhancement of jasmonate-mediated antiherbivore defense responses in tomato by acetic acid, a potent inducer for plant protection. *Front. Plant Sci.* 10. doi: 10.3389/fpls.2019.00764

Chermenskaya, T. D., Burov, V. N., Maniar, S. P., Pow, E. M., Roditakis, N., Selytskaya, O. G., et al. (2001). Behavioral responses of western flower thrips, *frankliniella occidentalis* (Pergande), to volatiles from three aromatic plants. *Int. J. Trop. Insect. Sci.* 21, 67–72. doi: 10.1017/S1742758400020063

Cloyd, R. A. (2016). Western flower thrips (Thysanoptera: Thripidae) and insecticide resistance: an overview and strategies to mitigate insecticide resistance development. *J. Entomol. Sci.* 51, 257–273. doi: 10.18474/JES16-15.1

De Almeida, L. F. R., Frei, F., Mancini, E., De Martino, L., and De Feo, V. (2010). Phytotoxic activities of Mediterranean essential oils. *Molecules* 15, 4309–4323. doi: 10.3390/molecules15064309

Degenhardt, J. (2009). Indirect defense responses to herbivory in grasses. *Plant Physiol.* 149, 96–102. doi: 10.1104/pp.108.128975

De Jager, C. M., Butôt, R. P. T., Klinkhamer, P. G. L., De Jong, T. J., Wolff, K., and van der Meijden, E. (1995). Genetic variation in chrysanthemum for resistance to *Frankliniella occidentalis*. *Entomol. Exp. Appl.* 77, 277–287. doi: 10.1111/j.1570-7458.1995.tb02325.x

Dicke, M., and Baldwin, I. T. (2010). The evolutionary context for herbivore-induced plant volatiles: beyond the 'cry for help'. *Trends Plant Sci.* 15, 167–175. doi: 10.1016/j.tplants.2009.12.002

Durr, T. D., Stratton, C. A., Dosoky, N. S., Satyal, P., and Murrell, E. G. (2022). Shared phytochemicals predict efficacy of essential oils against western flower thrips (*Frankliniella occidentalis*) in the greenhouse. *Chem. Biol. Technol. Agric.* 9, 62. doi: 10.1186/s40538-022-00328-w

Ebadollahi, A., Naseri, B., Abedi, Z., Setzer, W. N., and Changbunjong, T. (2022). Promising Insecticidal Efficiency of Essential Oils Isolated From Four Cultivated *Eucalyptus* Species in Iran against the Lesser Grain Borer, *Rhyzopertha Dominica* (F.). *Insects* 13, 517. doi: 10.3390/insects13060517

Erland, L. A., Rheault, M. R., and Mahmoud, S. S. (2015). Insecticidal and oviposition deterrent effects of essential oils and their constituents against the invasive pest *Drosophila suzukii* (Matsumura) (Diptera: Drosophilidae). *Crop Prot.* 78, 20–26. doi: 10.1016/j.cropro.2015.08.013

Escobar-Bravo, R., Klinkhamer, P. G., and Leiss, K. A. (2017). Induction of jasmonic acid-associated defenses by thrips alters host suitability for conspecifics and correlates with increased trichome densities in tomato. *Plant Cell Physiol.* 58, 622–634. doi: 10.1093/pcp/pcx014

Gharbi, K., and Tay, J. W. (2022). Fumigant Toxicity of Essential Oils against *Frankliniella occidentalis* and *F. insularis* (Thysanoptera: Thripidae) as Affected by Polymer Release and Adjuvants. *Insects* 13, 493. doi: 10.3390/insects13060493

He, M., and Ding, N. Z. (2020). Plant unsaturated fatty acids: multiple roles in stress response. *Front. Plant Sci.* 11. doi: 10.3389/fpls.2020.562785

Jiang, Y., Zhang, W., Chen, X., Wang, W., Köllner, T. G., Chen, S., et al. (2021). Diversity and biosynthesis of volatile terpenoid secondary metabolites in the *Chrysanthemum* genus. *Crit. Rev. Plant Sci.* 40, 422–445. doi: 10.1080/07352689.2021.1969504

Katerinopoulos, H. E., Pagona, G., Afratis, A., Stratigakis, N., and Roditakis, N. (2005). Composition and insect attracting activity of the essential oil of Rosmarinus officinalis. *J. Chem. Ecol.* 31, 111–122. doi: 10.1007/s10886-005-0978-0

Kesraoui, S., Andrés, M. F., Berrocal-Lobo, M., Soudani, S., and Gonzalez-Coloma, A. (2022). Direct and indirect effects of essential oils for sustainable crop protection. *Plants* 11, 2144. doi: 10.3390/plants11162144

Kessler, A., and Baldwin, I. T. (2002). Plant responses to insect herbivory: the emerging molecular analysis. *Annu. Rev. Plant Biol.* 53, 299–328. doi: 10.1146/annurev.arplant.53.100301.135207

Kherroubi, M., Zerrouk, I. Z., Rahmoune, B., Zaidat, S. A. E., Messadi, O., and Mouhouche, F. (2021). Evaluation of the potential insecticide activity of three plants essential oil against the chickpea seeds beetles, *Callosobruchus maculatus*. *Analele Universităţii din Oradea Fascicula Biologie* 28, 97–102.

Kim, H., Choi, Y., and Verpoorte, R. (2010). NMR-based metabolomic analysis of plants. *Nat. Protoc.* 5, 536–549. doi: 10.1038/nprot.2009.237

Kim, H. K., Choi, Y. H., and Verpoorte, R. (2011). NMR-based plant metabolomics: where do we stand, where do we go? *Trends Biotechnol.* 29, 267–275. doi: 10.1016/j.tibtech.2011.02.001

Kim, K. H., Yi, C. G., Ahn, Y. J., Kim, S. I., Lee, S. G., and Kim, J. R. (2015). Fumigant toxicity of basil oil compounds and related compounds to *Thrips palmi* and *Orius strigicollis*. *Pest Manage. Sci.* 71, 1292–1296. doi: 10.1002/ps.3925

Koschier, E. H. (2008). Essential oil compounds for thrips control–a review. *Nat. Prod. Commun.* 3, 1171–1182. doi: 10.1177/1934578X0800300726

Koschier, E. H., De Kogel, W. J., and Visser, J. H. (2000). Assessing the attractiveness of volatile plant compounds to western flower thrips *frankliniella occidentalis*. *J. Chem. Ecol.* 26, 2643–2655. doi: 10.1023/A:1026470122171

Koschier, E. H., Sedy, K. A., and Novak, J. (2002). Influence of plant volatiles on feeding damage caused by the onion thrips *Thrips tabaci*. *Crop Prot.* 21, 419–425. doi: 10.1016/S0261-2194(01)00124-7

Kumar, P., Mishra, S., Malik, A., and Satya, S. (2013). Housefly (Musca domestica L.) control potential of *Cymbopogon citratus* Stapf. (Poales: Poaceae) essential oil and monoterpenes (citral and 1, 8-cineole). *Parasitol. Res.* 112, 69–76. doi: 10.1007/s00436-012-3105-5

Kumar, A., Singh, S. P., and Bhakuni, R. S. (2005). Secondary metabolites of *Chrysanthemum* genus and their biological activities. *Curr. Sci.* 89, 1489–1501. Available online at: https://www.jstor.org/stable/24110912

Leiss, K. A., Choi, Y. H., Abdel-Farid, I. B., Verpoorte, R., and Klinkhamer, P. G. L. (2009a). NMR metabolomics of thrips (*Frankliniella occidentalis*) resistance in *Senecio* hybrids. *J. Chem. Ecol.* 35, 219–229. doi: 10.1007/s10886-008-9586-0

Leiss, K. A., Choi, Y. H., Verpoorte, R., and Klinkhamer, P. G. L. (2011). An overview of NMR-based metabolomics to identify secondary plant compounds involved in host plant resistance. *Phytochem. Rev.* 10, 205–216. doi: 10.1007/s11101-010-9175-z

Leiss, K. A., Maltese, F., Choi, Y. H., Verpoorte, R., and Klinkhamer, P. G. L. (2009b). Identification of chlorogenic acid as a resistance factor for thrips in chrysanthemum. *Plant Physiol.* 150, 1567–1575. doi: 10.1104/pp.109.138131

LoPresti, E. F., Pearse, I. S., and Charles, G. K. (2015). The siren song of a sticky plant: columbines provision mutualist arthropods by attracting and killing passerby insects. *Ecology* 96, 2862–2869. doi: 10.1890/15-0342.1

Macel, M., Visschers, I. G. S., Peters, J. L., Kappers, I. F., De Vos, R. C. H., and Van Dam, N. M. (2019). Metabolomics of thrips resistance in pepper (*Capsicum* spp.) reveals monomer and dimer acyclic diterpene glycosides as potential chemical defenses. *J. Chem. Ecol.* 45, 490–501. doi: 10.1007/s10886-019-01074-4

Mežaka, I., Kronberga, A., Berga, M., Kaļāne, L., Pastare, L., Skudriņš, G., et al. (2023). Biochemical and Physiological Responses of *Cucumis sativus* L. to Application of Potential Bioinsecticides—Aqueous *Carum carvi* L. Seed Distillation By-Product Based Extracts. *Agriculture* 13, 1019. doi: 10.3390/agriculture13051019

Mirnezhad, M., Romero-González, R. R., Leiss, K. A., Choi, Y. H., Verpoorte, R., and Klinkhamer, P. G. (2010). Metabolomic analysis of host plant resistance to thrips in wild and cultivated tomatoes. *Phytochemical Analysis: Int. J. Plant Chem. Biochem. Techniques* 21, 110–117. doi: 10.1002/pca.1182

Negahban, M., Moharramipour, S., and Sefidkon, F. (2007). Fumigant toxicity of essential oil from *Artemisia sieberi* Besser against three stored-product insects. *J. Stored Prod. Res.* 43, 123–128. doi: 10.1016/j.jspr.2006.02.002

Nerio, L. S., Olivero-Verbel, J., and Stashenko, E. (2010). Repellent activity of essential oils: a review. *Bioresource Technol.* 101, 372–378. doi: 10.1016/j.biortech.2009.07.048

Nilon, A., Robinson, K., Pappu, H. R., and Mitter, N. (2021). Current status and potential of RNA interference for the management of tomato spotted wilt virus and thrips vectors. *Pathogens* 10, 320. doi: 10.3390/pathogens10030320

Pan, S., Zhang, J., Pan, H., Li, K., and Wu, J. (2021). Herbivore identity and intensity interact to influence plant metabolic response to herbivory. *Arthropod-Plant Interact.* 15, 285–298. doi: 10.1007/s11829-021-09823-7

Rahman, M. M., Keya, S. S., Sahu, A., Gupta, A., Dhingra, A., Tran, L. S. P., et al. (2024). Acetic acid: a cheap but chief metabolic regulator for abiotic stress tolerance in plants. *Stress Biol.* 4, 34. doi: 10.1007/s44154-024-00167-9

Rajput, L. B., Gilal, A. A., Bukero, A., and Wahocho, N. A. (2017). Impact of different oils as biopesticide against sucking insect pests in cotton. *J Basic Appl Sci.* 13, 34–40. doi: 10.6000/1927-5129.2017.13.06

Razzaq, A., Sadia, B., Raza, A., Khalid Hameed, M., and Saleem, F. (2019). Metabolomics: A way forward for crop improvement. *Metabolites* 9, 303. doi: 10.3390/metabo9120303

Reitz, S. R. (2009). Biology and ecology of the western flower thrips (Thysanoptera: thripidae): the making of a pest. *Fla Entomol* 92, 7–13. doi: 10.1653/024.092.0102

Reitz, S. R., and Funderburk, J. (2012). "Management strategies for western flower thrips and the role of insecticides," in *Insecticides–pest engineering*. Ed. F. Perveen (InTech, Rijeka, Croatia), 355–384.

Reitz, S. R., Maiorino, G., Olson, S., Sprenkel, R., Crescenzi, A., and Momol, M. T. (2008). Integrating plant essential oils and kaolin for the sustainable management of thrips and tomato spotted wilt on tomato. *Plant Dis.* 92, 878–886. doi: 10.1094/PDIS-92-6-0878

Rice, P. J., and Coats, J. R. (1994). Insecticidal properties of several monoterpenoids to the house fly (Diptera: muscidae), red flour beetle (Coleoptera: tenebrionidae), and southern corn rootworm (Coleoptera: chrysomelidae). *J. Econ. Entomol.* 87, 1172–1179. doi: 10.1093/jee/87.5.1172

Riefler, J., and Koschier, E. H. (2009). Behavior-modifying activity of eugenol on *Thrips tabaci* Lindeman. *J. Pest Sci.* 82, 115–121. doi: 10.1007/s10340-008-0229-6

Roeder, K. A., and Behmer, S. T. (2014). Lifetime consequences of food protein-carbohydrate content for an insect herbivore. *Funct. Ecol.* 28, 1135–1143. doi: 10.1111/1365-2435.12262

Saberi Riseh, R., Gholizadeh Vazvani, M., Ebrahimi-Zarandi, M., and Skorik, Y. A. (2022). Alginate-induced disease resistance in plants. *Polymers* 14, 661. doi: 10.3390/polym14040661

Tripathi, A. K., Prajapati, V., Aggarwal, K. K., and Kumar, S. (2001). Toxicity, Feeding Deterrence, and Effect of Activity of 1,8-cineole from *Artemisia annua* on Progeny Production of *Tribolium castanaeum* (Coleoptera: Tenebrionidae). *J. Econ. Entomol.* 94, 979–983. doi: 10.1603/0022-0493-94.4.979

Trouvelot, S., Héloir, M. C., Poinssot, B., Gauthier, A., Paris, F., Guillier, C., et al. (2014). Carbohydrates in plant immunity and plant protection: roles and potential application as foliar sprays. *Front. Plant Sci.* 5. doi: 10.3389/fpls.2014.00592

van Zwieten, R., Bierman, T. V., Klinkhamer, P. G. L., Bezemer, T. M., Vrieling, K., and Kodger, T. E. (2024). Mimicking natural deterrent strategies in plants using adhesive spheres. *Proc. Natl. Acad. Sci. U.S.A.* 121, e2321565121. doi: 10.1073/pnas.2321565121

Verdeguer, M., Sánchez-Moreiras, A. M., and Araniti, F. (2020). Phytotoxic effects and mechanism of action of essential oils and terpenoids. *Plants* 9, 1571. doi: 10.3390/plants9111571

Villa-Ruano, N., Pérez-Hernández, N., Zepeda-Vallejo, L. G., Quiroz-Acosta, T., Mendieta-Moctezuma, A., Montoya-García, C., et al. (2019). ^{1}H-NMR based metabolomics profiling of citrus juices produced in veracruz, méxico. *Chem. Biodivers* 16, e1800479. doi: 10.1002/cbdv.201800479

Walling, L. (2000). The myriad plant responses to herbivores. *J. Plant Growth. Regul.* 19, 195–216. doi: 10.1007/s003440000026

frontiers | Frontiers in Plant Science

TYPE Original Research
PUBLISHED 25 February 2025
DOI 10.3389/fpls.2025.1557544

OPEN ACCESS

EDITED BY
Marta Sousa Silva,
University of Lisbon, Portugal

REVIEWED BY
Michał Rurek,
Adam Mickiewicz University, Poznań, Poland
Alma Angelica Del Villar Martinez,
National Polytechnic Institute (IPN), Mexico

*CORRESPONDENCE
Shunghong Cheng
1999033@ynau.edu.cn
Hongxing Cao
caohx@catas.cn

RECEIVED 08 January 2025
ACCEPTED 05 February 2025
PUBLISHED 25 February 2025

CITATION
Xu W, John Martin JJ, Li X, Liu X, Cheng S and Cao H (2025) Transcriptional and metabolic analysis of oleic acid synthesis in seedless and tenera oil palm species. *Front. Plant Sci.* 16:1557544. doi: 10.3389/fpls.2025.1557544

Transcriptional and metabolic analysis of oleic acid synthesis in seedless and tenera oil palm species

Wen Xu[1,2], Jerome Jeyakumar John Martin[2], Xinyu Li[2], Xiaoyu Liu[2], Shunghong Cheng[1*] and Hongxing Cao[2*]

[1]College of Tropical Crops, Department of Forestry, Yunnan Agricultural University, Pu'er, China, [2]Coconut Research Institute, Chinese Academy of Tropical Agricultural Sciences, Wenchang National Key Laboratory for Tropical Crop Breeding, Haikou, Wenchang, China

The oil palm (*Elaeis guineensis* Jacq.) is a perennial oilseed crop whose mesocarp produces palm oil rich in the unsaturated fatty acid oleic acid, known for its oxidative stability and cardiovascular health benefits. However, the regulatory mechanisms and pathways responsible for variations in oleic acid biosynthesis during fruit development remain inadequately elucidated. The study examined the mesocarp of oil palm fruits from three developmental stages in seedless and Tenera varieties to evaluate oleic acid content. Fruits from Seedless (MS) and Tenera (MT) oil palms, pollinated for 95 days (MS1 and MT1), 125 days (MS2 and MT2), and 185 days (MS3 and MT3), were analyzed using metabolomics via liquid chromatography-tandem mass spectrometry (LC-MS/MS). RNA sequencing was conducted to profile gene expression associated to oleic acid biosynthesis and accumulation. Differential genes and metabolites were mapped and functionally enriched through KEGG pathway analysis. The result revealed that *SAD*, *FabD*, *LACS6*, *BC*, *FabB*, and *FabI* were positively associated with oleic acid content, whereas *LACS9* exhibited either a negative or strongly negative correlation. By integrating metabolomic and transcriptomic techniques, this study elucidates the distinct mechanisms of oleic acid biosynthesis in seedless and thin-shelled oil palm varieties. These findings provide a scientific foundation for enhancing oleic acid content and improving the quality of oil palm-derived products.

KEYWORDS

oil palm, oleic acid biosynthesis, transcriptome, metabolome, lipid metabolism

1 Introduction

The oil palm (*Elaeis guineensis* Jacq.) is one of the most important oil crops globally, renowned for its superior productivity compared to other oilseed crops. Its oil yield is approximately eight to ten times greater than that of soybean and rapeseed, respectively, making it the most productive oil crop worldwide (Papilo et al., 2022). The mesocarp of oil

palm fruit is the primary oil-producing tissue, containing predominantly 38–45% palmitic acid (C16:0) and 38–44% oleic acid (C18:1) (Dussert et al., 2013; Morcillo et al., 2021).

Oleic acid, a monounsaturated fatty acid, is known for its exceptional oxidative stability, which supports immune regulation and helps prevent cardiovascular diseases (Katariya et al., 2021). After ingestion, oleic acid undergoes hydrolysis in the stomach and enters the bloodstream intact as glycerol monoesters (Voon et al., 2019). Moreover, studies suggest that high-oleic oil palm can generate an estimated economic value of $1,500 per hectare annually when oleic acid content exceeds 65% (Sambanthamurthi et al., 2002). In comparison, high-oleic acid rapeseed oil typically contains 75–84% oleic acid (Chang et al., 2022). As a result, oleic acid holds significant nutritional and economic value. Consequently, the developing oil palm varieties with elevated oleic acid content through genetic enhancement has become a critical objective in breeding programs (Bahariah et al., 2021).

Previous research has identified key enzyme genes involved in oleic acid synthesis in oil palm. Sun et al. (2016) successfully cloned Δ12-desaturase, a gene associated with the biosynthesis of long-chain polyunsaturated fatty acids (LC-PUFAs), and demonstrated that *egFAD12* exhibited peak activity in oil palm fruits 120–140 days after pollination. This enzyme facilitates the conversion of oleic acid to linoleic acid. Ben Ayed et al. (2022) performed a comparative analysis of 24 *FAD2* sequences from different species and identified two single nucleotide polymorphisms (SNPs), SNP373 and SNP718, associated with oleic and linoleic acid content. These SNPs were shown to regulate *FAD2* activity, either reducing or increasing oleic acid levels. Additionally, Bahariah et al. (2023) utilized a multiplex CRISPR/Cas9 platform to successfully induce mutations in the *EgFAD2* gene, located on chromosome 8, and the *EgPAT* gene (also known as *EgFATB-1*), found on chromosomes 3 and 7. This approach aims to reduce the activity of the *PAT* and *FAD2* enzymes, thereby enhancing oleic acid content. To achieve high levels of 18:1 for improved oil stability and human health, *FAD2* has become a prime target for disruption using the powerful genome editing tool CRISPR/Cas9 (Okuzaki et al., 2018; Al Amin et al., 2019; Do et al., 2019). Wei et al. (2024) further identified six enzyme genes—*BC*, *ACC*, *FabB*, *FabI*, *FabG*, and *FabD*—that promote oleic acid accumulation during oil palm fruit development.

An AGAMOUS-like MADS-box transcription factor, *EgAGL9*, was identified through expression profiling at various developmental stages of the oil palm pericarp. Research by Zhang et al. (2022) demonstrated that *EgAGL9* interacts with the enzyme genes *EgSAD*, *EgTSA*, and *EgSDH* in the fatty acid synthesis pathway, leading to a substantial reduction in the proportion of unsaturated fatty acids, including oleic, linoleic, and linolenic acids. Additionally, *EgMADS2* has been shown to regulate *EgDGAT* expression, significantly decreasing linoleic acid content while increasing oleic acid levels in transgenic embryos (Li et al., 2020). A full-length cDNA encoding *EgLACS9* was also cloned from oil palm pericarp. Overexpression of *EgLACS9* in the *LACS*-deficient *Saccharomyces cerevisiae* strain YB525 resulted in reduced levels of C18:1 (oleic acid) and C18:2 (linoleic acid) (Wang et al., 2021). Moreover, downregulation of the transcription factor *EgGRP2A* resulted in decreased expression of *EgFATA* and a concomitant reduction in oleic acid content (Luo et al., 2024). A seed-like fruit-specific complex network has been established in the mesocarp of oil palm.NF-YA3, NF-YC2, and ABI5 directly activate WRI1-1 and a subset of FA synthesis genes. NF-YA3 also physically interacts with NF-YC2, ABI5 and WRI1-1 to form transcription complexes that regulate gene expression. WRKY40 cooperates with WRKY2 to repress ABI5, resulting in the synthesis of oils and oils (Yeap et al., 2017). Additionally, researchers have explored the biosynthesis, transport, key enzymes and their regulation of C18 UFAs, especially the emerging regulatory network involving transcription factors and upstream signaling pathways (He et al., 2020). The findings collectively contribute to understanding the genetic regulation of oleic acid synthesis and highlight potential targets for genetic improvement to enhance oil quality.

Although initial investigations into oleic acid in oil palm have been conducted, there is a lack of comprehensive studies examining the variation in oleic acid content across different oil palm varieties and developmental stages. This study utilized high-throughput sequencing technology for transcriptomics and liquid chromatography-tandem mass spectrometry (LC-MS/MS) for metabolomics to examine the changing patterns of oleic acid during oil palm growth and development. By analyzing the differences in oleic acid content across various oil palm varieties, this research elucidates the dynamic characteristics of oleic acid at different developmental stages and provides a scientific foundation for enhancing the quality of oil palm.

2 Materials and methods

2.1 Experimental materials

The experimental samples were collected from oil palm fruits of seedless and thin-shelled varieties, harvested at different developmental stages from the Coconut Research Institute of the Chinese Academy of Tropical Agricultural Sciences (19°33′N, 110° 47′E), located at the institute's oil palm test site. The samples consisted of mesocarp tissue obtained from oil palm fruits at three distinct developmental stages: 95 days (early developmental stage: MS1 and MT1), 125 days (mid-developmental stage: MS2 and MT2), and 185 days (late developmental stage: MS3 and MT3) post-pollination. For each developmental stage, three biological replicates were taken, ensuring a robust representation of the variation within each stage. Following collection, all samples were immediately stored in liquid nitrogen at -80°C to preserve metabolomic and transcriptomic integrity for subsequent analysis. These stored samples were then subjected to high-throughput sequencing and liquid chromatography-tandem mass spectrometry (LC-MS/MS) for in-depth investigation of the metabolic and transcriptional profiles.

2.2 Metabolomics analysis and data processing

Mesocarp samples were prepared for metabolomic analysis using an ExionLC ultra-high-performance liquid chromatography (UHPLC) system coupled with a SCIEX QTRAP 6500+ tandem mass spectrometer. Metabolite extraction involved tissue homogenization, solvent extraction, and filtration to ensure sample integrity and reproducibility. Metabolite separation was conducted under optimized chromatographic conditions, and detection was performed in multiple reaction monitoring (MRM) mode for high sensitivity and specificity. Raw mass spectrometry data were processed with Analyst 1.6.3 software, including peak detection, alignment, and integration. Metabolite identification was achieved by matching spectral data with local lipid databases, while spectral peaks across samples were aligned and corrected for variability. Absolute metabolite concentrations were determined from integral peak areas. Differentially abundant metabolites were identified through orthogonal partial least squares discriminant analysis (OPLS-DA), with selection criteria including a variable importance in projection (VIP) score of ≥ 1, a fold change of ≥ 2 for upregulation, or ≤ 0.5 for downregulation. Results from MRM mode were visualized in Supplementary Figure S2, and identified metabolites were further analyzed to provide insights into oleic acid biosynthesis, elucidating developmental and varietal differences in oil palm.

2.3 Mesocarp RNA extraction and high throughput sequencing

Total RNA was extracted from mesocarp tissues collected at 95, 125, and 185 days after pollination using a commercial RNA isolation kit (Tiangen Biotech, China), following the manufacturer's protocol, with homogenization performed under liquid nitrogen to preserve RNA integrity. RNA quality and integrity were assessed using an Agilent 2100 Bioanalyzer, with samples achieving RNA integrity number (RIN) values ≥ 7.0 deemed suitable for downstream applications. Purity was evaluated using A260/A280 and A260/A230 ratios measured on a NanoDrop spectrophotometer, while RNA concentrations were quantified with a Qubit RNA assay kit. The cDNA fragments underwent end repair, A-tailing, adapter ligation, and PCR amplification, with library quality assessed using an Agilent 2100 Bioanalyzer and concentrations determined via qPCR. After passing the library check, different libraries are pooled according to the effective concentration and the target downstream data volume required for Illumina sequencing, and 150bp paired-end reads are generated. Four types of fluorescently labeled dNTP, DNA polymerase, and junction primers are added to the sequencing flow cell for amplification. When extending the complementary strand of each sequencing cluster, each fluorescently labeled dNTP added releases corresponding fluorescence, which is then captured by the sequencer, and converted into sequencing peaks by the computer software, thus obtaining the sequence information of the fragment to be sequenced.

Raw data were filtered using fastp v 0.19.3, mainly removing reads with adapters; when the N content of any sequencing read exceeded 10% of the number of bases in the read, the paired reads were removed; when the number of low-quality (Q<=20) bases in any sequencing read exceeded 50% of the number of bases in the read, the paired reads were removed. All subsequent analyses were based on clean reads. reference genomes and their annotation files were downloaded from the indicated websites, indexes were constructed using HISAT v2.1.0, and clean reads were aligned to the reference genomes. Differentially expressed genes (DEGs) were identified using DESeq2 with stringent criteria: false discovery rate (FDR) < 0.05 and |log2FoldChange| ≥ 1. Identified DEGs underwent further analysis, including Nr functional annotation, enrichment analysis, and other bioinformatics approaches, to explore their roles in metabolic and regulatory pathways.

2.4 Statistical analysis

Data analysis was performed using Excel 2019 and SPSS software. For graphical representation, Origin 2022 and GraphPad Prism 9.5 were utilized. Venn diagrams and heatmaps were generated using the online tool available at https://www.omicshare.com/tools/. Statistical significance was determined based on the appropriate tests for each data set, with p-values < 0.05 considered statistically significant.

3 Results and analyses

3.1 Analysis of the dynamics of oleic acid metabolites in the pulp of seedless and thin-shelled oil palms at different stages of development

Studies on oleic acid metabolites in the pulp of seedless and thin-shelled oil palm varieties at various developmental stages revealed that the free fatty acid composition in the pulp consisted of 13 unsaturated and 17 saturated fatty acids, with oleic acid being the dominant fatty acid. In the seedless oil palm variety, oleic acid content gradually increased from 277.30 nmol/g at the MS1 stage to 31,536.14 nmol/g at the MS2 stage, reaching a peak of 32,992.80 nmol/g at the MS3 stage. This increase represented 15.64%, 58.81%, and 56.66% of the total free fatty acid content at each respective stage. Furthermore, oleic acid accounted for 64.27%, 75.44%, and 69.31% of the total unsaturated fatty acids at these stages (Figures 1A–C).

In the thin-shelled oil palm variety, oleic acid content increased from 4,549.25 nmol/g at the MT1 stage to 26,021.06 nmol/g at the MT2 stage, reaching a maximum of 30,396.86 nmol/g at the MT3 stage. This corresponded to 48.85%, 56.88%, and 50.51% of the total free fatty acid content, respectively. Oleic acid also made up 68.87%, 78.2%, and 73.31% of the total unsaturated fatty acids at the respective stages (Figures 1A–C).

The increase in oleic acid content from the MT1 to MT2 stage was greater in seedless oil palm (31,258.84 nmol/g) than in thin-

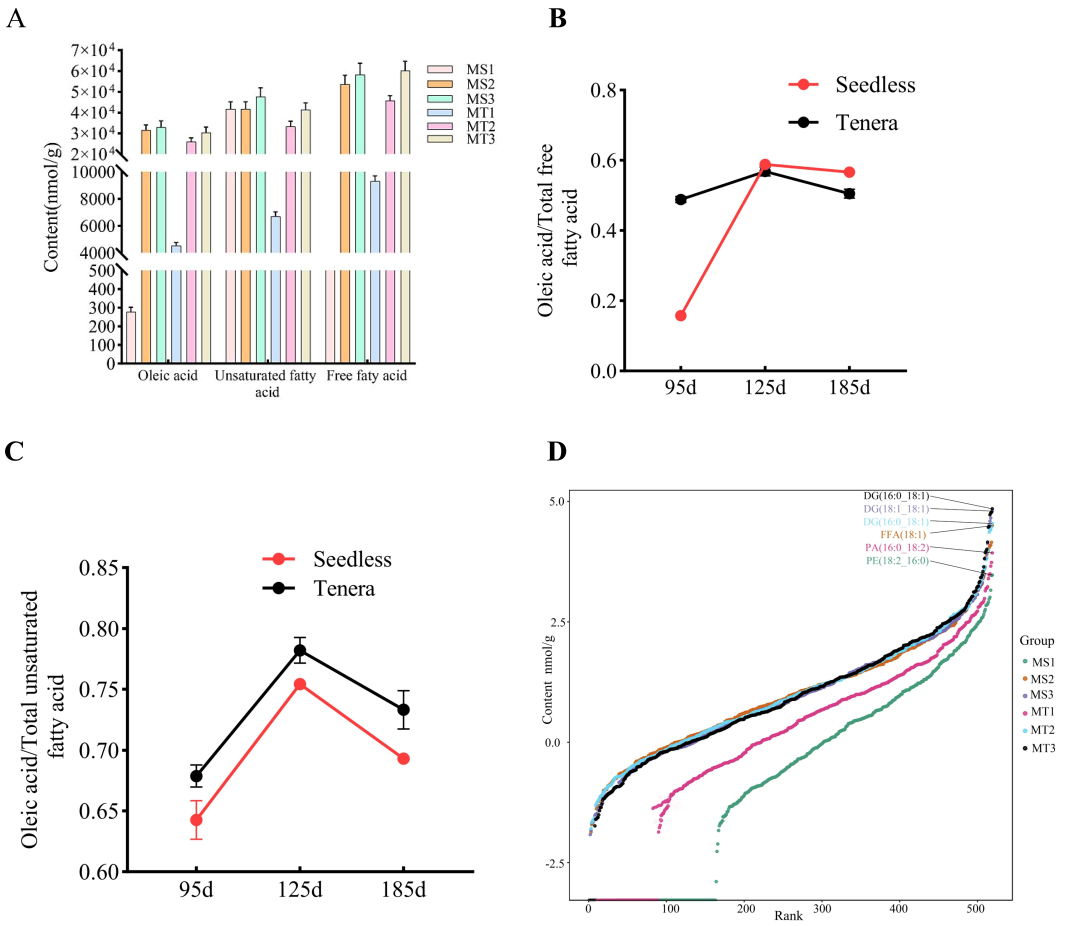

FIGURE 1
Dynamic changes of oleic acid content in Seedless and Tenera oil palm at different developmental stages. **(A)** Dynamics of oleic acid, unsaturated fatty acids, and total free fatty acids **(B)** Oleic acid as a percentage of total free fatty acids **(C)** Oleic acid as a percentage of total unsaturated fatty acids **(D)** Dynamic distribution of substances in all substance groups. Each point in the graph represents a lipid molecule. The vertical coordinate represents the corresponding content (log10 conversion) of each lipid molecule, and the lipid molecules with the highest contents are labelled. Different color curves represent different groupings.

shelled oil palm (21,471.81 nmol/g). From mid-development onwards, the oleic acid content of seedless oil palm exceeded that of thin-shelled oil palm, and the oleic acid content of the two varieties of oil palm reached a maximum at a later stage of development, a trend reflecting the pattern of unsaturated fatty acid content of the two varieties. The contribution of lipids in the pulp of the two varieties of oil palm at different developmental stages is as follows: at the early stage of development of the seedless species (MS1), the highest content of phosphatidylethanolamine (18:2_16:0), at the middle stage of development of the fruit (MS2), the highest content of fatty acids in the fruit pulp is said to be oleic acid (18:1), and at the late stage of development (MS3), the highest content of glycerol diesters (18:1_18:1). MS3), the highest content in the pulp was triglycerides (18:1_18:1); in the early stage of development of thin-shelled species of oil palm (MT1), the highest content in the pulp was phosphatidic acid (16:0_18:2), and in the middle stage of development of thin-shelled species of oil palm (MT2) and the late stage of development (MT3), the highest content in the pulp was triglycerides (16:0_18:1) (Figure 1D).

3.2 Differential metabolite analysis of comparative groups across developmental periods

Differential metabolite analysis was conducted across different developmental periods of oil palm, using criteria of fold-change ≥ 2 or fold-change ≤ 0.5 and VIP ≥ 1. A total of 19 differential metabolites were identified through comparisons of three developmental stages of oil palm (Table 1). In the comparison between the MS1 vs. MT1 stage, 12 differential metabolites were found, consisting of 11 up-regulated metabolites and 1 down-regulated metabolite (Figure 2A). At the MS2 vs. MT2 stage, 7 differential metabolites were identified, with 1 up-regulated metabolite and 6 down-regulated metabolites (Figure 2B). Finally, at the MS3 vs. MT3 stage, 9 differential metabolites were observed, with 4 up-regulated and 5 down-regulated metabolites (Figure 2C).

Three metabolites were commonly differential across all three comparison groups (Figure 2D): tridecanoic acid (Lipid-B-N-0017), myristic acid (Lipid-B-N-0005), and palmitoleic acid (Lipid-B-N-

TABLE 1 Differential metabolites in different comparison groups of oil palm mesocarp in Seedless and Tenera oil palm.

Comparable Group	Lipid Metabolites ID	Up/Down
MS1 VS. MT1	Lipid-B-N-0030; Lipid-B-N-0051; Lipid-B-N-0039; Lipid-B-N-0034;Lipid-B-N-0028; Lipid-B-N-0026; Lipid-B-N-0013; Lipid-B-N-0008; Lipid-B-N-0007; Lipid-B-N-0006; Lipid-B-N-0005	Up
	Lipid-B-N-0017	Down
MS2 VS. MT2	Lipid-B-N-0005	Up
	Lipid-B-N-0010;Lipid-B-N-0026;Lipid-B-N-0019;Lipid-B-N-0017;Lipid-B-N-0003;Lipid-B-N-0050	Down
MS3 VS. MT3	Lipid-B-N-0010;Lipid-B-N-0013;Lipid-B-N-0005;Lipid-B-N-0012	Up
	Lipid-B-N-0027;Lipid-B-N-0029;Lipid-B-N-0026;Lipid-B-N-0019;Lipid-B-N-0017	Down

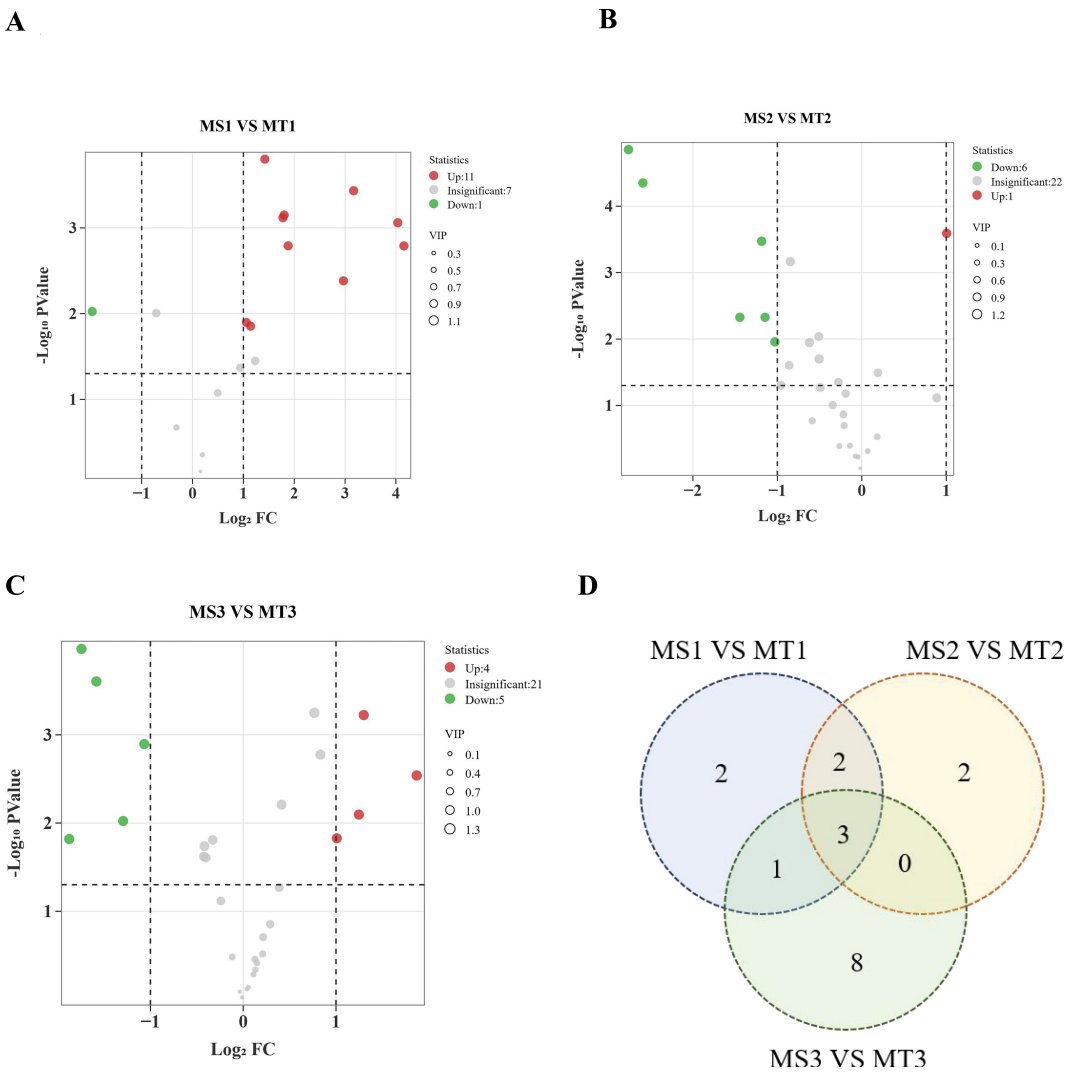

FIGURE 2
Statistics of different metabolites of oil palm in Seedless and Tenera **(A-C)**. **(A-C)** are volcano plots of MS1 VS MT1, MS2 VS MT2 and MS3 VS MT3 differential metabolites, respectively **(D)** Venn map. Each point represents a metabolite, with the horizontal axis showing the logarithm of the fold change between the two sample varieties (Log2 fold change) and the vertical axis representing the significance of the variable (VIP). Larger absolute values on the horizontal axis indicate greater significance of the difference. Green dots denote down-regulated metabolites, red dots represent up-regulated metabolites, and gray dots indicate metabolites with significant changes.

0026) (Table 2). Among these, only myristic acid was consistently up-regulated across all stages, while tridecanoic acid was the only metabolite consistently down-regulated. Palmitoleic acid was up-regulated in the early developmental stages but down-regulated in the mid- and late stages. Additionally, oleic acid (Lipid-B-N-0028) was up-regulated during the early stages of development. These findings offer valuable insights into the dynamic changes of fatty acid metabolites in the pulp of oil palm across different developmental stages.

3.3 Analysis of significantly differentially expressed genes at different developmental periods

Analysis of differentially expressed genes (DEGs) across developmental periods in oil palm revealed significant up- and down-regulation of gene expression. A comparison of transcriptome data between the two oil palm varieties at each growth stage during three developmental periods (MS1 vs. MT1, MS2 vs. MT2, and MS3 vs. MT3) identified 7140, 4881, and 4686 DEGs, respectively. Of these, 3159, 2395, and 2567 were up-regulated, while 3991, 2491, and 2129 were down-regulated (Figure 3A). Across all three comparative groups, a total of 1401 genes were significantly differentially expressed (Figure 3B). Additionally, 454 up-regulated and 626 down-regulated genes were common across both oil palm varieties in the three developmental periods (Figures 3C, D).

3.4 Enrichment analysis of significantly differentially expressed genes of oil palm fruits at different developmental periods

Enrichment analysis of significantly differentially expressed genes (DEGs) in oil palm fruits across different developmental periods, integrating metabolome data with transcriptome data and referencing KEGG metabolic pathway information, revealed that free fatty acids were enriched in five key lipid metabolism pathways of oil palm (Figures 4A–C). The five fatty acids with significant differences in the fatty acid biosynthesis pathways of oil palm, including those from Seedless and Tenera species, were two unsaturated fatty acids—oleic acid and palmitoleic acid—and three saturated fatty acids—palmitic acid, lauric acid, and myristic acid. These fatty acids corresponded to 37 differential genes (Table 3).

NR annotation of the 37 significantly differentially expressed genes in Seedless and Tenera oil palm species highlighted that genes such as *SAD*、 *FabD*, *LACS6*, *LACS9*, *FabB*, *BC*, and *FabI* were highly expressed during oil palm fruit development. Regarding the dynamic changes in the expression of these enzyme genes, *SAD* and *BC* exhibited a trend of increasing and then decreasing expression during fruit development in both seedless and thin-shelled oil palms, peaking at the middle developmental stage (Figures 5A, B). *LACS6* expression increased and peaked at the late developmental stage, while *LACS9* expression patterns differed between the two varieties: in seedless oil palm, *LACS9* expression was highest at MS1 and then decreased, whereas in thin-shelled oil palm, *LACS9* expression was lowest at MT1, subsequently increased, and peaked at MT3 (Figure 5C). *FabB* expression increased with development in thin-shelled oil palm and peaked at MT3 (Figure 5D), and the expression patterns of *FabD* and *FabI* increased and then decreased, reaching a maximum during the middle developmental stage (Figures 5E, F).

The dynamic changes in the content of the five differential metabolites were correlated with the expression changes of these seven enzyme genes (Figure 5; Tables 4, 5). The results indicated that *SAD*, *FabD*, *LACS6*, *BC*, *FabB*, and *FabI* were positively correlated with oleic acid content in both oil palm varieties, while *LACS9* exhibited a negative correlation with these five free fatty acids (Tables 4, 5). This suggests that the expression of these enzyme genes (*SAD*, *FabD*, *LACS6*, *BC*, *FabB*, and *FabI*) promotes oleic acid accumulation in the pulp, while *LACS9* expression inhibits this accumulation.

4 Discussion

The study revealed a significant increase in oleic acid levels during the developmental stages of oil palm fruits in both seedless and thin-shelled varieties, with pronounced accumulation occurring in the middle stage. By the late stage, the oleic acid content stabilized. In the late developmental stage, oleic acid content stabilized. Throughout the developmental process, the seedless species consistently exhibited higher oleic acid levels compared to the thin-shelled species. These results provide a foundational basis for the development of high-oleic-acid planting materials and strategies to enhance oleic acid content.

TABLE 2 Detailed information on common differential metabolites in the three comparison groups.

Lipid Metabolites ID	Lipid Metabolites	Q1 (Da)	Molecular Weight	Ionization model	Formula
Lipid-B-N-0026	FFA(16:1)	253.216755	254.22458	[M-H]-	C16H30O2
Lipid-B-N-0017	FFA(30:0)	451.44965	368.36543	[M-H]-	C24H48O2
Lipid-B-N-0005	FFA(14:0)	227.201105	228.20893	[M-H]-	C14H28O2

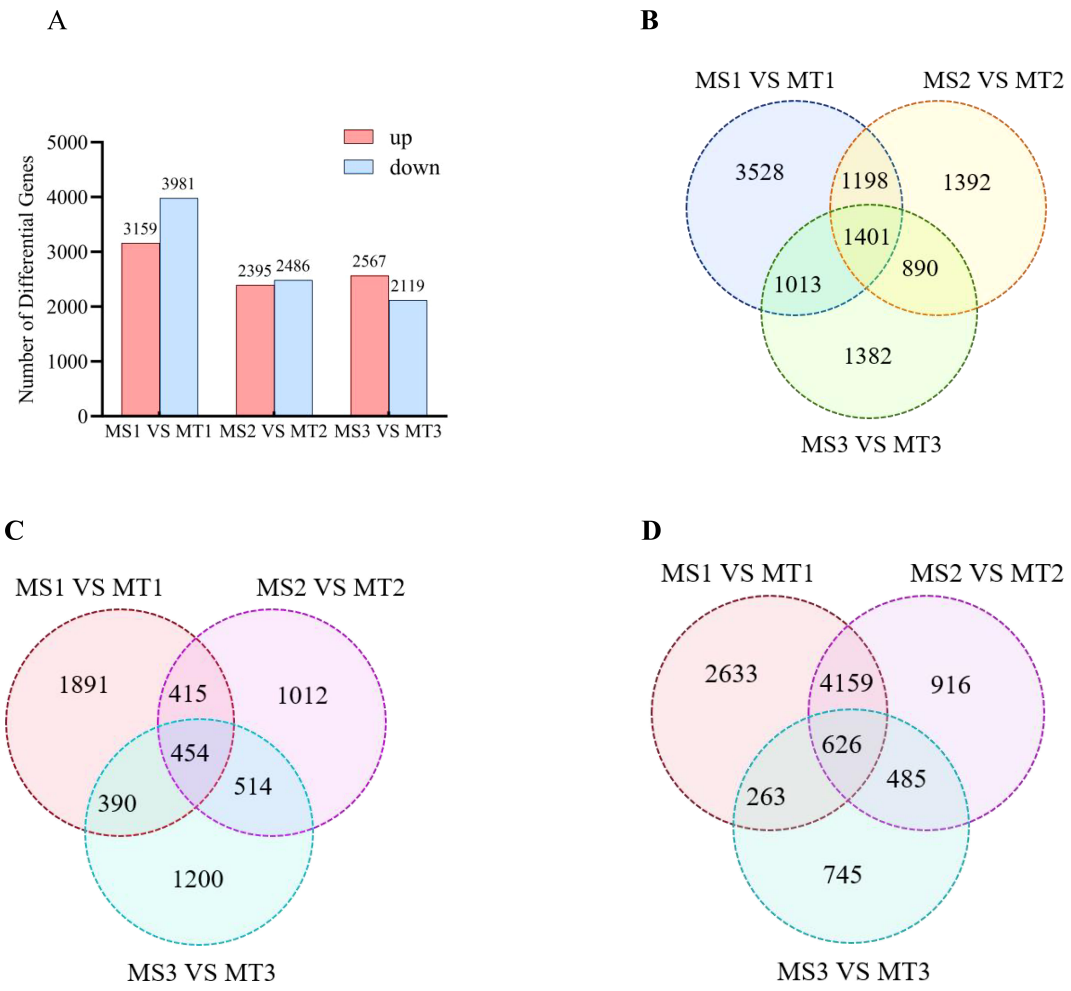

FIGURE 3
Statistics of different genes of oil palm in Seedless and Tenera **(A)** Histogram **(B)** Venn map of up/down-regulated differential genes **(C)** Venn map of up-regulated differential genes **(D)** Venn map of down-regulated differential genes.

4.1 *LACS* family genes exhibit distinct roles in oleic acid biosynthesis

Previous research supports these findings, highlighting the conserved roles of *LACS* family genes across different plant species. In Arabidopsis thaliana, most of the *LACS* family genes (comprising nine members) have been well characterized, with distinct functions in lipid metabolism (Zhang et al., 2018). Notably, *LACS6* in Arabidopsis has been implicated in the activation of fatty acids for storage lipid synthesis, aligning with our observations in oil palm. Additionally, studies in other crops have revealed similar patterns. For instance, two *LACS6* enzyme genes were found to exhibit strong correlations between their expression levels and metabolite content in oil-producing tissues. Specifically, *LACS6* showed high expression in the pulp, with peak expression occurring during the mid-to-late developmental stages (MT3 period), which is consistent with our findings in oil palm. Similar trends were also reported in stalked lentils (Bao et al., 2021), where *LACS6* expression was closely associated with increased lipid accumulation during key developmental phases. Zhong et al. (2023) reported that the expression of nearly all *LACS* genes was significantly higher in high-seeded oilseed cotton compared to low-seeded varieties, highlighting their importance in seed oil production. Similarly, in kale-type oilseed rape, *BnLACS2* plays a crucial role in seed oil biosynthesis, exhibiting substrate preferences for fatty acids such as 14:0, 16:0, 18:0, 18:1, and 22:1 (Ding et al., 2020). Furthermore, *LACS* genes have been shown to exhibit distinct expression patterns across different tissues and developmental stages (Ayaz et al., 2021). For instance, earlier research found that overexpression of *EgLACS9* in oil palm led to a significant reduction in palmitic, oleic, and linoleic acids (Wang et al., 2021), which is consistent with our observation that LACS9 may inhibit oleic acid accumulation in seedless oil palms. In contrast, *LACS6* has been identified as key enzyme in activating long-chain fatty acids for cellular lipid synthesis and degradation through β-oxidation (Shockey et al., 2002). In the present study, the *LACS6* exhibited a positive correlation with the five major free fatty acids in seedless oil palm (Table 4), indicating its role in enhancing the synthesis of these

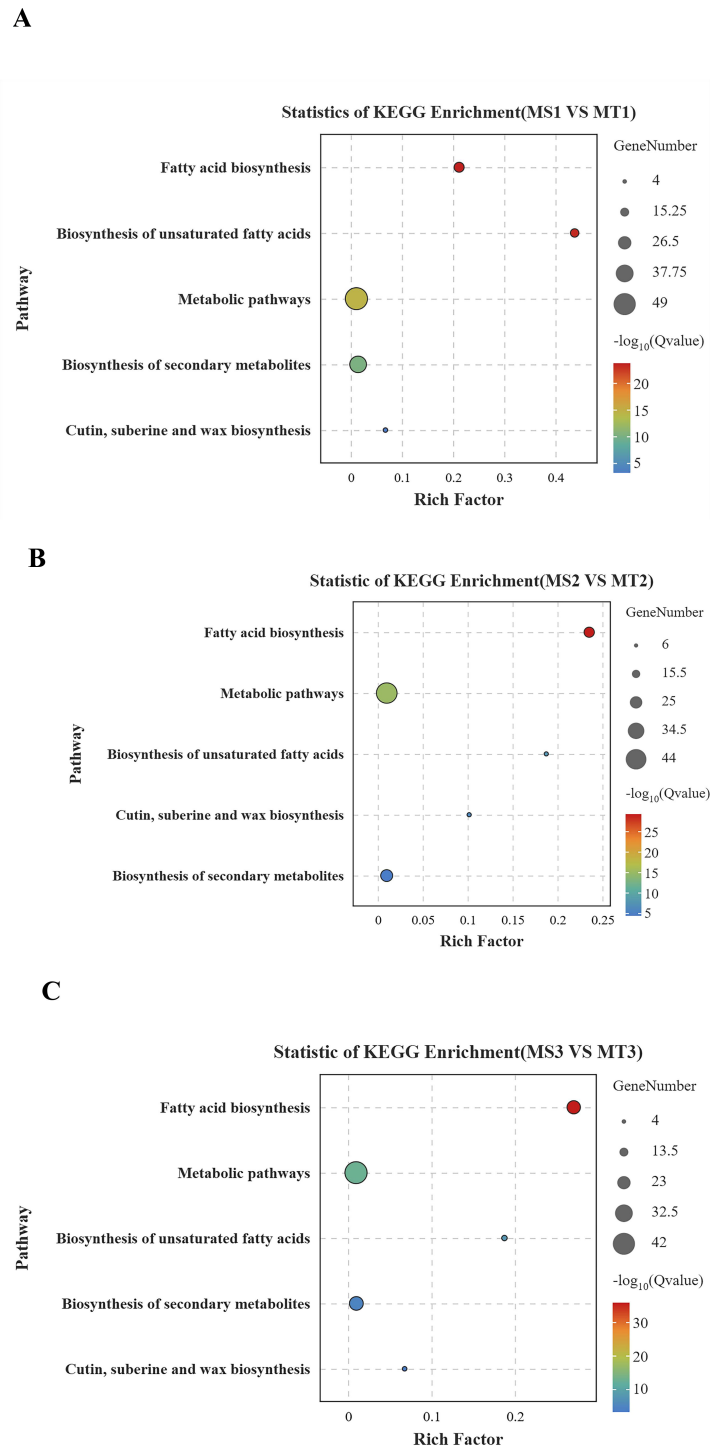

FIGURE 4
Bubble map of KEGG enrichment in oil palm fruit at different developmental periods. **(A)** differential gene KEGG results for MS1 vs MT1; **(B)** differential gene KEGG results for MS2 vs MT2; **(C)** differential gene KEGG results for MS3 vs MT3. The size of the circle indicates the number of different genes, and the larger the circle, the more genes. q value is a p-value that has been verified by multiple factors.

fatty acids in this variety. However, in thin-shelled oil palm, *LACS6* showed a negative correlation with lauric acid but positive correlation with palmitic acid, oleic acid, palmitoleic acid, and myristic acid (Table 5). This suggests that *LACS6* may promote the synthesis of these four fatty acids while inhibiting the lauric acid production in the mesocarp of thin-shelled oil palm.

4.2 *BC* genes promote oleic acid production

The *BC* gene plays an important role in fatty acid biosynthesis by catalyzing the biotin carboxylation reaction (Laseke et al., 2023). In the present study, *BC* exhibited a positive correlation with the

TABLE 3 Differential lipid metabolites and gene statistics of fatty acid biosynthesis (ko00061) pathway at different developmental periods of Seedless and Tenera oil palm mesocarp.

Comparable group	Lipid Metabolites ID	Lipid Metabolites	Genes ID
MS1 VS MT1	Lipid-B-N0028	FFA(18:1)Oleic acid	LOC105034511;LOC105035520;LOC105039456;LOC105042279;LOC105057927;LOC105061240;LOC105061231;LOC105040700;LOC105044978;LOC105048199;LOC105051934;novel.3082;LOC105050555;LOC105037839;LOC105049670;LOC105051176;novel.3968;LOC105050310
	Lipid-B-N0026	FFA(16:1) Palmitoleic acid	
	Lipid-B-N0007	FFA(16:0) Palmitic acid	
	Lipid-B-N-0005	FFA(14:0) Myristic acid	
MS2 VS MT2	Lipid-B-N0026	FFA(16:1) Palmitoleic acid	LOC105034507;LOC105035520;LOC105042279;LOC105042280;LOC105060936;LOC105058955;LOC105035642;LOC105039221;LOC105038382;LOC105040698;LOC105040700;novel.3082;LOC105050555;ElguCp049;LOC105051176;LOC105042027;LOC105056688;LOC105047747;LOC105050310;LOC105048939
	Lipid-B-N0005	FFA(14:0) Myristic acid	
	Lipid-B-N-0003	FFA(12:0) Lauric acid	
MS3 VS MT3	Lipid-B-N-0026	FFA(16:1) Palmitoleic acid	LOC105034507;LOC105034511;LOC105035520;LOC105039456;LOC105042279;LOC105061231;LOC105035641;LOC105040698;LOC105040700;LOC105044978;novel.3082;LOC105049274;ElguCp049;LOC105058068;LOC105037839;LOC105042027;LOC105056688;novel.2764;LOC105047747;LOC109506086;PTE;LOC105050310;LOC105048939
	Lipid-B-N-0005	FFA(14:0) Myristic acid	

levels of five free fatty acids in the pulp of seedless oil palm (Table 4), suggesting that *BC* may facilitate the synthesis of these fatty acids in this variety. Interestingly, in thin-shelled oil palm, ***BC*** showed a contrasting pattern- it was negatively correlated with lauric acid but positively correlated with palmitic acid, palmitoleic acid, oleic acid, and myristic acid (Table 5). This indicates that the expression of the *BC* enzyme gene may enhance the synthesis of the four fatty acids while simultaneously inhibiting the production of lauric acid in thin-shelled oil palm.

4.3 Role of *SAD* genes in promoting oleic acid biosynthesis

SAD genes play a pivotal role in fatty acid biosynthesis by catalyzing the desaturation of stearic acid (C18:0) to oleic acid (C18:1), a key step in the production of unsaturated fatty acids (Liu et al., 2020). In hybrid oil palm, the expression of *OeSAD1*, *OeSAD2*, and *OeSAD3* has been observed to increase during early developmental stages before declining in later stages, highlighting their dynamic role in lipid metabolism (Wang et al., 2022). Similarly, in peony seeds, *SAD1* and *SAD2* have been shown to catalyze the desaturation of C18:0 to C18:1, underscoring their importance in the biosynthesis of unsaturated fatty acids (Li et al., 2021). In the present study, *SAD* genes exhibited a positive correlation with palmitic acid, palmitoleic acid, oleic acid, myristic acid, and lauric acid in the pulp of seedless oil palm (Table 4). This suggests that *SAD* may promote the synthesis of these fatty acids during fruit development in seedless varieties. However, in thin-shelled oil palm, *SAD* genes showed a positive correlation with palmitic acid, palmitoleic acid, oleic acid, and myristic acid, but a negative correlation with lauric acid (Table 5). This indicates that *SAD* may enhance the synthesis of the former four fatty acids while suppressing lauric acid production in thin-shelled varieties. The result suggest that the dual role of *SAD* genes in regulating fatty acid composition, depending on the oil palm variety and developmental stage. The positive correlation between *SAD* and oleic acid in both seedless and thin-shelled oil palms underscores its critical role in promoting oleic acid biosynthesis. At the same time, the contrasting effects on lauric acid production suggest that *SAD* may act as a regulatory switch, modulating the balance between saturated and unsaturated fatty acids.

4.4 *FabB*, *FabD*, and *FabI* genes drive oleic acid accumulation in oil palm mesocarp

The *FabB*, *FabD*, and *FabI* genes play critical roles in the fatty acid biosynthesis pathway, contributing significantly to the accumulation of oleic acid in the mesocarp of oil palm. *FabB* acts as an activator of fatty acid synthase (FAS) and functions as a β-oxoacyl-ACP synthase, catalyzing the addition of acyl-ACP to malonyl-ACP to form β-oxoacyl-ACP, a key step in fatty acid synthesis II pathway (Lee et al., 2013). Enzymes encoded by the *FabA* and *FabB* genes are known to introduce double bonds in decane precursors, which are elongated into unsaturated fatty acyl chain such as the 16:1Δ9 and 18:1Δ11 essential for functional membrane phospholipids (Wei et al., 2024). In microalgae *fabB/F* has been identified as playing a key role in the elongation of medium fatty acids (C < 18) and the conversion of cis-16:1 to cis-18:1 (Gong and Miao, 2019). In this study, *FabB* was positively correlated with palmitic acid and myristic acid, oleic acid, and lauric acid in the pulp of seedless oil palm (Table 4). In thin-shelled oil palm, *FabB* showed positive correlation with palmitic acid, myristic acid, oleic acid, and palmitoleic acid but a negative correlation with lauric acid (Table 5). The results suggest that *FabB* supports the production of palmitic acid, myristic acid, and oleic acid in both seedless and thin-shelled oil palm varieties, while also enhancing lauric acid synthesis in seedless species and inhibiting its formation in thin-shelled species during fruit development.

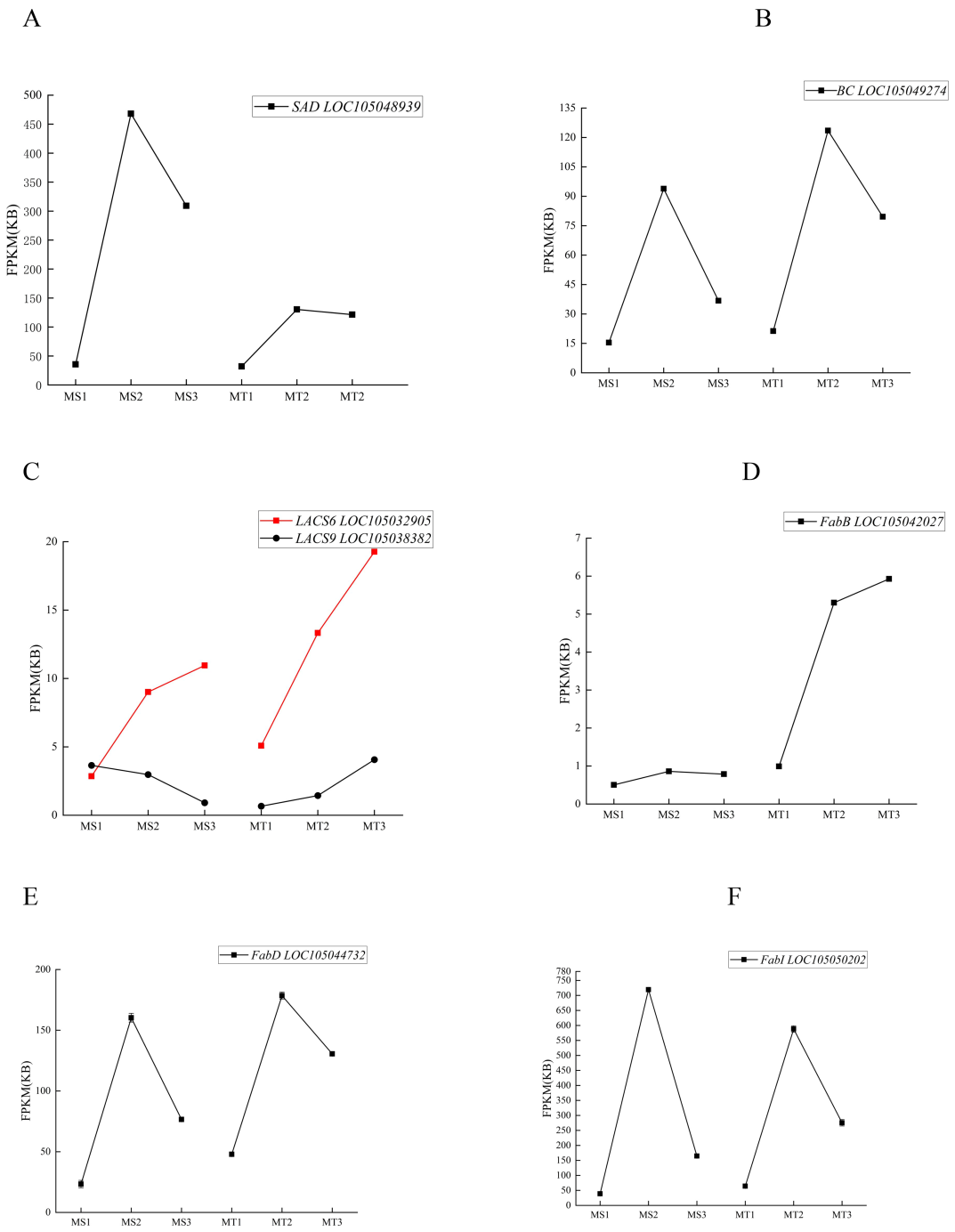

FIGURE 5
The expression levels of key enzyme genes changed dynamically in different developmental stages of seedless and Tenera oil palm **(A-F)**.

FabD is a crucial enzyme in the type II fatty acid synthesis pathway, responsible for transferring malonyl groups from malonyl coenzyme A to acyl carrier protein (ACP) to form malonyl-ACP and free coenzyme A-SH (Magnuson et al., 1993). In this study, *FabD* was positively correlated with the levels of five free fatty acids in the pulp of seedless oil palm (Table 4), and with oleic acid content in the pulp of Tenera oil palm (Table 5). The results suggest that the *FabD* likely facilitates oleic acid synthesis in both seedless and thin-shelled oil palm species.

FabI catalyzes the final step in type II fatty acid biosynthesis and is widely utilized for the production of pharmacologically relevant chiral intermediates, such as palmitic and oleic acids, due to its unique properties in reduction and asymmetric enantioselective catalysis (Zhou et al., 2023). In this study, the *FabI* was positively correlated with palmitic and oleic acid content in the pulp of seedless oil palm (Table 4). Additionally, *FabI* showed a strong positive correlation with oleic acid in the pulp of thin-shelled oil palm, with a notably high expression levels during the middle stage

TABLE 4 Correlation analysis of fatty acid content and enzyme genes in Seedless oil palm.

Gene ID	Enzyme name	Oleic acid	Myristic Acid	Palmitic acid	Palmitoleic acid	Lauric acid
LOC105044732	*FabD*	0.762	0.840	0.843	0.609	0.707
LOC105032905	*LACS6*	0.956	0.916	0.911	0.979	0.763
LOC105038382	*LACS9*	-0.973	-0.966	-0.965	-0.937	-0.693
LOC105049274	*BC*	0.677	0.771	0.775	0.505	0.663
LOC105048939	*SAD*	0.912	0.956	0.959	0.807	0.809
LOC105047027	*FabB*	0.714	0.801	0.806	0.550	0.687
LOC105050202	*FabI*	0.607	0.710	0.715	0.425	0.617

TABLE 5 Correlation analysis of fatty acid content and enzyme genes in Tenera oil palm.

Gene ID	Enzyme name	Oleic acid	Myristic Acid	Palmitic acid	Palmitoleic acid	Lauric acid
LOC105044732	*FabD*	0.854	0.666	0.733	0.689	-0.940
LOC105032905	*LACS6*	0.952	0.994	0.994	0.982	-0.674
LOC105038382	*LACS9*	-0.946	-0.981	-0.985	-0.959	0.644
LOC105049274	*BC*	0.820	0.611	0.682	0.638	-0.934
LOC105048939	*SAD*	0.951	0.848	0.890	0.858	-0.911
LOC105047027	*FabB*	0.880	0.718	0.777	0.736	-0.943
LOC105050202	*FabI*	0.693	0.454	0.532	0.488	-0.904

of development (Table 5). These findings suggest that the *FabI* plays a significant role in promoting oleic acid synthesis.

5 Conclusion

Significant differences in oleic acid content were observed between seedless and thin-shelled oil palms at various developmental stages. During the early developmental period, oleic acid content was higher in thin-shelled oil palms compared to seedless species. This difference may be attributed to the high expression of *LACS9* in seedless oil palms, which could inhibit oleic acid accumulation. In contrast, the elevated expression of *FabB* and *LACS6* genes in the thin-shelled oil palms appeared to promote oleic acid accumulation in thin-shelled oil palms. The mid-developmental stage emerged as crucial for oleic acid synthesis, with genes such as *FabD*, *LACS6*, *BC*, *SAD*, *FabB*, and *FabI* exhibiting high expression, levels, lead to a significant increase in oleic acid content during this period. By the late developmental stage, oleic acid levels stabilized, with comparable levels observed in both seedless and thin-shelled varieties, This stabilization likely resulted from distinct regulatory mechanisms involving the expression of *LACS9* and *LACS6*. These findings provide a theoretical foundation for selecting germplasm with high oleic acid content and breeding oil palm varieties enriched in unsaturated fatty acids. Future research incorporating proteomic analyses will be essential to identify differentially accumulated enzymes and establish stronger connections between transcriptomic changes and metabolite profiles. Such approaches will offer deeper insights into the regulatory mechanisms governing oleic acid biosynthesis, enabling more precise strategies for metabolic engineering and crop improvement.

Data availability statement

The datasets presented in this study can be found in online repositories. The names of the repository/repositories and accession number(s) can be found in the article/Supplementary Material.

Author contributions

WX: Conceptualization, Methodology, Writing – original draft, Writing – review & editing. JJ: Conceptualization, Data curation, Writing – original draft, Writing – review & editing. XL (3rd Author): Data curation, Investigation, Writing – original draft, Writing – review & editing. XL (4th Author): Validation, Visualization, Writing – original draft, Writing – review & editing. SC: Formal analysis, Supervision, Writing – original draft, Writing – review & editing.

HC: Formal analysis, Funding acquisition, Project administration, Supervision, Writing – original draft, Writing – review & editing.

Funding

The author(s) declare financial support was received for the research, authorship, and/or publication of this article. This research work was financially supported by the National Key R&D program of China (2023YFD2200700), China Agriculture Research System (CARS-14-2-31), Central Public Interest Scientific Institution Basal Research Fund for Chinese Academy of Tropical Agricultural Sciences (No. 1630152022001)and Protection of species and variety resources on tropical palm of Ministry of Agriculture and Rural Affair (No. 1820003).

Conflict of interest

The authors declare that the research was conducted in the absence of any commercial or financial relationships that could be construed as a potential conflict of interest.

Generative AI statement

The author(s) declare that no Generative AI was used in the creation of this manuscript.

Publisher's note

Supplementary material

The Supplementary Material for this article can be found online at: https://www.frontiersin.org/articles/10.3389/fpls.2025.1557544/full#supplementary-material

References

Al Amin, N., Ahmad, N., Wu, N., Pu, X., Ma, T., Du, Y., et al. (2019). CRISPR-Cas9 mediated targeted disruption of FAD2-2 microsomal omega-6 desaturase in soybean (Glycine max. L). *BMC Biotechnol.* 19, 9. doi: 10.1186/s12896-019-0501-2

Ayaz, A., Saqib, S., Huang, H., Zaman, W., Lü, S., and Zhao, H. (2021). Genome-wide comparative analysis of long-chain acyl-CoA synthetases (LACSs) gene family: A focus on identification, evolution and expression profiling related to lipid synthesis. *Plant Physiol. Biochem.* 161, 1–11. doi: 10.1016/j.plaphy.2021.01.042

Bahariah, B., Masani, M. Y. A., Fizree, M.P.M.A.A., Rasid, O. A., and Parveez, G. K. A. (2023). Multiplex CRISPR/Cas9 gene-editing platform in oil palm targeting mutations in EgFAD2 and EgPAT genes. *J. Genet. Eng. Biotechnol.* 21, 3. doi: 10.1186/s43141-022-00459-5

Bahariah, B., Masani, M. Y. A., Rasid, O. A., and Parveez, G. K. A. (2021). Multiplex CRISPR/Cas9-mediated genome editing of the FAD2 gene in rice: a model genome editing system for oil palm. *J. Genet. Eng. Biotechnol.* 19, 86. doi: 10.1186/s43141-021-00185-4

Bao, W. Q., Ao, D., Wang, L., Ling, Z. H., Chen, M. S., Bai, Y., et al. (2021). Dynamic transcriptome analysis identifies genes related to fatty acid biosynthesis in the seeds of Prunus pedunculata Pall. *BMC. Plant Biol.* 21, 152. doi: 10.1186/s12870-021-02921-x

Ben Ayed, R., Chirmade, T., Hanana, M., Khamassi, K., Ercisli, S., Choudhary, R., et al. (2022). Comparative analysis and structural modeling of elaeis oleifera FAD2, a fatty acid desaturase involved in unsaturated fatty acid composition of american oil palm. *Biol. (Basel)* 11, 529. doi: 10.3390/biology11040529

Chang, T., Wu, J., Wu, X., Yao, M., Zhao, D., Guan, C., et al. (2022). Comprehensive evaluation of high-oleic rapeseed (Brassica napus) based on quality, resistance, and yield traits: A new method for rapid identification of high-oleic acid rapeseed germplasm. *PloS One* 17, e0272798. doi: 10.1371/journal.pone.0272798

Ding, L. N., Gu, S. L., Zhu, F. G., Ma, Z. Y., Li, J., Li, M., et al. (2020). Long-chain acyl-CoA synthetase 2 is involved in seed oil production in Brassica napus. *BMC Plant Biol.* 20, 21. doi: 10.1186/s12870-020-2240-x

Do, P. T., Nguyen, C. X., Bui, H. T., Tran, L. T. N., Stacey, G., Gillman, J. D., et al. (2019). Demonstration of highly efficient dual gRNA CRISPR/Cas9 editing of the homeologous GmFAD2-1A and GmFAD2-1B genes to yield a high oleic, low linoleic and α-linolenic acid phenotype in soybean. *BMC Plant Biol.* 19, 311. doi: 10.1186/s12870-019-1906-8

Dussert, S., Guerin, C., Andersson, M., Joët, T., Tranbarger, T. J., Pizot, M., et al. (2013). Comparative transcriptome analysis of three oil palm fruit and seed tissues that differ in oil content and fatty acid composition. *Plant Physiol.* 162, 1337–1358. doi: 10.1104/pp.113.220525

Gong, Y., and Miao, X. (2019). Short chain fatty acid biosynthesis in microalgae synechococcus sp. PCC 7942. *Mar. Drugs* 17, 255. doi: 10.3390/md17050255

He, M., Qin, C. X., Wang, X., and Ding, N. Z. (2020). Plant unsaturated fatty acids: biosynthesis and regulation. *Front. Plant Sci.* 11. doi: 10.3389/fpls.2020.00390

Katariya, A., Gajera, V., Lambole, V., Shah, D., and Joshi, H. (2021). Review on: role of oleic acid in various disease. *Int. J. Pharm. Sci. Rev. Res.* 197–205. doi: 10.47583/ijpsrr.2021.v67i02.031

Laseke, A. J., Boram, T. J., Schneider, N. O., Lohman, J. R., and St Maurice, M. (2023). Allosteric Site at the Biotin Carboxylase Dimer Interface Mediates Activation and Inhibition in Staphylococcus aureus Pyruvate Carboxylase. *Biochemistry* 62, 2632–2644. doi: 10.1021/acs.biochem.3c00280

Lee, S., Lee, S., Yoon, Y. J., and Lee, J. (2013). Enhancement of Long-Chain Fatty Acid Production in Escherichia coli by Coexpressing Genes, Including fabF, Involved in the Elongation Cycle of Fatty Acid Biosynthesis. *Appl. Biochem. Biotechnol.* 169, 462–476. doi: 10.1007/s12010-012-9987-y

Li, C., Hu, L., Que, B., Hu, Y., Guo, Y., Zhang, M., et al. (2021). Expression profiles of genes involved in fatty acid and lipid biosynthesis in developing seeds of Paeonia ostii. *Genes Genomics* 43, 885–896. doi: 10.1007/s13258-021-01102-2

Li, S. Y., Zhang, Q., Jin, Y. H., Zou, J. X., Zheng, Y. S., and Li, D. D. (2020). A MADS-box gene, EgMADS21, negatively regulates EgDGAT2 expression and decreases polyunsaturated fatty acid accumulation in oil palm (Elaeis guineensis Jacq.). *Plant Cell Rep.* 39, 1505–1516. doi: 10.1007/s00299-020-02579-z

Liu, G., Wu, Z., Peng, Y., Shang, X., Xie, Y., and Arnold, R. J. (2020). Transcriptome analyses reveals the dynamic nature of oil accumulation during seed development of Plukenetia volubilis L. *Sci. Rep.* 10, 20467. doi: 10.1038/s41598-020-77177-w

Luo, S., Huang, J., Jin, L., Zou, J., Zheng, Y., and Li, D. (2024). Transcription factor EgGRP2A regulates EgFATA expression and promotes oleic acid accumulation in oil palm (Elaeis guineensis). *J. Plant Physiol.* 299, 154263. doi: 10.1016/j.jplph.2024.154263

Magnuson, K., Jackowski, S., Rock, C. O., and Cronan, J. E. Jr. (1993). Regulation of fatty acid biosynthesis in Escherichia coli. *Microbiol. Rev.* 57, 522–542. doi: 10.1128/mr.57.3.522-542.1993

Morcillo, F., Vaissayre, V., Serret, J., Avallone, S., Domonhédo, H., Jacob, F., et al. (2021). Natural diversity in the carotene, tocochromanol and fatty acid composition of crude palm oil. *Food Chem.* 365, 130638. doi: 10.1016/j.foodchem.2021.130638

Okuzaki, A., Ogawa, T., Koizuka, C., Kaneko, K., Inaba, M., Imamura, J., et al. (2018). CRISPR/Cas9-mediated genome editing of the fatty acid desaturase 2 gene in Brassica Napus. *Plant Physiol. Biochem.* 131, 63–69. doi: 10.1016/j.plaphy.2018.04.025

Papilo, P., Marimin, M., Hambali, E., Machfud, M., Yani, M., Asrol, M., et al. (2022). Palm oil-based bioenergy sustainability and policy in Indonesia and Malaysia: A systematic review and future agendas. *Heliyon* 8, e10919. doi: 10.1016/j.heliyon.2022.e10919

Sambanthamurthi, R., Akmar, A. S. N., and Parveez, G. K. A. (2002). Genetic manipulation of the oil palm - challenges and prospects. *Planter* 78, 547–562.

Shockey, J. M., Fulda, M. S., and Browse, J. A. (2002). Arabidopsis contains nine long-chain acyl-coenzyme a synthetase genes that participate in fatty acid and glycerolipid metabolism. *Plant Physiol.* 129, 1710–1722. doi: 10.1104/pp.003269

Sun, R., Gao, L., Yu, X., Zheng, Y., Li, D., and Wang, X. (2016). Identification of a Δ12 fatty acid desaturase from oil palm (Elaeis guineensis Jacq.) involved in the biosynthesis of linoleic acid by heterologous expression in Saccharomyces cerevisiae. *Gene* 591, 21–26. doi: 10.1016/j.gene.2016.06.039

Voon, P. T., Lee, S. T., Ng, T. K. W., Ng, Y. T., Yong, X. S., Lee, V. K. M., et al. (2019). Intake of palm olein and lipid status in healthy adults: A meta-analysis. *Adv. Nutr.* 10, 647–659. doi: 10.1093/advances/nmy122

Wang, M., Li, R., Cao, H., Jin, L., and Li, X. (2022). Cloning and expression analysis of the oil palm Δ9 stearoyl-ACP dehydrogenase EgSAD gene. *J. Trop. Crops* 43, 235–243. doi: 10.3969/j.issn.1000-2561.2022.02.002

Wang, Y., Zhao, J., Chen, H., Zhang, Q., Zheng, Y., and Li, D. (2021). Molecular cloning and characterization of long-chain acyl-CoA synthetase 9 from the mesocarp of African oil palm (Elaeis guineensis Jacq.). *Scientia Hortic.* 276, 109751. doi: 10.1016/j.scienta.2020.109751

Wei, L., Yang, C., John Martin, J. J., Li, R., Zhou, L., Cheng, S., et al. (2024). Metabonomics and transcriptomic analysis of free fatty acid synthesis in seedless and tenera oil palm. *Int. J. Mol. Sci.* 25, 1686. doi: 10.3390/ijms25031686

Yeap, W. C., Lee, F. C., Shabari Shan, D. K., Musa, H., Appleton, D. R., and Kulaveerasingam, H. (2017). WRI1-1, ABI5, NF-YA3 and NF-YC2 increase oil biosynthesis in coordination with hormonal signaling during fruit development in oil palm. *Plant J.* 91, 97–113. doi: 10.1111/tpj.13549

Zhang, Q., Jin, Y.-h., Zou, J.-x., Zheng, Y.-s., and Li, D.-d. (2022). Characterization and functional analysis of the MADS-box EgAGL9 transcription factor from the mesocarp of oil palm (Elaeis guineensis Jacq.). *Plant Sci.* 321, 111317. doi: 10.1016/j.plantsci.2022.111317

Zhang, C., Maddelein, M.-L., Wai-Yin-Sun, R., Gornitzka, H., Cuvillier, O., and Hemmert, C. (2018). Pharmacomodulation on Gold-NHC complexes for anticancer applications – is lipophilicity the key point? *Eur. J. Medicinal Chem.* 157, 320–332. doi: 10.1016/j.ejmech.2018.07.070

Zhong, Y., Wang, Y., Li, P., Gong, W., Wang, X., Yan, H., et al. (2023). Genome-wide analysis and functional characterization of LACS gene family associated with lipid synthesis in cotton (Gossypium spp.). *Int. J. Mol. Sci.* 24, 8530. doi: 10.3390/ijms24108530

Zhou, J., Zhang, L., Wang, Y., Song, W., Huang, Y., Mu, Y., et al. (2023). The molecular basis of catalysis by SDR family members ketoacyl-ACP reductase fabG and enoyl-ACP reductase fabI in type-II fatty acid biosynthesis. *Angewandte Chemie-international Edition* 62, e202313109. doi: 10.1002/anie.202313109

frontiers | Frontiers in Plant Science

TYPE Original Research
PUBLISHED 05 March 2025
DOI 10.3389/fpls.2025.1537924

OPEN ACCESS

EDITED BY
Marta Sousa Silva,
University of Lisbon, Portugal

REVIEWED BY
Andrey Stoyanov Marchev,
Bulgarian Academy of Sciences, Bulgaria
Jianwen Qiao,
Yan'an University, China

*CORRESPONDENCE
Yubo Zhang
zyb781210@sina.com

†These authors have contributed equally to this work

RECEIVED 02 December 2024
ACCEPTED 11 February 2025
PUBLISHED 05 March 2025

CITATION
Hu X, Xu W, Zhang Y, Pan S, Xie Y, Liao R, Yang S, Wu Y and Deng D (2025) Microstructure observation and flavor substances excavation of Yunyan 87 tobacco leaves with different oil contents.
Front. Plant Sci. 16:1537924.
doi: 10.3389/fpls.2025.1537924

Microstructure observation and flavor substances excavation of Yunyan 87 tobacco leaves with different oil contents

Xianfeng Hu[1†], Wei Xu[2†], Yubo Zhang[1*], Shouhui Pan[3], Yanlan Xie[1], Rui Liao[2], Shenggang Yang[2], Youxiang Wu[2] and Daomao Deng[3]

[1]College of Agriculture, Anshun University, Anshun, Guizhou, China, [2]Raw Material Supply Center, China Tobacco Guizhou Industrial Co Ltd., Guiyang, Guizhou, China, [3]Production Technology Center, Guizhou Province Tobacco Company Anshun Company, Anshun, Guizhou, China

Introduction: The oil content of tobacco leaves is intimately associated with their aromatic characteristics. This study aims to explore the microstructure and distinctive flavor substances of Yunyan 87 high-oil-content tobacco leaves.

Methods: The microstructure and characteristic flavor substances of Yunyan 87 tobacco leaves with different oil contents were analyzed using scanning electron microscope (SEM) and comprehensive two-dimensional gas chromatography coupled with time-of-flight mass spectrometry (GC×GC-TOF MS).

Results: The results indicate that the surface of high-oil tobacco leaves was characterized by a high density of glandular hairs, primarily composed of short-stalked glandular hairs featuring enlarged glandular heads. A total of 1551 flavor substances were detected in high-oil tobacco leaves, compared to 1500 metabolites were identified in low-oil tobacco leaves. Among these flavor substances, eight exhibited up-regulated, while three were down-regulated. Notably, the oil-related substances hexadecanoic acid methyl ester and the aroma-related substances nonanoic acid methyl ester and pseudoionone were found to be significantly more abundant in high-oil tobacco leaves compared to their low-oil counterparts. Consequently, hexadecanoic acid methyl ester may serve as a reliable indicator for evaluating the oil content in tobacco leaves, while nonanoic acid methyl ester and pseudoionone could play crucial roles as flavor substances influencing the aroma of tobacco leaves.

Discussion: These findings provide a theoretical foundation for future research on the regulatory mechanisms underlying the synthesis of aroma-producing flavor substances in tobacco leaves.

KEYWORDS

flavor substances, hexadecanoic acid methyl ester, nonanoic acid methyl ester, pseudoionone, tobacco oil content

1 Introduction

Tobacco (*Nicotiana tabacum* L.) serves as a cash crop that plays a crucial role in the economies of numerous countries (Wang and Yan, 2013; Yin et al., 2019). The aroma of tobacco represents a complex perception by the human olfactory system in response to the volatile organic compounds (VOCs) emitted by combusted tobacco leaves. High-quality tobacco leaves are characterized by a mellow taste, distinctive flavor, and rich aroma. The precursors of tobacco aroma include sugars, pigments, amino acids, polyphenols, and alkaloids, all of which make a significant contribution to the aroma quality of tobacco products (Zhang et al., 2013; Qin et al., 2020; Liu et al., 2022). The flavor substances in tobacco leaves can be categorized into alcohols, aldehydes, ketones, acids, esters, and phenols based on their functional groups (Forehand et al., 2000). Researchers employed non-targeted metabolomics to identify the substances responsible for aroma generation before and after the baking of K326 tobacco and to assess their relevance to the quality of tobacco leaves. Among the 584 metabolites analyzed, 44 were identified as aroma - related metabolites, including alcohols, aldehydes, phenols, and organic acids (Zou et al., 2023). The variety, maturity, cultivation conditions, altitude, climate, and processing technology of tobacco significantly influence the composition and concentration of its aromatic components. Yan et al (Yan et al., 2020). reported that the application of active organic carbon in the soil enriches the aromatic substances present in tobacco leaves. Compared with pure chemical treatment, the combined application of biochar and chemical fertilizers as well as high - carbon and chemical fertilizer treatment can increase soil carbon and nitrogen contents, and enhance the levels of neutral aromatic substances in tobacco leaves by 19. 38% and 28. 90% respectively (Yan et al., 2020a). The researchers discovered that the abundance of aromatic substances in Changchun tobacco leaves sourced from Jilin Province was greater than that in Nanxiong tobacco leaves obtained from Guangdong Province (Qin et al., 2021). Furthermore, the aroma of tobacco leaves is closely associated with their oil content, leaves with higher oil content exhibit a more pronounced aroma. An enhanced oil content not only augments the softness of tobacco leaves but also elevates their grade and quality, thereby yielding a more robust flavor. Nevertheless, studies on the differences in the microstructures and flavor substances among tobacco leaves with diverse oil contents are rarely reported.

Flavor omics is widely used to analyze the flavor characteristics of various foods, including alcohol, tea, fruits, chili peppers, and meat products, etc (Huang et al., 2022; Wang et al., 2022; Yang et al., 2022; Gu et al., 2023; Ruan et al., 2023; Li et al., 2024; Lin et al., 2024). Comprehensive two-dimensional gas chromatography time-of-flight mass spectrometry (GC×GC-TOF MS) is characterized by high throughput, precision, sensitivity, and reproducibility, and is thus widely applied in flavor omics. Chen et al (Chen et al., 2024). conducted a comprehensive analysis of the flavor characteristics of rapeseed protein isolates treated with phytase and ethanol using GC×GC-TOF MS. They found that this treatment led to a decrease in carboxylic acid substances with acidic odors and an increase in ester substances that contribute to the fruity and sweet aroma of the rapeseed protein isolates. Schwanz et al (Schwanz et al., 2019). employed GC×GC-TOF MS in combination with chemometrics to analyze the chemical sensory markers in cigarette smoke derived from diverse tobacco varieties, thereby establishing a correlation among key chemical sensory markers, tobacco varieties, and cultivation practices. In conclusion, GC×GC-TOF MS characterized by prominent advantages including high - resolution capability, high sensitivity, and the capacity to rapidly analyze numerous compounds in complex samples, provides a comprehensive analytical methodology for the investigation of flavor substances.

The oil content of tobacco leaves is a crucial indicator for quality evaluation. Tobacco leaves with higher oil content are characterized by improved aroma quality. This paper is aimed at exploring the microstructure and distinctive flavor substances of Yunyan 87 high-oil-content tobacco leaves. The Yunyan 87 tobacco leaves, characterized by different oil contents, were analyzed using scanning electron microscope (SEM) and GC×GC-TOF MS to elucidate the microstructure and distinctive flavor substances present in high-oil content Yunyan 87 tobacco leaves. This research provides a theoretical foundation for further exploration of the synthesis and regulatory mechanisms underlying aroma-producing characteristic flavor substances in tobacco leaves.

2 Materials and methods

2.1 Materials

Ethanol (99. 8%) was procured from Aladdin Holding Group Co. , Ltd. (Beijing, China). Sodium chloride, anhydrous ethanol, and isoamyl acetate were sourced from Sinopharm Chemical Reagents Co. , Ltd. (Shanghai, China). Electron microscope stationary liquid and phosphate buffered saline (PBS) were obtained from Wuhan Xavier Biotechnology Co. , Ltd. (Wuhan, China), while osmic acid was purchased from Shanghai Kanglang Biotechnology Co. , Ltd. (Shanghai, China).

2.2 Sensory evaluation of tobacco leaves

Five tobacco sensory evaluation experts from Guizhou Zhongyan Industrial Co. , Ltd. evaluated ten Yunyan 87 dry tobacco leaf samples for indicators such as aroma quality, aroma quantity, miscellaneous gas, thrill, sweet feeling, and oil content. The specific criteria are as follows:

1. *Aroma quality*: relatively good (7. 6–9. 0), above-average (6. 1–7. 5), moderate (4. 6–6. 0), below-average (3. 1–4. 5), poor (≤3).
2. *Aroma quantity*: sufficient (7. 6–9. 0), adequate (6. 1–7. 5), available (4. 6–6. 0), less (3. 1–4. 5), very less (≤3).
3. *Miscellaneous gas*: very light (7. 6–9. 0), light (6. 1–7. 5), moderate (4. 6–6. 0), heavy (3. 1–4. 5), very heavy (≤3).

4. *Thrill*: very small (7. 6–9. 0), small (6. 1–7. 5), moderate (4. 6–6. 0), large (3. 1–4. 5), very large (≤3).
5. *Agreeable aftertaste*: comfortable (7. 6–9. 0), relatively comfortable (6. 1–7. 5), moderate (4. 6–6. 0), inadequate (3. 1–4. 5), tongue stagnation (≤3).
6. *Sweet feeling*: significant (7. 6–9. 0), relatively significant (6. 1–7. 5), still significant (4. 6–6. 0), moderate (3. 1–4. 5), weak (≤3).
7. *Oil content*: rich (++++), more (+++), slightly (++), less (+).

Based on the evaluation results, samples with high oil content were selected for subsequent analysis and designated as H samples, while those with low oil content were labeled as L samples.

2.3 Assessment of agronomic traits in tobacco leaves

The lengths, widths, and single - leaf dry weights of tobacco leaves with high oil content and those with low oil content were measured separately. Each measurement was repeated three times, and the average values were calculated. The high - oil and low - oil tobacco leaves were evaluated in terms of the color, oily texture, and softness of dried tobacco leaves, and photographs were taken. The leaf shape index was calculated according to Equation 1 as follows:

$$\text{Leaf shape index} = \text{leaf length}/\text{leaf width} \quad (1)$$

2.4 Observation microscopic morphology of tobacco leaves

Yunyan 87 dried tobacco leaves with high - oil and low - oil contents were punched and sampled in such a way as to minimize mechanical damage, and the area of the tissue blocks did not exceed 3 mm^2. The samples were gently rinsed with PBS, and the surface intended for scanning was carefully protected and marked. Subsequently, the samples were rapidly positioned in an electron microscope fixative solution and fixed at room temperature for 2 hours. Then, the samples were transferred to 4°C for storage. The fixed samples were rinsed three times with 0. 1 M PBS (pH 7. 4), each rinse lasting 15 min. An osmium acid solution (1%) was prepared using 0. 1 M PBS (pH 7. 4) and incubated at room temperature in the dark for 1 - 2 hours. Afterward, it was rinsed three times with 0. 1 M PBS (pH 7. 4), each rinse lasting 15 min. The samples were treated with 30, 50, 70, 80, 90, 95, 100, and 100% alcohol for 15 min and finally treated with isoamyl acetate for 15 min. The samples were placed in a critical point dryer for drying. The tobacco leaves were placed close to the conductive carbon film double-sided adhesive and on the sample table of the ion sputtering instrument for gold spraying for approximately 30 s. Scanning electron microscopy (SEM, SU8100, HITACHI, Tokyo, Japan) was utilized to observe and capture images.

2.5 Flavor substances detection of tobacco leaves

Based on the sensory evaluation results of the Yunyan 87 oil content carried out by Guizhou China Tobacco Industry Co. , Ltd. , dry tobacco samples with high oil content were selected and labeled H-1, H-2, and H-3, while dry tobacco samples with low oil content were named L-1, L-2, and L-3. Tobacco leaves were mailed to Suzhou Panomik Biomedical Technology Co. , Ltd. (Jiangsu, China) for testing to clarify the characteristic flavor substances of Yunyan 87 tobacco leaves with high-oil content.

2.5.1 Preparation of internal standard solution

An appropriate quantity of the standard (deuterated n - hexanol - d13) was transferred and dissolved in a 50% ethanol aqueous solution. A single - standard mother liquor at a concentration of 10 mg/L was prepared, and the stock solution was refrigerated at 4°C.

2.5.2 Flavor substances extraction

Place the sample in a 15 mL centrifuge tube and dilute the ethanol concentration in the sample to 10% (v/v) with a saturated sodium chloride aqueous solution. The 5 mL of diluted liquor samples was transferred to 20 mL headspace sampling bottles, and 10 μL of the internal standard solution was added to the sample. The transferred sample was incubated for 10 min at 50°C. Before adsorbing the sample, the solid-phase microextraction (SPME) extraction head was aged at 270°C for 10 min. Subsequently, the aged SPME extraction head was transferred to the incubation room, and the sample was adsorbed for 30 min at 50°C. After adsorption, the SPME extraction head was transferred to the gas chromatography (GC) inlet, desorbed at 5 min at 250°C, and then aged for 10 min at 270°C post-injection.

2.5.3 GC×GC analysis

The LECO Pegasus BT 4D (LECO, St. Joseph, MI, USA) GC×GC-TOF MS chromatographic system consists of an Agilent 8890A gas chromatograph (Agilent Technologies, Palo Alto, CA, USA), a dual-stage jet modulator, and a split/splitless injection module. The mass spectrometric system is a high-resolution TOF mass spectrometer. The separation system comprises a first-dimensional chromatographic column, namely Rxi-5Sil MS (30 m × 0. 25 mm × 0. 25 μm, Restek) (Restek, USA), which is suitable for the preliminary separation of volatile and non-polar compounds, and a second-dimensional chromatographic column, namely Rxi-17Sil MS (1. 5 m × 0. 15 mm × 0. 15 μm, Restek) (Restek, USA), which enables secondary orthogonal separation via selective differences. High-purity helium gas (99. 999%) is used as the carrier gas, and an electronic flow controller is employed to maintain a constant flow rate of 1. 0 mL/min, ensuring the reproducibility of retention times. For the first-dimensional chromatographic column Rxi-5Sil MS, the initial temperature is set at 40°C and maintained for 3 min. Subsequently, the temperature is increased at a rate of 5°C/min until it reaches 180°C, after which it is held at this temperature for 1 min. Thereafter, the

temperature is further raised at a rate of 4°C/min to 250°C and finally maintained at this final temperature for 3 min. The temperature program of the second-dimensional chromatographic column Rxi-17Sil MS is 5°C higher than that of the first-dimensional chromatographic column. The modulator temperature is always 15°C higher than the column temperature of the second-dimensional chromatographic column, with a modulation period of 8 s, effectively avoiding peak broadening and improving the two-dimensional separation efficiency. The injection system features a high-temperature injection port of 250°C, designed to accommodate various injection modes (pulsed/splitless), enabling effective vaporization of high-boiling-point components (Savareear et al., 2019).

2.5.4 Mass spectrum conditions

The mass spectrometer detector LECO Pegasus BT 4D (LECO, St. Joseph, MI, USA) was employed in this study. The temperature of the mass spectrometric transfer line was set at 250°C, which helps to ensure the stability and accuracy of the analytes during transmission. The ion source temperature was maintained at 250°C, enabling the sample molecules to acquire sufficient energy for efficient ionization. The acquisition rate was 200 spectra/s, allowing for the rapid acquisition of a large amount of mass spectral data while ensuring data integrity. The electron impact ionization energy was set at 70 eV, under which most organic compounds can achieve stable ionization and generate characteristic fragment ions, facilitating the qualitative and quantitative analysis of the samples. The detector voltage was adjusted to 2028 V to ensure accurate detection and amplification of the mass spectral signals, while avoiding signal distortion or increased noise caused by excessively high or low voltages, thereby improving the quality of the mass spectral data. The mass spectrometric scanning range was set from m/z 35 to 550, which can cover the molecular ion peaks and major fragment ion peaks of most organic compounds, showing good adaptability for analyzing various components in complex samples (Tran and Marriott, 2007).

2.6 Analysis of flavor substances

Flavor substances primarily comprise volatile flavor components, including hydrocarbons, aldehydes, esters, acids, ketones, alcohols, ethers, phenols and heterocyclic substances. These substances are generated through a series of intricate biochemical reactions during the processing of flavor precursors. Using the PubChem database and classyfire software, the types of detected flavor substances were annotated and analyzed, and the number and relative contents of flavor substances corresponding to each category were analyzed (Li et al., 2023).

2.6.1 Screening of flavor substances

The screening conditions of different substances were as follows: p value < 0. 05+VIP > 1 in t test or one-way ANOVA test. The experiment adopts aggregated hierarchical clustering, each object was classified into one class, and these classes were merged into larger and larger objects until the end. The data was scaled by pheatmap package, and the hierarchical cluster diagram of relative quantitative values of substances was obtained.

2.6.2 Analysis of sensory flavor characteristics

The flavor of the product comprised the recognizable taste and smell characteristics and a complex of unrecognizable ones. The flavor molecules database (FlavorDB) (https://cosylab.iiitd.edu.in/flavordb) was utilized to analyze and compare the sensory flavor of the substances (Maldonado et al., 2003; Hu et al., 2024). Based on the FlavorDB database, igraph was used to construct the network diagram of sensory flavor.

2.7 Statistical analysis

Analysis of variance (ANOVA) was carried out using Statistix 8. 1 (Tallahassee, FL, USA), and the comparison processing method was based on the least significant difference test at the level of 0. 05. Principal component analysis (PCA) was used to downscale and classify the metabolic data to obtain more reliable and intuitive results. All flavor substances in the targeted flavor omics and sensory annotation were obtained from the FlavorDB.

3 Results and discussion

3.1 Sensory flavor evaluation of tobacco leaves

A sensory evaluation of ten tobacco leaves was carried out, focusing on multiple aspects such as aroma quality, aroma quantity, miscellaneous gas, thrill, sweet feeling, and oil content. The results presented in Supplementary Table 1, indicate that sample 1 received the highest total score of 42. 5, while sample 10 obtained the lowest score of 36. 8. Notably, sample 1 of tobacco leaves was characterized by a high oil content, whereas sample 10 exhibited a low oil content. Therefore, sample 1 with sufficient oil content and sample 10 with low oil content were selected for further research and were designated as sample H and sample L, respectively.

3.2 Agronomic characteristics of tobacco leaves

The dry average leaf length, average leaf width, leaf shape index, and average single leaf weight of tobacco leaves with different oil content were determined. As illustrated in Figure 1, the average leaf length of high-oil tobacco leaves was significantly greater than that of low-oil tobacco leaves, measuring 71. 06 cm and 61. 23 cm, respectively. Although the average leaf width and average single leaf weight of high-oil tobacco leaves were higher than those of low-oil tobacco leaves, the differences were not statistically significant. The leaf shape index shows that tobacco leaves with both levels of oil content were needle - shaped, and this shape was more pronounced in high - oil tobacco leaves.

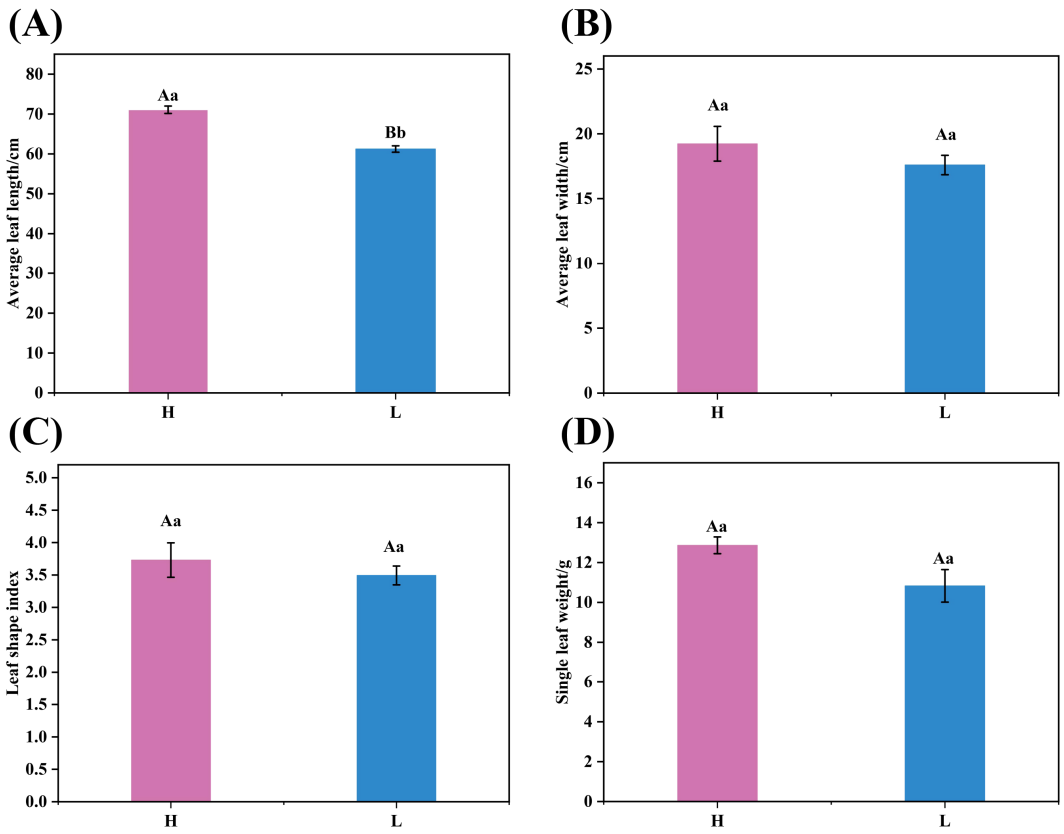

FIGURE 1
Agronomic characteristics of tobacco leaves. **(A)**Average leaf length, **(B)** average leaf width, **(C)** leaf shape index, and **(D)** single leaf weight. The letters 'H' and 'L' denote high oil content and low oil content tobacco leaves, respectively. In the bar chart, means sharing the same letter are not significantly different from each other as determined by ANOVA and Duncan's test ($p < 0.05$).

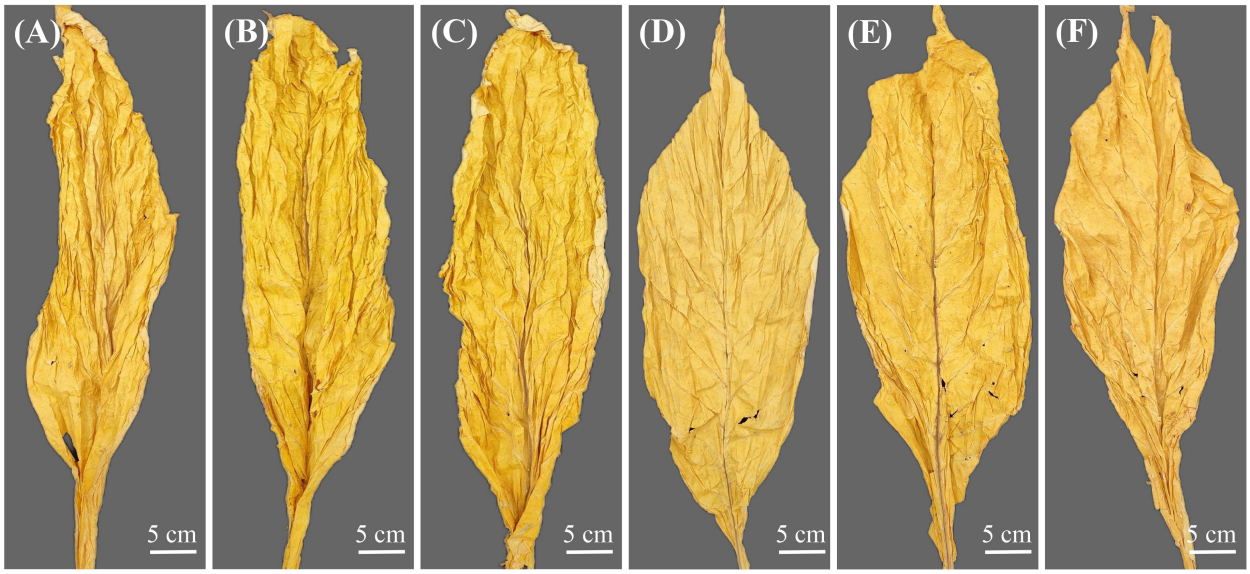

FIGURE 2
Appearance morphology of dried tobacco leaves with different oils contents. **(A–C)** high-oil tobacco leaves, **(D–F)** low-oil tobacco leaves.

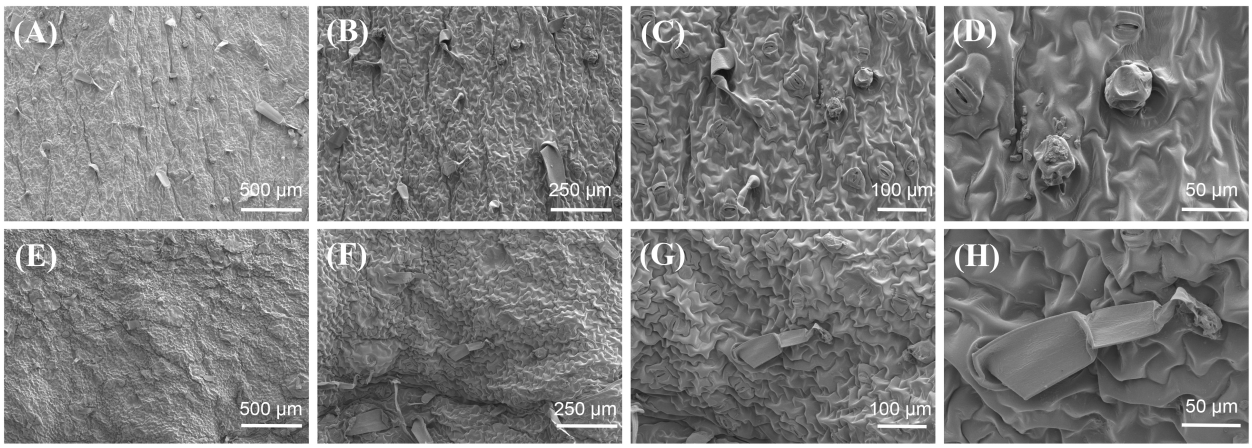

FIGURE 3
Microscopic morphology of dried tobacco leaves with different oils contents. **(A–D)** high-oil dry tobacco leaves, **(E–H)** low-oil dry tobacco leaves.

3.3 Appearance morphology of dried tobacco leaves

Through the appearance evaluation of dry tobacco leaves with different oil contents, it was found that the front and back of high-oil-content tobacco leaves were generally similar in color. The leaves were of medium thickness, with delicate leaf tissue and obvious suppleness (Figures 2A–C). Moreover, the color of the high-oil tobacco leaves was orange and mature, the leaf structure was loose, the oily feeling was strong, and the color fullness and uniformity of the tobacco leaves were excellent. Nevertheless, the low-oil-content tobacco leaves had stiff and thin leaves, poor oiliness, and weak chromaticity (Figures 2D–F).

3.4 Microscopic morphology of tobacco leaves

The glandular hairs of plants are specialized multicellular structures that originate from epidermal cells and form the first line of defense against abiotic and biotic stresses by forming physical barriers and secreting various substances (Dunn et al., 2011; Djoumbou et al., 2016; Garg et al., 2018). The glandular hairs present on the surface of tobacco leaves possess secretory functions within the epidermal glandular structures of plants. Based on their morphological and structural characteristics, tobacco glandular hairs can be classified into two types: long-stalked glandular hairs and short-stalked glandular hairs. The long-stalked glandular hairs are composed

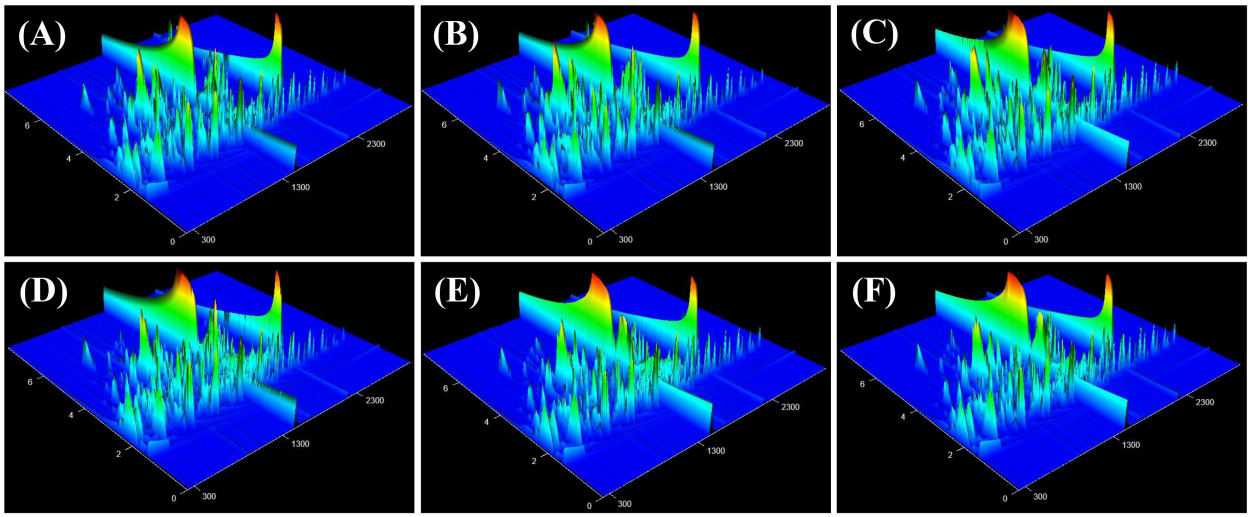

FIGURE 4
Total ion flow chromatogram of tobacco leaves with different oil contents. **(A–C)** high-oil dry tobacco leaves, **(D–F)** low-oil dry tobacco leaves.

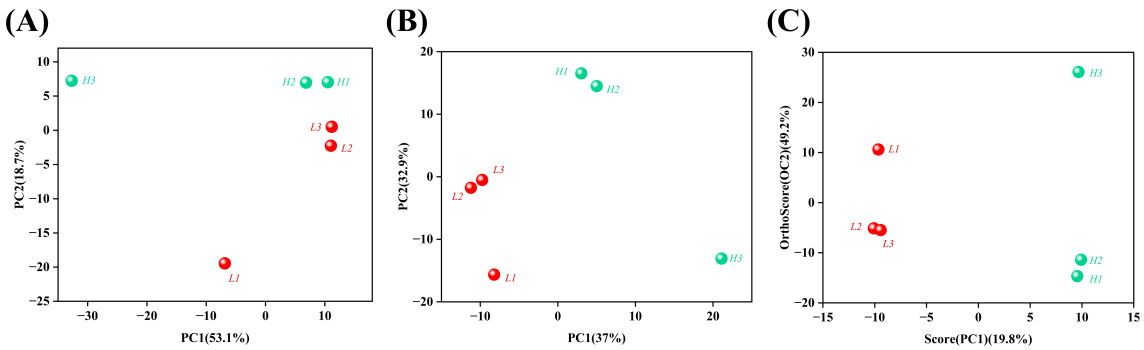

FIGURE 5
Principal component analysis (PCA) of tobacco leaves with different oil contents. **(A)** PCA Score Plot, **(B)** PLS-DA Score Plot, **(C)** OPLS-DA Score Plot. The letters 'H' and 'L' denote high oil content and low oil content tobacco leaves, respectively.

of a multicellular stalk and either a unicellular or multicellular head. In contrast, the short-stalked glandular hairs consist of a unicellular stalk and a multicellular head (Song et al., 2022). The glandular hairs on the surface of tobacco leaves primarily secrete essential oils, resins, waxes, sugars, alcohols, ketones, alkanes, and other substances, which are associated with the aroma and taste of tobacco leaves and the resistance characteristics of tobacco (Wang et al., 2001; Yan et al., 2021). The micro - morphologies of high - oil and low - oil tobacco samples were observed by scanning electron microscopy (SEM). The SEM results of tobacco leaves indicate that the surface glandular hairs of tobacco leaves with high-oil content were richer than those of tobacco leaves with low-oil content (Figure 3). Most glandular hairs on the surface of high-oil tobacco leaves were short-stalked glandular hairs, with enlarged glandular heads and rich secretions, cuticle ornamentation was relatively sparse. The results indicated that the oil content of tobacco leaves might be associated with the density and morphology of the glandular hairs on their surfaces.

3.5 Total ion flow chromatogram

The components isolated through chromatography are subsequently introduced into the mass spectrometer, which performs continuous scanning to gather data. A mass spectrogram was obtained from each scan, and all the ion intensities in each mass spectrogram were added to obtain the total ion current intensity. In this study, GC×GC-TOF MS was employed to analyze the volatile components of tobacco samples with high and low oil contents. The abscissa and ordinate represent the one-dimensional and two-dimensional retention times (in seconds), respectively (Figure 4). The color and peak height reflect the intensity of the ion response, with a redder color indicating a higher response strength. The overall peak occurrence rate in the three-dimensional total ion current chromatogram of each sample was satisfactory, suggesting that the samples contained a large number of volatile substances.

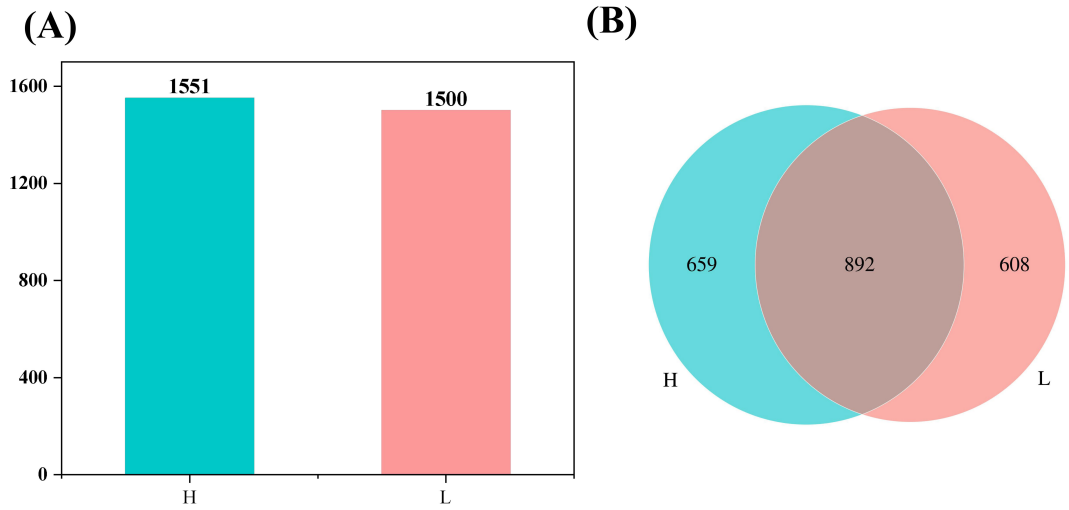

FIGURE 6
Statistical analysis of identification flavor substances of tobacco leaves with different oil contents. **(A)** Column chart of the number of identification substances; **(B)** Venn diagram of the number of identification substances. The letters 'H' and 'L' denote high oil content and low oil content tobacco leaves, respectively.

3.6 Principal component analysis

The principal component analysis (PCA) model reflects the original state of the metabolomic data, facilitating an understanding of the overall data situation. In particular, it is helpful for identifying and eliminating abnormal samples and enhancing the accuracy of the model. The score of each sample for each principal component represents its spatial coordinates within the calculated mathematical model, intuitively reflecting the distribution of each sample in the model space. The degrees of aggregation and dispersion of the samples can be visualized in the PCA score chart. The closer the distribution points of the samples, the closer the composition and concentration of the variables/molecules contained in these samples. As illustrated in Figure 5, each point was segregated into two clusters. The tobacco samples with low and high oil contents were positioned on the left and right sides of PC1, respectively. PCA revealed that there was a significant difference in the flavor substances between tobacco leaves with high oil content and those with low oil content.

3.7 Statistical analysis of identification flavor substances

The tobacco leaves with different oil contents were analyzed, revealing the detection of 1551 flavor substances in high-oil tobacco and 1500 flavor substances in low-oil tobacco. Within the detectable range, the flavor substances detected in high-oil tobacco leaves were found to be more plentiful than those in low-oil tobacco leaves. As illustrated in Figure 6, a total of 892 types of flavor substances were identified in both high-oil and low-oil tobacco. Among them, 659 types of specific flavor substances were detected in high-oil tobacco. This indicates that the specific flavor substances in high-oil tobacco samples were more numerous than those in low-oil tobacco samples.

3.8 Analysis of flavor substances of tobacco leaves

Flavor results from the interaction among taste, pre-nasal olfactory perception, and post-nasal olfactory perception and is frequently termed taste and aroma (Meyberg et al., 1991). Flavor substances consist of esters, acids, hydrocarbons, aldehydes, ketones, alcohols, ethers, phenols, and heterocyclic substances, which are produced via a series of complex biochemical reactions during the processing of flavor precursors (Gang et al., 2001). The PubChem database and classyfire software were employed to analyze the differences in the relative content of flavor substances between high-oil and low-oil tobacco leaves. As shown in Figure 7, the proportions of alcohols (9. 33%), aldehydes (5. 45%), ketones (9. 01%), esters (4. 86%), carboxylic acids (1. 58%), heterocyclic substances (22. 13%) and other volatile substances (39. 61%) in high-oil tobacco leaves were higher than those in low-oil tobacco leaves. The relative content of hydrocarbons in high-oil tobacco leaves (8. 02%) was found to be lower than that in low-oil tobacco leaves (12. 88%). Neutral aromatic substances in tobacco, including alcohols, ketones, and esters, play a crucial role as flavor substances in enhancing the quality of tobacco products (Kroumova and

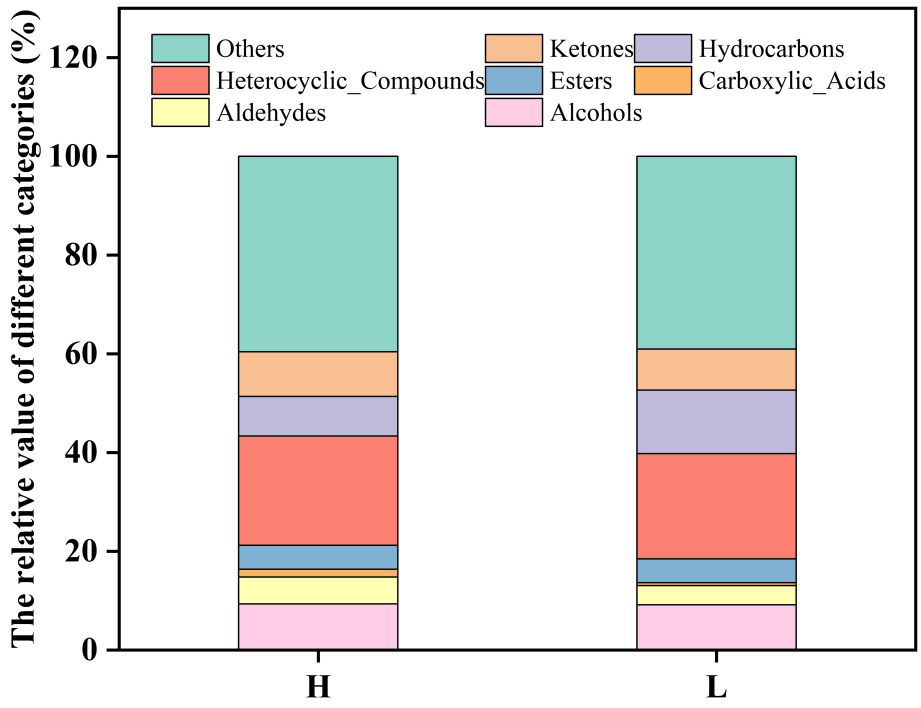

FIGURE 7
Analysis of flavor substances in tobacco leaves with different oils. The letters 'H' and 'L' denote high oil content and low oil content tobacco leaves, respectively.

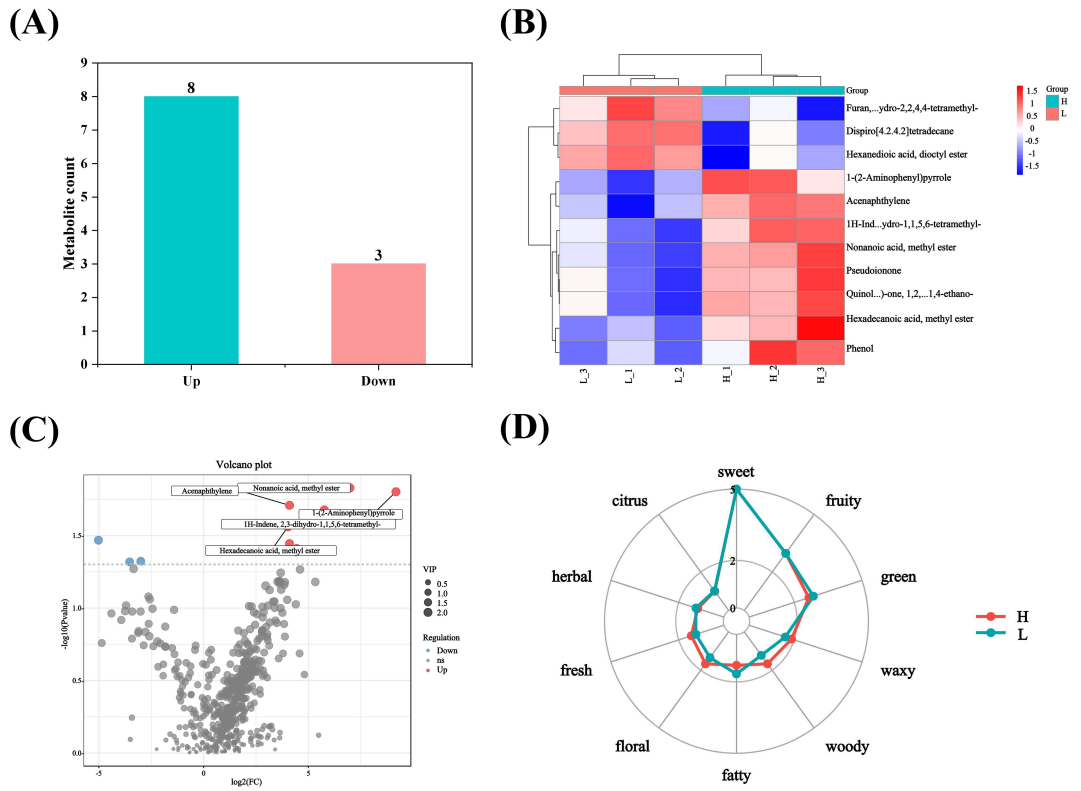

FIGURE 8
Screening of various substances in tobacco leaves and analysis of their sensory flavor characteristics. **(A)** Statistical column chart of different flavor substances; **(B)** heat map of different flavor substances; **(C)** volcano plot of different flavor substances; **(D)** sensory flavor characteristic chart of tobacco leaves with different oil contents. The letters 'H' and 'L' denote high oil content and low oil content tobacco leaves, respectively.

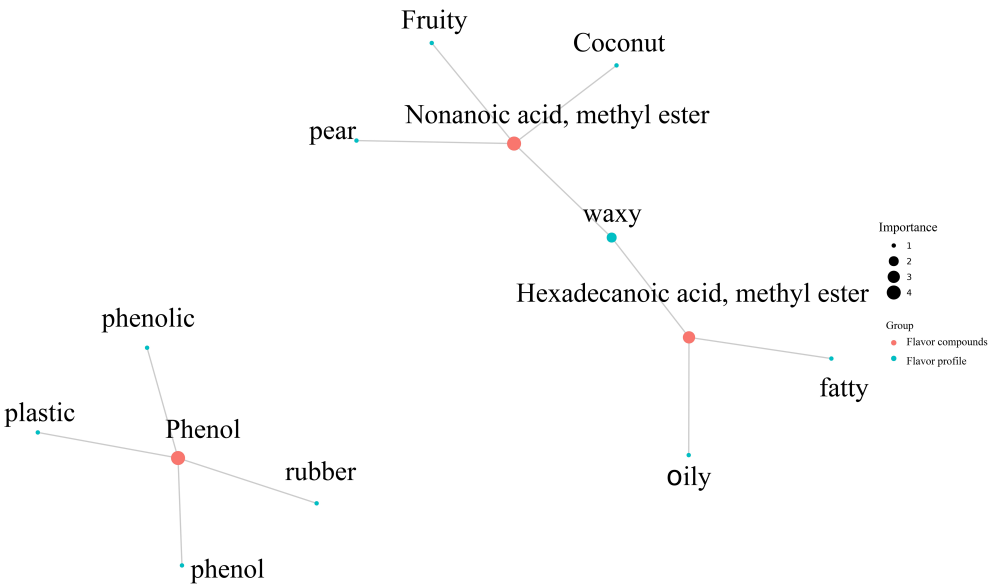

FIGURE 9
Correlation network diagram of sensory flavor characteristics and flavor substances.

Wagner, 2003; Goff and Klee, 2006). The main esters identified in tobacco leaves were ethyl octanoate, ethyl oleate, ethyl laurate, hexadecanoic acid methyl ester, and nonanoic acid methyl ester. The majority of esters in tobacco are higher fatty acid esters, which can serve as carriers of flavor substances and soften the smoke.

3.9 Screening of different flavor substances

After screening, different flavor substances were identified in the list of high-oil and low-oil tobacco leaves. The optional screening conditions for the related substances were p-value <0. 05 + VIP >1 in the t-test or one-way ANOVA. As shown in Figure 8, the comparison of low-oil and high-oil tobacco leaves were presented. The screening outcomes for various flavor substances revealed that there were 573 distinct metabolites in high-oil and low-oil tobacco leaves. Among them, eight metabolites were significantly up-regulated, while three were significantly down-regulated. The significantly down-regulated flavor substances included dispiro [4. 2. 4. 2] tetradecane; furan, tetrahydro-2,2,4,4-tetramethyl; hexanedioic acid, dioctyl ester. The flavor substances that were up-regulated included 1-(2-Aminophenyl) pyrrole; 1*H*-indene, 2,3-dihydro-1,1,5,6-tetramethyl; pseudoionone; acenaphthylene; hexadecanoic acid methyl ester; nonanoic acid methyl ester; phenol; quinolin-6(7 *H*)-one, 1,2,3,4,8,8a-hexahydro-1,4-ethano. The oil-related substance hexadecanoic acid methyl ester and aroma-related substances nonanoic acid methyl ester and pseudoionone were significantly higher in the high-oil tobacco than in the low-oil tobacco. Therefore, the content of hexadecanoic acid methyl ester can be used as an important indicator for evaluating the oil content of tobacco leaves, and nonanoic acid methyl ester and pseudoionone may be important substances influencing the aroma of tobacco leaves.

3.10 Analysis of sensory flavor characteristics

The differences in sensory flavor characteristics between high-oil and low-oil tobacco leaves was compared using the FlavorDB. Ten attributes were used to describe the sensory flavor of tobacco leaves, namely: sweet, fruity, green, waxy, fatty, woody, fresh, citrus, herbal, and floral. As depicted in Figure 8D, the sensory flavors of fresh, floral, woody, and waxy notes in high-oil tobacco leaves were more pronounced than those in low-oil tobacco leaves. The analysis of sensory flavor characteristics indicated that the predominant flavors of high - oil and low - oil tobacco samples were honey and sweetness. Based on the FlavorDB, igraph was employed to construct a network diagram depicting the relationship between the flavor substances and sensory characteristics (Figure 9). The green circles denote sensory characteristics, while the red circles represent flavor substances. The size of the green circles is proportional to the number of flavor substances associated with the sensory characteristics, with larger circles indicating greater importance of the sensory characteristics. The larger the red circle, the greater the number of sensory characteristics associated with the flavor compound, and the more significant the role of the flavor substance. For example, the flavor substance hexadecenoic acid methyl ester influences the oil, fat, and fatty content of tobacco leaves. Meanwhile, nonanoic acid methyl ester, which has a coconut aroma, enhances the fruit aroma of tobacco leaves.

4 Conclusion

The oil content of tobacco leaves serves as a crucial index for quality assessment. Tobacco leaves with higher oil content have sufficient aroma and superior aroma quality. This study aims to explore the microstructure and distinctive flavor substances of Yunyan 87 high-oil-content tobacco leaves. We analyzed Yunyan 87 tobacco leaves with different oil levels using SEM and GC×GC-TOF MS. It was found that the glandular hairs on the surface of Yunyan 87 leaves with high oil content were more abundant than those on the surface of Yunyan 87 leaves with low oil content. The majority of glandular hairs on the surface of high-oil tobacco leaves were characterized by short stalks and enlarged glandular heads, with rich secretions and relatively sparse cuticle ornamentation. Overall, a total of 1551 flavor substances were detected in the high-oil tobacco samples, whereas 1500 flavor substances were identified in the low-oil tobacco samples, suggesting that the high-oil tobacco contains a greater abundance of small molecular weight metabolites. Among these flavor substances, eight were found to be up-regulated, while three were down-regulated. Notably, compared with those in low - oil tobacco samples, the levels of oil - related substances (such as hexadecanoic acid methyl ester) and aroma - related substances (including nonanoic acid methyl ester and pseudoionone) were significantly higher in high - oil tobacco samples. The content of hexadecanoic acid methyl ester could potentially serve as a crucial indicator for assessing the oil content of tobacco leaves. Meanwhile, nonanoic acid methyl ester and pseudoionone may play significant roles in modulating the aroma of these leaves. This research offers a theoretical foundation for future investigations into the regulatory mechanisms and synthesis pathways related to the aroma-generating traits of tobacco.

Data availability statement

The original contributions presented in the study are included in the article/Supplementary Material. Further inquiries can be directed to the corresponding author.

Author contributions

XH: Conceptualization, Data curation, Formal analysis, Methodology, Resources, Writing – original draft, Writing – review & editing. WX: Conceptualization, Formal analysis, Methodology, Supervision, Writing – original draft, Writing – review & editing. YZ: Data curation, Investigation, Methodology, Project administration, Software, Supervision, Writing – original draft, Writing – review & editing. SP: Data curation, Formal analysis, Project administration, Writing – original draft, Writing – review & editing. YX: Data curation, Formal analysis, Methodology, Writing – original draft, Writing –

review & editing. RL: Data curation, Investigation, Project administration, Software, Writing – original draft, Writing – review & editing. SY: Funding acquisition, Investigation, Methodology, Writing – original draft, Writing – review & editing. YW: Conceptualization, Formal analysis, Methodology, Project administration, Writing – original draft, Writing – review & editing. DD: Conceptualization, Data curation, Project administration, Writing – original draft, Writing – review & editing.

Funding

The author(s) declare that financial support was received for the research, authorship, and/or publication of this article. The authors are grateful for the support from Guiyan Brand Raw Material-customization of Anshun Ziyun High-oil Tobacco Leaves Development and Application Project (ASXY-HX (2022) No. 001), Top-notch Young Talents Project of Guizhou Provincial Department of Education (Qian Jiao Ji (2024) No. 344), Guizhou Provincial Department of Education Youth Project (Qian Jiaoji (2024) No. 210), Qianzhong Characteristics Key Laboratory of Plant Protection Informatization (Qian Jiao Ji (2022) No. 052).

Conflict of interest

Authors WX, RL, SY, and YW were employed by the company China Tobacco Guizhou Industrial Co Ltd. SP and DD were employed by the company Guizhou Province Tobacco Company Anshun Company.

The remaining authors declare that the research was conducted in the absence of any commercial or financial relationships that could be construed as a potential conflict of interest.

Generative AI statement

The author(s) declare that no Generative AI was used in the creation of this manuscript.

Publisher's note

Supplementary material

The Supplementary Material for this article can be found online at: https://www.frontiersin.org/articles/10.3389/fpls.2025.1537924/full#supplementary-material

References

Chen, Y., Tao, X., Hu, S., He, R., Ju, X., Wang, Z., et al. (2024). Effects of phytase/ethanol treatment on aroma characteristics of. *Food. Chem.* 431, 137119. doi: 10.1016/j.foodchem.2023.137119

Djoumbou, F. Y., Eisner, R., Knox, C., Chepelev, L., Hastings, J., Owen, G., et al. (2016). Classyfire: automated chemical classification with a comprehensive, computabl taxonomy. *J. Cheminform.* 8, 61. doi: 10.1186/s13321-016-0174-y.eCollection2016

Dunn, W. B., Broadhurst, D., Begley, P., Zelena, E., Francis McIntyre, S., Anderson, N., et al. (2011). Procedures for large-scale metabolic profiling of serum and plasma using gas chromatography and liquid chromatography coupled to mass spectrometry. *Nat. Protoc.* 6, 1060–1083. doi: 10.1038/nprot.2011.335

Forehand, J. B., Dooly, G. L., and Moldoveanu, S. C. (2000). Analysis of polycyclic aromatic hydrocarbons, phenols and aromatic amines in particulate phase cigarette smoke using simultaneous distillation and extraction as a sole sample clean-up step. . *J. Chromatogr. A* 898, 111–124. doi: 10.1016/S0021-9673(00)00827-X

Gang, D. R., Wang, J., Dudareva, N., Nam, K. H., Simon, J. E., Lewinsohn, E., et al. (2001). An investigation of the storage and biosynthesis of phenylpropenes in sweet basil. *Plant Physiol.* 125, 539–555. doi: 10.1104/pp.125.2.539

Garg, N., Sethupathy, A., Tuwani, R., Nk, R., Dokania, S., Iyer, A., et al. (2018). FlavorDB: a database of flavor molecules. *Nucleic. Acids Res.* 46, D1210–d1216. doi: 10.1093/nar/gkx957

Goff, S., and Klee, H. (2006). Plant volatile compounds: sensory cues for health and nutritional value. *Science.* 311, 815–819. doi: 10.1126/science.1112614

Gu, W., Wei, Y., Fu, X., Gu, R., Chen, J., Jian, J., et al. (2023). HS-SPME/GC×GC-TOFMS based flavoromics and antimicrobial properties of the aroma components of. *Zanthoxylum motuoense. Foods.* 12, 12112225. doi: 10.3390/foods12112225

Hu, R., Cai, Z., Ji, L., Wu, Y., and Ma, X. (2024). High-flux recovery of aromatic compounds from tobacco extract using an MCM-41/PDMS hybrid membrane. *Sep. Purif. Technol.* 340, 126822. doi: 10.1016/j.seppur.2024.126822

Huang, Q., Dong, K., Wang, Q., Huang, X., Wang, G., An, F., et al. (2022). Changes in volatile flavor of yak meat during oxidation based on multi-omics. *Food. Chem.* 371, 131103. doi: 10.1016/j.foodchem.2021.131103

Kroumova, A. B., and Wagner, G. J. (2003). Different elongation pathways in the biosynthesis of acyl groups of trichome exudate sugar esters from various solanaceous plants. *Planta.* 216, 1013–1021. doi: 10.1007/s00425-002-0954-7

Li, R., Shi, J., Li, C., Ren, X., Tao, Y., Ma, F., et al. (2023). Characterization of the key odorant compounds in Qinguan apples (malus × domestica). *LWT-Food. Sci. Technol.* 184, 115052 doi: 10.1016/j.lwt.2023.115052

Li, X., Zhang, B., Li, W., Zhao, Y., Lyu, X., You, X., et al. (2024). Unraveling the chemosensory characteristics dependence of sauce-flavor baijiu on regionality using descriptive sensory analysis and quantitative targeted flavor omics. *Food. Chem.* 441, 138274. doi: 10.1016/j.foodchem.2023.138274

Lin, L., Fan, W., Xu, Y., Zhu, D., Yang, T., and Li, J. (2024). Characterization of key odorants in Chinese texiang aroma and flavor type baijiu (Chinese liquor) by means of a molecular sensory science approach. *J. Agric. Food. Chem.* 72, 1256–1265. doi: 10.1021/acs.jafc.3c07053

Liu, A., Yuan, K., Li, Q., Liu, S., Li, Y., Tao, M., et al. (2022). Metabolomics and proteomics revealed the synthesis difference of aroma precursors in tobacco leaves at various growth stages. *Plant Physiol. Bioch* 192, 308–319. doi: 10.1016/j.plaphy.2022.10.016

Maldonado, R. G., Rodriguez, B. E., Sanchez, C. A., Rodriguez, S. R., and Sanchez, S. (2003). Production of tobacco aroma from lutein. specific role of the microorganisms involved in the process. *Appl. Microbiol. Biot* 62, 484–488. doi: 10.1007/s00253-003-1315-6

Meyberg, M., Krohn, S., Brümmer, B., and Kristen, U. (1991). Ultrastructure and secretion of glandular trichomes of tobacco leaves. *Flora.* 185, 357–363. doi: 10.1016/S0367-2530(17)30495-4

Qin, G., Zhao, G., Canbin, O., and Liu, J. (2021). Aroma components of tobacco powder from different producing areas based on gas chromatography ion mobility spectrometry. *Open Chem.* 19, 442–450. doi: 10.1515/chem-2020-0116

Qin, Y., Bai, S., Li, W., Sun, T., Galbraith, D. W., Yang, Z., et al. (2020). Transcriptome analysis reveals key genes involved in the regulation of nicotine biosynthesis at early time points after topping in tobacco (*Nicotiana tabacum* L.). *BMC. Plant Biol.* 20, 30. doi: 10.1186/s12870-020-2241-9

Ruan, S., Luo, H., Wu, F., He, L., Lai, R., and Tang, X. (2023). Organic cultivation induced regulation in yield formation, grain quality attributes, and volatile organic compounds of fragrant rice. *Food. Chem.* 405, 134845. doi: 10.1016/j.foodchem.2022.134845

Savareear, B., Escobar-Arnanz, J., Brokl, M., Saxton, M. J., Wright, C., Liu, C., et al. (2019). Non-targeted analysis of the particulate phase of heated tobacco product aerosol and cigarette mainstream tobacco smoke by thermal desorption comprehensive two-dimensional gas chromatography with dual flame ionisation and mass spectrometric detection. *J. Chromatogr. A.* 1603, 327–337. doi: 10.1016/j.chroma.2019.06.057

Schwanz, T. G., Bokowski, L. V. V., Marcelo, M. C. A., Jandrey, A. C., Dias, J. C., Maximiano, D. H., et al. (2019). Analysis of chemosensory markers in cigarette smoke from different tobacco varieties by GC×GC-TOF MS and chemometrics. *Talanta.* 202, 74–89. doi: 10.1016/j.talanta.2019.04.060

Song, Z., Wang, P., Chen, X., Peng, Y., Cai, B., Song, J., et al. (2022). Melatonin alleviates cadmium toxicity and abiotic stress by promoting glandular trichome development and antioxidant capacity in *Nicotiana tabacum*. *Ecotox. Environ. Safe* 236, 113437. doi: 10.1016/j.ecoenv.2022.113437

Tran, T. C., and Marriott, P. J. (2007). Characterization of incense smoke by solid phase microextraction- Comprehensive two-dimensional gas chromatography (GC×GC). *Atmos. Environ.* 41, 5756–5768. doi: 10.1016/j.atmosenv.2007.02.030

Wang, E., Wang, R., DeParasis, J., Loughrin, J. H., Gan, S., and Wagner, G. J. (2001). Suppression of a P450 hydroxylase gene in plant trichome glands enhances natural-product-based aphid resistance. *Nat. Biotechnol.* 19, 371–374. doi: 10.1038/86770

Wang, X., Xu, R., Tong, X., Zeng, J., Chen, M., Lin, Z., et al. (2022). Characterization of different meat flavor compounds in Guangdong small-ear spotted and yorkshire pork using two-dimensional gas chromatography–time-of-flight mass spectrometry and multi-omics. *LWT-Food. Sci. Technol.* 169, 114010. doi: 10.1016/j.lwt.2022.114010

Wang, X., and Yan, Y. (2013). Entropy coefficient assessment of mulch drip irrigation scheme in tobacco fields. *Adv. Mater. Res.* 726-731, 3077–3083. doi: 10.4028/www.scientific.net/AMR.726-731.3077

Yan, X., Guan, Y., Liu, X., Lei, B., Wang, Z., Zhang, H., et al. (2021). *NtCycB2* gene knockout enhances resistance to high salinity stress in *Nicotiana tabacum*. *Ind. Crop Prod.* 171, 113886. doi: 10.1016/j.indcrop.2021.113886

Yan, S., Niu, Z., Yan, H., Zhang, A., and Liu, G. (2020a). Influence of soil organic carbon on the aroma of tobacco leaves and the structure of microbial communities. *Curr. Microbiol.* 77, 931–942. doi: 10.1007/s00284-020-01895-7

Yan, S., Zhao, J., Ren, T., and Liu, G. (2020). Correlation between soil microbial communities and tobacco aroma in the presence of different fertilizers. *Ind. Crop Prod.* 151, 112454doi: 10.1016/j.indcrop.2020.112454

Yang, Y., Qian, M. C., Deng, Y., Yuan, H., and Jiang, Y. (2022). Insight into aroma dynamic changes during the whole manufacturing process of chestnut-like aroma green tea by combining GC-E-Nose, GC-IMS, and GC×GC-TOF MS. *Food. Chem.* 387, 132813. doi: 10.1016/j.foodchem.2022.132813

Yin, F., Karangwa, E., Song, S., Duhoranimana, E., Lin, S., Cui, H., et al. (2019). Contribution of tobacco composition compounds to characteristic aroma of Chinese faint-scent cigarettes through chromatography analysis and partial least squares regression. *J. Chromatogr. B. Analyt. Technol. Biomed. Life. Sci.* 1105, 217–227. doi: 10.1016/j.jchromb.2018.12.001

Zhang, J., Zhao, C., Chang, Y., Zhao, Y., Li, Q., Lu, X., et al. (2013). Analysis of free amino acids in flue-cured tobacco leaves using ultra-high performance liquid chromatography with single quadrupole mass spectrometry. *J. Sep. Sci.* 36, 2868–2877. doi: 10.1002/jssc.201300450

Zou, L., Su, J., Xu, T., Ji, X., Wang, T., Chen, Y., et al. (2023). Untargeted metabolomics revealing changes in aroma substances in flue-cured tobacco. *Open Chem.* 21, 20220326. doi: 10.1515/chem-2022-0326

frontiers | Frontiers in Plant Science

TYPE Original Research
PUBLISHED 24 March 2025
DOI 10.3389/fpls.2025.1530673

OPEN ACCESS

EDITED BY
Marta Sousa Silva,
University of Lisbon, Portugal

REVIEWED BY
Shouchuang Wang,
Hainan University, China
Kourosh Vahdati,
University of Tehran, Iran

*CORRESPONDENCE
Hongxing Cao
hongxing1976@163.com

†These authors have contributed equally to this work

RECEIVED 19 November 2024
ACCEPTED 06 February 2025
PUBLISHED 24 March 2025

CITATION
Zhang R, John Martin JJ, Liu X, Li X, Zhou L, Li R, Fu X, Li W and Cao H (2025) Joint analysis of transcriptional metabolism for flavonoid synthesis during different developmental periods in oil palm exocarp. *Front. Plant Sci.* 16:1530673. doi: 10.3389/fpls.2025.1530673

Joint analysis of transcriptional metabolism for flavonoid synthesis during different developmental periods in oil palm exocarp

Ruimin Zhang[1,2†], Jerome Jeyakumar John Martin[2†], Xiaoyu Liu[2], Xinyu Li[2], Lixia Zhou[2], Rui Li[2], Xiaopeng Fu[2], Wenrao Li[3] and Hongxing Cao[2*]

[1]National Key Laboratory of Germplasm Innovation and Utilization of Fruit and Vegetable Horticultural Crops, College of Horticulture and Forestry, Huazhong Agricultural University, Wuhan, China, [2]Coconut Research Institute, Chinese Academy of Tropical Agricultural Sciences, Wenchang, China, [3]School of Life Sciences, Henan University, Kaifeng, Henan, China

To identify candidate genes for breeding oil palm varieties with high flavonoid content through molecular biotechnology, this study analyzed the metabolomes and transcriptomes of oil palm exocarp at different developmental stages using LC-MS/MS and RNA-Seq techniques. The green fruiting type (FS) oil palm exocarp at 95 days (FS1), 125 days (FS2), and 185 days (FS3) after pollination served as the materials. The enzyme genes F3H, CHS, ANS, and DFR were positively correlated with Quercetin-3-O-sambubioside. DFR also showed positive correlations with Afzelechin, Epiafzelechin, and Baimaside. In contrast, F3H, CHS, and ANS were negatively correlated with Hesperetin-7-O-glucoside. Additionally, CYP73A, UGT73C6, FG2-1, and FG2-2 were negatively correlated with Afzelechin, Epiafzelechin, Quercetin-3-O-sambubioside, and Baimaside, while CYP75A was negatively correlated with Epiafzelechin, Quercetin-3-O-sambubioside, and Baimaside. These results suggest that F3H, CHS, ANS, and DFR play a role in promoting Quercetin-3-O-sambubioside* synthesis, with DFR further enhancing the production of Afzelechin, Epiafzelechin, and Baimaside. On the other hand, F3H, CHS, and ANS may inhibit Hesperetin-7-O-glucoside synthesis. Meanwhile, CYP73A, UGT73C6, FG2-1, and FG2-2 appear to suppress the synthesis of multiple flavonoids, including Afzelechin, Epiafzelechin, Quercetin-3-O-sambubioside*, and Baimaside. Lastly, CYP75A is implicated in suppressing Epiafzelechin, Quercetin-3-O-sambubioside*, and Baimaside synthesis. These findings provide a foundation for future molecular breeding efforts targeting flavonoid-rich oil palm varieties.

KEYWORDS

oil palm, metabolomics, transcriptomics, flavonoids, biosynthesis

1 Introduction

The oil palm (Elaeis guineensis Jacq.), a member of the palm family (Palmae), is a perennial tree native to South and Central America. As one of the most important woody oilseed crops in tropical regions, it has high economic value due to its efficient oil production. Its primary products include palm oil, extracted from the mesocarp, and palm kernel oil, derived from the kernels, both of which have extensive applications in the food, chemical, and bioenergy industries (John Martin et al., 2022). While research on oil palm has extensively focused on lipid metabolism and stress responses, the control of flavonoid biosynthesis in the fruit remains relatively unexplored. Flavonoids are vital secondary metabolites responsible for pigmentation, plant defense mechanisms, and have implications for human health due to their antioxidant properties. In oil palm, anthocyanins are a significant subclass of flavonoids found in the exocarp, contributing to the fruit's coloration and maturity indicators. The biosynthesis of flavonoids occurs via complex metabolic pathways and is regulated by various genes and transcription factors (Yang et al., 2024b).

Flavonoids have diverse biological functions, including antioxidant and antimicrobial properties. For instance, the high antioxidant capacity of blueberries is attributed to their flavonoid content (Kalt et al., 2020). Studies have shown that flavonol glycosides are related to the astringency and bitterness of tea, with polyphenol oxidase (PPO) playing a dominant role in catalyzing flavonol glycosides in tea leaves (Guo et al., 2021). Additionally, polyphenol oxidase in walnuts exhibits resistance to environmental stress (Khodadadi et al., 2020). In rice, flavonoids like naringenin confer resistance to bacterial pathogens, while sakuranetin imparts resistance to fungal pathogens (Murata et al., 2020). Additionally, flavonoids contribute to pigmentation, such as anthocyanin accumulation in grape skins, which enhances pigmentation (Jiu et al., 2022). In root growth, flavonoids play a role in promoting development through the stimulation of flavonol biosynthesis in Arabidopsis thaliana (Tan et al., 2019). Moreover, flavonoids are involved in pollen development and contribute to the promotion of self-incompatibility during pollination in Brassica oleracea (Lan et al., 2017). High levels of flavonoid oil palm may help protect against a wide range of diseases, for example, in corn, high levels of flavonoids have powerful anti-inflammatory and anti-cancer activity (Casas et al., 2014). Flavonoids found in citrus fruits have considerable nutritional value in the treatment of cardiovascular disease (Testai and Calderone, 2017).

Flavonoids represent the largest group of polyphenolic compounds, comprising approximately 8,000 distinct flavonoid metabolites. Flavonoids can be categorized into the following main types: chalcones, flavanones, flavanonols, flavonoids,flavonols, flavanols, isoflavones, and more (Shen et al., 2022). Studies have demonstrated that oil palm possesses a high flavonoid content (Zain et al., 2021). Flavonoid biosynthesis is a complex metabolic process that primarily occurs through the phenylpropanoid pathway, converting the amino acid phenylalanine into various flavonoid compounds. This pathway is crucial for the production of numerous secondary metabolites that play significant roles in plant physiology, protection, and interactions with the environment. The figure depicts the flavonoid biosynthesis pathway, starting from 4-Coumaroyl-CoA, a precursor in the phenylpropanoid pathway. The enzyme Chalcone Synthase (CHS) catalyzes its conversion into chalcones such as Isoliquiritigenin and Naringenin chalcone, which are then cyclized by Chalcone Isomerase (CHI) into flavanones Liquiritigenin and Naringenin, respectively. Naringenin serves as a central intermediate, branching into various products: Hesperetin, Isosakuranetin, 8-C-Glucosyl-naringenin, and Apigenin, which can further glycosylate into Vitexin. Through the action of Flavanone 3-Hydroxylase (F3H), Naringenin converts into Dihydrokaempferol, which serves as a precursor for different flavonoids. Kaempferol is synthesized by Flavonol Synthase (FLS), while Leucopelargonidin, a precursor for anthocyanin Pelargonidin, forms via Dihydroflavonol Reductase (DFR) and Anthocyanidin Synthase (ANS). Taxifolin is another derivative that can lead to Leucocyanidin and eventually (-)-Epicatechin through similar enzymatic steps. These flavonoids contribute to pigmentation, UV protection, and stress responses, with the pathway tightly regulated by enzymes like CHS, CHI, F3H, FLS, DFR, and ANS (Zhang et al., 2024) (Figure 1). In the biosynthetic pathway of flavonoids and flavonols, all three differential metabolites —kaempferol, lignans, and quercetin—were down-regulated. Additionally, eight differential enzyme genes were identified within the pathway, among which F3'H was found to be associated with the differential metabolites (Yang, 2023). Regulation of flavonoid biosynthesis is intricately controlled by several transcription factors, including the R2R3-MYB, bHLH, and WD40 protein families. These proteins form complexes that determine the expression patterns of the biosynthesis genes, enabling the plants to adapt their flavonoid profiles according to developmental and environmental cues. For example, in *Arabidopsis*, the TT2, TT8, and TTG1 mix to regulate proanthocyanidin biosynthesis, demonstrating the complexity of regulatory mechanisms across different species (Falcone Ferreyra et al., 2012). In another study, flavonoid biosynthesis appears to involve specific transcription factors, notably AcMYB5 and AcMYB194, which have been annotated as potential regulators in the biosynthetic pathway (Lai et al., 2023).

Currently, transcriptomics and metabolomics play a very crucial role in the cultivation of various plant species (Sadat-Hosseini et al., 2020; Zhou et al., 2024). The study of different metabolites and genes involved in the flavonoid synthesis pathway in the exocarp of oil palm fruits is still in the preliminary stage. Therefore, this study hypothesizes that five differential metabolites and nine enzyme genes play a pivotal role in flavonoid synthesis in the exocarp of oil palm. By integrating transcriptomic and metabolomic data from the exocarp of green-fruited oil palm (FS) at various developmental stages, this research aims to identify key candidate genes and metabolites involved in flavonoid biosynthesis. The findings of this study will contribute valuable insights for the future cultivation and utilization of oil palm varieties, as well as for the identification and development of high-flavonoid resources and products.

2 Materials and methods

2.1 Experimental materials

The experimental materials used in this study were derived from the green-fruited oil palm variety (O×G Amazon), cultivated at the

Coconut Research Institute of the Chinese Academy of Tropical Agricultural Sciences Oil Palm Research Base, located in Wenchang City, Hainan Province, China (19°33'N, 110°47'E). Fruit exocarp was harvested at three different developmental stages: 95 days after pollination (early fruit development, FS1), 125 days (rapid fruit accumulation, FS2) and 185 days (stable fruit development, FS3). At each developmental stage, three biological replicates were collected. Each replicate consisted of pooled exocarps from a minimum of 10 fruits to ensure representation of the biological variation. The exocarps were carefully peeled from the fruit and immediately flash-frozen in liquid nitrogen, then stored at -80°C for subsequent analyses.

2.2 Experimental procedures

2.2.1 Determination and analysis of flavonoid metabolites

For metabolomic analysis, the frozen exocarp samples were ground into a fine powder using a liquid nitrogen-cooled mortar and pestle. The powdered samples were extracted with a solvent mixture of n-hexane, acetone, and ethanol in a 1:1:1 (v/v/v) ratio. The extraction was performed at room temperature for 30 minutes, followed by filtration through a 0.22 μm nylon membrane to remove particulates. The resulting filtrates were analyzed for flavonoid metabolites using High-Performance Liquid Chromatography-Mass Spectrometry (HPLC-MS).

The HPLC system (Agilent 1200 Series, Agilent Technologies, USA) was coupled to a mass spectrometer (TripleTOF 5600, AB SCIEX, USA). The chromatographic separation was performed on a C18 column (Zorbax Eclipse Plus C18, 4.6 mm × 150 mm, 5 μm particle size, Agilent Technologies). The mobile phase consisted of solvent A (0.1% formic acid in water) and solvent B (0.1% formic acid in acetonitrile). The gradient elution program was as follows: 0-5 min, 5-20% B; 5-10 min, 20-50% B; 10-15 min, 50-90% B; 15-20 min, 90-100% B. The flow rate was set to 0.5 mL/min. Mass spectrometry was performed using electrospray ionization (ESI) in negative ion mode, with the ionization voltage set at -4.5 kV and the source temperature at 500°C. Data were collected in both Full Scan and MS/MS modes, and analyzed using Analyst 1.6.3 and MultiQuant 3.0.3 software. Differential metabolites were identified based on fold change ≥ 2 or fold change ≤ 0.5. Statistical significance was determined using one-way ANOVA (SPSS 26.0, IBM, USA).

2.2.2 Total RNA extraction and high-throughput sequencing

Total RNA was extracted from the exocarp samples using the Plant Total RNA Extraction Kit (Roche, Switzerland), following the manufacturer's protocol. RNA integrity was assessed by electrophoresis on a 1% agarose gel, while RNA concentration and purity were measured using a NanoPhotometer spectrophotometer (Implen, Germany) and Qubit 2.0 Fluorometer (Thermo Fisher Scientific, USA). The quality of RNA was further confirmed with the Agilent 2100 Bioanalyzer (Agilent Technologies, USA).

RNA samples that passed quality control were used to construct sequencing libraries. Library preparation and sequencing were performed using the Illumina TruSeq RNA Library Prep Kit (Illumina, USA), followed by sequencing on the Illumina NovaSeq 6000 platform (Illumina, USA), generating paired-end 150 bp reads.

2.2.3 Transcriptome data analysis and differentially expressed genes

Raw transcriptomic data were processed for quality control using fastp v0.19.3 (Chen et al., 2018). Clean reads were aligned to the oil palm reference genome (provided by the Oil Palm Genome Database) using HISAT v2.1.0. Gene expression levels were quantified using Fragments Per Kilobase of Transcript Per Million Fragments Mapped (FPKM) calculated by StringTie v1.3.4d. Differentially expressed genes (DEGs) were identified using DESeq2 v1.22.1 with a False Discovery Rate (FDR) < 0.05 and |log2Fold Change| ≥ 1. KEGG pathway enrichment analysis was conducted to identify biological pathways significantly associated with the flavonoid biosynthesis pathway.

2.2.4 Integration of metabolomic and transcriptomic data

Pathways enriched in differentially expressed metabolites and genes were compared against the KEGG database (https://www.genome.jp/kegg). A hypergeometric test was used to identify significant pathways containing more than 25 shared entries, with the top 25 pathways selected based on the lowest p-values. Correlations between genes and metabolites were investigated using Pearson's correlation analysis (R v4.0.5), with a threshold of correlation coefficient > 0.80 and p-value < 0.05 for selecting significant gene-metabolite relationships.

2.2.5 Statistical analysis

Statistical analyses were conducted using SPSS 26.0 (IBM Corp., USA) and R software (v4.0.5). Data are presented as means ± standard deviation (SD), with statistical significance set at $p < 0.05$. Differential metabolites were identified based on fold change (FC) ≥ 2 or ≤ 0.5. Differentially expressed genes (DEGs) were identified using DESeq2 with an FDR-adjusted p-value < 0.05 and |log2Fold Change| ≥ 1. Pathway enrichment analysis was performed using the KEGG database.

3 Results and analysis

3.1 Metabolomic analysis of oil palm exocarp flavonoids

3.1.1 Composition and classification of flavonoids in the oil palm exocarp at different developmental stages

During the development of the oil palm exocarp, a total of 274 flavonoids were identified and classified into nine distinct groups: 104 flavonoids, 88 flavonols, 7 chalcones, 20 dihydroflavonoids, 6 dihydroflavonols, 9 anthocyanins, 17 flavanols, 15 other flavonoids, and 8 isoflavones. Within these categories, flavonoids exhibited the highest relative content, followed by flavonols, with dihydroflavonols had the lowest relative content. Throughout the developmental stages (FS1 to FS3), the relative contents of

flavonoids, chalcones, anthocyanins, and flavanols increased initially before decreasing. In contrast, the relative contents of dihydroflavonoids, dihydroflavonols, flavonols, and isoflavonoids showed a consistent decline, whereas other flavonoids displayed a consistent upward trend (Figure 2). The overall relative flavonoid content increased initially and subsequently declined (Figure 3). Metabolomic analysis of the FS1 to FS3 developmental stages identified 92 flavonoid metabolites based on screening criteria (Variable Importance in Projection, VIP ≥ 1, Fold_Change ≥ 2, or Fold_Change ≤ 0.5). Of these, 71 metabolites were down-regulated, and 21 were up-regulated. Flavonoids and flavonols comprised the largest proportion of the differential metabolites. Prominent flavonoids included Diosmetin (5,7,3'-Trihydroxy-4'-methoxyflavone), Gnetifolin B, Demethoxysudachitin, Jaceosidin, Vitexin, Isovitexin, and Diosmetin-7-O-rutinoside (Diosmin). Significant flavonols comprised Rhamnocitrin, Rehderianin I, Isorhamnetin-3-O-gallate, and Limocitrin-3-O-galactoside (Table 1). The relative content of different flavonoid species in the oil palm exocarp during the FS1-FS3 period was clustered (Figure 4). Analysis of the results revealed that the relative content of three flavonoid compounds—Peonidin-3-O-glucoside, Cyanidin-3-O-rutinoside (Keracyanin), and Cyanidin-3-O-glucoside (Kuromanin)—increased from FS1 to FS2, then decreased to FS3, with levels lower than those in FS1.

The relative contents of the flavonoid compounds Hesperetin-7-O-glucoside and Quercetin-3-O-Sambubioside-5-O-Glucoside were lower in FS1, increased in FS2, and decreased in FS3 although, remained higher than in FS1.Isovitexin*, Vitexin*, Taxifolin (Dihydroquercetin), Kaempferol-3-O-galactoside (Trifolin), *Quercetin-3-O-sambubioside*, and eight other flavonoids showed a continuous decrease in relative content from FS1 to FS3. Cyanidin-3-O-glucoside (Kuromanin) and Epiafzelechin increased in relative content from FS1 to FS2 and decreased in FS3.

3.1.2 Analysis of differential metabolites of flavonoids in the exocarp of oil palm fruits at different developmental periods

The number of significantly up-regulated and down-regulated metabolites was determined by analyzing the metabolomic data of oil palm fruits during FS1-FS3 based on the screening criteria (variable importance in projection, VIP) ≥ 1, Fold Change ≥3 or Fold_Change ≤ 0.5 (Figure 5). In FS1 vs FS2, there were 12 metabolites showing increased levels, such as hesperetin-7-O-glucoside, diosmetin (5,7,3'-Trihydroxy-4'-methoxyflavone), gnetifolin B, and persicogenin (5,3'-dihydroxy-7,4'-dimethoxyflavanone), along with 1 metabolite showing decreased levels. In the FS1 vs FS3 comparison, hesperetin-7-O-glucoside, 3,5,4'-Trihydroxy-7-methoxyflavone (rhamnocitrin), diosmetin (5,7,3'-trihydroxy-4'-methoxyflavone), and gnetifolin B exhibited decreased levels, while 14 other metabolites showed significant increases. Conversely, isorhamnetin-3-O-arabinoside, epiafzelechin, avicularin (quercetin-3-O-alpha-L-Arabinofuranoside)*, and 27 other metabolites displayed significant decreases. In FS2 vs FS3, three metabolites showed increased levels: persicogenin (5,3'-dihydroxy-7,4'-dimethoxyflavanone), 5,4'-dihydroxy-3,7-dimethoxyflavone (kumatakenin), and 4',5-dihydroxy-3',5'-dimethoxyflavone. Meanwhile, the metabolites with decreased levels included epiafzelechin, avicularin (quercetin-3-O-α-L-arabinofuranoside)*, and 19 others. The number of up- and down-regulated differential metabolites initially increased and then decreased as fruit development progressed. No differential metabolites were observed in the comparisons of FS1 vs. FS2, FS1 vs. FS3, and FS2 vs. FS3. A total of 11 common differential metabolites, including Hesperetin-7-O-glucoside, Diosmetin (5,7,3'-Trihydroxy-4'-methoxyflavone), and Gnetifolin B, were identified in both FS1 vs. FS2 and FS1 vs. FS3. Persicogenin (5,3'-dihydroxy-7,4'-dimethoxyflavanone) was a shared differential metabolite in FS1 vs. FS2 and FS2 vs. FS3. Additionally, 16 co-occurring differential metabolites, such as Pectolinarigenin*, Epiafzelechin, and Avicularin (Quercetin-3-O-α-L-arabinofuranoside)*, were found in both FS1 vs. FS3 and FS2 vs. FS3.

3.2 Analysis of differential genes in different developmental periods of oil palm pericarp

Transcriptome analysis of the oil palm exocarp during developmental stages of FS1, FS2, and FS3 revealed significant differential gene expression. Genes were screened based on criteria of |log2Fold Change| ≥ 1 and FDR < 0.05. In the FS1 vs. FS2 comparison, 1,152 genes were genes (e.g., LOC105048385, LOC105052646,

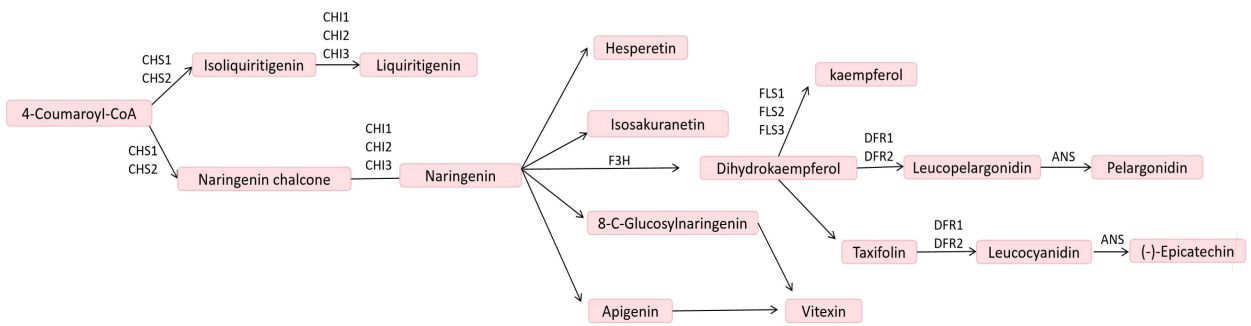

FIGURE 1
Flavonoid biosynthetic pathway (Zhang et al., 2024). CHS, chalcone synthase; CHI, chalcone isomerase; F3H, flavanone 3-hydroxylase; FLS, flavonol synthase; DFR, dihydroflavonol reductase; ANS, anthocyanidin synthase.

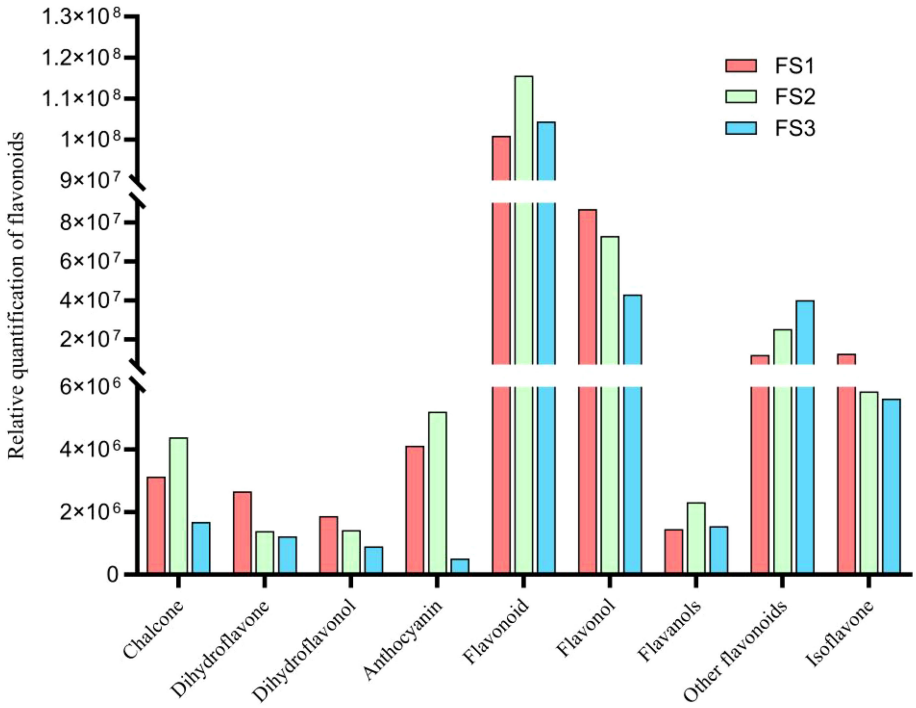

FIGURE 2
Changes in relative quantification of various flavonoid compounds in the exocarp of oil palm fruits at different developmental periods (FS1-FS3).

LOC105058257) while1,765 genes were down-regulated (e.g., LOC105049188, LOC105058893, LOC105056795) (Figure 6A). For the FS1 vs. FS3 comparison showed 2,740 up-regulated genes (e.g., LOC105032120, LOC105058752, LOC105049762) and 3,171 down-regulated genes (e.g., LOC105038978, LOC105041013, LOC105048687). Whereas, in FS2 vs. FS3 comparison, 2,969 genes were up-regulated (e.g., LOC105041978, LOC105035259, LOC105050452) while 3,102 were down-regulated (e.g., LOC105036076, LOC105035725, LOC105034160). As the fruit development progressed, the number of down-regulated genes consistently exceeded the up-regulated genes, with an overall increase in the counts of both up- and down-regulated genesacross all developmental comparisons (FS1 vs. FS2, FS1 vs. FS3, and FS2 vs. FS3). Across the three developmental stages, 676 differentially expressed genes were identified as common, suggesting shared regulatory pathways or functional roles throughout the fruit's development (Figure 6B).

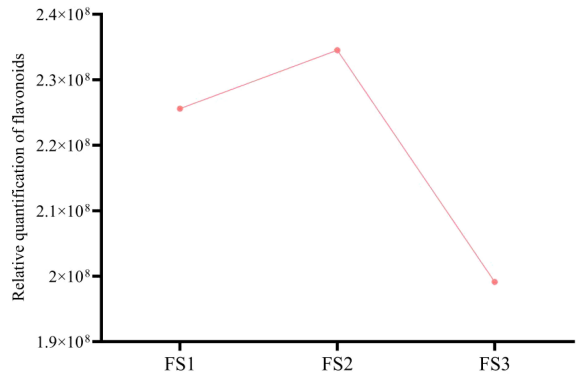

FIGURE 3
Changes in the total relative quantification of exocarp flavonoid compounds during different developmental periods (FS1-FS3) of oil palm fruits.

3.3 Joint analysis of metabolic transcriptome data of oil palm fruits at different developmental periods

The joint analysis of flavonoid metabolome and transcriptome data from oil palm fruits at various developmental stages revealed that differential metabolites and genes were primarily enriched in five pathways: flavonoid biosynthesis, anthocyanin biosynthesis, flavonoid and flavonol biosynthesis, phytometabolic, and secondary metabolite biosynthesis pathways (Figure 7). In the comparison between FS1 and FS2, the flavonoid biosynthesis pathway exhibited the highest number of enriched metabolites (3) and was the most significantly enriched pathway (Figure 7A). In FS1 vs. FS3, the anthocyanin biosynthesis pathway showed the most significant enrichment with five metabolites, while the flavonoid and flavonol biosynthesis pathways had the highest number of enriched metabolites but lacked significant enrichment (Figure 7B). Similarly, in FS3 vs. FS3, the anthocyanin biosynthesis pathway remained the most significantly enriched, with five metabolites, whereas the flavonoid and flavonol biosynthesis pathway contained six enriched metabolites but was not significantly enriched (Figure 7C).

10.3389/fpls.2025.1530673

TABLE 1 Relative quantification of flavonoids in oil palm exocarp across developmental stages.

Compounds	Class	Relative quantification of flavonoids at different developmental periods		
		FS1	FS2	FS3
Apigenin-6-C-glucoside (Isovitexin)*	Flavones	2019620.46	1462332.49	397627.64
5,7,3',5'-tetrahydroxy-6-methylfavanone	Flavones	93071.33	1824800.72	3941462.31
Diosmetin (5,7,3'-Trihydroxy-4'-methoxyflavone)*	Flavones	91445.73	1890541.58	3870042.83
Apigenin-8-C-Glucoside (Vitexin)*	Flavones	1932329.11	1525720.73	392020.71
5-Hydroxy-6,7,3',4'-tetramethoxyflavone	Flavones	3621.42	4943.89	17790.89
7,8-Dihydroxy-5,6,4'-trimethoxyflavone	Flavones	6050.10	9531.87	53277.67
6,7,8-Tetrahydroxy-5-methoxyflavone*	Flavones	93548.48	1857192.87	3645527.51
Luteolin-7,3'-di-O-glucoside	Flavones	162889.32	139912.74	8753.91
Chrysoeriol-5-O-glucoside	Flavones	526864.69	293592.78	117382.02
Demethoxysudachitin	Flavones	11691.19	137549.42	436256.74
Luteolin-7-O-(6''-sinapoyl)glucoside	Flavones	1072242.03	1074463.99	111278.89
4',5,7-Trihydroxy-3',6-dimethoxyflavone (Jaceosidin)*	Flavones	13910.22	148175.09	458275.68
5,7-Dihydroxy-3',4',5'-trimethoxyflavone	Flavones	9256.37	14342.01	82467.76
Tricin-7-O-(2''-feruloyl)glucoside	Flavones	705475.59	379078.63	30544.53
Luteolin-8-C-glucoside (Orientin)	Flavones	3564656.88	2605266.90	415992.50
Dihydroxy-dimethoxyflavone*	Flavones	3525.66	6988.13	0
3,5,7,2'-Tetrahydroxyflavone; Datiscetin	Flavones	20328.63	74437.94	122016.34
Gnetifolin B*	Flavones	941174.91	16393090.11	35568924.91
Luteolin-7-O-(6''-malonyl)glucoside*	Flavones	216449.81	97127.35	23363.70
4',5-Dihydroxy-3',5'-dimethoxyflavone	Flavones	8942.47	9446.69	77285.43
Luteolin-6-C-glucoside (Isoorientin)	Flavones	11555755.99	9329137.41	1015143.69
Pedaliin*	Flavones	382916.18	284639.15	86978.89
5,4'-Dihydroxy-3,6,7,3'-tetramethoxyflavone-4'-O-glucoside	Flavones	36036.67	27360.98	3692.06
[6-[2-(3,4-Dihydroxyphenyl)-5,7-dihydroxy-4-oxochromen-3-yl] oxy-3,4,5-trihydroxyoxan-2-yl]methyl acetate*	Flavones	3720338.06	3613463.21	887874.70
Hispidulin-7-O-(6''-O-p-Coumaroyl)Glucoside	Flavones	97833.66	72511.46	21128.34
3'-O-Methyltricetin-5-O-glucoside*	Flavones	487740.17	469753.54	115474.60
Hispidulin-8-C-glucoside	Flavones	149344.35	119091.50	24789.94
Isosaponarin(Isovitexin-4'-O-glucoside)	Flavones	161405.28	116599.92	32567.78
Tricin-4'-O-glucoside*	Flavones	295466.28	131533.29	66169.24
Luteolin-7-O-gentiobioside	Flavones	149272.48	170131.18	2477.02
Pectolinarigenin*	Flavones	3730.26	6213.40	0
Tricin-7-O-Glucuronide	Flavones	7875.15	7337.83	1392.99
Diosmetin-7-O-rutinoside (Diosmin)*	Flavones	269546.51	254449.49	52761.57
Chrysoeriol-8-C-glucoside (Scoparin)	Flavones	182647.11	110342.50	18930.53
Persicogenin (5,3'-dihydroxy-7,4'-dimethoxyflavanone)	Flavanones	1992.98	0	41497.84
Cirsilineol (4',5-Dihydroxy-3',6,7-trimethoxyflavone)	Flavanones	22014.28	41071.45	244873.34

(Continued)

10.3389/fpls.2025.1530673

TABLE 1 Continued

Compounds	Class	Relative quantification of flavonoids at different developmental periods		
		FS1	FS2	FS3
6-C-Glucosyl-2-Hydroxynaringenin	Flavanones	1151798.93	465535.10	224516.94
Aromadendrin-7-O-glucoside*	Flavanonols	885655.49	445495.90	218380.16
Taxifolin(Dihydroquercetin)	Flavanonols	28975.09	14020.04	6989.04
Hesperetin-7-O-glucoside	Flavanones	0	14521.49	4347.09
Taxifolin-3'-O-glucoside	Flavanonols	23067.85	12120.56	5368.11
Cyanidin-3-O-glucosylrutinoside	Anthocyanidins	19352.46	38290.65	6583.67
Peonidin-3-O-rutinoside	Anthocyanidins	154751.58	212483.70	12214.78
Cyanidin-3-O-(6"-O-p-coumaroyl)glucoside-5-O-glucoside	Anthocyanidins	45218.46	92330.09	11701.11
Cyanidin-3-O-rutinoside (Keracyanin)	Anthocyanidins	1058218.61	1862488.86	148579.56
Cyanidin-3-O-glucoside (Kuromanin)	Anthocyanidins	2343141.57	2362212.82	203875.44
Peonidin-3-O-glucoside	Anthocyanidins	67177.65	94717.09	5368.97
Cyanidin-3-O-(6"-O-malonyl)glucoside	Anthocyanidins	129740.70	270682.02	21457.54
3,5,4'-Trihydroxy-7-methoxyflavone (Rhamnocitrin)	Flavonols	91664.13	1956973.69	3879757.90
Quercetin-3-O-arabinoside	Flavonols	498076.14	294867.03	85321.06
5,4'-Dihydroxy-3,7-dimethoxyflavone(Kumatakenin)	Flavonols	134861.11	102067.47	966492.75
Morin-3-O-lyxoside	Flavonols	442938.92	285097.41	88199.58
Isorhamnetin; 3'-Methoxy-3,4',5,7-Tetrahydroxyflavone	Flavonols	86015.33	81902.51	11329.95
Kaempferol-3-O-(6"-malonyl)glucoside*	Flavonols	173294.87	74263.53	21421.32
Avicularin(Quercetin-3-O-α-L-arabinofuranoside)*	Flavonols	21592.29	10916.24	0
Morin	Flavonols	516432.66	504732.50	104138.66
Quercetin-7-O-(6"-malonyl)glucoside	Flavonols	732565.40	814849.33	176289.48
Rehderianin I	Flavonols	10467.99	123745.49	368656.02
Kaempferol-7-O-glucoside	Flavonols	375446.56	104576.34	43461.22
Isorhamnetin-3-O-(6"-acetylglucoside)	Flavonols	613569.29	420904.76	130610.11
Kaempferol-3-O-(6"-malonyl)galactoside*	Flavonols	166364.22	78066.59	16638.27
Kaempferol-3-O-galactoside (Trifolin)	Flavonols	93021.63	89114.60	17092.06
Isorhamnetin-3-O-(6"-malonyl)glucoside*	Flavonols	320042.32	262264.19	67188.85
Quercetin-3-O-sambubioside*	Flavonols	25208.77	14377.96	3114.81
Quercetin-3-O-(2"-O-acetyl)glucuronide	Flavonols	97622.57	69844.51	21525.05
Sexangularetin-3-O-glucoside-7-O-rhamnoside	Flavonols	5471675.85	3281744.78	1200804.43
Kaempferol-3-O-(6"-O-acetyl)glucoside	Flavonols	689470.35	296202.82	81782.25
8-Methoxykaempferol-7-O-rhamnoside	Flavonols	154721.96	136070.06	20165.95
Quercetin-3-O-glucoside (Isoquercitrin)	Flavonols	101017.68	60105.78	17693.22
Quercetin-3-O-galactoside (Hyperin)*	Flavonols	660741.22	385887.87	109223.27
Isorhamnetin-3-O-gallate	Flavonols	6732.05	20249.67	31132.22
Quercetin-3-O-apiosyl(1→2)galactoside*	Flavonols	23259.11	13121.89	4333.19
Quercetin-3-O-sophoroside (Baimaside)	Flavonols	16808.76	15141.60	1872.83

(Continued)

TABLE 1 Continued

Compounds	Class	Relative quantification of flavonoids at different developmental periods		
		FS1	FS2	FS3
Isorhamnetin-3-O-arabinoside	Flavonols	4303.43	1477.51	0
Limocitrin-3-O-galactoside	Flavonols	15554.59	17825.99	3745.71
Isorhamnetin-3-O-rutinoside-7-O-rhamnoside*	Flavonols	1112235.95	648935.04	263874.17
Morin-3-O-xyloside*	Flavonols	26754.62	19111.44	4583.89
Catechin-(7,8-bc)-4α-(3,4-dihydroxyphenyl)-dihydro-2-(3H)-one	Flavanols	25419.29	23563.74	6071.30
Epicatechin gallate*	Flavanols	7779.88	82904.80	9679.12
Gallocatechin 3-O-gallate	Flavanols	12158.19	51681.34	34475.50
Afzelechin (3,5,7,4'-Tetrahydroxyflavan)	Flavanols	24295.13	23868.02	4363.36
Epiafzelechin	Flavanols	7921.84	8118.93	0
O-Demethylforbexanthone	Other Flavonoids	499311.66	781147.08	117582.58
1,3,6-trihydroxy-2,5,7-trimethoxyxanthen-9-one	Other Flavonoids	550157.70	141463.00	13894.27
9,11-dimethoxy-2h-[1,3]dioxolo[4,5-b]xanthen-10-one*	Other Flavonoids	973870.96	16543900.64	35670120.09
1,3,6,8-tetrahydroxy-2,5-dimethoxyxanthen-9-one	Other Flavonoids	44424.85	14830.60	4258.32
1,2,4,5-tetrahydroxy-7-(hydroxymethyl)anthracene-9,10-dione	Other Flavonoids	151027.76	75128.35	32235.14
Iristectorigenin A*	Isoflavones	16447.14	139368.46	447987.42
Genistein-8-C-glucoside	Isoflavones	375945.39	279778.97	69260.90
Iristectorin A*	Isoflavones	323003.98	126168.33	69286.04
Genistein-7-O-galactoside*	Isoflavones	5254.35	4093.33	0

The values represent the relative abundance of each compound, measured in arbitrary units, as determined by metabolomics analysis. Compounds marked with an asterisk (*) denote isomeric forms identified during the study. Each compound is categorized into subclasses such as Flavones, Flavanones, Flavanonols, Anthocyanidins, Flavanols, Isoflavones, and Other Flavonoids. This classification highlights the diverse flavonoid profiles across developmental stages, providing insights into their dynamic changes and potential roles during oil palm exocarp development. (In Figures 1–3 and Table 1, the relative quantification is the integrated peak area of the substance in the sample, the peak area is actually the peak area of the peak at the retention time of the quantified ion of the corresponding substance, which represents its specific response intensity, and the higher the intensity of this response, the larger the peak area, which represents the larger the relative content of its substance in the sample.)

Among the identified pathway, the plant metabolic and secondary metabolite synthesis pathways were identified as the primary routes for synthesis and metabolism in plants, with most metabolites and genes enriched in fruit stages (FS). In the flavonoid biosynthesis pathway (Ko00941) (Table 2), metabolites such as Eriodictyol (5,7,3',4'-Tetrahydroxyflavanone), Afzelechin (3,5,7,4'-Tetrahydroxyflavan), and Epiafzelechin were co-enriched, along with Naringenin-7-O-Neohesperidoside (Naringin)*, Hesperetin-7-O-glucoside, and eight other differential metabolites. Additionally, 47 differentially expressed genes, including LOC105054663, LOC105054281, LOC105035842 were enriched. In the flavonoids and flavonols biosynthesis pathway (Ko00944) (Table 3), 10 differential metabolites such as Isovitexin*, Vitexin*, and Vitexin-2"-O-rhamnoside, as well as 18 differential genes including LOC105036086, LOC105055415, and LOC105058071 were enriched.

Within the flavonoid biosynthetic pathways, three differential metabolites and eight differential genes were enriched in FS1 VS FS2, five differential metabolites and 11 differential genes in FS1 VS FS3, and five differential metabolites and 14 differential genes in FS2 VS FS3. In the flavonoids and flavonols biosynthesis pathway, no differential metabolites or genes were enriched in FS1 VS FS2, whereas 10 differential metabolites and seven differential genes were enriched in FS1 VS FS3, and seven differential metabolites and six differential genes were enriched in FS2 VS FS3. Based on the results, suggest that the flavonoid biosynthesis pathway, flavonoids and flavonols biosynthesis pathway play important roles in the development and maturation of oil palm fruits, and promote flavonoids synthesis in the exocarp of oil palm during these stages.

In the flavonoid biosynthesis pathway (Ko00941) and the biosynthesis pathway of flavonoids and flavonols (Ko00944), Nr annotation of 65 significantly differentially expressed genes identified nine key enzyme genes—F3H, CHS, ANS, CYP75A, DFR, UGT73C6, and FG2—were highly expressed during oil palm fruit development (Table 4). Among the dynamic changes in the expression of these nine key enzyme genes (Figure 8), the expression of three genes, LOC105054663, LOC105036364, and LOC105048473 (encoding the enzyme F3H, CHS, and DFR), showed a decreasing trend from FS1-FS3., This trend aligned with the changes in the levels of metabolites such as Afzelechin, Quercetin-3 -O-sambubioside*, and Baimaside. In contrast, the expression of LOC105054281 (encoding ANS) increased initially and then decreased during the

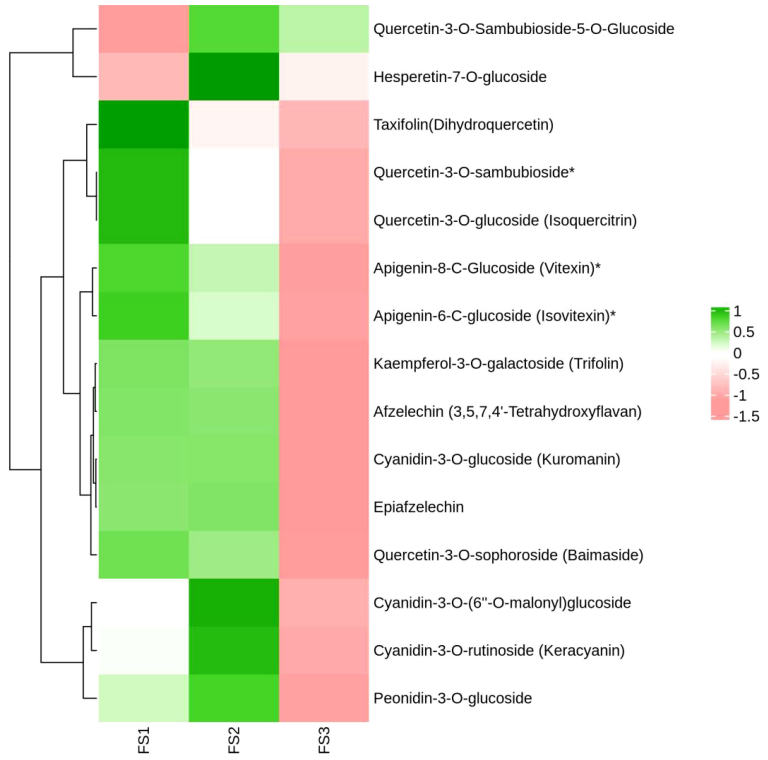

FIGURE 4
Clustering heat map of relative quantification of exocarp flavonoids in oil palm fruits at different developmental periods (FS1~FS3). (The horizontal coordinates are the different periods of the samples, the vertical coordinates are the differential metabolites, the different colors are the colors filled with the different values obtained from the standardized treatment of different relative contents (green represents high content, red represents low content), the dendrogram on the left side of the heat map represents the results of the hierarchical clustering of the differential metabolites, and the annotated strips on the right side of the clustering map correspond to the substances.)

FS1-FS3 period, correlating with the fluctuations in the levels of metabolites Epiafzelechin and Hesperetin-7-O-glucoside. The changes in the expression of these nine enzyme genes were correlated with the dynamic fluctuations in the content of the five differential metabolites. Notably the genes LOC105054663, LOC105036364, LOC105054281, and LOC105048473 (enzyme genes: F3H, CHS, ANS, and DFR) showed a significant positive correlation with Quercetin-3-O- sambubioside*. Additionally, LOC105048473 (enzyme gene: DFR) exhibited a significant positive correlation with Afzelechin, Epiafzelechin and Baimaside.

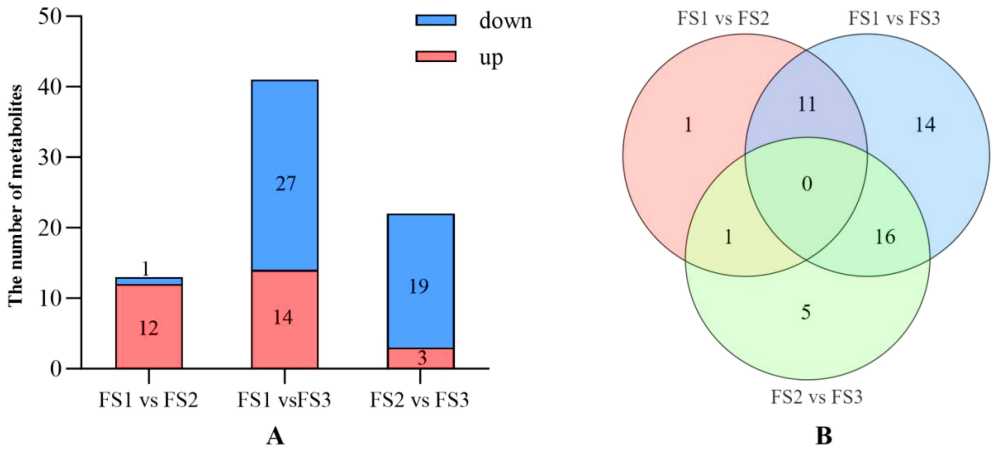

FIGURE 5
Differential statistics of flavonoid metabolites in the exocarp of oil palm fruits at different developmental stages (FS1-FS3). **(A)** Comparison of the number of upregulated and down-regulated metabolites and the trend of change at each stage of FS1 VS FS2, FS1 VS FS3, FS2 VS FS3. **(B)** Number of the same differential metabolites at each stage of FS1 VS FS2, FS1 VS FS3, FS2 VS FS3.

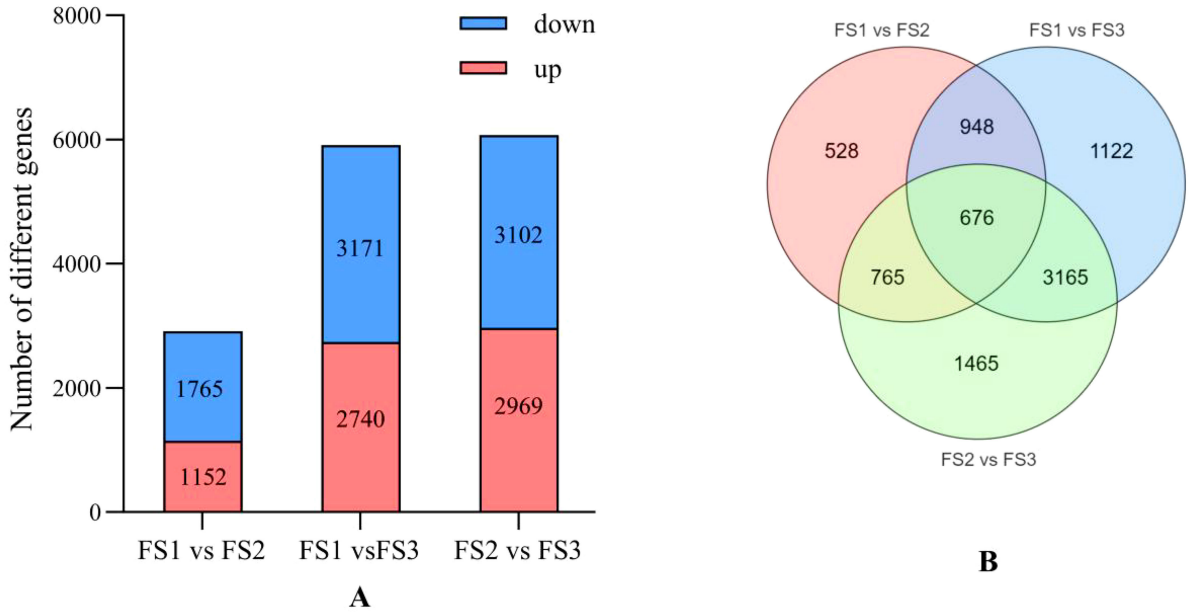

FIGURE 6
Differential statistics of flavonoid differential genes in the exocarp of oil palm fruits at different developmental stages (FS1-FS3). **(A)** Comparison of up-regulated and down-regulated differential genes and the trend of change at each stage of FS1 VS FS2, FS1 VS FS3, FS2 VS FS3. **(B)** Number of identical differential genes at each stage of FS1 VS FS2, FS1 VS FS3, FS2 VS FS3.

Conversley, LOC105054663, LOC105036364, and LOC105054281 (encoding F3H, CHS, ANS) displayed a significant negative correlation with Hesperetin-7-O-glucoside. Furthermore, the genes LOC105050451, LOC105055415, LOC105057418, and LOC105057419 (encoding CYP73A, UGT73C6, FG2-1, FG2-2 respectively) showed a significant negative correlation with Afzelechin, Epiafzelechin, *Quercetin-3-O- sambubioside*, and Baimaside. Finally, LOC105036086 (encoding CYP75A) exhibited a significant negative correlation with Epiafzelechin, Quercetin-3-O-sambubioside*, Baimaside.

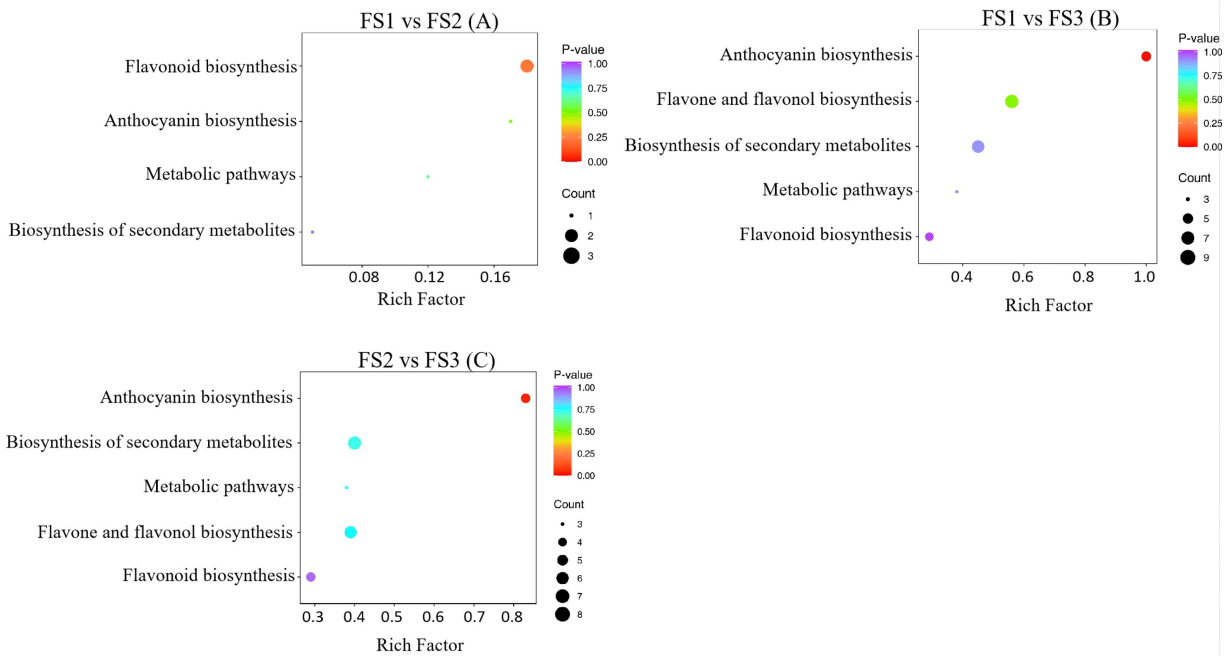

FIGURE 7
These three images **(A–C)** are described separately in the body of the article, and the images are framed the same way, so they do not need to be described separately again in the tag.

TABLE 2 Statistics of differential metabolites and differential genes related to flavonoid biosynthesis pathway (Ko00941) in exocarp of oil palm at different developmental stages (FS1-FS3).

	Differential metabolites	Differential gene ID
FS1 vs FS2	Naringenin-7-O-Neohesperidoside(Naringin)* Taxifolin(Dihydroquercetin) Hesperetin-7-O-glucoside	LOC105054663;LOC105036364;LOC105060373;LOC105054281; LOC105035842;LOC105058232;LOC105058071;LOC105034344
FS1 vs FS3	Apigenin-8-C-Glucoside (Vitexin)*, Taxifolin(Dihydroquercetin), Epiafzelechin, Galangin (3,5,7-Trihydroxyflavone), Hesperetin-7-O-glucoside	LOC105054663;LOC105050451;LOC105036364;LOC105060373; LOC105054281;LOC105035842;LOC105058232;LOC105058071; LOC105052441;LOC105034344 ;LOC105037012
FS2 vs FS3	Apigenin-8-C-Glucoside (Vitexin)*, Taxifolin(Dihydroquercetin), Epiafzelechin, Eriodictyol, Afzelechin	LOC105054663;LOC105052309;LOC105050451;LOC105036364; LOC105060373;LOC105045978;LOC105035842;LOC105058232; LOC105058071;LOC105052441;LOC105037012;LOC105040724; LOC105048473;LOC105041901

* means isomers.

TABLE 3 Statistics of differential metabolites and differential genes related to the biosynthesis pathway of flavonoids and flavonols in exocarpons of oil palm at different developmental stages (FS1-FS3) (Ko00944).

	Differential metabolites	Differential gene ID
FS1 vs FS2	\	\
FS1 vs FS3	Nicotiflorin*,Isovitexin*,3,7-Di-O-methylquercetin,Vitexin*,Vitexin-2”-O-rhamnoside,Trifolin,Vitexin-2”-O-rhamnoside,Cynaroside*, Isoquercitrin, Baimaside	LOC105058071;LOC105036086;LOC105041901;LOC105045491; LOC105055415;LOC105057418;LOC105057419
FS2 vs FS3	Isovitexin*,Vitexin*,Vitexin-2”-O-rhamnoside,Trifolin,Vitexin-2”-O-rhamnoside,Isoquercitrin, Baimaside	LOC105058071;LOC105036086;LOC105041901;LOC105057418; LOC105036426;LOC105057419

“” indicates that differential metabolites and differential genes on the flavonoid biosynthesis pathway (ko00941) were not detected. * means isomers.

TABLE 4 Correlation analysis of key enzyme gene expression levels and relative contents of main flavonoids during the development of oil palm fruit.

Gene Id	Genes	camomile	Epifriedelanol	Hesperidin 7-O-glucoside	Quercetin-3-O-sambubioside*	Baimaside
LOC105054663	*F3H*	0.65	0.73*	-0.88**	0.80**	0.68*
LOC105036364	*CHS*	0.70*	0.79*	-0.83**	0.82**	0.74*
LOC105054281	*ANS*	0.67*	0.76*	-0.87**	0.82**	0.69*
LOC105048473	*DFR*	0.81**	0.88**	-0.69*	0.86**	0.82**
LOC105050451	*CYP73A*	-0.90**	-0.96**	0.41	-0.89**	-0.89**
LOC105036086	*CYP75A*	-0.74*	-0.86**	0.66	-0.90**	-0.80**
LOC105055415	*UGT73C6*	-0.92**	-0.9**	0.58	-0.89**	-0.94**
LOC105057418	*FG2-1*	-0.87**	-0.95**	0.53	-0.90**	-0.85**
LOC105057419	*FG2-2*	-0.89**	-0.97**	0.46	-0.90**	-0.87**

“*” indicates a significant correlation ($P<0.05$), “**” indicates an extremely significant correlation ($P<0.01$).

In summary, F3H, CHS, ANS, and DFR may positively regulate Quercetin-3-O-sambubioside*. DFR may positively regulate the levels of Afzelechin Epiafzelechin and Baimaside. On the other hand, F3H, CHS, and ANS may downregulate the content of Hesperetin-7-O-glucoside. CYP73A, UGT73C6, FG2-1, and FG2-2 may negatively regulate Afzelechin, Epiafzelechin, Quercetin-3-O-sambubioside*, and Baimaside. Finally, CYP75A may downregulate the levels of Epiafzelechin, Quercetin-3-O-sambubioside*, Baimaside.

4 Discussions

High-flavonoid oil palm varieties have great nutritional and medicinal potential due to their rich bioactive compounds. Oil palm leaves contain higher polyphenols than green tea, including flavonoids like epigallocatechin and catechin, offering benefits such as protection against cancer, diabetes, hypertension, neurodegenerative diseases, and cardiovascular health (Mohamed,

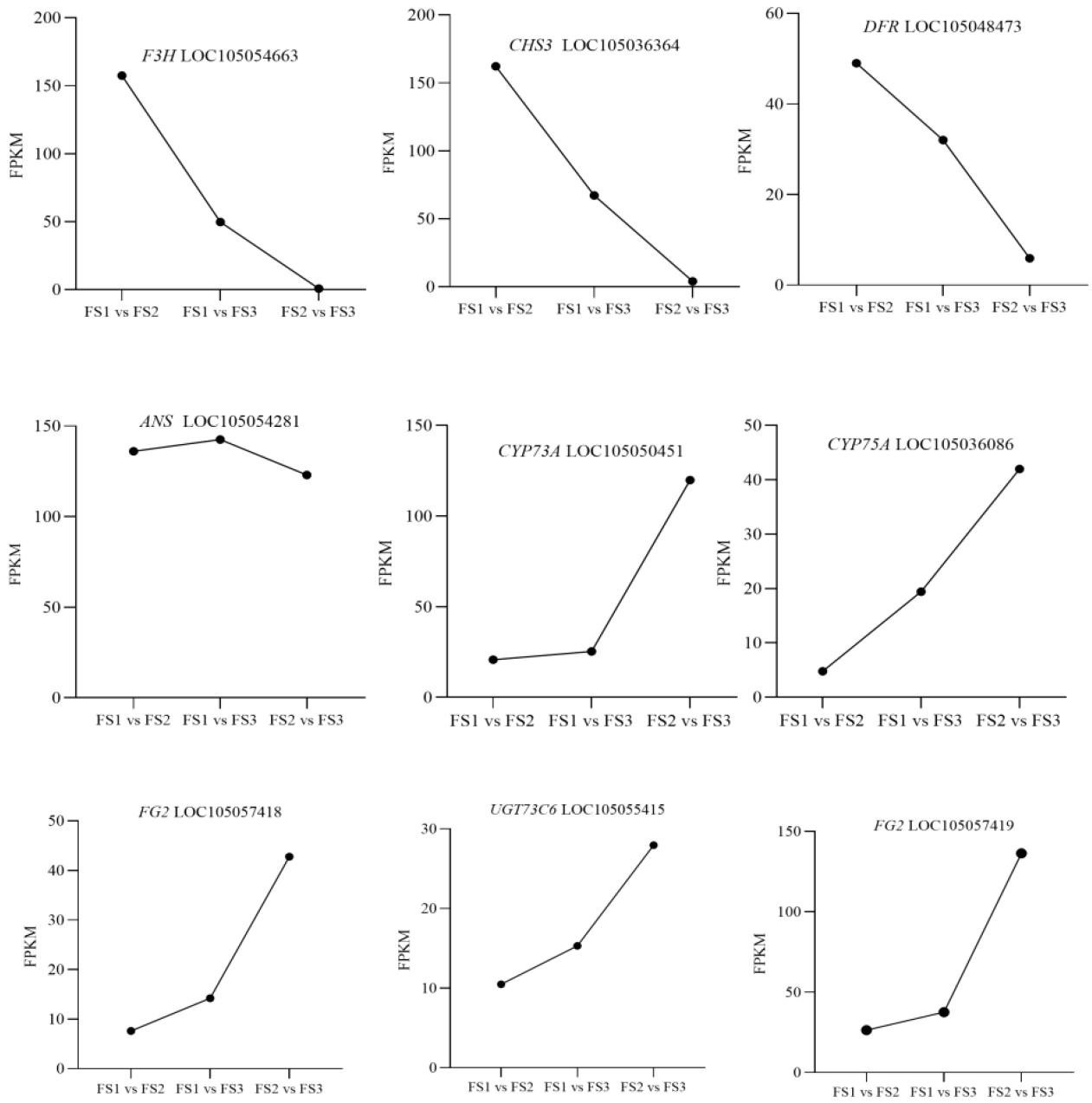

FIGURE 8
Dynamic changes of the relative contents of key enzyme genes in different stages of oil palm fruit (FS1~FS3). F3H:flavanone 3-hydroxylase, CHS: chalcone synthase, DFR:dihydroflavonol reductase, ANS:anthocyanidin synthase, CYP73A:Cytochrome P450 73A, CYP75A:Cytochrome P450 75A, FG2:flavonol-3-O-glucoside L-rhamnosyltransferase, UTG: UDP-glycosyltransferase,.

2014). The Palm Fruit Bioactive Complex (PFBc), derived from palm oil, is rich in antioxidants and polyphenols, which reduce inflammation and improve cognitive function, particularly during aging (Hewlings et al., 2021). Genetic engineering and conventional breeding can enhance the nutritional value of palm oil by increasing carotene and vitamin E content, which provide antioxidative and cardioprotective benefits (Ithnin et al., 2023).

Flavonoids serve diverse functions in plants, including antibacterial and antifungal activities, as well as roles in plant coloration, root growth, and pollen development. In this study, we explored the variations in flavonoid accumulation in oil palm at different stages (FS1-FS3) using metabolomics techniques. The results showed that the primary pathways for flavonoid synthesis in oil palm exocarp were the flavonoid biosynthesis pathway and the flavonoid and flavonol biosynthesis pathway. Additionally, the differential metabolite Afzelechin, Epiafzelechin, Hesperetin-7-O-glucoside, Quercetin-3-O-sambubioside*, and Baimaside, were closely associated with flavanoid content in oil palm pericarp.

Transcriptome sequencing is a widely utilized tool in the study of plant flavonoids. CHS is a key enzyme that catalyzes the first critical step in the flavonoid biosynthesis pathway (Wang et al., 2018), while DFR regulates the metabolic flux of flavonoids (Lei

et al., 2023). In this study, the expression of CHS and DFR in FS showed a continuous decline, a trend that was consistent with, and positively correlated to the relative content of metabolites such as Afzelechin, Quercetin-3-O-sambubioside*, and Baimaside. These finding suggest that CHS and DFR may play a positive regulatory role in the biosynthesis of flavonoids in oil palm exocarp. Similarly, the expression of F3H in FS also exhibited a continuous decrease, aligning with the relative contents of Afzelechin, Quercetin-3-O-sambubioside*, and Baimaside. A positive correlation was observed between the metabolites Quercetin-3-O-sambubioside* and Baimaside. Among the enzyme genes related to flavonoid synthesis, it was found that CHS and F3H were positively regulated in both the flavonoid biosynthesis and flavonoid and flavonol biosynthesis pathways (Yang et al., 2023). The expression of ANS in FS initially increased and then decreased during fruit ripening, reflecting the changes in the content of Epiafzelechin and Hesperetin-7-O-glucoside. Specifically, ANS expression was positively correlated with Epiafzelechin but negatively correlated with Hesperetin-7-O-glucoside. This pattern aligns with findings in the Azalea cultivar 'Fenhe', where down-regulation of ANS was associated with pink coloration (Xia et al., 2022). The expression levels of CYP73A, CYP75A, UGT73C6, and FG-2 in FS were consistently elevated, along with increased contents of Afzelechin, Epiafzelechin, and Quercetin-3-O-sambubioside*, Baimaside. This led to hypothesized that CYP73A, CYP75A, UGT73C6 and FG-2 play a negative regulatory role in the biosynthesis of flavonoids in the oil palm exocarp. In the context of Begonia exocarp browning, CYP73A has been identified as a key gene influencing flavonoid accumulation (Yang et al., 2024a). Meanwhile the enzyme gene CYP75A, and its associated gene family are closely associated to flavonoid biosynthetic enzymes and the regulation of pigments (Yuanyuan et al., 2023). Additionally, UGT73C6, a glycosyltransferase involved in flavonol glycoside biosynthesis in *Arabidopsis thaliana* (Patrik et al., 2003). Genes like FG2 and F3H are highly expressed in sour orange, which biosynthesis fortified flavonoid compounds with enhanced antioxidant activity to detoxify the deleterious effects of reactive oxygen species produced during drought stress (Rao et al., 2023). Flavonoid concentrations, particularly flavonols, are frequently linked to color changes in plants. For instance, in hibiscus, flavonol concentrations exhibit an inverse relationship with anthocyanin levels, playing a significant role in flower coloration and antioxidant activity (Mejía et al., 2023). In oil palm, previous research has distinguished between black-fruited and green-fruited varieties, with black coloration attributed to anthocyanins and carotenoids contributing to fruit coloration in both varieties (Suraninpong and Nuanlaong, 2022). This study revealed that the ratio of flavonol content to total flavonoid content in the oil palm pericarp ranged from 21.62% to 38.45%. Although few studies have explored flavonols in oil palm, the findings suggest that high flavonol content may contribute to color changes in the exocarp during fruit development. Therefore, hypothesized that a high content of flavonols may be related to color changes in FS oil palm exocarp.

The insights gained from this study have potential applications in the development of high-flavonoid oil palm varieties. Enhanced flavonoid content could improve the nutritional value of oil palm products. Further research could focus on manipulating key regulatory genes, such as CHS, F3H, DFR, and ANS, through genetic engineering or marker-assisted selection to achieve these goals. By advancing our understanding of flavonoid biosynthesis in oil palm, this study lays the groundwork for practical applications in agriculture, food, and biotechnology.

5 Conclusions

Study provides new insights into the flavonoid metabolism in oil palm, specifically in the mesocarp and exocarp. As the fruit develops and ripens, the relative content of flavonoids initially increases and then decreases, which may be influenced by the flavonoid biosynthetic pathway, enzyme gene regulation, and differential metabolites. Key genes such as F3H, CHS, ANS, and DFR are likely involved in promoting the synthesis of flavonoids like quercetin-3-O-sambubioside, afzelechin, epiafzelechin, and baimaside. Conversely, genes such as CYP73A, CYP75A, UGT73C6, and FG2 appear to suppress the synthesis of these flavonoids, suggesting complex regulatory mechanisms in the biosynthesis of flavonoids in oil palm fruits.

The findings of this study offer valuable genetic insights into the regulation of flavonoid synthesis and metabolism, laying the groundwork for future research into the molecular mechanisms underlying flavonoid biosynthesis in oil palm. To deepen our understanding, further investigations are needed to explore the functional roles of the nine key enzyme genes identified—F3H, CHS, ANS, DFR, CYP73A, CYP75A, UGT73C6, FG2-1, and FG2-2. Future work should include functional experiments to confirm these gene functions and examine their interactions with transcription factors. Ultimately, this research could contribute to the development of oil palm varieties with enhanced flavonoid content, offering new opportunities for product development and the sustainable utilization of oil palm.

Data availability statement

The datasets presented in this study can be found in online repositories. The names of the repository/repositories and accession number(s) can be found in the article/Supplementary Material. The data presented in the study are deposited in the NCBI repository, accession number PRJNA1236833.

Author contributions

RZ: Writing – original draft. JJ: Writing – review & editing, Data curation. XLiu: Conceptualization, Methodology, Writing – review & editing. XLi: Data curation, Writing – original draft. LZ: Conceptualization, Methodology, Writing – original draft. RL: Conceptualization, Data curation, Writing – original draft. XF: Data curation, Writing – original draft. WL: Methodology, Writing

– review & editing. HC: Formal Analysis, Supervision, Writing – review & editing.

Funding

The author(s) declare that financial support was received for the research and/or publication of this article. This study was supported by National Key R&D Program of China (No. 2023YFD2200700); Special Project for Basic Research Operating Costs of the Chinese Academy of Tropical Agricultural Sciences (No. 1630152022001); Demonstration and Dissemination of Key Technologies for Oil Palm Production in Indonesia (GHYF2024019); and Henan Province Science and Technology Research Project (NO. 232102320272).

Conflict of interest

The authors declare that the research was conducted in the absence of any commercial or financial relationships that could be construed as a potential conflict of interest.

Generative AI statement

The author(s) declare that no Generative AI was used in the creation of this manuscript.

Publisher's note

Supplementary material

The Supplementary Material for this article can be found online at: https://www.frontiersin.org/articles/10.3389/fpls.2025.1530673/full#supplementary-material

References

Casas, M. I., Duarte, S., Doseff, A. I., and Grotewold, E. (2014). Flavone-rich maize: an opportunity to improve the nutritional value of an important commodity crop. *Front. Plant Sci.* 5, 440. doi: 10.3389/fpls.2014.00440

Chen, S., Zhou, Y., Chen, Y., and Gu, J. (2018). *fastp: an ultra-fast all-in-one FASTQ preprocessor* Vol. 34 (Oxford, England: Bioinformatics), i884–i890.

Falcone Ferreyra, M. L., Rius, S. P., and Casati, P. (2012). Flavonoids: biosynthesis, biological functions, and biotechnological applications. *Front. Plant Sci.* 3. doi: 10.3389/fpls.2012.00222

Guo, X. Y., Lv, Y. Q., Ye, Y., Liu, Z. Y., Zheng, X. Q., Lu, J. L., et al. (2021). Polyphenol oxidase dominates the conversions of flavonol glycosides in tea leaves. *Food Chem.* 339, 128088. doi: 10.1016/j.foodchem.2020.128088

Hewlings, S. J., Draayer, K., and Kalman, D. S. (2021). Palm Fruit Bioactive Complex (PFBc), a source of polyphenols, demonstrates potential benefits for inflammaging and related cognitive function. *Front. Plant Sci.* 13, 1127. doi: 10.3390/nu13041127.13

Ithnin, M., Othman, A., Tahir, N. I. M., Banisetti, K. B., Abd Halim, M. A., and Rajesh, M. K. (2023). "Oil palm: Genome designing for improved nutritional quality," in *Compendium of crop genome designing for nutraceuticals*. Ed. C. Kole (Springer Nature Singapore, Singapore), 1–41. doi: 10.1007/978-981-19-4169-6_22

Jiu, S., Guan, L., Leng, X., Zhang, K., Haider, M. S., Yu, X., et al. (2022). The role of VvMYBA2r and VvMYBA2w alleles of the MYBA2 locus in the regulation of anthocyanin biosynthesis for molecular breeding of grape (Vitis spp.) skin coloration. *Plant Biotechnol. J.* 19, 1216–1239. doi: 10.1111/pbi.13543

John Martin, J. J., Yarra, R., Wei, L., and Cao, H. (2022). Oil palm breeding in the modern era: challenges and opportunities. *Plants* 11, 1395. doi: 10.3390/plants11111395

Jones, P., Messner, B., Nakajima, J. I., Schaffner, A. R., and Saito, K. (2003). UGT73C6 and UGT78D1, glycosyltransferases involved in flavonol glycoside biosynthesis in Arabidopsis thaliana. *J. Biol. Chem.* 278, 43910–43918. doi: 10.1074/jbc.m303523200

Kalt, W., Cassidy, A., Howard, L. R., Krikorian, R., Stull, A. J., Tremblay, F., et al. (2020). Recent research on the health benefits of blueberries and their anthocyanins. *Adv. Nutr. (Bethesda Md.)* 11, 224–236. doi: 10.1093/advances/nmz065

Khodadadi, F., Tohidfar, M., Vahdati, K., Dandekar, A. M., and Leslie, C. A. (2020). Functional analysis of walnut polyphenol oxidase gene (JrPPO1) in transgenic tobacco plants and PPO induction in response to walnut bacterial blight. *Plant Pathol.* 69, 756–764. doi: 10.1111/ppa.13159

Lai, J., Li, C., Zhang, Y., Wu, Z., Li, W., Zhang, Z., et al. (2023). Integrated transcriptomic and metabolomic analyses reveal the molecular and metabolic basis of flavonoids in areca catechu L. *J. Agric. Food Chem.* 71, 4851–4862. doi: 10.1021/acs.jafc.2c08864

Lan, X., Yang, J., Abhinandan, K., Nie, Y., Li, X., Li, Y., et al. (2017). Flavonoids and ROS play opposing roles in mediating pollination in ornamental kale (Brassica oleracea var. acephala). *Mol. Plant* 10, 1361–1364. doi: 10.1016/j.molp.2017.08.002

Lei, T., Huang, J., Ruan, H., Qian, W., Fang, Z., Gu, C., et al. (2023). Competition between FLS and DFR regulates the distribution of flavonols and proanthocyanidins in Rubus chingii Hu. *Front. Plant Sci.* 14, 1134993. doi: 10.3389/fpls.2023.1134993

Li, Y., Zhao, X., Zhang, M. M., He, X., Huang, Y., Ahmad, S., et al. (2023). Genome-based identification of the CYP75 gene family in Orchidaceae and its expression patterns in Cymbidium goeringii. *Front. Plant Sci.* 13, 1243828. doi: 10.3389/fpls.2023.1243828

Mejía, J. J., Sierra, L. J., Ceballos, J. G., Martínez, J. R., and Stashenko, E. E. (2023). Color, antioxidant capacity and flavonoid composition in hibiscus rosa-sinensis cultivars. *Molecules* 28, 1779. doi: 10.3390/molecules28041779

Mohamed, S. (2014). Oil palm leaf: A new functional food ingredient for health and disease prevention. *Front. Plant Sci.* 5. doi: 10.4172/2157-7110.1000300

Murata, K., Kitano, T., Yoshimoto, R., Takata, R., Ube, N., Ueno, K., et al. (2020). Natural variation in the expression and catalytic activity of a naringenin 7-O-methyltransferase influences antifungal defenses in diverse rice cultivars. *Plant J.* 101, 1103–1117. doi: 10.1111/tpj.14577

Rao, M. J., Feng, B., Ahmad, M. H., Tahir ul Qamar, M., Aslam, M. Z., Khalid, M. F., et al. (2023). LC-MS/MS-based metabolomics approach identified novel antioxidant flavonoids associated with drought tolerance in citrus species. *Front. Plant Sci.* 14, 1150854. doi: 10.3389/fpls.2023.1150854

Sadat-Hosseini, M., Bakhtiarizadeh, M. R., Boroomand, N., Tohidfar, M., and Vahdati, K. (2020). Combining independent *de novo* assemblies to optimize leaf transcriptome of Persian walnut. *PloS One* 15, e0232005. doi: 10.1371/journal.pone.0232005

Shen, N., Wang, T., Gan, Q., Liu, S., Wang, L., and Jin, B. (2022). Plant flavonoids: Classification, distribution, biosynthesis, and antioxidant activity. *Food Chem.* 383, 132531. doi: 10.1016/j.foodchem.2022.132531

Suraninpong, P., and Nuanlaong, S. (2022). Comparative transcriptome profiling and molecular marker development for oil palm fruit color. *Sci. Rep.* 12, 15507. doi: 10.1038/s41598-022-19890-2

Tan, H., Man, C., Xie, Y., Jun, Y. J., and Fang, C. J. (2019). A crucial role of GA-regulated flavonol biosynthesis in root growth of Arabidopsis. *Mol. Plant* 12, 521–537. doi: 10.1016/j.molp.2018.12.021

Testai, L., and Calderone, V. (2017). Nutraceutical value of citrus flavanones and their implications in cardiovascular disease. *Nutrients* 9, 502. doi: 10.3390/nu9050502

Wang, Z., Yu, Q., Shen, W., El-Mohtar, C. A., Chun, Z. X., and Gmitter, F. J. (2018). Functional study of CHS gene family members in citrus revealed a novel CHS gene

affecting the production of flavonoids. *BMC Plant Biol.* 18, 1–13. doi: 10.1186/s12870-018-1418-y

Xia, X., Gong, R., and Zhang, C. (2022). Integrative analysis of transcriptome and metabolome reveals flavonoid biosynthesis regulation in Rhododendron pulchrum petals. *BMC Plant Biol.* 22, 401. doi: 10.1186/s12870-022-03762-y

Yang, N. (2023). *Joint transcriptome and metabolome analysis of flavonoid content differences during the growth of golden sunflower Anemones* (Inner Mongolia Agricultural University). doi: 10.27229/d.cnki.gnmnu.2023.001245

Yang, C., Sun, N., Qin, X., Liu, Y., Sui, M., Zhang, Y., et al. (2024a). Multi-omics analysis reveals the biosynthesis of flavonoids during the browning process of Malus sieversii explants. *Physiologia Plantarum* 176, e14238. doi: 10.1111/ppl.14238

Yang, C., Zhang, S., John Martin, J. J., Fu, X., Li, X., Cheng, S., et al. (2024b). An in-depth study of anthocyanin synthesis in the exocarp of virescens and nigrescens oil palm: metabolomic and transcriptomic analysis. *BMC Plant Biol.* 24, 910. doi: 10.1186/s12870-024-05607-2

Zain, M. S. C., Yeoh, J. X., Lee, S. Y., Afzan, A., and Shaari, K. (2021). Integration of choline chloride-based natural deep eutectic solvents and macroporous resin for green production of enriched oil palm flavonoids as natural wound healing agents. *Antioxidants* 10, 1802. doi: 10.3390/antiox10111802

Zhang, M., Zhang, J., Xiao, Q., Li, Y., and Jiang, S. (2024). Reduction of flavonoid content in honeysuckle via Erysiphe lonicerae-mediated inhibition of three essential genes in flavonoid biosynthesis pathways. *Front. Plant Sci.* 15. doi: 10.3389/fpls.2024.1381368

Zhou, L., Sun, X., Iqbal, A., Yarra, R., Wu, Q., Li, J., et al. (2024). Revealing the aromatic sonata through terpenoid profiling and gene expression analysis of aromatic and non-aromatic coconut varieties. *Int. J. Biol. Macromolecules* 280, 135699. doi: 10.1016/j.ijbiomac.2024.135699

Frontiers in
Plant Science

Cultivates the science of plant biology and its applications

The most cited plant science journal, which advances our understanding of plant biology for sustainable food security, functional ecosystems and human health.

Discover the latest Research Topics

See more →

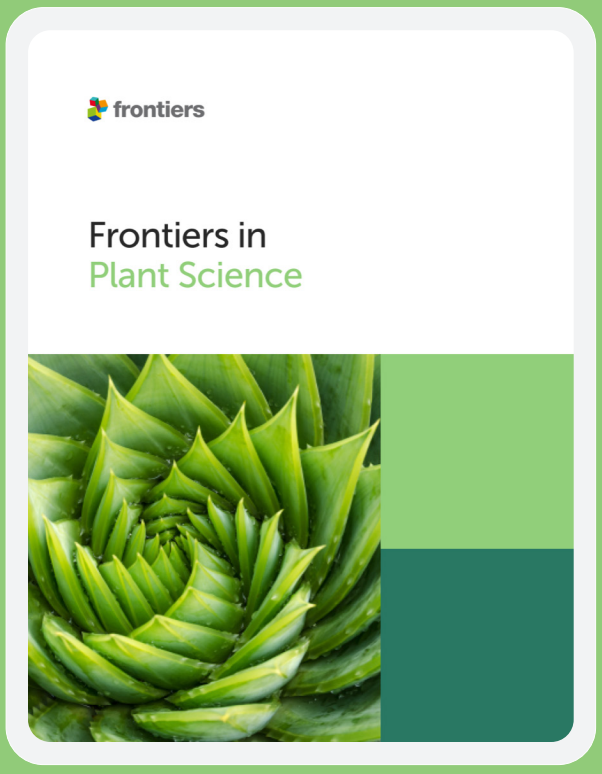

Frontiers

Avenue du Tribunal-Fédéral 34
1005 Lausanne, Switzerland
frontiersin.org

Contact us

+41 (0)21 510 17 00
frontiersin.org/about/contact